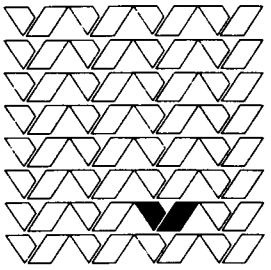
vinçotte

Quality assurance - Quality control - Survey
P.O. Box 11
B - 1640 Rhode-St-Genèse Tel : 02. 358 35 80 Telex : 225 50

ARCHIVES

NUCLEAR SAFETY DIVISION



OECD ORGANISATION FOR ECONOMIC CO-OPERATION AND DEVELOPMENT
COMMITTEE ON THE SAFETY OF NUCLEAR INSTALLATIONS
CSNI REPORT N° 46

PROCEEDINGS

OF THE SPECIALISTS' MEETING ON

RELIABILITY OF THE ULTRASONIC INSPECTION OF AUSTENITIC MATERIALS

Brussels, Belgium
29 - 30 May 1980

Hosted by the
ASSOCIATION VINCOTTE

Editor : P. CAUSSIN — Association Vinçotte

FOREWORD

The ultrasonic inspectability of austenitic materials and components is a controversial subject of discussion in the international nuclear circle since those materials were specified for major parts of primary systems of both light water and sodium cooled nuclear reactors. Initially those materials were deemed uninspectable by ultrasonics. However in the early seventies special techniques did appear and were immediately tested on site. In view of the preliminary results, large research programs were launched all over the world to improve the performances, to understand the difficulties, and to establish the confidence level of ultrasonics applied to nuclear austenitic materials. In the mean time, existing ultrasonic testing techniques were systematically applied on primary and auxiliary circuits and cladding areas. Specific service problems such as intergranular stress corrosion cracking, sub-cladding cracking, peculiar geometries also required development of adapted techniques.

Informed of those developments by its Working Group on Safety Aspects of Steel Components of Nuclear Installations, the OECD (Organization for Economic Co-operation and Development) - Committee for the Safety of Nuclear Installations (CSNI) decided to gather all known specialists of these problems to make up the state of the art and draw recommandations for further actions. At the invitation of the OECD - Nuclear Energy Agency (NEA), a programme group was established (appendix 1) and Association VINCOTTE of Belgium hosted and organized the specialist meeting. 84 invited delegates from three international organizations and 14 american, asian and european countries gathered in Brussels for a two days debate.

The reader will find in the next pages, the 24 reports presented as well as short summaries of discussion periods. From these three major points emerged :

- the knowledge of the behaviour of ultrasonic waves in austenitic materials has made essential progresses. It shows that a successful ultrasonic inspection depends often on the previous knowledge of the macrostructure involved. Therefore the participants recommended that material standards be more stringent to assess more reproducible austenitic macrostructures and that specific non-destructive methods be developed to test on site the peculiarities of actual materials.

- At present the ultrasonic inspection of austenitic materials can be effective with a high level of preparation and a carefull choice of probes and instruments. Furthermore new techniques based on signal analysis theories appear and some already are at the stage of industrial demonstration. The participants were of the opinion that they might bring soon significant improvements.

- All trials and new developments presented were based upon specific test pieces. However due to the reported variability of austenitic structures, such pieces do not provide a satisfactory basis for comparison. Therefore the participants strongly recommended that a worldwide international programme be organized to collect common sets of pieces, to objectively compare all available techniques using these, and to draw specific recommandations. Such a programme was though to be initiated by 1985.

To conclude the foreword, I would like to thank all individuals and organizations who helped me to organize this meeting. First of all my thanks go to OECD for its support and specifically to Mr. P. OLIVER for his advices and his aid. I am also very glad to aknowledge the very effective help I got from all Programme Group members and session chairmen. Last but not least, my thanks go also to Association VINCOTTE for its financial support, and to the personnel of its Public Relation Service for its very effective management of all practical aspects of the meeting.

P. CAUSSIN
Engineer - Section Head
Association Vinçotte
Belgium

CONTENTS

SESSION 1 : FUNDAMENTALS — Page

- The effect of anisotropy on the propagation of ultrasonic waves in austenitic stainless steel — 2
  A. JUVA, Technical Research Centre of Finland
  J. LENKKERI, University of Oulu, Finland

- Contribution to improving ultrasonic testing of thick bimetallic welds — 25
  B. TRUMPFF, J-P. LAUNAY, J-J. OLIVERA
  Framatome, France

- Some fundamental aspects of testing austenitic steel structures by ultrasonics — 41
  W. OPPERMAN, H.A. CROSTACK
  Dortmund University, F.R. Germany

- Utilization of a Fisher linear discriminant function in IGSCC detection — 55
  J-L. ROSE, M-J. AVIOLI, Drexel University, USA
  M.E. LAPIDES, Electric Power Research Institute, USA

- On the applicability of ultrasonic testing techniques for coarse grain austenitic welds — 93
  E. NEUMANN, M. ROEMER, R. SCHENK, K. MATTHIES
  Federal Institute for Material Testing, F.R. Germany

- Overview of Argonne National Laboratory efforts on ultrasonics NDE of stainless steel welds — 119
  D.S. KUPPERMAN, K.J. REIMANN
  Argonne National Laboratory, USA

SESSION 2 : INSTRUMENTS AND METHODS

- Longitudinal wave ultrasonic inspection of austenitic weldments — 150
  B.S. GRAY, R.J. HUDGELL, H. SEED
  United Kingdom Atomic Energy Authority

- Ultrasonic testing technique of fuel cladding tubes for FBR - Grass echo suppression technique — 169
  M. IGARASHI, T. SHIBATA, M. MIURA
  Power Reactor and Nuclear Fuel Development Corporation, Japan

Page

- Experience of ultrasonic inspections of fillet and butt welds in austenitic steel in Heysham and Hartlepool A.G.R.'s — 188
  J.R. TOMLINSON, A-R. WAGG
  Central Electricity Generating Board, United Kingdom

- Improved ultrasonic inspection of austenitic stainless steel components by signal averaging techniques — 201
  S. KRAUS, K. GOEBBELS
  Fraunhofer - Institut für Zerstörungsfreie Prüfverfahren, F.R. Germany

- Multiple-bearing-angle (MBA) crack detector for cladded pipe examinations — 214
  G. GRUBER
  Fraunhofer - Institut für Zerstörungsfreie Prüfverfahren, F.R. Germany

- Flaw-to-grain echo enhancement by split-spectrum processing — 232
  V.L. NEWHOUSE, N.M. BILGUTAY, J. SANIIE
  Purdue University, USA

- Ultrasonic Imaging techniques in non-destructive evaluation — 244
  S. GANAPATHY
  University of Michigan, USA

- Ultrasonic inspection of stainless steel pipe weldments for IGSCC — 265
  M.E. LAPIDES
  Electric Power Research Institute, USA

  Written contribution shortly introduced by
  J.L. ROSE
  Drexel University, USA

SESSION 3 : INDUSTRIAL PRACTICE

- Application of ultrasonic testing techniques on austenitic welds for fabrication and in-service inspection — 286
  X. EDELMANN
  Sulzer Brothers Limited, Switzerland

- Recent experiences in the ultrasonic examination of austenitic steel components — 304
  M. KROLL, E. FISCHER, M. STERNISCHA, H.D. WALLHEINKE
  Kraftwerk Union, F.R. Germany

Page

- Present practice on ultrasonic in-service inspection through austenitic stainless steel on nuclear piping in Spain 333
  J.B. PEREZ PRAT
  Tecnatom S.A, Spain

- Detection of underclad defects by non-destructive testing 349
  J-P. LAUNAY, J-C. LECOMTE, P. MARTIN, A. THOMAS
  Framatome, France

- Sizing of cracks perpendicular to stainless steel overlay by ultrasonic testing 374
  T. SAITOH, Japan Steel Works
  S. TAKAHASHI, Chiyoda Chemical Engineering and Construction Co, Ltd, Japan

SESSION 4 : RELIABILITY

- Report on a survey of ultrasonic testing in austenitic weld material 396
  S. SANDBERG, Tekniska Roentgen Centralen, Sweden

- Ultrasonic examination of stainless steel E.B. welds by an immersion technique 403
  G. TORRIDA, G. ANTONIOLA, D. LATERZA
  Fiat T.T.G. S.p.A., Italy

- Factors affecting the reliability of the ultrasonic examination of austenitic components 421
  P. CAUSSIN, J. CERMAK, D. VERSPEELT
  Association Vinçotte, Belgium

- Detectability of intergranular stress corrosion cracking using field proven ultrasonic techniques 441
  C.E. LAUTZENHEISER, W.C. MAC GAUCHEY
  Southwest Research Institute, USA

- Ultrasonic inspection reliability for primary piping systems 456
  F.L. BECKER
  Battelle Northwest Laboratory, USA

PANEL SESSION 481

Appendix : Programme Group 493

SESSION 1 : FUNDAMENTALS

Chairmen : X. EDELMANN, Sulzer Brothers Limited, Switzerland

K. GOEBBELS, Fraunhofer - Institut für Zerstörungsfreie Prüfverfahren, F.R. Germany

The effect of anisotropy on the propagation of ultrasonic waves in austenitic stainless steel.

A. JUVA - Technical Research Center of Finland
J. LENKKERI - University of Oulu, Finland

ABSTRACT

Austenitic stainless steel single crystals were used for measuring ultrasonic velocities and attenuations for both longitudinal and shear wave modes in certain crystallographic orientations. Calculations of the orientation dependence of the velocities as well as energy flux deviations were performed using the velocity measured in the 110 direction.

Using the single crystal data the attenuation caused by Rayleigh scattering was calculated corresponding to polycrystalline materials. The attenuation was 2.5 times higher than in ferritic steel with similar grain size.

In a spherical single crystal specimen some unexpected phenomena occurred. The reasons for these phenomena were analyzed. In the sphere 111 lattice directions were the most favourable for the propagation of ultrasound whereas the 100 directions were very poor. The propagation in the 110 directions was between that of the 111 and 100 directions. However, these results at least partly depend on the spherical shape of the specimen.

To study the effects of grain size and orientation polycrystalline welded and casted specimens having a 100 fibre texture were studied and the results were analyzed using calculations based on the single crystal measurements. For longitudinal waves in polycrystalline specimens the 45° direction to the axis of the columnar grains gave remarkably lower attenuation values than other directions. It was also observed

that the attenuation of the longitudinal waves parallel to the grains was slightly lower than perpendicular to them. For propagation of shear waves the 0° and 90° directions to the columnar grain axis were most favourable. In the perpendicular case the shear wave had to be polarized parallel to the grain axis to obtain maximum penetration. The observed phenomena were explained on the basis of velocity and energy flux calculations.

I INTRODUCTION

Ultrasonic examination of austenitic stainless steel welds and castings is restricted by the strong attenuation of ultrasound. The attenuation of ultrasound depends on various parameters among which grain size and texture have an important role. However, when comparing the theories and results of several researchers, it must be concluded that the effects of grain size and texture are not yet clear (Caussin, 1978).

In the following the effects of grain size and texture are analyzed on the basis of measurements made in austenitic stainless steel single crystals as well as in strongly textured polycrystalline specimens.

Theoretically the attenuation of ultrasound is smaller in a single crystal than in polycrystalline materials because the scattering at grain boundaries is missing. In a single crystal the attenuation is rather low in low index lattice directions. In more complicated lattice directions the direction of energy flux i.e. propagation direction deviates from the wave front normal i.e. from the easy propagation direction leading to high apparent attenuation. The ultrasound velocity and energy flux varies in different lattice directions depending on the elastic anisotropy of the material. In polycrystalline materials the grain boundary scattering is also the larger the more anisotropic the material is i.e. the more the acoustic impedances of the adjacent grains differ from each other.

Depending on the relationship between the ultrasonic wave length λ and the average grain size D, Papadakis

(1965) gave the well known equations for the attenuation a caused by grain boundary scattering:

Rayleigh scattering when $\lambda >> D$: $a = K_1 f^4 D^3$ (1)

stochastic scattering when $\lambda \sim D$: $a = K_2 f^2 D$ (2)

diffusive scattering when $\lambda < D$: $a = K_3 D^{-1}$ (3)

where f is the frequency of the ultrasound. The coefficients K_1, K_2 and K_3 depend on the elastic anisotropy of the crystals.

For the Rayleigh and stochastic scattering the coefficients K_1 and K_2 include a factor $\mu^2 = (c_{11}-c_{12}-2c_{44})^2$, where c_{11}, c_{12} and c_{44} are the three independent elastic coefficients of a cubic crystal. In an isotropic crystal $\mu = 0$, which means that no scattering exists. On the contrary, in anisotropic materials, the scattering is very strong.

The advantages of using low frequency under conditions, where the Rayleigh and stochastic scattering exist, are very apparent because the frequency affects the scattering by its 4th and 2nd power in Eqs. (1) and (2). On the other hand according to equation (3) the frequency has no influence on the diffusive scattering. In deformed materials the grain size is usually smaller than the wave length and thus Rayleigh scattering predominates, and the attenuation a decreases with decreasing grain size D. In castings and welds the grain size is usually larger than the wave length and consequently mainly diffusive scattering occurs the attenuation a decreasing when the grain size D increases.

could be performed in all possible orientations. However, some practical difficulties occurred, which are discussed later in this paper.

To measure the attenuation and velocity in different directions in the polycrystalline materials several specimens were fabricated. Cylinders with 30 mm diameter and 30 mm length as well as 30x30x30 mm cubes were fabricated with their axes in different directions. These specimens were used only for longitudinal wave measurements. All of the interesting directions were available. Immersion techniques with focussed probes as well as an interferometer were applied.

For being able to study the attenuation of the shear wave mode in the 0°, 45° and 90° directions to the columnar grains also triangular specimens were made. Immersion technique was used also for these studies. Varying the angle of incidence in water, either longitudinal or shear waves could be generated in the specimen.

Another experimental arrangement applying a special device was used to obtain accurate velocity values for both longitudinal and polarized shear waves. These measurements were performed to determine the elastic coefficients and anisotropy of the single crystal. For these measurements a 5 mm thick plate was cut from the single crystal. The orientation of the surfaces parallel to the 110 plane was checked by X-ray Laue photographs. The angle of misorientation was less than 1°. The velocities of the longitudinal mode and two different transverse modes with polarization in 001 and $1\bar{1}0$ directions, respectively, were measured by a 10 MHz pulse-echo-overlap apparatus similar to that of Hellier et al. (1975). X-cut and Y-cut quartz transducers attached to the sample by phenylsalicylate were used for the longitudinal and transverse waves, respectively.

One transducer in each measurement operated as both transmitter and receiver. In the ultrasonic equipment the time base of the oscilloscope is triggered by a signal generator with a frequency selected so that two echoes of the echo-train are in accurate overlap on the screen of the oscilloscope. The output of the same signal generator is also divided by 10, 100 or 1000 in a frequency divider and lead to trigger the pulsed oscillator, which produces the ultrasonic pulses. The transit time between the selected echoes is the inverse of the frequency of the signal generator. This corresponds to the exact overlap. The absolute accuracy in the determination of the ultrasonic velocity is about 0.1 % but small changes of about 0.005 % in the velocity arising from e.g. temperature changes may be detected.

The density of the sample measured by hydrostatic weighing is 8057.5 kgm^{-3}, which was used in calculations of the elastic coefficients.

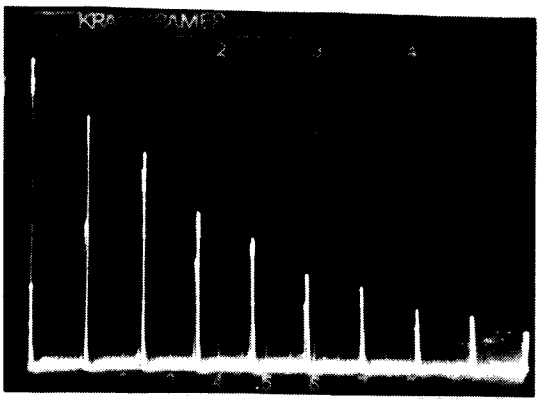
Plate-like specimens were also cut from the polycrystalline materials A and B. However, because of the strong attenuation the measurements at 10 MHz were possible only in few directions.

3 RESULTS

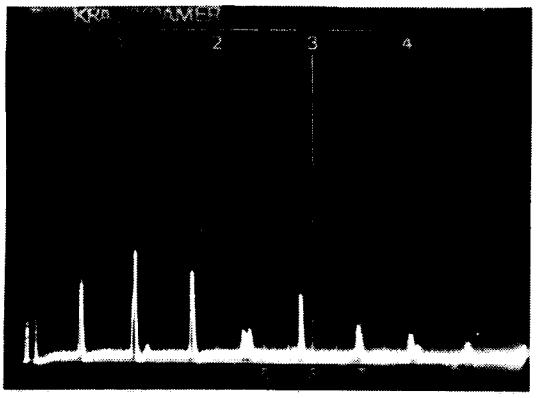
3.I SINGLE CRYSTAL MEASUREMENTS

The screen displays obtained with the single crystal sphere in the directions 111, 110 and 100 using a 2 MHz transducer are presented in Fig. 3. In other directions no back wall echoes were obtained. In each measurement the second back wall echo was less sensitive to the variation of the angle of incidence. When adjusting the second echoes to the 0-level of the screen

a.



b.



c.

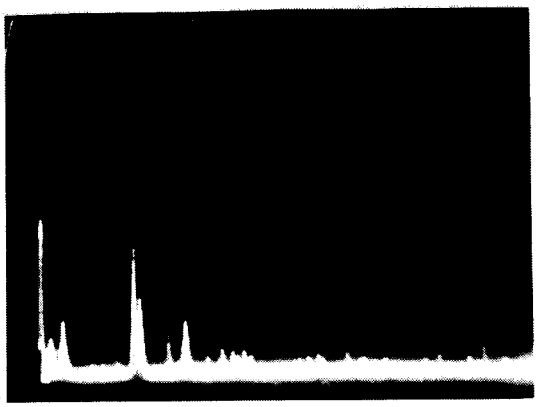


Fig. 3. Screen displays obtained in the single crystal sphere in the directions a) 111, b) 110, and c) 100.

Table 2 Velocities and attenuations measured from the single crystal specimens.

Specimen	Mode	Direc-tion	Polar-ization	v, m/s	a,dB/cm
plate	long.	110	110	6085	0.67
plate	trans.	110	001	4014	1.17
plate	trans.	110	$1\bar{1}0$	2086	1.87
sphere	long.	111	111	6300	-
sphere	long.	110	110	6080	-

the superiority of the 111 directions was recognized. In the 110 directions an amplification increase of 8 dB was needed compared to the 111 directions. In the 100 directions the needed increase of amplification was 22 dB.

The velocities measured from the single crystal sphere with the interferometer as well as the velocities and attenuations obtained from the plate like specimen with the pulse-echo-overlap method are given in Table 2.

3.2 MEASUREMENTS IN TEXTURED POLYCRYSTALS

The longitudinal wave velocity and attenuation measured with a 2 MHz transducer in the polycrystalline cubes at angles 0°, 45° and 90° with respect to the columnar grain axis are given in Table 3. The attenuation in the 45° direction is clearly the lowest in both materials. The parallel direction (0°) is the second best direction and the perpendicular one (90°) is clearly the worst. These results are in agreement with those obtained by Baikie et al., 1976 and Kupperman et al., 1976.

The results obtained with the cylindrical specimens also prove the superiority of the 45° direction. In all other directions the attenuation was so strong that even the first back wall echo was not obtained. Fig. 4a gives a typical screen display representing these

2 EXPERIMENTAL PROCEDURES

An austenitic stainless steel single crystal, and two polycrystalline strongly textured materials were studied. The single crystal was delivered by Aremco Products, USA. Due to difficulties in growing the single crystal, the final sample consisted of a few separate grains. One of those was, however, large enough for this study. A 30 mm diameter sphere was spark cut from the large crystal. The shape and surface quality of the specimen were finished with extreme care by polishing and etching. In Fig. 1a the single crystal sphere is seen etched before final cutting off from the cylinder. Some primary lattice directions can be seen on the sphere. On the final polished and etched surface in Fig. 1b the cubic lattice symmetry can be seen.

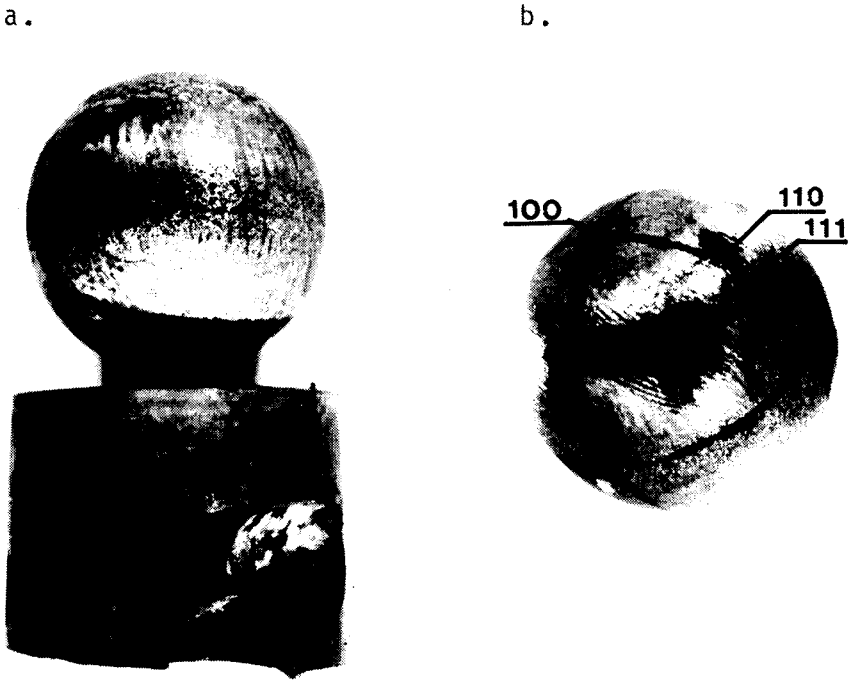


Fig. 1. The spherical single crystal. a) etched before final cutting, b) finished.

One of the polycrystalline materials (material A) was produced with submerged arc overlay welding. Its cross

section perpendicular to the welding direction is presented in Fig. 2a. The other material (B) was a slice of a continuously casted slab, a macrograph of which is seen in Fig. 2b. In both materials a clear solidification texture can be seen. With X-ray diffraction measurements a strong 100 texture was observed in the solidification direction of material A. In material B a texture consisting of both 100 and 111 poles was recognized, the former being the stronger. The chemical compositions of the materials are given in Table 1.

a. b.

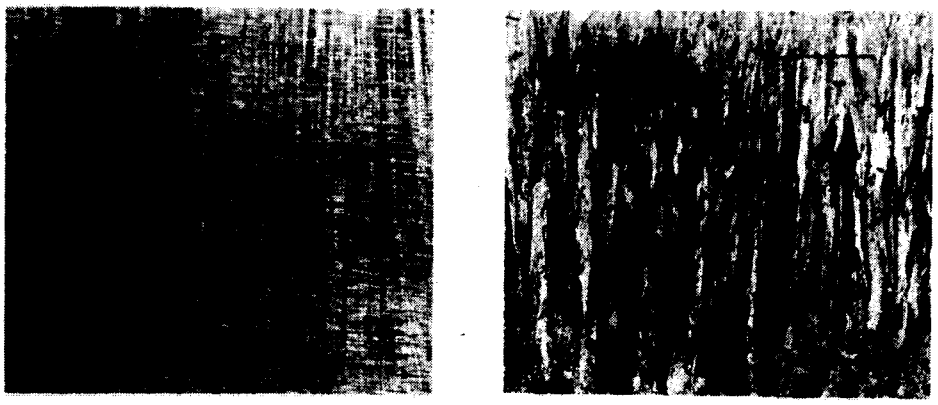


Fig. 2. Macrographs of a) weld material A (scale 1.75:1) and b) casting B (scale 1:1.5).

Table 1. Chemical compositions of the materials used for the studies.

Material	Composition %													
	C	Si	Mn	S	P	Cr	Ni	Mo	Cu	Ti	Al	W	V	Nb
single crystal	0.05	0.04	0.02	0.005	0.005	14.5	14.5	2.5	0.03	-	-	-	-	-
weld, A	0.03	0.6	1.58	0.027	0.027	18.0	9.5	0.12	0.15	0.002	0.10	0.10		0.05
casting, B	0.02	0.71	0.84	0.014	0.017	19.3	11.6	2.47	0.06	0.00	-	-	0.03	-

The attenuation and velocity in the spherical single crystal were measured both with immersion techniques with focussed probes and using an interferometer with different frequencies. Only longitudinal wave measurements were made with this specimen. The spherical form was assumed to be very useful because measurements

directions. The attenuation was clearly lowest for the 45° direction. The characteristics of material A in the 45° direction were: v_L = 5910...6090 m/s, and a = 1.7 dB/cm. A typical display for the 45° direction is shown in Fig. 4b. The previously mentioned difference between the attenuations in 0° and 90° directions was not observed here because of the scattering effect at the convex surface of the cylinders.

Table 3 The longitudinal velocity v_L and attenuation a measured at 2 MHz in different directions with respect to the columnar grain axis in materials A and B using 30x30x30 mm cubic specimens.
x) In this direction no back wall echoes were obtained.

Material	Direction	v_L, m/s	a, dB/cm
A	0°	5000-5030	1.2-1.3
A	45°	6000-6040	0.7-0.8
A	90°	5140-5280	2.3-2.8
B	0°	5220	1.8
B	45°	6140	1.0-1.3
B	90°	x)	x)

a. b.

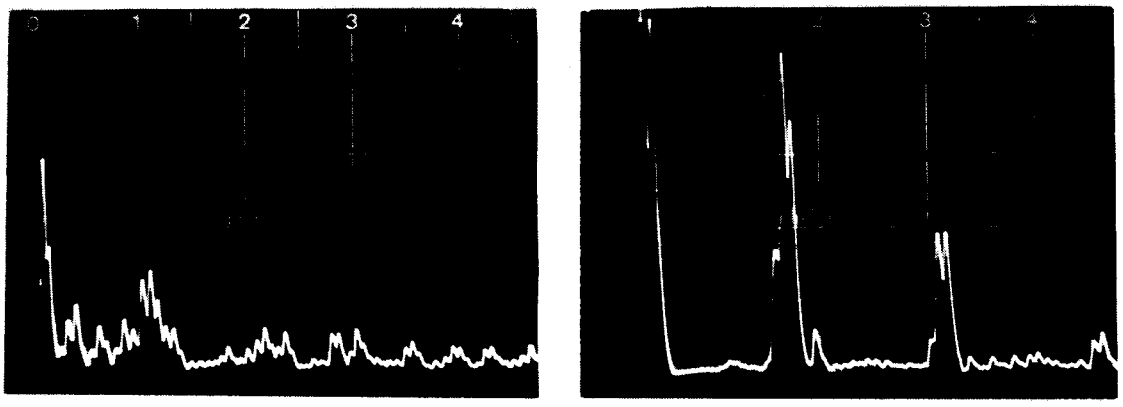


Fig. 4. Screen displays obtained from cylindrical specimens of material A using the same amplification.
a) parallel to the columnar grain axis
b) in 45° direction to the columnar grain axis.

The results obtained from the plate like specimens using the pulse-echo-overlap method with 10 MHz are given in Table 4. The tests were made in directions

0°, 45° and 90° both in the welded material A and in the casting B. However, results were obtained only in the directions and with the modes given in Table 4.

Table 4 The results obtained from the polycrystalline plate-like specimens at 10 MHz.

Material	Mode	Direc-tion	Polar-ization	v, m/s	a, dB/cm
A	long.	0°	-	5308	5.9
A	trans.	0°	90°	3960	7.4
A	long.	45°	-	6228	6.0
A	trans.	90°	0°	4060	9.7
B	long.	45°	-	6287	5.8

The results obtained from the triangular specimens of materials A and B using immersion technique are visualized in Fig. 5. The only angles of incidence in water in which a back wall echo from the specimen could be obtained are shown in the figure. Velocity measurements support the conclusion that for 10° and 11° angles of incidence the mode is longitudinal and for 16° transversal.

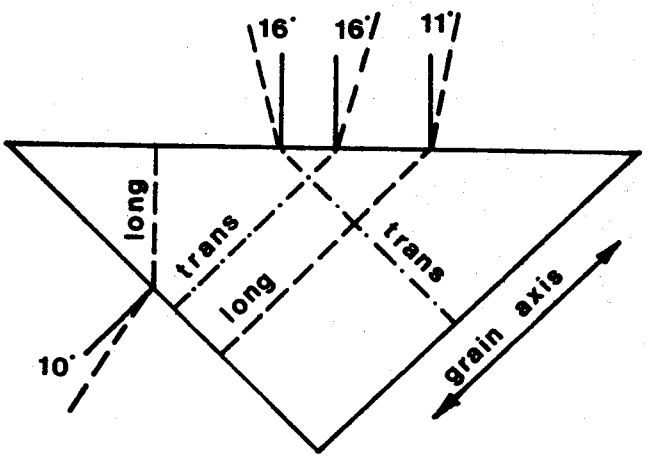


Fig. 5. Angles of incidence in water and wave modes in triangular specimens.

In the direction parallel to the grain axis both longitudinal and transversal modes seem to penetrate the material. However, in the perpendicular direction only the transversal mode and in the 45° direction only the longitudinal mode can be created in the material.

4 THEORETICAL CONSIDERATIONS

4.I THE ELASTIC COEFFICIENTS

The elastic coefficients of a cubic crystal are related to the velocities of ultrasonic waves in the 110 directions through the equations:

$$\rho v_L^2 = 1/2\ (c_{11} + c_{12} + 2c_{44})$$

$$\rho v_{T_1}^2 = c_{44} \qquad (3)$$

$$\rho v_{T_2}^2 = 1/2\ (c_{11} - c_{12}),$$

where v_L is the longitudinal wave velocity, and v_{T_1} and v_{T_2} are the transverse wave velocities with the polarization in the 001 and $1\bar{1}0$ directions, respectively. The three independent elastic coefficients c_{11}, c_{12} and c_{44} are then obtained from the velocity measurements in one crystal direction of the 110 type. The calculated coefficients for the present austenitic steel single crystal are: $c_{11} = 2.036 \times 10^{11}\ Nm^{-2}$, $c_{12} = 1.335 \times 10^{11}\ Nm^{-2}$ and $c_{44} = 1.298 \times 10^{11}\ Nm^{-2}$.

The velocities v_i ($i = 1, 2, 3$) in an arbitrary crystal direction with mutually orthogonal polarization vectors (r_i, s_i, t_i) obey an equation of motion which in a crystal of cubic symmetry has a form of three simultaneous equations (Truell et al., 1969):

$$(A_{11} - \rho v^2)r + A_{12}s + A_{13}t = 0$$

$$A_{21}r + (A_{22} - \rho v^2)s + A_{23}t = 0 \qquad (4)$$

$$A_{31}r + A_{32}s + (A_{33} - \rho v^2)t = 0,$$

where

$$A_{11} = c_{44} + (c_{11} - c_{44})n_x^2,$$
$$A_{21} = A_{12} = (c_{12} + c_{44})n_x n_y$$

$$A_{22} = c_{44} + (c_{11} - c_{44})n_y^2,$$
$$A_{31} = A_{13} = (c_{12} + c_{44})n_x n_z$$

$$A_{33} = c_{44} + (c_{11} - c_{44})n_z^2,$$
$$A_{32} = A_{23} = (c_{12} + c_{44})n_y n_z$$

and n_x, n_y and n_z are the direction cosines of the wave front normal.

The values of v are obtained from the condition that the determinant formed by the coefficients of r, s and t in Eq. (4) must be zero. This condition leads to a cubic equation for v^2 and three real and positive values for v in each crystal direction. For each value of v the corresponding polarization vector may then be obtained from Eq. (4). In each direction the three values of v correspond to the three modes with mutually orthogonal polarization vectors. In special symmetry directions such as the 100, 110 and 111 directions one of them is a pure longitudinal mode and the other two pure transverse modes. In an arbitrary direction there are one quasilongitudinal and two quasitransversal modes.

4.2 ORIENTATION DEPENDENCE OF THE VELOCITIES

The Eqs. (4) were solved by computer for 25 different directions of the wave front normal, (Fig. 6). The wave front normals corresponded to 25 pairs of angles α and β (Fig. 7), which varied from 0° to 90° and from 0° to 45°, respectively, with intervals of 15°. The values of velocity and polarization direction in the other parts of the direction space are obtained by sym-

metry. The velocities in four different crystal planes corresponding to four different values of β are presented in Fig. 8. The orientation dependence of the velocity is much stronger for the transverse modes than for the longitudinal mode. The longitudinal velocity is highest for the 111 directions and lowest for the 100 directions.

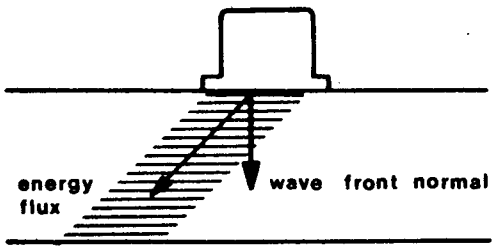


Fig. 6. Visualization of the wave front normal and the direction of energy flux i.e. "propagation direction".

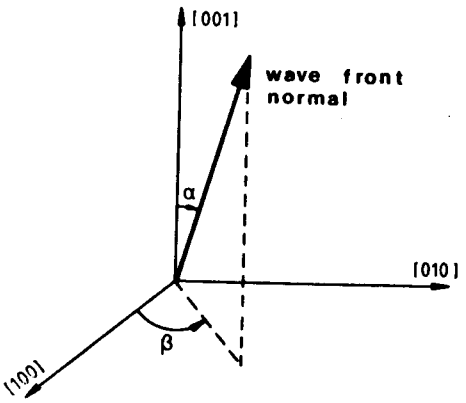


Fig. 7. Angles α and β defining the wave front normal direction.

4.3 ENERGY FLUX DEVIATION

In an elastically isotropic medium the wave front normal direction is also the direction of energy flux (propagation direction) of the ultrasonic pulse (Fig. 6). In an anisotropic medium the direction of energy flux deviates from the wave front normal except in some symmetry directions of the crystal. The direction of the energy flux of the pulse is the normal of the corresponding "slowness surface" (Auld, 1973). The slow-

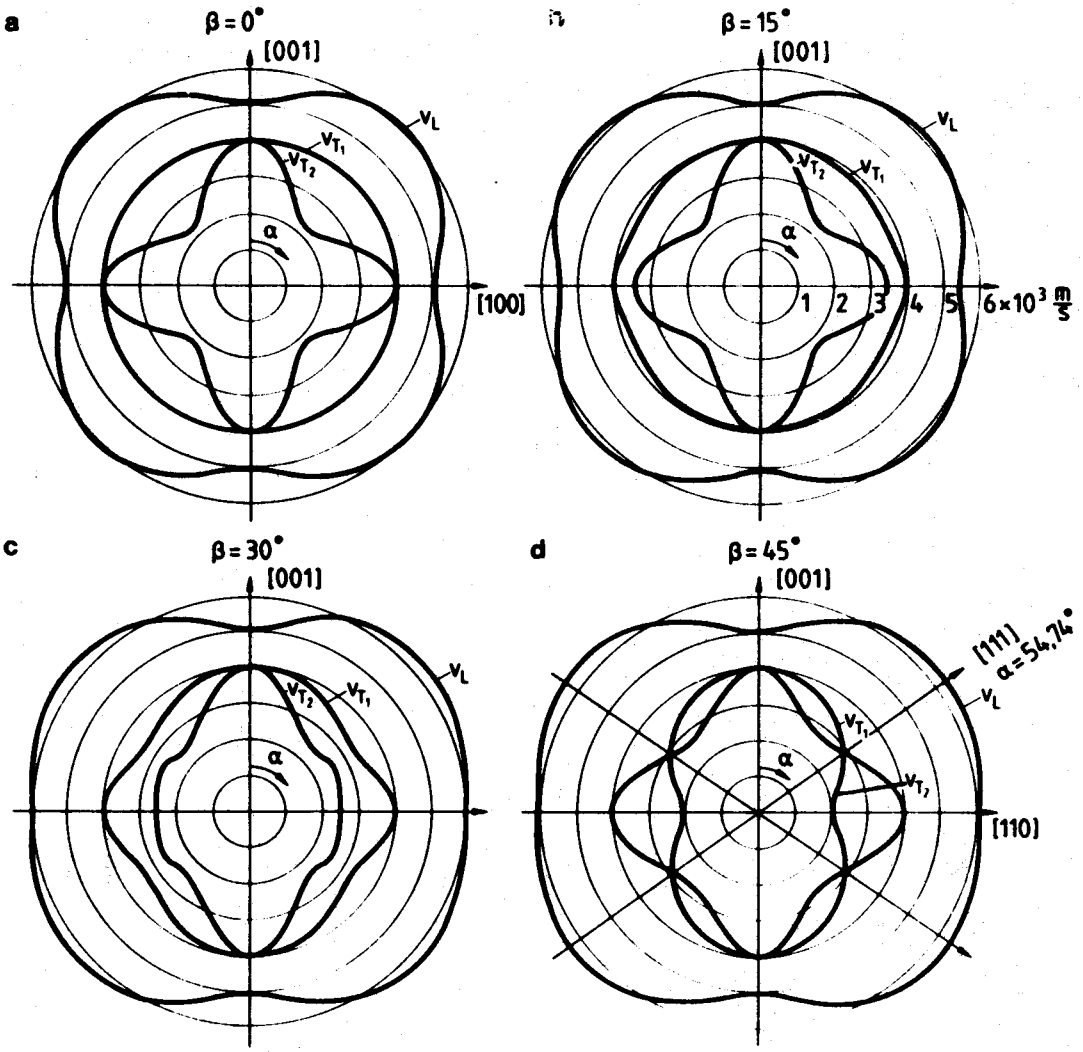


Fig. 8. Orientation dependence of velocity in four crystal planes presented in polar coordinates.

ness furface means the resiprocal of the velocity presented as a function of crystal direction. Cross sections of the slowness surfaces corresponding to the angle β of 0°, 15°, 30° and 45° are presented in Fig. 9.

5 DISCUSSION

The experiments made on the single crystal sphere may be compared to the calculations presented in chapter 4. The observation that measurements were possible

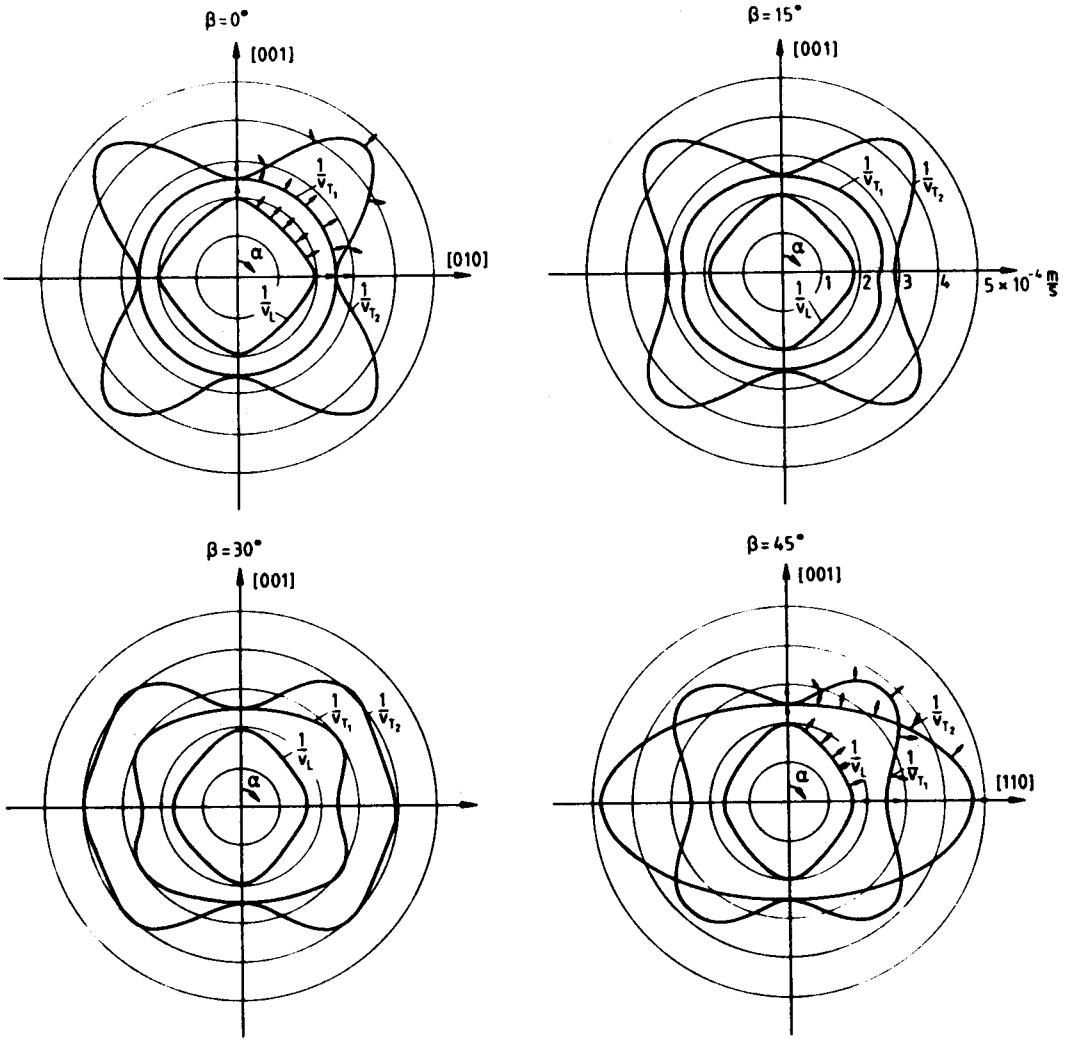


Fig. 9. Cross sections of the slowness surfaces corresponding to $\beta = 0^\circ$, 15°, 30° and 45°. The small arrows in a) and d) represent the directions of energy flux.

only in some symmetry directions of the crystal is consistent with the fact that the direction of energy flux differs from the wave front normal. Therefore an ultrasonic pulse aimed to be sent through the sphere deviates from the exact diagonal direction and no echo pattern is obtained in an arbitrary direction of the single crystal sphere.

In the symmetry directions 100, 110 and 111 the measurements should be possible because here the energy flux is parallel to the wave front normal. In the 110

and 111 directions the echo pattern was indeed obtained. In the 111 directions the amplitude decay was exponential but in the 110 directions the amplitude fluctuated quite irregularly from echo to echo as seen in Fig. 3. In the 100 directions only one echo was visible in Fig. 3c. A possible reason for this is that the curvature of the slowness surface is quite strong in the vicinity of the 100 direction as seen in Fig. 9. Thus even a small deviation of the wave front normal from the ideal 100 direction causes a strong deviation in the direction of the energy flux. Therefore, the beam having a width of a couple of millimeters diverges strongly in the 100 direction. On the contrary, in the 111 directions the slowness surface is quite flat near the 111 direction and the normal of the surface i.e. the energy flux is quite accurately in the 111 direction in spite of small deviations in the wave front normal direction. Both the experiments and the curvature of the slowness surface indicate that the situation in the 110 directions is somehow intermediate between the cases of 100 and 111 directions.

Even in the 111 directions the echo pattern was quite sensitive for small changes in the direction of the incident ultrasonic beam. A misorientation of about 2° decreased drastically the amplitudes of the echoes of odd order numbers but left the amplitudes of the even echoes unchanged as seen in Fig. 10. A possible reason for this is suggested in Fig. 11. In the vicinity of the 111 directions of the sphere it may be possible that the pulse reflects back and forth in the sphere along a slightly V-shaped path. This may be the case if the wave front normal coinsides with the normal of the surface of the sphere in the reflection points A and B in Fig. 11. In this case every second echo does not hit or only partly hits the receiver.

The values of the longitudinal wave velocities in the 111 and 110 directions of the sphere are in fairly good

a. b.

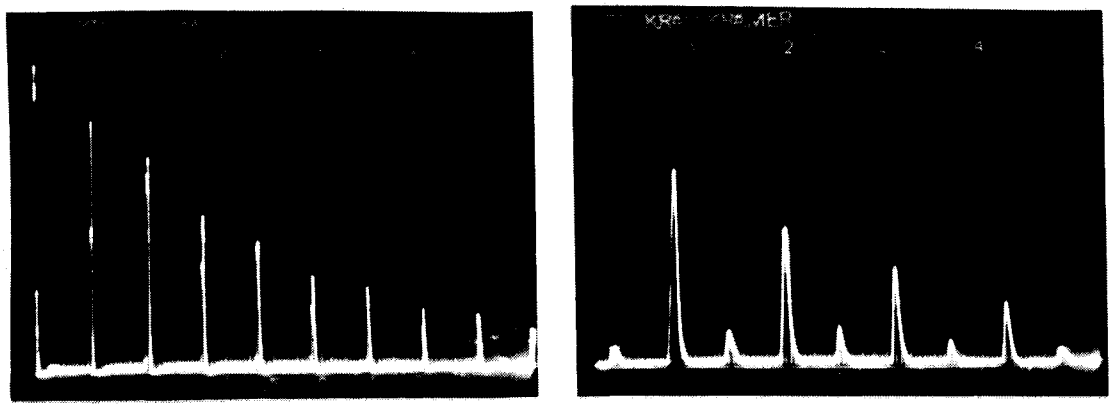


Fig. 10. The effect of a small misorientation (about 2°) on the echo pattern obtained in the 111 direction of the single crystal sphere. a) no misorientation b) 2° misorientation.

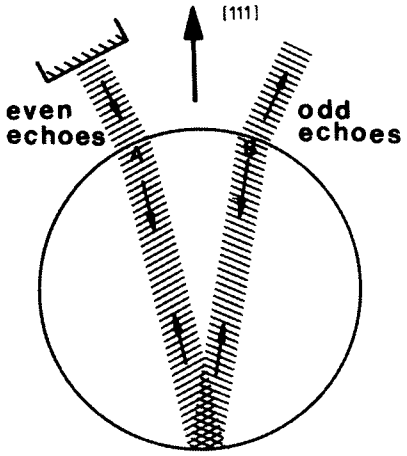


Fig. 11. A possible explanation for the effect illustrated in Fig. 10. The situation is strongly exaggerated. In real conditions, if the incident beam deviates only 2° from 111 direction, also the odd number echoes partly hit the receiver.

agreement with the more accurate values measured in the plate shaped single crystal.

In polycrystalline materials under conditions of Rayleigh ($\lambda >> D$) and stochastic ($\lambda \sim D$) scattering the attenuation can be estimated through Eqs. (1) and (2) using the measured single crystal elastic coefficients. If for example the grain size is 0.1 mm and

the freguency 5 MHz, the condition for Rayleigh scattering is obeyed and the attenuation is 1.07 dB/cm for longitudinal waves and 7.32 dB/cm for shear waves. The values are about 2.5 times higher than for body centred cubic iron with corresponding grain size and frequency.

In crystalline materials with coarse grain size ($D > \lambda$) as for example in welds and castings usually diffusive scattering (Eq. 3) occurs. In these materials the situation is much more complicated. In the polycrystalline samples A and B with strong fibre texture the velocity is lower along the fibre-like grains than in other directions. The velocity along the grains is close to the velocity in the 100 directions of the single crystal. This supports the X-ray diffraction measurements confirming that the texture is of 100 type. With regards to the observation that the attenuation is lowest in the 45° direction to the fibre axis and essentially stronger in all other directions, no simplified correlation between velocity and attenuation can be given although the attenuation very often decreases with increasing velocity.

The situation in the direction perpendicular to the grain axis (90°) may be discussed referring to Fig. 8a. This figure shows that in the plane perpendicular to a 100 type crystal direction the angular dependence of the longitudinal velocity is considerable. A polycrystalline sample with a 100 type fibre texture may be considered to consist of grains having either $\alpha = 0°$ and different values of β, or $\beta = 0°$ and different values of α as in Fig. 8a. The velocity therefore varies from grain to grain leading to strong reflections at the grain boundaries and therefore to strong attenuation.

In the direction of the fibre axes (0°) the velocity is equal in every grain if the directions of the fibre

axes are accurately in a 100 direction. The experimental attenuation is, however, quite strong. The reason is believed to be similar to that discussed in the case of the single crystal sphere. Because of the strong curvature of the slowness surface near the 100 direction the beam diverges rapidly leading to many reflections at the sidewalls of fibre-like grains. This leads to spurious pulses and deteriorated echo train seen as a strong apparent attenuation.

In the 45° direction to the fibre axes in each grain α is 45° but β has random values in different grains. From Figs. 8a-d it is seen that the longitudinal velocity is only weakly dependent on β if α is 45°. Therefore, the reflections from the grain boundaries are quite weak. The slowness surface in Fig. 9 is also quite flat in the regions where α is near 45° and the beam divergency is therefore believed to be weaker than in other directions.

It can be seen from the Figs. 8 and 9 that the shear wave velocity depends strongly on the propagation direction and on the polarization direction. This means that the attenuation in a polycrystalline sample caused by the grain boundary scattering is still stronger for shear waves than for longitudinal waves. In the experiments made both in plate-like and triangle shaped samples the measurements for shear waves were possible only in two directions i.e. in the parallel direction (0°) and in the perperpendicular direction (90°) providing that the polarization is parallel to the fibre axis. These observations are clarified by analysing Figs. 8 or 9. In the 100 directions the shear wave velocity is independent of the polarization direction. Hence the velocity is the same in the direction of grain axes and the attenuation is much lower than in an arbitrary direction. From Figs. 8a or 9a it may be seen that if the propagation direction of

shear waves is perpendicular to a 100 axis the velocity of the fast shear wave mode v_{T_1} in Fig. 8a is independent of the propagation direction in this 100 plane. In this case the fast shear wave is the shear wave having the polarization in the 100 direction. In a textured sample with the propagation direction perpendicular to the fibre axis v_{T_1} is therefore equal in all of the grains and the attenuation is fairly low.

6 CONCLUSIONS

The effects of anisotropy on the propagation of ultrasound in austenitic stainless steels is considerable. Particularly in the coarse grain weld and cast materials where diffusive grain boundary scattering occurs the situation is very complicated. The solidification texture in welds and castings causes big differences in attenuations, velocities and propagation angles of both wave modes in different scanning directions. Explanations can be given for all of the observed phenomena on the basis of theoretical calculations. However, the link between practical NDT of austenitic welds and castings and the information of this study is not quite clear. The authors, however, hope that the results of this study can be helpful to understand the difficulties associated with practical ultrasonic inspections of these materials.

7 REFERENCES

Auld, B. A., 1973: Acoustic fields and waves in solids.Vol. II, New York: John Wiley a Sons, p. 12.

Baikie, B. L., Wagg, A. R., Whittle, M. J. and Yapp,

D., 1976: Ultrasonic inspection of austenitic welds. J. Br. Nucl. Energy Soc. 15, p. 257-261.

Caussin, P., 1978: Ultrasonic testing of austenitic stainless steel structures. OECD, SINDOC (78) 190, 29 p.

Hellier, A. G., Palmer, S. B. and Whitehead, D. G., 1975: An integrated circuit pulse-echo-overlap facility for measurement of velocity of sound. J. Phys. E: Sci. Instrum. 8, p. 352-354.

Kupperman, D. S. and Reimann, K. J., 1976: Effects of microstructure on ultrasonic examination of stainless steel. CSNI-Specialists' Meeting on the Ultrasonic Inspection of Reactor Components, Risley, Sept. 27-29, 10 p.

Papadakis, E. P., 1965: Revised grain-scattering formulas and tables. J. Acoust. Soc. Am. 37, p. 703-710.

Truell, R., Elbaum, C. and Chick, B. B., 1969: Ultrasonic methods in solid state physics. New York: Academic Press, p. 12.

Contribution to improving ultrasonic testing of thick bimetallic welds

B. TRUMPFF, J-P. LAUNAY, J.J. OLIVERA, Framatome, France

ABSTRACT

The need for safety of nuclear power installations is forcing engineers to finds ways and means of efficiently testing austenitic welds joints.

In view of the advantages of ultrasonic testing, which is used with success for ferritic weld joints, development of more effective methods for austenitic weld inspection is an important objective in the nuclear industry.

FRAMATOME is cooperating with WESTINGHOUSE, ELECTRICITE DE FRANCE and the COMMISSARIAT à l'ENERGIE ATOMIQUE to determine the capabilities and reliability of ultrasonic testing procedures for detecting flaws in austenitic steels and bimetallic weldments.

A particular section of FRAMATOME's work, performed at the INSA Laboratory in Lyon, is concerned with the study of thick bimetallic welds between forged and cast stainless and ferritic steels.

Conventional ultrasonic testing of such weldments is rendered difficult or inefficient by considerable background noise, important anisotropy in ultrasonic wave propagation and spurious echos.

An analytical study of ultrasonic wave propagation was carried out to design the best suited transducers for examination of two kinds of thick bimetallic welds. (wave, frequency, refracted angle in steel damping and sound field).

This study included several points :

- 1°) Metallurgical structure of the various areas of each weldment.
- 2°) Ultrasonic wave propagation (velocity and attenuation) at various frequencies performed on cylindrical samples removed from various areas of each weldment.
- 3°) Principal parameters for ultrasonic testing (wave mode, frequency and refracted angle in steel) of artificial flaws machined in flat test blocks representative of each weldment (3 mm diameter side drilled woles and 3 x 3 mm notches).

The results of this study contribute towards the design and choice of probes best suited to inspection of these austenitic welds.

The use of these special probes which are manufactured in FRAMATOME and INSAS' LABORATORIES considerably improves detection of natural and artificial reflectors.

1. INTRODUCTION

The need for safety of nuclear power installations is forcing engineers to find ways and means of efficiently testing austenitic weld joints.

In view of the advantages of ultrasonic testing, which is used with success for ferritic weld joints, development of more effective methods for austenitic weld inspection is an important objective in the nuclear industry.

FRAMATOME is cooperating with WESTINGHOUSE, ELECTRICITE DE FRANCE and the COMMISSARIAT A L'ENERGIE ATOMIQUE to determine the capabilities and reliability of ultrasonic testing procedures for detecting flaws in austenitic steels and bimetallic weldments.

A particular section of FRAMATOME's work, performed at the INSA Laboratory in Lyon, is concerned with the study of thick bimetallic welds between forged and cast stainless and ferritic steels.

Ultrasonic testing of such weldments is complicated by the phenomenon of "anisotropic scattering" which produces considerable background noise, spurious echoes and anisotropic attenuation of ultrasonic waves.

An analytical study of the ultrasonic wave propagation in the various areas of two kinds of thick bimetallic welds enables us to determine the characteristics of special probes which will be tested on artificial and actual flaws.

2. METALLURGY

2.1. Description of the two bimetallic joints

2.1.1. Weldment (I) between forged ferritic and forged austenitic steels

This weldment is composed of 5 areas (fig. 1) :

(A) forged ferritic low carbon steel (SA 508 Cl. 3),
(B) buttering composed of 24 Cr - 12 Ni stainless steel for the first layer and 20 Cr - 10 Ni - 3 Mo for the other layers, applied with a covered electrode,
(C) homogeneous weld composed of 20 Cr - 10 Ni - 3 Mo stainless steel, applied with a covered electrode,
(D) forged austenitic stainless steel (Z 3 CND 17-12),
(E) cladding composed of 24 Cr - 12 Ni stainless steel for the first layer and 20 Cr - 10 Ni - 3 Mo for the other two layers, applied using automatic technique.

2.1.2. Weldment (II) between cast ferritic and cast austenitic steels

This weldment is also composed of 5 areas (fig. 2) :

(A) cast ferritic low carbon steel (SA 216 grade WCC),
(B) buttering with the same composition as 2.1.1. (B),
(C) homogeneous weld with the same composition as 2.1.1. (C),
(D) cast austenitic stainless steel (Z 3 CND 17-12),
(E) cladding with the same composition as 2.1.1. (E) but applied with a covered electrode.

2.2. Metallographic study

2.2.1. Weldment (I) (fig. 1) :

(A) forged ferritic steeld :

micrographic examination (m.e) revealed a very fine grained ferrite and cementite texture (the grain size according to AFNOR A 04.102 is G = 11).

(B) buttering :

macrographic examination (M.E) revealed the edges of the successive weld runs and unidirectional crystallization perpendicular to the weld preparation and to these runs. The grains follow the heat paths in the weld during cooling and they often grow epitaxially from one weld run to another. The grains are columnar in shape; they are about 1 mm wide and up to several centimeters long.

m.e. revealed :

- in a plane perpendicular to the weld axis, a ferrite lattice (7 %) marking the limits of austenitic matrix crystallization. Important variations in the lattice shape occur between two weld runs,
- in a plane parallel to the weld axis, a regular ferrite lattice without any special direction.

(C) homogeneous weld :

M.E. revealed variable crystallization around a principal axis coinciding with the axis of symmetry of the preparation. The dendritic texture has the same characteristics as in 2.2.1. (B).

(D) forged austenitic stainless steel :

m.e. revealed a classical austenitic twinned texture (G = 3 to 4).

(E) cladding :

The dendritic texture has the same characteristics as in 2.2.1 (B).

2.2.2. Weldment (II) (fig. 2) :

(A) cast ferritic steel :

m.e. revealed a very fine-grained ferrite and lamellar perlite texture (G = 10),

(B) buttering : same texture as in 2.2.1 (B),

(C) homogeneous weld : same texture as in 2.2.1 (C),

(D) cast austenoferritic stainless steel :

M.E. revealed a coarse texture with streaked grains. These grains are equiaxial on the edge (grain size 3 mm); but in central area, the grains increase to 4 mm x 10 mm in size and are perpendicular to the weld axis.

m.e. revealed a coarse texture with a thick ferrite lattice (30 %),

(E) cladding : same texture as in 2.2.1 (E).

3. ULTRASONIC WAVE PROPAGATION

3.1. Measurement methods

Cylindrical samples (19.4 or 35.3 mm in diameter) were taken from the various areas of each weldment parallel to its axis.

The study of ultrasonic longitudinal wave propagation (attenuation and velocity) was performed using the apparatus shown in fig. 3 : the cylindrical samples were placed between transmitting and receiving transducers (two Panametrics V 115, Ø 0.75", 10 MHz broadband with plexiglass lenses) so that the beam passed through the diameter of the specimen. The ultrasonic longitudinal beam propagation characteristics of the samples were studied by rotating them in the beam.

3.1.1. Attenuation measurements

Owing to the choice of tuning of Panametrics 5052 PR pulser-receiver and Hewlett Packard 141 T Spectrum Analyser, a constant frequency spectrum level was obtained on ferritic samples for frequency between 1 and 5 MHz. This level was considered as the reference level. For anisotropic samples, attenuation was plotted against this level for angles increasing 5° at a time.

3.1.2. Velocity measurements

Only velocity curves were plotted for non interface cylindrical samples. Velocity and attenuation measurements were obtained from the same screen displays.

3.2. Results

3.2.1. Ultrasonic longitudinal wave propagation in the various areas of weldment (I)

3.2.1.1. Ferritic forged steel

- Attenuation : isotropic. A constant level of between 1 and 5 MHz was considered as reference.
- Velocity : constant at 5950 m/s.

3.2.1.2. Austenitic forged stainless steel

- Relative attenuation : isotropic. Relative attenuation was negligeable foi low frequencies (1 MHz) but increased in upper frequency ranges. We found a relative attenuation coefficient α ie.

$$\alpha \left[\text{dB/Cm}\right] = 0.04 \quad f^2 \left[\text{MHz}\right] \quad \text{with} \qquad 3 \text{ MHz} \leqslant f \leqslant 5 \text{ MHz}$$

- Velocity was constant at 5790 m/s.

3.2.1.3. Dendritic areas (buttering and homogeneous weld)

- Relative attenuation was anisotropic and the variations of attenuation observed was markedly cyclic, having a period of 90°.
  Attenuation was weaker at low frequencies and the gap between maximum and minimum decreased at lower frequencies.
  These extremes remained unaltered when frequency was varied.
  The axis of least attenuation was regularly observed at an angle of 45° to the grain alignment axis of the dendritic texture.
  A specimen curve is given in fig. 4.

  It seems that attenuation in this kind of dendritic texture was caused by curvature of the incident beam as :

  1) only slight variations in background noise was observed when sample was rotated;
  2) in an angular position with transmitted signal reduced to minimum, a stronger signal was obtained when a 2 mm receiving transducer was displaced perpendicularly with respect to the incident ultrasonic beam.

- Velocity was anisotropic, the variation was cyclic with a periode of 90°.
  In the homogeneous weld (fig. 5), the maximum velocity was 6120 m/s and the minimum 5250 m/s (difference of 15 %).

  In the buttering, the maximum velocity was 6280 m/s and the minimum 5270 m/s (difference of 16 %).

  The maximum velocity corresponds to the maximum attenuation.
  However it should be noted that these measurements only indicate "apparent" attenuation and velocity in the incident ultrasonic beam direction owing to beam curvature phenomenon.

3.2.1.4. Global attenuation

In fig. 6, attenuation was plotted as a function of angular position for each cylindrical sample. For a given scanning surface, the direction of least attenuation corresponds to the minimum when attenuation curves for cylindrical samples representing the various areas through which ultrasonic waves pass to reach a given point in the weld are superimposed.

3.2.2. Ultrasonic longitudinal wave propagation in the various areas of weldment (II)

3.2.2.1. Ferritic cast steel and dendritic areas

- Attenuation and velocity : same results as in 3.2.1.1. and 3.2.1.3.

3.2.2.2. Austenoferritic cast stainless steel

Variations were small enough to enable the sample to be considered as isotropic for attenuation and velocity.

- Attenuation was slight at 1 MHz but greatly increased at higher frequencies ie $\alpha \left[\text{dB/cm}\right] = 0.7 \quad f \left[\text{MHz}\right]$ with $2 \text{ MHz} \leq f \leq 5 \text{ MHz}$.

3.2.2.3. Global attenuation

In fig. 7, we plotted attenuation as a function of angular position for each cylindrical sample.

4. OPTIMIZATION OF DETECTION OF ARTIFICAL REFLECTORS

Various artificial reflectors (3 mm diameter side drilled holes and 3 x 3 mm notches) are machined in 50 mm wide test-blocks representative of each weldment (fig. 8).

The tests were performed under water with following variables : wave mode, refraction angle in steel and frequency.

To detect reflectors, several factors were taken into consideration : the crossing of the water/steel interface, attenuation particular to each material for a given angle of incidence, the crossing of interfaces between steels if it occurs, and variation in the path of ultrasounds according to the angle of incidence.

4.1. The effect of wave mode

The tests performed with longitudinal waves gave better results than with transverse waves at same frequency or wavelength.

4.2. The effect of refraction angle in steel

Each reflector was examined from both surfaces for refracted angles in steel increasing in 10° steps. We used a CGR Ultrasonic R 7 flaw detector and a Panametrics V 305 (0. 75" in diameter - 2.25 MHz) transducer. The reference amplification (0dB) was obtained for an amplitude signal 6/7 the height of the screen on a 2 mm diameter side drilled hole machined at a depth of 50 mm in a ferritic test-block possessing the same ultrasonic properties as the IIS block. At each measurement position, the amplification needed to produce an amplitude signal 6/7 the height of the screen, the apparent ultrasonic sound path and the signal to noise (S/N) ratio were plotted.

4.2.1. Weldment (I)

1) The two parent materials (ferritic forged steel and austenitic forged stainless steel) are very permeable to ultrasonic waves : this permeability is not very different in these two materials. On the other hand, the dendritic textures of the buttering, the cladding and the homogeneous weld are very difficult to cross and induced phenomena such as : high degree of anisotropic attenuation, very low signal to noise ratio, curvature of the ultrasonic beam and spurious echoes.

2) In each of the four possible scanning directions, all the reflectors were detected if the angle θ refracted in the steel is such that $40° \leq \theta \leq 50°$, as already noted in fig. 6.

3) The mean difference in amplitude for echos associated with a line of reflectors at the same depth was generally smaller for $\theta \geq 40°$.

4) Only $\theta = 45°$ allowed a S/N ratio > 12 dB for all the reflectors and in the four scanning directions (an exception however : S/N 9 dB in the screen display for hole n° 2 examined from the cladded surface through austenitic stainless steel parent material).

5) There were many structural spurious echoes at small refracted angles ($\theta \leq 30°$) and angles close to weld preparation angles (15° and 30°).

6) The location of reflectors was poorly situated for high refracted angles ($\theta \geq 60°$), due to curvature of the ultrasonic beam in the dendritic textures for long sound paths.

A refracted angle θ - 45° is therefore the best suited direction to inspect the maximum volume of this weldment and gave the best conditions for detection and location of flaws.

This confirms the directions pointed out by the ultrasonic propagation study in the cylindrical samples (§ 3.2.1.4., fig. 6).

4.2.2. Weldment (II)

1) Various areas of the joint possessed different ultrasonic propagation characteristics :

   - the ferritic steel is very permeable to ultrasonic waves;
   - the coarse grained texture of the austenitic cast stainless steel produced a drastic and non uniform attenuation in ultrasound, the S/N ratio being very small (some reflectors 65 mm deep were not detected);
   - the dendritic textures as in 4.2.1.1.

2) As the parent materials were not symmetrical, the detection of the artificial flaws varied greatly with respect to direction :

   - when examining from the ferritic steel side, all the reflectors (except the notch n° 9) are detected when $\theta = 45°$;
   - when examining from cast stainless steel side, reflectors situated at a depth of 25 mm were detected for $\theta \leqslant 60°$, while the 55 mm deep reflectors were no longer detected : the sound path in this steel must be reduced to detect the reflectors near the opposite surface.

3) The S/N ratio was very low for tests performed from the cast stainless steel side.

4) There were many structural spurious echoes at small refracted angles ($\theta \leqslant 30°$) and also at angles close to weld preparation angles (10° and 20°).

5) The location of reflectors was poorly situated for small ($\theta \leqslant 10°$) and high ($\theta \geqslant 60°$) refracted angles owing to a long sound path in the dentritic textures of the buttering and the homogeneous weld.

   A $40° \leqslant \theta \leqslant 45°$ refracted angle in steel is therefore the best-suited direction to inspect the maximum volume of this weldment and provides the best conditions for flaw detection and location.

   This also confirms the directions pointed out by the ultrasonic propagation study in the cylindrical samples (§ 3.2.2.3., fig. 7).

4.3. The effect of frequency

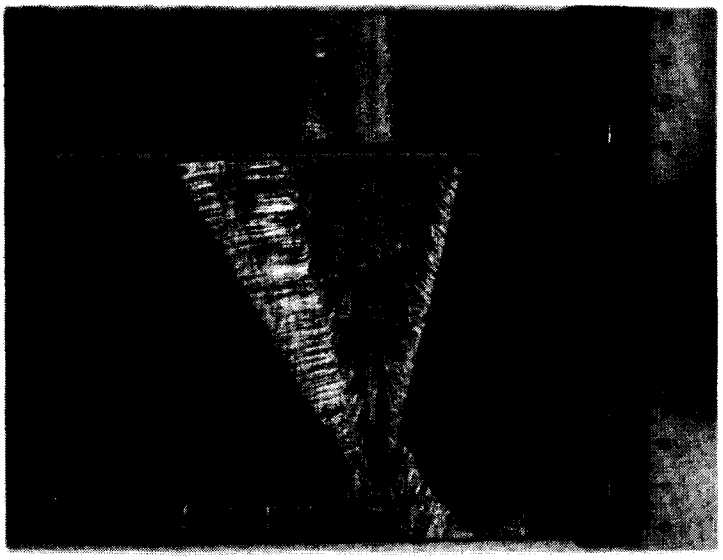
A Panametrics V 115 (Ø 0.75" - 10 MHz broadband) transducer was connected to the Panametrics 5052 PR Pulser Receiver.
30 mm (weldment I) or 25 mm (weldment II) deep side drilled holes were examined with longitudinal waves at a 45° refracted angle in the steel.

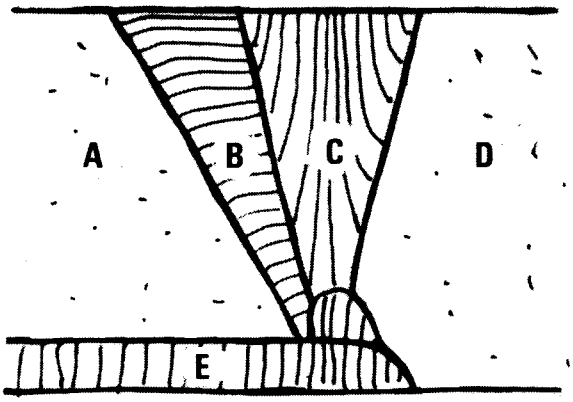
The -3 dB frequency spectrum bandwidth for signals obtained from each reflector showed that 1.5 MHz was well suited for both weldments.

5. CONCLUSIONS

The above results make it possible to define the characteristics of suitable probes : they should emit longitudinal waves at 1.5 MHz at an angle of 45° in steel.

At the present time, FRAMATOME is testing some special probes manufactured in both its own and in INSA'S Laboratories.
Other commercially available probes, specially manufactured for inspection of austenitic welds, will also be tested. The transducers giving the best results will be used for testing representative blocks with actual flaws.





Macrograph

Area A :

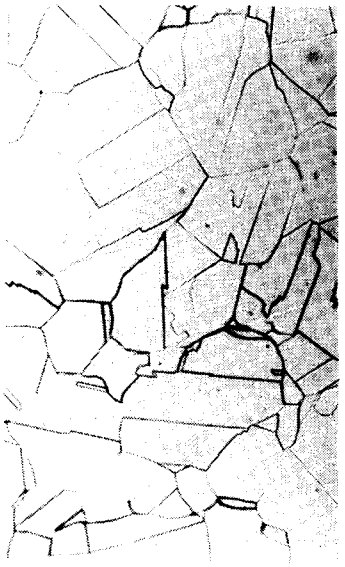
Ferritic forged steel parent material.



X 100

Area D :

Austenitic forged stainless steel parent material.

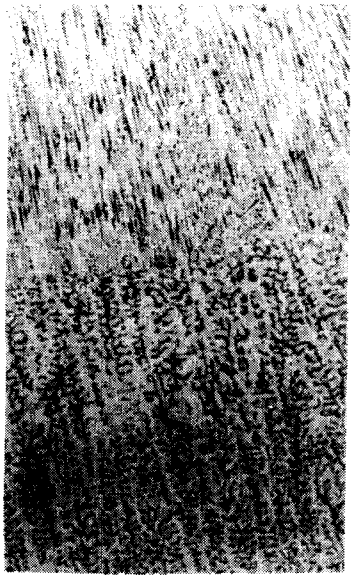


X 100

Area C :

Manual metal arc buttweld (austenitic steel).

Perpendicular to weldment skin.



X 100

Area C :

Manual metal arc buttweld (austenitic steel).

Parallel to the weldment skin.

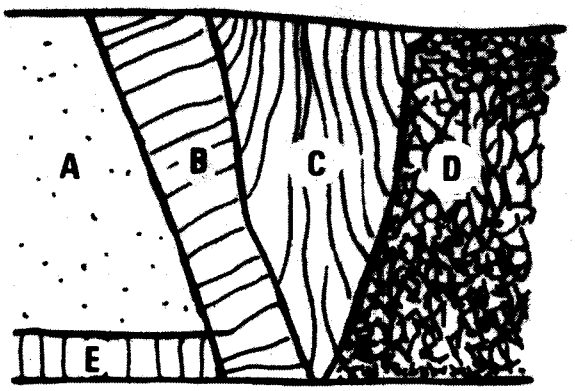


X 100

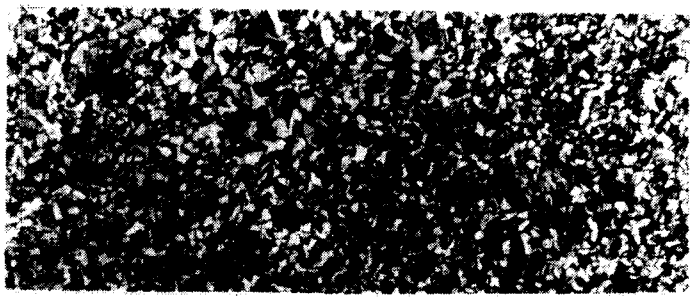
Micrographs.

Fig. 1 - Weldment (I) - Metallography





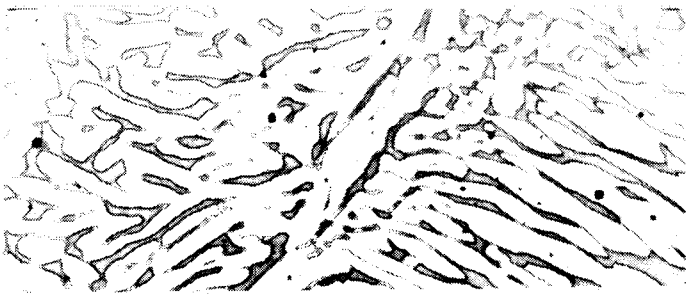
Macrograph



Area A :

Ferritic cast steel parent material.

X 100



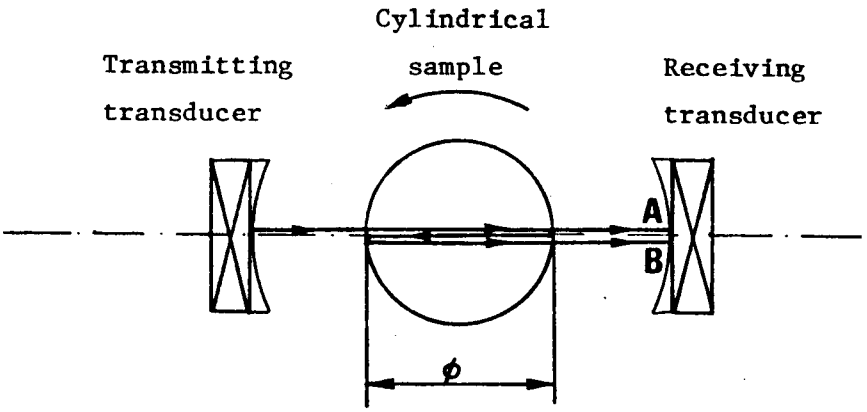
Area D :

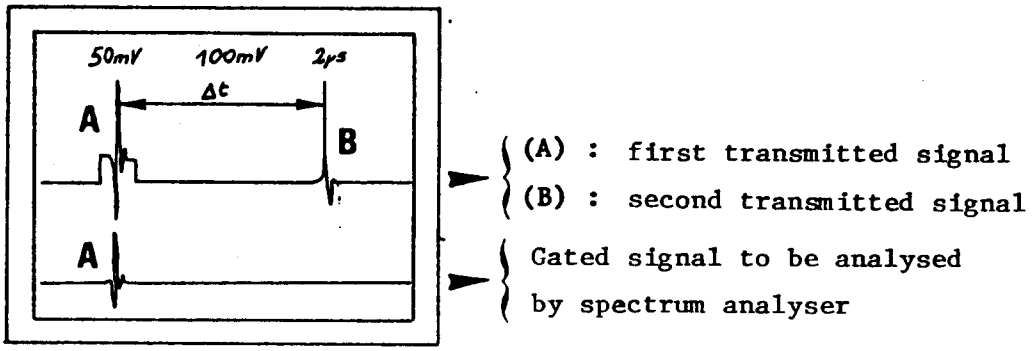
Austenoferritic cast stainless steel parent material.

X 100

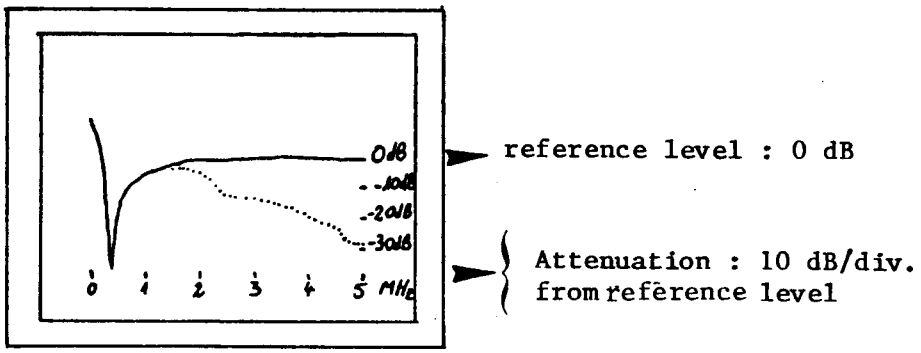
Micrographs.

Fig. 2 - Weldment (II) - Metallography





screen display



frequency spectrum

longitudinal wave velocity in the cylindrical sample : $v = \frac{2\phi}{t}$

Fig. 3 : Attenuation and velocity measurement methods.

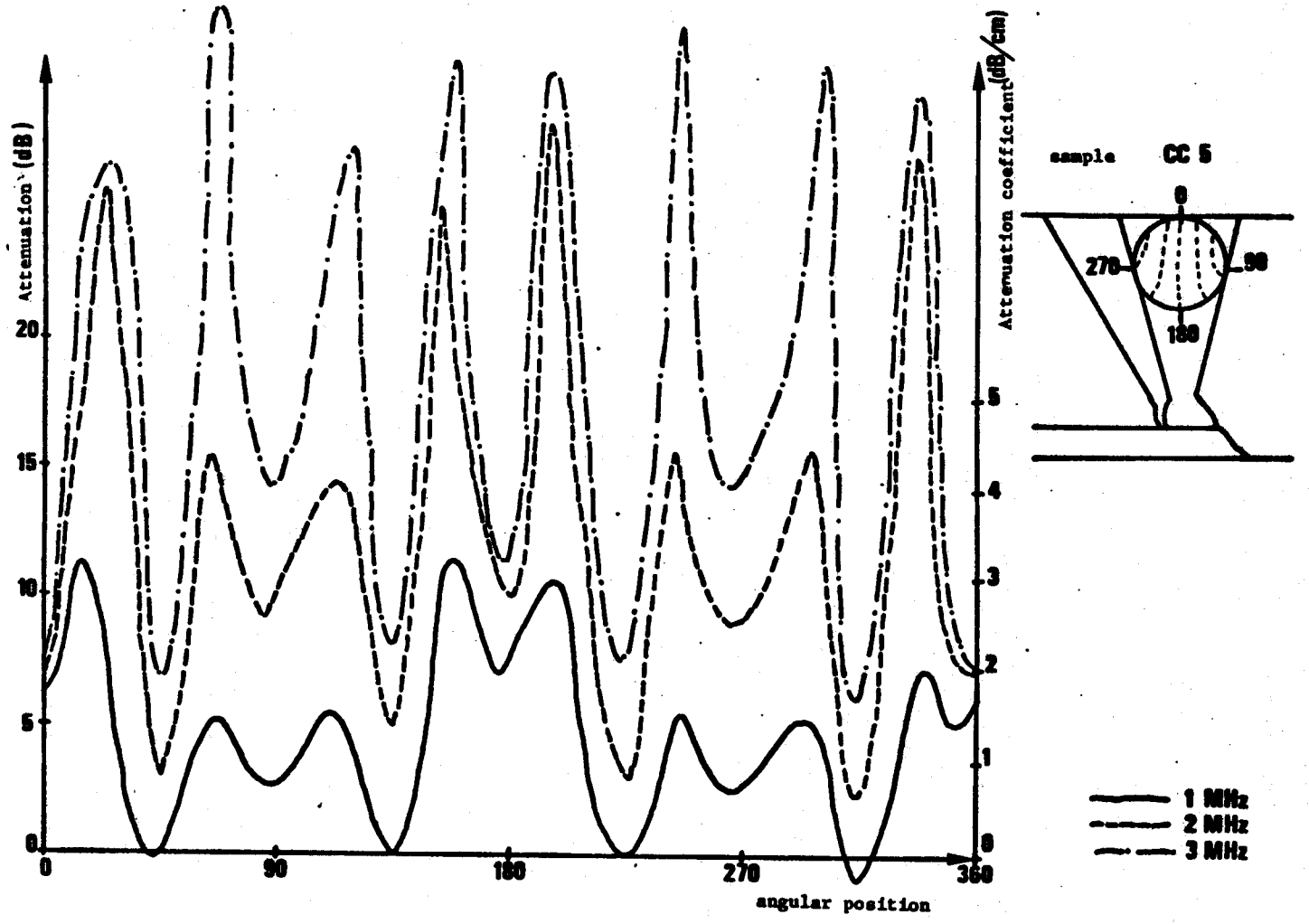


Fig. 4 - Longitudinal wave attenuation in the manual metal arc buttweld Weldment (I) , area (C).

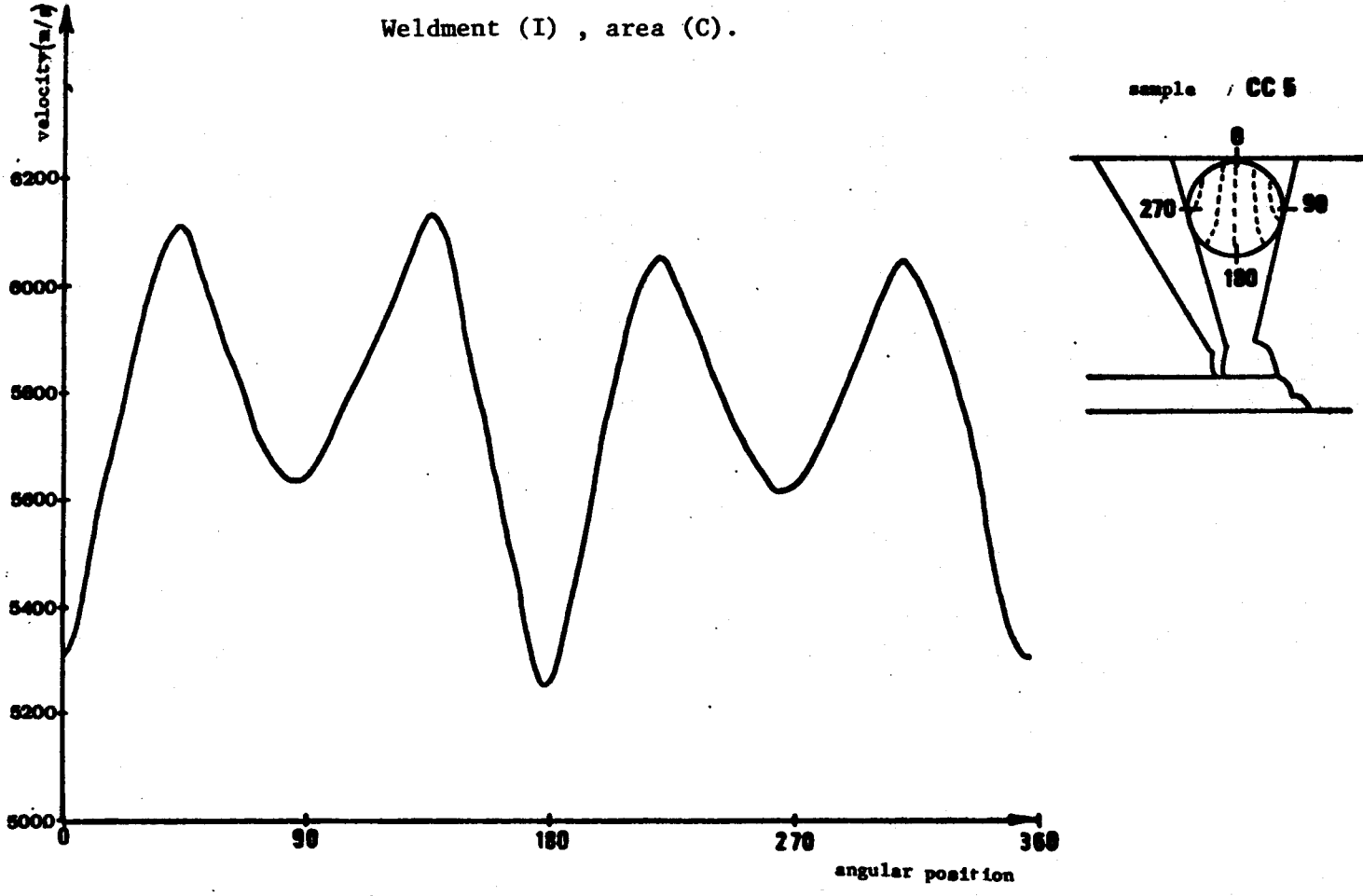


Fig. 5 - Longitudinal wave velocity in the manual metal arc buttweld Weldment (I) , area (C)

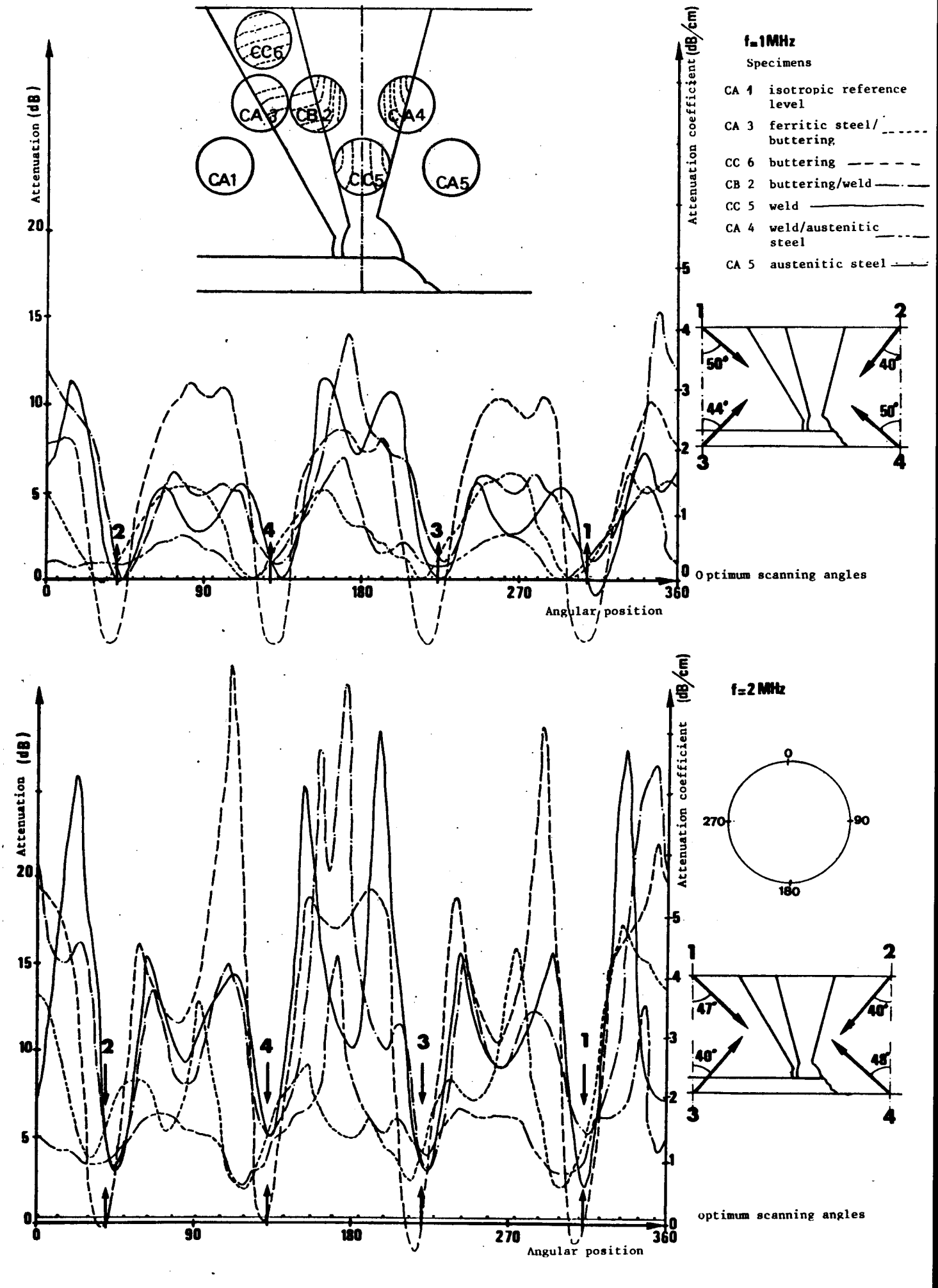


Fig. 6 - Weldment (I) Attenuation in the various cylindrical samples at 1 and 2 Mhz

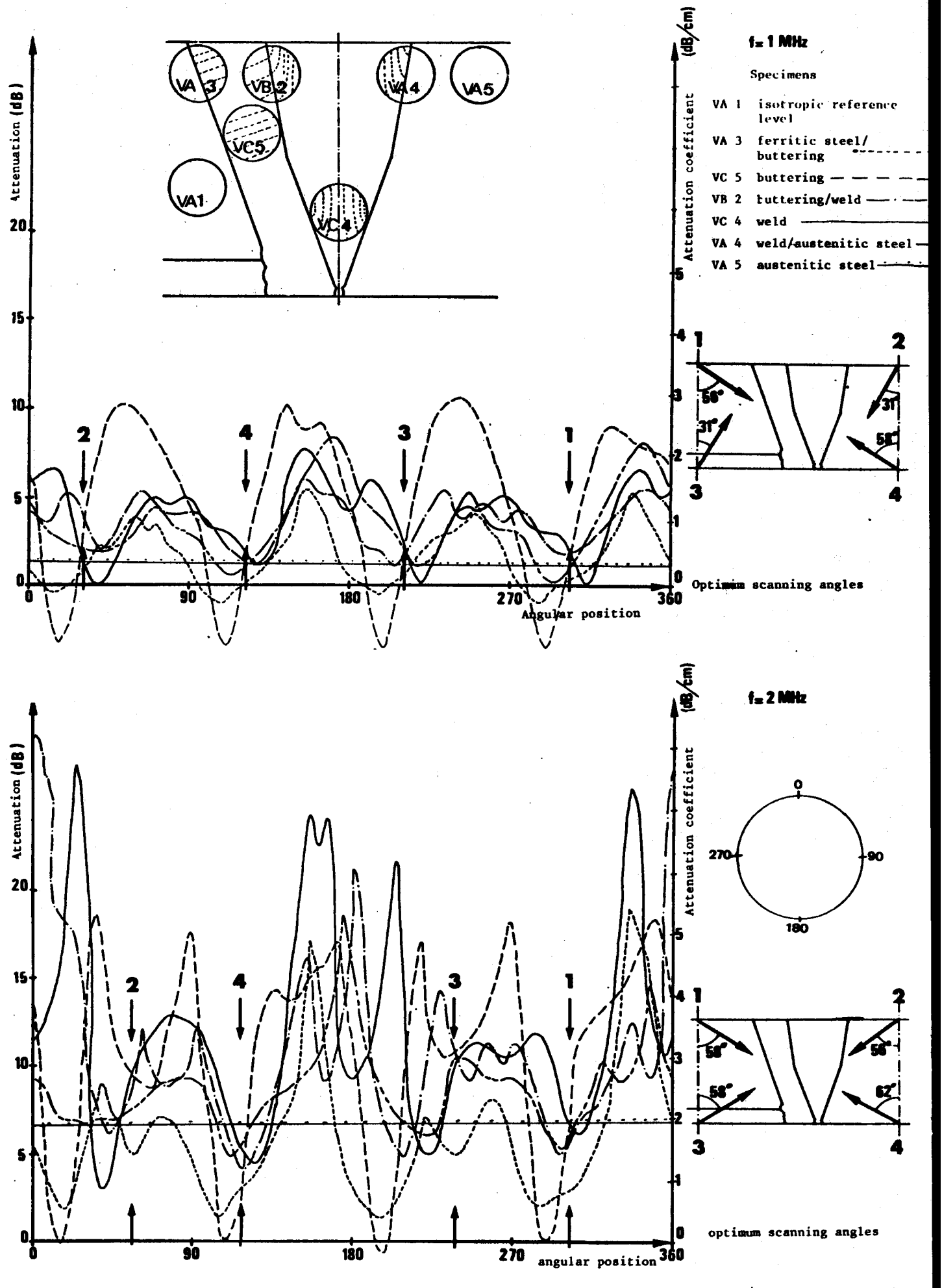
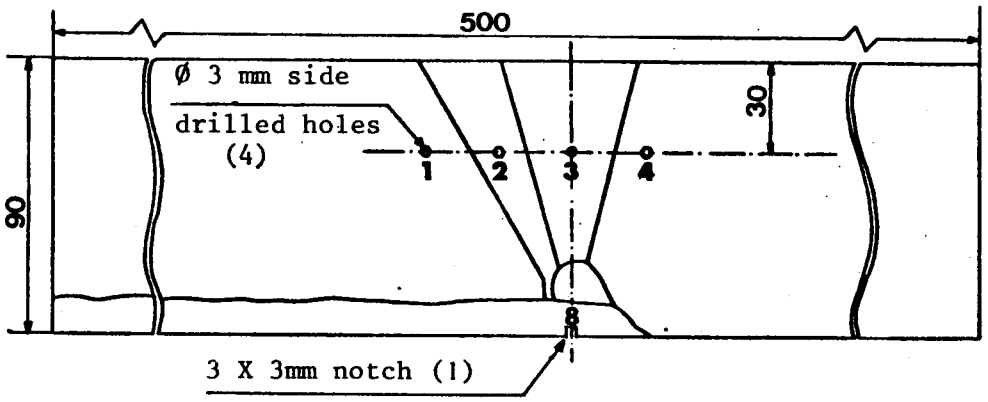
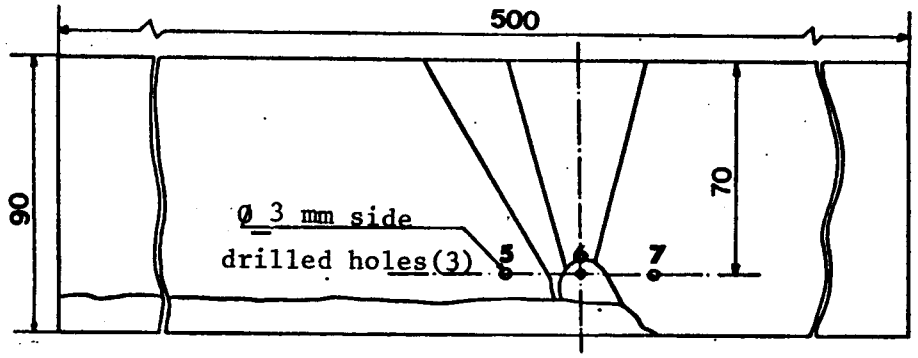
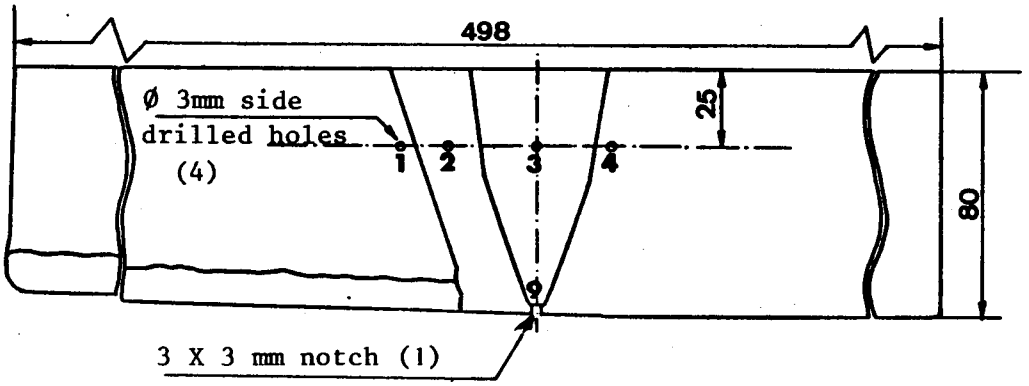


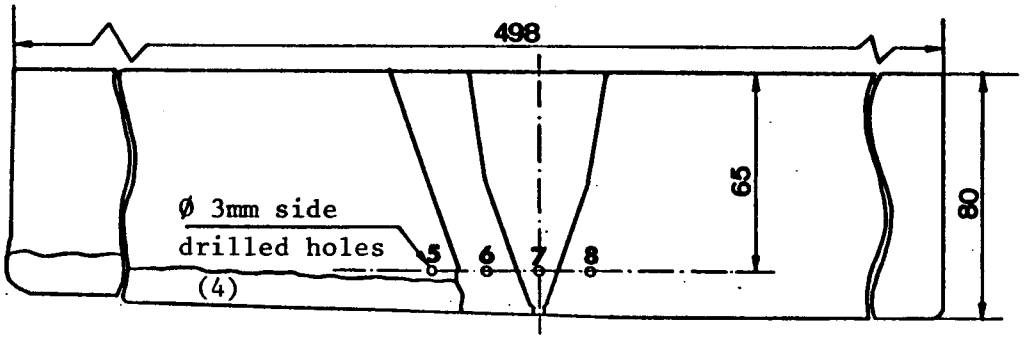
Fig 7 - Weldment (II) - Attenuation in the various cylindrical samples at 1 and 2 Mhz





Weldment (I)





Weldment (II)

Fig. 8 - Test-blocks with machined reflectors

Some fundamental aspects of testing austenitic steel structures by ultrasonics

W. OPPERMAN, H.A. CROSTACK
Dortmund University, F.R. Germany

ABSTRACT

A number of essential influencing factors in the ultrasonic testing of austenitic materials are discussed in conjunction with calculations and practical measurements. The work establishes that for the detection of defects optimum frequency ranges exist and that by staying within these ranges, the signal-to-noise (S/N) ratio and also the evaluation of defects in materials producing marked ultrasonic scatter can be improved. The effect of spectral distribution of the pulse being dominant over that of pulse duration was noted.

1. INTRODUCTION

In the ultrasonic testing of materials with high attenuation, difficulties are encountered which grow particularly when there is marked scatter. Such scatter occurs in very coarsegrained and inhomogeneous materials as a result of which the S/N ratio is markedly reduced whereby defect identification is rendered more difficult. This situation gives rise to two problems when testing marked scatter-producing, and therefore also austenitic materials. The first problem involves detecting defects, that is to say identifying them even in materials generating a great deal of scatter. The second problem concerns evaluation of defect indication and hence interpretation of defect size, shape and location (for example by the DGS-Diagram). The problem of defect detection which is substantially dependent on raising the S/N ratio, and the techniques whereby this may be achieved, have already been reported on [1].

One of these techniques, the so-called CS-Technique [2; 3], is based on the fact that by specific electrical excitation of the transducer, the spectrum of the acoustic pulse receives a desired defined composition. Apart from the already mentioned advantage provided by the reduction of scatter [1] and the resultant improvements in materials testing [2; 4; 5], this technique offers some further features that make it appear especially suited to basic research into the interaction between ultrasound and reflector. These are :

- Possible variation of frequency at constant bandwidth.
- Variation of bandwidth at constant centre frequency.
- Variable duration and form of pulses, the effects of which are, of course, associated with the spectral distribution.
- Concentration on specific frequency ranges. As a result, a very high acoustic energy is available in these ranges which is particularly useful in basic studies.

These features make the CS-Technique appear particularly advantageous to basic research into the relationship between the S/N ratio and the pulse duration as well as the pulse spectrum.

2. INFLUENCE OF SPECTRAL DISTRIBUTION

Apart from the noise reduction [1] which were calculated on the basis of simplified assumptions for basic studies and are compared with the white noise itself, some further influencing factors exist in practical testing, particularly in defect evaluation. These are the transducer with its frequency-dependent transfer function, the sound field which depends upon the d/λ - ratio of the transducer, and finally the sound field of the defect which depends upon the d/λ - ratio of the reflector but is also affected by losses of divergence. Therefore, the defect indication is subject to a dual influence by the test frequency.

However, these relationships become particularly difficult and confusing if, instead of using monochromatic wave trains, spectra are employed whose composition may change. This possible change of the spectra is illustrated briefly in the following example - fig. 1 - which shows the frequency spectra of a gated sine wave and those of a sine wave also gated but having superimposed on it a $(1-\cos \omega t)^4$ function. If these pulse, or the spectra shown, are applied to a wide-band transducer (12 mm dia) which, in turn, transmits them to a cylindrical hole (6 mm dia) to a depth of penetration of 100 mm, the spectra shown in the second row of fig. 1 result. The gated sine wave in particular exhibits a rise of the higher frequencies and a reduction of the lower frequencies in the defect response. If, however, the ultrasonic pulse is subject, to a certain amount of damping due to Rayleigh scatter (0.26 dB/cm at 4 MHz - third row of fig. 1), the high-frequency components which actually contribute more to defect identification, are increasingly damped whilst the low-frequency components are raised. At higher levels of damping, e.g. approximately 0.78 dB/cm at 4 MHz, a value which is at times exceeded by a considerable margin in austenitic castings, this can lead to a situation where the defect response contains hardly any frequency components of the actual test frequency of 5 MHz. In the case of the gated sine wave the defect is actually tested with frequencies around 2.5 MHz rather than 5 MHz. By contrast, the pulse designated $\sin^4$ has a considerably more favourable shape. Under the same conditions it also undergoes de-mixing. However, since the spectrum falls off abruptly on either side, the de-mixing is also drastically limited so that the defect is tested, and hence also evaluated, with approximately the same frequency band even when high attenuation is present.

To achieve positive defect identification, it is important to use not only a single frequency since otherwise there is the danger that at certain angles the defect will not be detected. On the one hand the CS-Technique distinctly limits the spectrum while, on the other, it considerably broadens the main maxima compared with the gated sine wave, so that a defined frequency band with several nearly equivalent frequency components are available for defect detection.

The shifts in the frequency spectrum which may be produced even in gated sine waves by unfavourable switch-on and switch-off functions, naturally manifest themselves to an appreciably greater extent as soon as wide-band transducers are used in the conventional mode. These transducers have, in the recent past, been very widely advocated for testing austenitic materials [6]. While they are, initially, eminently suited to defect detection, they do have inherent risks when it comes to defect evaluation. To illustrate this, fig. 2 gives the frequency spectrum of a broad-band 2.25 MHz-transducer. The spectrum was determined on a fine-grained hemisphere by the impulse-echo-technique [7]. In the testing of an austenitic casting with a grain size of approximately 1 according to ASTM the echo from a 6 mm hole at a depth of about 65 mm consists preferably of frequency components below 1 MHz. Therefore, the nominal frequency of 2.25 MHz specified here shifts in the evaluation to less than 1 MHz. This causes considerable difficulties to the evaluation parameters since the divergence of the sound field naturally changes considerably with the frequency. Thus, the frequency or wave length directly acts on the near-field length and hence on evaluation scales such as, for example, the DGS-Diagram. For evaluation of the defect it is hence necessary either to have precise knowledge of these processes of de-mixing of the pulse as it travels to the defect, a demand which, at the time of writing, appears virtually impossible to meet, or to set from the very start test parameters in such a way that their modification due to sound damping will be insignificant.

These considerations apply, to the formation of the sound field of the defect and hence to defect evaluation when sound damping is present. If additional scatter occurs, optimum ranges for the test exist since, fundamentally, there are different functional relationships between frequency and scatter on the one hand and frequency and defect size and location on the other. For an optimum test, maintaining these optimum ranges is, therefore, extremely important. This situation is shown in fig. 3 for a 4 mm cylindrical hole at a depth of 100 mm. The left-hand row covers the various spectra based on the assumption of white noise as the impinging acoustic spectrum while on the right-hand side the specified transfer function of a transducer is superimposed. In the left-hand row the response of the 4 mm hole acting as reflector is plotted vs. the white noise. So long as this occurs without damping, the amplitude of the reflector rises with increasing frequency. If scatter does occur, the damping of the sound on its way to the reflector will not only cause the echo from the reflector to be damped in the high frequency range but, additionally, there will occur (in the region of the Rayleigh-scatter with the 4th power of the frequency) noise signals. The latters grow faster with the frequency than does the defect-generated signal. If damping through scatter is around 0.23 dB/cm at 4 MHz, the reflector signal can no longer be separated from the noise signal above 4 MHz. With this more coarse-grained structure the scatter amplitude rises more rapidly with the frequency. This, however, entails two requirements.

One is that it is very important to maintain the optimum test frequency range and hence to narrow down the test range in order to obtain sensitive defect detection. In particular, the sharp cutoff of high-frequency improves the S/N ration while the cutoff of low-frequency components which contribute little to defect identification, reduces particularly divergence losses. Adherence to a specific test range which is indicated in broken lines in the right-hand row of graphs, becomes particularly important whenever there is marked scatter, that is to say when the scatter curve begins at very early frequencies and rises very rapidly.

A defined test range is further of significance when there are small defects which will only register at very high frequencies and are incapable of generating strong signals. This means particularly that whenever this test range becomes very narrow, in other words when the limits of conventional test methods are reached, the CS-Technique will yield a substantial improvement in defect detection. The improvements obtainable in the S/N-ratio through the CS-Technique and adherence to specific test ranges therefore depend upon the existing coefficient of scatter and upon the size of the defect. The improvement will be relatively minor when there is a low degree of scatter and the defect is very large. In testing austenitic materials, even using special transducers for varying depths, the CS-Technique yielded improvements in many instances of about 6 to 10 dB over the conventional technique [2].

The prerequisite for an optimum test, i.e. the maintenance of specific ranges or, as mentioned above, the comparison between the conventional and the CS-Technique under optimum conditions, depends largely upon knowledge of the range having the optimum S/N ratio. Determining this range by the conventional technique is difficult. Here, again, the CS-Technique offers a comparatively easy way of determining the spectra of defects and noise in dependence upon the frequency. By choosing the test frequency, a spectroscopy of the two quantities is simply carried out. By way of illustration, fig. 4 gives the echo from a 6 mm drilled hole at a depth of 65 mm and the scatter signal a short distance in front of the defect, i.e. at a depth slightly less than 65 mm, in the aforementioned coarse-grained austenitic casting. It will be noted that the amplitude of the defect signal rises already at low frequencies while that of the noise signal does not start to respond until about 1.7 MHz. That the maximum amplitude of the noise signal is greater at approximately 2.3 MHz than that of the defect signal is due in part to the shortest distance and in part to interferences. Here, de-mixing of the acoustic pulse is not yet as complete as at the depth of the defect. This measurement is made by continuously varying the centre frequency by the CS-Technique. In order not to lose the axial resolution the pulse still has a relatively broad bandwidth. However, in order to obtain a very narrow-band spectrum so as to be able to use it in a comparison with the calculation referred to at the beginning of the section, the centre frequency of the transmitted pulse is used directly for filtering the echo on the reception side to a narrow band within the preselected time window. In this way a very effective spectroscopy is possible with the simpliest means.

S/N ratios measured in this way correspond largely to the calculations presented in fig. 3. Since the calculations are initially based on monochromatic wave trains (Fourier transformations), they demand in the ideal case an infinitely narrow frequency band for analysis. These demands are, however, of relatively little significance to S/N determination as required in the practical application of ultrasonics. The operator must distinguish on the screen of an US-test monitor the echo procuded by the defect from the noise. To determine this S/N ratio as it occurs in practice, two time windows are set, one of which determines the noise some way in front of the defect while the second screens out the echo from the defect and directly compares the two echoes with each other. If one shows this S/N ratio in dependence upon the variation of the centre frequency, the same tendency results in principle - fig. 5. The maximum S/N ratio is at approximately 1.5 MHz and hence distinctly below the limit at which the scatter amplitudes of the spectrum rise sharply. Compared with the S/N ratio as indicated by the spectra, the value of the S/N ratio in the case of the short pulse of fig. 5 is reduced through the integration over a larger band within the frequency range. The value is, however, in most cases still higher than that obtainable with transducers under normal excitation.

In US-testing austenitic materials, the use of wide-band transducers presents particular problems because these transducers still have a relatively broad spectrum in the test zone which is close to the surface. The high-frequency components present here cause relatively high scatter amplitudes and therefore a lower S/N ratio. With increasing depth this pulse undergoes de-mixing so that its frequency spectrum slips into the optimum range. Here, positive and sensitive defect identification is possible. As the pulse travels further, i.e. penetrates to greater depths, further de-mixing of the pulse is due to damping so that its frequency spectrum shifts to lower values. In consequence of this it may happen that the pulse again slips out of the optimum range and overlooks smaller defects at greater depths due to the low-frequency components which are primarily present. Hence the S/N ratio deteriorates again. It follows from this that with wide-band transducers the S/N ratio is either dependent upon depth, or one would have to select for each defect depth a transducer with a specifically suited spectrum.

3. INFLUENCE OF PULSE LENGTH

The investigations clearly confirm the great influence of the frequency on the scatter amplitudes, and asshown on the divergence and the formation of the defect sound field. As the S/N ratios are limited to a relatively narrow frequency range, adherence to this optimum frequency range definitely commends itself. Here, the CS-Technique already yields a distinct advantage because it is able to largely stay within this range and yet forms relatively short pulses so that the axial resolution is not lost. On the other hand, however, currently accepted thinking is that especially broad-band and, in accordance with the current form of excitation, extremely short pulses are capable of raising the S/N ratio [6]. It is argued that a pulse-excited transducer which transfers

this broad spectrum, generates a very short pulse whose interference capability, particularly in depth, is considerably restricted. From this it is concluded that the scatter amplitude must necessarily fall. The successes achieved with such broad-band transducers then led also to the demand that extremely short, broad-band pulses be used - which, however, invariably also involve high-frequency components. In juxtaposition to this is the statement - confirmed by these investigations - that high-frequency components cause particularly high scatter amplitudes.

These two opposite statements lead to the question of whether this influence of pulse length affects the scatter signal to a more marked degree than does the frequency spectrum. To clarify this question, the practical S/N ratio was determined for a pulse of 1.5 µsec and one of 3 µsec length (fig. 6), using the same workpiece with its 6 mm dia. hole drilled to a depth of 65 mm. The spectra of these two pulses, designated S21.5 and S23, respectively, are also shown in fig. 6. In this particular case, the frequency "zero" represents the centre frequency which is used as the variable quantity for the S/N ratio. It will be noted that the 3 µsec long pulse has a narrower frequency band than the 1.5 µsec pulse, its spectrum being symmetrical about the centre frequency which means that it also extends towards the left. The results obtained by measurement of the S/N ratios are interesting inasmuch as the longest pulse distinctly yields the best S/N ratio. However, the range within the shortest pulse with the broadest spectrum yields lower S/N ratio values, it does nevertheless retain these almost constant over a wide range.

The explanation of this is provided by the width of the spectrum. At low frequencies, the short pulse has the better S/N ratio. When the centre frequency is very low, there is as yet no significant occurence of scatter components. The high-frequency components contained in the short pulse, however, already contribute to improved defect detection. When the centre frequency for the long and short pulse extends into the optimum S/N ratio, the high-frequency components of the shortest pulse generate more scatter so that the S/N ratio is lowered. If, however, the centre frequency is shifted towards very high frequencies with extremely strong damping, the short pulse has the possibility of de-mixing itself towards low frequencies more than the long pulse is able to. For the range of the optimum S/N ratio at this centre frequency, the shortest pulse contains components of lower frequency and higher amplitude and hence S/N ratios lying within the optimum range so that defect detection is increased. Therefore, the decisive influencing factor is not the pulse length but rather the spectrum, its composition and the modification it undergoes on its journey through the workpiece.

While in this coarse-grained austenitic material a shift of the optimum centre frequency for the S/N ratio will already be noticed, these relationships become more pronounced when testing an austenitic weld in a 9 mm thick plate (fig. 7). When directing ultrasonic pulses at the considerably smallest defect (side-drilled hole, 1.5 mm dia), the same tendencies as those previously noted will be observed with respect to the size of the S/N ratio. The longest pulse

distinctly yields the best S/N ratio and this more particularly, at the highest centre frequencies. As the pulses grow shorter, the range of a good S/N ratio again widens but the maximum value falls and shifts towards low frequencies which is understandable whilst the high frequencies, in short pulses generate scatter components.

This statement concerning the considerably greater influence of the test frequency or its spectrum on the scatter amplitudes, compared with that of the pulse duration, is also confirmed by another experiment involving the ultrasonic irradiation of three different materials using a broad-band transducer with a rated nominal frequency of 2.25 MHz. The resultant spectra are shown in fig. 8. The first material is a finegrained steel plate whose rear wall echo is shown in the high-frequency pulse and in its spectrum. The second is a cast iron plate with a strong sound-damping characteristic, in other words a material causing absorption and scatter, whose rear wall echo is shown at two different distances. The third is hard rubber which causes absorption only. This experiment provides that particularly the marked de-mixing of the frequency spectrum in cast iron goes hand in hand with a lengthening of the pulse. After passing through an 80 mm thick piece of cast iron the pulse is already so long that its beginning and end are no longer visible on the oscilloscope whereas the absorption-causing piece of hard rubber which exhibits a relatively mild fall-off towards the high frequencies, still forms a relatively short pulse. Hence, the originally short duration of the pulse is no longer present at the defect site when there is sound damping. The pulse, and hence its axial resolution at this point, has lengthened considerably through modification of its spectral content compared with the pulse at the point of entry into the material. It follows from this that the spectrum plays a substantially greater role than does the duration of the pulse.

The CS-Technique is capable of providing an improvement in the testing of such marked scatter-producing austenitic materials. For one thing, defect detection can be increased through utilization of the optimum S/N ratio, the particular advantage being that the given spectrum is also maintained over different depths of the workpiece. For another, maintaining these data constant over the depth of the workpiece makes for considerably improved defect evaluation. The example of an austenitic forging will illustrate these two facts - fig. 9. In this forging, which measures approximately 250 mm by 360 mm, there are a 3 mm dia. side-drilled hole about 50 mm below the surface and a flat bottom hole about 350 mm below the surface. The optimum test range is between about 0.9 and 1.3 MHz. Above these frequencies, there is a relatively sharp rise in the noise level. The results obtained for these two defects by the conventional technique and by the CS-Technique are compared. By the conventional technique, it may very well be possible for a 1 MHz resonant transducer to detect the flat bottom hole before the back wall echo with a S/N ratio of more than 10 dB. However, due to its resonant design this transducer is not capable of detecting the 50 mm deep drilled hole as its pulses are too long. If, by contrast, a wide-band 2.25 MHz transducer is employed, it will detect the drilled hole at a distance of 50 mm relatively distinctly; its pulse, however, is so weakened at a greater depth that a back wall echo will not even be observed.

If the same transducers are excited by the CS-Technique within this 1 to 1.3 MHz range, the resonant 1.0 MHz transducer will detect the very close defect due to the shortening of the pulse facilitated by the CS-Technique while the 2.25 MHz transducer will not only detect that same defect, using a test frequency of 1.3 MHz, but will also detect the defect close to the back wall with a considerably improved S/N ratio. In fact, it was even able to detect some smaller natural reflectors located in-between. By maintaining the test data constant, the test range is appreciably extended. The axial resolution, compared with the 2.25 MHz transducer used in the conventional mode, is admittedly somewhat lower but the S/N ratio rises to values which cannot be determined from these scope traces.

4. SUMMARY

In testing coarse-grained materials, defect detection suffers from unfavourable S/N ratios. With respect to this, calculations and practical measurements are presented which prove that there exist within the transfer function of a transducer optimum frequency ranges for defect detection. The practical application of these findings demands that specific frequency ranges be adhered to during the test.

Staying within these frequency ranges provides not only an improved S/N ratio but also an extension of the test range and a substantial improvement in defect evaluation. Moreover, the frequency spectrum exercises a greater influence on the S/N ratio than does the length of the pulse. The CS-Technique which selects specific frequency ranges and permits defined measurements should be applied especially in those cases where the evaluation of defects causes problems. The use of DGS-diagrams and the like in testing coarse-grained materials should thereby be improved.

Some examples of ultrasonic tests of austenitic castings, austenitic forgings and thin-walled austenitic weld seams are illustrated.

References:

/1/ Goebbels, K., M. Römer, H.-A. Crostack
Quantitativer Vergleich verschiedener Ultraschall-Prüfverfahren zur Verbesserung des Signal/Rausch-Abstandes beim Vorliegen kohärenten Untergrundes
Materialprüfung 21 (1979) Nr. 8

/2/ Crostack, H.-A.
Beitrag zur Verbesserung der Ultraschallprüfung beim Ermitteln von Fehlern in schwer prüfbaren Werkstücken
Habilitationsschrift Universität Dortmund, 1978

/3/ Crostack, H.-A.
Untersuchungen zur Steuerung von Ultraschallimpulsen und ihr Einsatz in der zerstörungsfreien Werkstoffprüfung
Europäische Vortragstagung zerstörungsfreie Materialprüfung 24.-26.4.1978 Mainz

/4/ Becker, H., M. Vogt
Ultraschallprüfung austenitischer Schmiedestücke mit neuartiger Sendetechnik
Fachberichte Hüttenpraxis Heft 10, S. 915

/5/ Stelling, H.-A., H.-A. Crostack
Untersuchungen zur Optimierung der Ultraschallprüfung von Gußeisenwerkstoffen
Europäische Vortragstagung zerstörungsfreie Materialprüfung 24.-26.4.1978 Mainz

/6/ Just, T. etal
Leistungsfähigkeit verschiedener Ultraschallprüftechniken an austenitischen Probeschweißungen mit natürlichen Testfehlern
Materialprüfung 19 (1977) Nr. 12, 488

/7/ Crostack, H.-A., K.-F. Walder
Calibration of Transducers
next time in "Ultrasonics"

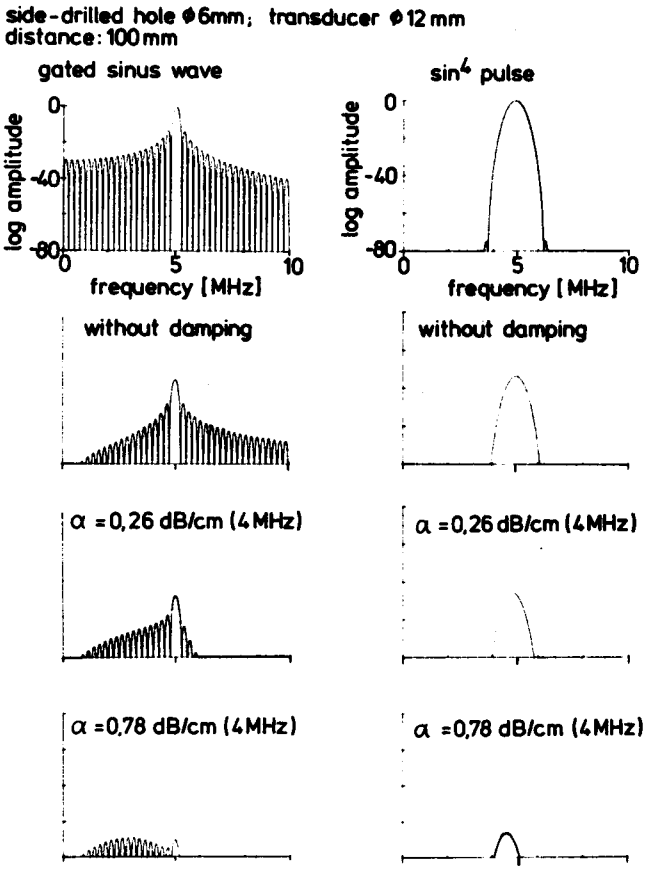


Fig. 1: Influence of Pulse Shape on Flaw Spectrum

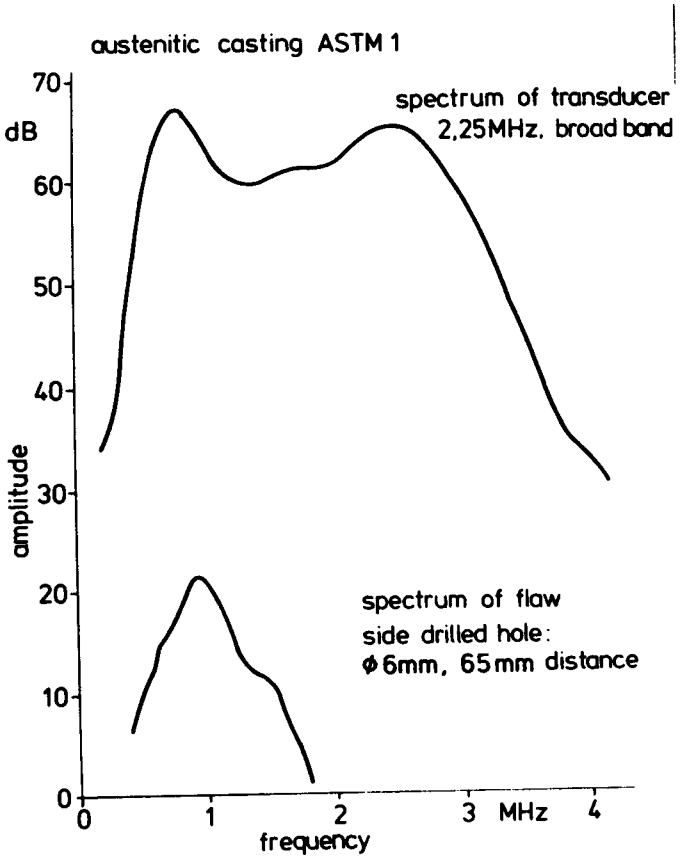


Fig. 2: Influence of Scattering on Flaw Spectrum

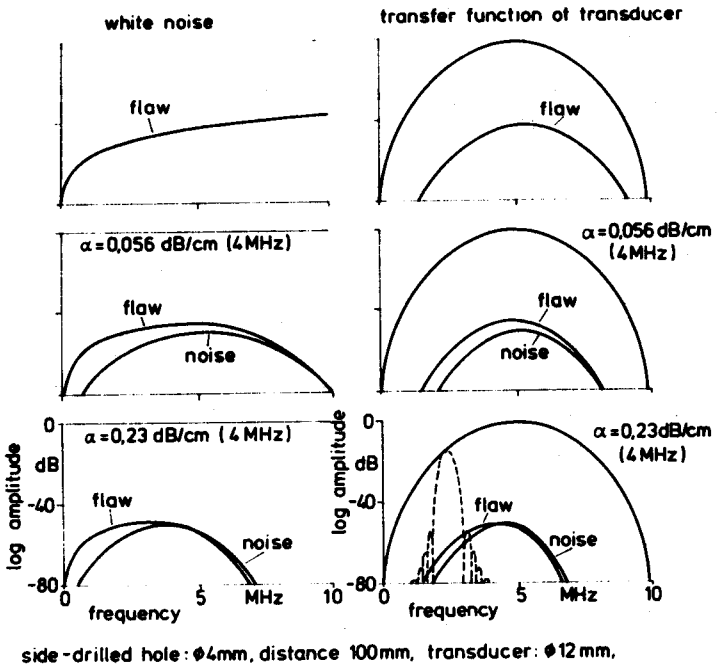


Fig. 3: Influence of Spectra on S/N-Ratio

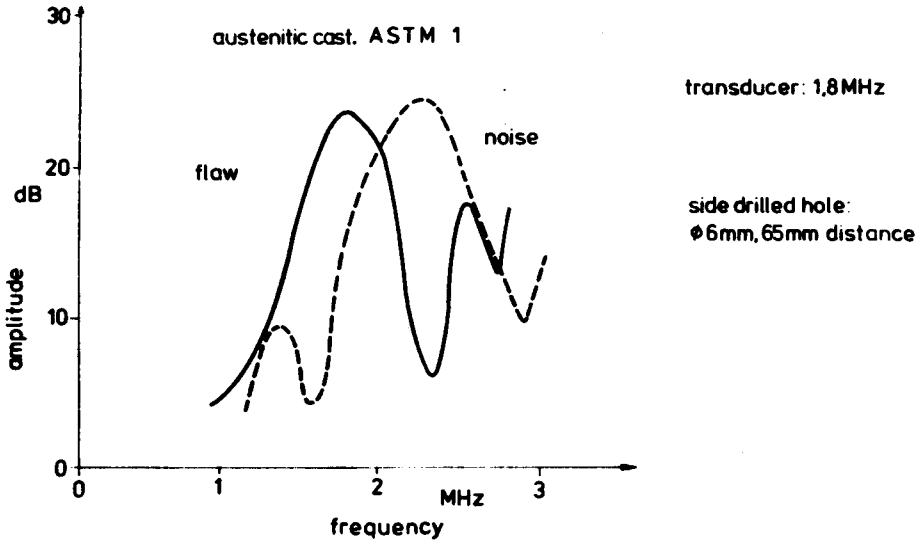
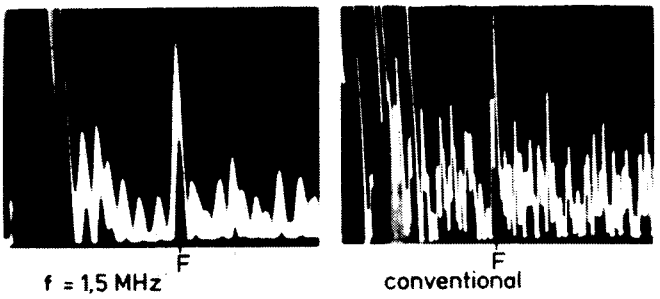
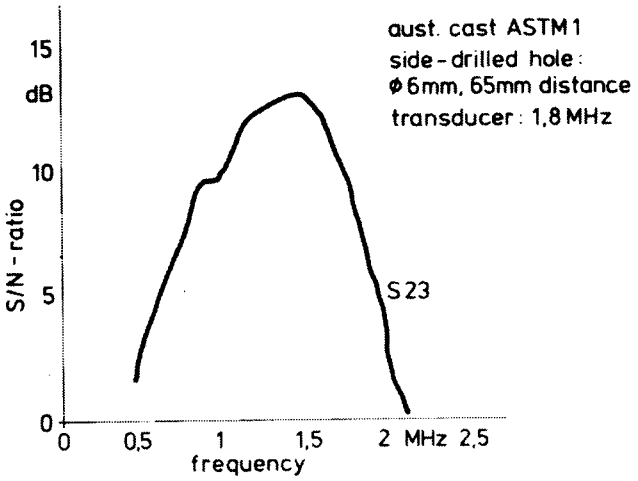


Fig. 4: Comparison of Spectra





F = flaw-echo

Fig. 5: Influence of Test-Frequency on S/N-Ratio

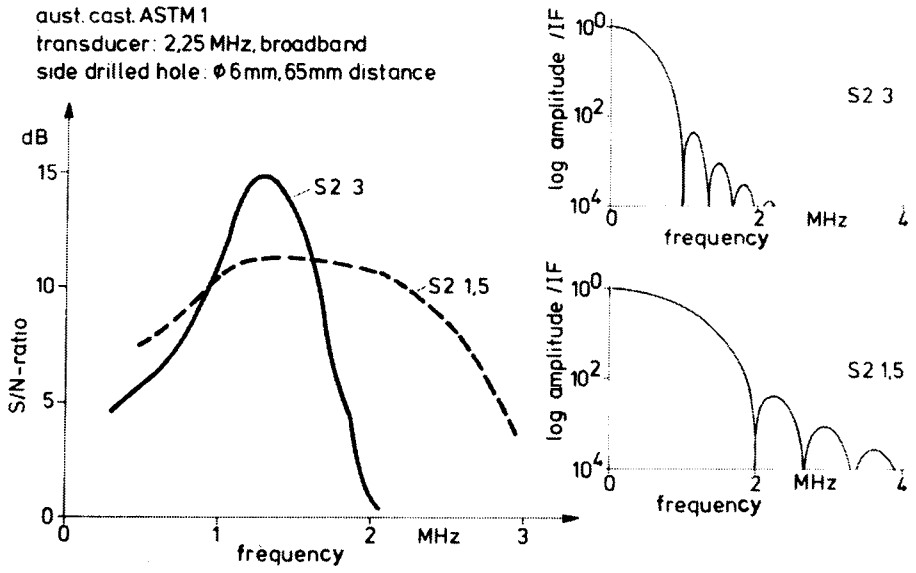


Fig. 6: Influence of Pulse Length on S/N-Ratio

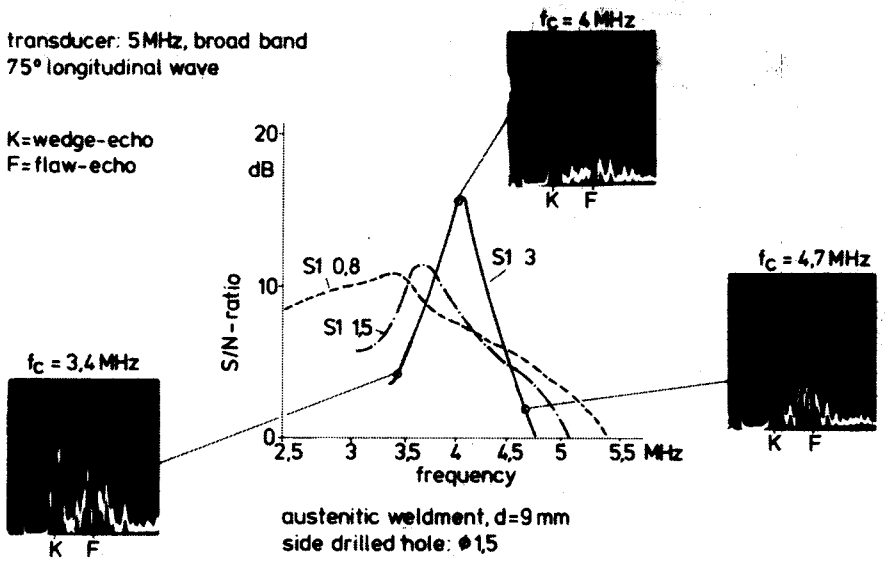


Fig. 7: Influence of Pulse Parameters on Flaw Detection

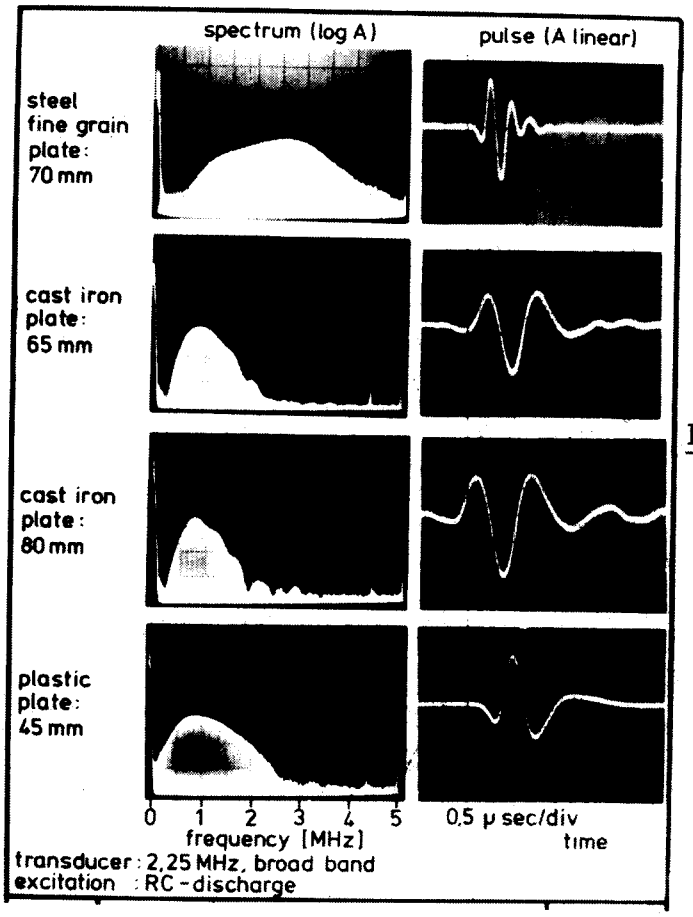


Fig. 8: Influence of Attenuation on Pulse Parameters

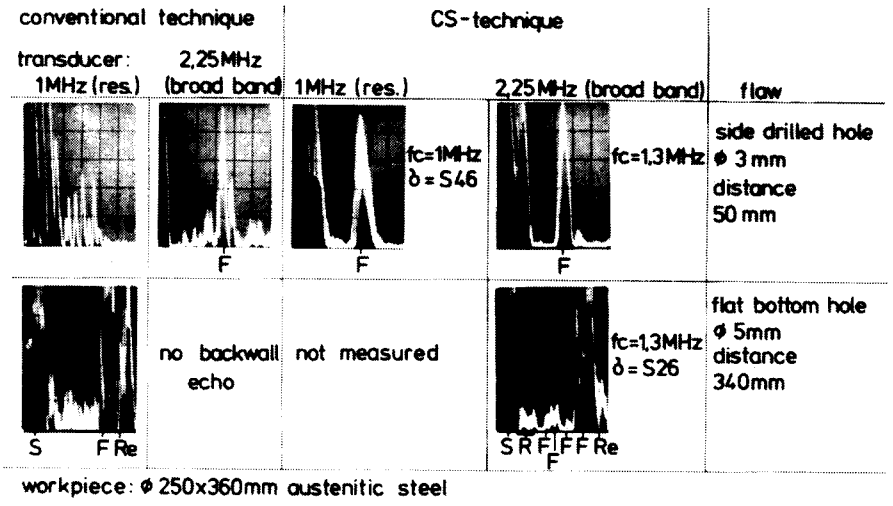


Fig. 9: Comparison of US-Techniques

Utilization of a Fisher linear discriminant function in IGSCC detection

J.L. ROSE, M.J. AVIOLI - Drexel University, USA
M.E. LAPIDES, Electric Power Research Institute, USA

ABSTRACT

A Fisher Linear Discriminant function is used to separate geometric indications from IGSCC indications in 304 stainless steel piping. Excellent performance on a variety of test samples has been achieved. A transducer selection criteria is outlined that enables us to locate reflectors efficiently. Dual element angle beam transducers are used for thick pipes and single element angle beam transducers are used for thin pipes. Excellent signal to noise ratio and gain is achieved with these transducers. Following the transducer selection process, an algorithm selection criteria is established as a function of both pipe diameter and thickness. The algorithms are all Fisher Linear Discriminant functions that make use of such features as rise time of the RF waveform envelope, pulse duration, fall time, partial power between 1.5 and 2.0 MHz in the power spectral response and a second partial power between 2.0 and 2.5 MHz.

Physics is used to explain the excellent performance of the dual angle beam transducers and also to explain the usefulness of the five features listed above. Physical considerations include grain scattering, forward and backscatter concepts, transducer focusing effects, specular reflection characteristics of a notch and of a single crack, and random scattering characteristics from geometric reflectors.

Results are presented in the paper for a variety of test specimens. The training data is described in detail followed by a complete test data analysis. Engineering interpretations of sensitivity and specificity are outlined, sensitivity being defined as the capability of finding cracks in the crack population, and specificity defined as a capability of finding geometries in the complete geometric population. Overall performance of the algorithms in a rating study on thick wall pipe was approximately 80%. Improved algorithm performance is also suggested by way of a data acquisition retake philosophy and a circumferential integration philosophy. Consideration of a circumferential intergration procedure improved the overall algorithm performance to about 87%.

In order to review the pattern recognition studies associated with the establishment of the Fisher Linear Discriminant function, a tutorial review and analysis of all of the data acquired on thick wall pipes are analyzed using probability density function analysis, two-space scatter diagrams, self-tested Fisher Linear Discriminants, sorting tree techniques, followed by a template matching program. These studies show that the rating study carried out on the thick wall pipe was close to optimum as far as utilization of the five signal features are concerned.

INTRODUCTION

The subject of IGSCC detection has received considerable attention in recent years. Ongoing research work on this and related problem areas can be found in ref. [1]. Work reported in this paper describes procedures for separating IGSCC signals from geometric type reflection signals, geometric indications including counterbore, root, and crown type situations. Preliminary work on this subject is reported in papers by Rose and Singh [2, 3, 4]. Similar work utilizing an adaptive learning philosophy is reported in ref. [5].

A transducer and algorithm selection criteria is outlined in this paper that provides us with a procedure for effectively locating reflectors and then for characterizing the reflectors. A dual element angle beam transducer is used in some of the work. Details of this transducer are reported in ref. [6]. The dual element angle beam transducer has excellent gain and signal to noise ratio for inspecting 304 austenitic stainless steel piping.

Physics is also used to explain the excellent performance of the dual angle beam transducers and also to explain the usefulness of the five features used in pattern recognition. Physical considerations include grain scattering, forward and backscatter concepts, transducer focusing effects, specular reflection characteristics of a notch and of a single crack, and random scattering characteristics from the geometric reflectors.

A two-space scatter diagram of selected time domain and frequency domain features has shown promise for solving this difficult classification problem [2, 3, 4]. A Fisher Linear Discriminant function is used in this work that improves the overall prediction capability considerably. Details of the Fisher Linear Discriminant function are reported in ref. [7] and ref. [8]. Features included in this study are rise time of the RF waveform envelope, pulse duration, fall time, partial power between 1.5 and 2.0 MHz of the power spectral response, and a second partial power between 2.0 and 2.5 MHz.

Results are presented in the paper for a variety of test specimens, the test specimens containing intergranular stress corrosion cracking produced from a special graphite wool technique [9]. The training data is described in detail followed by a complete test data analysis. Engineering interpretations of sensitivity and specificity are outlined, sensitivity being defined as the capability of finding cracks in the crack population, and specificity defined as a capability of finding geometries in the complete geometric population. Improved algorithm performance is also suggested by way of a data acquisition retake philosophy.

Overall performance of the algorithms in a rating study on thick wall pipe was approximately 80%. Consideration of a circumferential integration procedure improved the overall algorithm performance to about 87%.

In order to review the pattern recognition studies associated with the establishment of the Fisher Linear Discriminant function, a tutorial review and analysis of all of the data acquired on thick wall pipes are analyzed using probability density function analysis, sorting tree techniques, followed by a template matching program. These studies show that the rating study carried out on the thick wall pipe was close to optimum as far as utilization of the five signal features are concerned.

A discussion and comparison of the rating results on thick wall pipe with the tutorial review presentation is also presented in the paper.

DATA ACQUISITION METHODOLOGY FOR TRAINING PURPOSES FOR THE RATING STUDY

The development of a simplified pattern recognition algorithm to discriminate IGSCC from geometric reflectors in nuclear reactor piping is complicated by variations in pipe wall thicknesses. The data used in this study, for training purposes, were taken from three different size pipe sections as follows:

A - 4" schedule 80 (.337" thick) 29 IGSCC, 70 crown
10" schedule 40 (.32" thick) 33 crack, 24 geometries

B - 10" schedule 60 (.5" thick) 55 IGSCC, 15 root

C - 12" schedule 100 (.875" thick) 25 IGSCC, 34 geometries
26" schedule 80 (1.3" thick) 17 IGSCC, 17 counterbore, 22 root

This study sought to determine the effects of pipe thickness on an IGSCC detection system.

Pipe thickness has an effect on the location of IGSCC in relation to the weld itself. See Figure 1. Due to varying stress concentrations and other factors, cracking in larger diameter (and therefore, larger thickness) pipes occurs closer to the weld root indications when dealing with larger pipes, due to their proximity to the expected sight of cracking. On the other hand, cracks in smaller thickness pipes may be located so as to allow the ultrasonic beam to rebound and record an echo from the weld crown. Furthermore, since the pipe wall is relatively thin, the additional arrival time of the crown indication will not be as evident as with thicker pipe. Thus, crown indications are often a problem with smaller size pipes. As expected, crown indications only showed up with the 4" dia. specimen, while root and counterbore signals appeared with the 4", 10", 12", and 26" dia. pipes.

The dual element transducer was preferred, due to its reduction of grain noise and resultant high SNR [6]. The smaller single element unit, however, was used with the smaller size pipes to provide adequate contact over most of the transducer's surface. Both transducers were checked prior to their use for appropriate frequency content and pulse shape characteristics.

Prior to ultrasonic examination, available records and penetrant testing results were studied to determine the most probable locations of cracking in the specimens.

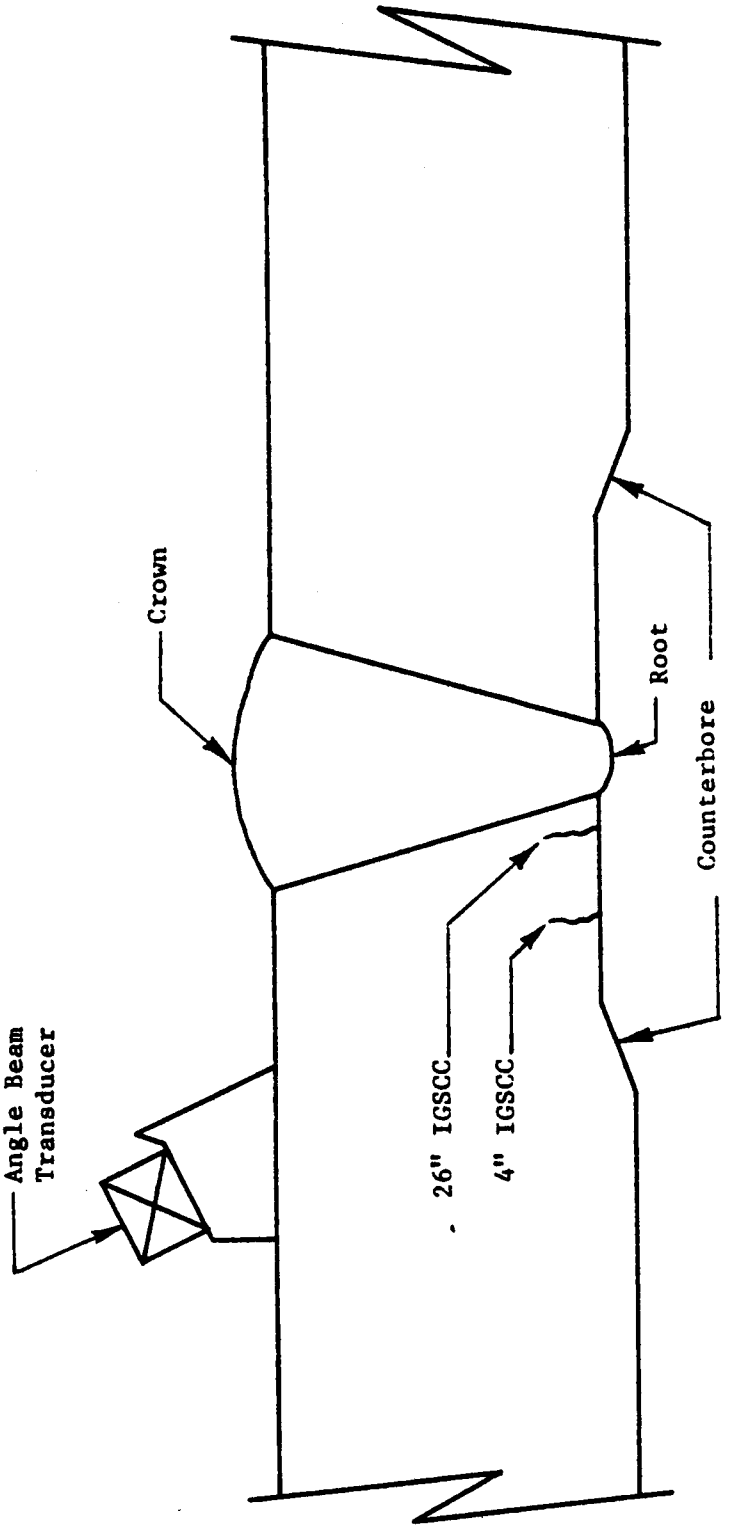


Figure 1. Relative Locations of IGSCC for Different Thickness Pipes

The data acquisition system is diagrammed in Figure 2. Its major components are:

Aerotech UTA-2 Pulser-Receiver
Tektronix 7704 Oscilloscope
Biomation 8100 Analog-to-Digital Converter
Hewlett-Packard 1200A Oscilloscope
PDP 11/05 Minicomputer with Hard and Floppy Disks
Tektronix Graphics Terminal and Hard Copy Unit

Actual data taking was started by following a standard procedure to set the "gate": that portion of time after the transmitted pulse which contains the signal to be studied. To set the gate, the transducer was placed so as to obtain a direct reflection from the edge of the pipe sample to be tested. The fact that the indication is from the edge is verified by the damping technique: the operator places his finger at the pipe edge and checks for attenuation of the signal. The point in time of the start of this echo is noted. The actual gate is set slightly back in time from this to account for wave velocity variations in the heat affected zone and decreased path length due to counterbore. The offset is approximately 10% for smaller diameter (4") pipes, and 15-20% for the larger sizes.

With the gate set, the transducer was moved around the circumference of the pipe, near the weld in question, using mineral oil as an acoustic couplant. When an indication was found which could be identified as either crack or geometry, it was taken as data. Data was taken in the vicinity of a 1/2 skip distance value from the weld centerline. This identification was accomplished with the records mentioned previously; in addition, it should be noted that the damping technique can be used to verify many geometry indications.

The actual recording of data was two-part. First, the location of the point on the pipe, instrument settings, and type of indication were hand-recorded. Second, the signal was digitized and sent to the computer, where it was stored on a magnetic disk for future use. The signals were averaged 32 times before storage to improve their signal-to-noise ratios. Enough of each signal was stored as was thought necessary to make a decision, their lengths varying from 5 to 20 microseconds.

FEATURE EXTRACTION

Due to a very large variance in the amplitude values for crack as well as geometry indications, it was concluded that amplitude information alone could not be used for the reflector classification problem. Sample results are contained in Table 1.

A total of five features found to work best from a large list of features were therefore extracted from each stored signal:

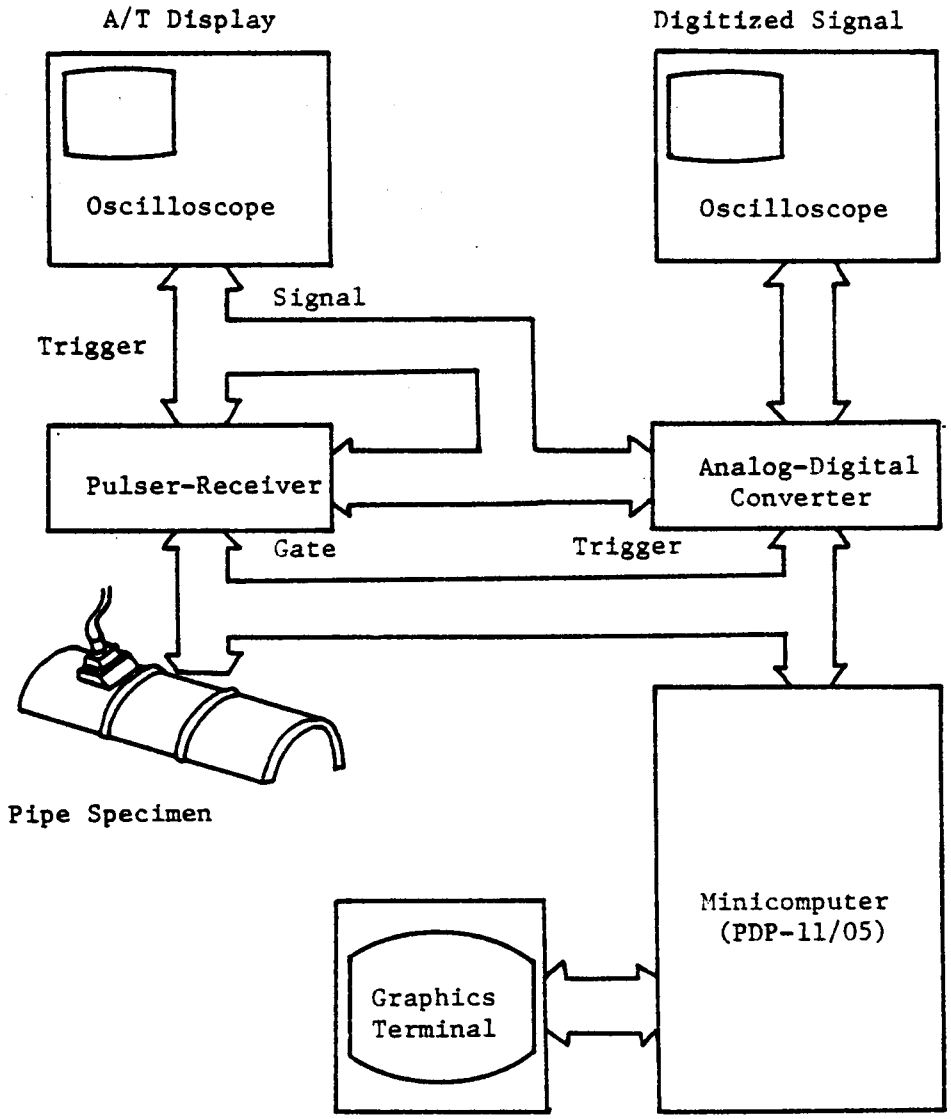


Figure 2. Block Diagram of Data Acquisition System

Table 1. Sample Amplitude Results in mV for a 26" Pipe Specimen

	Maximum	Minimum
Crack	3343.2	566.4
Root	1288.56	326.6
Counterbore	714.6	197.12

Feature 1. The duration of the pulse as measured from 20% to 20% of maximum amplitude

Feature 2. The rise time of the pulse as measured from 20% to 90% of maximum amplitude

Feature 3. The fall time of the pulse as measured from 90% to 20% of maximum amplitude

Feature 4. The partial power contained in the 1.5 to 2 MHz band of the signal's frequency spectrum

Feature 5. The same as Feature 4 but from 2 to 2.5 MHz

Envelope generation made use of a Hilbert Transform. Details are outlined below.

Any real signal can be represented as the real part of a complex signal called the pre-envelope.

$$\underline{x}(t) = x(t) + j\,\hat{x}(t)$$

where $\underline{x}(t)$ = pre-envelope
$x(t)$ = signal
$\hat{x}(t)$ = Hilbert Transform of $x(t)$

The Hilbert Transform is defined as:

$$\hat{x}(t) = \frac{1}{\pi}\int_{-\infty}^{\infty}\frac{x(\tau)}{t-\tau}\,d\tau$$

This is simply the convolution of $\frac{1}{\pi t}$ and the real signal.

In the frequency domain

$$\hat{X}(\omega) = \begin{cases} -j\,F(\omega) & \omega > 0 \\ 0 & \omega = 0 \\ j\,F(\omega) & \omega < 0 \end{cases}$$

and

$$\hat{x}(t) = \int_{0}^{\infty} -j\,F(\omega)\,e^{j\omega t}\,d\omega + \int_{-\infty}^{0} j\,F(\omega)\,e^{j\omega t}\,d\omega$$

The envelope of a signal is defined as:

$$E(t) = |\underline{x}(t)| = \sqrt{x(t)^2 + \hat{x}(t)^2}$$

Therefore, to generate the envelope of a particular signal, it is necessary to obtain its Hilbert Transform. This is most easily accomplished by generating the Fourier Transform of the original signal and then multiplying the positive frequency portion by $-j$, the negative frequency portion by j and setting the $\omega = 0$ value to zero. Upon inversion, this is the Hilbert Transform.

The original signal components and the Hilbert Transform components are squared point by point and then added together. The square root of this sum is the envelope.

It should be noted that the partial power features were obtained using a sliding band pass filter. This was used to mimick possible analog circuitry. The filter was 3 dB down at .25 MHz on either side of the filter center frequency and the roll-off rate was 20 dB/octave, again on either side of the center frequency.

TRANSDUCER AND ALGORITHM SELECTION

A transducer and algorithm selection chart is outlined in Table 2. Once a particular pipe thickness and diameter are known, Table 2 can be used to select an appropriate pattern recognition algorithm. The training base used to develop the algorithm is also listed in Table 2. All of the useful algorithms referred to in Table 2 are listed for reference purposes in Table 3. Transducer specifications are listed in Table 4. The transducer and algorithm selection criteria outlined above was generated according to the data acquisition methodology section for five features followed by a Fisher Linear Discriminant technique [7, 8].

Some of the transducer selection considerations are outlined next.

Physical Considerations of the Dual Element Angle Beam Probe

Selection of a dual element probe was based on a number of items. The dual element transducers consist of acoustically and electronically separated transmitting and receiving elements. The transmitting and receiving elements are positioned at an angle to each other, as illustrated in Figure 3. The dual element angle beam transducer design is shown in Figure 4. The improved SNR of the dual element angle beam transducer in a high noise environment could be explained by the fact that the receiver element is only receptive to the energy emanating from a zone where the ultrasonic beams related to each element overlap, or in other words, on the directivity pattern of the transmitting and receiving transducer. It can be argued that a dual-element transducer for a fixed design range has the capability of providing SNR equal to a single-element transducer, if not better. This type of transducer is usually designed for a fixed thickness range and its application beyond this intended design function results in poor performance. In order to carry out complete volumetric examinations of reason, their application has been rather limited. Additional benefits of the dual element probe are outlined in Figure 5. A computer program is used to evaluate sound pressure field variations produced by a number of dual element angle beam transducers in order to obtain an optimally designed transducer.

The results of a computer model aimed at determining the optimal transducer shape and such other design parameters as roof angle, separation distance between elements, and height of the transducer above interface, etc. for various pipe sizes is outlined in [6]. Pressure profiles can be used to study changes in the focal distances and lateral resolution of the transducers. Precise focal point position can also be studied.

Table 2. MACC Transducer and Algorithm Selection Chart

	Dia. < 10"	Dia. ≥ 10"
Thickness < .4"	U1 single element Algorithm 1-1 Training Base A	
.4" ≤ Th ≤ .8"		U2 dual element Algorithm 2-2 Training Base B
Thickness > .8"		U2 dual element Algorithm 3-2 Training Base C

Training Base

A - 4" schedule 80 (.337" thick) 29 IGSCC, 70 crown
10" schedule 40 (.32" thick) 33 crack, 24 geometries

B - 10" schedule 60 (.5" thick) 55 IGSCC, 15 root

C - 12" schedule 100 (.875" thick) 25 IGSCC, 34 geometries
26" schedule 80 (1.3" thick) 17 IGSCC, 17 counterbore, 22 root

Table 3. Algorithms

Algorithm 1-1

-.0145451 = -.00395259RT - .00465021PD + .0171996P1 - .0749970P2
Expected performance of 90.7% sensitivity, 67% specificity, 0% retake

Algorithm 1-1 (alternate)

-.00704321 = -.00291599RT - .0020665PD
Expected performance of 60% sensitivity, 55.7% specificity, 0% retake

Algorithm 2-2

Th = -.0265993PD + .0639162P1 - .000457078P2
Th > .0431121 - crack
-.0597 < Th < -.0431 → retake
Th < .0597492 - geometry
Expected performance of 96% sensitivity, 57.1% specificity, 8.6% retake

Algorithm 3-2

Th = -.0004228RT - .007969PD + .0341P1 - .0555P2
Th > -.0044 - crack
-.007 < Th < -.0044 → retake
Th < -.007 - geometry
Expected performance of 90% sensitivity, 77% specificity, 18% retake

Note: if -.006 to -.0085 expected 95, 69, 11,
if -.00875, 95, 57, 0
for a reference pulse of
.7 μsec RT, 2.01 μsec PD, ≈1.75 MHz, CF

Table 4. Transducer Specifications

I. Transducer U1, Single Element Angle Beam Transducer

a. Transducer shape - circular

b. Diameter - 0.375"

c. Center frequency - "1.5 MHz"

d. Frequency content - "Intermediate"
(a bandwidth of approximately 1.5 MHz)

e. Transducer shoe to produce angles of 45° in carbon steel

f. Transducer shoe width - 0.624"

g. Specifics:

KB-Aerotech PN3815-2
A24070

with standard parallel inductor tuning

II. Transducer U2, Dual Element Angle Beam Transducer (see Figure 3)

a. Transducer shape - square

length = 3/8 inch
width = 3/8 inch

b. Separation Distance Q - 0.08 cm

c. Roof Angle β - 5°

d. Incident Angle α - 32°
(as required to yield 45° angle in carbon steel)

e. Height of the transducer above the interface TH - 0.5 cm

f. Center frequency - 1.5 MHz

g. Frequency content - "Intermediate"

h h. Transducer shoe width - 0.855"
effective shoe width - 0.83"

i. Specifics:

KB-Aerotech J288133

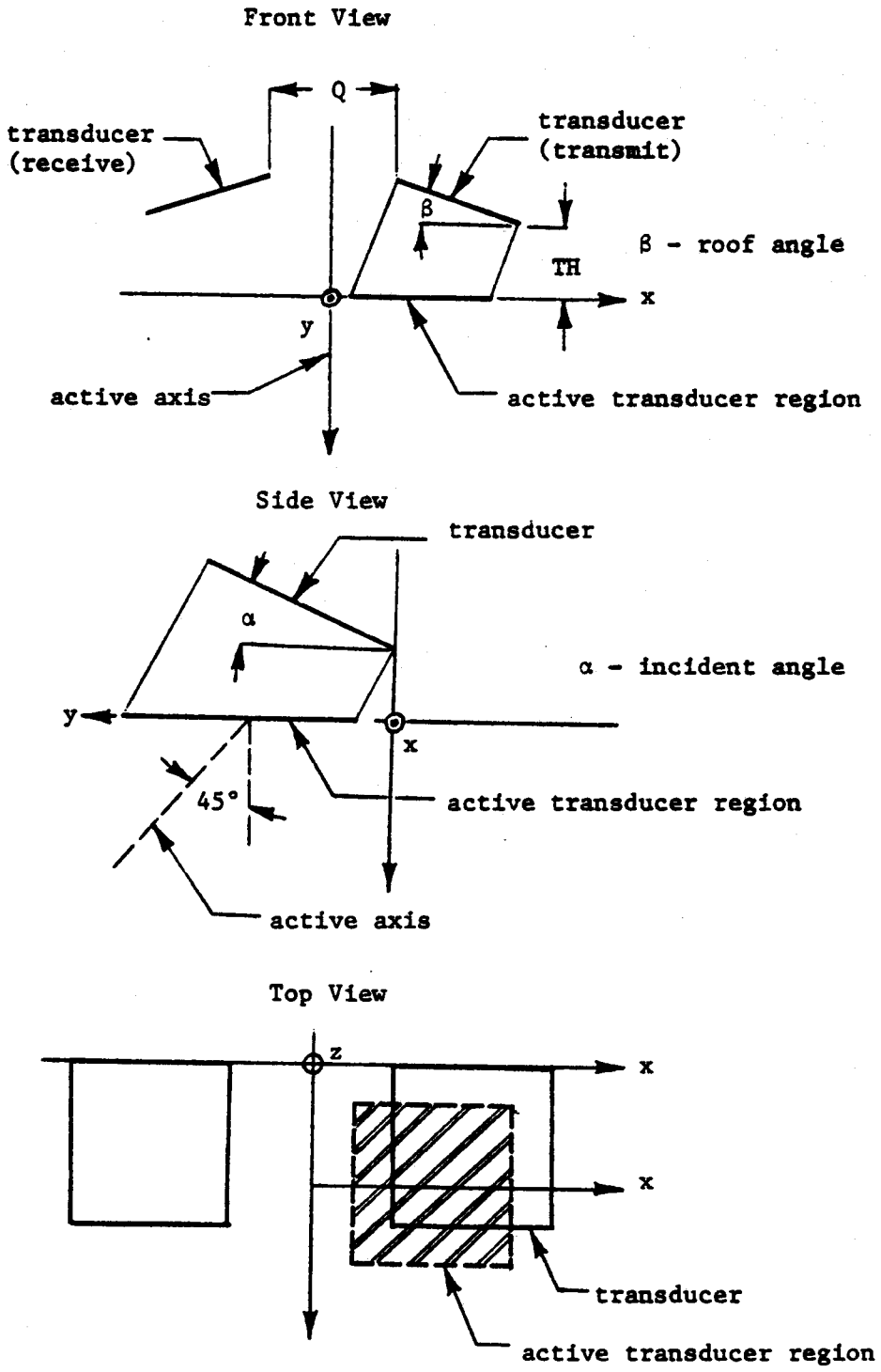


Figure 3. Dual Element Active Axis Computation Concept

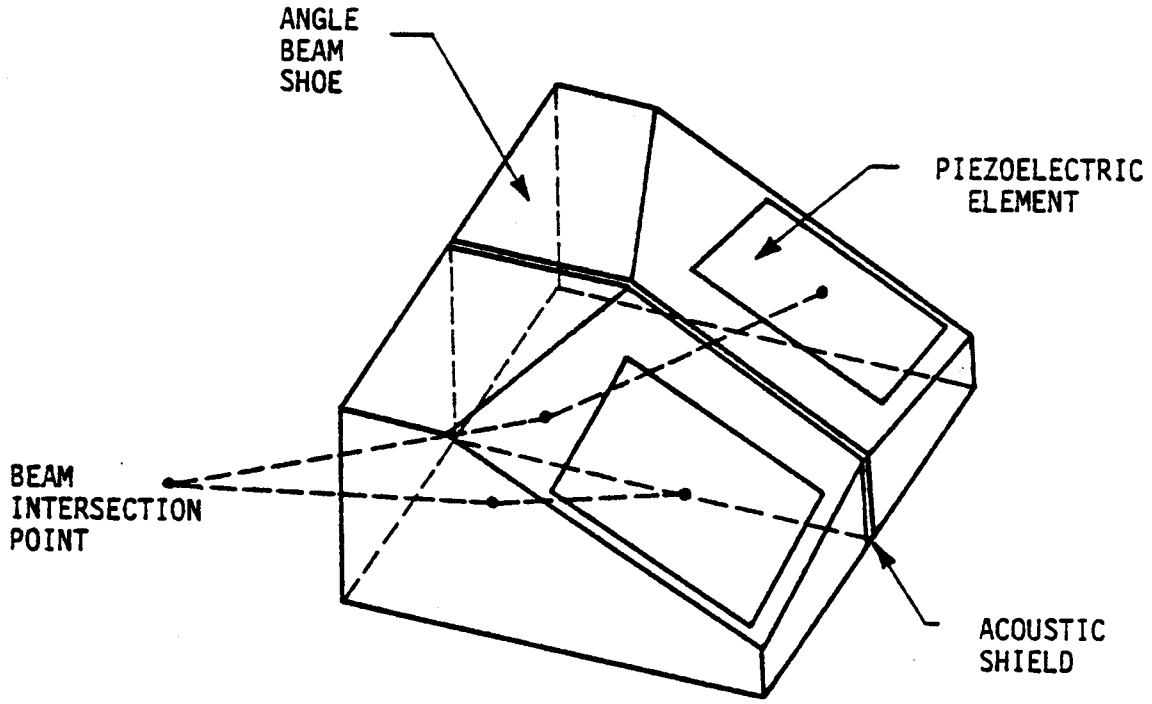
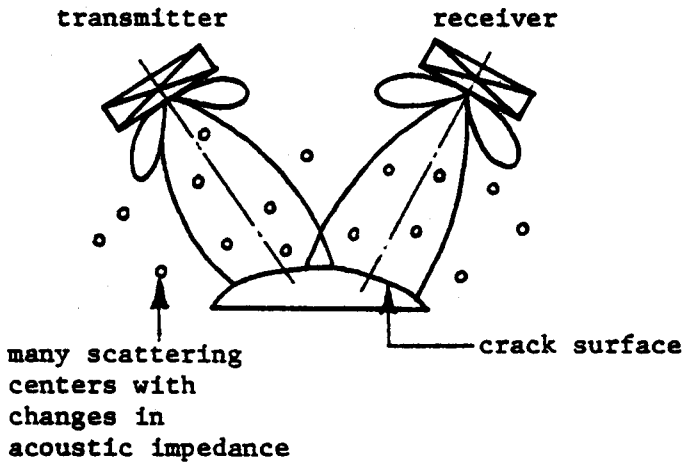


Figure 4. Dual Element Angle Beam Transducer Design



1. Directivity of the sending transducer is towards a crack surface with many grain scattering centers in its way.

2. Directivity of scattering centers are much more concentrated towards the sending transducer compared to the receiving transducer, especially when considering the cumulative effect of all grain scattering that occurs along the path from the sending transducer to the crack surface in question.

3. Grain scattering as the wave travels from the crack surface to the receiver will not impinge on the receiving transducer since directivity is back scattered in the direction of the crack surface.

4. Focusing of the ultrasound beam at a particular depth provides us with the maximum reflected signal from the crack area. (Grain scattering magnitudes are therefore smaller, hence leading to an improved S/N ratio.)

Figure 5. Physical Explanation of Dual Probe Values in SS Pipe Inspection

Shoe Width Determination

Shoe width was an important consideration. The inspection of steel pipes for weld area defects in this work was performed with shear wave transducer assemblies. A shoe is attached to the active transducer element in order to introduce sound energy at some angle other than normal. Discounting pipe wall thickness, the effective introduction of energy into a pipe is therefore a function of shoe and couplant contact.

When using either a single element or a dual element probe, the operator quite often uses a technique known as signal peaking. Signal peaking is a process whereby the inspector skews the transducer until he obtains a maximum amplitude signal. Curved shoes, shoes shaped for a particular pipe geometry, do not lend themselves conveniently to this type of inspection. Many indications are obtained with the transducer assembly in a position skewed off normal. Therefore, effective pipe inspection requires the use of transducers with flat-faced shoes.

The problem addressed here then, is to have a dual or single element transducer selection criteria based on flat shoes and various diameters of stainless steel pipe.

A flat surface abutted against a curved surface forms a line of contact. The contact is greatest when the transducer is parallel to the axis of the pipe and minimum when it is perpendicular to the axis (assuming a rectangular shoe; i.e. not square). The introduction of ultrasonic energy into this interface situation would be limited if this line were the only path available. Fortunately, liquid couplants are used and these not only increase the effective energy path, but reduce the area of contact problem when skewing the transducer.

The geometrical situation is shown in Figure 6.

This couplant layer thickness is very important. One would prefer to get as much ultrasonic energy as possible into the pipe being ispected. That is, minimum reflection of energy is desired at the oil-pipe interface. For completeness, the dual element configuration is shown in Figure 7.

The couplants used most often are similar to mineral oil with respect to their acoustical properties. The pipes usually inspected are stainless steel. It has been found that a frequency of 1.5 MHz is somewhat better than other frequencies for the inspection of stainless steel. A typical situation then, would involve mineral oil with 1.5 MHz ultrasonic energy propagating through it into steel. This information and layered media theory taken from Brekovskikh [10] indicates that maximum transmission of energy occurs when the oil layer varies from 2/5 λ to 3/5 λ.

Referring to Figure 6, if $L_1 = 2/5\ \lambda$ and $L_2 = 3/5\ \lambda$, then best transmission would be in effect.

Layer thickness is obviously a function of shoe width. This formula is easily derived and has been used in our transducer selection criteria to make sure that the shoe is not too large.

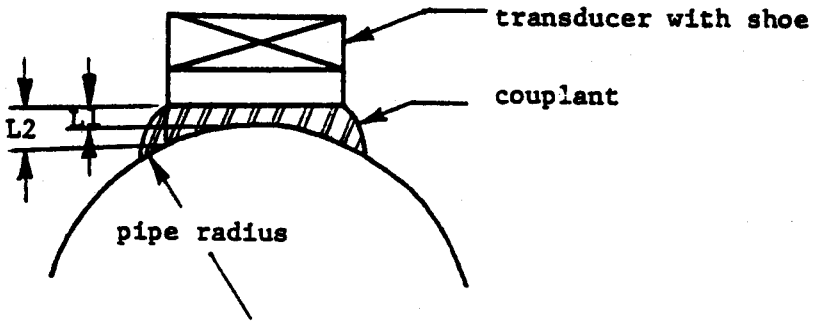


Figure 6. Transducer, Couplant, and Pipe Interfacing for Shoe Width Analysis

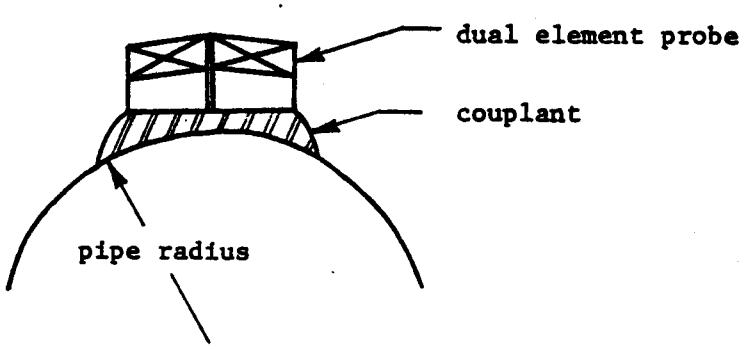


Figure 7. Dual Element Interfacing Configuration for Shoe Width Analysis

RATING RESULTS

A series of tests was conducted on five different graphite-wool type Japanese pipes [9]. In order to evaluate the performance of the transducers and algorithms contained in the transducer and algorithm selection chart, only thick wall pipes were considered in this study. Excellent results were obtained and are listed in Table 5. A photograph of one of the test specimens is included as Figure 8.

The reference pulse for the dual element transducer used in this study is shown for reference purposes in Figure 9. This data was taken by the edge of pipe B5-B6 at a half "V" distance.

An additional concept of circumferential integration was considered at this time. In order to see if circumferential integration would help, points in error were studied with neighboring points to see if spatial averaging could improve our prediction. If neighboring points were both correct, it was assumed that circumferential integration was possible. If two error points, side by side, had neighboring points that were correct, circumferential integration was also assumed as positive. On the other hand, three errors in a row led us to believe that circumferential integration would not help. A study of the data acquisition on the five Japanese pipes produced the following results. Of 17 incorrect answers, 15 could now be called correct using circumferential integration. It might be possible, therefore, to raise the overall index of performance by about 7% by employing circumferential integration.

ADDITIONAL PATTERN RECOGNITION STUDIES FOR A TUTORIAL REVIEW OF OUR ALGORITHM DEVELOPMENT PROCEDURES

It was decided to carry out some additional work on pattern recognition in order to determine an upper limit on algorithm performance for the five Japanese pipes available in our laboratory. Archival type data was acquired from areas both in the graphite-wool region and in areas where dye penetrant indications were clearly shown. Results of these additional studies are reported on the following pages. The studies serve as a tutorial review of our algorithm development procedures.

Probability Density Function Analysis

Considerations from physics and observation of the data taken from five 12" schedule 100 Japanese pipes showed that five features were most useful in studying discrimination capability between intergranular stress corrosion cracking and geometric type reflectors in the pipes. In order to study the distributions of these features for the crack and geometric type reflectors, a series of probability density function curves were generated. Figures 10 through 14 show the resulting PDF curves for rise time, pulse duration, fall time, partial power P1, and partial power P2, respectively. Results obtained were excellent, showing that smaller rise times generally come about for cracks with very dispersive results for geometric type reflectors. Reduced pulse duration values were also smaller for cracks and spread very substantially for geometric type reflectors. The partial power feature from 1.5 to 2.0 MHz for cracks was compact and well-defined compared to very

Table 5. Index of Performance Values on the Five Japanese Pipes

B5-B6	Sensitivity	$\frac{8}{11}$ = 73%
	Specificity	$\frac{7}{11}$ = 64%
	Overall	$\frac{15}{22}$ = 68%
C5-C6	Sensitivity	$\frac{25}{25}$ = 100%
	Specificity	$\frac{21}{25}$ = 84%
	Overall	$\frac{46}{50}$ = 92%
C7-C8	Sensitivity	$\frac{6}{8}$ = 75%
	Specificity	$\frac{15}{20}$ = 75%
	Overall	$\frac{21}{28}$ = 75%
D5-D6	Sensitivity	$\frac{13}{16}$ = 81%
	Specificity	$\frac{23}{29}$ = 79%
	Overall	$\frac{36}{45}$ = 80%
D7-D8	Sensitivity	$\frac{11}{15}$ = 73%
	Specificity	$\frac{19}{25}$ = 76%
	Overall	$\frac{30}{40}$ = 75%
ALL PIPES	Sensitivity	$\frac{63}{75}$ = 84%
	Specificity	$\frac{85}{110}$ = 77%
	Overall	$\frac{148}{185}$ = 80%

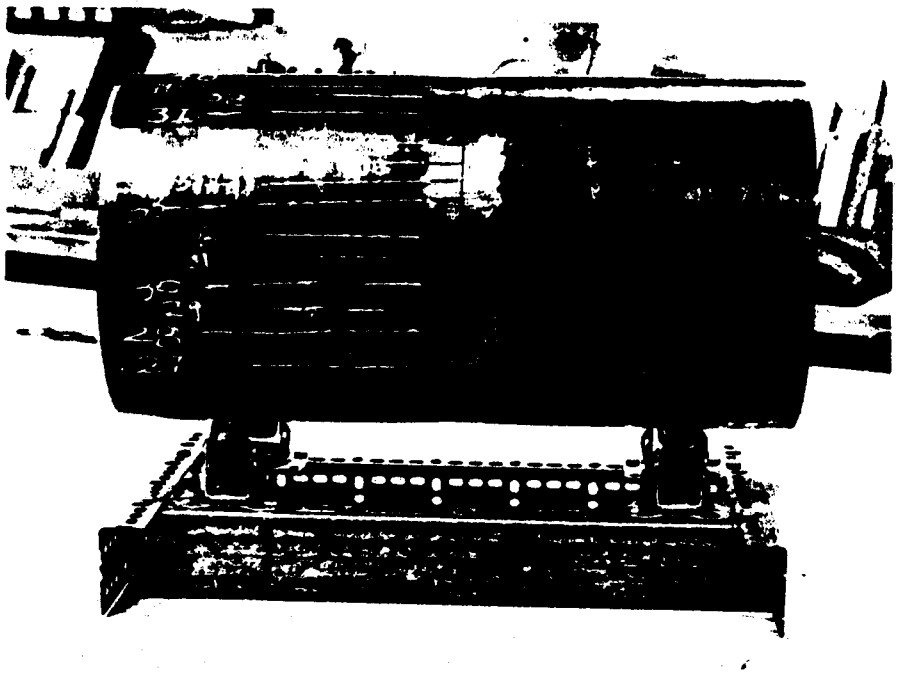
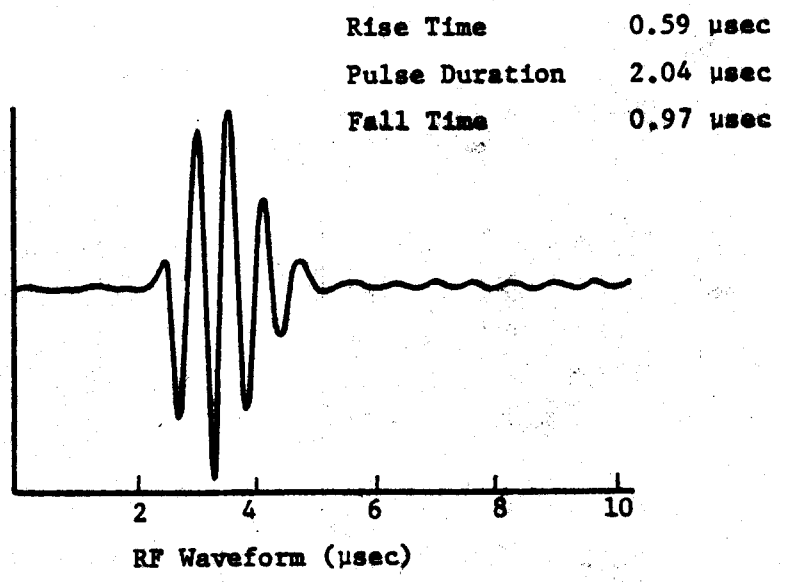


Figure 8. Japanese Pipe Specimen 12" Schedule 100 on Test Stand (D7-D8)



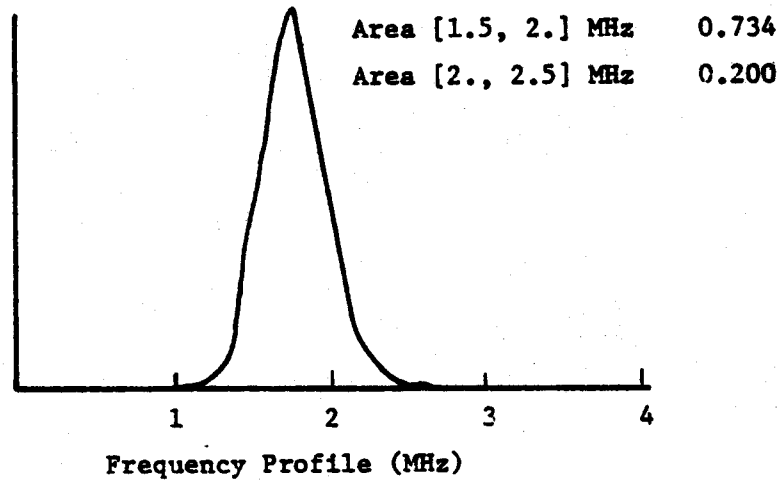


Figure 9. Dual Element Angle Beam Reference Waveform Characteristics from the Edge of Test Specimen B5-B6

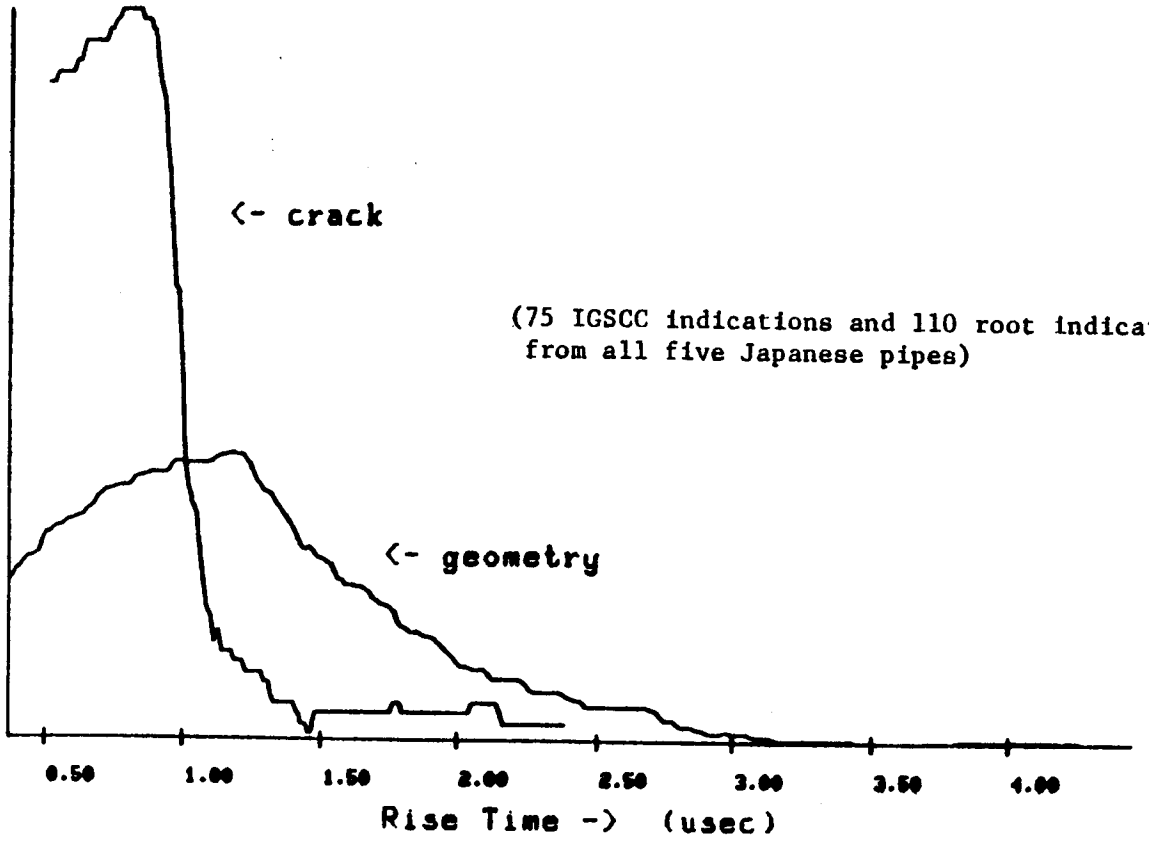


Figure 10. PDF Curves Showing Rise Time vs. Frequency of Occurrence for Cracks and Geometries

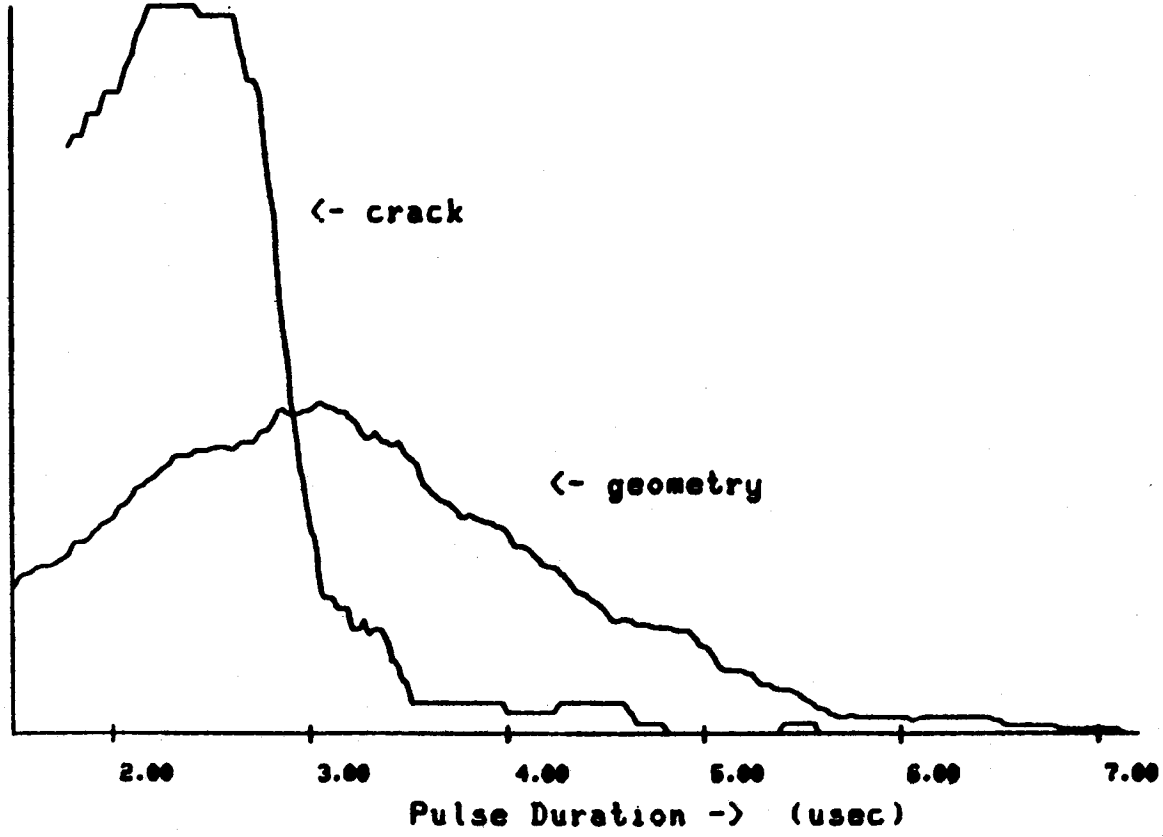


Figure 11. PDF Curves Showing Pulse Duration Vs. Frequency of Occurrence for Cracks and Geometries

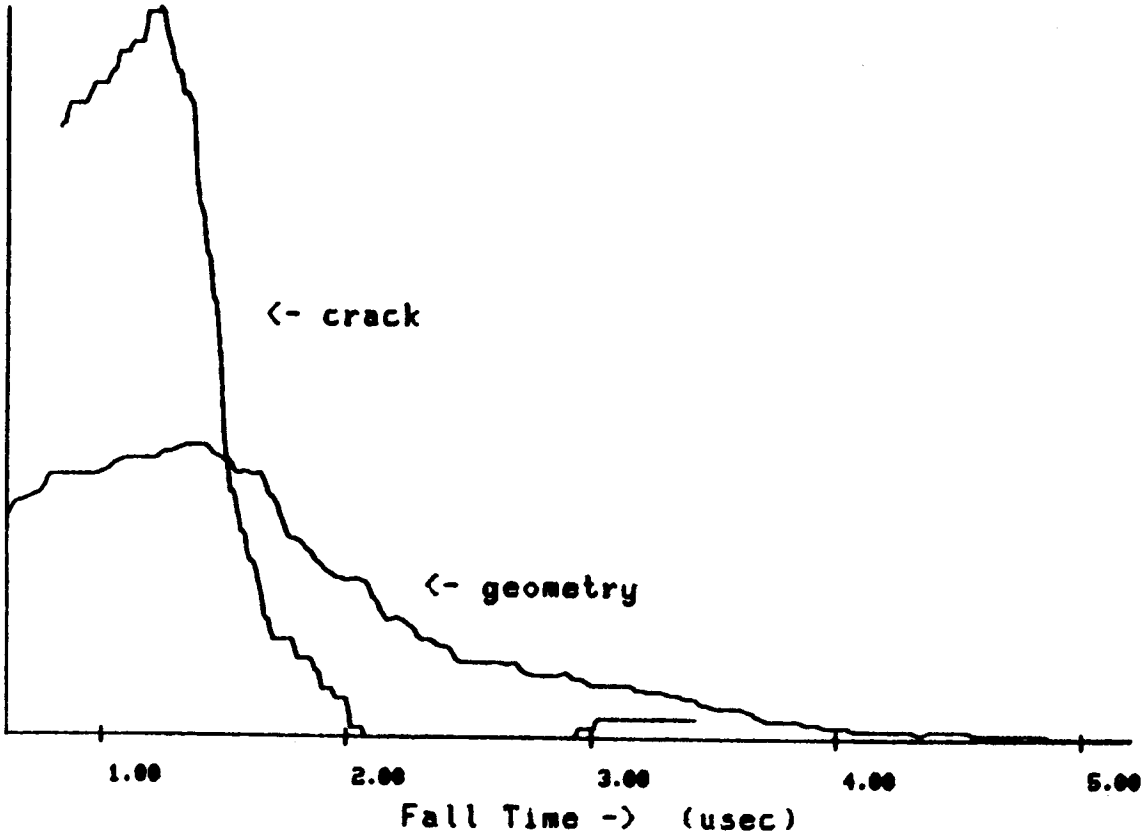


Figure 12. PDF Curves Showing Fall Time Vs. Frequency of Occurrence for Cracks and Geometries

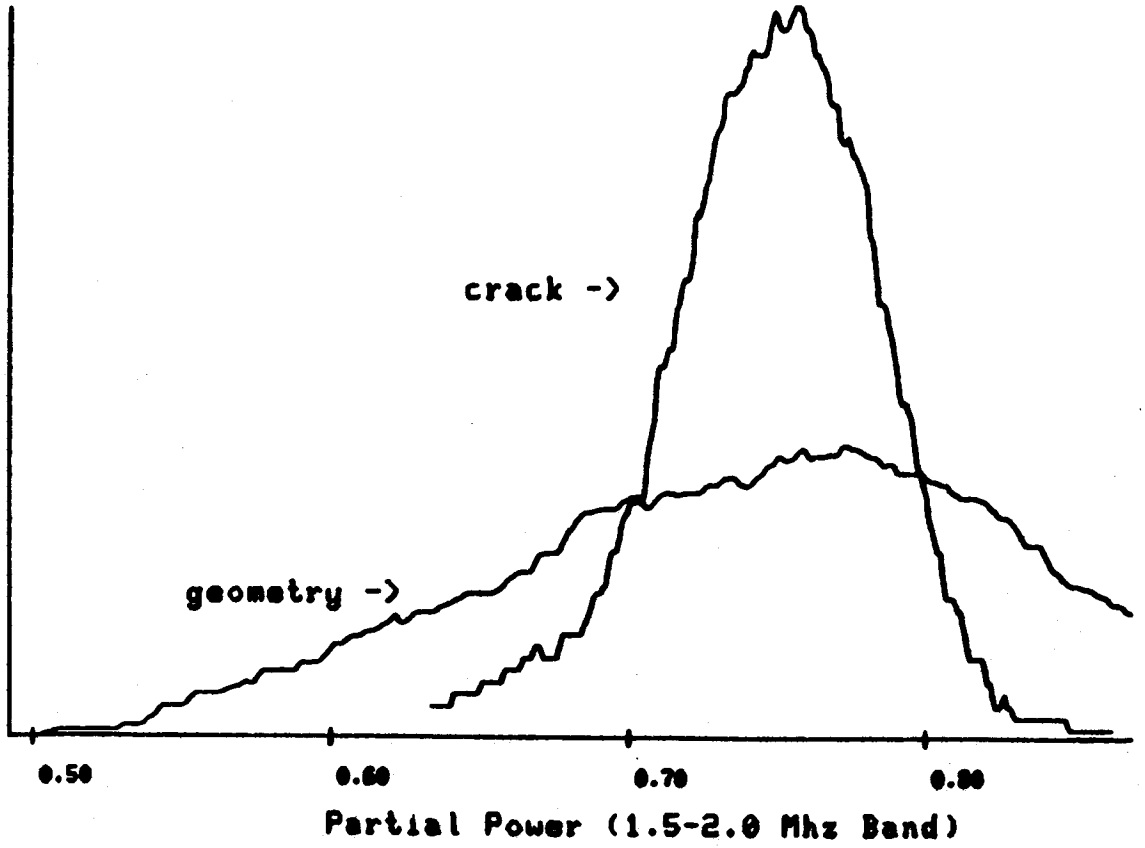


Figure 13. PDF Curves Showing a Spectral Power Feature Vs. Frequency of Occurrence for Cracks and Geometries

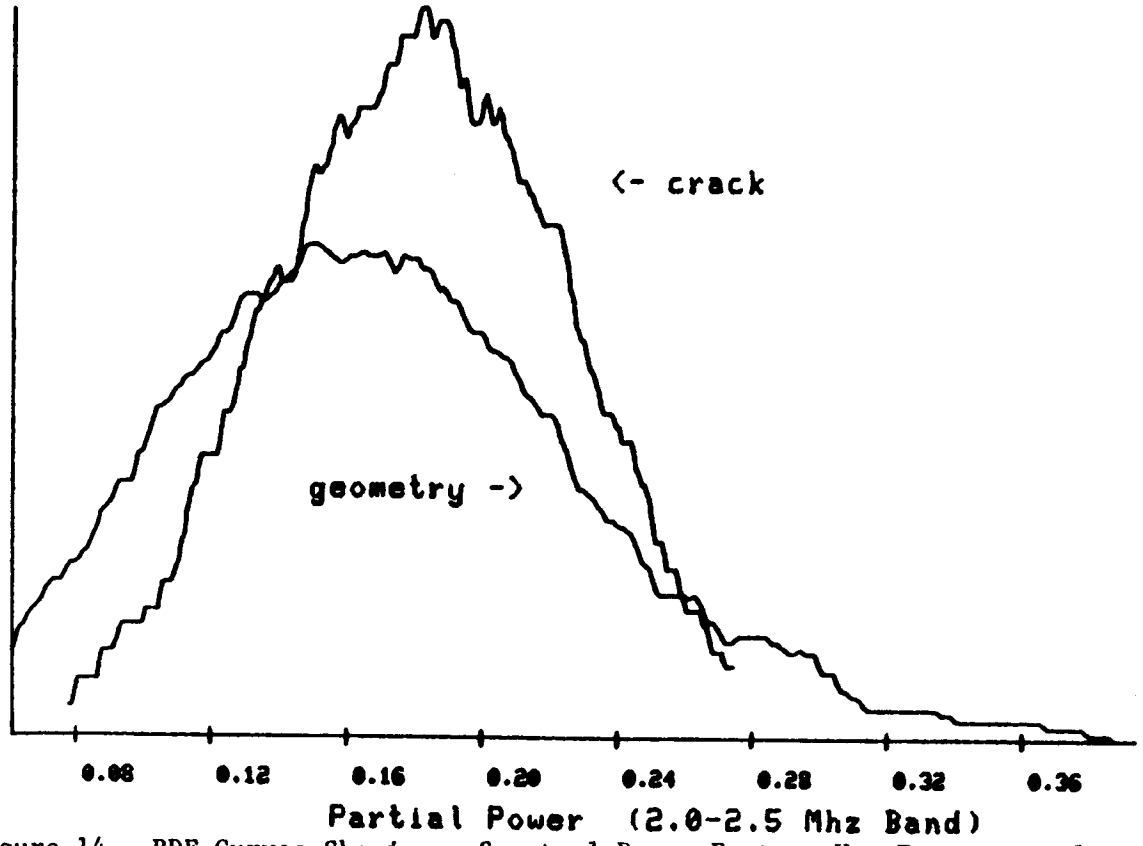


Figure 14. PDF Curves Showing a Spectral Power Feature Vs. Frequency of Occurrence for Cracks and Geometries

dispersive results for geometric type reflectors. The feature of fall time also showed some promise being smaller for crack and dispersive for geometric indications.

Probability density function curves can be used in a number of ways. They can be used to develop two-space scatter diagrams that are easy to analyze from a visual inspection point of view. Quite often one feature is not sufficient for solving a classification problem. On the other hand, two features have shown great promise for signal classification. Obviously, if five features are examined, ten two-space scatter diagrams could be produced, each producing different index of performance values. The best features from the probability density function analysis can be used to study the most promising two-space diagrams. If results are still not acceptable, the PDF input with the best feature information can be used to extend our analysis into N-space; say for example, with a Fisher Linear Discriminant technique.

Sorting trees can also be established from an analysis of PDF curves. This technique ensures us that classification potential based on a single feature measurement would not be overlooked. Sorting tree algorithms can also be established as a switching system that classifies signals as crack or geometric immediately, based on certain feature values and then subjects all remaining data to a more advanced pattern recognition algorithm.

Some of these concepts and a few additional extensions that make use of PDF analysis are explained on the following pages.

Two-Space Scatter Diagrams

It is convenient to study a plot of one feature versus another in order to seek out clusters of data ideally, of course, looking for a geometric cluster and a crack cluster. A search for these clusters is very easily carried out in two-dimensional space. As an alternative to cluster analysis, one might recognize in two-space a linear decision surface that seems to separate the data nicely into two classes. Selection of this line, of course, can vary the sensitivity and specificity of the pattern recognition algorithm selected for this study. Of ten two-space scatter diagrams that are possible in this five feature study, two sample two-space scatter diagrams are illustrated in Figure 15 and 16. The resulting sensitivity and specificity for the partial power versus pulse duration curve shown in Figure 15 is 87% and 58%, respectively. The overall performance is 70%. In Figure 16 the resulting index of performance values are improved slightly, being 85%, 63%, and 72% for the sensitivity, specificity, and overall performance, respectively. Many other topics of interest in pattern recognition can be studied quite readily with the aid of two-space scatter diagrams. As an example, sensitivity, specificity, and overall performance can be plotted as a function of either the X or Y coordinate intercept for the straight line shown in Figures 15 and 16. A retake philosophy could also be established that actually considers two parallel lines on the two-space scatter diagrams with the interior region being called a retake zone. This concept is illustrated in Figure 17. Inpsection has indicated that this procedure can ususally produce a marked improvement in algorithm performance as a data retake experiment usually forces the data points to fall futher away from the decision surface.

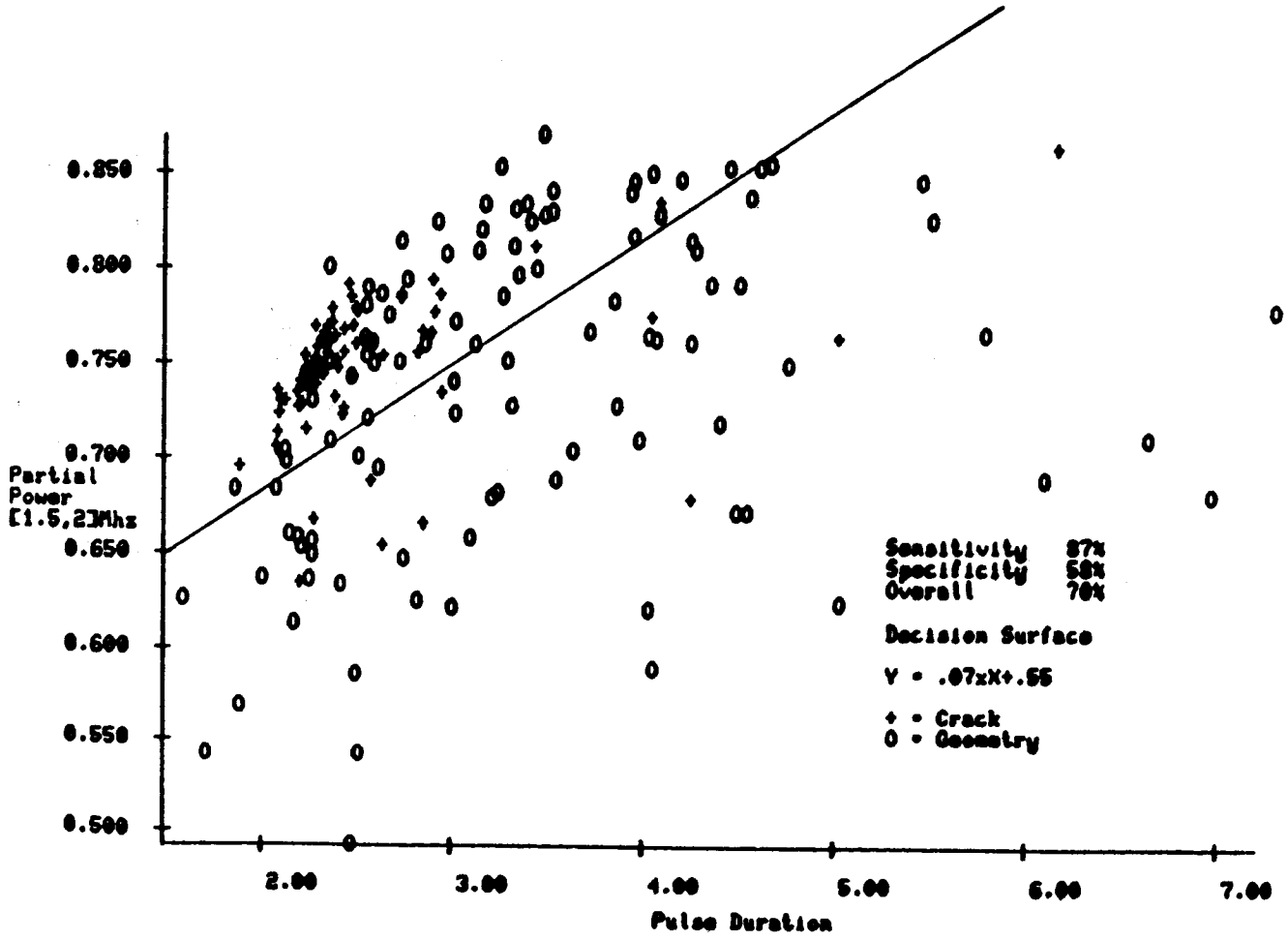


Figure 15A. Two-Space Scatter Diagram Showing Pulse Duration Vs. Partial Power P1

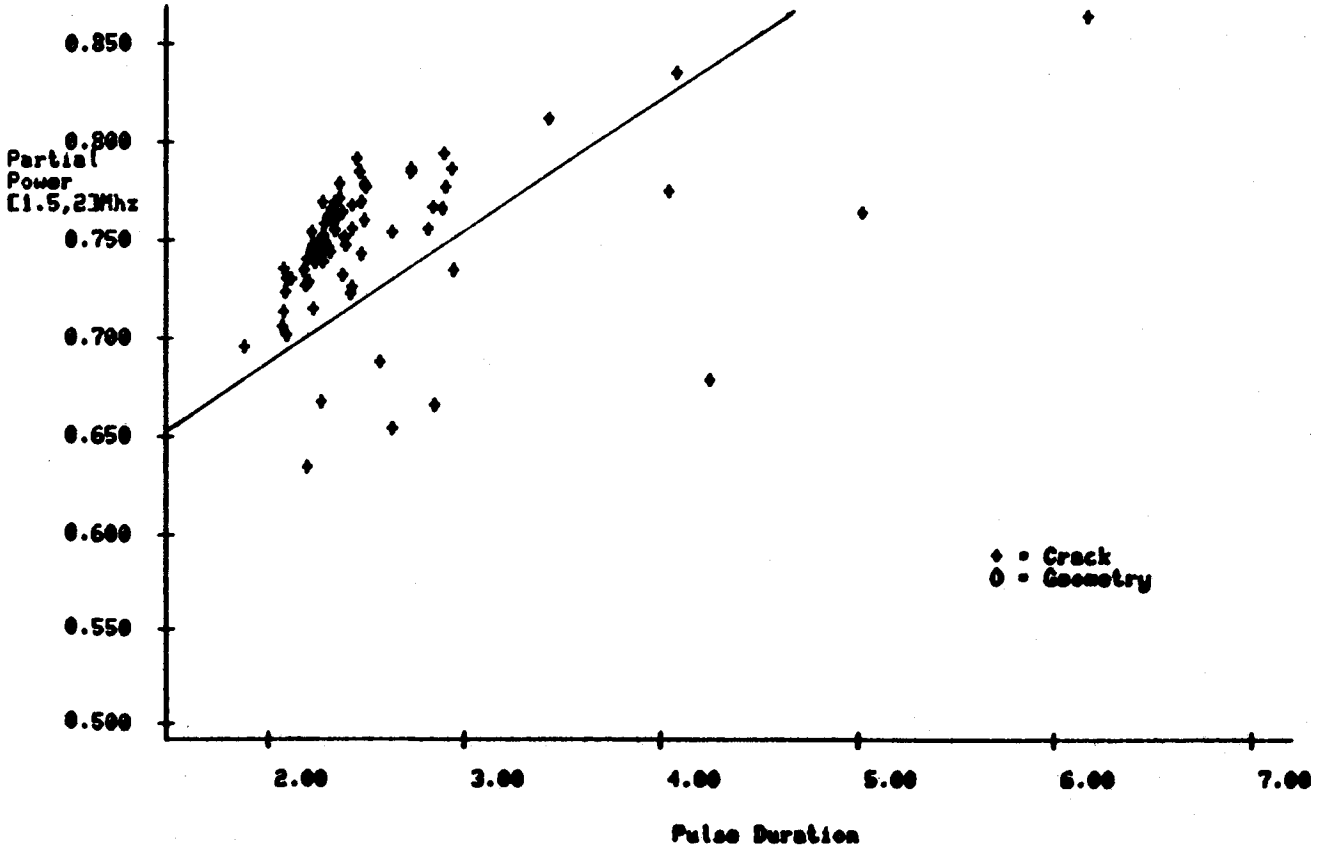


Figure 15B. Two-Space Scatter Diagram of Cracks Only for Pulse Duration vs. Partial Power P1

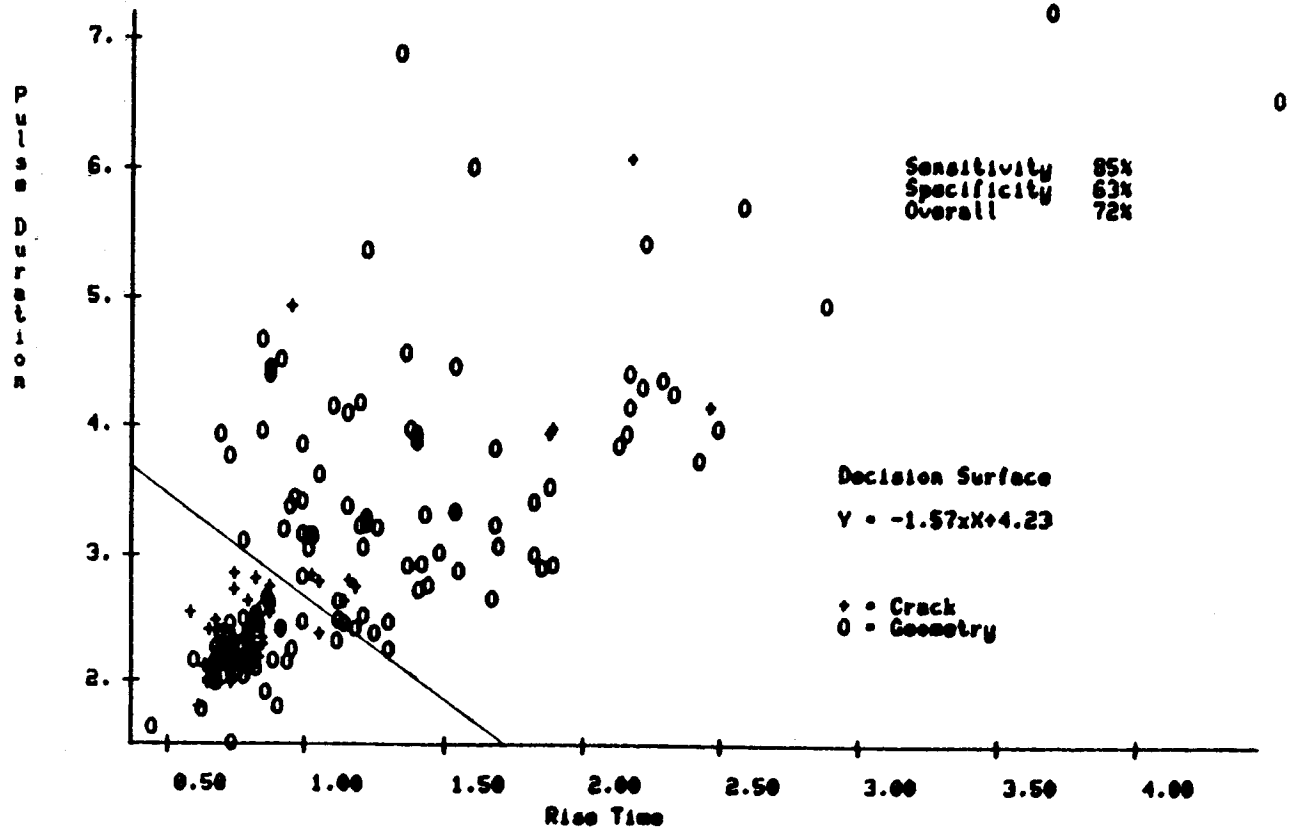


Figure 16A. Two-Space Scatter Diagram Showing Rise Time Vs. Pulse Duration

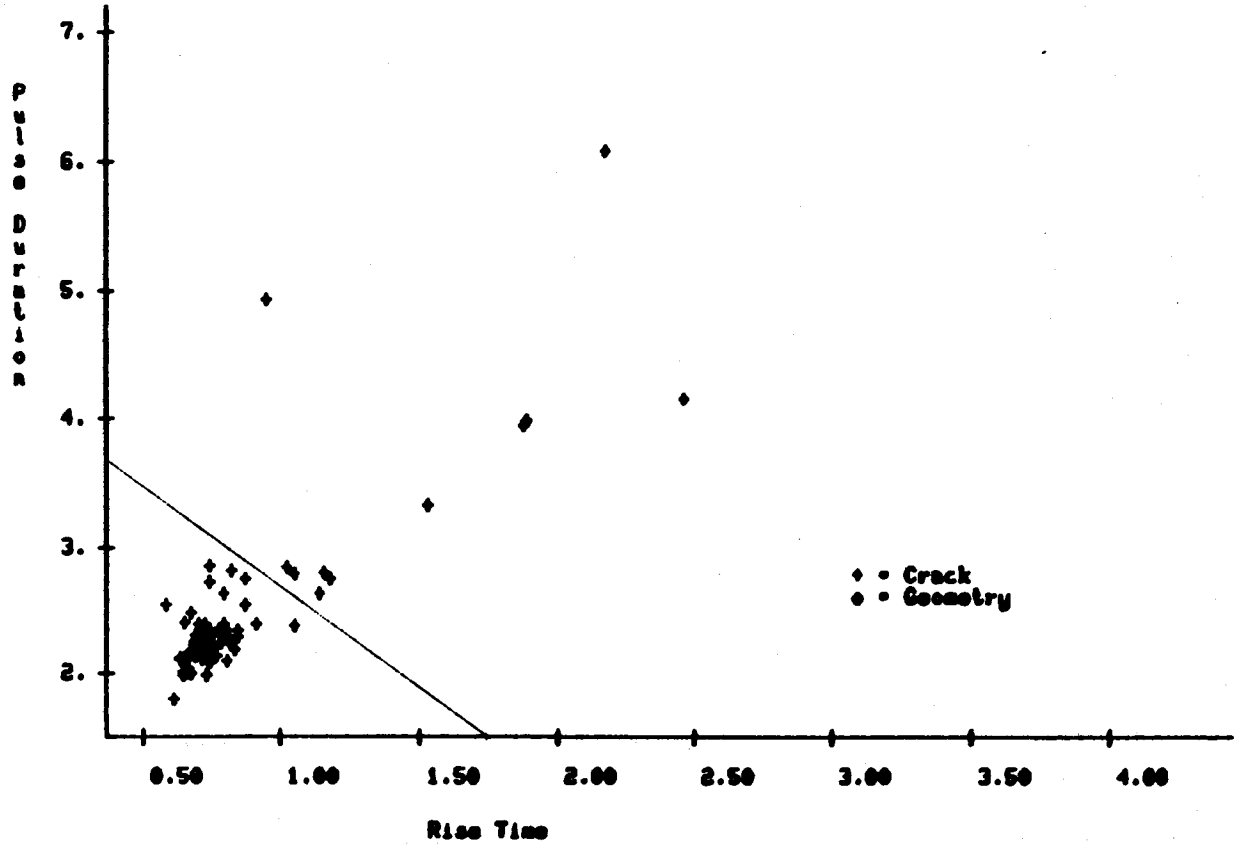


Figure 16B. Two-Space Scatter Diagram of Cracks Only for Rise Time Vs. Pulse Duration

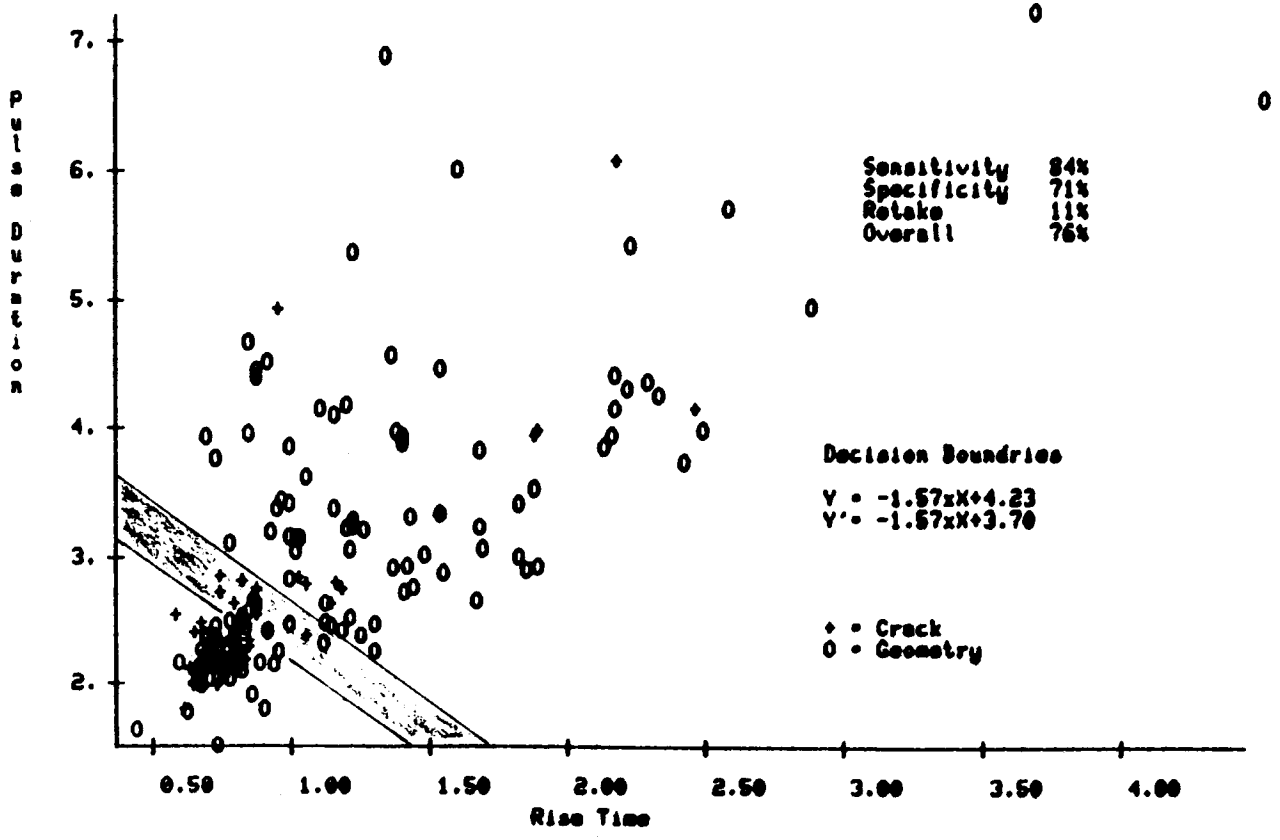


Figure 17. Two-Space Scatter Diagram Showing Rise Time Vs. Pulse Duration with a Retake Zone for Improved Performance

Fisher Linear Discriminant

Some work reported in the past has shown the versatility of the Fisher Linear Discriminant function as a pattern recognition algorithm development procedure in signal classification. Based on the results of the engineering evaluation analysis, it was decided to study the effectiveness of four features in the Fisher Linear Discriminant. Rise time, pulse duration, the partial power feature P1, and the partial power feature P2 were used. The resulting sensitivity, specificity, and overall performance was 84%, 77%, and 80%, respectively. It is very simple to modify the threshold used in the Fisher Linear Discriminant function which can change the algorithms performance. A plot of sensitivity and specificity versus threshold is illustrated in Figure 18. A 77% sensitivity value, 77% specificity value, and hence 77% overall performance can be obtained with a threshold of about 1.80. An increase in sensitivity of say to 90% causes a significant reduction in specificity to about 60% for a threshold value of about 2.00. An engineering decision on algorithm selection is required at this point that is based on both inspection reliability and economics.

The retake philosophy to improve algorithm performance was also studied in this case. In this case, a retake percentage of 14.0% produces a sensitivity of 88.1%, specificity of 69.6% and overall performance of 77.4% for an upper threshold of 1.917 and a lower threshold of 1.6888, the algorithm being

$$\text{Threshold} = -.675000RT - .565664 + 5.31333P1 - .0906331P2$$

Sorting Tree Analysis

Many different sorting tree arrangements could be considered in this study. One that seemed reasonably useful is diagrammed in Figure 19. In this case, feature values of the five features were compared with feature values that would guarantee a high probability of the signal being a crack-like reflector, these numbers taken from the PDF curves. The high sensitivity is effected by calling the majority of reflectors cracks. Therefore, the geometries were sorted first knowing that crack calls contained many geometries. Results for the sorting tree arrangement shown in Figure 19 are as follows: sensitivity, 81%; specificity, 81%; overall performance, 81%. It should be pointed out that performance is somewhat improved by selecting an interval for the P1 feature. Typical linear algorithms do not, in general, deal with these situations.

Template Matching of Feature Vectors

It is possible to develop a pattern recognition algorithm by using a minimum distance classifier that actually compares an unknown feature vector to a prototype feature vector for a crack and a geometric indication. The test vector is classified as either crack or geometry according to a distance measure providing us with a degree of closeness to a cluster in feature space. This technique also provides us with a modified matched filter methodology that is often useful in signal classification analysis.

Prototype vectors of cracks and geometries may be generated in a number of ways For this study the vectors were obtained by using the mean vectors of each class and secondly the median vectors of each class. The four features, rise time, pulse duration, partial power P1, and partial power P2, were used.

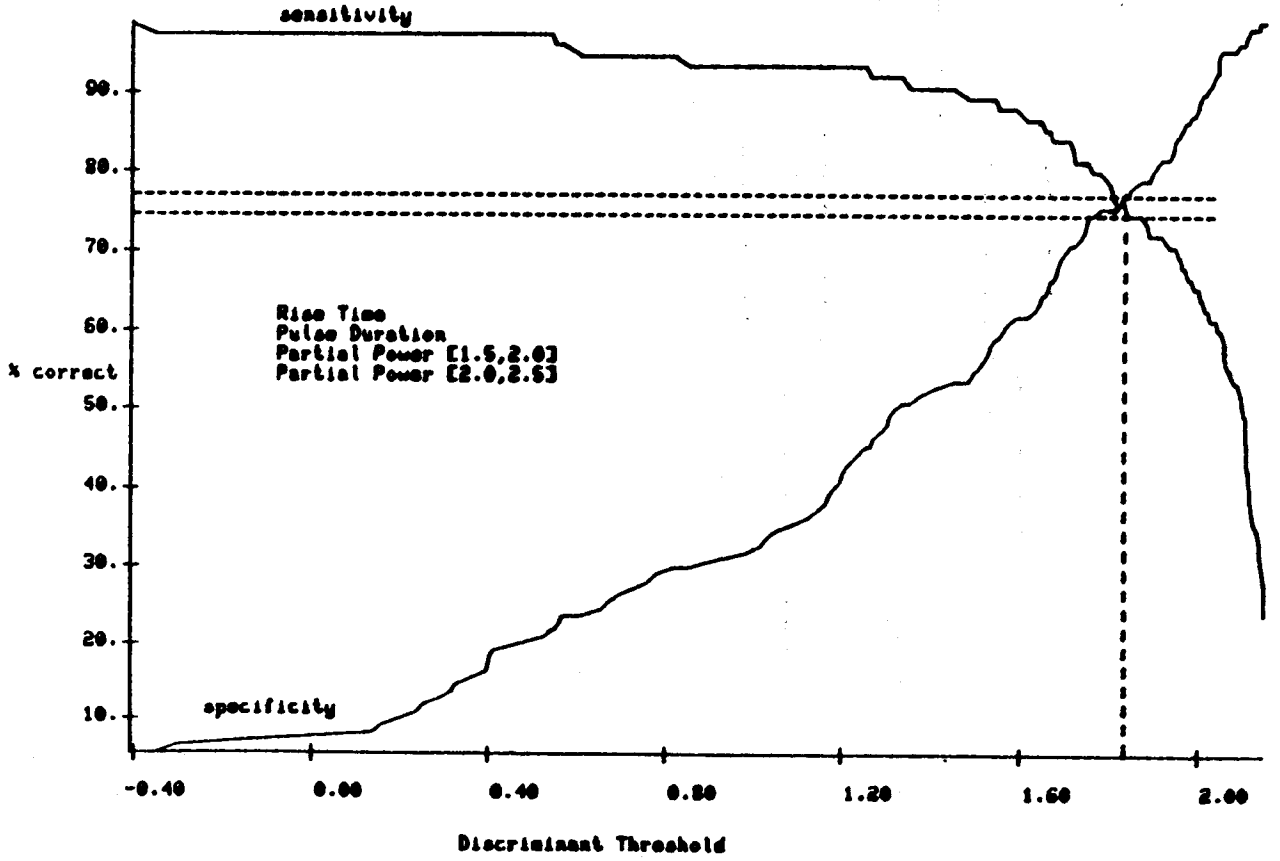


Figure 18. A Plot Showing Sensitivity and Specificity Vs. Threshold

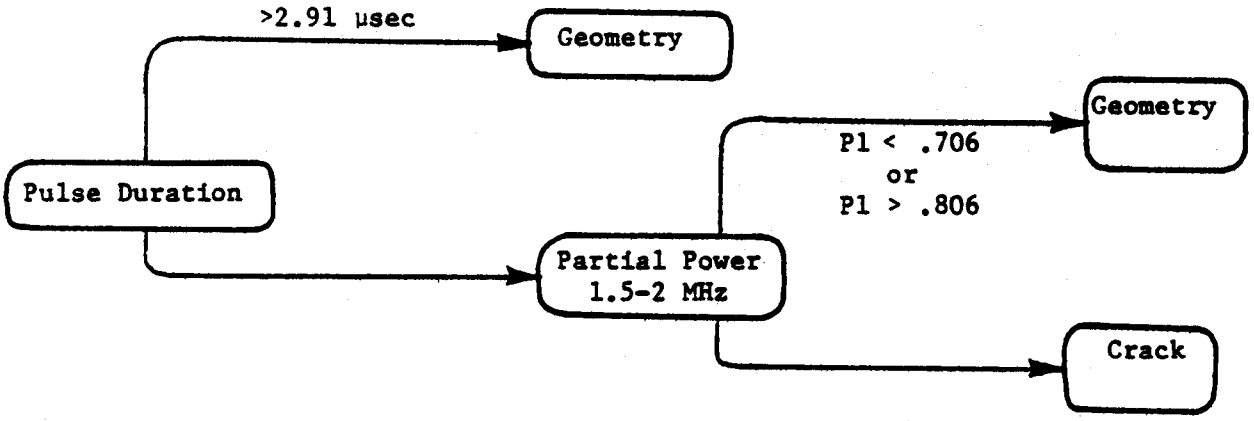


Figure 19. Sorting Tree Arrangement Possibility for the Five Japanese Pipes

Bias was decreased by normalizing the feature values. Without normalization, distance measures would have been strongly biased toward pulse duration, its range being on the order of 1 to 10 in magnitude whereas other features ranged from .3 to 3 in magnitude. The results for this study are shown below.

	Unnormalized		Normalized	
	Mean	Median	Mean	Median
Sensitivity	91%	81%	92%	92%
Specificity	60%	63%	62%	69%
Overall	72%	70%	74%	78%

As indicated above, using the median normalized vectors as prototypes produced the best overall performance.

CONCLUDING REMARKS

1. Results from the rating study for thick pipes was encouraging, the sensitivity, specificity, and overall performance being 84%, 77%, and 80%, respectively. The tutorial review procedure that led to a new algorithm produced little improvement, in this case, providing us with a sensitivity, specificity, and overall performance of 88%, 69%, and 77%, respectively.

2. Circumferential integration procedures could improve the overall performance by about 7%.

3. Threshold modification can be used to increase sensitivity or specificity with the tradeoffs depending on the economic situation and required inspection reliability.

4. Algorithm selection is not unique. Similar results can be obtained for a large number of different algorithms. As an example, the two algorithms used in this paper, the first used in the rating study on thick pipes, and the second generated from the tutorial review procedure, were similar in nature, but significantly different with respect to the coefficients used in the Fisher Linear Discriminant function. Signs were logical. Less influence on the partial power P2 was obvious in the tutorial algorithm. This, of course, was expected from the PDF curves. In the rating algorithm, PD was more influential than RT, but in the tutorial algorithm, both were important. Additional studies and the variations with pipe thickness must still be carried out.

5. The original algorithm listed in Table 2 for 12" schedule 100 pipe was tried on the data acquired for tutorial purposes on the five Japanese pipes. It was expected to obtain an upper level of sensitivity, specificity, and overall performance of about 88%, 69%, and 77%, respectively, these figures coming about as a result of a Fisher tutorial development on all of the Japanese pipe data. In this exercise, however, without the benefit of a retake procedure, the sensitivity, specificity, and overall index of performance for 185 data sets was 78%, 73%, and 75%, respectively. Additional work must be

carried out on algorithm selection retake influences and algorithm similarities in order to understand fully algorithm utilization.

6. Algorithm improvement may still be possible by modifying the transducer system, perhaps to a dual tandem configuration, etc. There is obviously no substitute for clever data acquisition that makes use of the physics of wave propagation in an attempt to acquire all mode conversion and scattering information.

7. Algorithm improvement could also be possible by incorporating more features into the analysis. Probability density function analysis is a valuable aid in feature selection. Additional data on more pipes will improve the feature base, and hence algorithm development procedure.

8. Additional work on intermediate and thin wall pipe must still be carried out in order to test the transducer and algorithm selection concepts presented in this paper.

REFERENCES

1. Nondestructive Evaluation Program, Progress in 1979. EPRI NP-1234-SR, Special Report, December 1979.

2. Rose, J. and Singh, G. P., "Ultrasonic Pattern Recognition Study of IGSCC in Stainless Steel Piping," Project 892-1, EPRI NP-891, September 1978.

3. Rose, Joseph L. and Singh, Gurvinder P., "A Pattern Recognition Reflector Classification Feasibility Study in the Ultrasonic Inspection of Stainless Steel Pipe Welds," British Journal of Nondestructive Testing, Vol. 21, No. 6, November 1979.

4. Rose, J. L. and Singh, G. P., "Stress Corrosion Cracking Vs. Geometric Reflector Classification Analysis for 304 Austenitic Stainless Steel Pipe Weld Specimens," presented and published in the proceedings of the Ninth World Conference on NDT, Melbourne, Australia, November 1979.

5. Shankar, R., Mucciardi, A. N., Lawrie, W. E., and Stein, R. N., "Development of Adaptive Learning Network for Pipe Inspection," Project 770, EPRI NP-688, March 1978.

6. Rose, Joseph L. and Singh, Gurvinder P., "An Analysis of the Dual-Element Angle Beam Transducer," to be published in a research supplement to Materials Evaluation, July 1980.

7. Rose, J. L. and Thomas, G. H., "The Fisher Linear Discriminant Function for Adhesive Bond Strength Prediction," British Journal of Nondestructive Testing, Vol. 21, No. 3, May 1979.

8. Thomas, G. H. and Rose, J. L., "A Generalized Adhesive Bond Strength Prediction Algorithm Based on Ultrasonic Signal Analysis," presented and published in the proceedings of the Ninth World Conference on NDT, Melbourne, Australia, November 1979.

9. Kavamoto and Lapides, "Production of Controlled Intergranular Stress Corrosion Cracking of Large Pipes," part of a special report, RP 1448-7, Nondestructive Evaluation Program, Progress in 1979. EPRI NP-1234-SR, Special Report, December 1979.

10. Brekhovskikh, L. M., Waves in Layered Media, London/New York: Academic Press, 1960, pp. 50-51.

ACKNOWLEDGMENTS

The Electric Power Research Institute is acknowledged for their support of this work. Computer hardware support from Krautkramer-Branson, Inc. is also appreciated.

On the applicability of ultrasonic testing techniques for coarse grain austenitic welds

E. NEUMANN, M. ROEMER, R. SCHENK, K. MATTHIES
Federal Institute for Materials Testing, F.R. Germany

ABSTRACT

On the following items it shall be reported :

- Ultrasonic probe techniques to overcome ultrasonic attenuation due to grain scattering and their performance. This includes such techniques as limitation of the sensitivity range by transmitter-receiver probes and focusing probes and the evaluation of flaw indications.

- Use of broad band longitudinal ultrasonic pulses. This includes discussion of the problem of ultrasonic scattering and the problem of transmission of ultrasonic signals by scattering media evaluating the power spectra of the ultrasonic signals.

- On the problem of matching between ultrasonic probe and ultrasonic flaw detector.

- Signal processing methods as inverse filtering and non linear signal processing.

I. Introduction

Until now ultrasonic testing of coarse grained austenitic welds is a difficult problem. Recently special testing techniques have been developed to overcome ultrasonic attenuation due to grain scattering [1-5]. If the attenuation coefficient is smaller than 0,3 dB/mm at the frequency of the ultrasonic pulse testing could successfully be carried out. Nevertheless for ultrasonic testing coarse grain austenitic materials it is necessary to decide case by case which technique to apply. The basis of reliable ultrasonic testing is to perform ultrasonic testing with reference blocks of the same type of construction as the component under test.

For the development of testing codes for coarse grained austenitic materials especially the relationship between materials structure and ultrasonic testability has to be investigated. But already at present it seems to be sure that only the combination of different optimization procedures concerning the ultrasonic testing system leads to sufficient reliable ultrasonic inspection results. Such procedures are:

- Damping of the ultrasonic probes to produce short, broadband ultrasonic pulses.
- Selection of such types of ultrasonic waves, which possibly

do not interact with grain structure e.g. longitudinal waves or polarized transversal waves.
- Limitation of the sensitivity range of the ultrasonic probes by suitable shaping the probes' sound field to reduce grain scattering.
- Acoustic and electrical matching of transducer and ultrasonic flaw detector as a transfer system [6].
- Application of signal processing methods to increase the signal to noise ratio:

  - Use of transmitter-pulses of variable frequency and bandwith [7]
  - after reception of the signals e.g. averaging methods [2] inverse filtering or multiplicative mixing.

2. On ultrasonic scattering and transmission of ultrasonic signals through coarse grain austenitic material

Because of the dependence of sound velocity on the direction of propagation within the austenitic crystal ultrasound is scattered statistically when propagating through coarse grained polycrystaline austenitic materials. Additionally discontinuities of acoustic impedance at the grain boundaties lead to partial reflexion of ultrasound.

Fig. 1 shows the result of this scattering process. The amplitude of the indication from a cylindrical drill hole (Ø 3 mm) in an austenitic cast testpiece is shown as a function of frequency. It is decreasing strongly with increasing frequency.

On the other hand the amplitude of scatter indications, which by measurement of time of flight using a time window seem to originate from the neighbourhood of the test flaw is nearly independent on frequency. This seems to be contrary to the law that ultrasonic scattering is dependent on frequency by a power of two to four of frequency.

The interpretation is that one has to deal with multiple scattering of ultrasound. By this effect the high frequency part of the ultrasound is restricted to the vicinity of the ultrasonic probe while the low frequency part of ultrasound is spreading over the whole volume of the testpiece. But in both cases the soundpathes caused by multiple scattering are reaching the meter range. So the amplitude of scatter indications measured are dependent on the experimental arrangement. Measuring in pulse-echo technique as usually is done in ultrasonic testing the attenuation as a function of time of flight is constant for all scatter indications and not dependent on their frequency. So the measured spectrum of scatter indications is determined by the ultrasonic probe's characteristic spectrum itself. Measuring with two ultrasonic probes in a through transmission arrangement a strong dependence of amplitude of scatter indications is seen as has been shown just recently [8].

The result of these measurements is the choice of ultrasonic frequency. On the one hand one has to avoid decreasing signal to noise ratio with increasing frequency. On the other hand one has to avoid a poor resolution of flaws by choosing a testing frequency lower than 1 MHz. So it has been proven to be a good compromise for austenitic weld joints with wall thickness up to 60 mm to

choose a frequency range between 1,5 - 2,0 MHz.

To reduce the negative influence of ultrasonic scattering on testability of coarse grain materials the use of short longitudinal wave pulse is favourable. As a result interference effects between different grain boundary echoes are reduced. So high amplitudes scatter indications ("grass") are avoided.

When using long, narrow banded ultrasonic pulses it may happen that by interference of different grain boundary echoes false indications are generated. These false indications are not easy to discriminate from real indications. One means to suppress false indications is inverse filtering of the signal, as it is shown in fig. 17, 18. Inverse filtering is a method to increase the bandwidth of a signal supplementary. Generally speaking the amplitude of scattered ultrasound is proportional to the root of the ultrasonic pulse lenghth:

$$A_{scat} \sim \sqrt{\Delta x}$$

This means that reducing the pulse length by a factor of 10 the signal to noise ratio will increase by 10 dB [2].

The interaction between materials structure and ultrasonic pulses can be estimated by frequency analysis as the pulse lenghth and pulse spectrum are connected by the Fourier transform. In fig. 2 three power spectra are shown:

- -spectrum of a backwall echo from a material with low attenuation (quartz) representing the characteristic spectrum of the ultrasonic probe itself,
- spectrum of a backwall echo from austenitic cast material,
- spectrum of the scatter indications within a certain time window in the neighbourhood of the backwall echo from austenitic cast material.

From the spectrum of the backwall echoes it can be seen that the austenitic coarse grain material is acting as a low-pass filter on the ultrasonic pulse. Depending upon the length if the sound path the effective testing frequency and the bandwidth are reduced. The example is showing that the effective frequency is reduced from 2 MHz to 1 MHz and the bandwidth (6dB-width) corresponding from2 MHz to 1 MHz. So it seems that the broadband ultrasonic probe is matching its spectral characteristics to the testing problem . The effective testing frequency now is shifted to a frequency range, where the noise spectrum has not its maximal amplitude.

Fig.3 is demonstrating the calculated influence of coarse grain material of attenuation $\alpha_{f_{centre}} \approx 0,3 \frac{dB}{mm}$ and sound path s = 100 mm on ultrasonic signals of different bandwidths. The result is that the bandwidth is decreasing in both cases, the pulses are growing longer. But the broad banded pulse is still short enough to avoid interference of grain boundary indications.

The amplitude is decreasing by 38 dB in the case of the narrow banded pulse but only by 24 dB in the case of the broad banded pulse.

So under all circumstances broad banded ultrasonic pulses are better suited to test coarse grain material than narrow banded pulses. As for the optimal band width of the ultrasonic pulse the following considerations are valid.

The spectrum of the scatter indications is identical with the spectrum of the back wall echo from the low attenuation material (the probe's characteristic spectrum). The main spectral characteristics of the scatter indications evidently are determined by the ultrasonic probe itself. This is conform with the above measurements that the amplitude of scatter indications is not frequency dependent.

So it seems not to be favourable too to use extremly short, broadbanded ultrasonic pulses [9]. It is necessary much more to find a compromise between scatter indications of higher frequency and false indications generated by interference of narrow banded grain boundary echoes.

Fig. 4 is demonstrating this factual situation. Ultrasonic pulses and spectra of a narrow banded, a broad banded and an extremly broad banded probe measured in low attenuation material are shown. Moreover the A-scans of the backwall echo in austenitic cast material are shown. The backwall echoes are overshooting by 10 dB to demonstrate the grain scatter indications. As can be seen the best signal-to-noise ratio is achieved with the fairly broad banded system. The extremly broad banded system is not favourable because the high-frequency portion of the spectrum is contributing to the grain scatter indications while the signal with information doesn't contain high frequency components. On the other hand the narrow banded system is generating false indications by interference of grain boundary reflections. In the case of a fairly broad banded system where the measured spectra of scatter indications and of signals with information are in the same frequency range the signal-to-noise ratio is highest.

As can be seen from fig. 5 the frequency spectrum of grain scattering indications varies considerably depending on the probes position on the surface of a specimen. By sharp frequency tuning of a narrow band ultrasonic system to frequency windows in the spectrum of grain scattering indications a high signal to noise ratio would be obtained. Unfortunately it is not possible to get a good signal to noise ratio by sharp frequency tuning of a narrow band system, because of the severe fluctuations of scatter indications as a function of probe position on the specimen's surface. This can be concluded from the spectrum averaged over different probe positions.

3. Ultrasonic probe techniques

3.1 Use of longitudinal ultrasonic waves.

For ultrasonic testing coarse grained austenitic welds, it has been shown that longitudinal waves are best suitable because the influence of coarse grain structure on the signal to noise ratio is lower than with transversal waves [10]. Following this theoretical estimation the increase in signal-to-noise ratio using longitudinal waves should be about 11 dB. Experimentally the increase of the signal-to-noise ratio is found to be only about 4 dB (fig. 16). The reason for this might be that not only Rayleigh scattering is occuring but phase scattering too.

3.2 Longitudinal wave single transducer probes

In many cases of testing austenitic weld joints a sufficient signal-to-noise ratio is obtained by using longitudinal waves instead of tranversal waves and using a sound field of lower divergence [3]. By reducing the sound field's diameter the scatter indications are reduced. The dimensions of the sound field are adapted to the testing problem by calculating the transducer dimensions using the Kirchhoff' diffraction theory in the Fraunhofer approximation [11-13].

3.3 Longitudinal wave transmitter receiver probes

3.3.1 Operating principle

The need for more efficient reduction of the sensitivity area of the probe in more difficult cases of testing austenitic weld joints is leading to transmitter receiver probes [14] and to focussing probes [15-17, 20].
As Richter pointed out 1968 [18], the coherent noise occuring during ultrasonic testing of coarse grained weld metal may be reduced by using a transmitter receiver method. The lobes of the two transducers of the probe are inclined towards one another so that they are crossing in the first half skip distance. Their crossing area is the sensitive area of the probe. Only ultrasound coming from this area is registered with a significant signal amplitude. The coherent scattering is coming no longer from the area passed by the ultrasonic pulse, but only from the sensitivity area of the probe while the signal of a reflector remains nearly as high as with a single transducer probe. The level of the coherent scattering is given by the lateral and azimutal extension of the sensitivity area as well as by the actual extension of the sensitivity area between the position of the reflector and the receiver. The possibility to limit the sensitivity area in axial direction is an important advantage of transmitter receiver probes. According the required extension and position of the sensitivity area of a transmitter-receiver probe, the transducer dimensions are calculated by Kirchhoff diffraction theory. Testing experiences with welded components have shown, that the extension of the sensitivity area in lateral and azimutal direction should be 15-20 mm. The decrease in sensitivity at the zone edges may be 6 dB.

Fig.6 shows examples of distance-amplitude-correction (DAC) curves of probes with plane coupling surfaces obtained at 3 mm flat bottom holes as a function of reflector depth and projection distance. Especially in cases of complex shaped surfaces of the specimen, the DAC-curves have to be measured with a suitable reference specimen of equal scale containing test reflectors.

3.3.2 On the evaluation of ultrasonic flaw indications

For testing austenitic welds especially in the case of complicated geometrical conditions, defects classification is based on comparisons with reference reflectors using distance-amplitude-corrections curves. For each specimen under test reference blocks welded under same conditions as the specimen itself have to be used. Reference reflectors for time-base and sensitivity setting are cylindrical drill holes in almost all cases. However sometimes flat bottom holes are used, for instance when testing cladded specimen for subcladding cracks.

The correlation between the echo height and the diameter of flat bottom holes as reference reflectors was evaluated experimentally for transmitter-receiver probes. A fine grain austenitic steel test block was used containing flat bottom holes (3, 6, 10, 15 mm Ø) in the depth b = 25 mm. Fig. 7 represents the relative amplitude ΔV of the echo indications as a function of equivalent flaw size (diameter of the flat bottom holes). The amplitude ΔV is related to the amplitude of the echo-indication of the 3 mm Ø flat bottom hole, for which is $\Delta V = 0$. The straight line shows the theoretical dependence between echo height and equivalent reflector size using a single transducer probe: The signal amplitude increases by 12 dB when the diameter of the reflector is doubled. One measures the same dependence of the echo height when varying the diameter of the flat bottom hole for transmitter-receiver probes. Only at large sizes of flat bottom holes the results measured with transmitter-receiver probes are deviating from the 12 dB-law: Now the measured amplitudes are lower than those measured with a single transducer probe.

3.3.3 Application of transmitter-receiver probes to thick-walled specimens.

Because of the limitation in the sensitive range of the probes for the testing of thick walled parts, several angular transmitter receiver probes have to be employed whose sensitive ranges cover the whole weld under inspection. Fig. 8 shows an example of dividing the weld seam in testing zones. The weld in a 60 mm thick plate has been divided into four testing zones in depth. The ultrasonic testing with transmitter-receiver probes is performed within half the skip distance. The angle of incidence has to be adapted to the zone depth and, if possible, to the preferred orientation of the expected flaws. For the surface testing zone, the angle of incidence is chosen to be 70°. Experiments with test-flaws near the surface (for instance with slots of1 mm height and width), have shown that a reflector near the surface is detectable with a sufficient signal to noise ratio. The angles of incidence for the second and the third testing zone are smaller to reduce the lengths of the sound paths. For the testing zone at the opposite surface an angle of 45° has been chosen, in this case exploiting the reflection of an angle mirror for flaw detection.

3.3.4 Application if transmitter-receiver probes to thin-walled specimens.

There are thoroughly different problems in the case of thin-walled (6-12 mm) austenitic welded specimens as for instance welded tubes (100-700 mm Ø). The main problem with ultrasonic testing austenitic welds, coarse grained dendritic material is of less importance. Because of the low wall-thickness heat dissipation after welding i s relatively fast. So formation of coarse grain in the weld metal solidifying at first fine grained is restrained. Moreover the sound path in the weld metal does not exceed 15-20 mm. Therefore it seems possible to choose a higher ultrasonic frequency than 2 MHz. Especially welds with excessive reinforcement and root convexity are difficult to test ultrasonically because of the problem of geometric indications. To solve this problem increased resolving power of the ultrasonic pulses and increased accuracy of reflector location are necessary.

Increased resolving power is achieved by choosing a frequency range of ultrasonic pulses between 4 and 6 MHz which is fairly attenuated in the austenitic weld metal. Furthermore the sound field is

adapted to the volume to be inspected by the Kirchhoff diffraction theory. The projected distance between the front of the ultrasonic probe and weld crown is about 20 mm. Thus grinding of the weld is no longer necessary.

Increased accuracy of reflector location is achieved by mechanized inspection using an automated ultrasonic probe manipulator.

Testing results obtained with artificial flaws are shown in fig. 9 [1].

Because of the relatively fine grained weld material it is sufficient in many cases to use longitudinal wave single transducer probes for welds in thin-walled austenitic specimens. Certainly these probes have to be specially tailored too: According the required extension of the ultrasonic beam the transducer dimensions have to be calculated according to diffraction theory taking into account the curvature of the surface.

In a laboratory scale ultrasonic testing can be done using immersion techniques as shown in fig. 10. This has the following advantages compared with the usual contact technique of coupling:

- No influence of the coupling layer on testing results,
- Free choice of angle of incidence,
- Use of (larger) focussing probes possible because adaption of the probes coupling surface to the specimens surface is not necessary.

Practical solutions for ultrasonic testing systems using immersion technique are shown in figs. 11, 12.

3.4 Focussing probes

The improvement of the signal-to-noise ratio by ultrasonic testing with focussing probes is due to the limitation of the sensitivity area to the focal area.
On the focussing of sound field by curved piezoelectric membranes and lenses has been already reported extensively [15-17, 19].
It shall be reported here on the focussing of sound fields by means of Fresnel zone-plates [20].
It is the advantage of Fresnel zone-plates that they have short focal distances coupled with a high degree of focussing. Focussing of the sound field by a Fresnel zone-plate is resulting from phenomena of diffraction. The Fresnel zone-plate is placed directly in front of a piezoelectric membrane. A zone-plate consists of a central circular opaque zone together with a set of combined opaque ring zones, fig. 13. All zones have the same surface area, namely the area of the central circle: $F_1 = \pi \cdot f_p \cdot \lambda$, ($f_p$ = focal length), λ being the ultrasonic wavelength. The series of zone radii is given by: $r_n = \sqrt{n \cdot f_p \cdot \lambda}$, n being an integer. This zone-plate is acting as a focussing lens with a focal length f_p.
The reversal zone-plate is acting as a focussing lens, too. Hence it follows that only a part of the incident sound pressure can be concentrated in the focal point by an obstruction zone-plate. Therefore we use a third type of zone-plate, suggested by Lord Rayleigh [21] for optical systems, as shown in the bottom part of the fig. 13. It is called a phase reversal zone-plate. Either the

ring zones or the reverse zones are covered with transparent rings of thickness d, such that (N-1) d = $\lambda/2$, N being an integer. The path difference of $\lambda/2$ represents a π -phase change, i.e. a relative phase reversal. The contributions of these rings are adding to the contributions of the reverse ring zones. Fig. 14 shows a focussing probe with a reversal zone plate consisting of 5 zone rings and the Schlieren-optical representation of the sound field in water. Fig. 15 shows the measured sound pressure distribution in the focal point perpendicular to the acoustical axis and the sound pressure distribution along the acoustical axis in the focal area.

3.5 Comparison of performance of different inspection techniques

To estimate the performance of different ultrasonic inspection techniques quantitative statistical methods have been applied for the evaluation of the results [22]. An austenitic test weld was inspected containing a great number of intentionally produced, natural flaws, e.g. pores, slags, lacks of fusion etc. Altogether 27 different longitudinal flaws were evaluated by inspection from two sides of the weld .
The position and the approximate size of these flaws were taken from a radiographic inspection. Fig. 16 gives the testing results obtained with transversal wave single transducer-, longitudinal wave single transducer-, longitudinal wave focus-,and longitudinal wave transmitter receiver probes, all with $\alpha = 60°$ and $\lambda \approx 3$ mm.

The cumulative echo height distributions of flaw indications p_{Detect} and of scatter indications p_{Scat} are given in a probability diagram as a function of relative gain setting ΔV /dB/. $\Delta V = 0$ dB corresponds to the sensitivity setting for the 3 mm flat bottom hole indication on 80 % of full screen.

The left hand curves p_{Detect} show the cumulating echo height distribution of the flaw indications. The echo heights are measured by that gain setting ΔV where echo heights reach 80 % of full screen. The curves p_{Detect} represent the flaw detection probability as a function of variable reference level ΔV.

The right hand curves P_{Scat} show the cumulative echo height distribution of the grain scattering indications. The echo heights of the scattering indications are measured too by that gain setting ΔV where echo heights of scattering indications reach 80 % of full screen. P_{Scat} is the probability that a noise signal exceeds the reference level ΔV, so that it is taken as a flaw signal.

The detectability of flaws in coarse grained materials is determined exclusively by the echo height of scatter indications. Therefore the noise level $\Delta V = R_1$ is defined as that gain setting at which the cumulative echo height distribution of the grain scatter indications reaches the value 1 %. This means that the noise level is that level which is exceeded by 1 % of all scatter indications while 99 % of all scatter indications fall below that level. By this measuring method the signal-to-noise ratio may determined objectively and reproducibly the error of measurements being not larger than 2 dB.

From these diagrams the quality criteria may be taken by which the performance of the different ultrasonic testing techniques may be judged :

1.) The maximal flaw detection probability at the gain setting corresponding to the noise limit R_1 : transmitter-receiver probe 87 %, focussing probe 79 %, longitudinal wave single transducer probe 59 %, tranversal wave single transducer probe 48 %.

2.) The signal-to-noise ratio taken for the reference reflector 3 mm flat bottom hole : transmitter-receiver probe 11 dB, focussing probe 11 dB, longitudinal wave single transducer probe 7 dB, transversal wave single transducer probe 2,5 dB.

4. Deconvolution (inverse filtering) and non-linear signal-processing

It has been already stated, that short ultrasonic pulses will cause less grass indications than longer ones. Due to that fact a further increase of the bandwidth of the transfer system transmitter-probe-specimen-probe-receiver was tried. For that purpose the falling slopes of the pulse spectrum near the bandlimits were lifted by an inverse filter, which had been realized in a computer. After that procedure of inverse filtering it turned out, that the amplitude of grass indications decreased compared to that of flaw indications, i.e. the signal-to-noise ratio was increased. The reason for this effect is the further reduction of the coherence length of the ultrasonic pulse which results in a decreased capability of forming interferences. For this type of signal processing it is meaningless with which bandwidth the ultrasonic pulse really propagates through the material. One can assume for sound propagation that the laws of linearity and causality are valuable. Therefore it is possible to correct the transfer characteristics by an inverse filter also after receiving of the signal, i.e. it is possible to amplify the weak components of the signal near the band limits more so that, the coherence lengths of the signal will apparently be reduced. As this type of inverse filtering needs a digital computer and is additionally time consuming, it has been tried to establish approximately an inverse filter by use of an electrical cicuit. The improvements gained by this are shown in fig. 17, 18.

Further improvements can be expected by employing non-linear methods of signal processing, e.g. by multiplicative mixing of single frequency components of the signal, fig. 19 [23, 24].

References

/1/ Neumann, E., Roemer, M., Just, T., Matthies, K. Nabel, E.
Development and Improvement of Ultrasonics Testing Techniques for Austenitic Nuclear Components;
Proc. Int. Conf. NDE in the Nuclear Industry, 13. - 15. Februar 1978, Salt Lake City, Utah, USA, p. 84

- Neumann, E., Römer, M., Schenk, R., Nabel, E.
Status of Ultrasonic Testing for Coarse Grained Austenitic Material; Proceedings of the 9th World Conference on Non-Destructive Testing, Section 4E, Melbourne, 18.-23.11.79

- Matthies, K., Neumann, E., Römer, M.
Über die Ultraschallprüfung von austenitischen geschweißten Rohren; Vortragstagung Zerstörungsfreie Materialprüfung, DGZfP e.V., 12.-14. Mai 1980, Göttingen

/2/ Goebbels, K.
Gefügebeurteilung mittels Ultraschall-Streuung;
Materialprüfung 17, 231 (1975)

- Kraus, S., Goebbels, K.
Improvement of signal-to-noise ratio for the ultrasonic testing of coarse-grained materials by signal averaging techniques; Proc. 1st Int. Symp. Ultras. Materials Characteriz., NBS, Gaithersburg, Juni 1978

- Kraus, S., Goebbels, K., Neumann R.
Der Einsatz von Signalmittelungsverfahren zur Verbesserung des Signal-Rausch-Abstandes bei der Ultraschall-Prüfung; Vortragstagung Zerstörungsfreie Materialprüfung, DGZfP e.V., 21.-23. Mai 1979, Lindau

- Goebbels, K., Römer, M., Crostack, H.-A.
Quantitativer Vergleich verschiedener Ultraschall-Prüfverfahren zur Verbesserung des Signal-Rausch-Abstandes beim Vorliegen kohärenten Untergrundes; Materialprüfung 21 (1979) Nr. 8, S. 261/267

- Goebbels, K.
Structure Analysis by Scattered Ultrasonic Radiation, Chap. 4 in Research Techniques in Nondestructive Testing, edt. by R.S. Sharpe, Academic Press Inc., London, 1980

/3/ Edelmann, X., Hornung, R.
Erfahrungen im Prüfen von austenitischen Schweißverbindungen; Material und Technik, Band 5 (1977), S. 19/29

- Edelmann, X.
Betrachtungen zur praktischen Anwendung der Ultraschallprüfung von austenitischen Schweißverbindungen;
Europäische Vortragstagung Zerstörungsfreie Materialprüfung, DGZfP e.V., 24.-26. April 1978, Mainz, Germany, Band 3, S. 729

- Edelmann, X.
Wiederkehrende Prüfung mit Ultraschall an austenitischen Schweißverbindungen im Hauptkühlsystem von Druckwasserreaktoren; Internationales Symposium "Neue Verfahren der zerstörungsfreien Werkstoffprüfung und deren Anwendung in der Kerntechnik", 17.-19. Mai 1979, Saarbrücken

- Edelmann, X.
Application of Ultrasonic Testing Techniques on Austenitic Welds for Fabrication and Inservice Inspection; 3rd Int.

Conf. on Nondestructive Evaluation in the Nuclear Industry 11./13. Februar 1980, Salt Lake City, Utah, USA; American Society for Metals (ASM), Metals Park, Ohio 44073

[4] von Klot, R.
Verbesserung des Signal/Rausch-Verhältnisses bei der Ultraschallprüfung durch Einsatz der Signalmittelungstechnik; Fachausschüsse Sonderprüfverfahren und Ultraschallprüfverfahren, DGZfP e.V., 24. Februar 1977, Berlin, Germany, DGZfP 1977 - 500, p. 107

[5] Ganglbauer, O., Scheidl, H., Reindl, H., Frielinghaus, R.
Beitrag zur Ultraschallprüfung austenitischer Schweißnähte; Vortragstagung Zerstörungsfreie Materialprüfung, DGZfP e.V., 21.-23. Mai 1979, Lindau

- Ganglbauer, O., Frielinghaus, R., Wallner, F.
Contribution to the Ultrasonic Testing of Austenitic Welds Using Longitudinal Angle Beam Probes; Proceedings of the 9th World Conference on Non-Destructive Testing, Section 3B-14, Melbourne, 18.-23.11.79

- Frielinghaus, R.
Possibilities of Ultrasonic Testing of Austenitic Welds Using Longitudinal Angle Beam Probes; Proceedings of the 9th World Conference on Non-Destructive Testing, Section 3B-13, Melbourne, 18.-23.11.79

[6] Nabel, E., Matthies, K., Möhrle, W., Wüstenberg, H.
Gedanken zur elektrischen Anpassung von Ultraschall-Prüfkopf-Gerät; Vortragstagung Zerstörungsfreie Materialprüfung, DGZfP e.V., 12.-14. Mai 1980, Göttingen

[7] Crostack, H.-A., Deutsch, V., Steffens, H.-D., Stelling, H.-A., Vogt, M.
Ultraschallprüfung mit Sendeimpulsen stufenlos veränderlicher Frequenz und steuerbarer Spektralverteilung; Materialprüfung 20 (1978) Nr. 10 S. 372/77

- Crostack, H.-A., Steffens, H.-D.
Application of Controlled Ultrasonic Pulses in NDT; Proceedings of the 9th World Conference on Non-Destructive Testing, Section 4E-3, Melbourne, 18.-23.11.79

- Oppermann, W., Crostack, H.-A.
Grundlegende Aspekte bei der US-Prüfung von schallstreuenden Werkstoffen mit Signalen der CS-Technik; Vortragstagung Zerstörungsfreie Materialprüfung, DGZfP e.V., 12.-14. Mai 1980, Göttingen

[8] Hecht, A., Cherian, P., Neumann, E., Mundry, E.
Untersuchungen zur Ultraschallstreuung in austenitischen Stählen; Vortragstagung Zerstörungsfreie Materialprüfung, DGZfP e.V., 12.-14. Mai 1980, Göttingen

[9] Schenk, R., Hecht, A., Neumann, E., Schmid, R.
Einfluß der Signalübertragung bei der Ultraschallprüfung grob strukturierter Bauteile; Vortragstagung Zerstörungsfreie Materialprüfung, DGZfP e.V., 12.-14. Mai 1980, Göttingen

[10] Wüstenberg, H., Just, T., Möhrle, W., Kutzner, J.
Zur Bedeutung fokussierender Prüfköpfe für die Ultraschallprüfung von Schweißnähten mit austenitischem Gefüge; Materialprüfung 19 (1977) Nr. 7, S. 246/51

[11] Neumann, E., Kuhlow, B., Römer, M., Matthies, K.
Ultrasonic testing of austenitic components of sodium cooled fast reactors; Specialist Meeting In-service inspection and monitoring of LMFBRS, 9.-11. März 76, Int. Atomic Energy Agency, Bensberg, Germany, IWGFR/10, p. 57

[12] Kuhlow, B., Römer, M., Neumann, E., Matthies, K.
Ultrasonic Testing of Austenitic Steel Weld Joints; 8th WCNDT, 6.-11. September 1976, Cannes, France, 3 H 6

[13] Wüstenberg, H., Schulz, E., Möhrle, W., Kutzner, J.
Zur Auswahl der Membranform bei Winkelprüfköpfen für die Ultraschallprüfung; Materialprüfung 18, 223 (1976)

[14] Neumann, E., Wüstenberg, H., Nabel, E., Leisner, W.
Ultraschallprüfung von Schweißverbindungen austenitischer Stähle; Vortragstagung Zerstörungsfreie Materialprüfung, DGZfP e.V., 20.-21. Mai 1974, Nijmegen, Ndl., Materialprüfung 16, 395 (1974)

[15] Schlengermann, U.
Schallfeldausbildung bei ebenen Ultraschallquellen mit fokussierenden Linsen; Acustica 30, 291 (1974)

[16] Wüstenberg, H., Kutzner, J., Möhrle, W.
Fokussierende Prüfköpfe zur Verbesserung der Fehlergrößenabschätzung bei der Ultraschallprüfung von dickwandigen Reaktorkomponenten; Materialprüfung 18, 152 (1976)

[17] Schulz, E., Wüstenberg, H., Erhard, A., Möhrle, W.
Praktischer Einsatz der Fokuskopftechnik in der Ultraschallprüfung; Vortragstagung Zerstörungsfreie Materialprüfung, DGZfP e.V., 21.-23. Mai 1979, Lindau, Germany

[18] Richter, H.-U.
Zur Ultraschallprüfung austenitischer Schweißverbindungen; Die Technik 23, 610 und 692 (1968)

[19] Grützmacher, J.
Ultraakustischer Richtstrahler, Z. techn. Physik 17, 166 (1936)

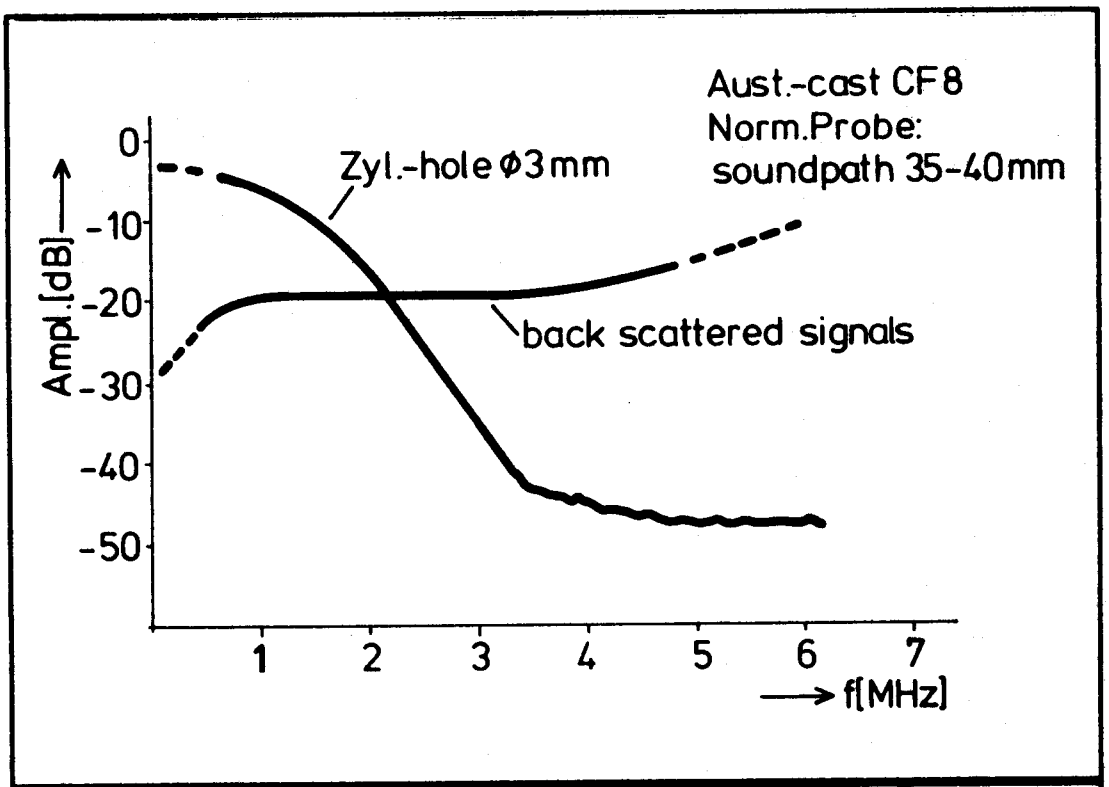
[20] Römer, M., Neumann, E., Kuhlow, B., Mundry, E.
Fresnel'sche Zonenplatte zur Schallfeldfokussierung; Materialprüfung 21 (1979), Nr. 10, S. 363/365

[21] Wood, R. W., Phil. Mag., 45, 511 (1898)

[22] Just, T., Römer, M., Neumann, E., Mundry, E.
Vergleich der Leistungsfähigkeit verschiedener Ultraschallprüftechniken für grobkristalline Werkstoffe mittels statistischer Methoden; Europäische Vortragstagung Zerstörungsfreie Materialprüfung, DGZfP e.V., 24.-26. April 1978, Mainz, Germany, Band 2, S. 323

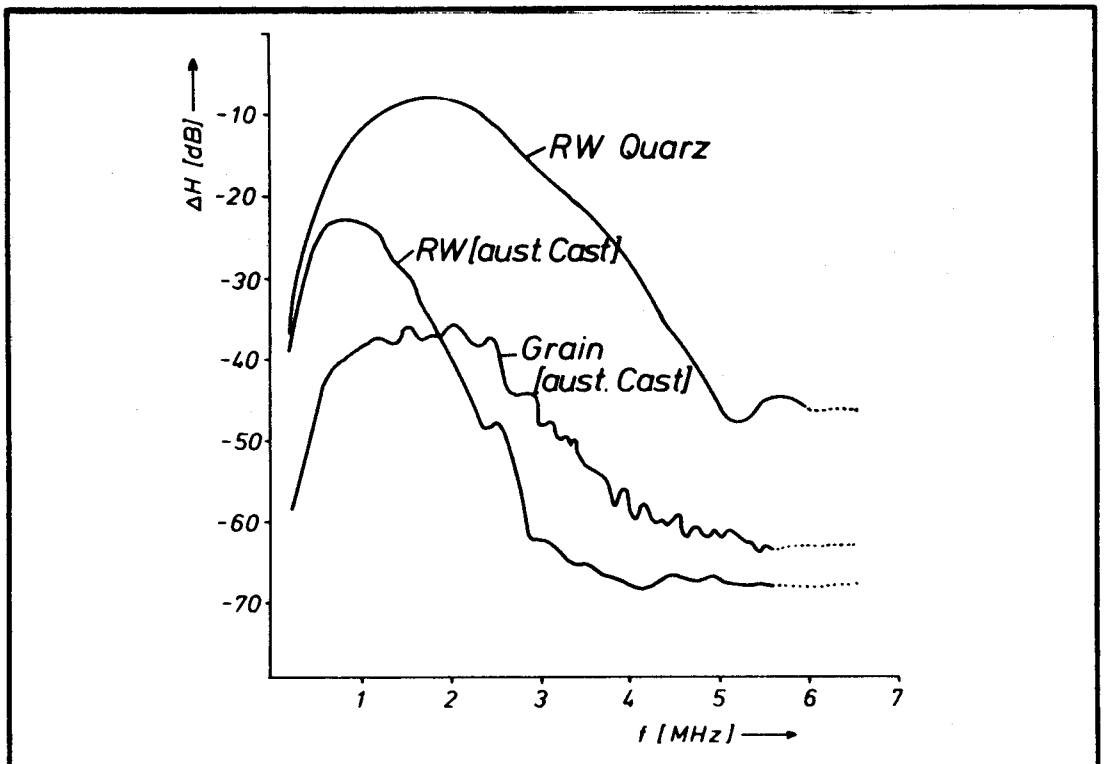
[23] Nabel, E., Just, T.
Diskussionsbeitrag zur Verbesserung des Signal/Rausch-Verhältnisses bei der Ultraschallprüfung grobkörniger Werkstoffe; Vortragsveranstaltung "Neuere Verfahren zur Analyse von Ultraschall-Befunden" der DGZfP-Fachausschüsse Sonderprüfverfahren und Ultraschall-Prüfverfahren, BAM Berlin, 24.2.1977, Berichtsband DGZfP 1977-500, S. 119

[24] Bundesanstalt für Materialprüfung, partial report "Ultraschallprüftechnik" in the final report RS 143 - "Null- und Wiederholungsprüfung von austenitischen Reaktorbehältern und -komponenten mit Ultraschallverfahren"; INTAT 77.19/23. 77019.3 (Interatom, Bergisch-Gladbach 1, Germany), March 1977



B A M Berlin	Influence of ultrasonic scattering in an austenitic cast material on the flaw detectability	Labor 6.24 80 62 1026

Fig. I



B A M Berlin	Ultrasonic power spectra	Labor 6.24 79 62 922

Fig. 2

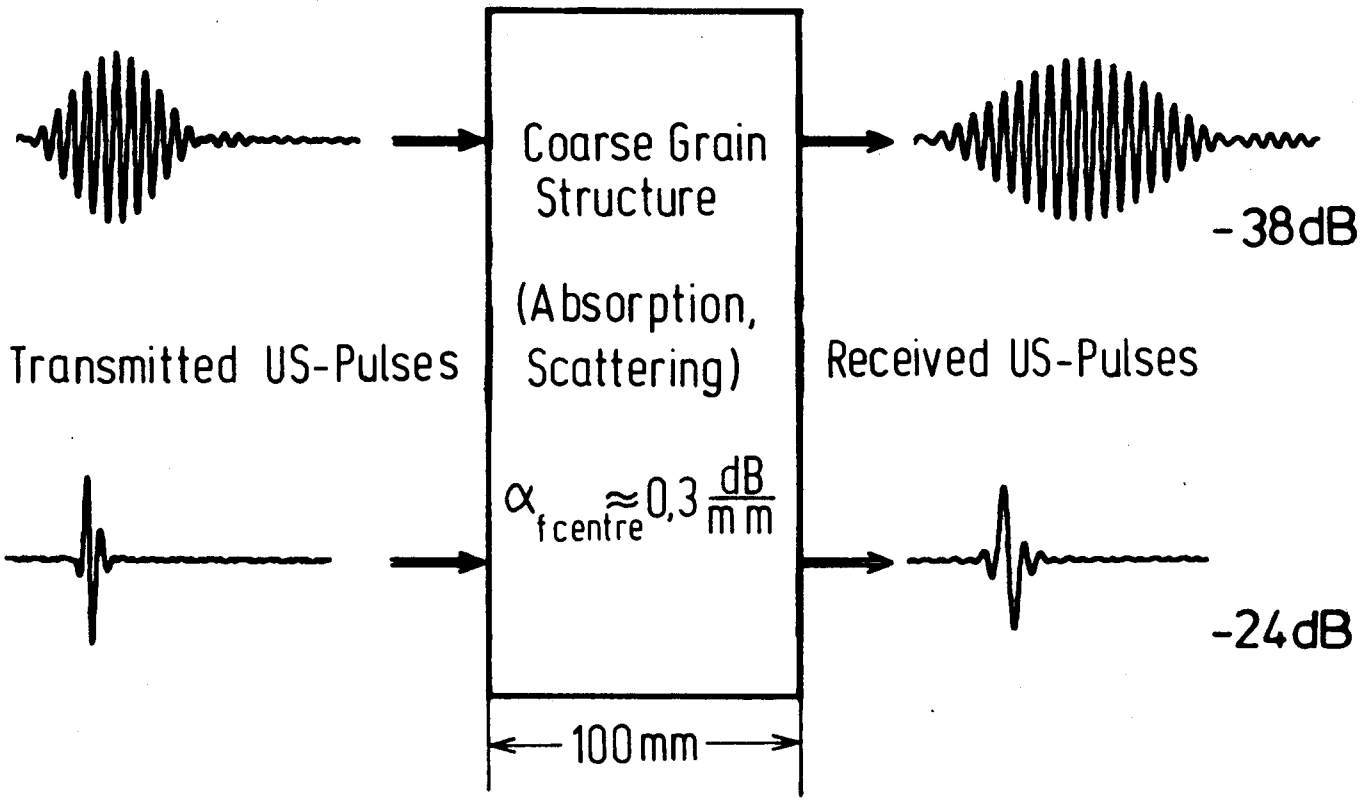


Fig. 3: Calculated influence of coarse grain material on ultrasonic pulses

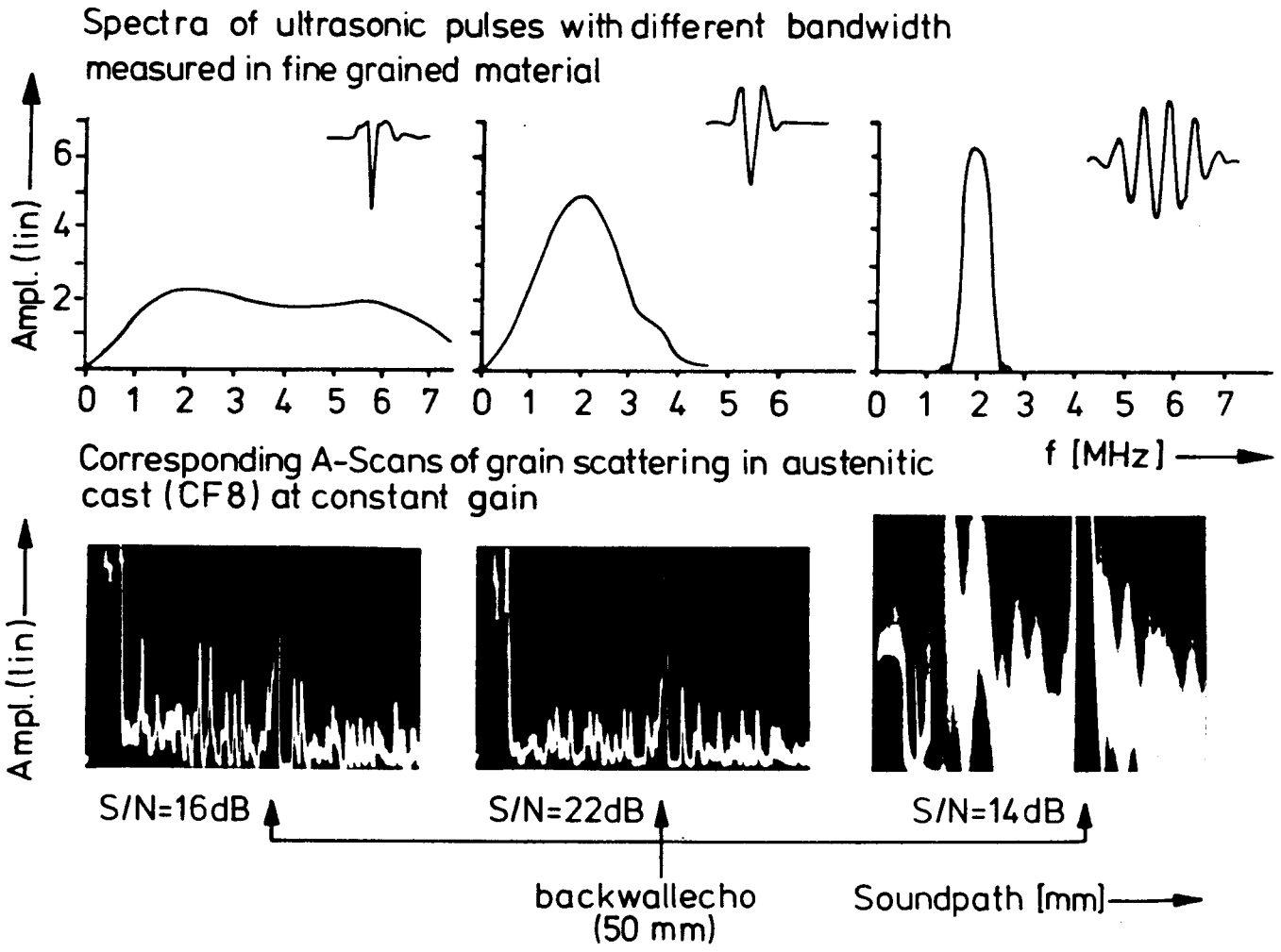
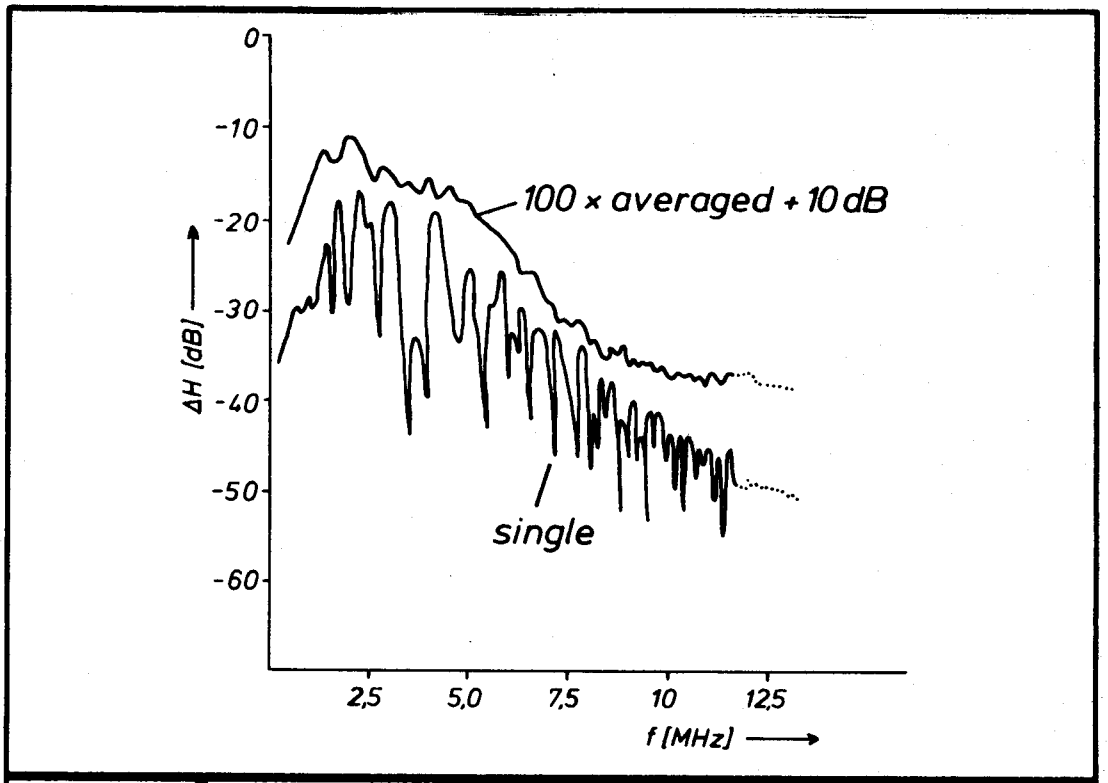


Fig. 4: Influence of the bandwith of ultrasonic probes on the signal-to-noise ratio



B A M Berlin	Power spectra of ultrasonic backscattering	Labor 6.24 79 62 924

Fig. 5

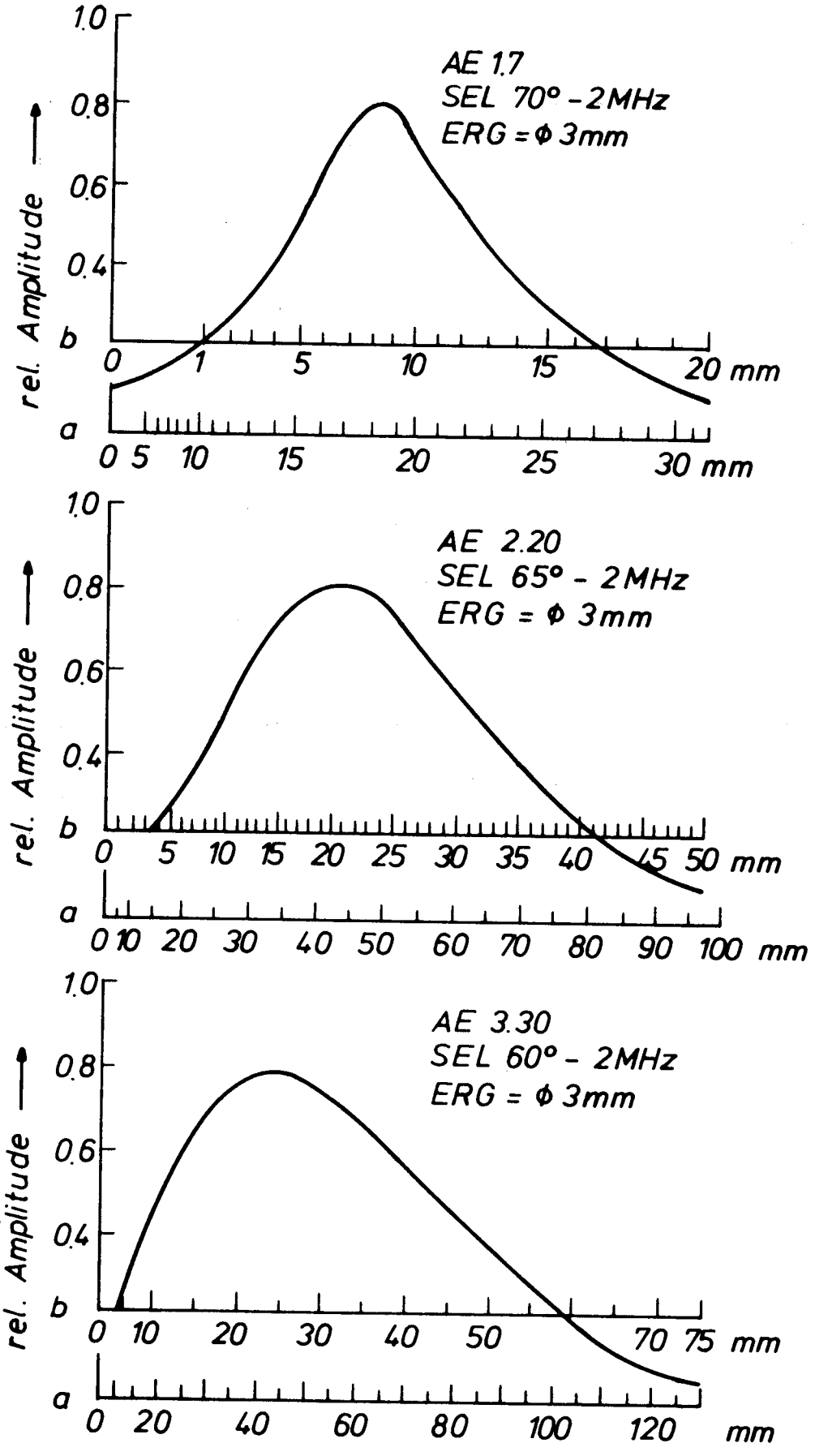
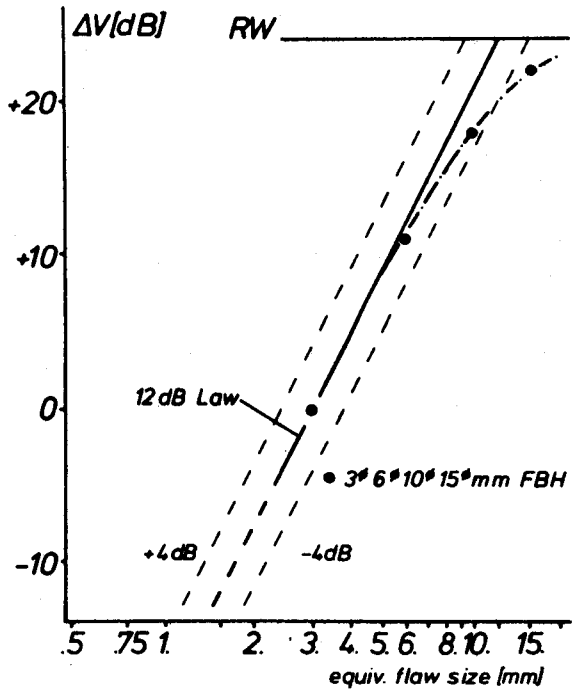

1.0
0.8
0.6
0.4
rel. Amplitude
AE 1.7
SEL 70° - 2MHz
ERG = Φ 3mm
b
0 1 5 10 15 20 mm
a
0 5 10 15 20 25 30 mm
1.0
0.8
0.6
0.4
rel. Amplitude
AE 2.20
SEL 65° - 2MHz
ERG = Φ 3mm
b
0 5 10 15 20 25 30 35 40 45 50 mm
a
0 10 20 30 40 50 60 70 80 90 100 mm
1.0
0.8
0.6
0.4
rel. Amplitude
AE 3.30
SEL 60° - 2MHz
ERG = Φ 3mm
b
0 10 20 30 40 50 70 75 mm
a
0 20 40 60 80 100 120 mm

Fig. 6



B A M Berlin	Dependence of echoamplitude ΔV from equivalent flaw size for a transmitter-receiver probe	Labor 6.24 80 62 1027

Fig. 7.I

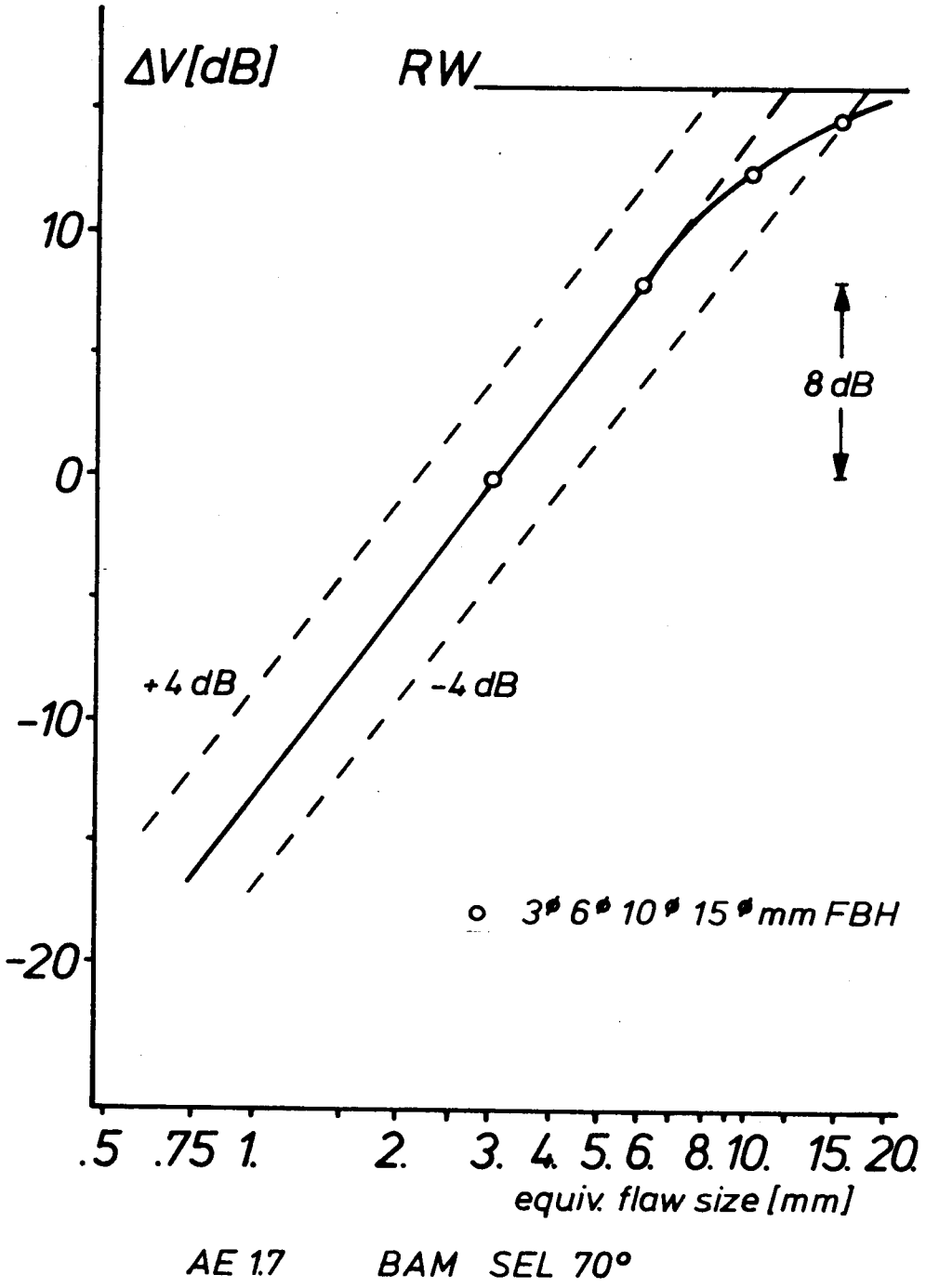

ΔV[dB]
RW
10
0
-10
-20
8 dB
+4 dB
-4 dB
3 6 10 15 mm FBH
.5 .75 1. 2. 3. 4. 5. 6. 8. 10. 15. 20.
equiv. flaw size [mm]
AE 1.7 BAM SEL 70°

Fig. 7.2

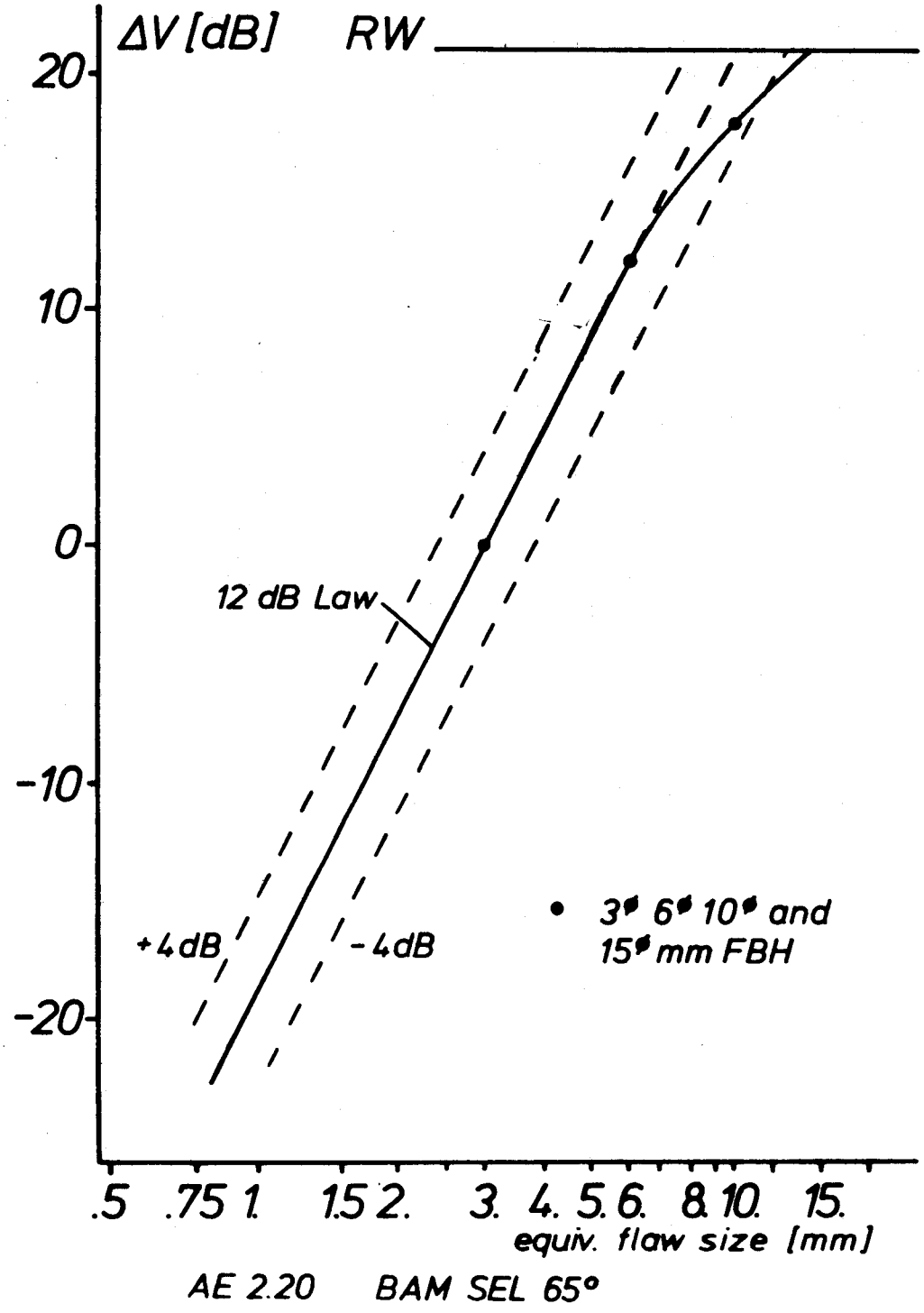
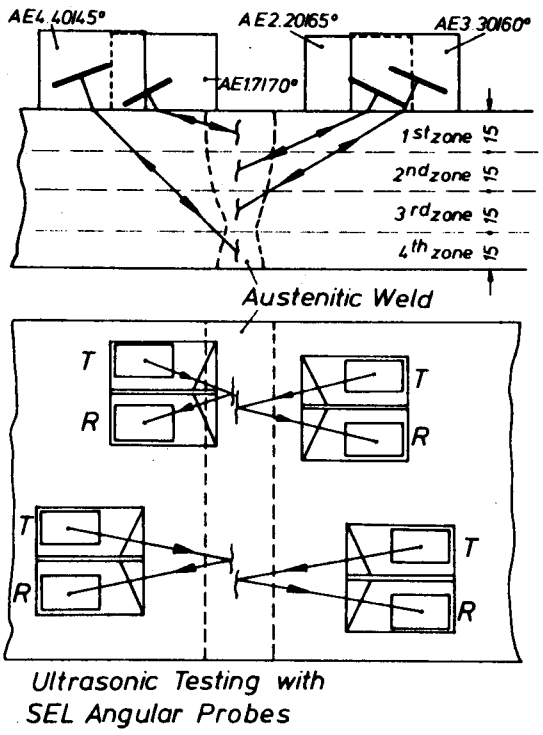

ΔV [dB]
RW
20
10
0
-10
-20
12 dB Law
+4dB
-4dB
• 3ø 6ø 10ø and
15ø mm FBH
.5 .75 1. 1.5 2. 3. 4. 5. 6. 8. 10. 15.
equiv. flaw size [mm]
AE 2.20 BAM SEL 65°

Fig. 7.3



Ultrasonic Testing with
SEL Angular Probes

B A M Berlin	SEL - Technik Tiefenzoneneinteilung	Labor 6.24 79 62 962

Fig. 8

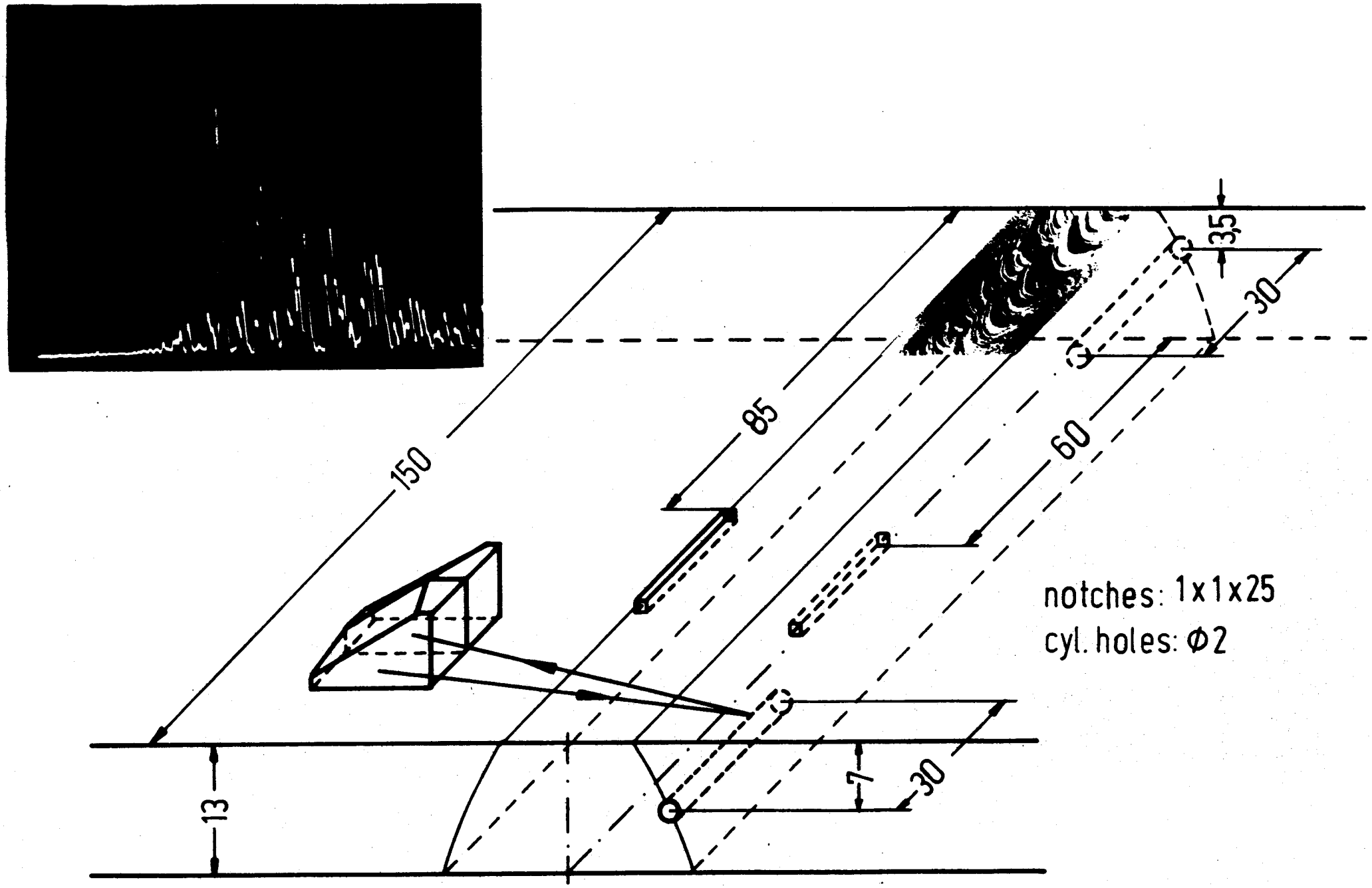
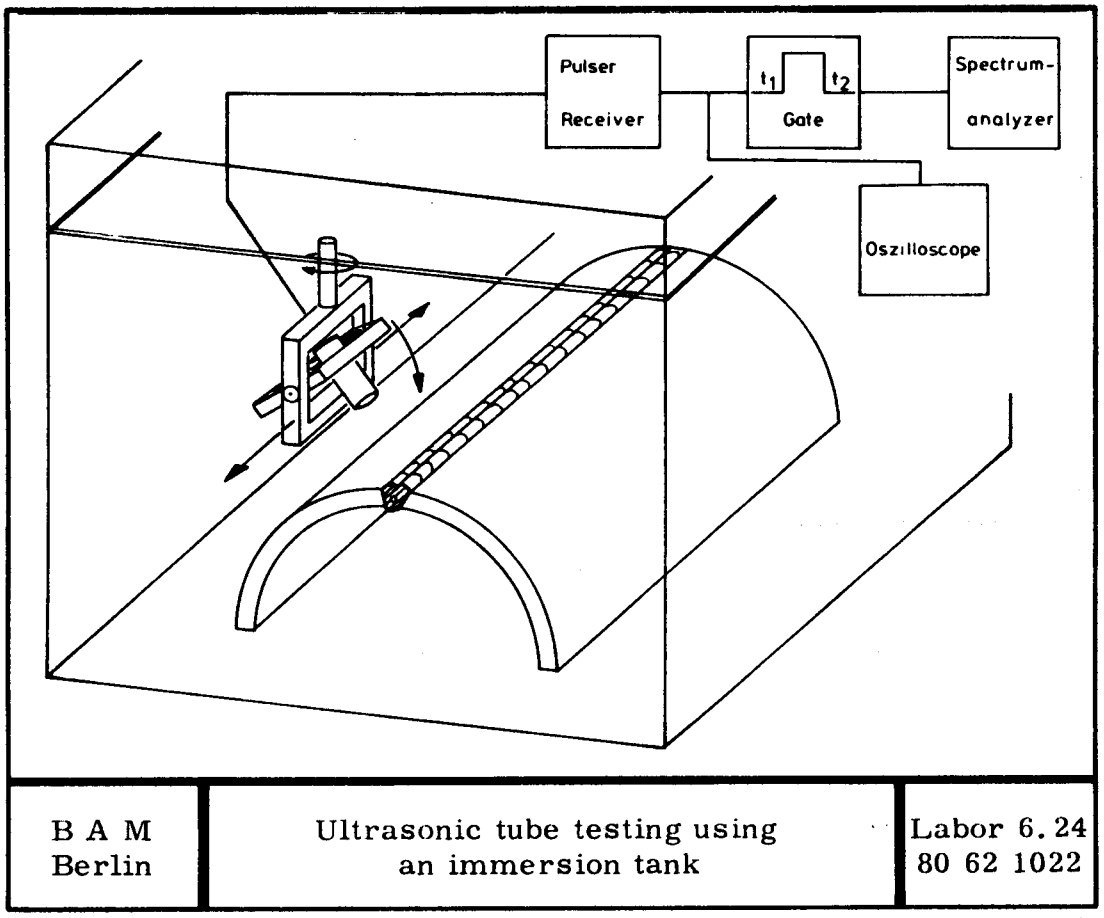


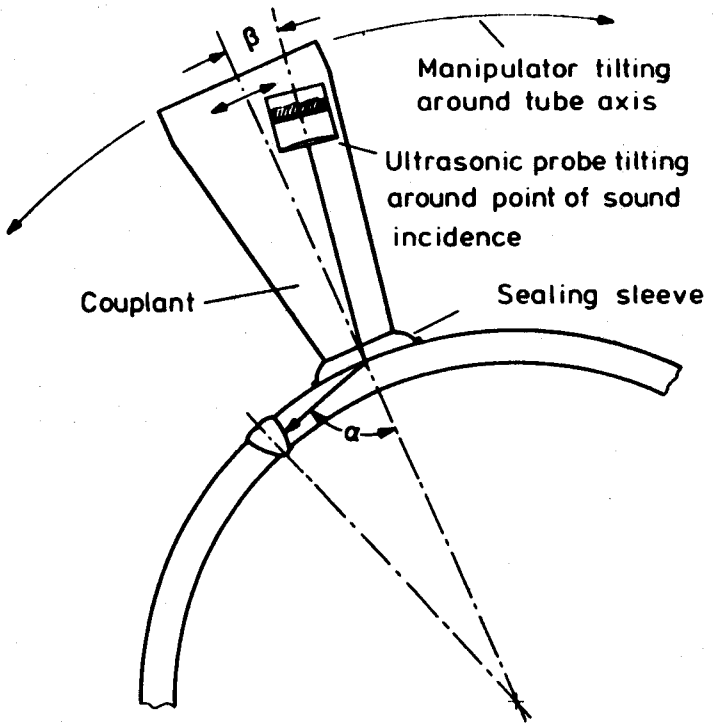
Fig. 9



B A M Berlin	Ultrasonic tube testing using an immersion tank	Labor 6.24 80 62 1022

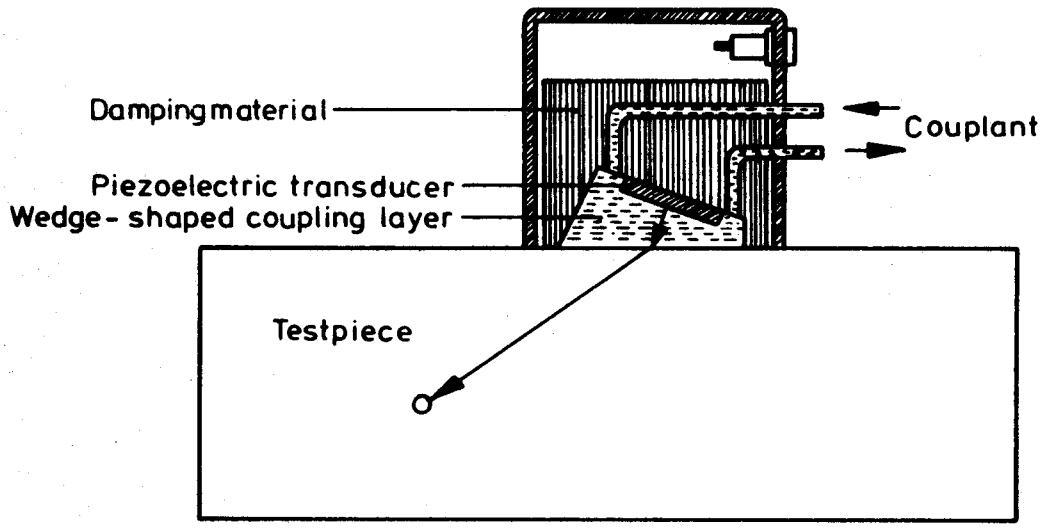
Fig. 10

Fig. II



B A M Berlin	Manipulator for Ultrasonic tube testing	Labor 6.24 80 62 1016

Fig. I2



B A M Berlin	Ultrasonic angle beam probe with wedge-shaped coupling layer	Labor 6.24 80 62 1018

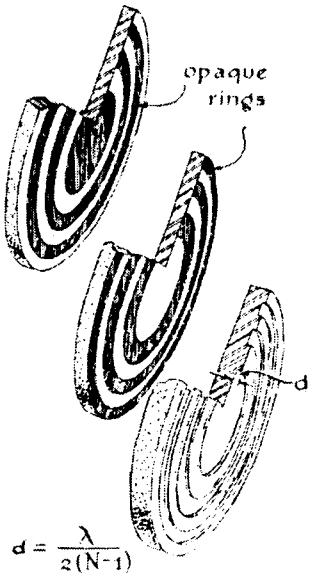


Fig. I3: Two types of obstruction zone plates and the phase reversal zone plate (below).(After J. Strong, Concepts of Classical Optics, Freeman & Co., San Francisco and London, 1958)

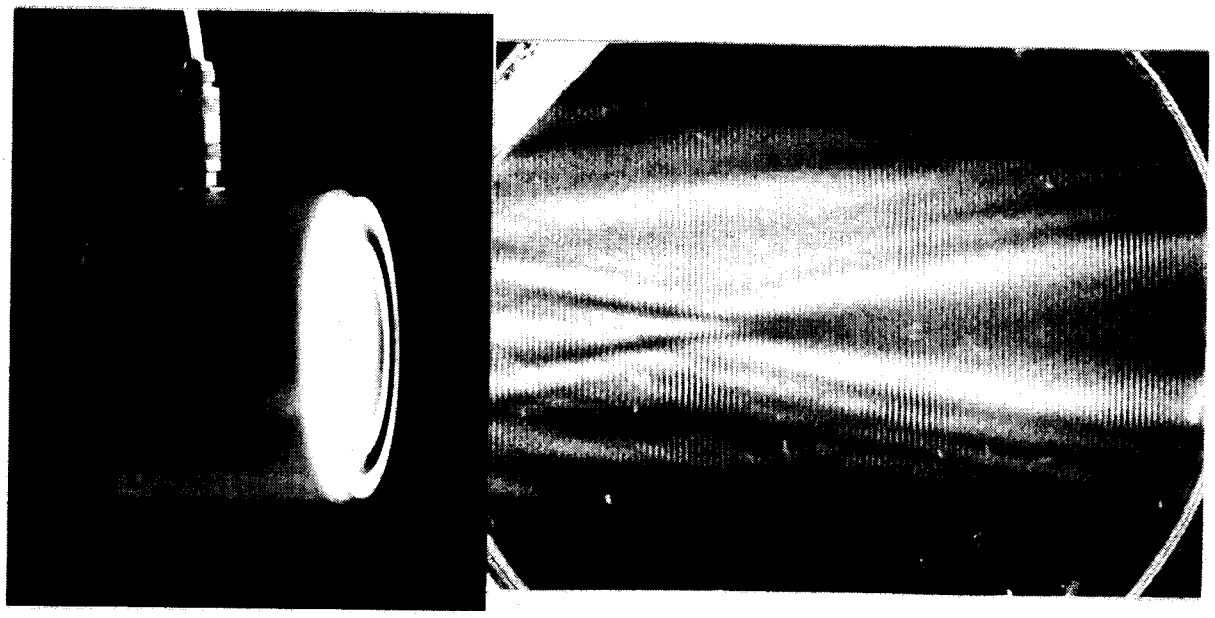


Fig. I4: Focussing probe with a reversal zone plate and Schlierenoptical representation of the sound field in water

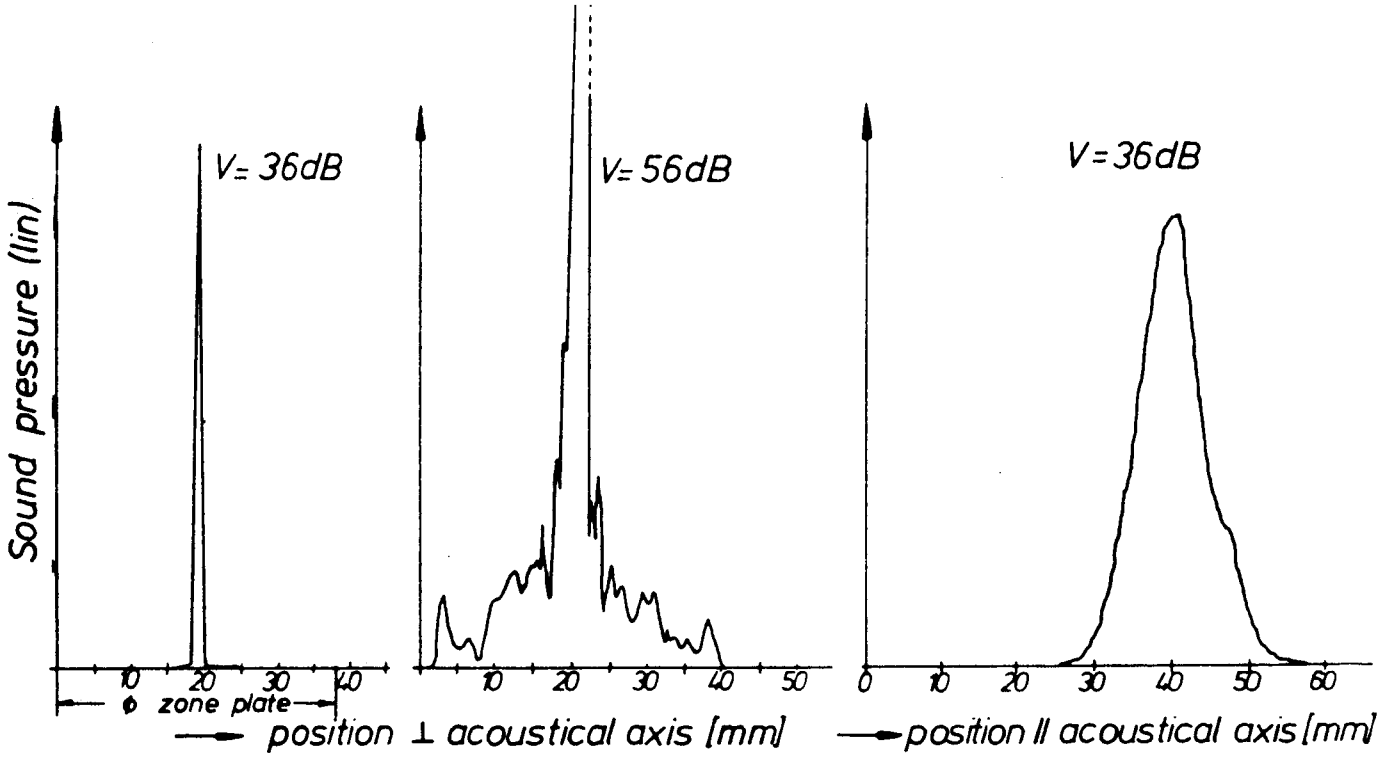


Fig. 15: Measured sound pressure distribution in the focal point perpendicular to the acoustical axis and along the acoustical axis in the focal area of a focussing probe with a reversal zone plate.

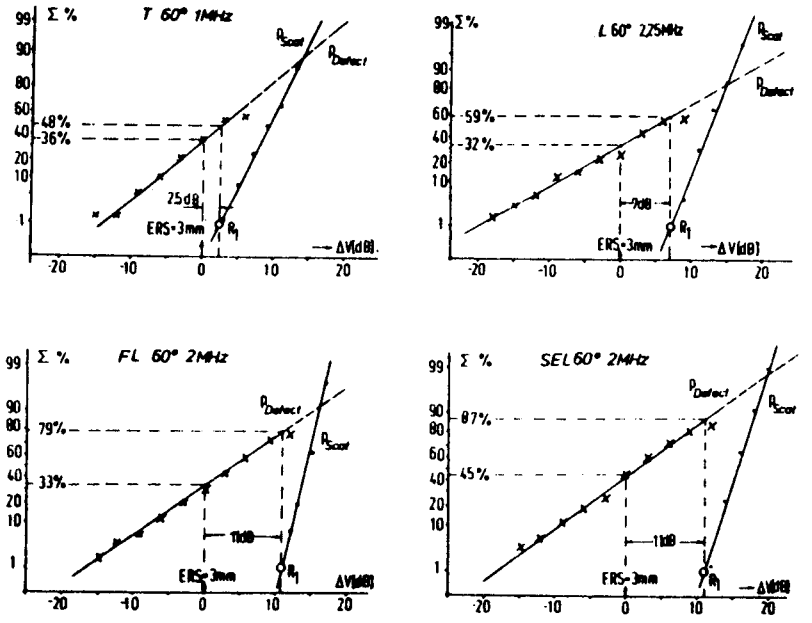


Fig. 16: Cumulative echo height distributions of flaw indications p_{Detect} and scatter indications p_{Scat} as functions of relative gain setting ΔV from an austenitic test weld. T= transversal wave single transducer-, L=longitudinal wave single transducer-; FL=longitudinal wave focus-, and SEL=transmitter-receiver probe. $\alpha = 60^{\circ}$ $\lambda \approx 3$ mm.

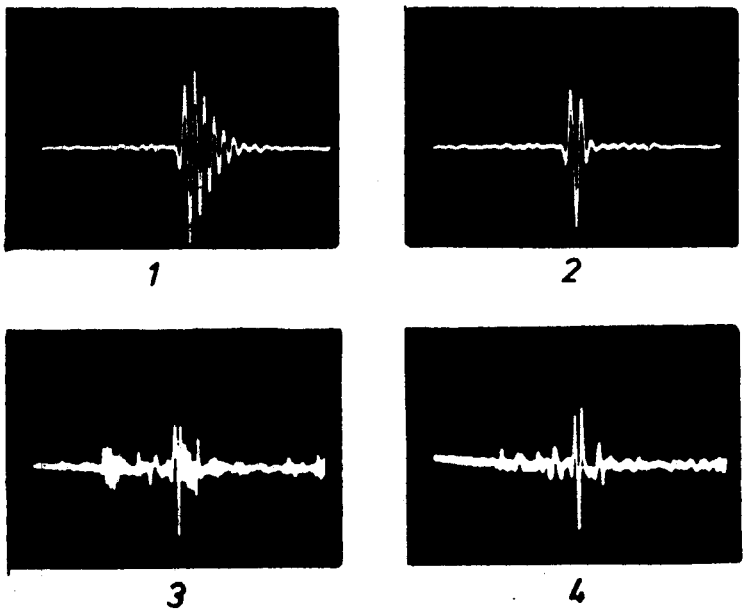
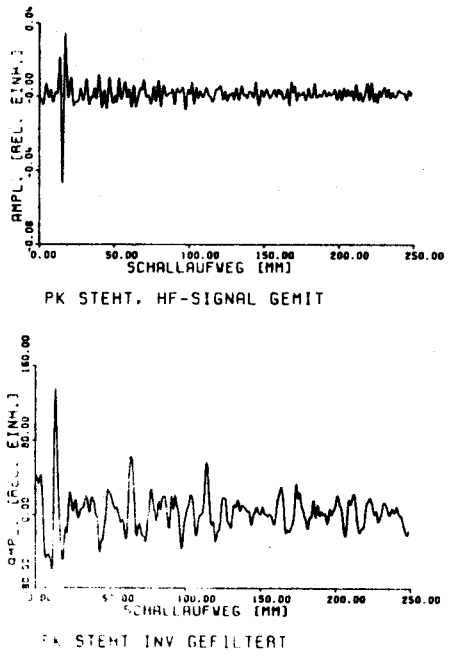


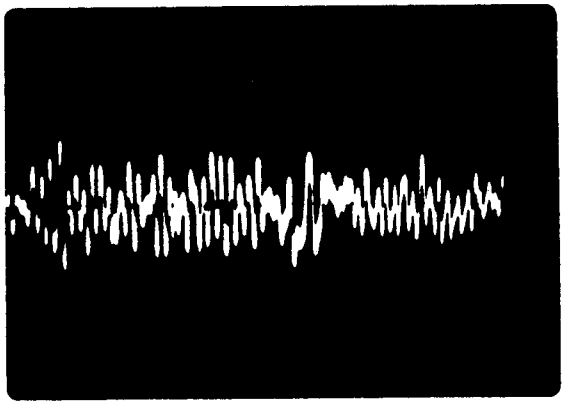
Fig. 17: Inverse filtering of ultrasonic signals by use of an electrical circuit:
1 and 2: Rear wall echo before and after inverse filtering.
3 and 4: Echo indication from a cylindrical drill hole (Ø 2 mm) in coarse grained weld metal before and after inverse filtering. The "ghost" indication is disappearing by inverse filtering.
f = 2 MHz.



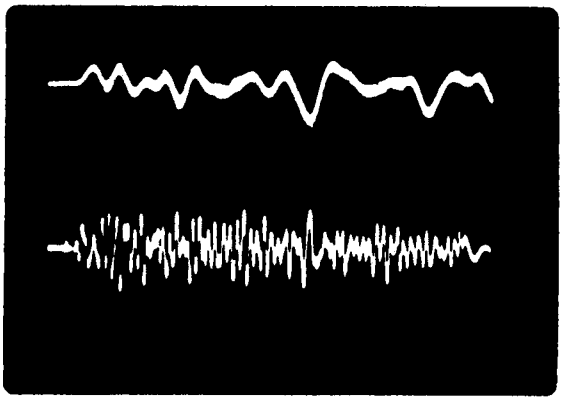
HF-presentation of the sequence of backwall-echoes starting with the second echo

Same signal after inverse filtering. Now the third and fourth backwallecho are discriminated

Fig. 18: Inverse filtering of a sequence of backwall echoes. Austenitic cast, 50 mm wallthickness, normal probe, 1 MHz.

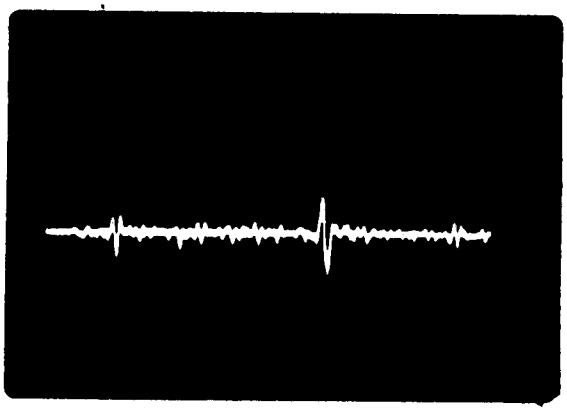


$f(t)$



$f_u(t)$

$f_o(t)$



$f_u(t) \cdot f_o(t) = s(t)$

Fig. 19: Improvement of the signal-to-noise-ratio by multiplicative mixing. The signal f(t) (backwall echo from austenitic cast, 50 mm wall thickness, normal probe, 1 MHz) is splitted in a low frequency part $f_u(t)$ and a high frequency part $f_o(t)$. Multiplicative mixing $f_u(t).f_o(t)=s(t)$ is resulting in an improved signal-to-noise-ratio.

Overview of Argonne National Laboratory efforts on ultrasonic NDE of stainless steel welds.

D.S. KUPPERMAN, K.J. REIMANN
Argonne National Laboratory, USA

ABSTRACT

An overview of Argonne National Laboratory efforts on ultrasonic NDE of stainless steel welds will be presented. Data on velocity of sound and signal amplitude variations in stainless steel weld metal as well as data on deviations of longitudinal and shear beams will be discussed and compared with model calculations. Variations in sound velocity with propagation direction has been observed to be as large as 45% for shear and 14% for longitudinal waves. Beam deviations as large as $\sim 22°$ for longitudinal, $\sim 45°$ for SV, and $\sim 22°$ for SH waves have been detected experimentally. Comparison of experimental results with model calculations assuming an orthotropic symmetry for the weld metal are reasonably good. The implications for nondestructive examination of weld metal are discussed. Advantages of spatial averaging of coherent ultrasonic noise to improve signal-to-noise ratios in ultrasonic inspections are presented. Significant improvements in signal-to-noise ratios can be observed for detection of reflectors in weld metal. Efforts to assess the adequacy of conventional ultrasonic testing techniques for detection of intergranular stress-corrosion cracking (IGSCC) in stainless steel reactor piping are presented. Difficulty in detecting field-induced IGSCC was reduced through the use of a single-element focused transducer.

* Review supported by the U. S. Nuclear Regulatory Commission.

I. INTRODUCTION

This paper will present a review of efforts at Argonne National Laboratory (ANL) on ultrasonic inspection of stainless steel welds. The topics to be discussed include results on wave propagation in stainless steel weld metal, spatial averaging techniques to minimize coherent ultrasonic noise from the weld metal microstructure, and problems associated with optimization of conventional ultrasonic techniques to detect intergranular stress-corrosion cracking (IGSCC) in reactor piping.

II. WAVE PROPAGATION IN AUSTENITIC STAINLESS STEEL WELD METAL

The microstructure of austenitic stainless steel weld metal is acoustically anisotropic. Consequently, the ultrasonic inspection of austenitic stainless steel weld metal is difficult, and the acoustic properties are not easily understood. Many investigators, some of them mentioned below, have studied the propagation of ultrasonic waves in stainless steel weld metal and the implications for flaw detection.[1-19]

Yoneyama et al. [7] have studied the cause of false indications sometimes observed in austenitic stainless steel welds and have demonstrated that shear-wave signals can be reflections caused when the acoustic beam deviates from the anticipated path and follows the lines of grain growth. Baikie et al. [8] showed the orientation dependence of longitudinal wave

velocity and demonstrated that the apparent attenuation of longitudinal waves at 2 MHz in stainless steel weld metal varied with propagation direction relative to the columnar grain axis. The minimum attenuation occurred for waves propagating at about 45° to the grain axis (the direction of maximum wave velocity). Tomlinson et al. [9] interpreted Baikie's data on the basis of beam deviation, concluding that the variation in apparent attenuation may be primarily due to the variation in beamwidth (and deviation) with propagation direction, with the smallest beamwidth observed for directions of maximum velocity. In a recent report, Adler et al. [10] discuss anisotropic structural materials (stainless steel welds and centrifugally cast pipe) and illustrate how anisotropy must be accounted for when employing frequency analysis for flaw characterization. Some data are presented on the relative apparent attenuation of longitudinal waves as a function of propagation direction, in qualitative agreement with Baikie [8]. In previous publications by the present authors [19], the variation in frequency spectra with microstructure, including polarization effects, has been examined.

The three main factors that contribute to the ultrasonic attenuation are grain-boundary scattering, mode conversion, and the phenomenon of beam steering, in which the ultrasonic beam is guided towards the direction of maximum ultrasonic velocity in the weld [9]. Spurious signals, which cannot be correlated with component geometry or actual flaws, contribute to the difficulties in interpreting the results. The difficulties encountered, as well as the high attenuation in the weld metal, have been discussed in the literature [2-12, 14, 17, 18]. However, for coarse-grain materials, proper selection of the acoustic mode and an understanding of the acoustic propagation characteristics when the weld metal is inspected may enhance the reliability and sensitivity and lead to an improved ultrasonic testing method.

Experimental Procedure

Experimental results were obtained for a "V"-type multipass shielded-metal arc weld, 1-cm^3 coupons from welded Type 304 stainless steel tensile specimens made available for this study, and three $\sim$1-cm^3 single crystals of austenitic stainless steel. The single-crystal sample compositions were 19Cr-10Ni, 19Cr-14Ni, and 19Cr-19Ni.

The original welded plate (300 x 150 x 50 mm) from which other specimens were cut was Type 304 stainless steel with Type 308 stainless steel weld metal. The weld was a "V" type with a 77° included-angle, multipass shielded-metal arc. This specimen was cut in half along the long dimension. From one half, a 24 x 25 x 38 mm weld-metal coupon was removed for ultrasonic examination, as shown in Fig. 1. The 1-cm^3 tensile-specimen coupons were the source of velocity-of-sound and attenuation data for propagation direction 45° to the columnar-grain axis.

Velocity-of-sound data were acquired with an Intervalometer employing the pulse-echo-overlap method [20, 21]. Normal-incidence 2.25-MHz and 5-MHz shear- and longitudinal-wave transducers were employed. These transducers and an Aerotech UTA3 pulser-receiver system were used for flaw detection. A shear-wave couplant or epoxy was used to couple shear waves directly into the weld metal. An X-ray diffractometer 2θ scan method was used to evaluate the crystallographic texture in the weld samples.

Experimental Results

A. Elastic Constants

To obtain the single-crystal elastic constants for stainless steel, the longitudinal velocity and slow and fast shear velocities were measured

along the <110> propagation direction of each single crystal. The elastic constants C_{44}, C_{11}, and C_{12} are determined from the following relationships:

$$C_{44} = \rho V^2_{t_1} ,$$

$$C_{11} = \rho(V^2_{\ell} + V^2_{t_2} - V^2_{t_1}) ,$$

and

$$C_{12} = \rho(V^2_{\ell} - V^2_{t_2} - V^2_{t_1}) ,$$

where V_{ℓ} is the longitudinal velocity, V_{t_1} the shear, and V_{t_2} the slow shear. Table I shows the results (average of the 3 single-crystal samples) for velocity of sound and elastic constants. The uncertainty in the latter

TABLE I

Velocity of Sound and Elastic Constants for Stainless Steel

V_{ℓ} <110>	6.062×10^5 cm/s	C_{11}	$20.5 \pm 0.2 \times 10^{11}$ dynes/cm^2
V_{t_1} <110>	3.957×10^5 cm/s	C_{12}	$13.3 \pm 0.2 \times 10^{11}$ dynes/cm^2
V_{t_2} <110>	2.130×10^5 cm/s	C_{44}	$12.5 \pm 0.5 \times 10$ dynes/cm^2
ρ	8.01 g/cm^3		

measurements includes a slight error (<0.2 percent for C_{11}) due to misorientation of the <110> crystallographic axis from the cubic-face normal and path-length measurement. The data could be corrected for the misorientation, but this uncertainty is much smaller than that due to the other errors combined. These values are within 5 percent (for C_{11} and C_{44}) and

10 percent (for C_{12}) of values found in the literature for 304 stainless steel [12, 22].

B. Microstructure

Columnar grains up to 10 mm in length and 1 mm in width, essentially parallel to the z-axis, can be observed. In the weld metal the X-ray results indicated a strong preferred <100> orientation in the z-direction. The X-ray diffraction data are, of course, obtained only from the surface of the specimen interrogated.

C. Velocity of Sound in Weld Metal

Our results (refer to Fig. 4) for longitudinal-wave velocity are consistent with those of [9] and [10] but only qualitatively consistent with the shear-wave results of [10]. (The present data show greater anisotropy.) A variation in velocity of 14 percent for longitudinal and 45 percent for shear waves is observed here. The maximum velocity for longitudinal waves is in a direction $\sim$45° to the columnar grain axis, whereas this is the direction of minimum shear velocity. The maximum velocity for shear waves is in a drection perpendicular with polarization parallel, to the grain axes (these are the directions of low longitudinal velocity.) Velocity measurements parallel, perpendicular, and at 45° to the grain axes were sufficient to verify the theoretical results, as these are the directions of minimum and maximum velocity.

D. Attenuation

As was reported in [9], the present experimental observations have shown that longitudinal waves propagating at $\sim$45° to the long axis of the columnar grains exhibit the least attenuation. This is confirmed in the present study,

where pulse-echo signals obtained from 1-cm^3 weld-metal coupons show that ultrasonic waves propagating at 45° to the grain axes have 1.5-3 dB/cm less attenuation than waves propagating parallel or perpendicular to the columnar grains.

The results for shear waves are different. It has been observed here that shear waves propagating across the grain axis, but with polarization parallel to the grain axis, transmitted signals with 3 dB/cm less attenuation than shear waves propagating in other directions, including 45° to the grains axis. The significance of these results with regard to flaw detection will be discussed in later sections of this paper.

Theory

The coarse-grain character and anisotropy of stainless steel weld metal suggest that, in a model which describes the region of the weld where the columnar grains are vertical, an assumption can be made that the sample has orthotropic symmetry [23]. The effectiveness of the model can be checked by comparing the predicted and measured ultrasonic velocities in various propagation directions. The following discussion (a) indicates how the velocity in various directions can be predicted for the weld metal, and (b) discusses the phenomenon of beam steering, which can have a great effect on apparent attenuation of both longitudinal and shear waves. The discussion begins with the simple example of a single crystal of stainless steel and concludes with the model previously described.

Calculations of velocity and deviations in the 100 and 110 plane for single-crystal Type 304 stainless steel were performed by Musgrave's method [1, 13, 15], using elastic constants from single-crystal specimens of Table I. The results are plotted in Figs. 2-3. The deviation is labeled

positive if it is in the same direction as the increment of the angular-velocity direction cosine, and negative if it is in the opposite direction. Curves derived are similar in shape to curves obtained by Musgrave for nickel [1]. The figures show that the quasilongitudinal velocity can vary from 6.4×10^3 to 5.1×10^3 m/s and the shear-wave velocities from 4.0×10^3 to 2.1×10^3 m/s. The angle between velocity vector and energy ray can amount to 22° for longitudinal waves, 50° for vertically polarized (SV) shear waves, and 35° for horizontally polarized (SH) shear waves in single crystals of stainless steel. The results for single crystals are presented for the 110 plane so that they can be compared with the weld-metal results (Figs. 4-5). These curves clearly show how velocity surface, wave surface, and energy-ray deviations are modified in going from a single crystal to the orthotropic symmetry of the weld metal. The coarse-grain structures exhibit symmetry around one axis (the z-axis), and there will be five independent elastic constants [16]:

$$\bar{C}_{11D} = \bar{C}_{22D} = \bar{C}_{11} + \frac{3\gamma C}{20} \qquad \bar{C}_{33D} = \bar{C}_{11} + \frac{2\gamma C}{5}$$

$$\bar{C}_{44D} = \bar{C}_{55D} = \bar{C}_{44} - \frac{\gamma C}{5} \qquad \bar{C}_{66D} = \bar{C}_{44} + \frac{\gamma C}{20}$$

$$\bar{C}_{13D} = \bar{C}_{23D} = \bar{C}_{12} - \frac{\gamma C}{5} \qquad \bar{C}_{12D} = \bar{C}_{12} + \frac{\gamma C}{20}$$

where $\bar{C}_{ij}$ is the elastic constant for polycrystalline materials [10]. The texture anisotropy factor γ can be derived from the following considerations:

(a) In the 001 plane (cross section of a grain), the ultrasonic velocity should be independent of direction of incidence.

(b) The velocities parallel to the z-axis (the axis of symmetry) should be the same as given by C_{11} and C_{44} in a single crystal.

These restrictions establish the value $\gamma = 1$. Using the relations C_{ijD} and the same single-crystal elastic constants used previously, velocity surfaces and deviation were calculated for coarse-grain structures of Type 304 stainless steel. The results are plotted for the 110 plane in Figs. 4-5. Examination of the velocity curves indicates that in the 110 plane the quasilongitudinal velocity can vary between 6.2×10^3 and 5.1×10^3 m/s, while the shear-wave velocities can assume values between 4.0×10^3 and 2.4×10^3 m/s, and 4.0×10^3 and 3.2×10^3 m/s. The deviation of longitudinal waves can be as large as 21°, while that of shear waves can reach values of 44° or 13°, depending on polarization. Calculated values of velocity in discrete directions were within 10 percent of values obtained by measurements on a columnar-grain structure of weld metal.

The above theoretical considerations lead to a better understanding of consequences that will be encountered in the practical application of ultrasonic testing of structures with preferred orientations, such as stainless steel welds.

Discussion

The simple weld-metal model described above accounts reasonably well for the experimental data on velocity of sound and is in qualitative agreement with the data for attenuation.

Experimental observations of longitudinal waves by previous investigators indicate that waves propagating at ~45° to the long axis of the dendrites have the least attenuation [9]. In the present study, ultrasonic pulse-echo signals obtained from 1-cm^3 weld-metal coupons showed that longitudinal ultrasonic waves propagating at 45° to the dendrites undergo 1.5-3 dB/cm less

attenuation than waves propagating parallel or perpendicular to the dendrites (in general agreement with [9]). These results indicate that the convergence of ultrasonic beams along the propagation direction of maximum velocity may be the major factor in the attenuation of longitudinal waves. In Fig. 5, the energy-ray deviation is indicated for longitudinal waves. A negative slope for $\Delta = 0$ is the point of maximum convergence without deviation of the beam. A positive slope indicates divergence. The maximum convergence occurs at $\sim 50°$. This implies that a beam propagating along this direction would not necessarily deviate from the straight path and would experience a focusing effect. The experimental results indicating maximum beam intensity along a direction $\sim 45°$ to the dendrites are consistent with the predicted observation that the beam tends to focus when traveling along a direction of maximum velocity. Fig. 6 illustrates this point for longitudinal as well as shear waves.

The results for shear waves are not as clear as for longitudinal. Maximum shear velocities occur for waves propagating (a) parallel to the dendrites and (b) perpendicular to the dendrites, with polarization parallel to them. The minimum velocity is along a direction 45° to the grain axes with polarization in the 110 plane. The current experimental observation is that shear waves propagating across the columnar grains with polarization parallel to the grains axes have at least 3 dB/cm less attenuation than all other signals, including those from waves propagating at 45° to the columnar-grain axes. (This is qualitatively consistent with the theoretical predictions.) For shear waves traveling parallel to the grains, one observes a difference in attenuation for various polarizations which is not predicted. This may be due to variation in mode-conversion characteristics (the grains are not exactly parallel to the wave-propagation direction) or to a structure which

is not as symmetric about the z-axis as assumed. For shear waves traveling perpendicular to the long axis of the grain, grain-boundary scattering may be an important factor, since the acoustic-impedance mismatch across the dendrites varies considerably for different polarizations (and thus different wavelengths). This is suggested by the observation that the frequency spectrum varies with polarization. With high-velocity (long-wavelength) waves, higher frequencies are transmitted than with low-velocity (short-wavelength) waves [5,18]. The mismatch is least for waves polarized along the grain axis and greatest for waves polarized across them. In the latter case, scattering would help explain the larger-than expected variation in attenuation with polarized shear waves propagating across the columnar grains.

In order to help establish the adequacy of the model in predicting beam deviations for shear waves, a cylinder has been cut from the weld coupon of Fig. 1 to measure the deviation of the shear beams. A method employing a pitch-catch mode and normal-incidence shear-wave transducers is being used in an attempt to measure the deviation. Fig. 7 shows the arrangement. An epoxy is used along with two 2.25-MHz transducers and 1-cm^2 curved plexiglass "shoes." The transducers can be moved around the cylinder in steps by removing and reglueing the transducer to find the angle of maximum signal transmission and thus the beam-deviation angle. Although many difficulties are encountered with this simple method, data show significant beam deviations. The preliminary data are quantitatively consistent with the model predictions for vertically polarized (SV) waves, but only qualitatively for horizontally polarized (SH) waves. Nevertheless, the prediction that the sharpest deviation ($\sim$ 22°) for SH waves occurs for

waves propagating at ∿45° to the columnar grain axis is verified experimentally. In addition, a zero deviation for SV waves occurs for a propagation direction of ∿45° to the grain axis, as predicted. Furthermore, a large positive deviation (∿45°) for $\psi \sim 67°$ and a negative deviation ($\sim 22°$) for $\psi \sim 22°$ are observed.

Flaw Detection

The detectability of artificial reflectors placed in stainless steel weld metal is affected by wave mode (longitudinal or shear) and by variations in the polarization of the shear waves that are used.

A 2.25-MHz 13-mm-diameter Panametrics broad-band shear-wave transducer was used to detect a 2.4-mm-diameter side-drilled hole in a weld metal sample. With SH shear waves propagating at about 45° to the columnar grain axis, the reflection from the hole could be readily distinguished from the noise. However, with SV shear waves (45° angle to grain axis) the reflection from the hole could not readily be observed. The SV shear waves are used for conventional shear-wave inspection in which a longitudinal-mode crystal and wedge generate shear waves via mode conversion at the wedge/metal-surface interface. With a 2.25-MHz, 13-mm-diameter gamma-series longitudinal-wave transducer manufactured by Aerotech, the hole could also be readily distinguished from the background noise, although the longitudinal wave has less resolution because of the longer wavelength and ringing. These results are consistent with those presented earlier. For ultrasonic inspection of piping, SH shear waves, with particle motion perpendicular to the plane formed by the incident and reflected beams, would be preferable for two reasons:

(a) Spurious signals are reduced, since SH waves cannot be mode converted to longitudinal waves at the pipe inner wall, whereas SV waves can.

(b) As we have shown, SH waves with the specific geometry described here can penetrate stainless steel weld metal better than 45° SV waves, because of the anisotropic nature of the weld. Thus, defects in the HAZ of a weld could be detected from the opposite side of the weld with SH waves.

Generating SH waves, however, is difficult because normal-incidence shear waves must be employed (requiring a very viscous or solid couplant). The use of electromagnetic acoustic transducers (EMATs), which are noncontacting, may eventually alleviate this problem. Although the practical application of EMATs for routine reactor inspection is still in the future, they are currently being tested in Germany for stainless steel inspection.

III. ULTRASONIC DETECTION OF INTERGRANULAR STRESS-CORROSION CRACKS

The numerous problems associated with the in-service ultrasonic detection of IGSCC in nuclear reactor piping are well known: (a) Many geometrical reflectors are present; (b) the coutour of the weld on the ID surface is unknown; (c) ultrasonic signals from the cracks are weak; (d) the weld crown interferes with transducer movement; (e) the working environment is poor (high temperature, humidity, and radiation levels); (f) pipe access is limited; (g) ultrasonic attenuation varies from one pipe region to another; (h) the weld metal produces ultrasonic "noise"; and (i) reference standards are unsatisfactory. A program was carried out at ANL [25] to optimize the parameters associated with conventional ultrasonic in-service inspection techniques. The results of the study indicated that no single conventional

ultrasonic probe would optimally detect all the crack types (longitudinal, transverse, slanted, skewed) that might be expected in nuclear reactor piping. If a flaw of a specific size and orientation is sought, then some improvement can be made in detection capability. Some details of the program are discussed below.

Weld Geometry

Machine preparation and grinding can result in spurious ultrasonic reflections at the pipe ID, severely limiting inspectability of the HAZ. In this study, coupons were obtained from three azimuthal positions of a pipe-to-elbow section of 102-mm (4-in.) bypass piping. This pipe section was removed from service because of numerous ultrasonic indications. Sectioning of the pipe revealed no cracks; the signals, which varied in amplitude, were all from geometrical reflectors. This problem is not confined to bypass lines. In a section of 660-mm (26-in.) piping, signals can be obtained simultaneously from the root bead and land (step). A crack signal originating between the root and land would probably be obscured by the echoes from the geometrical reflectors. Inspectability could be improved by having the land in machine-prepared pipes at least two wall thicknesses beyond the root bead. In addition, the weld crown can interfere with the motion of the transducer (particularly 13-mm probes), limiting detection of ultrasonic echoes from the region of the weld fusion line. Smoothed weld crowns would alleviate this problem.

Attenuation of Ultrasonic Signals

Another inspection problem is the variability in ultrasonic attenuation among base metal, HAZ, and weld metal. A 2.25-MHz, 13-mm-dia transducer was

used to detect identical 13 x 1.3-mm EDM notches in the HAZ and base metal of a piece of 102-mm (4-in.) piping. A variation of almost 10 dB between base metal and HAZ was noted, with a further loss of ∿ 10 dB as the signal passed through the weld metal. Careful calibration procedures employing actual field piping or very good mock-up samples will be required to compensate for this attenuation variation. Notches in a reference welded pipe section were found to be advantageous for setting the sweep position. EDM notches (0.5 to 1.0 mm deep) in the HAZ of mock-up pipes would be useful for setting up an in-service test. EDM notches at the weld fusion line can indicate potential difficulties in detection of cracks near that location. Pipes with laboratory-induced IGSCC would provide an even more effective reference.

Use of Focused Probes

The application of focused probes to in-service ultrasonic testing could, in principle, improve the detection probability of IGSCC because of the narrower ultrasonic beam. This was found to be the case for small reflectors. In a plot of amplitude versus EDM notch depth for two transducers (one focused, one not), the signal-to-noise ratio for an ultrasonic echo from a small notch (0.13 mm deep) using the focused probe was more than double that with the unfocused probe.

The importance of a high signal-to-noise ratio is suggested by laboratory results obtained on a core spray line pipe section. This pipe contained six short (< 25 mm) field-induced cracks which, on the basis of available data, were estimated to be 2.8-4.8 mm deep. The cracks were partially skewed relative to the pipe longitudinal axis. Because such cracks are difficult to detect, a comparison could be made of defect-detection probabilities with various ultrasonic probes. Four transducers were evaluated. The cracked

area was scanned 10 times with each transducer, giving a maximum of 60 possible "detections" per transducer. The total time for each set of 10 scans varied from 30 to 35 min. Binomial distribution statistics were used to estimate the upper 95% confidence limit on the probability of missing one of the flaws in one scan of the pipe. The results are shown in Table II.

TABLE II

Probabilities That Nonthroughwall Stress-corrosion Cracks in Pipe 10-24A Will Escape Detection on a Single Pass by Various Transducers[a]

Transducer Serial Number	Transducer Frequency, MHz	Size, mm	Type	Miss Probability	Upper 95% Confidence Limit
015957	2.25	6	unfocused	0.63	0.75
016443	2.25	13	unfocused	0.52	0.65
016506	2.25	13	focused	0.42	0.55
015956	1.0	13	unfocused	0.72	0.83

[a]All transducers are Aerotech miniature shear-wave probes with replaceable wedges. A Branson 303B pulser-receiver was used (serial number 507070). The beam angle was 45°, and flat wedges were employed. The probabilities are those obtained with a single transducer under a specific set of conditions and are not to be interpreted as absolute values for the cracks examined; only the relative effectiveness of the four probes is evaluated.

The data, although limited, suggest that the focussed transducer was better for detecting these small flaws. These results with respect to the relative merits of the probes are consistent with those obtained for 102-mm pipes with small artificial reflectors.

Frequency Selection

The two major factors that determine the optimum frequency for inspecting stainless steel piping are diffraction (spreading) of the ultrasonic beam and scattering from the grain boundaries. In the present case, the

apparent attention α can be expressed as

$$\alpha = \alpha_D + \alpha_S \quad ,$$

where α_D is the loss due to diffraction and α_S is the loss due to grain-boundary (Rayleigh) scattering. For this scattering, $\lambda >> D$ where λ is ultrasonic wavelength and D is grain size. For a transducer of radius a generating longitudinal waves, α_D is about 1 dB for each a^2/λ. The Rayleigh scattering term for this case is

$$\alpha_S \propto f^4 \quad ,$$

where f = frequency. The result is that the system behaves as if it were a "band-pass filter". Although this effect is observed primarily for longitudinal waves, a phenomenon that is at least qualitatively similar (that is, a minimum in apparent attenuation versus frequency) should occur for shear waves. In the ANL study, tests on stainless steel with 1-, 2.25- and 5-MHz, 13-mm-dia transducers showed empirically that a frequency of $\sim$ 2.25 MHz gave minimum attenuation. In another study [26] with 13-mm-dia transducers, in which more frequencies were tested, the best frequency was found to be 1.8 MHz. Note, however, that a smaller transducer would shift the minimum attenuation to a higher frequency, and a larger one would shift it to a lower frequency.

Use of Dual- Versus Single-element Probes

In the ANL study, a dual-element 2.25-MHz Panametrics transducer was compared with several single-element probes. The only advantage noted for the dual-element probe was in detection of skewed reflectors. Recently,

however, a more compact dual-element transducer has been made available commercially and is becoming more widely used for detection of IGSCC [27].

IV. SPATIAL AVERAGING

Another technique that has potential application to the improved detection of flaws in SS welds is spatial averaging. The problem in inspecting stainless steel, particularly around welds, often reduces to one of extracting the flaw signal from the noise signlas. This problem is often related less to electronic noise than to coherent noise; that is, scattering from grain boundaries, rough surfaces, or weld-metal interfaces. A signal-averaging method is demonstrated here for flat surfaces where the defect (crack or notch) is in the weld metal.

A weld scanner, shown schematically in Figure 8, has been designed and built at ANL to demonstrate the advantages of spatial averaging. Water is used as a couplant. Two transducers (T and R in Fig. 8) are operated in a pitch-catch mode to generate 45° ultrasonic waves in stainless steel samples. The projection of the pitch-catch included angle θ to a horizontal plane is varied between 60 and 90° in steps of $\sim 3°$, and the receiving signal is averaged over several transducer positions. Each step incorporates a pause, during which the ultrasonic trace of the "A-scan" is digitized by a transient recorder and stored in the memory of a Data General Corporation 2/10 minicomputer. The average of digitized traces from up to ten angular positions of the beams is printed out after the scan for a particular point in the sample is completed. As a result, one obtains a series of averaged A-scans and their overall average as the weld scanner moves across the specimen.

Several specimens have been inspected with this device. In the example presented here, the weld scanner was used to examine a flat weld by means of

refracted longitudinal waves (45° beam). Figure 9 shows three individual traces and the computer average of ten such traces (corresponding to ten values of θ). The transducer was positioned so that ~45° longitudinal waves were propagated in the weld metal. The averaged trace unambiguously shows the reflected longitudinal and shear wave and the shear wave mode converted from a longitudinal wave in the EDM-notch plane. These signals are not as evident in the individual traces. The water-metal interface is seen as the first large peak. With the scanner away from the notch but still over the weld metal, the averaged trace does not show the presence of a reflector. The present study demonstrates that coherent ultrasonic noise can be averaged so as to significantly enhance the signal-to-noise ratio for flaws in stainless steel weld metal.

Another demonstration of the enhancement of signal-to-noise ratios is provided by a simplified system in which an Aerotech miniature shear-wave transducer (6 mm, 2.25-MHz, 45° beam) was moved parallel to the plane of a crack (2 cm long and up to 2 mm deep) in a stainless steel tensile specimen. A Sonic Mark I pulser-receiver with video output was used. The smoothing of the rf traces can often enhance the ability to detect flaws with the signal-averaging process. In this example, the transducer was displaced parallel to the crack plane in 3-mm steps. During this motion, 10 video traces, covering a total transducer displacement of 27 mm, were averaged to obtain the final A-scan.

Figure 10 shows a typical averaged trace and five of the data sets in that average. The peak is the crack signal. If the transducer is moved to a position ahead of the crack so that the beam still passes partially through the weld metal but does not impinge on the crack, the signal average shows a reduced noise level.

V. SUMMARY

Data on sound velocity and attenuation have been acquired for stainless steel weld-metal samples and compared with theoretical predictions and efforts of other investigators. Sound velocity has been observed to vary with propagation direction by as much as 45 percent for shear waves and 14 percent for longitudinal waves. In addition, elastic constants have been measured for single crystals of stainless steel.

A simple model that describes the propagation of ultrasonic waves in Type 308 stainless steel weld metal is generally consistent with sound-velocity data and apparent attenuation for both longitudinal and transverse waves. The model assumes that the weld consists of a collection of long single-crystal grains with their long axes in the 100 crystallographic direction. These grains are arranged parallel to each other with a random orientation about the long axis (that is, the axis has orthotropic symmetry [20]). Velocity and energy-ray deviation curves have been calculated for stainless steel single-crystal and columnar-grain structures, using the elastic-constant data obtained in the present study. These results were compared with results from the literature.

It has been demonstrated that inspections of welds with ultrasonic waves at an angle of 45° to the axes of the grains are more successful when SH or longitudinal waves are used rather than conventional shear waves. Inspections parallel or perpendicular to the grains are most effective with shear waves of the proper polarization, rather than longitudinal waves. These observations are generally consistent with model predictions.

Work carried out at ANL on the optimization of parameters for detection of IGSCC by conventional ultrasonic means, and the potential use of spatial-

averaging techniques for improving signal to coherent noise ratios in ultrasonic testing, have also been presented. The results of the parameter optimization study suggest that (a) no single probe is adequate to detect all the types of cracks that are found in reactor piping, (b) the use of single-element focussed probes may improve the probability of detecting very small IGSCC, and (c) the variation in attenuation due to microstructural differences between HAZ and base metal necessitates the use of special reference pipes (including pipes with welds and possibly IGSCC) for effective interpretation of ultrasonic signals. The studies on horizontally polarized shear waves indicate that research and development work with electromagnetic acoustic transducers for application to stainless steel components should be significantly increased, as it may ultimately allow reactor components to be inspected with 45° SH waves. These may be more effective for inspection of V-type stainless steel welds than the conventionally used 45° SV waves.

Spatial averaging has been shown to be potentially useful in reducing spurious ultrasonic signals during testing of stainless steel welds by averaging out coherent ultrasonic noise.

Acknowledgments

We wish to thank H. W. Knott for obtaining the X-ray diffraction data, N. F. Fiore for supplying the stainless steel single crystals, and G. M. Dragel for the metallography work. C. L. Johnson, A. Winiecki, W. Deininger, and W. A. Ellingson contributed greatly to the work described in this paper.

References

[1] M.P.J. Musgrave, "On the propagation of elastic waves in aelotropic media. I: General principles; II: Media of hexagonal symmetry," Proc. R. Soc. London, Ser. A, vol. 226, pp. 339 and 356, 1954.

[2] E. Holmes, "Ultrasonic behavior in austenitic stainless steel," Appl. Mater. Res., p. 181, July 1963.

[3] E. Holmes and D. Beasely, "The influence of microstructure in the ultrasonic examination of stainless steel welds," J. Iron Steel Inst. London, vol. 200, p. 283, Apr. 1962.

[4] J.P. Pelseneer and G. Louis, "Ultrasonic testing of austenitic steel castings and welds," Br. J. Non-Destr. Test., vol. 16, p. 107, July 1974.

[5] S. Serabian, "Influence of attenuation upon the weld interrogation distance amplitude curve," Mater. Eval., vol. 32 (12), p. 265, Dec. 1976.

[6] J.J. Mech and T.E. Michaels, "Development of ultrasonic examination methods for austenitic stainless steel weld inspection," Mater. Eval., vol. 35 (7), p. 81, 1977.

[7] H. Yoneyama, S. Shibata, and M. Kishigami, "Ultrasonic testing of austenitic stainless steel welds," NDT Int., vol. 11, p. 3, Feb. 1978.

[8] B.L. Baikie, A.R. Wagg, M.J. Whittle, and D. Yapp, "Ultrasonic inspection of austenitic welds," J. Br. Nucl. Energy Soc., vol. 15 (3), p. 257, July 1976.

[9] J.R. Tomlinson, A.R. Wagg, and M.J. Whittle, "Ultrasonic inspection of austenitic welds," in Nondestructive Evaluation in the Nuclear Industry Conf. Proc., R. Natesh, Ed., American Society for Metals, p. 64.

[10] L. Adler, K.V. Cook, W.A. Simpson, D.K. Lewis, and D.W. Fitting, "Ultrasonic flaw detection and characterization in structural materials by spectral analysis," Oak Ridge Nat. Lab. Rep. ORNL/TM-6456, Oct. 1978.

[11] E. Neumann, M. Romber, T. Just, E. Nable, K. Mattheis, and E. Mundry, "Development and improvements of ultrasonic testing techniques for austenitic nuclear components," presented at Second Int. Conf. on Nondestructive Evaluation in the Nuclear Industry, Salt Lake City, UT, Feb. 13-15, 1978.

[12] S. Matsumoto and K. Kumura, "The relationship between grain size and ultrasonic attenuation coefficient in austenitic stainless steel and iron," Trans. Nat. Res. Inst. for Metals, vol. 14 (4), pp. 155-164, 1972.

[13] M.P.J. Musgrave and G.F. Miller, "The propagation of elastic waves in aeolotropic media. III: Media of cubic symmetry," Proc. R. Soc. London, Ser. A., vol. 235, p. 352, 1956.

[14] D.S. Kupperman and K.J. Reimann, "Microstructural effects and signal-enhancement techniques in ultrasonic examination of stainless steel," Argonne Nat. Lab. Rep. ANL-76-115, Sept. 1976.

[15] M.P.J. Musgrave, "The propagation of elastic waves in crystals and other anisotropic media," Rep. Prog. Phys., vol. XIII, p. 74, 1959.

[16] H. Pursey and H.L. Cox, "The correction of elasticity measurements on slightly anisotropic materials," Philos. Mag. (Ser. 7), vol. 45 (362), p. 295, 1954.

[17] I.N. Ermolov and B.P. Pilin, "Ultrasonic inspection with coarse grain anisotropic structures," NDT Int., vol. 9 (6), p. 275, Dec. 1976.

[18] D.S. Kupperman and K.J. Reimann, "Effect of shear wave polarization on defect detection in stainless steel weld metal," Ultrasonics, vol. 16 (1), p. 21, Jan. 1978.

[19a] D.S. Kupperman, K.J. Reimann, and N.R. Fiore, "Role of microstructure in ultrasonic inspectability of austenitic stainless steel welds," Mater. Eval., vol. 36 (5), p. 70, Apr. 1978; D.S. Kupperman and K.J. Reimann "Ultrasonic wave propagation and anisotropy in austenitic stainless steel weld metal" IEEE Trans. on Sonics and Ultrasonics, Vol. SU-27, No. 1, Jan. 1980, p. 7.

[20] E.P. Papadakis, "Ultrasonic phase velocity by the pulse-echo-overlap method incorporating diffraction phase corrections," J. Acoustic Soc. Amer., vol. 42, pp. 1045-1051, 1967.

[21] E.P. Papdakis, "New, compact instrument for pulse-echo-overlap measurements of ultrasonic wave transit times," Rev. Sci. Instr., vol. 47 (7), pp. 806-813, June 1976.

[22] M.C. Mangabek and N.F. Fiore, "Orientation dependence of dislocation damping and elastic constants in Fe-18Cr-Ni single crystals," Trans. AIME, vol. 252, p. 2363, Nov. 1968.

[23] B.R. Dewey, L. Adler, R.T. King, and K.V. Cook, "Application of anisotropic elasticity to centrifugally cast piping," Oak Ridge Nat. Lab. Rep. ORNL/TM-5994, Oct. 1977.

[24] L.C. Lynnworth, "Ultrasonic probes using shear wave crystals - Principles," Mater. Eval., vol. 25, p. 12, 1967.

[25] D.S. Kupperman, K.J. Reimann and W.A. Ellingson, "Evaluation of Ultrasonic Techniques for Detection of Stress Corrosion Cracks in Stainless Steel Piping," Electric Power Research Institute Report, NP-761, prepared by Argonne National Laboratory, June 1978.

[26] Study to Define NDE Research for Inspection of Stainless Steels, Electric Power Research Institute Report, NP-797-SR, August 1978.

[27] P. Singh and J. Rose, "The Dual Element Angle Beam Transducer," Summary paper, ASNT Fall Conference, October 15-18, 1979, St. Louis, MO, p. 197.

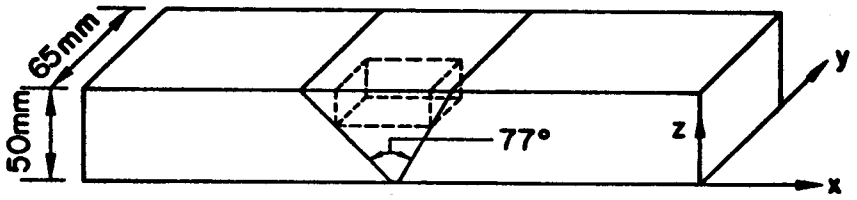


Fig. 1. Weld-metal coupon for acoustic-properties studies.

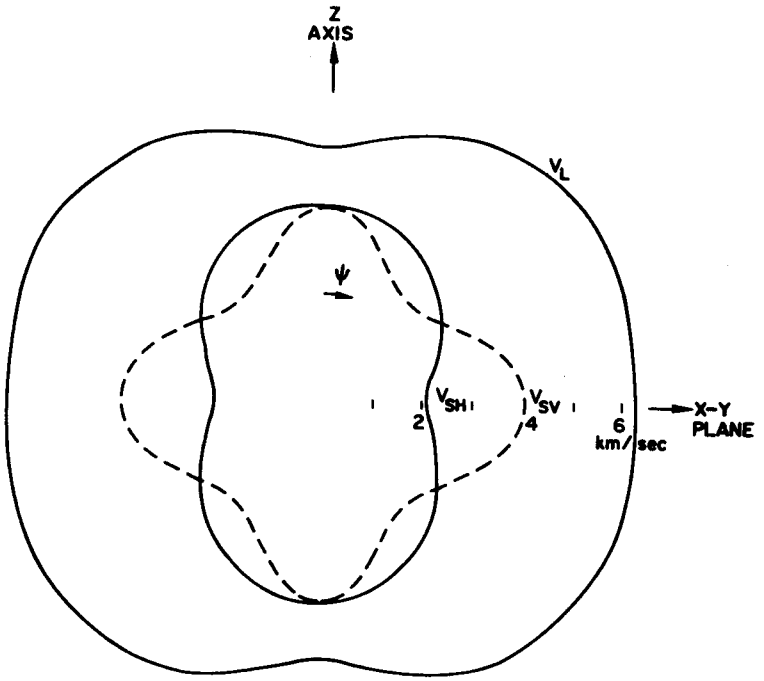


Fig. 2. Velocity-surface intersection with the 110 plane for single-crystal stainless steel.

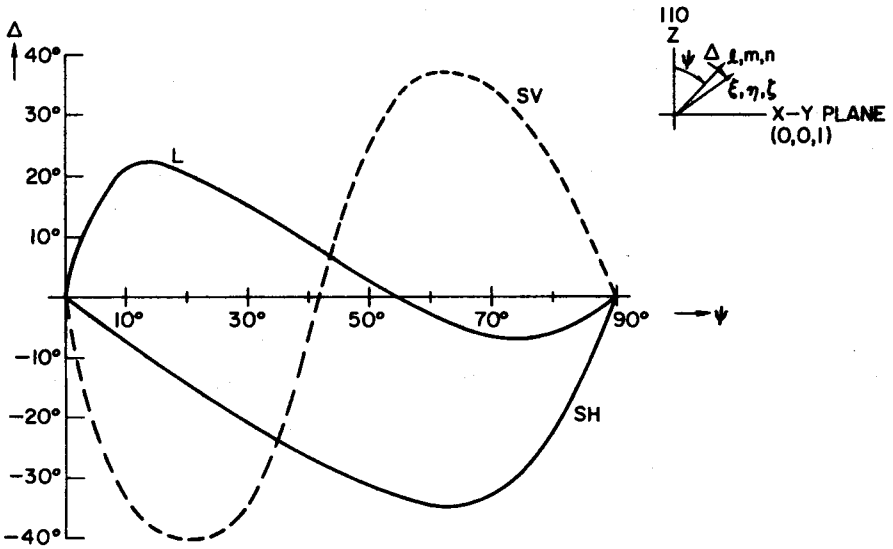


Fig. 3. Energy-ray deviation in the 110 plane for single-crystal stainless steel.

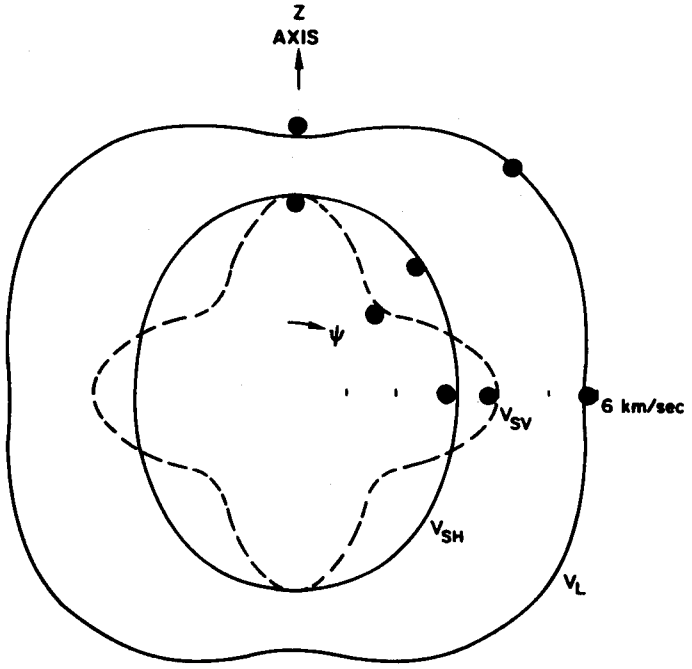


Fig. 4. Velocity-surface intersection with the 110 plane for columnar grain structure of stainless steel weld metal. Experimental data are shown.

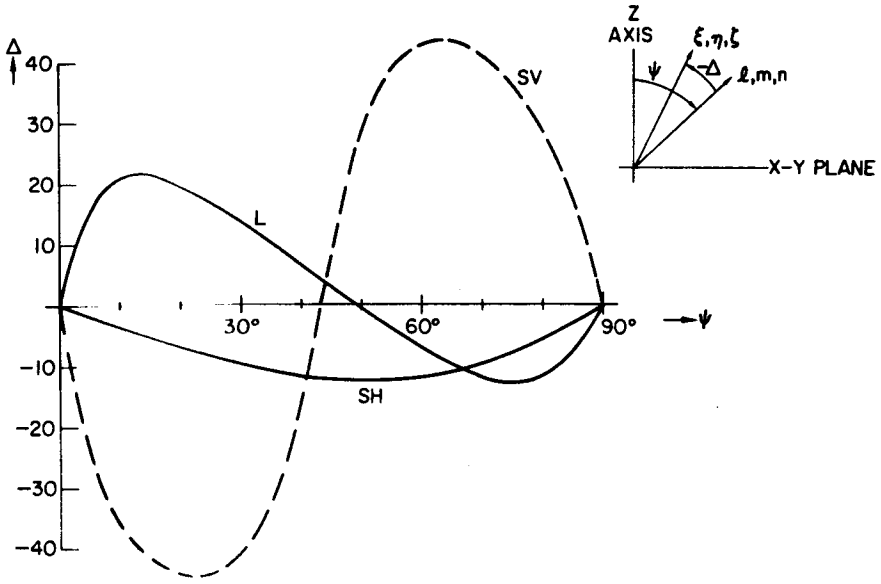


Fig. 5. Energy-ray deviation in the 110 plane for coarse-grain structure of stainless steel weld metal.

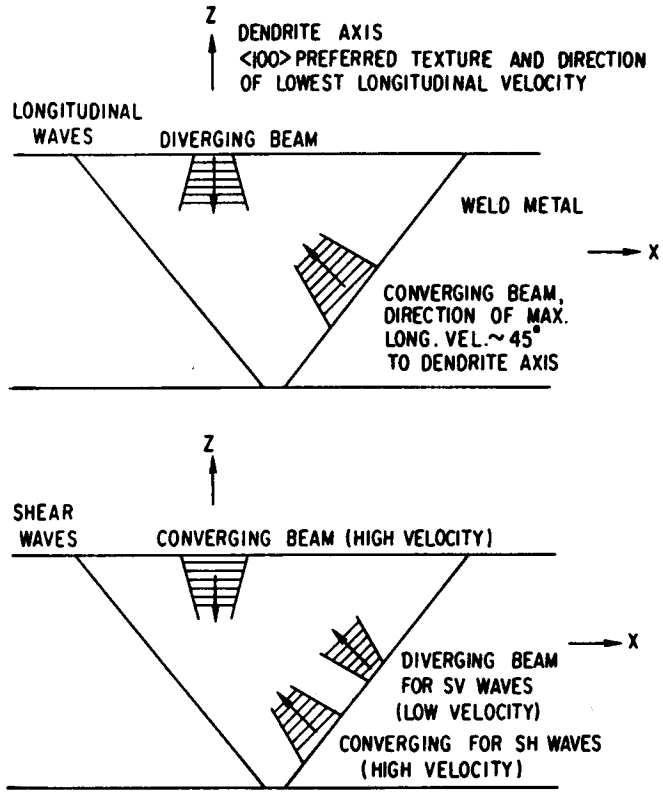
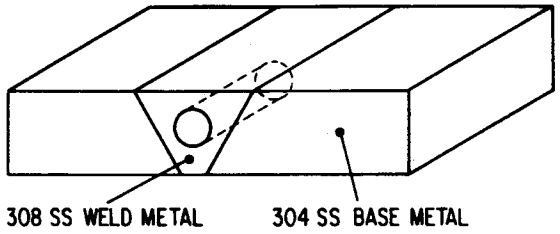


Fig. 6. Schematic representation of beam divergence and convergence for longitudinal and shear waves with propagation direction indicated by arrows.



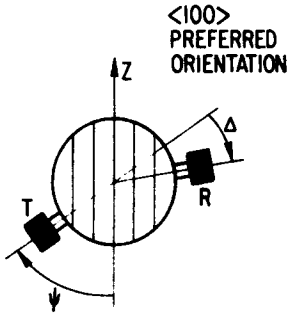


Fig. 7. Schematic representation of system for measuring shear-wave beam deviation. The cylinder used (2.5 cm long x 2 cm diameter) is cut from a 304 SS welded plate. The transmitted pulse (T) is propagated at an angle ψ with respect to the grain axis. The maximum received signal indicates the deviation angle Λ.

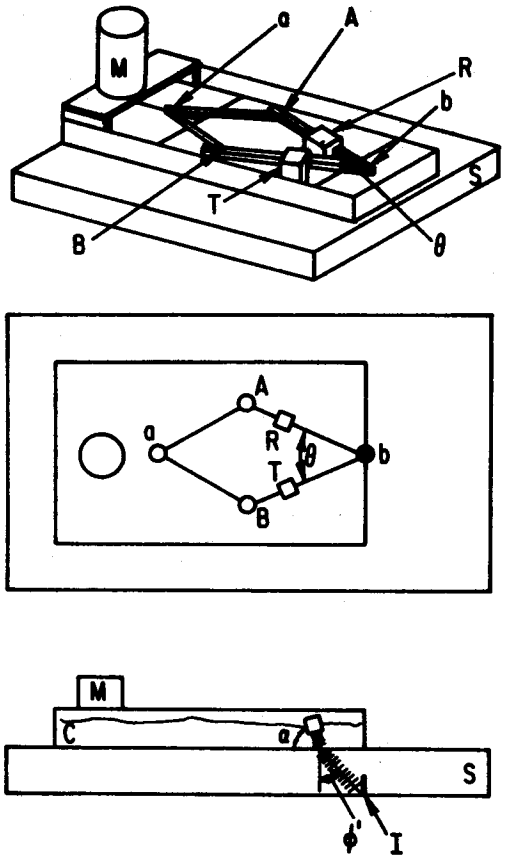


Fig. 8. Schematic representation of weld scanner. M = motor, C = couplant, S = sample, I = point of intersection of ultrasonic beams, α = incident angle in water, θ = scan angle, b = fixed pivot point, R = receiving transducer, T = transmitting transducer, and ϕ' = angle of refreaction in the sample.

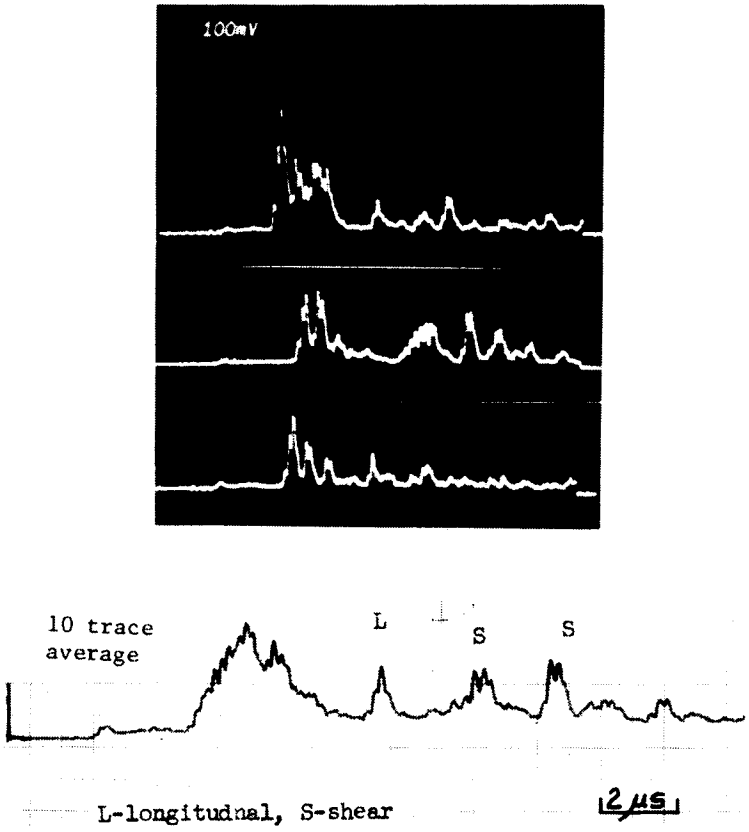


Fig. 9. Three individual traces and computer average of 10 traces from improved notch-detection system shown in Fig. 8, with a stainless steel weld metal sample. Refracted longitudinal (L) and two shear (S) waves can be seen.

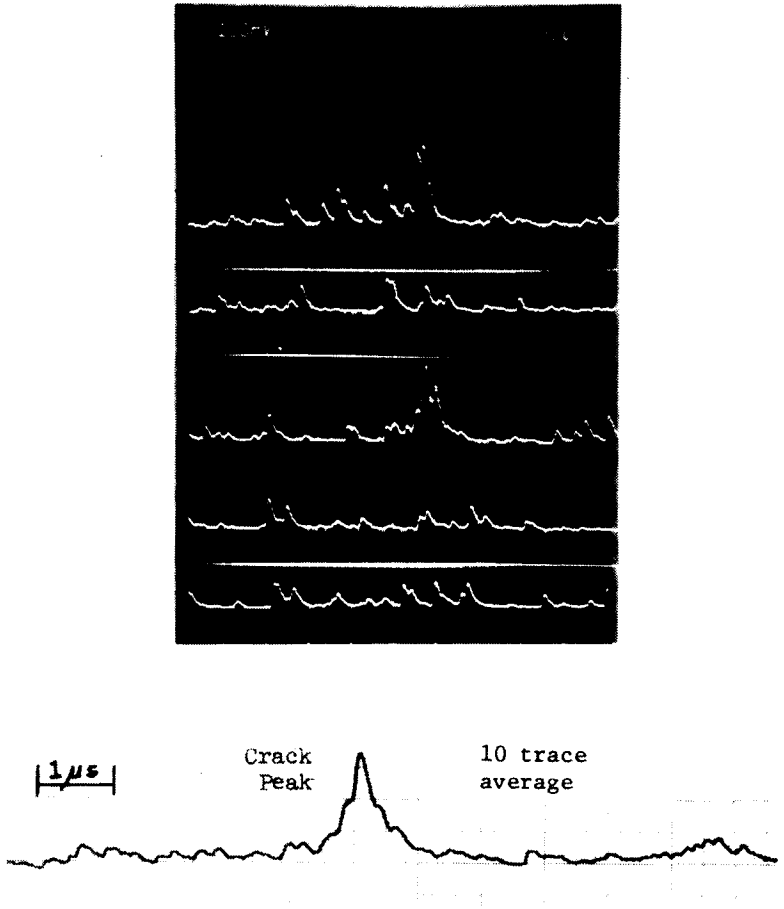


Fig. 10. Five oscilloscope traces and computer average of ten traces with beam reflecting off crack plane in 1-cm-thick stainless steel weld metal sample.

SESSION 2 : INSTRUMENTS AND METHODS

Chairmen : C.E. LAUTZENHEISER, Southwest Research Institute, USA

A. THOMAS, Framatome, France

Longitudinal wave ultrasonic inspection of austenitic weldments

B.S. GRAY, R.J. HUDGELL, H. SEED
United Kingdom Atomic Energy Authority

ABSTRACT

Successful volumetric inspection of LMFBR primary circuits, and also much of the secondary circuit, is dependent on the availability of satisfactory examination procedures for austenitic welds. Application of conventional ultrasonic techniques is hampered by the anisotropic, textured structure of the weld metal and this paper describes development work on the use of longitudinal wave techniques. In addition to confirming the dominant effects of the weld structure on ultrasound propagation some results are given of studies utilising deliberately induced defects in Manual Metal Arc Welds in 50mm plate together with preliminary work on the inspection of narrow austenitic welds fabricated by automatic processes.

1. INTRODUCTION

Successful volumetric inspection of LMFBR primary circuits, and also much of the secondary circuits, is dependent on the availability of satisfactory examination procedures for welds made between plates of austenitic steels such as Type 316 and 304. In order to supplement radiography in the demonstration of the structural integrity of the reactor during construction and to meet possible requirements for in-service inspection there is a need to provide appropriate ultrasonic procedures.

Application of conventional ultrasonic techniques is hampered by the anisotropic, textured, structure of the weld metal and this paper describes development work on the use of longitudinal wave techniques which are generally regarded as preferable for the examination of thick sections. In addition to confirming the dominant effects of weld structure, and hence fabrication procedure, on ultrasound propagation some results are given of studies utilising deliberately induced defects in Manual Metal Arc (MMA) welds together with preliminary work on the inspection of narrow gap welds fabricated by automatic processes.

Since it is the principal material of interest in this context for the UK fast reactor development programme, all the work to be discussed makes use of type 316 austenitic steel specimens and work has concentrated on butt welds in 50mm thick rolled plates.

The paper closes with a brief descussion of some factors involved in the application of these results to the in-service inspection of a sodium cooled reactor.

2. BASIC THEORY AND CHOICE OF TECHNIQUE

Macrographs of three manual metal arc welds are shown in Figure 1 and reveal long columnar grains which begin at a fusion face and extend into the body of the weld. The grains follow the heat flow paths in the weld during cooling and can grow epitaxially from one weld run to another as shown. The columnar structure of such welds may be broken up by mechanical deformation, or modified by heat treatment above 1050°C, but these processes cannot usually be considered for large items of plant and thus it is not generally possible to modify the weld structure following initial fabrication.

Baikie et al[1] showed that the ultrasound propagation velocity and attenuation in a 316 MMA weld is direction dependent for longitudinal waves while Launay et al[2] reported similar results for the components of a transition weld between austenitic and ferritic material in addition to providing a concise record of the practical advantages on signal/noise ratio grounds of using longitudinal waves for ultrasonic pulse echo examination instead of shear waves. Tomlinson et al[3] had reported very similar attenuation data for Inconel 182 weld metal and alpha brass while their results on a single crystal of nimonic 80A proved that the attenuation variations are not due to a grain boundary

effect. Nevertheless, these anisotropic effects are not significant in measurements made on samples of rolled plate which is made up of a relatively homogeneous distribution of equiaxed grains.

While there have been numerous studies of the compositional and metallurgical phase variations in austenitic weld metal, there is a marked lack of published data on the detailed variation of the elastic properties of the material. However, X-ray diffraction results by Baikie et al(1) and Kupperman and Reimann(4) show a strong alignment of the 100 crystallographic directions of the face centred cubic structure of the weld metal along the long axis of the columnar grains. Theory indicates that such a structure will produce anisotropy of the type observed whether or not the grains are aligned in the plane perpendicular to their axes, and also lead to the deflection of ultrasound beams because the wave fronts are no longer necessarily normal to the propagation direction. Figure 2 illustrates this beam skewing phenomena with a comparison of some theoretical and experimental data for the angle of deviation of the beam of longitudinal (Cp) waves propagating through a block of weld metal.

Qualititatively similar effects are observed for shear waves. For S_V waves the skewing effect is greater than for Cp waves, and opposite in direction for most beam angles(5), and this contributes to the well known signal to noise ratio problems but the effect appears less for S_H waves(4,5). However, the use of S_H waves is currently impracticable for most applications and the remainder of this paper will be mainly confined to the consideration of longitudinal waves in order to investigate their potential effectiveness for NDT when utilising their advantage in signal to noise ratio. An important aspect, however, is the need to appreciate factors which mean that a longitudinal wave probe cannot be regarded as if it were merely a novel variety of shear wave probe.

3. STUDIES USING ARTIFICAL REFLECTORS

As part of the investigation of the effect of weld structure on ultrasound propagation, 1½mm diameter side drilled holes were introduced into several welds and they were examined with a series of probes using both manual and automated techniques. Table I shows the results of measurements of beam angle in a specimen of Type 316 rolled plate for the five longitudinal wave angle probes prepared using a series of perspex wedges and a 12mm diameter commercial transducer.

Reflections from the holes that could be detected in the weld specimens one and two were maximised and the range, probe position and reflection amplitude recorded. The welds were examined from either side and from both the upper and lower surfaces and it was generally found that the effective beam angle differed from that in plate material. Detailed examination of the data revealed that the longitudinal waves propagate along preferred paths at 45° to the long axis of the columnar grains.

This is illustrated in Figure 3 and may be seen to agree with qualitative expectations from Fig 2 where the variation of beam skewing for the angles reported in Table I is such as to deflect a beam towards the 45° preferred direction. In contrast, for a conventional normal compression probe examination there is a defocusing effect which results in major beam bending as is also shown in Figure 3 for weld specimen two.

The differences between the grain structures of the weld specimens one and two produce significant differences in the ultrasound propagation directions and indicate that relatively small differences in the detailed fabrication procedures are important. Work on the third specimen emphasises this. Figure 1c shows the grain structure of a weld produced in the horizontal-vertical position with appropriate choice of preparation while the welds depicted in Figures 1a and 1b were produced down-hand. For the horizontal-vertical weld the beam from a normal compression probe is favourably inclined to the grains whereas an angled beam is not, which is in direct contrast to the situation for the down-hand samples.

Clearly, the fact that the ultrasound propagation direction is a function of the grain structure makes it very difficult to accurately locate a reflector from probe position and A scan data in the conventional manner. From the data obtained during the examination of the two down-hand welds it was observed that the range values were approximately correct for the direct distance between probe emission point and reflector in spite of the beam skewing phenomena. Using a flaw detector calibrated using rolled plate velocity data the average range error was 2-5% and it was found that holes could be located satisfactorily by a triangulation technique provided that they were detectable from both sides of the weld. This is illustrated in Figure 4.

Finally for the MMA welds, the relative amplitudes of the maximum signals reflected from the holes in the down-hand welds were measured using the calibrated gain control of a flaw detector for the angle beam examinations and the results are shown in Figure 5. For each specimen the range of amplitudes for the reflections from side drilled holes is 8-12dB but the signal to noise ratio is at least 15dB which is high for austenitic welds.

Since the beam skewing and variable apparent attenuation are apparently confined to the weld metal it is of interest to examine the results obtained from an examination of narrow gap welds. The study has therefore included welds made by a special Tungsten Inert Gas (TIG) and an electron beam welding process which yield a smaller volume of weld metal than the MMA process and which can have a very different dendrite structure as shown in Figure 6.

As anticipated the beam paths in weld metal were found to be sufficiently short for beam skewing effects to be negligible for longitudinal waves while, in contrast to Figure 5, the variations in signal amplitude shown in Figure 7 are such that a useful distance amplitude correction curve can be constructed which would facilitate automated sentencing.

Figure 8 compares the results of simple automated raster scans of the electron beam weld using 45° shear and longitudinal waves. A wide time gate was used and in the illustration the amplitude of the gated signal is superimposed on the co-ordinate corresponding to the position of the probe emission point along the weld centre line which is marked. The side drilled holes are clearly detected but also of significance is the large signal generated by the fusion face during the shear wave examination.

For shear waves, the signal from the fusion face is greater than that for a 1½mm side drilled hole in the weld metal whereas the reverse is true for longitudinal waves. This result may be explained qualitatively by two effects. First there is a 25% difference between the velocity of S_V waves in plate and in the 45 degree direction in weld metal, but only a 5% difference for longitudinal waves. Thus the acoustic impedance mismatch at the fusion boundary is larger for the shear waves than for the longitudinal waves. Secondly, longitudinal waves are only weakly reflected by right angle corners as strong shear wave components are produced by mode conversion(7). Qualitatively similar effects were observed in our corresponding measurements on the narrow gap TIG weld but the shear wave signals from the fusion face were much weaker than for the electron beam weld. This difference presumably derives from the different grain direction shown in Figure 6 and the greater roughness of the fusion face in this TIG weld specimen.

4. STUDIES USING DELIBERATELY INDUCED DEFECTS

In order to examine the application of angled longitudinal wave techniques to actual inspections a number of deliberately defective MMA welds have been prepared using down-hand techniques. These specimens will ultimately be examined destructively to confirm the effectiveness of the examination techniques under laboratory conditions.

The weld defects used in the study included lack of fusion and cracking introduced into different positions in the section of welds with single Vee, double Vee and 'U' preparations. After welding the specimens were machined flat on all surfaces to remove the excess root penetration, the cap, and all distortion produced by welding.

All the welds were tested with angled and normal 2¼MHz longitudinal wave single crystal probes using both manual and automated techniques. A 12½mm diameter probe was used for the normal scans and for the angled scans a 25mm dia probe mounted on a 21° perspex wedge to give a nominal 45° beam. During the manual scans the probe was skewed slightly to maximise the signal but for the automated scans the beam centre line was kept normal to the weld centre line.

As with the samples containing artifical reflectors the specimens were examined ultrasonically from both sides of the weld using both upper and lower surfaces, and, in addition, an

orthodox radiographic examination was carried out.

Figure 9 illustrates the results for a lack of fusion defect for which the A scans were recorded in digital form during an automated examination in the geometry indicated in Fig 8a. These A scans are reproduced as a time series display in Fig 8b and the approximate location of the fusion boundaries sketched in. The echoes which originated from the region of a planned defect are clearly apparent.

The value of the exercise will be fully assessed on completion of the destructive examination but, if it is assumed that the deliberate defects are approximately of the size intended, then the work indicates that fairly small defects can be detected in the laboratory.

5. DISCUSSION

The work reported here confirms that ultrasound propagation is governed by the weld structure and hence that the fabrication procedure is very important. Indeed the effectiveness of any inspection using these techniques cannot be assessed without some knowledge of the grain structure. Therefore it is not possible to assess the effectiveness of an inspection solely with the use of data gathered during the inspection, weld fabrication data are essential.

A predictable grain structure is a pre-requisite for the use of these techniques but it is not clear that they could be used for welds produced by all available welding procedures. Thus some welding procedures produce columnar structures with little evidence of epitaxial growth from one weld run to another, as shown in Figure 10, and it is apparent that there will be no continuous preferred paths through such a weld. Further work is required to investigate the inspectability of a wider range of weld structures using longitudinal waves and, in particular, work is in progress on the effect of variations in the manual metal arc welding procedure.

The data of Figures 5 and 7 clearly indicate that signal amplitude is not a good guide to the size of any reflector while the spatial variation of the magnitude of beam skewing and consequent focusing effects rule out the use of dB drop techniques. Moreover, it is clearly virtually impossible to generate a useful DAC curve applicable to MMA welds and one of the most promising techniques to overcome this sizing problem is that under development by Silk(6) which is based on time of flight measurements of the diffracted signals from the edge of defects.

In addition to the problems referred to above and to the normal evolution required to convert laboratory techniques into field inspection procedures, application of ultrasonic inspection procedures to ISI of LMFBR involves consideration of a number of other important factors. Problems arising from the inspection temperature and choice of couplant are generally recognised, while the selection of calibration blocks has been

referred to above, but it is also necessary to consider the effects of sodium ingress on the detectability of surface breaking defects. Theoretical work by Temple(8) using idealised models clearly indicates that there is a threshold of crack width in the 10-100μ range below which the ultrasonic reflectivity of a sodium filled crack may be expected to decrease significantly.

Work in this area continues as part of the overall task of ensuring, in collaboration with the welding development engineers, that techniques are available to permit adequate inspection of LMFBR welds.

From a comparison of the results of the manual and automated examinations it may be concluded that the latter are generally more satisfactory and studies are in progress at RNL on the possible application of Pattern Recognition Techniques to further increase their effectiveness.

This paper has described experimental investigations on the application of longitudinal waves using probes with a centre frequency of 2¼MHz. Further work is required to investigate the possibility of there being an optimum frequency range of the type reported by Lautzenheiser and Greer(9) when using shear waves for the examination of thinner sections of austenitic material.

6. CONCLUSIONS

The experimental investigations described in this paper demonstrate that angled longitudinal waves show great promise as a practical inspection procedure for the detection of defects in austenitic welds. Nevertheless, since the propagation of ultrasound in austenitic weld metal is determined by the columnar structure of the weld, it is apparently essential that the fabrication procedure should be such as to yield a predictable, well ordered, grain structure and details of this procedure must be available to the ultrasonic examiner.

7. ACKNOWLEDGEMENTS

The permission of the Managing Director of the UKAEA, Northern Division to publish this paper is gratefully acknowledged.

8. REFERENCES

1. BAIKIE B L, WAGG A R, WHITTLE M J and YAPP D. 'Ultrasonic Inspection of Austenitic Welds'. IAEA/IWGFR Specialists Meeting on In-service Inspection and Monitoring of LMFBR's. Bensberg. March 1976.

2. LAUNAY J P, PETEUIL M and TRUMPFF B. 'Contribution to the improvement of ultrasonic testing of bi-metallic welds'. Presented to Conference on 'Periodic Inspection of Pressurised Components'. IMechE Conference Publications 1979-4 Paper C51/79 pp225-234.

3. TOMLINSON J R, WAGG A R and WHITTLE M J.
"Ultrasonic Inspection of Austenitic Welds". Second International Conference on Non-destructive Evaluation in the Nuclear Industry. Salt Lake City, February 13-15, 1978.

4. KUPPERMANN D S and REIMANN K J.
Effect of shear wave polarisation on defect detection in stainless steel weld metal. Ultrasonics. January 1978, pp21-27.

5. SILK M G, LIDINGTON B H and HAMMOND.
A Time Domain Approach to Crack Location and Sizing in Austenitic Welds. The Brit. J. of NDT - March 1980. Vol 22. No 2. pp55-61.

6. HUDGELL R J and SEED H.
Ultrasonic longitudinal wave examination of austenitic welds. The Brit. J. of NDT - March 1980. Vol 22, No 2. pp78-85.

7. KRAUTKRAMER J and H.
Ultrasonic testing of materials. Springer-Verlag, 2nd Edition, Section 1.63.

8. TEMPLE J A G.
Calculations of the reflection and transmission of ultrasound by cracks in steel filled with liquid sodium. Ultrasonics 1980 (to be published).

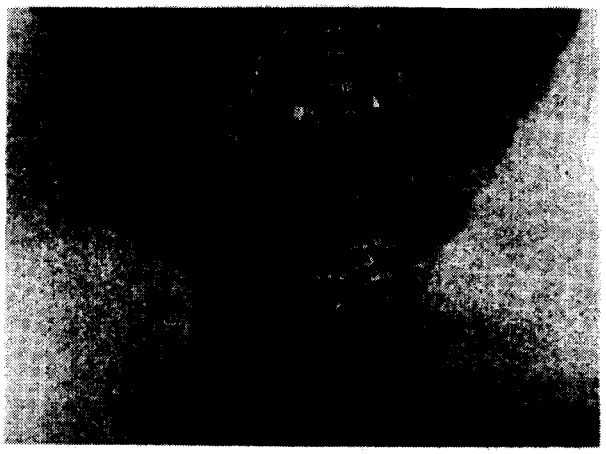
9. LAUTZENHEISER C E and GREER A S.
Ultrasonic inspection for stress, corrosion cracking in stainless steel. Presented to Conference on 'Periodic Inspection of Pressurised Components'. IMechE Conference Publications 1979-4. Paper C50/79. pp219-224.

TABLE I

LONGITUDINAL BEAM ANGLES IN 316 PLATE PRODUCED BY VARIOUS PERSPEX WEDGE ANGLES

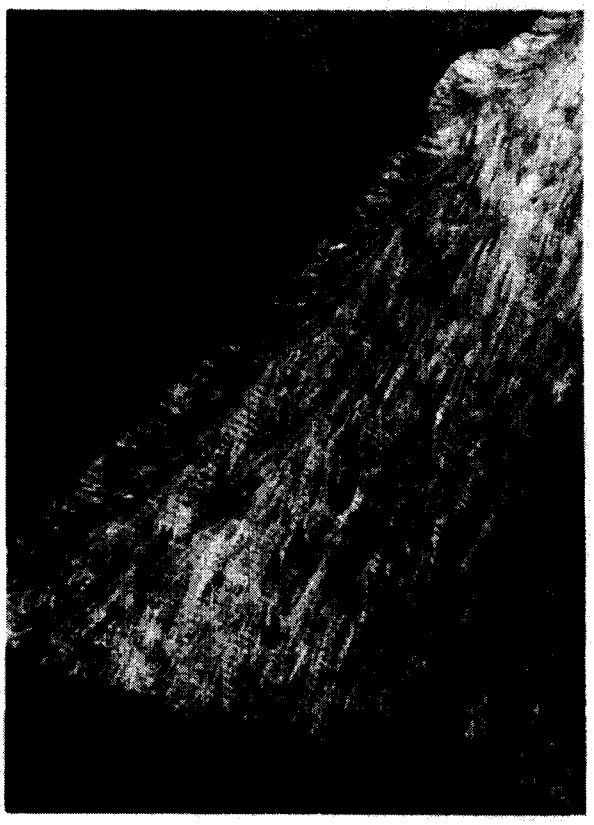
Perspex Wedge Angle (Degrees)	Beam Angle in Plate (Degrees)
18	39
19.5	42
21	48
22.5	51
24	57

(a) Specimen 1





(b) Specimen 2



(c) Specimen 3

FIG 1 MACROGRAPHS OF THREE MANUAL METAL ARC BUTT WELDS IN 50mm THICK PLATE

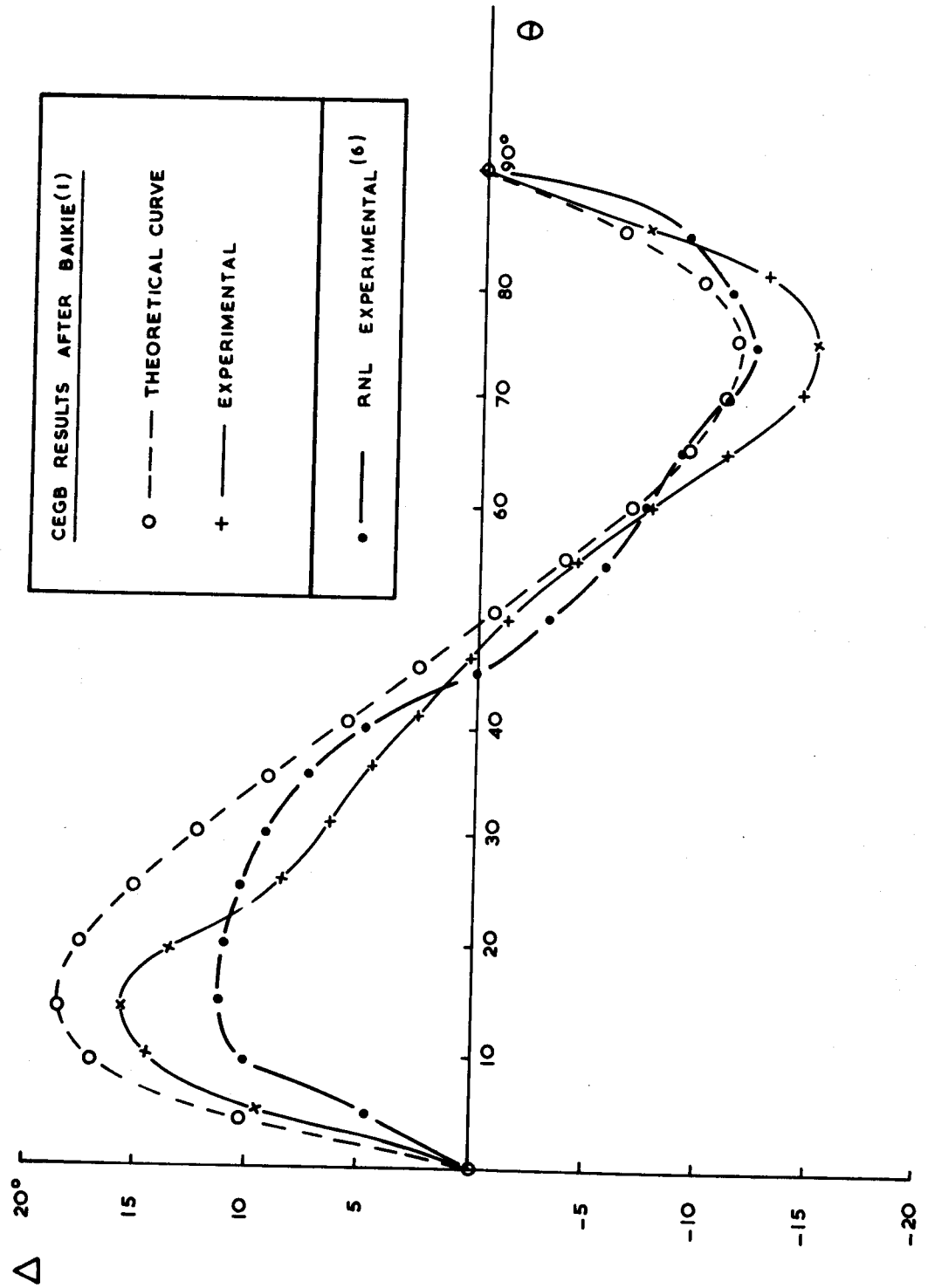


FIG. 2 SKEWING ANGLE Δ AS A FUNCTION OF THE ANGLE Θ BETWEEN THE NORMAL TO THE WAVE FRONT AND THE COLUMNAR GRAIN AXES

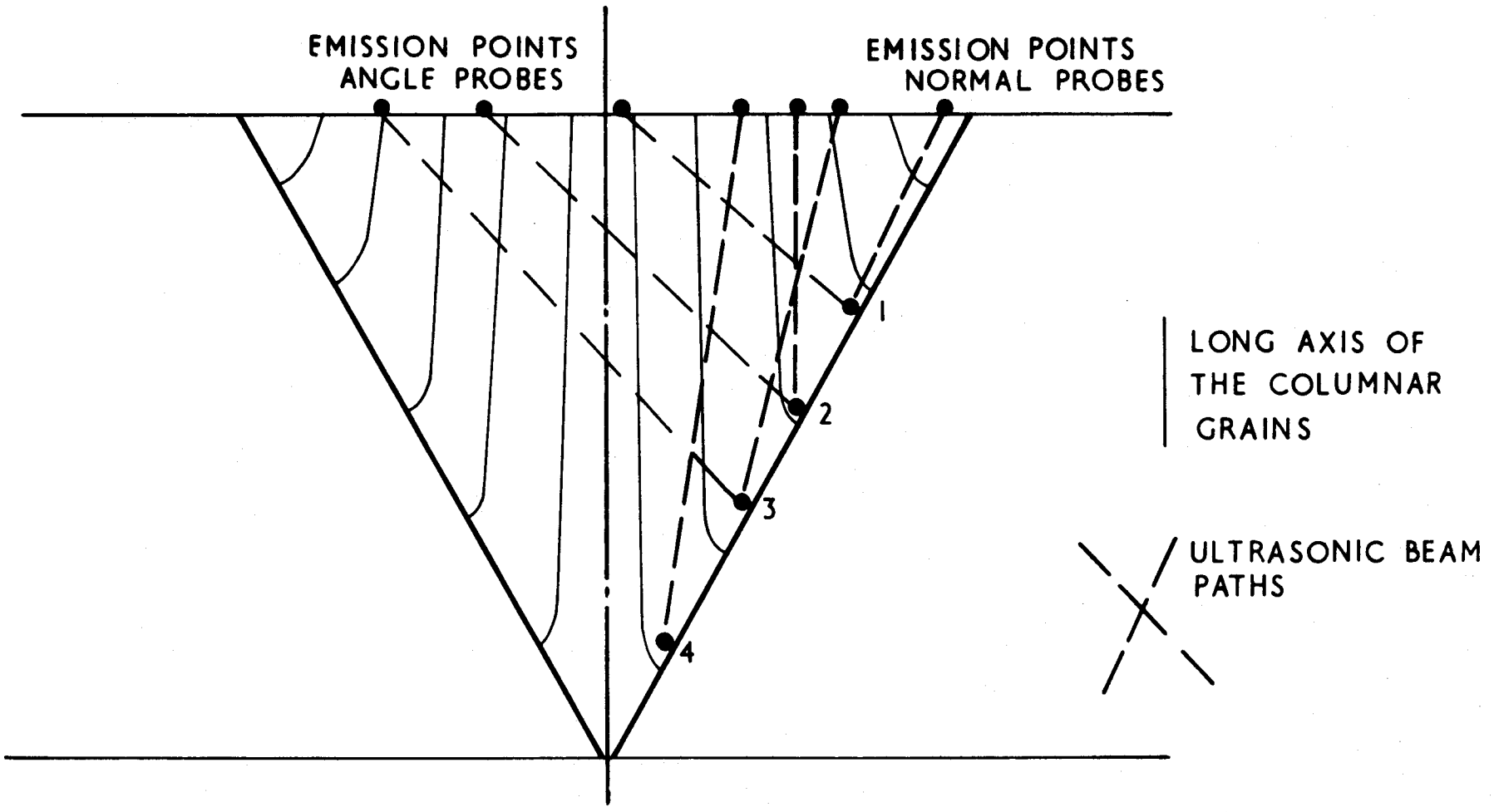
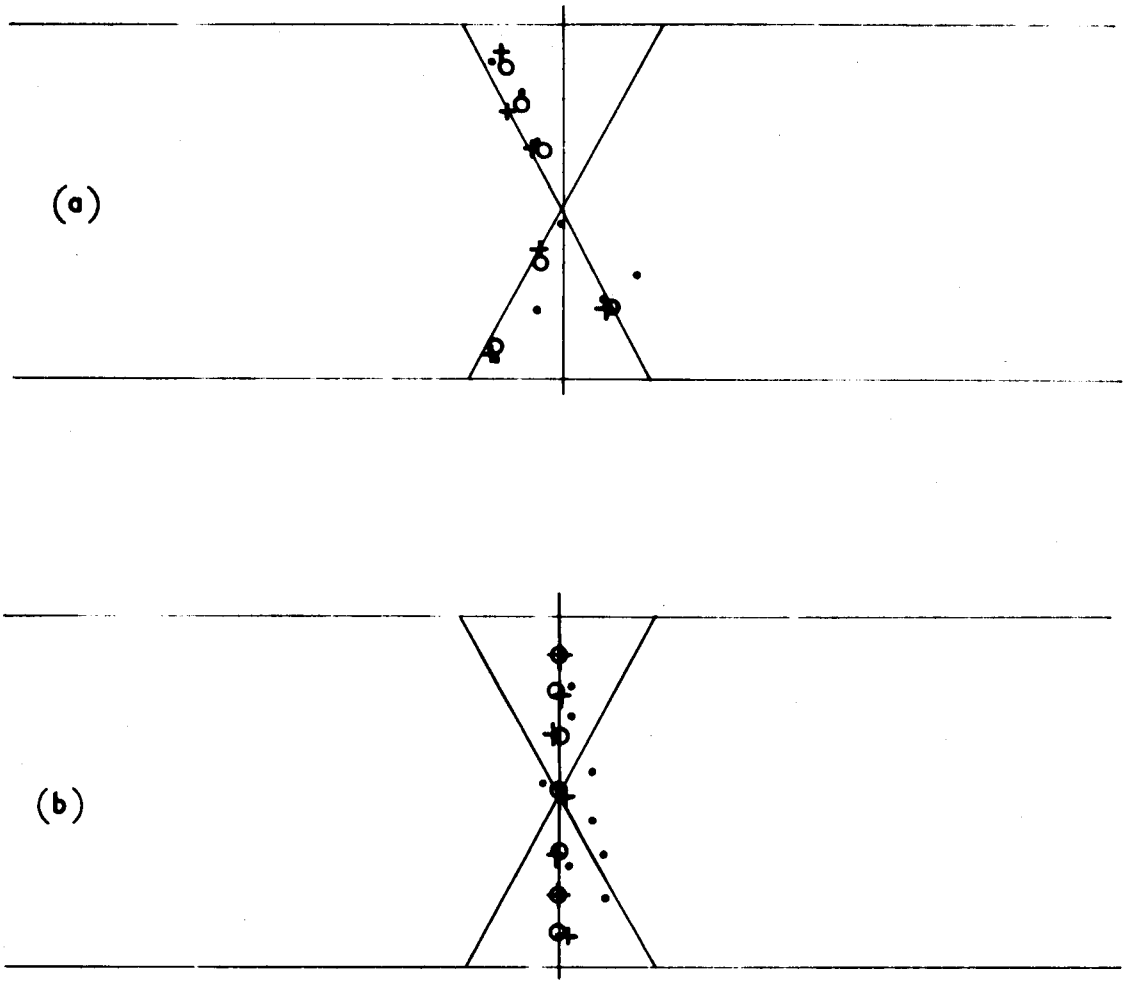


FIG. 3 THE DIRECTIONS OF THE MOST INTENSE PART OF BEAMS USING NORMAL / ANGLED PROBES FOR SPECIMEN 2



o SIDE DRILLED HOLES

• REFLECTOR POSITIONS USING CONVENTIONAL METHOD

+ REFLECTOR POSITIONS USING TRIANGULATION METHOD

FIG. 4 A COMPARISON OF REFLECTOR LOCATION USING CONVENTIONAL AND TRIANGULATION METHOD FOR AN MMA WELD

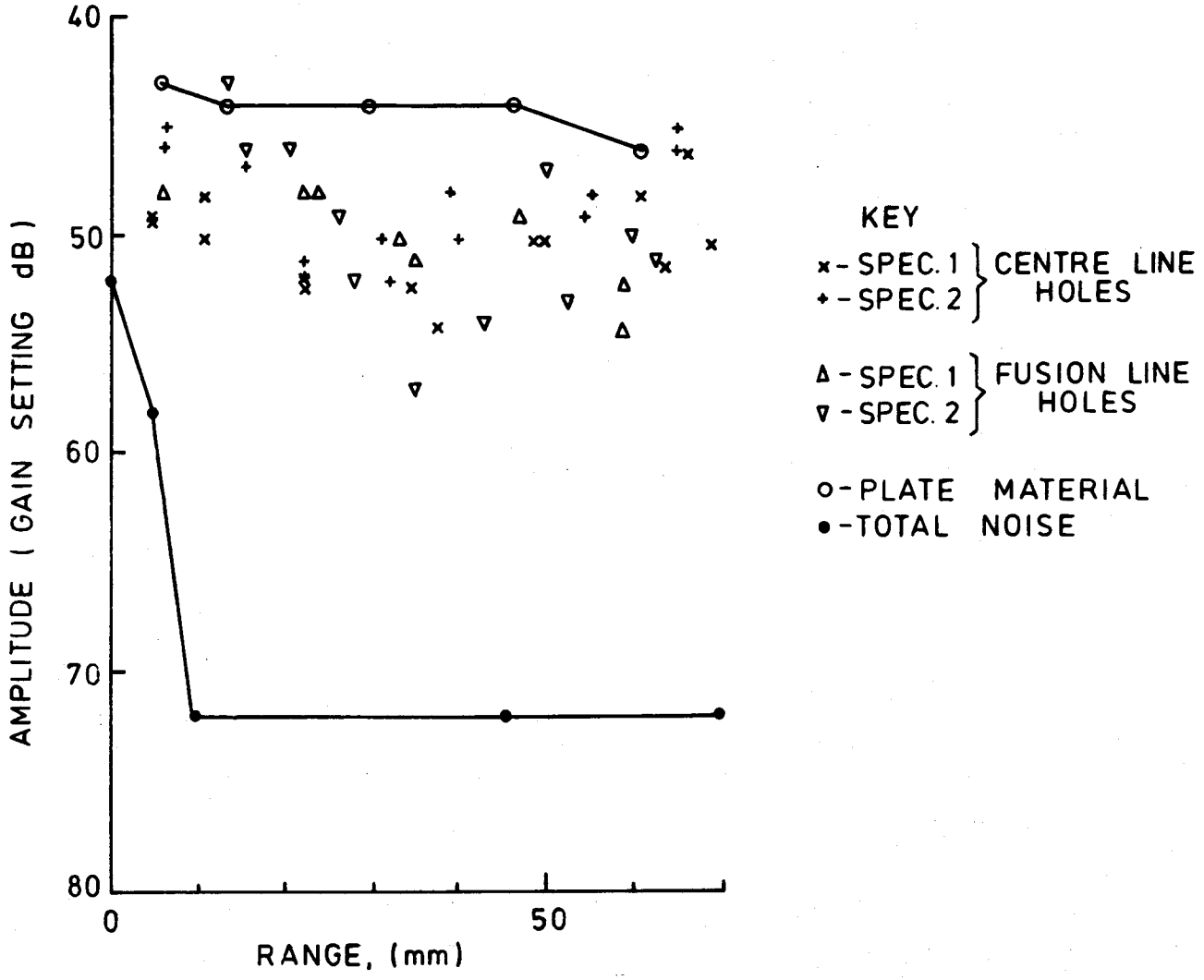
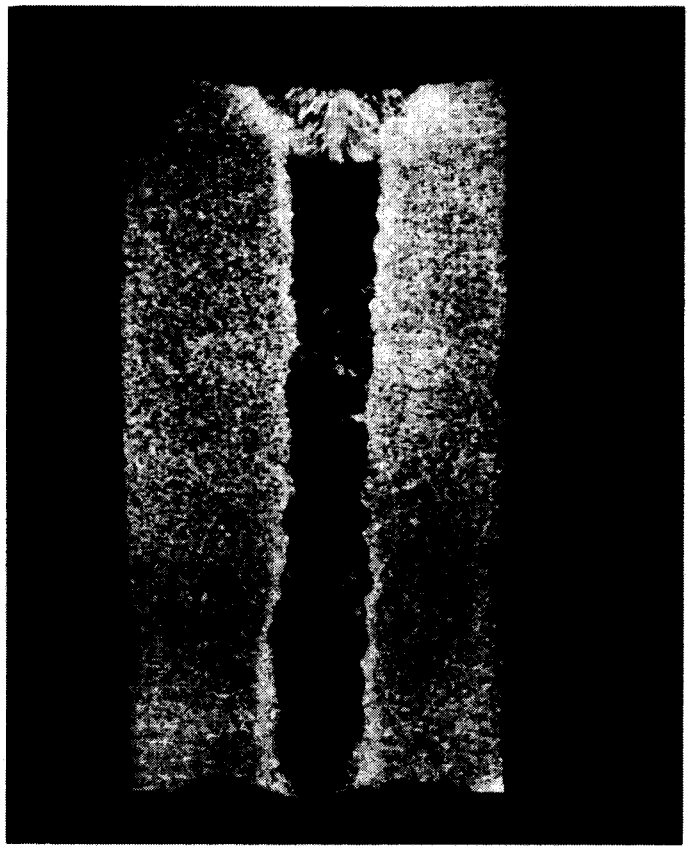


FIG. 5 AMPLITUDE RESULTS FOR DOWNHAND MMA WELDS WHEN EXAMINED FROM THE CROWN

(a)



TUNGSTEN INERT GAS WELD

(b)



ELECTRON BEAM WELD

FIG 6 MACROGRAPHS OF TWO NARROW GAP WELDS

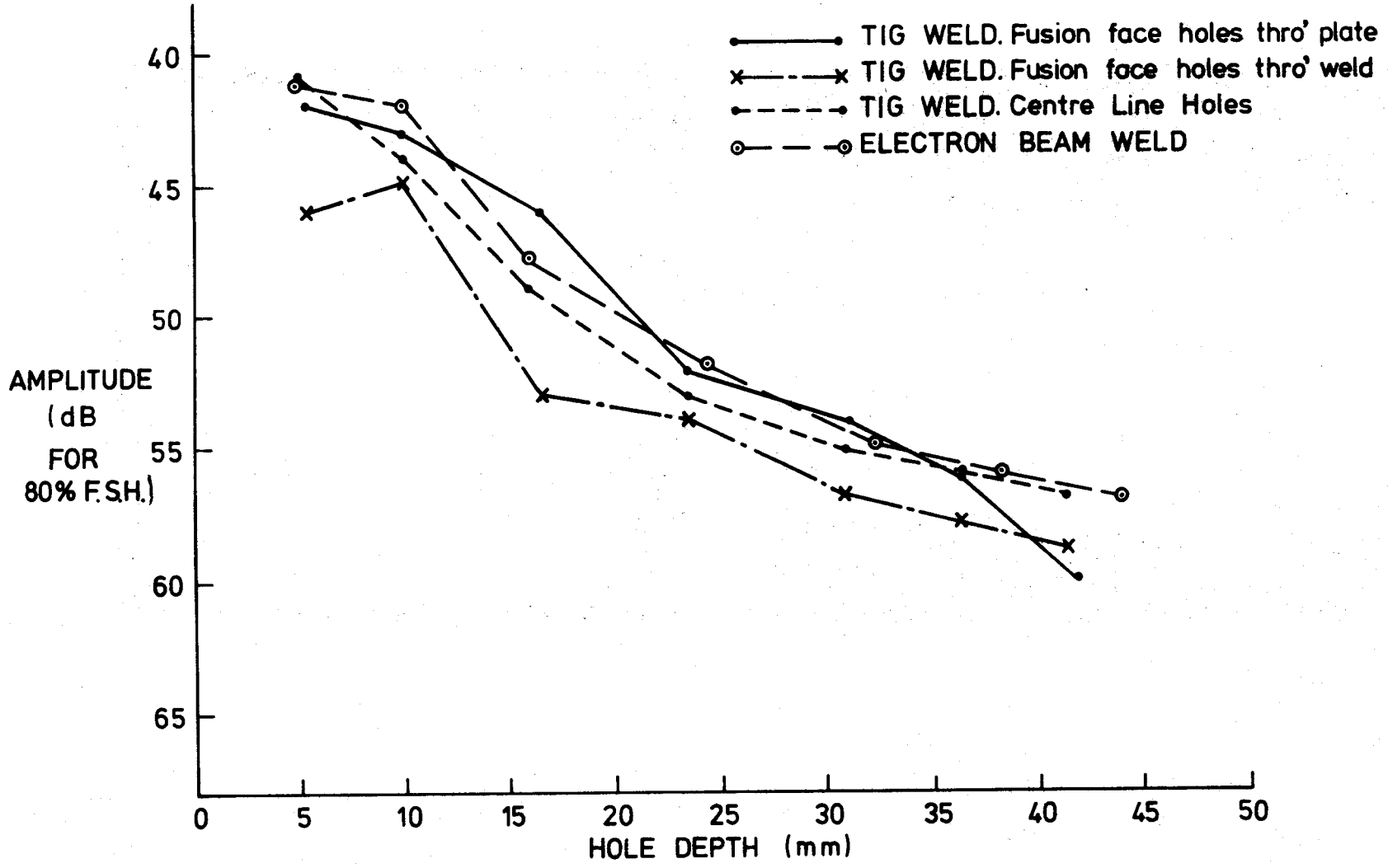


FIG. 7 AMPLITUDE RESULTS FOR TWO NARROW GAP WELDS WHEN EXAMINED FROM THE CROWN

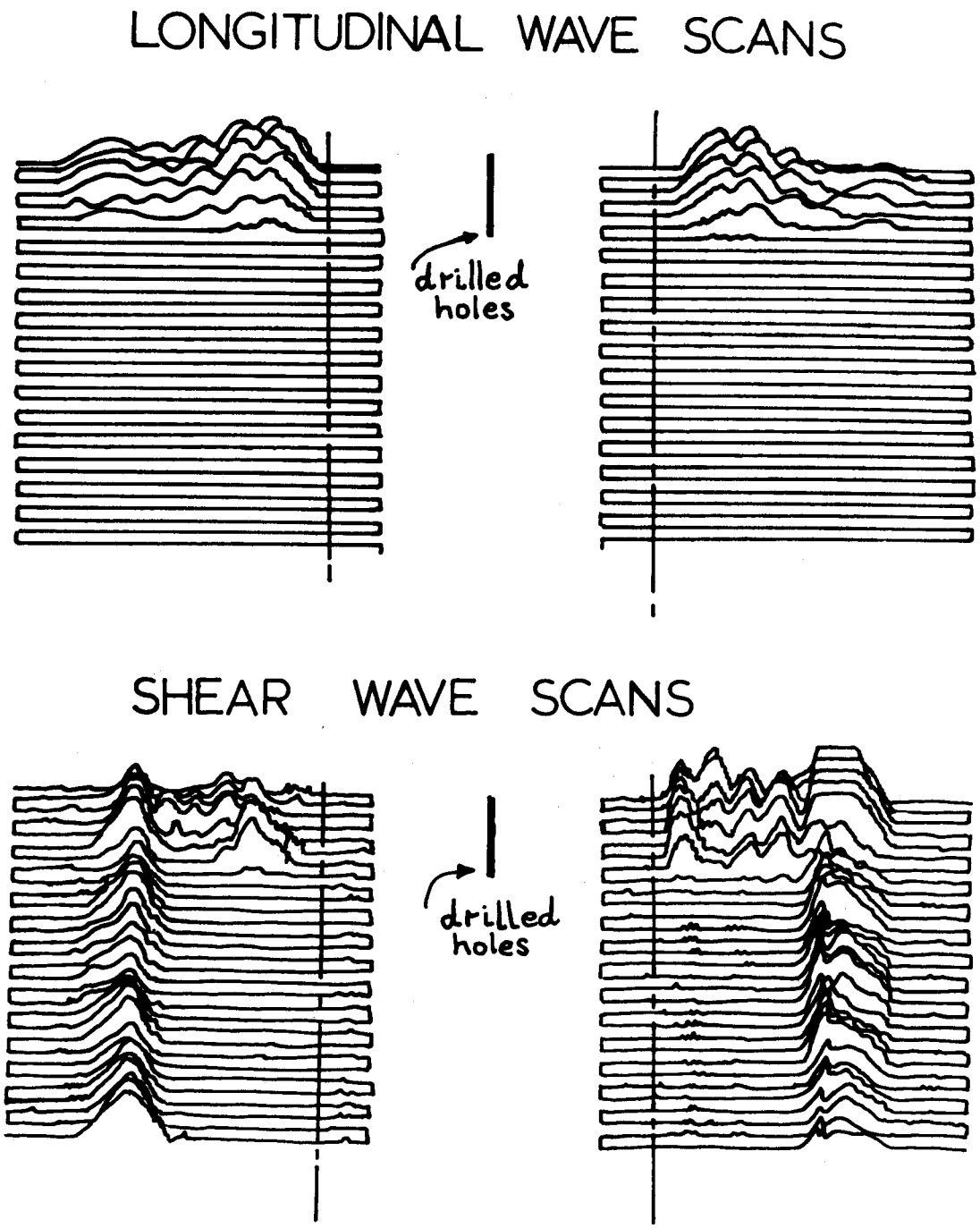
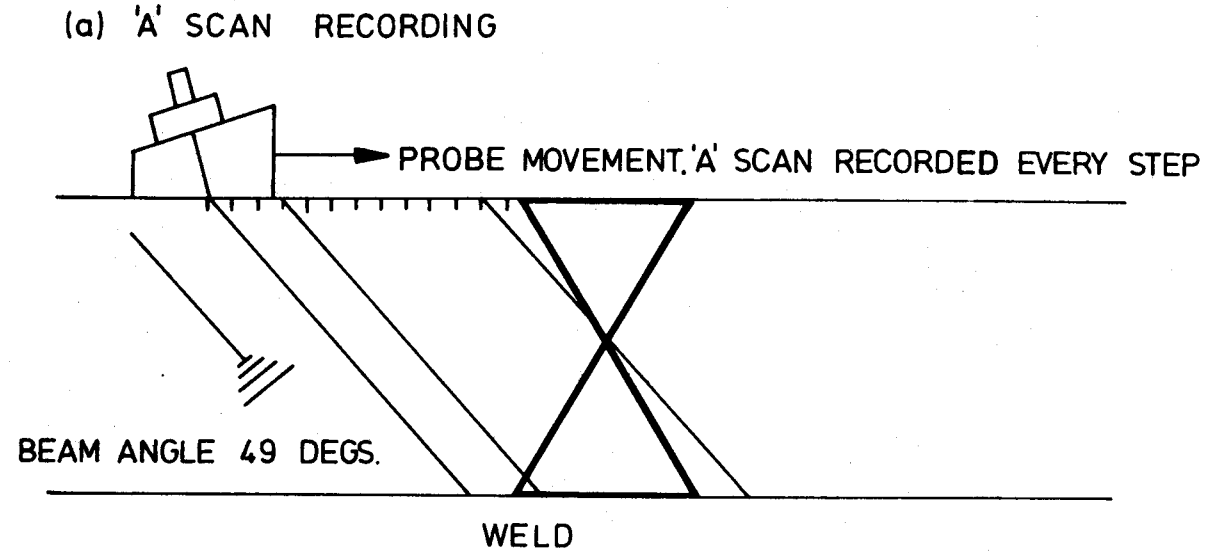


FIG. 8 RESULTS OF AUTOMATED SCANS, ANELECTRON BEAM WELD



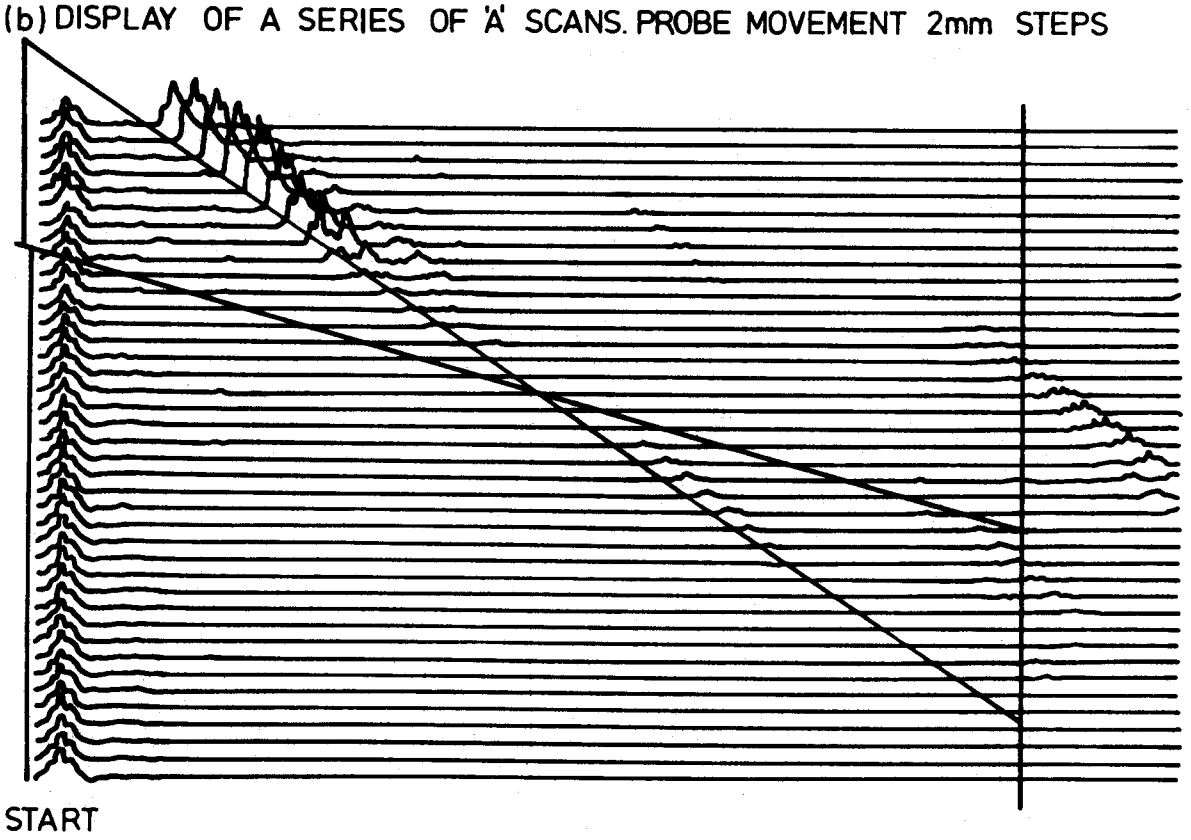
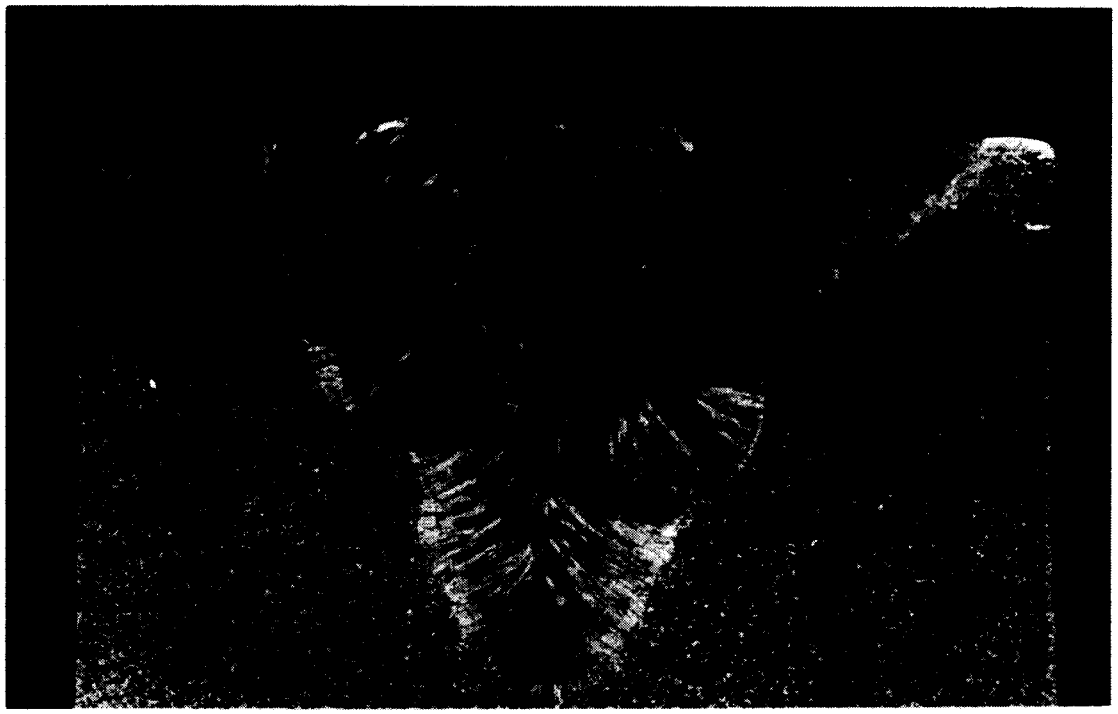


FIG. 9 THE RECORDING AND DISPLAY OF A SCAN DATA FOR A DELIBERATELY DEFECTIVE WELD



MACROGRAPH OF A SUBMERGED ARC BUTT WELD IN 25mm THICK PLATE

FIG. 10

Ultrasonic testing technique of fuel cladding tubes for FBR - Grass echo suppression technique

M. IGARASHI, T. SHIBATA, M. MIURA
Power Reactor and Nuclear Fuel Development Corporation, Japan

ABSTRACT

Type 316 stainless steel is applied for the fuel cladding tubes of FBR in Japan. Flaw of tubings are detected into details by ultrasonic test before those are constructed to fuel pins. The grain size of the stainless steel give an effect upon the results of the ultrasonic test. Especially when the grain size grows larger, grass echo increases and at the same time sensitivity of flaw detection deteriorates. To resolve the problems pointed out before, ultrasonic testing techniques to suppress grass echo is undergone. As a result of the test, two effective methods are found out. One is to give the adequate position of the ultrasonic transducers and another is to set characteristic frequency of the flaw detector's amplifier by that of transducers resonance frequency.

1. INTRODUCTION

Type 316 stainless steel is applied for the fuel cladding tubes of FBR in Japan.
The grain size of the stainless steel gives an effect upon the results of the ultrasonic test before those are constructed to the fuel pin.
When the grain size become larger, grass echo increase and at the same time sensitivity of flaw detection deteriorates.
To resolve the problems, ultrasonic testing techniques to suppress grass echo for large grain cladding tubes were developed.

2. TEST METHOD

2.1. Flaw detectors and transducers

The characteristics of the flaw detectors and transducers adopted to the tests are listed in Table 1.
To investigate the effect of the incident angle and of the flaw detectors upon the grass echo, UM-721 is used. NDT-102S and Mark II are used to examine the correlation between the frequency range and the grass echo.
To inspect thin wall specimen, focussing type transducer are necessary. Trial to suppress grass echo are undertaken with transducers of 0.3 and 0.5 mm in beam focus diameter.

2.2. Standard specimen

Standard specimens for the ultrasonic test are shown in fig. 1 and 2. These specimens are prepared to have different grain sizes. Artificial flaws are made at both the outside and inside surfaces of the standard specimens by the Electron Discharge Machining (EDM) method.

The reflector depths is given in both figure 1 and 2 in percent of wall thickness. Three levels, 5 %, 7 % and 10 %, are adopted as the nominal depth at Power Reactor and Nuclear Fuel Development corp'. And among these three nominal depths, the 7 % is used as the standard reference for judging of the integrity of fuel cladding tubes. The depth and the direction of flaws are given in both figures 1 and 2.

2.3. Ultrasonic testing method

Brief operation diagram of the ultrasonic testing method is given in fig. 3. Condition of ultrasonic test is summarized as follows,

1) Signals from inside and outside artificial flaws are adjusted at the same level.
2) Signals from artificial flaws are adjusted in proportion to the depth.
3) Signals levels from 7 % depth artificial flaws are adjusted to be larger than noise level.

The ultrasonic flaw detection tests are classified into two methods : either manually moving specimens or automatically moving them. The former is called "manual test" and the latter "automatic test".

3. RESULTS OF ULTRASONIC TEST

3.1. Transducer of 0.3 mm focus diameter

Result of the ultrasonic test for specimen no 1 which has small grain size is shown in fig. 4. The ultrasonic signal from inside and outside artificial flaws is proportional to the depth and no grass echo appears. The photograph inserted in the figure shows the signal of artificial flaws observed on an oscilloscope.
Fig. 5 shows result of ultrasonic test for specimen no 2 which has large grain size (ASTM grain size number 7.5). At this time, a grass echo which is equal to 10 % of the thickness of a cladding tube appears.
Under this circumstance the sensitivity of the flaw detection test is deteriorated. Larger the grain size is, higher the level of grass echo grows, and the inspection of 7 % thickness flaw becomes difficult.

The relation between incidence angles, longitudinal artificial flaw echoes and grass echos is found out with the manual test (fig. 6).
At maximum amplitude of artificial flaw echos, the level of grass echo remains low. The incidence angle at which signal levels of both inside and outside flaws are equal, is 25° and this angle is suitable for ultrasonic test. The results of the manual test of circumferential flaw are shown in fig. 7. About 24° is the proper incident angle for the circumferential flaw detection test.
For practical reasons, the automatic tests which simulate the actual conditions are undergone.
Fig. 8 shows the results of the automatic tests.
After the tests on the standard specimen that has large grain size with transducers of 0.3 mm focus diameter, the following two points become clear.

1) The detection of longitudinal 7 % thickness flaw is possible.

2) Echoes from circumferential 7 % thickness flaw are almost at the same level as of grass echoes and the detection is difficult.

3.2. Transducer of 0.5 mm focus diameter

The result obtained with the standard specimen no 2 using automatic test and the transducer of 0.5 mm focus diameter is shown in fig. 9.
When the incidence angle for the longitudinal direction is 23°, which is almost the same as that of transducer of 0.3 mm focus diameter, the incidence angle for the circumferential direction is 22.2°.
As may be seen from the fig. grass echoes were equivalent to those obtained on 7 % thickness reflectors for the circumferential direction.
When the detection of longitudinal flaws is made easy, the detection of circumferential ones is difficult.

3.3. Adjustment of transducer position for the detection of circumferential flaws

Fig. 10 shows the result of the ultrasonic test for the circumferential flaws of the standard specimen no 2.
When the incidence angle reaches 24.6°, the grass echoes decrease below the level of the 7 % thickness flaw echoes.
As this point, the linearity between the depth of artificial flaws and the level of flaw echoes is not observed.
Using the phenomenon that the grass echo is more attenuated than artificial flaw echoes, a trial to suppress the grass echo is made.
Measuring the flaw echoes after multiple reflection the air-metal interface is one of the simplest method to confirm the assumption.
In this purpose, the echoes were measured after 5 reflections. The results of the measurement are shown in fig. 11. When the incidence angle comes to 26°, the grass echoes fall below the 7 % thickness flaw echoes.
However it is necessary to use additional amplification for compensating for the attenuation due to the propagation over long distances.

3.4. The flaw detector and grass echo

Using the specimen with large grain size (ASTM grain size number 7.5), the relation between the frequency range of the flaw detector and the grass echo is examined.
At that time, the incidence angle of 24.5° is applied. Fig. 12, 13 and 14 indicates the relation between the frequency and the signal level of the standard specimen no 2. Grass echo is inclined to decrease when the transducer resonance frequency lies inthe lower frequency range af the flaw detector frequency response.

4. CONCLUSION

1) The circumferential ultrasonic detection of flaws in cladded fuel tubes is found more difficult than that of longitudinal ones.

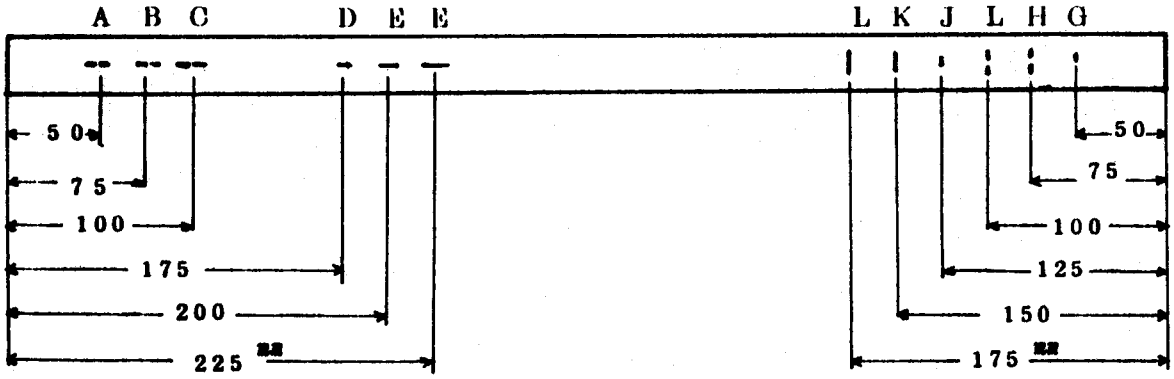
2) The accurate adjustment of the incidence angle is effective to suppress grass echo. An incidence angle of about 25° is good for the detection of the circumferential flaws according to this program.

3) Grass echo is inclined to decrease when the transducer resonance frequency lies in the lower frequency range of the flaw detector frequency response.

Flaw No	Longitudinal			Side	Flaw No	Circumferential			Side
	Depth	Width	Length			Depth	Width	Length	
A	4.9%	31μm	0.73mm	in	G	4.9%	27μm	0.72mm	in
B	7.2	32	0.74	"	H	6.9	28	0.73	"
C	9.3	33	0.73	"	I	9.1	29	0.72	"
D	5.0	26	0.73	out	J	4.9	26	0.73	out
E	7.1	28	0.73	"	K	7.1	28	0.73	"
F	9.1	28	0.74	"	L	9.1	28	0.73	"

inside diameter 5.6mm
outside diameter 6.5mm
thickness 0.45mm

Position



ASTM Grain size No=9.0

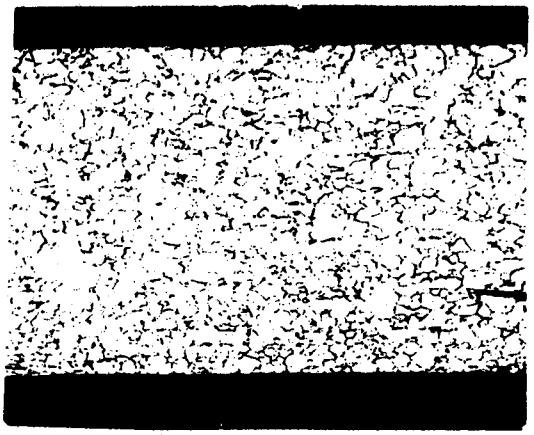
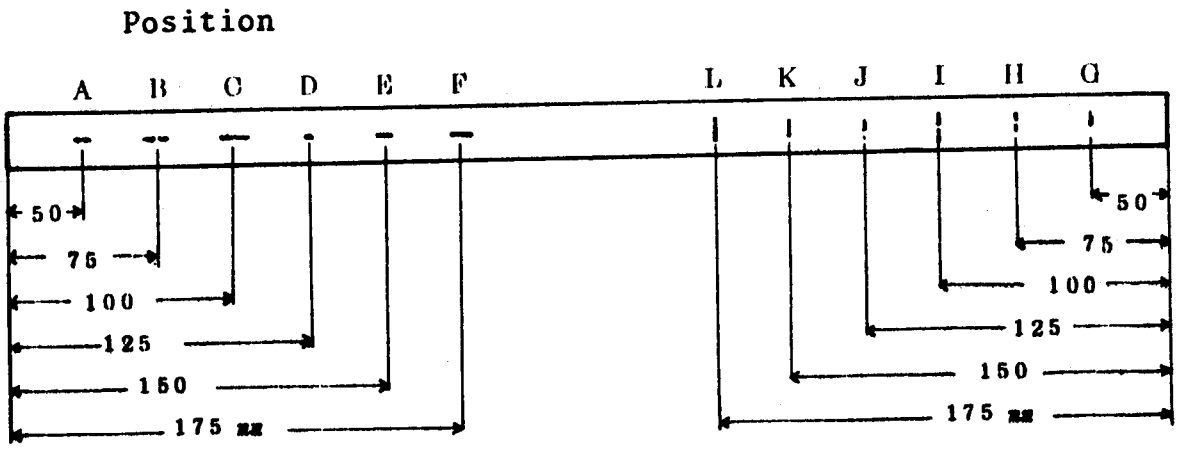


Fig.1. Summary of artificial flaw for standard specimen No1

Flaw No	Longitudinal			Side	Flaw No	Circumferential			Side
	Depth	Width	Length			Depth	Width	Length	
A	4.6%	31μm	0.76mm	in	G	4.6%	30μm	0.76mm	in
B	7.4	31	0.76	"	H	7.0	31	0.76	"
C	9.2	34	0.77	"	I	9.2	33	0.76	"
D	4.8	30	0.77	out	J	4.9	30	0.77	out
E	6.8	30	0.77	"	K	7.1	30	0.77	"
F	9.3	30	0.77	"	L	9.4	30	0.77	"

inside diameter 5.6mm
outside diameter 6.5mm
thickness 0.45mm



ASTM Grain size No=7.5

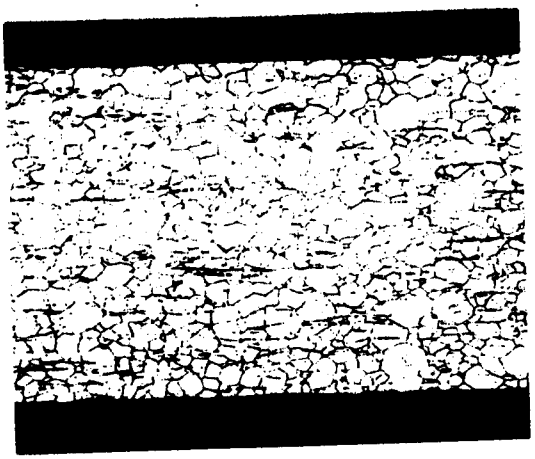


Fig.2. Summary of artificial flaw for standard spesimen No2

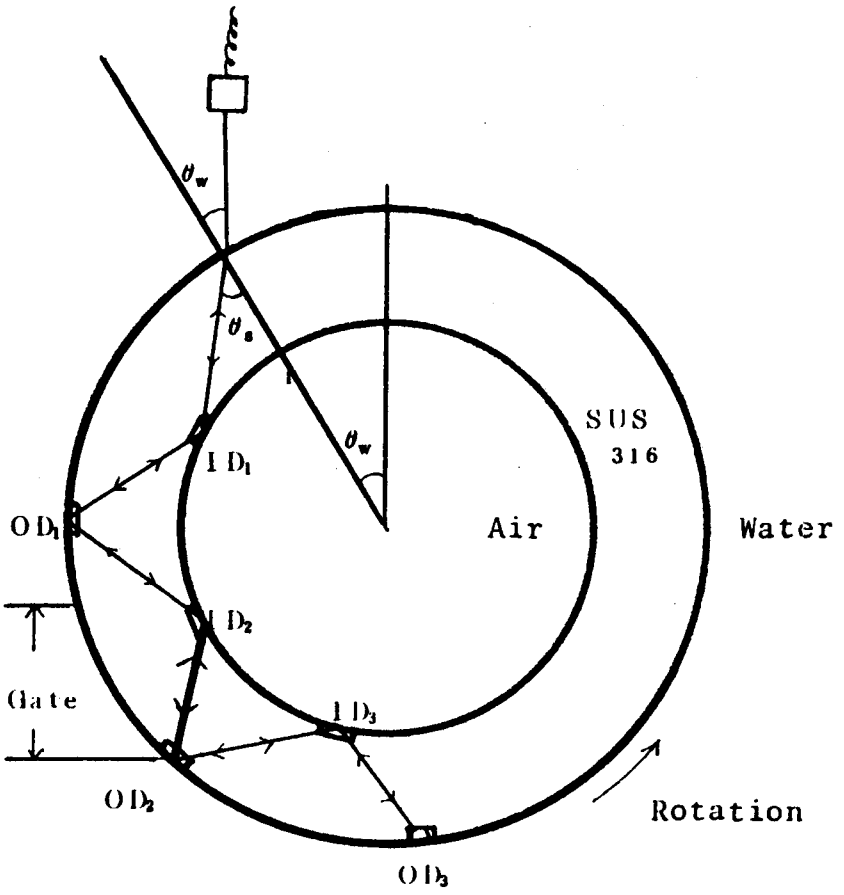
Flaw detectors

Name	NDT-102-S	UM 721	MARK II
Pulse Interval	6KHz	2KHz	10KHz
Frequency Range	7.0-16.9MHz	8.0-12.6MHz	3.4-12.6MHz

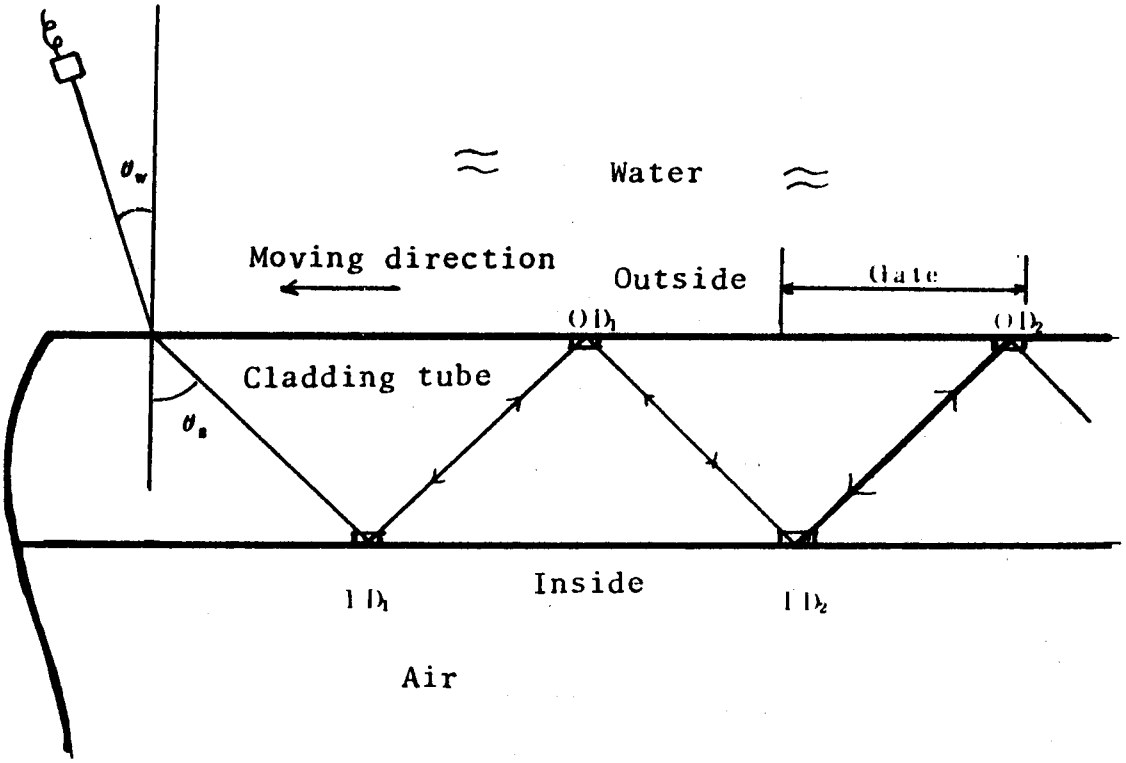
Transducers

Name	UZ 3-10-3	UZ 3-10-4
Resonant Frequency	Nominal 10MHz Practical 11.4MHz	Nominal 10MHz Practical 9.0MHz
Diameter of Transducer	4.5mm	4.5mm
Diameter of Focus(-3dB)	0.3mm	0.5mm

Table 1 Summary of flaw detectors and transducers



Testing method for longitudinal flaw



Testing method for circumfelential flaw

Fig.3. Operation diagram of ultrasonic testing

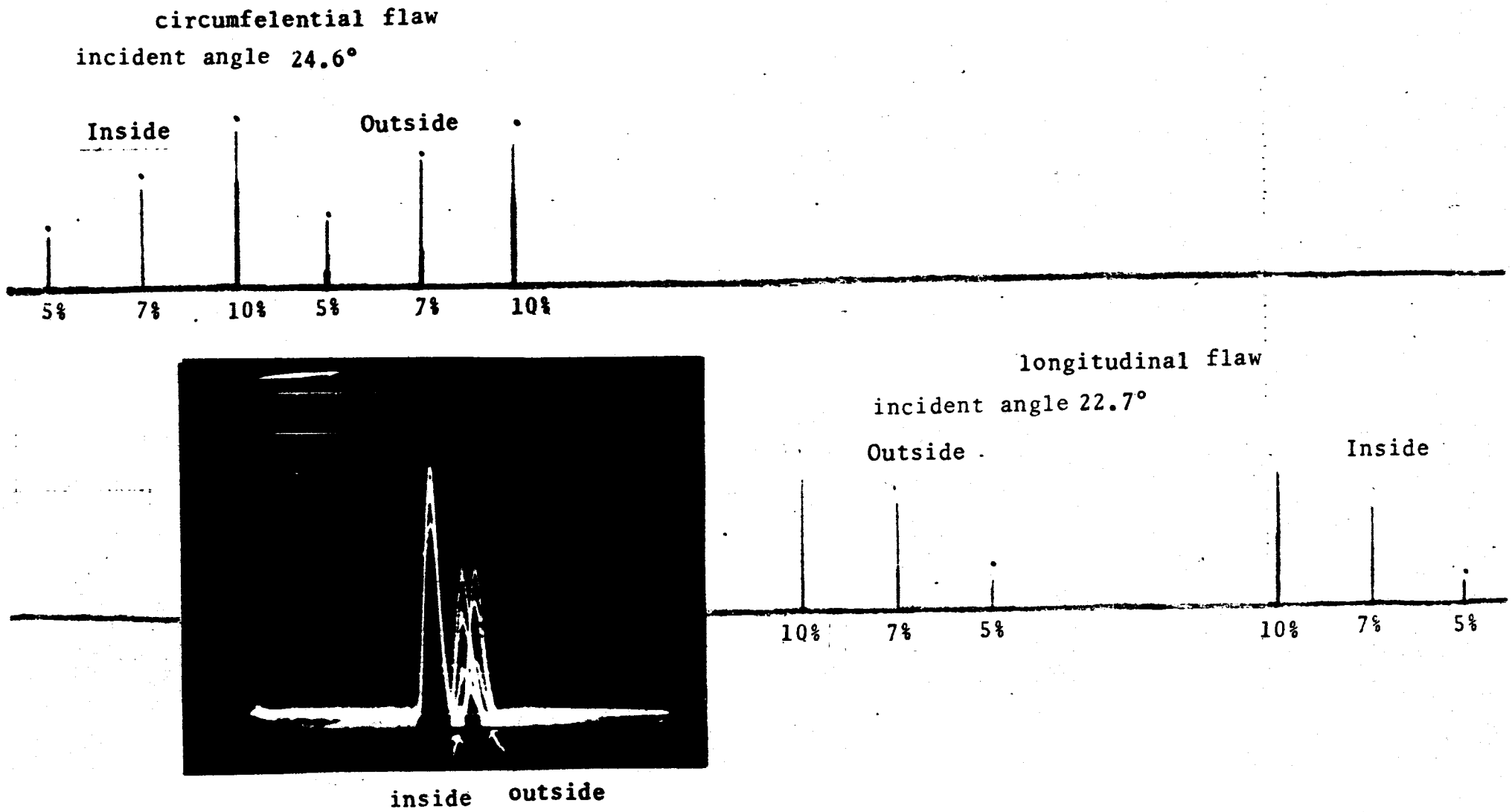


Fig.4. Result of ultrasonic test for standard specimen No 1.

Beam diameter: 0.3mm

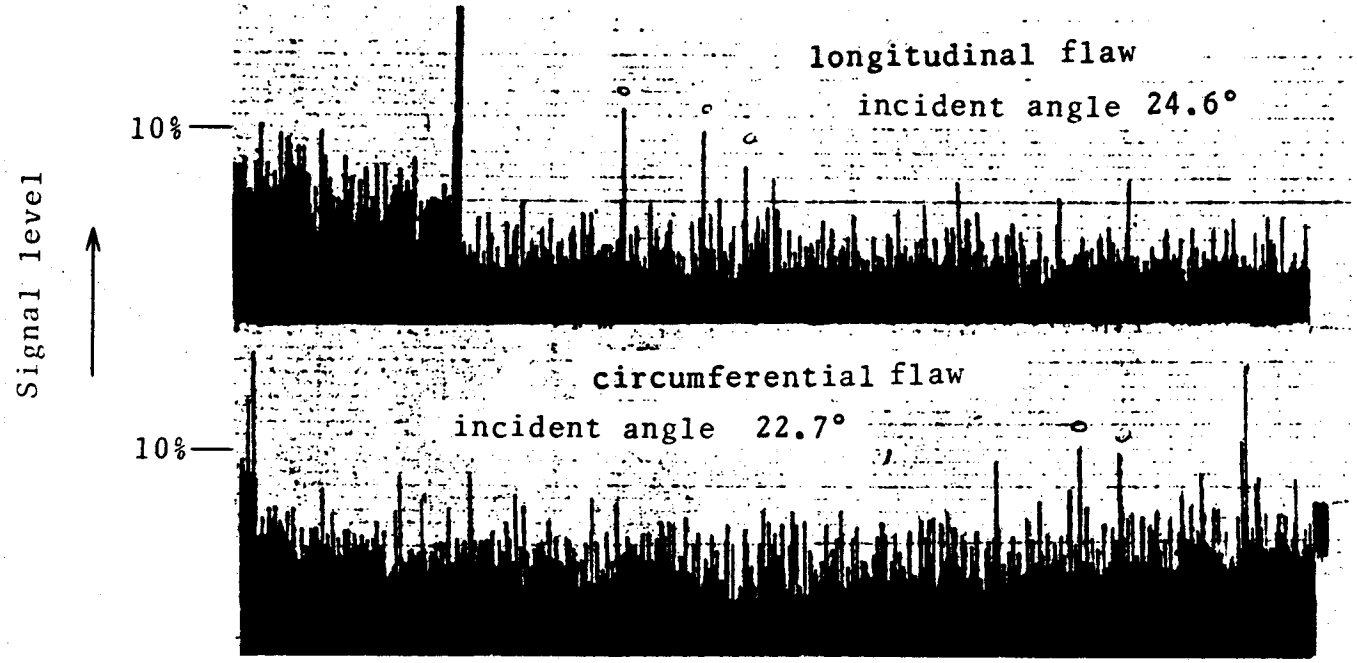


Fig.5. Result of ultrasonic test for standard specimen No 2
Beam diameter: 0.3mm

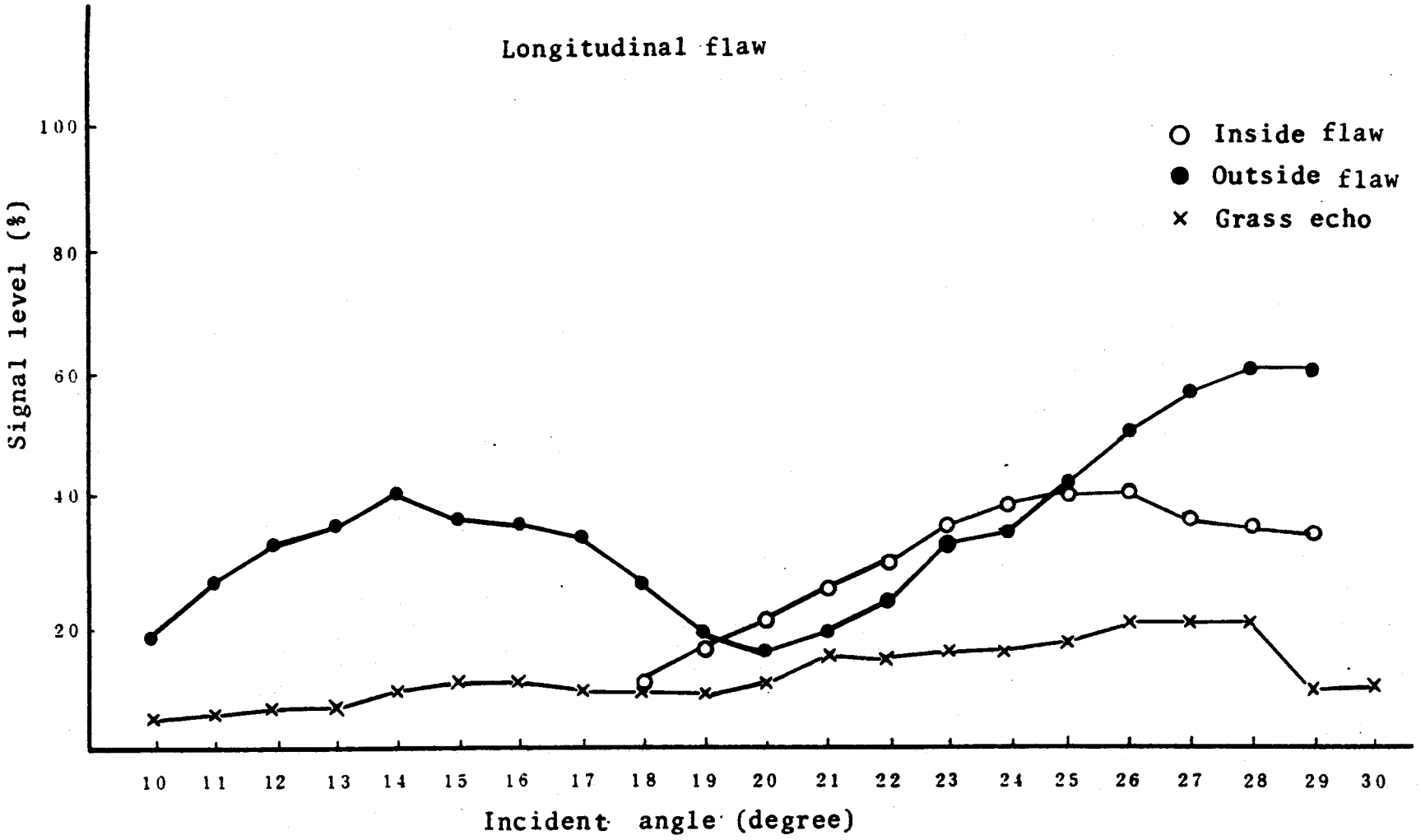


Fig.6. Relation between ultrasonic incident angle and signal level of inside flaw, outside flaw and grass echo

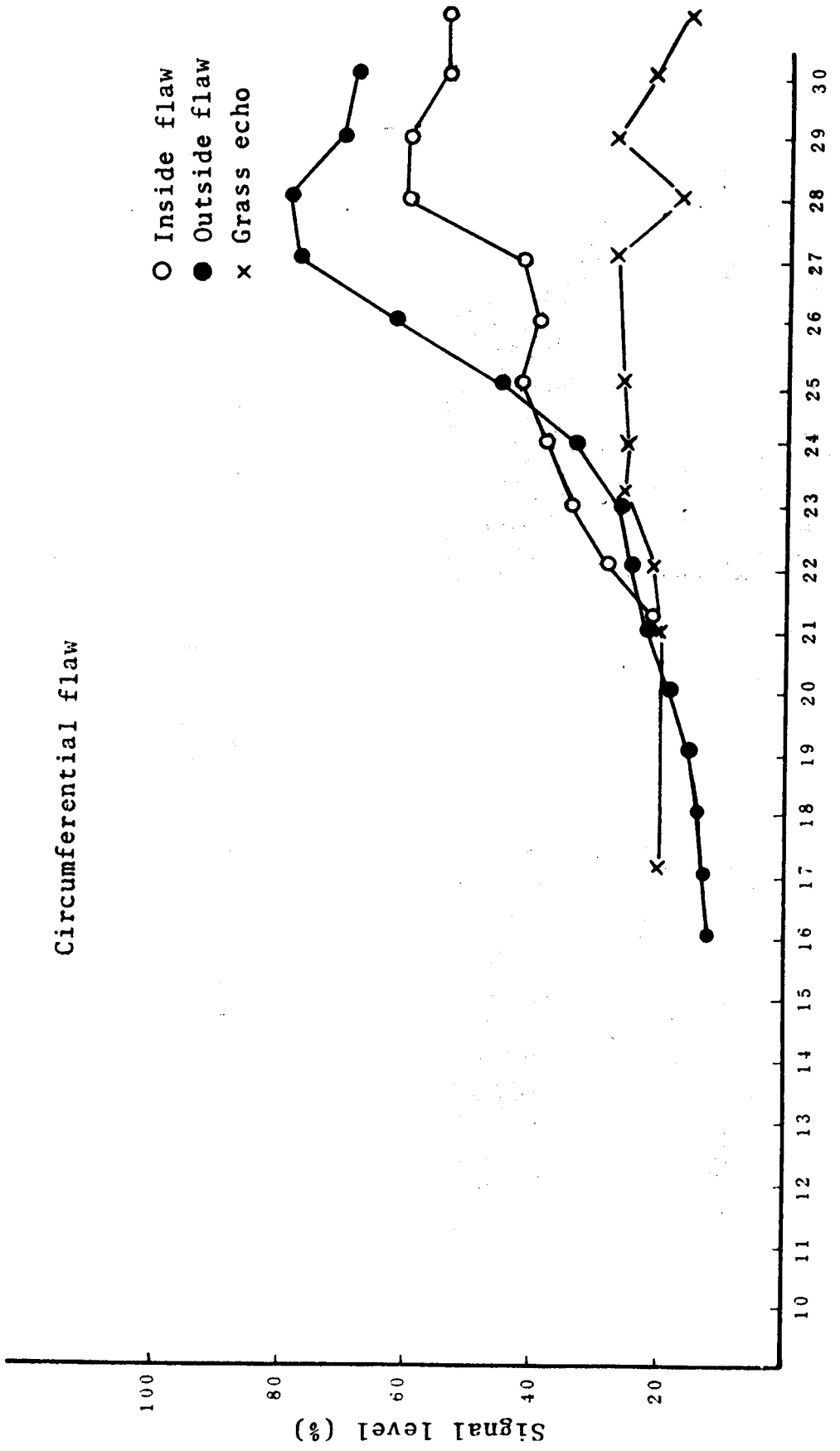


Fig.7. Relation between ultrasonic incident angle and signal level of inside flaw , outside flaw and grass echo

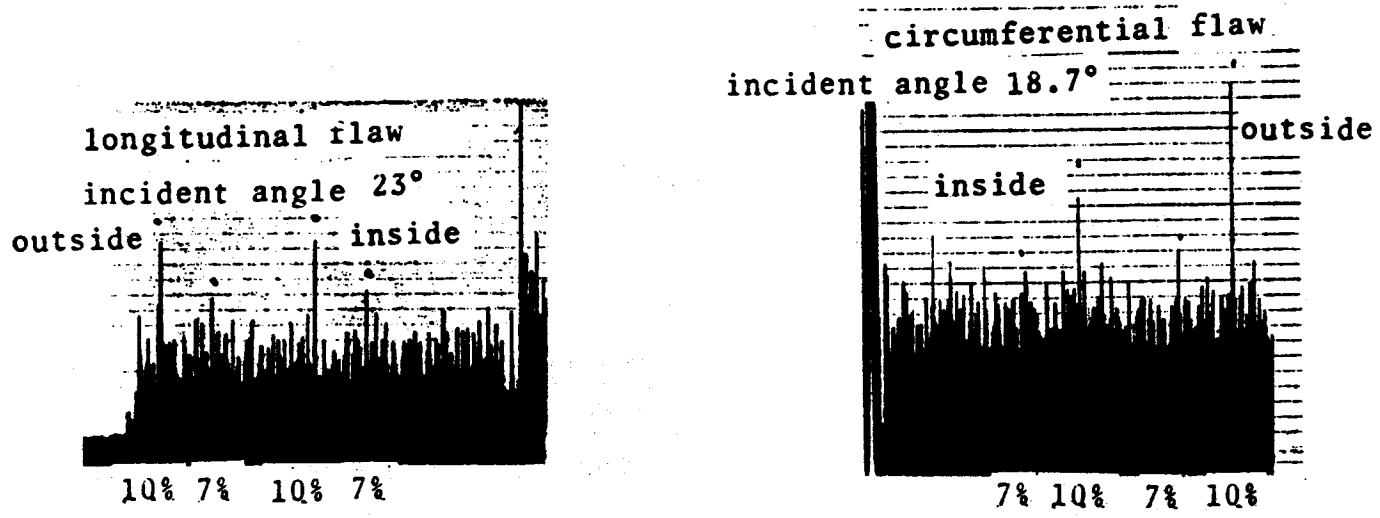


Fig.8. Result of automatical test for standard specimen No 2
Beam diameter: 0.3mm

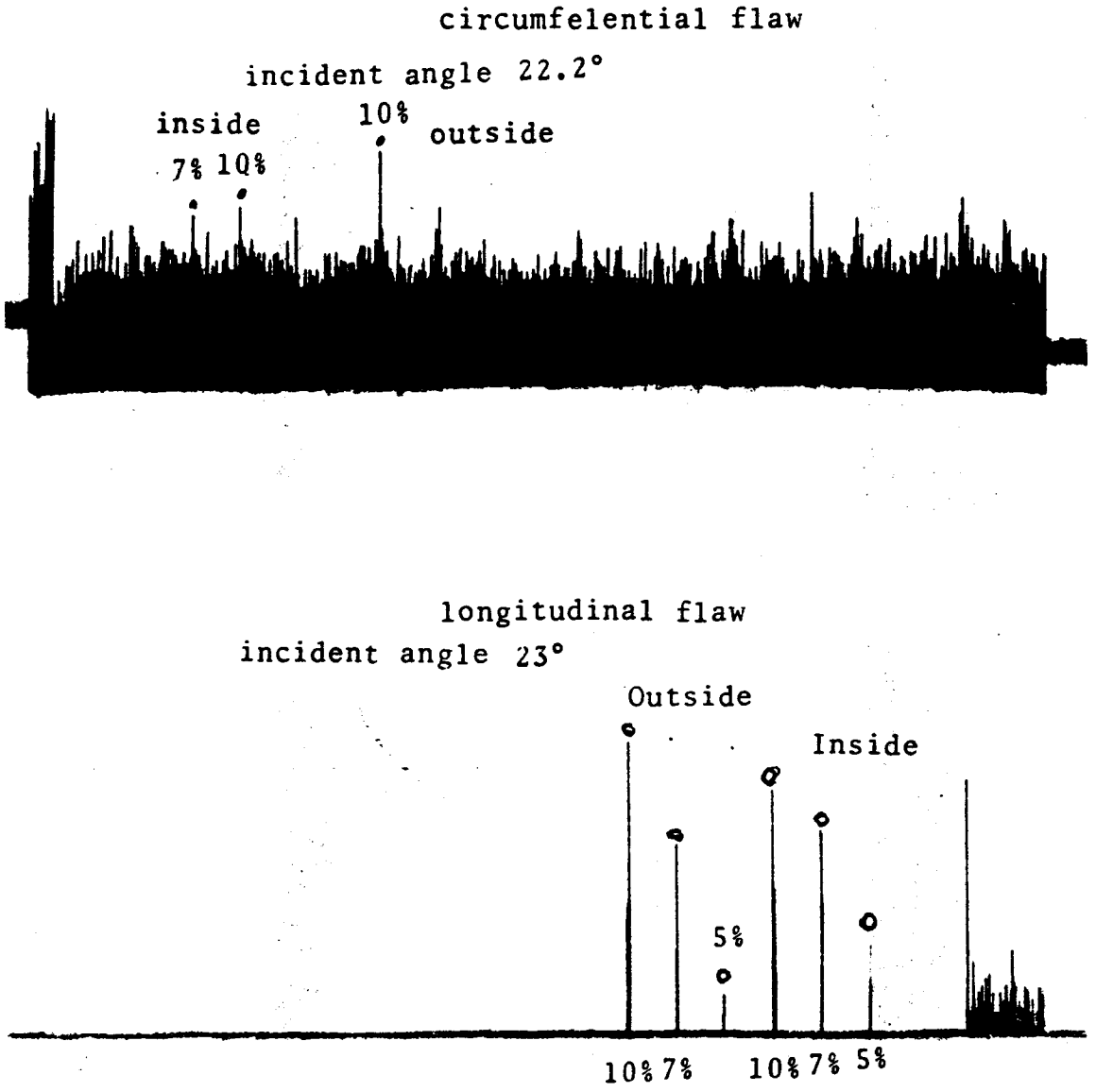


Fig.9. Result of ultrasonic test for standard specimen No 2
Beam diameter: 0.5mm

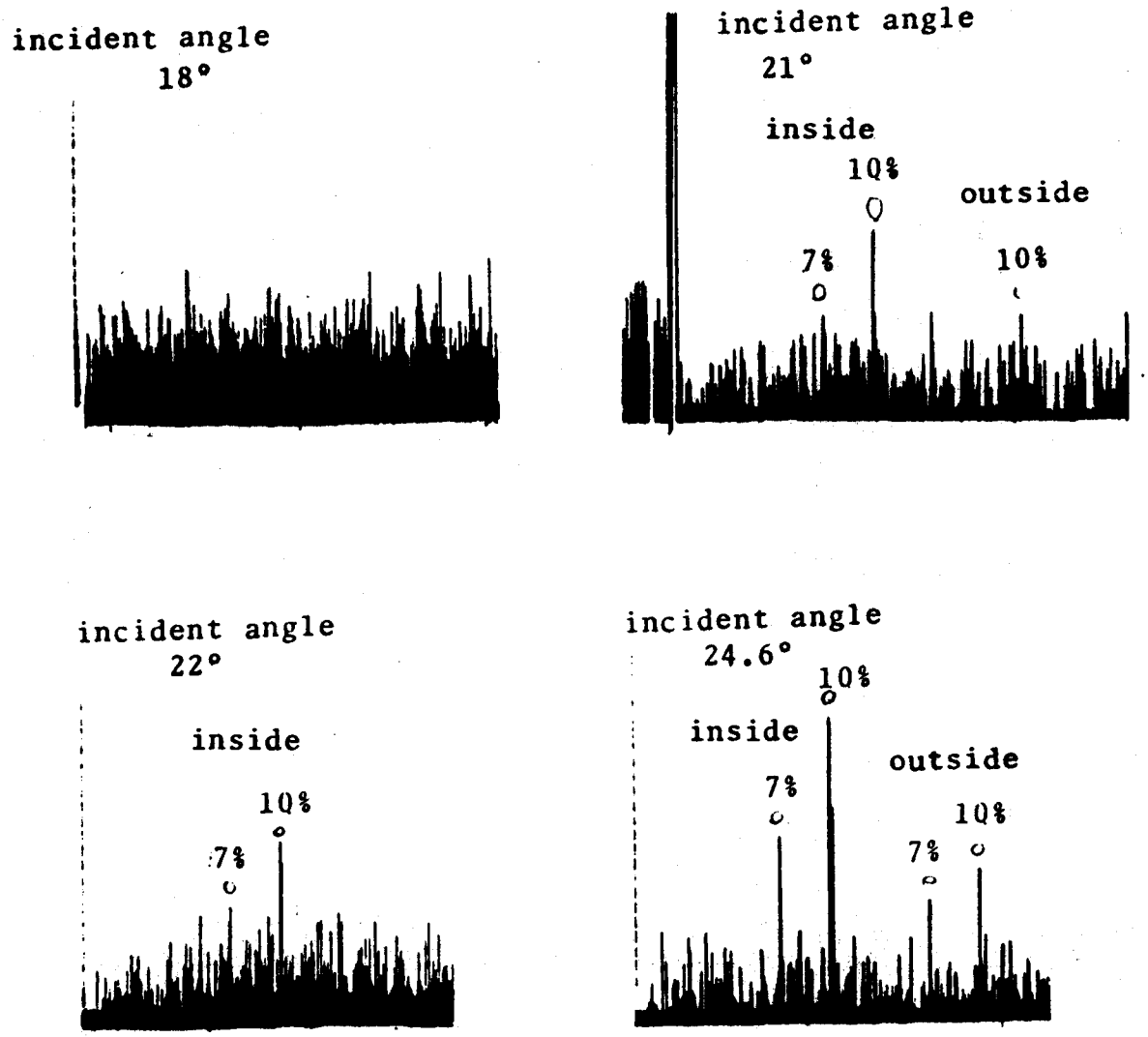


Fig.10. Result of ultrasonic test for circumferential artificial flaw
Beam diameter: 0.5mm

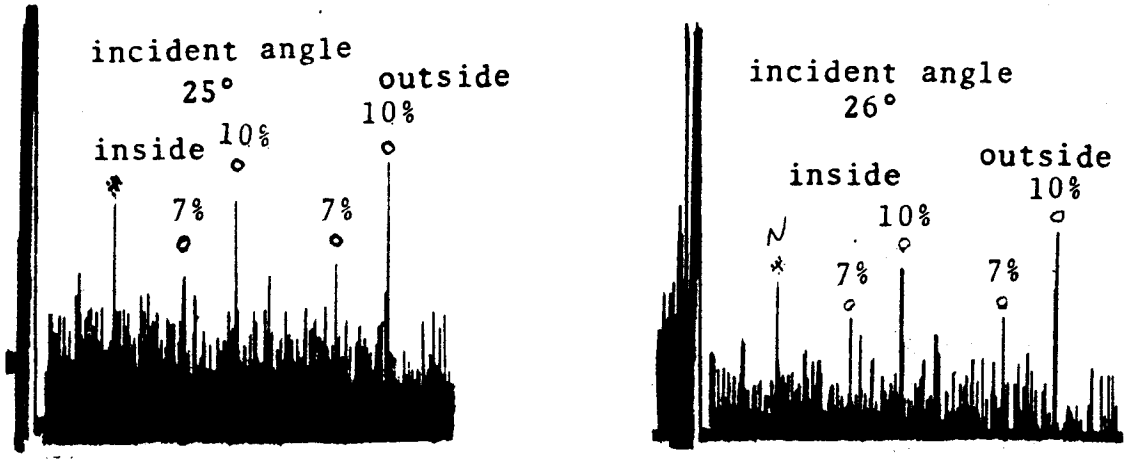
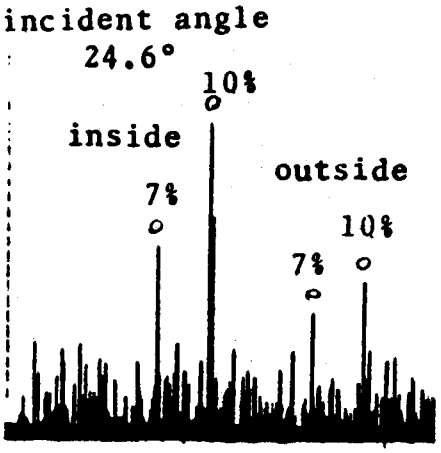
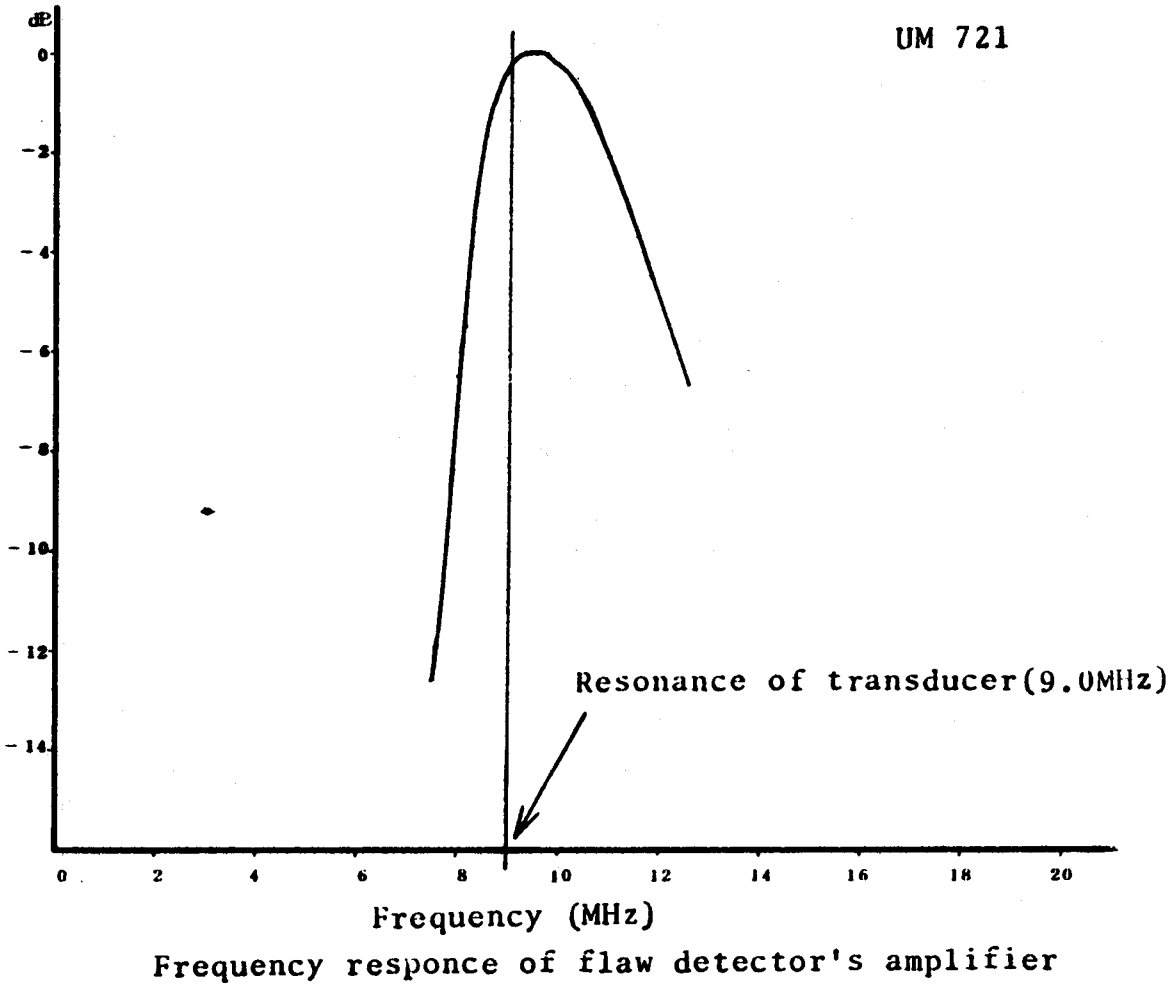


Fig.11. Result of ultrasonic test by 5th refrection for standard specimen No 2

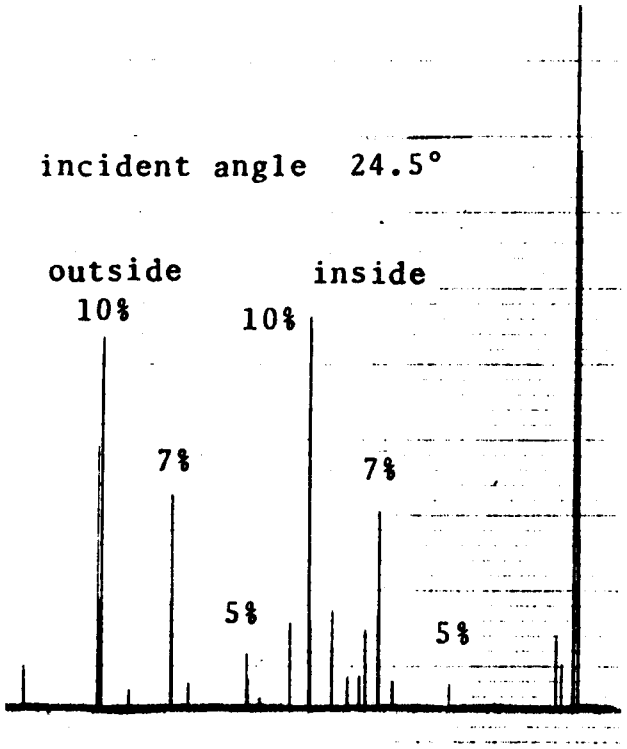
• Beam diameter: 0.5mm

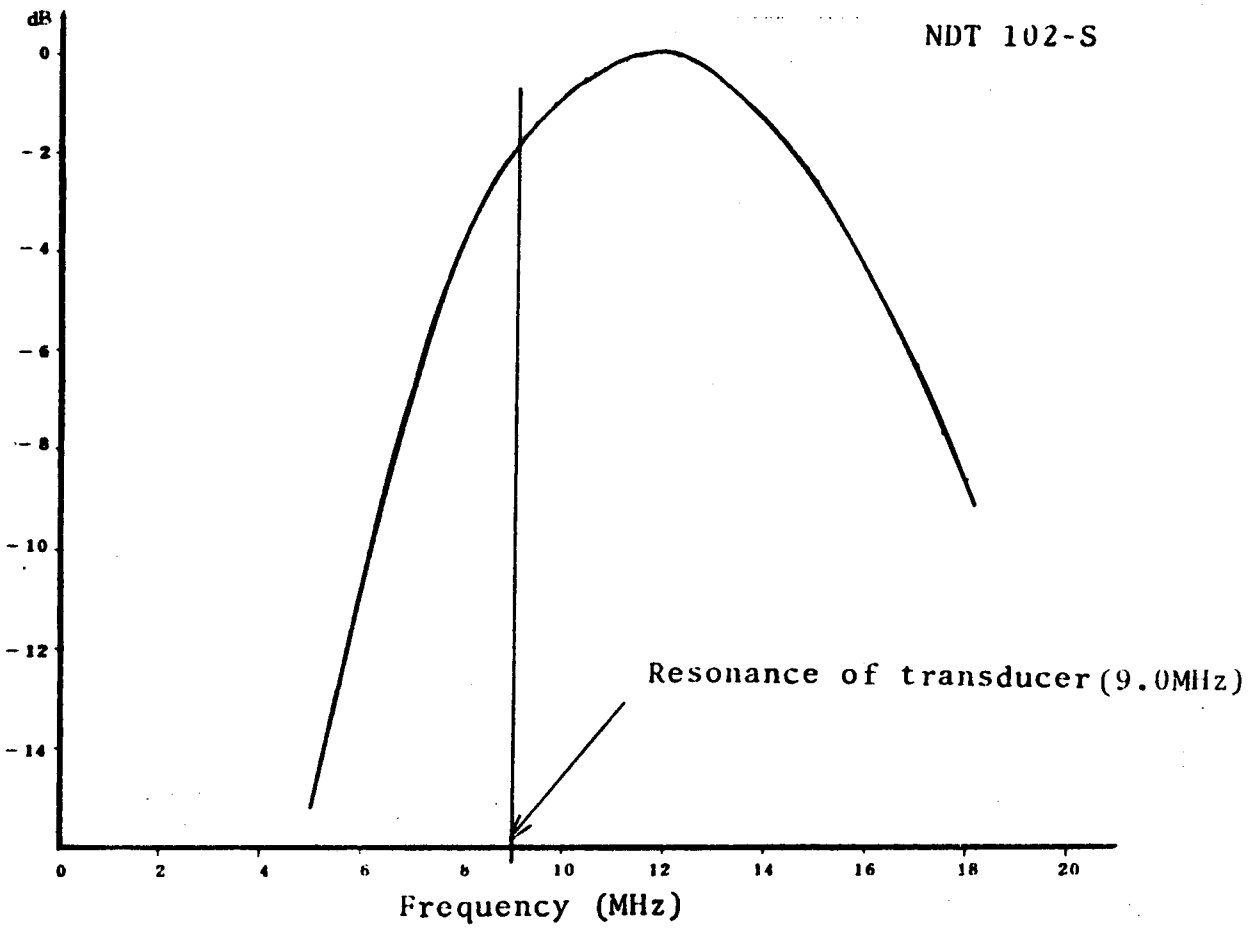




Frequency responce of flaw detector's amplifier

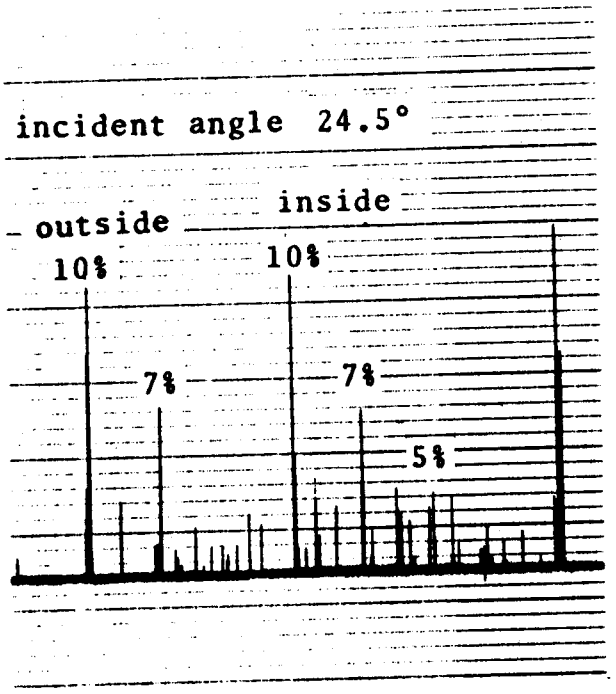
Fig.12. Grass echo of the standard specimen No2, and frequency range of flaw detector.

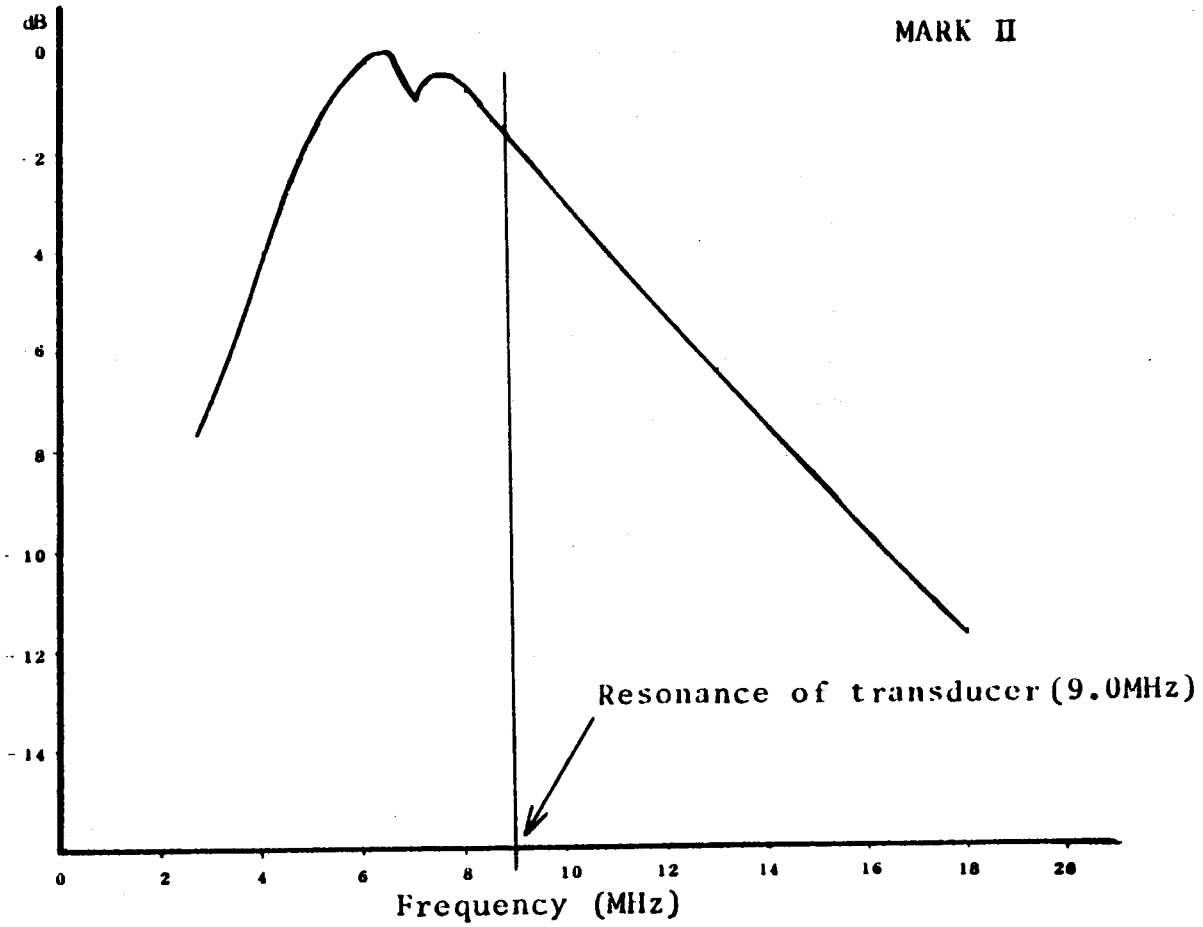




Frequency responce of flaw detector's amplifier

Fig.13. Grass echo of the standard specimen No2, and frequency range of flaw detector.





Frequency responce of flaw detector's amplifier

Fig.14. Grass echo of the standard specimen No2, and frequency range of flaw detector.

Experience of ultrasonic inspections of fillet and butt welds in austenitic steel in Heysham and Hartlepool A.G.R.'s

J.R. TOMLINSON, A.R. WAGG
Central Electricity Generating Board, United Kingdom

ABSTRACT

The experience of testing two designs of stainless steel (type 316) weldment in the boilers of the Heysham and Hartlepool Advanced Gas-Cooled Reactors is described.

The first weld discussed is a fillet weld (57 mm thick x 542 mm O.D.) joining superheater outlet headers to the concentric thermal sleeves. The unique feature of this inspection is the use of a welding procedure to produce columnar grains growing at 45° to the ultrasonic beams. The development work on which this is based has been extensively reported elsewhere; in this paper we concentrate on the practical difficulties of carrying out the inspection.

The inspection using straight beam short pulse compression wave probes is described in detail. Defect detection and sizing is based on evaluation of both direct echoes and obscuration of the back wall echo. Part of the inspection has been carried out with the assistance of a mechanical scanning jig; an X-Y recorder generates graphs of the test results. These graphs are analysed later to produce a description of defects in a form compatible with the acceptance standard.

Amongst the problems encountered have been the operator's unfamiliarity with the equipment, variations in attenuation and grass level and the magnitude of the task of data analysis.

Many indications from small pieces of welding slag and a geometrical echo not seen in the trial welds have made the task of analysis very tedious.

To date 100 of the 128 welds have been inspected. Although there have been regions of some welds that were declared uninspectable, no repairs have been necessary as a result of the inspection findings.

The second weld whose inspection is described is a manual metal arc butt weld in 19 mm wall x 102 mm O.D. pipe. This is the closing weld in an assembly carrying thermocouples into the superheater header. The presence of the thermocouples and an internal heat shield makes radiographic inspection very difficult. Ten such welds are to be inspected.

The ultrasonic inspection procedure, which has been demonstrated on trial welds containing artificial reflectors, involves the use of four probes. The root of the weld is inspected with a 60° shear wave beam passing entirely through the parent tube. A 60° shear wave beam and 45° and 0° compression wave beams are used to look for circumferential defects in the weld body. A 45° compression wave beam is also used to seek defects transverse to the weld. Conventional scanning, defect sizing and recording procedures are used.

Surprisingly, except in the inspection for transverse defects, no difficulties have been encountered with attenuation or grass. Echoes from the fusion face have been seen, and a nominal 60° shear wave beam has been found to propagate perpendicular to the inspection surface. No ultrasonic indications have been the cause of repairs. An indication on a radiograph in an area judged free of defects by ultrasonics was cut out. Visual examination during the repair confirmed that the defect was only a slight over-penetration of the weld bead into the bore of the pipe.

1. INTRODUCTION

The last ten years has seen a world-wide growth of interest in the possibility of applying ultrasonic testing methods to austenitic steel components. Prior to that the problems of inspecting such coarse-grained, anisotropic materials were recognised, but their causes were little understood. In recent years significant advances have been made in understanding the problem and in devising solutions. The contribution made in the C.E.G.B. to that understanding has been reported elsewhere (1). In this paper we review two applications of that work to post-fabrication inspections of austenitic welds incorporated in the boilers of the Heysham and Hartlepool Advanced Gas-Cooled Reactors (A.G.R.'s).

Figure 1 is a cross-section of the reactor design, showing the location of one of the eight pod boilers. The superheated steam outlet headers (4 per boiler) are located at the top of this structure where they pass through the concrete boiler closure head (Reference (2) gives more detail on the boiler design). As shown in Figure 2 the header is joined to the concentric thermal sleeve (necessary to protect the concrete from the high temperature of the reactor coolant gas) by a fillet weld. This is the first of the two welds whose inspection will be described. The header, the forging that forms the top of the thermal sleeve, and the weld itself are all made from AISI 316 steel. With 2 reactors at each site, there are 128 such welds to be inspected in all.

On No. 1 Reactor at each site 5 of the superheater headers are provided with additional thermocouples to monitor the temperatures of steam emerging from individual boiler tubes. The thermocouples pass into the steam space through a gland assembly mounted on top of the dome at the end of the header as shown in Figure 3. The ultrasonic inspection of the closing butt weld in this structure is the subject of the second part of this paper.

2. THERMAL SLEEVE TO SUPERHEATER HEADER WELD

2.1. Background to the Inspection

The integrity of this weld is vital to the safety of the reactor. Consequently it was deemed necessary to apply a volumetric non-destructive test to the structure after fabrication. The geometry of the weld prevents detection of defects on the fusion faces by radiography. Thus there was a need to develop an ultrasonic test procedure.

A fracture mechanics assessment of the likely stresses - both operational and residual from the welding process, combined with laboratory measurements of the creep strength of the weld metal lead to the definition of an acceptance standard for the fabrication of this structure. Fortunately it has proved possible to devise an ultrasonic inspection method which is capable of reliably detecting defects larger than 125 mm^2 in area, which is a lot smaller than the maximum size tolerable in this structure.

The strategy of NDT finally adopted includes a dye penetrant examination of the half-completed weld, and an ultrasonic inspection and a further dye-penetrant check on the fully machined weld.

2.2. Weld Design and Fabrication

As explained in reference (1) the design of the weld and the method of fabrication have been modified to suit the ultrasonic inspection. Here we describe briefly only the final design, - see Figure 4. The outside diameter of the header is 432 mm.

The body of the weld is built up in layers at 55° to the header axis, using manual metal arc welding. This procedure generates a columnar grain structure with the axes of the grains near 45° to the header axis. This orientation gives best transmission of ultrasonic beams radial to the header and parallel to its axis. There are slow variations in the grain orientation around the weld with more rapid fluctuations at the start-stop positions.

The weld is finally machined to the rectangular profile shown, with a surface roughness less than 3.2μm Ra.

2.3. Ultrasonic Procedure

A feature of the inspection procedure for this weld is its complexity; the final specification amounts to a 17 page document (3). It will only be possible to identify the main features of the technique here.

Four different beam directions are employed. These may be most simply categorized according to the surface through which the beams are injected.

(a) From the curved surface of the forging.
45° and 60° shear wave beams are used to detect defects lying on the fusion face to the forging. Miniature angle probes (8 mm x 9 mm crystal) and twin miniature angle probes of frequency 2 MHz are employed.

(b) From the flat surface of the weld.
Normal compression wave probes (5 MHz short pulse, 12.5 mm diameter crystal) are used to detect defects in the body of the weld and on the fusion face to the forging, and also to locate the root of the weld.

(c) From the curved surface of the weld.
Normal compression wave probes are used to detect defects in the body of the weld and on the fusion face to the header. Defects in any orientation, including axial cracks originating from the root, are detectable by their obscuration of the header bore echo. This inspection has been done with 5 MHz, 12.5 mm diameter crystal probes in contact, and in immersion (see 2.4. below).

In all the inspections the scanning sensitivity was chosen such that the sound scattered by the grain structure ("grass") occupied a certain fraction of the screen height - either 1/10 th or 1/20 th. Indications more than five times (14 dB) the height of the grass were to be reported and explored in more detail.

To understand the difficulties of defect sizing in these welds it is necessary to recognise that despite the close control over the welding, the effective attenuation of the beam is not constant. Figure 5 shows a typical plot of the amplitude of the header bore echo as a function of circumferential probe position. There are both slow variations in the attenuation over distances of order 200-400 mm (⅛ to ¼ of the circumference) and more rapid variations over distances of order 10-20 mm. The latter variations are on a scale comparable with the crystal diameter and result from variations in the insonified grains as the probe is moved. The longer range variations are assumed to result from deviations in the macroscopic alignment of the grains from the ideal inclination at 45° to the header axis. Both causes of variation make it difficult to apply conventional probe movement sizing methods (20 dB or 6 dB).

For the inspection through the forged ring these difficulties do not arise and sizing by probe movement methods is straight forward; from the flat surface of the weld there is no simple alternative - we must accept the consequent uncertainty in defect sizes. When inspecting through the curved surface two alternatives to probe movement methods present themselves.

The first may be described as a modified D.G.S. (A.V.G.) method. In this the amplitude of the defect signal is compared to the, partially-obscured, backwall signal. The method has been calibrated on a series of flat bottomed holes in a ferritic steel test block and checked with a model austenitic weld into which artificial reflectors were welded.

The second method of sizing is applicable to larger defects. This is essentially the same as that used for sizing of laminations in plate and relies on the obscuration of the header bore echo. It is appropriate to note that any areas in which the backwall echo is less than twice the height of the grass at the same range are reported as uninspectable and treated as defective in the assessment of the welds. Areas where the backwall echo is between 2 and 5 times the height of the grass (6 to 14 dB up) may at worst contain isolated defects less than 125 mm^2 in area.

2.4. Scanning Jig

Some form of continuous, analogue data recording system is desirable for the effective operation of any ultrasonic test system that relies on the obscuration of a standing echo. When the amplitude of this echo varies even in the absence of defects, because of variations in attenuation, this facility becomes essential.

This has been achieved with the use of a simple, hand-driven scanning jig and an X-Y recorder. The probe, which is coupled to the surface by a 35 mm-long oil column, and an indexing potentiometer are mounted on a ring which can be rotated around the weld. The slowly-leaking couplant is continuously replenished by a pump. The X-axis of the recorder represents circumferential position of the probe; the Y-axis is driven from the flaw detector via a logarithmic amplifier. By adjusting the gate delay either backwall echoes or defect echoes may be plotted. Figure 5 shows typical results.

These traces are the raw data for the analysis. They provide:-

(a) defect echo amplitudes as a function of probe position - from which defect dimensions according to the 20 dB or 6 dB methods can be found,

(b) relative amplitudes of defect and backwall echoes for the modified AVG sizing,

(c) backwall echo obscuration lengths for sizing big defects, and finally they form a very complete fingerprint of the weld which could be valuable if re-inspection was ever required.

2.5. Successes and Difficulties

Despite the complexity of the inspection process and the novelty of the welding procedure there have been no major difficulties. Just over 100 of the 128 welds have been inspected to date; no significant defects have been detected.

One problem not uncovered in work on the pre-production trial welds was the presence of an echo from the inner surface of the forged ring. This appeared on many production welds when the compression probe was placed on the curved surface of the weld, with its centre on the line of fusion to the forging (see Figure 4). Half of the beam is then incident at an angle of about 70° on the weld fusion face. Laboratory tests have confirmed that sufficient energy is reflected from this fusion face onto the inner surface of the forging for echoes to be obtained from that surface if it is machined in irregular steps, instead of the smooth profile shown in Figure 4.

The use of the scanning jig has greatly improved the ease of the inspection, while at the same time ensuring complete coverage of the weld surface and generating a very complete (and readily reproducible) record of the test results. In the early stages of the production inspection the ultrasonic operators were unfamiliar with the use of the chart recorder; now they can use it with as much facility as the flaw detector.

Probably the greatest difficulty associated with the use of the recorder is the magnitude of the task of analysing the large volume of data generated. Each weld generates 24 A3 size graphs of backwall echo and defect indications. In some welds a large number of small reflectors have been detected, particularly near the outer surface of the weld. Listing and sizing these indications, which are almost certainly innocuous slag, has proved time-consuming. There have also been small areas, near the root of the weld, where the attenuation has been high enough to prevent a proper inspection being carried out. Since these areas have to be treated as defective it is necessary to map out their sizes as carefully as if they were defects.

3. THERMOCOUPLE GLAND WELD

3.1. Background to the Inspection

This weld is a butt joint between two pieces of 102 mm O.D. x 19 mm wall 316 forged pipe. It is special because it is the closing weld in the assembly and hence has to be made with the thermocouples already threaded down the bore of the pipe. The thermocouples are protected from the heat of the welding process by an internal heat shield as shown in Figure 6. The presence of the heat shield and thermocouples make conventional radiographic procedures impossible. A double wall single image radiographic technique is being used on this weld but

it was clear from trials with welds containing artificial defects that this technique has only limited defect detection capabilities. An ultrasonic method that complements the radiography has accordingly been developed.

It was not felt worthwhile to carry out a full fracture mechanics assessment of these welds, which are therefore being accepted on the basis of a "radiographic" acceptance standard. Inevitably the results of the ultrasonic inspection are not directly compatible with this standard and a certain amount of interpolation between the capabilities of the ultrasonic technique and the requirements of the acceptance standard is necessary.

The weld is made by the manual metal arc process in the downhand position by rotating the assembly about a horizontal axis. This generates the columnar grain structure, symmetric about the weld centre-line, that is characteristic of this process. The weld cap is removed by grinding, with special care being taken to avoid the production of undulations in the surface.

3.2. Development of the Ultrasonic Procedure

The ultrasonic procedure was developed principally by the use of trial welds containing artificial defects. Three types of artificial defect were used:

(a) thin plates of 316 6 mm x 6 mm seal-welded onto the prepared tube ends to simulate lack of side-wall fusion,

(b) spark machined notches in the root and body of the weld simulating both longitudinal and transverse cracks (6 mm x 6 mm),

(c) short lengths of 316 tube 1.5 mm i.d. incorporated in the body of the weld simulating welding slag.

Of all these artificial defects, only the spark-machined slots transverse to the weld were difficult to detect using the probes as described below.

The inspection procedure for use on the production welds makes use of five different probe types - normal compression (5 MHz twin 6 mm x 3 mm crystals), 45° shear wave, 60° shear wave, 45° compression wave along the pipe and lastly 45° compression wave in the plane transverse to the pipe axis (all 5 MHz, 6 mm diameter crystals).

These are used to inspect the various parts of the weldment as follows.

Parent Tube This is checked for lamination-type flaws with the normal probe. Two 45° shear wave probes in a pitch and catch configuration are used to check on the shear wave velocity in the parent material and also to detect anomalous attenuation in the pipe (detected in the pipe used to make the trial welds).

Weld Root The 60° shear wave beam passing through parent material only is used. The 60° angle is preferred to the alternative 45° beam as it gives better discrimination between the signals from a truly defective root and those due to mild, and innocuous, over- or under-penetration of the root.

Weld Fusion Faces Both 45° and 60° shear wave beams are scanned from the half skip to full skip positions, again traversing only parent material. Weak echoes from the fusion face itself are seen at the full skip position.

Weld Body: Defects Along the Weld The 60° shear wave probe and 45° compression wave probe are used; sizing of indications is not attempted with the shear wave beam as this beam is liable to suffer severe deviations in direction as a result of the anisotropy of the weld metal (1). There was evidence from the trial welds of this probe generating a normal shear wave beam in the weld metal.

Weld Body: Defects Transverse to the Weld The 45° compression wave probe with a shoe contoured to fit this diameter of pipe is used.

The test sensitivities used are such that grass, while visible on the screen, presents no impediment to the inspection. The test sensitivities and reporting level are based on the results obtained with the trial welds. Defect sizing is based on the maximum amplitude method. Conventional manual scanning and data recording are employed.

3.3. Production Testing Experience

There are only 10 of these welds in all; consequently there has not been a large amount of data generated by the inspection of the production welds. No defects have been repaired on the strength of the ultrasonic test results. One weld however gave radiographic indications in the root area; the ultrasonic evidence pointed to the presence of a mild over penetration in this weld. Visual observation during the repair that was subsequently carried out confirmed the ultrasonic findings.

4. DISCUSSION

The inspections of the two welds described above have one feature in common - namely that an ultrasonic procedure was called for primarily because of the difficulties of radiographic inspection. We have not yet reached the stage where ultrasonic inspection of austenitic welds after fabrication is automatically required.

They are also similar in that the procedures used are relatively complex and each has been developed specifically for the particular weld geometry and process. As such their development and application are relatively costly in manpower terms. The development of the fabrication and inspection for the thermal sleeve to header weld illustrates what can be achieved - but only through the effective co-operation of a variety of skills. Figure 7 illustrates this by showing the involvement of the many groups and organisations involved in that work.

The organisations identified there are: NDTAC-NDT Applications Centre, MEL-Marchwood Engineering Laboratories, CERL-Central Electricity Research Laboratory, PITB-Production Inspection and Test Branch, GD&CD-Generation Design and Construction Division (all of which are parts of the C.E.G.B.) and B&W-Babcock & Wilcox (Operations) Ltd.

The two inspection procedures also have marked differences. That for the butt weld is superficially similar to that which would be applied to a ferritic weld; the peculiar geometry and greater thickness of the fillet weld required the application of more novel techniques. They also differ in the nature of the acceptance standard against which the ultrasonic results were judged. The fitness-for-purpose type of standard, based on fracture mechanics is easier to apply than the quality control type of standard originally written for use with radiography.

5. CONCLUSIONS

1. It is now possible to use ultrasonics to demonstrate the integrity of austenitic steel welds.

2. The procedures used will in general be specific to a particular component geometry and more complex in their application than those for ferritic welds.

3. The development of a successful inspection requires good liaison between designer, fabricator and inspector.

6. ACKNOWLEGEMENTS

This paper is published by permission of the Director General of the North Western Region of the C.E.G.B.

7. REFERENCES

1. Ultrasonic Inspection of Austenitic Welds by J.R. Tomlinson, A.R. Wagg and M.J. Whittle. Proc. Conf. on Non-Destructive Evaluation in the Nuclear Industry, Salt Lake City, 13-15 Feb. 1978, Am.Soc. Metals, 1978.

2. Helically Coiled Once-Through Steam Generators at Hartlepool and Heysham by P. Chambon. Proc. Conf. on Construction, Commissioning and Operation of AGR's, London, 26-27, May 1977. I. Mech.E., 1977.

3. A Specification for Ultrasonically Inspecting the Superheater Header to Thermal Sleeve Welds at Heysham and Hartlepool Power Stations - Revision 1 by A.R. Wagg and M.J. Whittle. C.E.G.B. Report No. NW/SSD/SR/100/78, Sept. 1978.

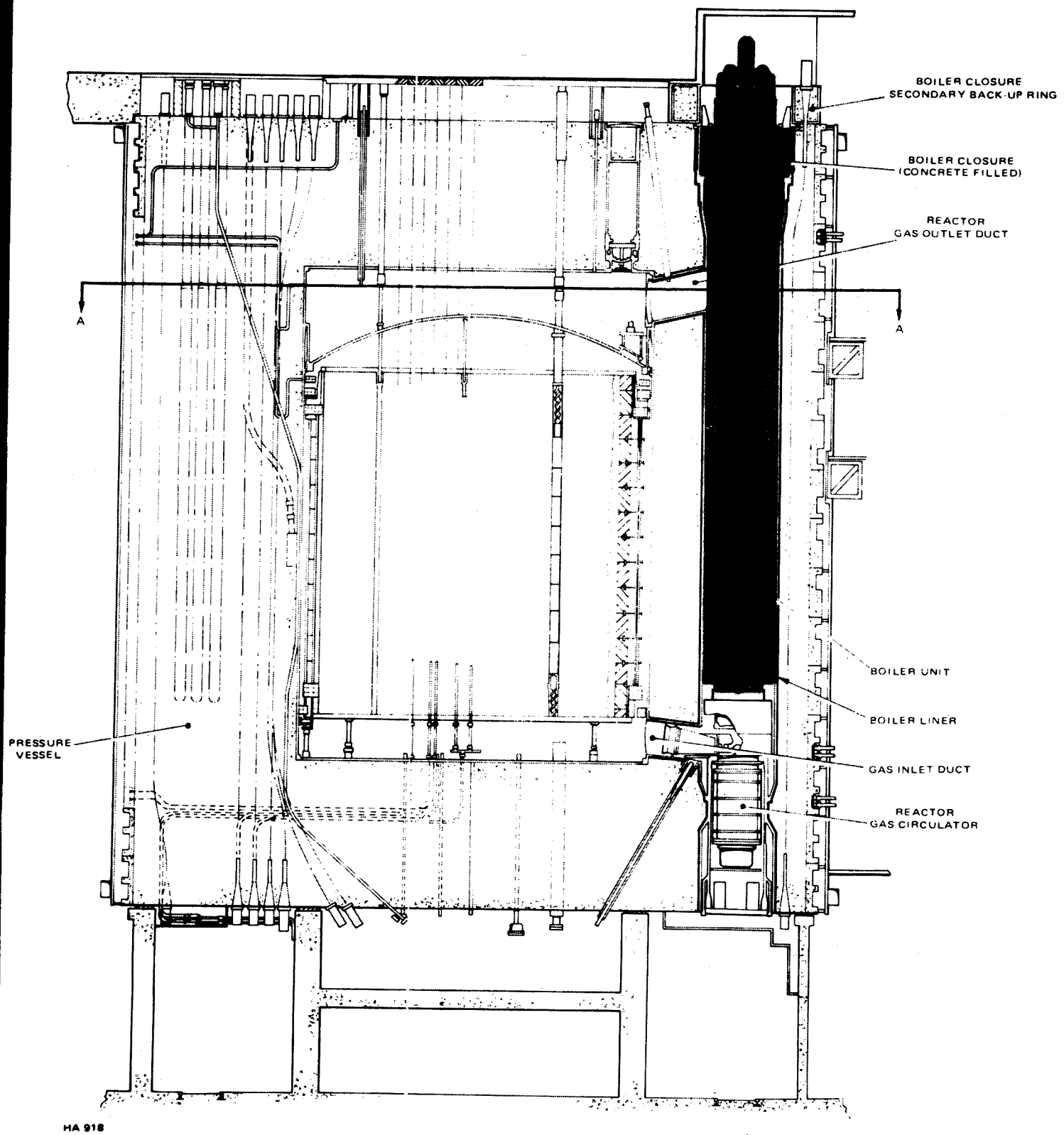


Fig.1 Cross Section of Heysham Reactor Showing Boiler

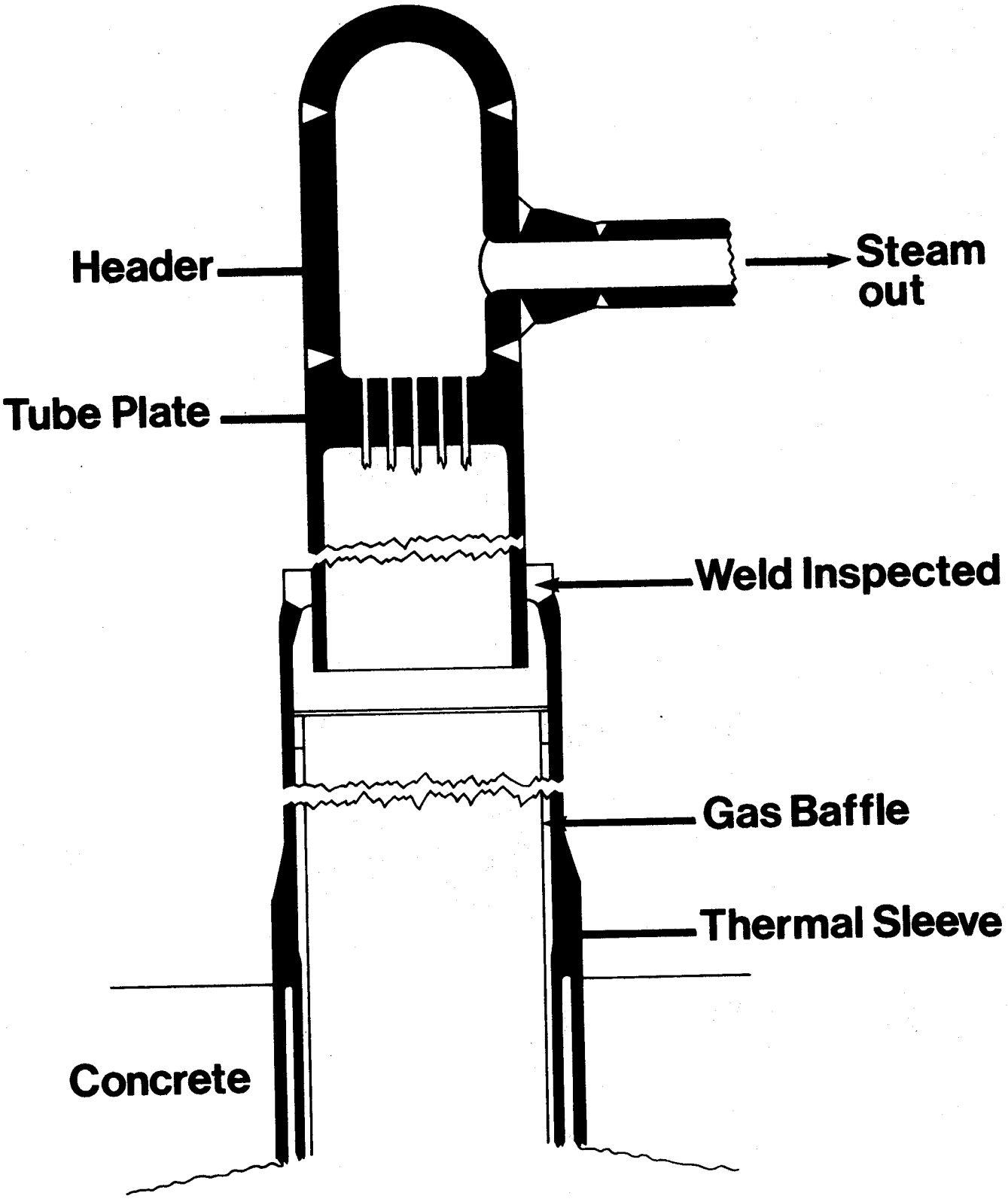


Fig. 2. Superheater Header and Thermal Sleeve

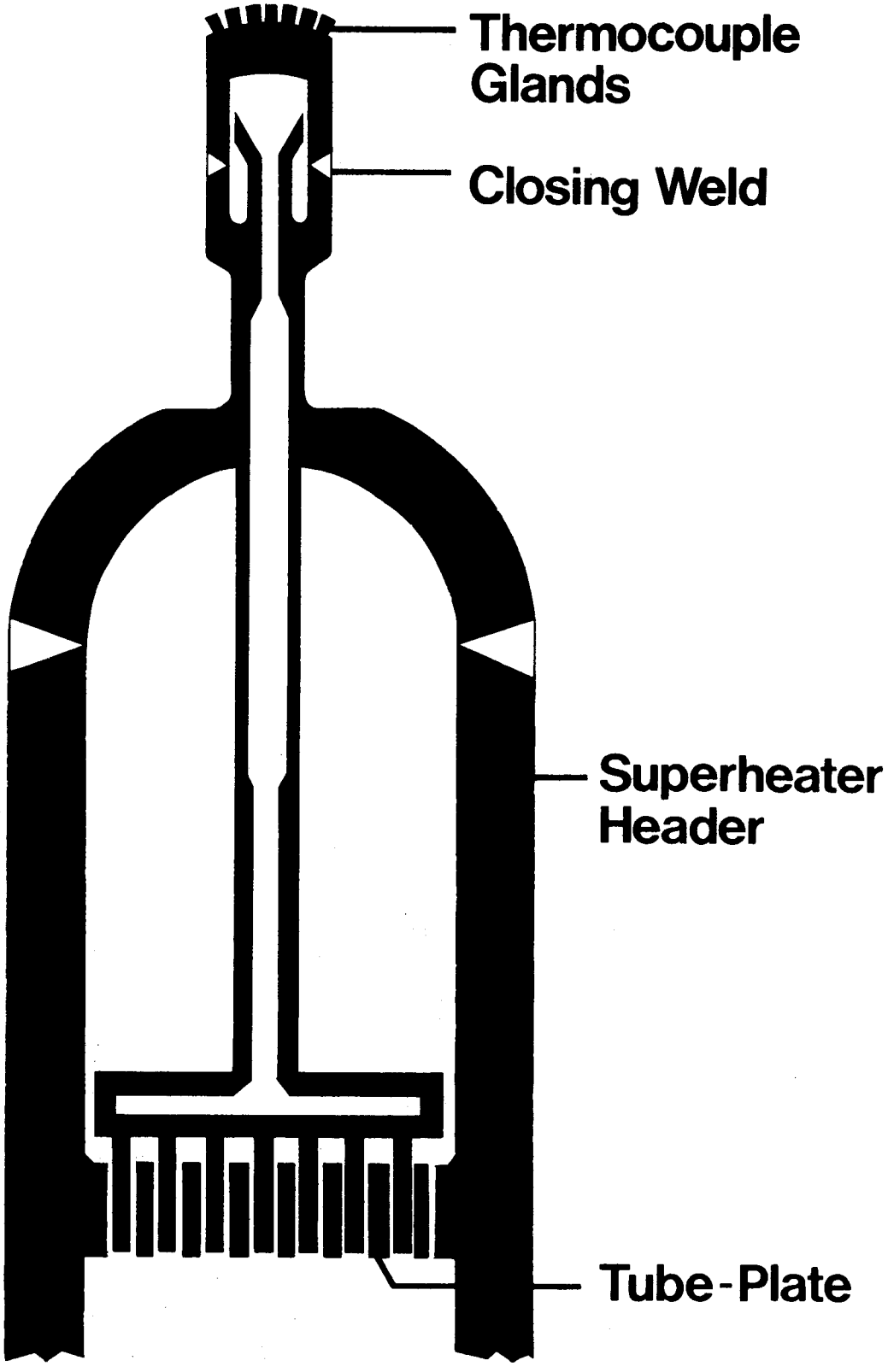


Fig.3 Thermocouple Assembly in Superheater Header

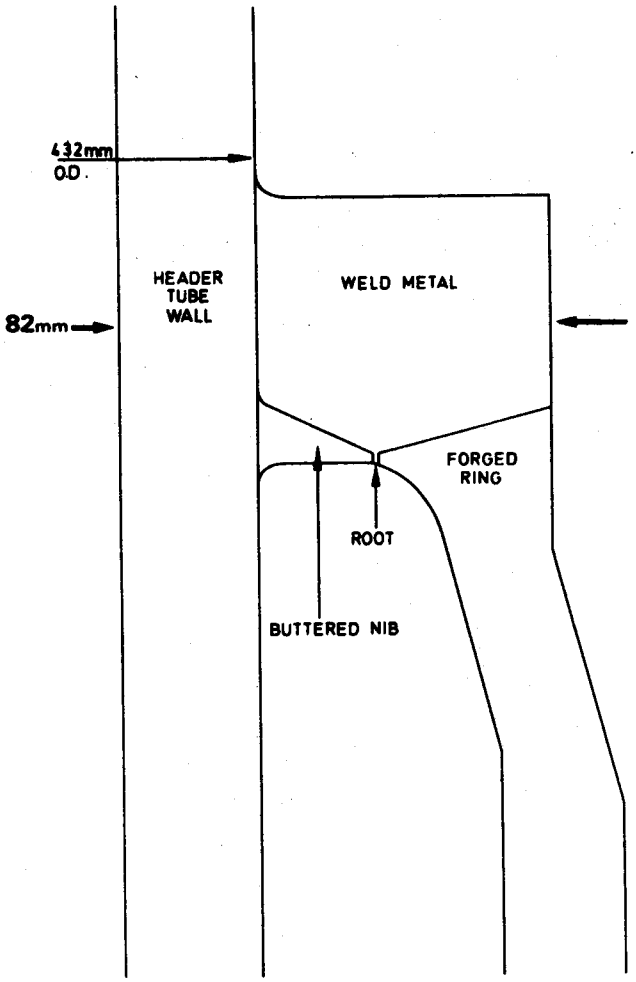


FIG.4. SUPERHEATER HEADER TO THERMAL SLEEVE WELD

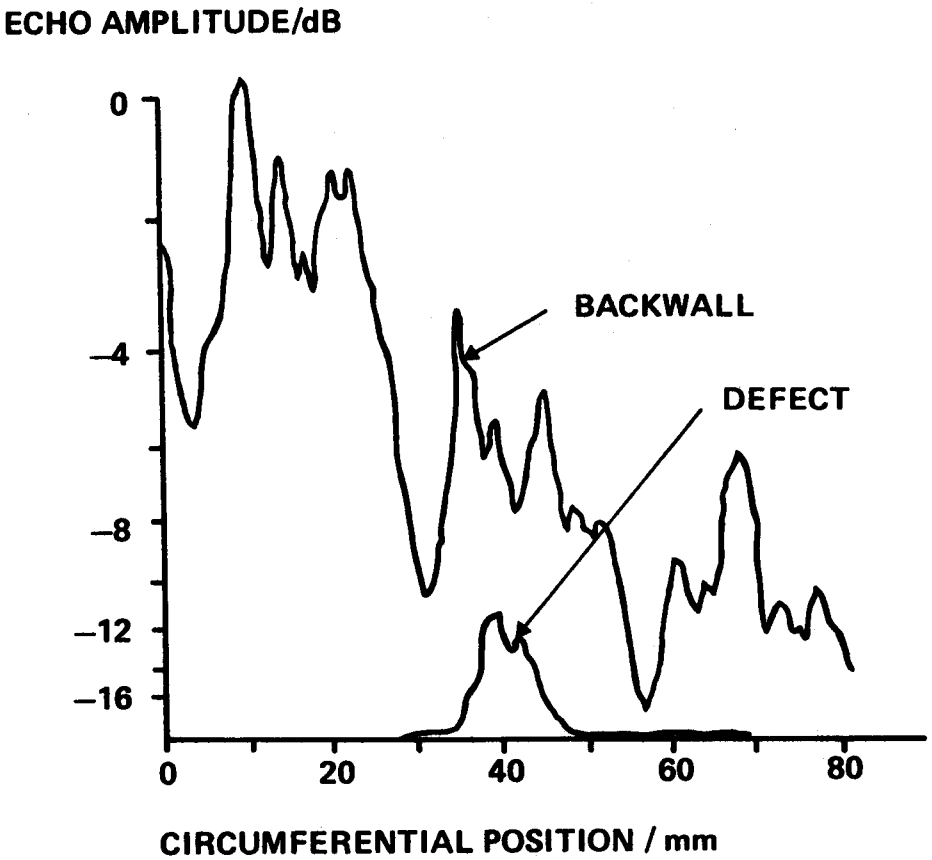


Fig.5 Backwall and Defect Echoes

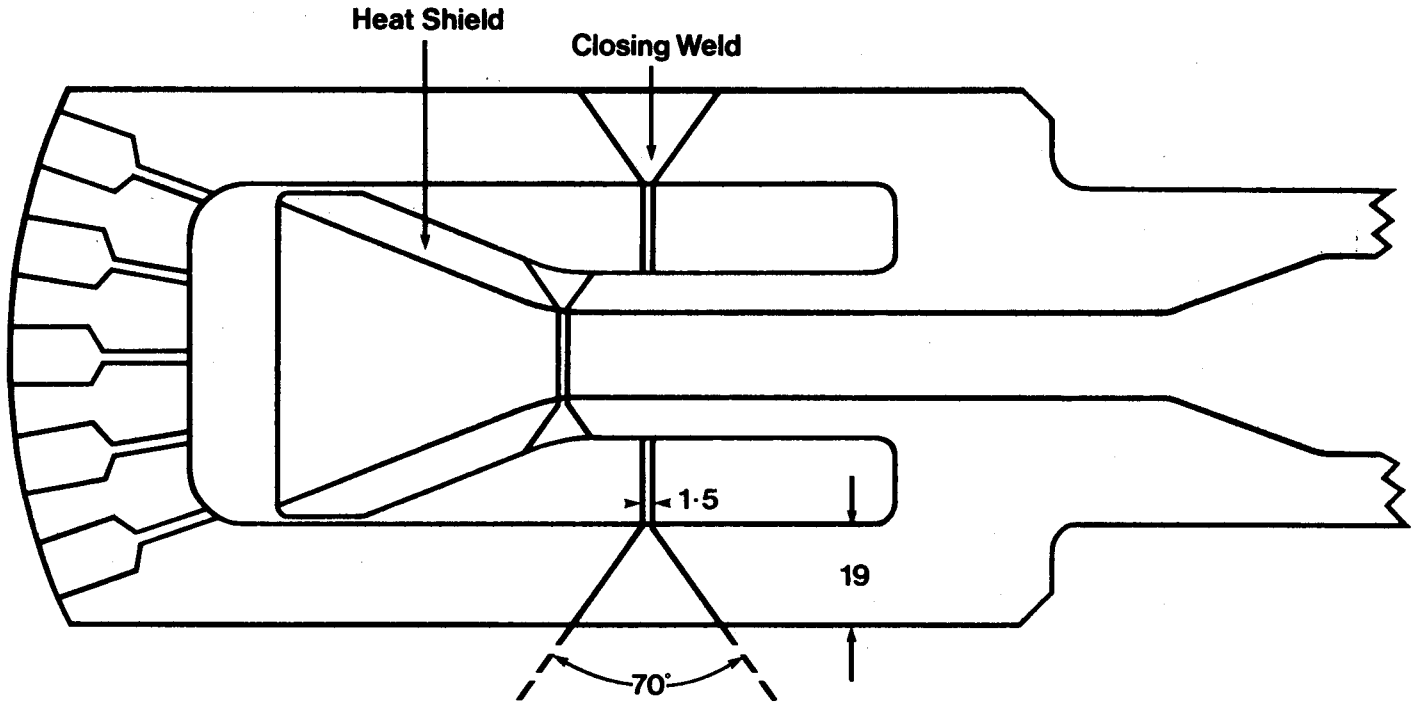


Fig. 6. Butt Weld in Thermocouple Assembly

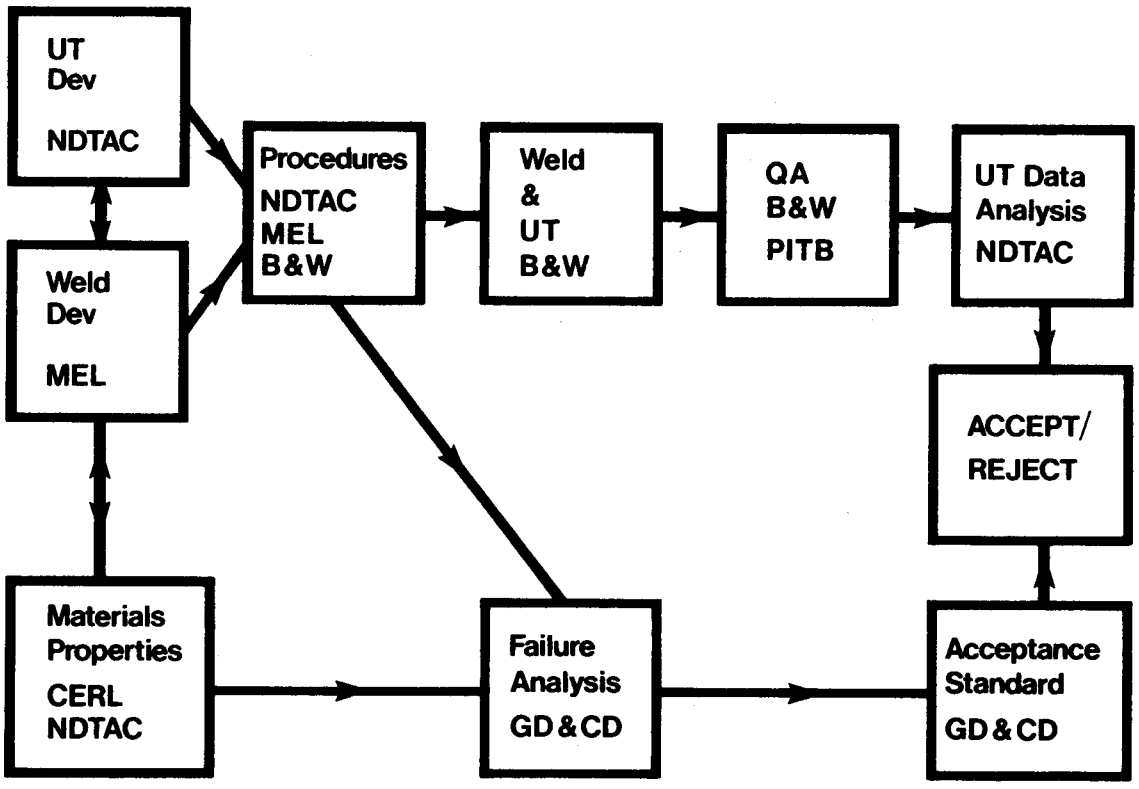


Fig. 7 Liason Between Specialist Groups

Improved ultrasonic inspection of austenitic stainless steel components by signal averaging techniques

S. KRAUS, K. GOEBBELS
Fraunhofer - Institut für Zerstörungsfreie Prüfverfahren, F.R. Germany

ABSTRACT

The ultrasonic inspection of stainless steel austenitic materials is highly restricted by backscattered ultrasound which is either caused by the coarse grained structure and by the high anisotropy and herewith related steps in acoustic impedance at grain boundaries. The backscattered signal can be of the same amplitude as the signal from the reflector. Today, worldwide a lot of research and development work is done to improve the ultrasonic inspectability of these components. Regarding the test arrangement as chain in the sense of the communication theory, consisting of the test block, the probe, the UT-device and the signal processing unit our work is connected with the last link of this chain. In the A-scan the backscattered signal appears as interference structure. The distribution of the amplitudes depends on the probe position upon the surface of the specimen, on the test frequency and on the angle of incidence. Small variations of these parameters cause great changes in the backscattered signal intereference structure, while the amplitude from a reflector remains constant. Adding up a certain number of A-scans from different positions, frequencies or angles, the signal-to-noise ratio (SNR) is improved. In this contribution will be reported about the physical background of backscattering, necessary to understand the method, the different signal averaging techniques (averaging analog or digital signals, high-frequency or video signals; spatial-, frequency-, directional averaging), the experimental set up (on-line signal averaging unit) and the results obtained at austenitic welds or castings with improvements in SNR up to 20 dB.

INTRODUCTION

As for the purpose of this meeting, the authors like to give a short review about their work concerning the improvement of signal-to-noise ratio (SNR) by signal averaging techniques. We have to thank the "Bundesministerium für Forschung und Technologie" for sponsoring this work in its "Reaktorsicherheitsforschungsprogramm".

For the ultrasonic inspection of coarse grained materials the signal-to-noise ratio as ratio between the amplitude of a defect indication A(x) and the amplitude of the scattered ultrasound $A_S(x)$, will be described in general by equation (1).

$$SNR = 20 \log A(x) / A_S(x) \quad [dB] \qquad (1)$$

The amplitude A(x) of the signal of interest (i.e. backwall-echo, defect echo), depending on the attenuation α in the material, is given by equation (2), disregarding beam diffraction.

$$A(x) = A_o \cdot e^{-\alpha x} \qquad (2)$$

with x: length of the sound path
A_o: maximum amplitude

The mean scattered amplitude $A_S(x)$ measured in pulse-echo technique as a function of the sound path x is proportional to the square root of the pulse length Δ and the scattering coefficient α_S.

$$A_S(x) = A_o \, (\Delta \cdot \alpha_S)^{1/2} \, e^{-\alpha x} \qquad (3)$$

By combining equations (2) and (3) according to equation (1), the SNR is

$$SNR = -10 \log (\Delta \cdot \alpha_S) \qquad (4)$$

As the diffraction is disregarded, as mentioned above, equation 4 is only exact if x equals 0. Furtheron, the scattering amplitude $A_S(x)$ is introduced as mean value. In the normal A scan, because of the interference of the scattered pulses, the scattering amplitudes can either be zero or 10 dB to 20 dB higher than this mean value for a fixed distance x.
All methods for improving the SNR when testing coarse grained materials can be more or less derived directly from equation (4). α_S and/or Δ must be influenced. This can be performed by one or more of the following methods.

In Fig. 1 the whole testing system is shown as chain in the sense of the communication theory. It consists of

specimen, probe, UT-device and signal processing unit. What about the specimen, the grain and dendritic structure can be varied by controlling the fabrication and the heat treatment during welding /1/.
What about the probe, the pulse length, wave mode and beam shape are variable. The pulse length and herewith the bandwidth depends on the damping of the probe. Wave modes can be longitudinal waves instead of transversal waves /2/ or polarized shear waves /3/, even electromagnetically excited. The focusing of the sound field can be done by lenses /4/, by separation of sending and receiving transmitter /5,6/ or by phased arrays /7/. Rising the testing frequency leads too to more focused sound beam; in some special cases, the testability can be improved by this method /8/. α_S and Δ can furtheron be controlled through the spectrum of the sending pulse. Using burst excitation instead of peak excitation, the spectrum of the pulse is controlled by pulse length and shape of the envelope; in this way, higher frequencies which contribute more to the scattering are drastically reduced /9/.

All the listed methods lead only to reduction of the height of the scattering amplitude, but do not smooth the interference structure itself. This is only possible by applying signal averaging techniques /10-12/. Last but not least, it must be mentioned, that today there is some effort in using other methods from the communication theory to improve signal-to-noise ratio.
In this paper will be reported about the signal averaging techniques.

Method

The already mentioned interference structure is the result of the reflections of the pulse at the grain boundaries in the sound beam and the superposition. This amplitude-

modulated signal has a frequency spectrum which is quite similar to that of the transmitting pulse; therefore it is coherent to the signal caused by reflection at a real defect. As we learned from the communication theory, improvements in SNR by signal averaging are only possible if the signal of interest and the noise are not coherent to each other. Therefore, we have to make the noise to a stochastic, incoherent one. This can be done by moving the probe over the surface of the test piece, by changing the testing frequency and/or by changing the angle of incidence. The methods are called:

- spatial signal averaging
- frequency signal averaging
- directional signal averaging

In all cases, small variations in position, frequency or angle cause strong variations in the interference structure while the signal of the defect remains constant - at least in first approximation - in amplitude and time-of-flight. This is shown in Fig. 2 for eight A scans from eight different positions on the surface separated by one grain diameter $d \approx 350$ µm. Adding more and more independent A scans, the improvement in SNR becomes better and better and the scattering amplitude fits to equation (3) (Fig. 3).

Here we had a plane-parallel specimen, the easiest case, if there are artificial or real defects, the moving must be performed with regard to the echo dynamic curve of the reflector.

The next two figures show the improvement in SNR by spatial averaging for longitudinal (Fig. 4) and transverse artificial weld defects (Fig. 5). For a two millimeter flat bottom hole, the SNR in the normal A scan is 0 dB; by averaging over 1024 A scans, SNR is improved for 15 dB.

For the transverse defect in an austenitic submerged arc weld, SNR is increased for 5 dB for the 3 mm flat bottom hole. Furthermore, there are detected two natural defects (slag inclusions we suppose) between the weld runnings, because we could find them with straight beam probes, too.

An example for frequency averaging is given in Fig. 6. For a 3 mm side drilled hole in an X-shaped austenitic weld, SNR is improved by changing the testing frequency between 3.7 MHz and 5.3 MHz and averaging 1024 times. When changing the angle of incidence while keeping constant the frequency, the effect is the same (Fig. 7).

The three averaging techniques mentioned above can be performed in different ways. Additionally can be varied:

- type of data processing
  (analog or digital signals)

- type of signals
  (high frequency of rectified signals)

- amplitude of A scan
  (wheighting by linear of exponential function).

It is depending on the testing problem what kind of method will be preferred. For a quantitative evaluation of the measurements in practical application there usually will be done linear digital averaging over rectified signals.

Measuring Device

The block diagram of such an on-line signal averaging device developed and built by IzfP is shown in Fig. 8. The ultrasonic equipment consists of an UT-device connected

with a probe which can be moved over the specimen surface in case of spatial averaging. A fast ADC and the averager-unit are the main parts of the signal processor. The averaged signals are displayed on a CRT, for documentation a plotter could be used. The instrument is controlled by a microcomputer. The averager-unit consists of 8 identically built modules with a throughput rate of $2.5 \cdot 10^6$ amplitude values per second each and a separate controller module.

Figure 9 shows the simplified timing diagram of an averager module. With a clock frequency of 50 MHz the averaging cycle of one module lasts 400 ns. The internal organization for memory read, memory write and process initialisation takes 60 ns. Reading takes 100 ns, adding and writing 80 ns each. The memory of each module is 1 k words by 18 bits. The application of 8 modules for parallel processing means a throughput rate of $2 \cdot 10^7$ amplitude values per second and a memory size of 8 K words by 18 bits. The performance time of the averaging process for 1024 A scans (400 µs each) is approximately 0.4 s.

Measurements

Figure 10 shows an improvement in SNR of 7 dB for a slag inclusion in an austenitic weld. The testing frequency was 2 MHz longitudinal waves. The thickness of the weld 60 mm.

Figure 11 shows for the same weld, the detection of lack of side wall fusion near the root. Angle of incidence: 45 degree. Testing frequency: 2.0 MHz; shear waves.

Figure 12 gives an interesting example for testing coarse grained casting not only with one of the methods mentioned above, but by combining two of them. Here we have

together the broadband transducer and the signal averaging method. The pulse length was only 1.5 wavelength, the frequency 2.5 MHz (longitudinal waves). With this transducer the porosity was already detectable in contrast to a not highly damped one. Additionally, averaging gives another 5 dB in SNR-improvement.

Outlook, Conclusion

With this contribution on the one hand, we tried to give an idea about the principle of signal averaging techniques for improved ultrasonic testing of coarse grained materials and on the other hand, to show the present status of the technique. What about the last point, we think that one great problem is solved, the problem of reducing the data processing time. We reached this aim by building up an on-line system in our own laboratory. Another improvement in the technique at all we shall reach by using electronically controlled phased arrays for spatial and directional averaging. At the moment, this work is going on.

The main problem to solve is, in our opinion, to concentrate further research and development efforts to investigate the possibility for combining the several methods for improving the SNR and to come by this to an optimized ultrasonic testing system for coarse grained materials /13/.

References

/1/ B.L. Baikie, A.R. Wagg, M.J. Whittle, D. Yapp: LMFBR Specialists Meeting, Bensberg 1976

/2/ H. Wüstenberg, T. Just, W. Möhrle, J. Kutzner: Materialprüfung, 19 (1977) 7, p. 246

/3/ D.S. Kupperman, N.V. Fiore, K.S. Reimann: Paper 2B8, VIII WCNDT, Cannes 1976

/4/ R. Saglio, M. Roule: Paper F05, VII ICNDT, Warszawa 1973

/5/ E. Neumann, H. Wüstenberg, E. Nabel, W. Leisner: Materialprüfung, 16 (1974) 12, p. 395

/6/ P. Caussin, OECD-NEA-Ref: SINDOC (78) 190

/7/ W. Gebhardt, F. Bonitz, H. Woll, V. Schmitz: IX WCNDT, Melbourne 1979

/8/ S. Kraus, K. Goebbels: IzfP-Bericht Nr. 760717-TW, Saarbrücken 1976 (available GRS, Köln)

/9/ H.-A. Crostack: Ultrasonics, 15 (1977), p. 253

/10/ S. Kraus, K. Goebbels: 1st Int. Symp. on Ultrasonic Mat. Charact., Gaithersburg, MD, June 1978

/11/ S. Kraus, R. Neumann, K. Goebbels: Proceedings Int. Symp. Saarbrücken 1979, p. 153-162

/12/ S. Kraus, R. Neumann, K. Goebbels: IX WCNDT, Melbourne 1979, Paper 4H5

/13/ K. Goebbels, M. Römer, H.-A. Crostack: Materialprüfung, 21 (1979) 8, 261-267

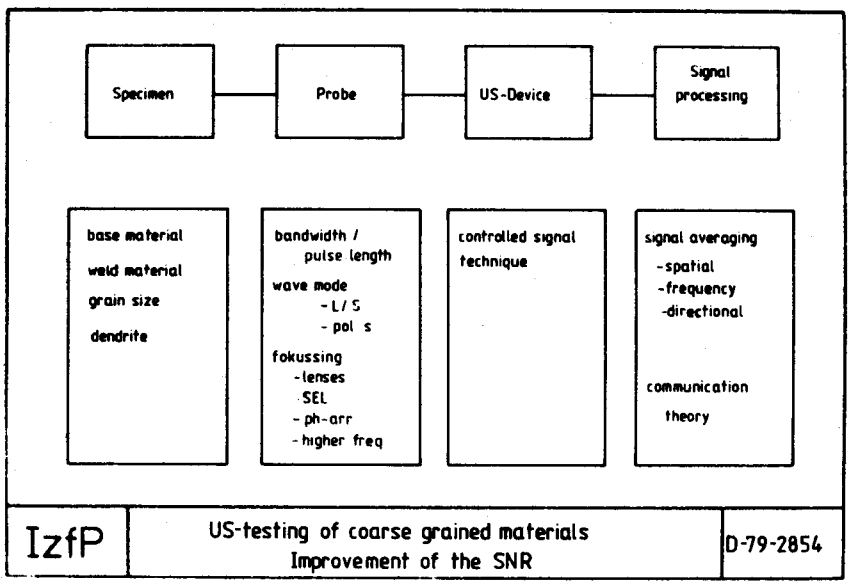


Fig. 1

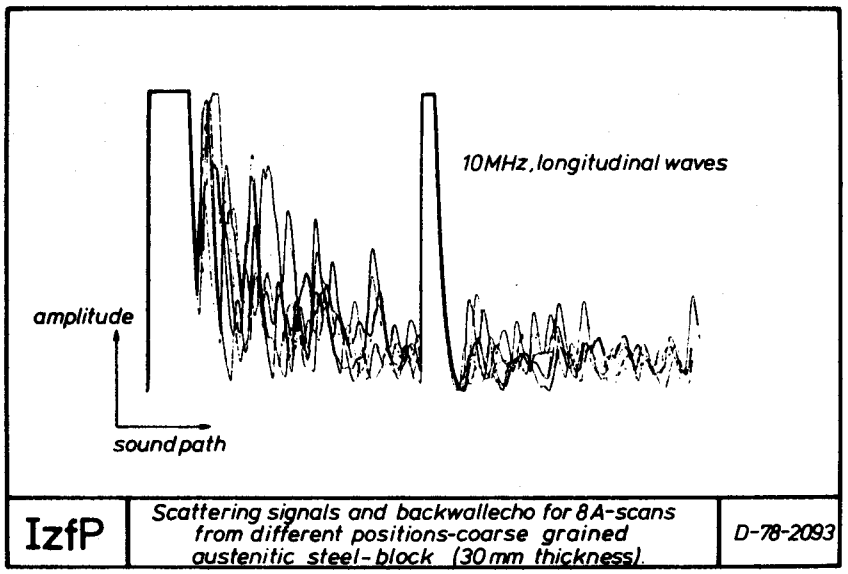


Fig. 2

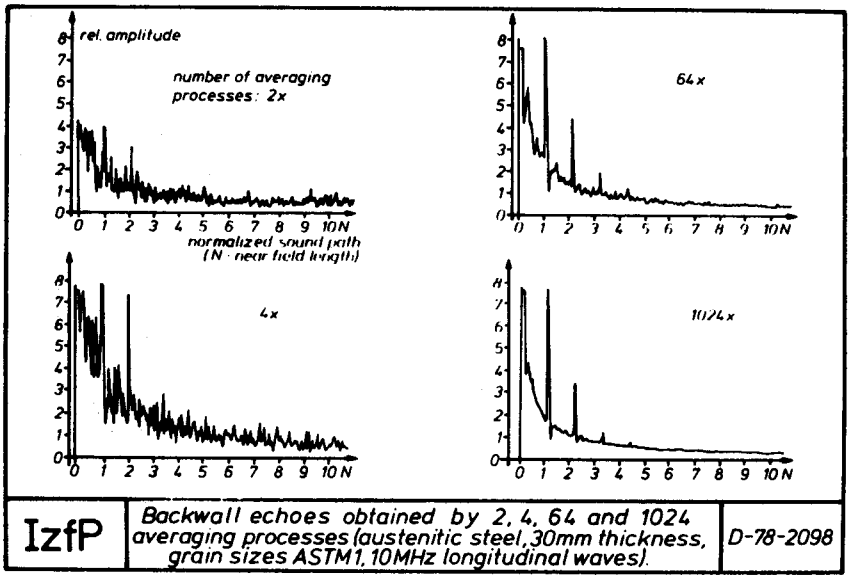


Fig. 3

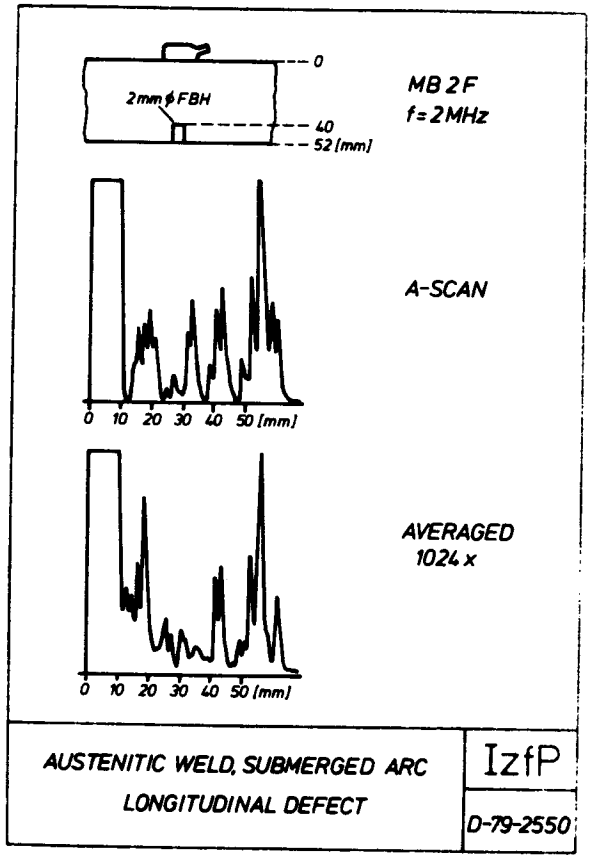

0
2mm ϕ FBH
40
52 [mm]
MB 2F
f = 2 MHz
A-SCAN
0 10 20 30 40 50 [mm]
AVERAGED
1024 x
0 10 20 30 40 50 [mm]
AUSTENITIC WELD, SUBMERGED ARC
LONGITUDINAL DEFECT
IzfP
D-79-2550

Fig. 4

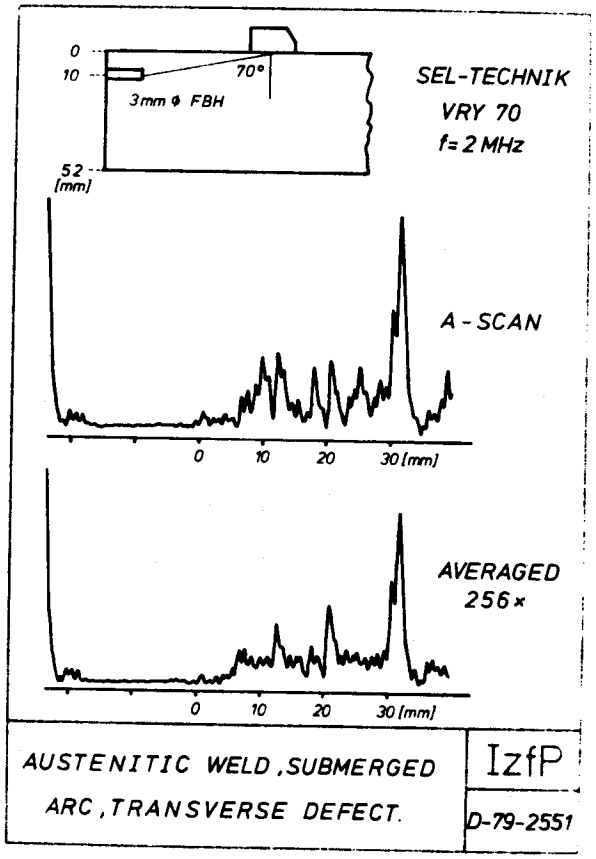

0
10
70°
3mm ϕ FBH
52 [mm]
SEL-TECHNIK
VRY 70
f = 2 MHz
A-SCAN
0 10 20 30 [mm]
AVERAGED
256 x
0 10 20 30 [mm]
AUSTENITIC WELD, SUBMERGED
ARC, TRANSVERSE DEFECT.
IzfP
D-79-2551

Fig. 5

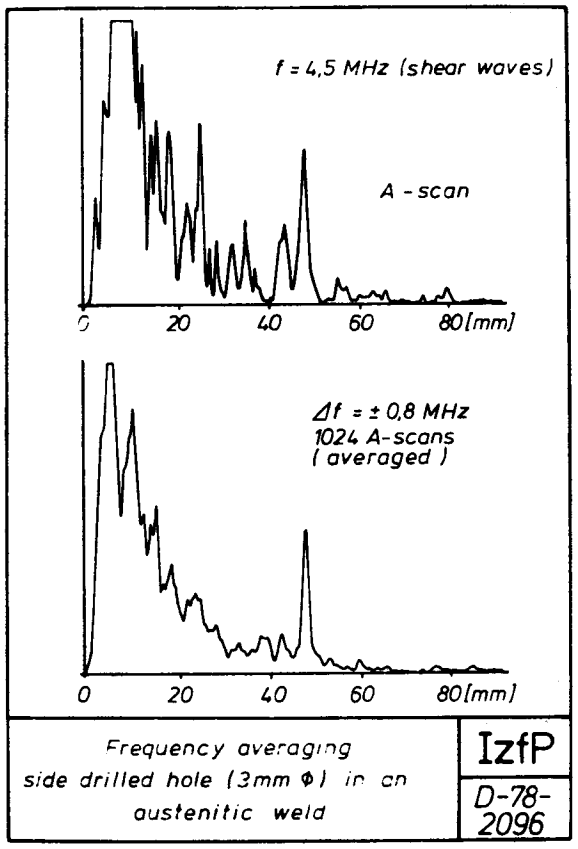

f = 4,5 MHz (shear waves)
A - scan
0
20
40
60
80 [mm]
Δf = ± 0,8 MHz
1024 A-scans
(averaged)
0
20
40
60
80 [mm]
Frequency averaging
side drilled hole (3mm Φ) in an
austenitic weld
IzfP
D-78-
2096

Fig. 6

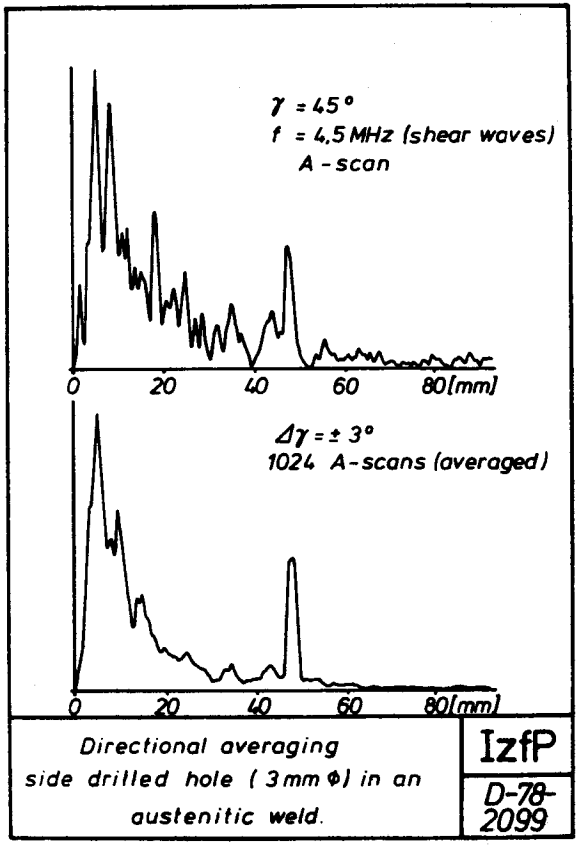

γ = 45°
f = 4,5 MHz (shear waves)
A - scan
0
20
40
60
80 [mm]
Δγ = ± 3°
1024 A-scans (averaged)
0
20
40
60
80 [mm]
Directional averaging
side drilled hole (3mm Φ) in an
austenitic weld.
IzfP
D-78-
2099

Fig. 7

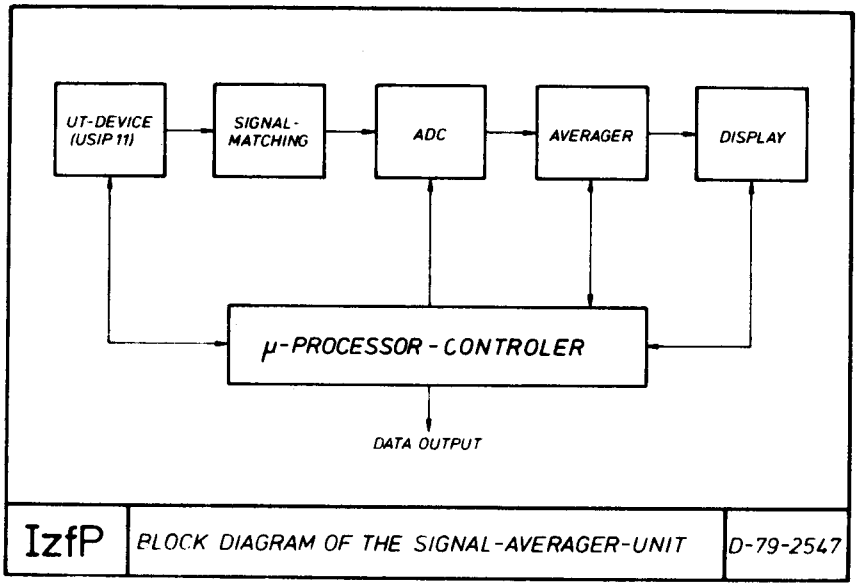

UT-DEVICE (USIP 11)
SIGNAL-MATCHING
ADC
AVERAGER
DISPLAY
μ-PROCESSOR-CONTROLER
DATA OUTPUT
IzfP
BLOCK DIAGRAM OF THE SIGNAL-AVERAGER-UNIT
D-79-2547

Fig. 8

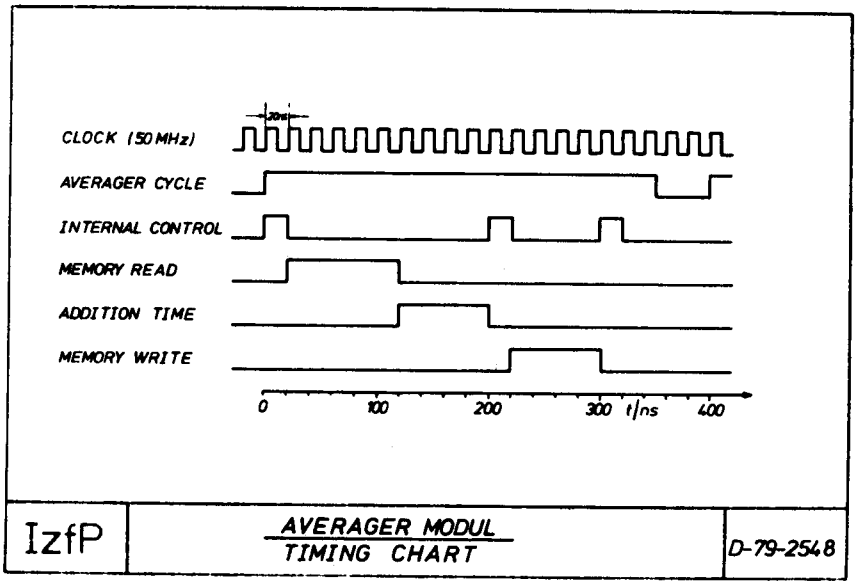

CLOCK (50 MHz)
AVERAGER CYCLE
INTERNAL CONTROL
MEMORY READ
ADDITION TIME
MEMORY WRITE
0
100
200
300
t/ns
400
IzfP
AVERAGER MODUL
TIMING CHART
D-79-2548

Fig. 9

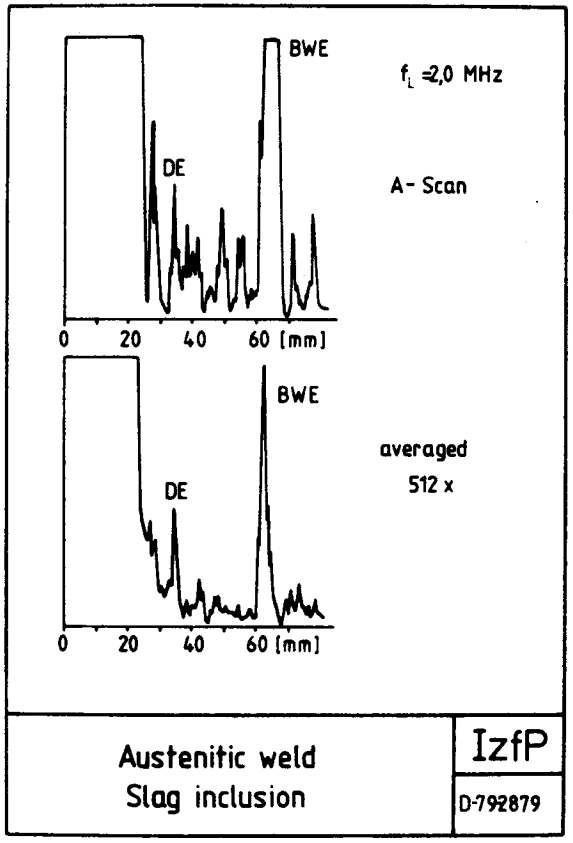


Fig. 10

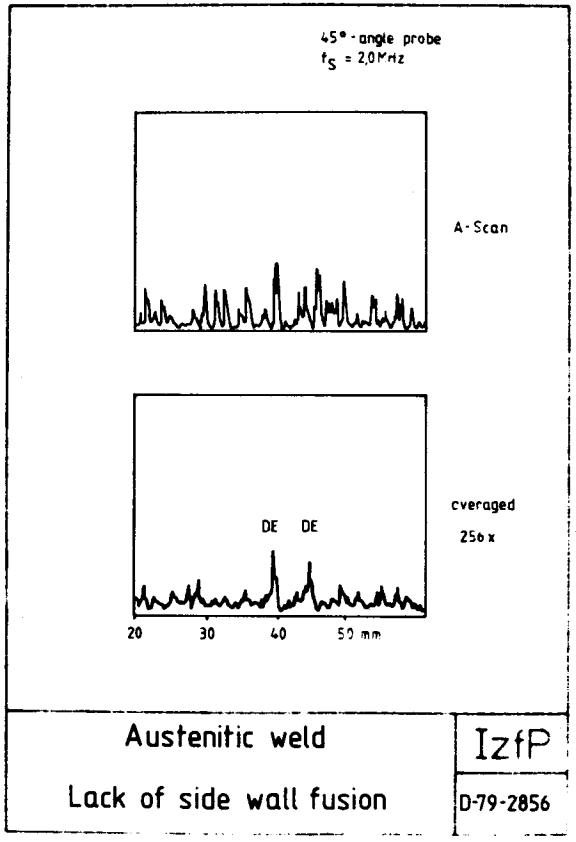


Fig. 11

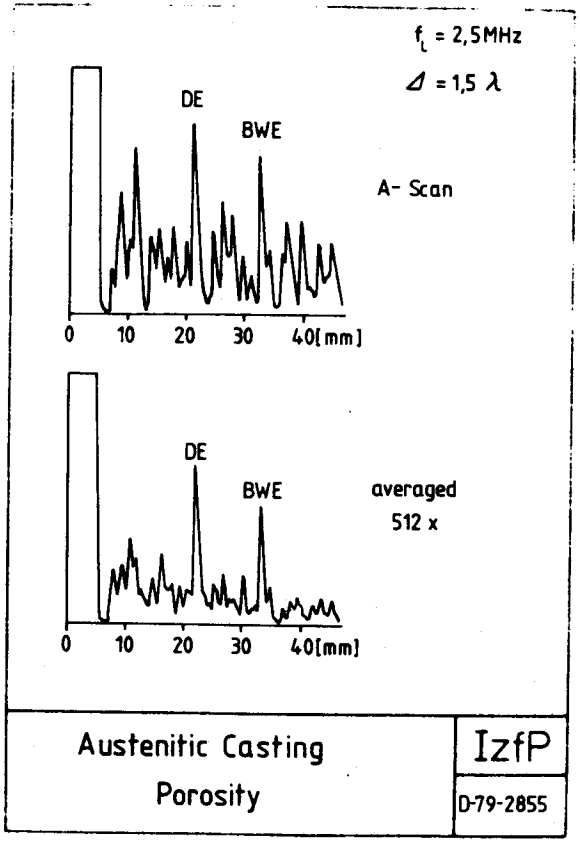


Fig. 12

Multiple - Bearing - Angle (MBA) crack detector for cladded pipe examinations.

G. GRUBER
Fraunhofer - Institut für Zerstörungsfreie Prüfverfahren, F.R. Germany

ABSTRACT

Two statistical ultrasonic techniques were developed to (1) aid in the selection of ultrasonically more readily inspectable cladded stainless steel components and (2) increase the realiability of detecting surface-breaking cracks in operating cladded piping systems. A method based on the satellite-pulse technique permits the quantification of variations in the shear-wave-velocity profile across clad-base material and weld-base material interfaces. To increase the reliability of crack detection through the introduction of redundancy into the ultrasonic inspection system, one of the anglebeam probes in a two-element nonplanar array transmits into the test material a nonevanescent longitudinal wave in addition to the usual shear wave. Results of proof-of-principle testing will be presented.

* Research Exchange Scientist from Southwest Research Institute, San Antonio, Texas

1. Introduction and Summary

Weldments and heat-affected zones (HAZ) of uncladded austenitic stainless steel piping systems are susceptible to intergranular stress corrosion cracking (IGSCC) in boiling water reactor (BWR) piping systems. Stainless steel corrosion-resistant cladding (CRC) has been applied to the inside surface of recirculation pipes in some BWR nuclear power plants so that the wrought structure be minimally susceptible to IGSCC.

The difficulties associated with the inservice inspection (ISI) of the welds and heat-affected zones of cladded recirculation pipes are well known [1-7]. The main problem appears to be not that of lack of sensitivity but that of too many "spurious indications", i.e., too much interference or "grass" which masks the small crack signals. The basic problem is the inability of the ultrasonic examiner to differentiate between the relevant ("signal", S) and irrelevant ("interference", I) parts of the highly-distorted, complex ultrasonic waveform received from a volume of cladded and/or welded structure. Tight cracks with irregular surfaces may have indications (signal echoes) too low to be separated from interference echoes originating either from the coarse microstructure of the clad/weld material (volume reverberation) or from the rough clad-base and weld-base material interfaces (surface reverberation) and thus escape detection. Conversely, interference echoes may be misinterpreted as having been caused by fatigue or stress corrosion cracks.

A synthesis of pertinent published works in the ultrasonic examination of austenitic welds of cladded piping systems has been performed. Deficiencies and capabilities of presently-employed or newly-proposed techniques for the ultrasonic examination of hard-to-inspect bimetallic stainless steel structures were assessed along with the adaptability of relatable signal generation, propagation, and processing technologies utilized in underwater acoustics, seismic communication, and medical ultrasonics. Innovative concepts and signal-to-interference ratio (SIR) enhancement choices were derived from a pattern-recognition rather than an amplitude-dependent approach through transfer of ideas from neighboring technical fields.

The development of a field-validated ultrasonic system, based on the feasibility-tested multiple-bearing-angle (MBA) crack detection technique, is the essence of recommendations for future work. If satisfactory correlations between the presence of narrow planar slits and certain readily-extractable ultrasonic signal features could be demonstrated not only with cladded test plates but also with fabricated mockups of welded cladded pipes, these relationships would be available for use in an effective/reliable volumetric examination which meets the requirements of Section XI of the American Society of Mechanical Engineers (ASME) Code.

2. Fabrication of Test Plates

The first step toward the development of a reliable ultrasonic system for the detection of fatigue or stress corrosion cracks that may develop in the recirculation pipes of some modern BWR nuclear power plants was the fabrication of cladded test plates (Fig. 1). These plates were used

to determine the main sources of interference and to establish the feasibility of half a dozen or so candidate techniques. The test plates were fabricated from materials and with cladding, heat treating, and welding procedures specified by the General Electric Company. In contrast to the field situation, however, the 12-mm thick Type 304 stainless steel "base" plates were cladded symmetrically on both sides with Type 308L stainless steel material. The clad thickness varies from 2.5 mm to 7.5 mm. Each plate contains four narrow slits ranging in depth from 0.5 mm to 5 mm. The slits are spaced 25 mm apart so as not to influence or otherwise bias the results of simulated-crack-detectability testing.

3. Main Sources of Interference

Since the interference echoes occupy a region of the time in which crack echoes could be present, it is important to establish the statistical characteristics of the main sources of interference. Unfortunately, not enough nondestructive evaluation (NDE) physics is available to provide us with guidance on the reflection, refraction, scattering, mode conversion, and other processes which may be involved. Concepts developed to model the propagation of ultrasonic signals in the inhomogeneous ocean with irregular upper and lower surfaces /8,9/ may be used to advantage in the ultrasonics of bimetallic stainless steel structures. There appear to be several, simultaneously-operating mechanisms responsible for the generation of interference echoes which hinder the detection of crack echoes. Sources of reduced SIR, which may explain the low signal-to-interference ratios encountered in the ultrasonic examination of the welds and heat-affected zones of cladded recirculation pipes, include the following deterministic and stochastic mechanisms:

(1) signal reduction associated with specular reflection of the ultrasound by discontinuities in the acoustical impedance profile at the bimetallic (base, clad, and weld metals) interfaces;

(2) signal reduction associated with refraction of the ultrasound by the discontinuities in the acoustical impedance profile at the bimetallic interfaces;

(3) volume reverberation due to multiple scattering from the coarse grains of the clad and weld materials;

(4) surface reverberation due to multiple scattering from the irregular bimetallic fusion lines; and

(5) random electronic noise.

The crack detection process is reverberation limited (rather than noise limited). This realization represents a major break from the ill-defined definition of "weld noise" or "grass" as the sum of those indications "originating in the weld area for which the source cannot be explained" (Reference 10).

Multiple backscattering from the grain boundaries in the interior of the clad and weld metals (volume reverberation) and that from the rough clad-base and/or weld-base material interfaces (surface reverberation) may produce a partially coherent interference wave field of large amplitude so as to obscure the signal wave field. The crack and reverberation echoes along the different metal paths overlap to give rise to a complex envelope for the received ultrasonic waveform which varies randomly (fluctuates) in a deterministically-unpredictable manner with slight movement of the pulse-echo transducer (probe) or shift in the center frequency of the transmitted pulse.

Upon the incident shear or longitudinal ultrasonic beam encountering an irregular base-clad or base-weld material interface, each hill and depression acts as a small localized surface scatterer so that the interference wave field received by the pulse-echo probe is the result of the superposition of a large number of waves of small amplitude and random phase. In contrast, the wave field received by the probe from the base of a surface-breaking crack remains largely coherent in space and time.

The performance of ultrasonic crack detection systems is also degraded by the randomly-oriented grain boundaries in the interior of the base, clad, and weld metals. The location and size of these volume scatterers are also randomly distributed.

In propagating from one point to another, portions of the ultrasonic energy is directed away and lost insofar as a particular receiver is concerned (deterministic mechanisms 1 and 2). Volume reverberation is always a source of interference in coarse-grained austenitic materials (stochastic mechanism 3). The multiple scatter of ultrasound by the irregular fusion lines of bimetallic structures also gives rise to random fluctuations of amplitude and phase in the received waveform (stochastic mechanism 4). For crack echoes with less than 10 dB signal-to-interference ratio, interpreting the received waveform (i.e., deciding the presence or absence of a crack based on the received, highly-distorted waveform) is marginal and completely unreliable for signals with less than 3 dB SIR.

4. Basic Experiments with Test Plates

Current understanding of the details of the physical phenomena in the ultrasonic examination of the welds and heat-affected zones of cladded stainless steel structures is limited, and does not permit the mathematical (deterministic or stochastic) derivation of the relationship between certain readily-extractable features of the received ultrasonic waveform and the relevant structure variables (e.g., state of cracking). The relationships which govern the statistical wave propagation phenomena in bimetallic structures must, therefore, be developed empirically by systematically varying the relevant material properties and ultrasonic parameters. Table 1 contains the lists of material properties and ultrasonic parameters which were varied.

Material Properties	Ultrasonic Parameters
Shear wave velocity distribution	Wave mode
Longitudinal velocity distribution	Dominant wavelength
Grain size distribution	Pulse length
Fusion line roughness distribution	Beam angle
Clad thickness distribution	Number of probes
	Separation of probes

Table 1. Variables Involved in Ultrasonic Crack Detection System Optimization Study

From the point of view of most SIR-reducing phenomena (i.e., reflection, refraction, and reverberation), uncontrolled/unknown variations in the sound velocity profile across the base-clad and base-weld material interfaces are considered to be undesired material properties. An ultrasonic creeping-wave method was developed to quantify the local variations in the shear-wave-velocity profile of cladded, welded, or otherwise bimetallic structures. The generation of the first pair of creeping waves by a hole drilled into the side of a homogeneous test specimen is shown in Fig. 2. The incident ultrasonic beam is aimed at the center of the void of diameter d so as to maximize the amplitude of the first pair of creeping waves which arrive at the pulse-echo shear wave probe after having traveled ("crept") once around the back surface of the void in opposite directions. For clarity, only the counterclockwise creeping wave is shown by the wiggly line from Q_1 to Q_2. When the ultrasound encounters the front surface of the void at point P, a specularly-reflected wave (R-wave) is sent back to the probe. A pair of Rayleigh-type surface waves is also produced by the incident wave at points Q_1 and Q_2 where the bulk-to-creeping-wave mode conversion is predicted to take place [11]. Each time the counterclockwise creeping wave reaches point Q_2, tangential reradiation, in the form of a tangentially-scattered bulk wave (S-wave) from the void during its circumvention, is launched at the desired detection angle to be received by the probe (Fig. 3 and 4). The delay time between the R pulse and its lagging "satellite" S pulse from a void of given diameter is inversely proportional to the shear velocity of the material surrounding the void [12]. The satellite-pulse technique for the determination of the variation of shear wave velocity across various base, clad, and weld material fusion lines in bi- or tri-metallic structures is based on the comparison of the separation in time-of-arrival between the main signal and the first in an infinite series of small associated pulses returned from side-drilled holes of the same diameter placed at various locations in a cladded, welded, or otherwise inhomogeneous stainless steel structure (Fig. 5). To obtain an estimate of the variability in ultrasonic shear-wave-velocity profile of cladded stainless steel piping systems, a series of measurements can be carried out on test plates fabricated with different base and clad materials, perhaps using different cladding, heat treating, and welding procedures.

A short-duration pulse was used to excite a highly-damped ultrasonic pulse-echo shear-wave probe with a center frequency of 4 MHz. The arrival time measurements were made directly from the radio-frequency (RF) waveforms displayed on the oscilloscope of a modified Sonic Mark I Ultrasonic Flaw

Detector. Using side-drilled holes of 2.50 mm diameter, the delay time ratio for stainless steel 304L and carbon steel 1020 was measured to be 1.04. This compares favorably with the expected shear velocity ratio of 1.05 as measured by a conventional ultrasonic technique. The creeping-wave shear velocity measurement technique may be used not only to determine local variations in the shear-wave-velocity profile of existing bimetallic structures but also to select acoustically better matched, and therefore ultrasonically more readily inspectable, bimetallic structures. Figure 6 shows two side-drilled holes; the upper hole was drilled into 304 stainless steel base material and the lower hole is located in 308L stainless steel clad material. An approximately 20% slower shear wave velocity was observed for the clad material (Figs. 7 and 8).

The absence of interference echoes before the R pulse and their presence both before and after the S pulse are quite noticeable in Fig. 8. This type of pulse spreading or waveform distortion may be explained as follows. Imagine a pulse of ultrasound to be incident upon the scatterers in a small volume V in an otherwise homogeneous metal. The scattering of the leading end of the pulse by the back scatterers in V may then arrive at the pulse-echo probe at the same instant as the scattering of the trailing end of the pulse by the front scatterers in V. The net effect of multiple scatter arrivals is pulse spreading. The reverberation caused by the scatterers lying within the ultrasonic beam at the range of interest and contained in the volume V increases with increasing pulselength.

5. Multiple Bearing Angle Crack Detector

In any statistical communication system, the SIR may be enhanced by a number of subsequently or simultaneously performed operations in the space, time, and/or frequency domains. The partly coherent nature of the interference field dictated that coherent detectors, based on forming the space, time, and frequency averages of the waveforms received from neighboring examination volumes, be considered as prime candidates for improving the reliability of ultrasonic inspection of the welds and heat-affected zones of cladded recirculation pipes [13-17]. The developed multiple-bearing-angle (MBA) crack detector offers superior performance over available ultrasonic techniques while being completely compatible with standard equipment and probes. The MBA crack detector utilizes the following SIR-enhancement techniques:

(1) Use of short pulses;
(2) Use of narrow beams;
(3) Use of both longitudinal and shear waves;
(4) Use of multiple bearing angles;
(5) Use of multiple frequencies;
(6) Array processing; and
(7) Spatial averaging.

In compiling this list, special consideration was given to assure compatibility of these techniques with each other. By definition, the best crack detector is the one which incorporates the demonstrable advantages of several of the listed techniques with minimum increases in system cost and complexity. Some solutions to the low-SIR problems encountered in the ultrasonics of bimetallic structures can be found in transmitted

pulse design (pulse shaping) or beamforming while others can be found in wave mode selection, pattern recognition, temporal averaging, array processing, and spatial averaging. The advantages of the listed techniques are briefly discussed.

(1) Use of Short Pulses

The volume or surface area where the reverberation echoes are produced in the welds and heat-affected zones of cladded pipes can be reduced by transmitting short pulses. Short pulses also provide for good range resolution and wide distribution of the transmitted ultrasonic energy in the frequency domain.

(2) Use of Narrow Beams

Beamforming provides another means for increasing the probability of detecting propagating IGSCC in cladded piping systems. The volume or surface area where reverberation echoes are produced can be reduced by restricting the transmitted beam. The bearing angle errors associated with signal and interference field amplitude and phase fluctuations can be reduced by the use of high-frequency, directional probes transmitting narrow beams. Beam restriction also provides for good lateral resolution

(3) Use of Both Longitudinal and Shear Waves

Splitting the transmitted energy in the time domain into two wave modes provides a further method for crack detection performance improvement. The detectability of cracks is affected by the wave mode. Longitudinal (L) waves may be better in some applications while shear (S) waves may be better in others. The sensitivity (probability of detection) or the specificity (probability of not false alarming) of the crack detector may be increased by combining the S-wave test with an L-wave test. These tests may be combined in series or in parallel (i.e., they may be performed in succession or simultaneously).

When the tests are combined in series, the inspected material is considered to be defective if it tests positive to each of the tests. The test specimen is considered to be free of defects if it tests negative to any of the tests. The series combination of tests enhances the specificity of the inspection by reduces its sensitivity.

When the tests are used in parallel, the inspected material is considered to be defective if it tests positive to any of the tests. The test specimen is considered to be free of defects if it tests negative to all tests. The parallel combination of tests enhances the probability of crack detection (sensitivity) although it reduces the specificity. To implement a combination of tests in parallel, it was decided to "resurrect" the L wave, made envanescent (i.e., suppressed) in the production of the standardized 45-degree S wave, by making the platform angle of the lucite wedge less than the usual value (37°) by about 8 degrees. This amounts to increasing the reliability of crack detection through the introduction of redundancy into the ultrasonic inspection system. The wedge-module design and the production of both a L wave and a S wave by one probe (Probe A) and only a S wave by another probe (Probe B) are presented below.

(4) Use of Multiple Bearing Angles

Splitting the transmitted energy in the space domain into several bearing angles provides still another method for improving the performance of the crack detector. Phase-locked multiple beams, produced by two or more probes connected in parallel to a common transmit-and-receive electronic system, may be employed to distinct advantage since it is unlikely that all transmitted pulses give rise to interference echoes in concert. The interference model assumed in this analysis consists of a statistically large number of statistically independent volume and surface reverberation sources (scattering centers) located at various distances and oriented at various angles relative to the multiple-bearing-angle (MBA) array shown in Fig. 9. The scattering centers are assumed to be uniformly distributed over all directions and all distances. Even though the examination volumes of the three beams L_a, S_a, and S_b seen in Fig. 10 are overlapping, the interference echoes received by the two probes may be assumed to be largely independent of one another and of the crack echoes.

For the purpose of introducing redundancy into the ultrasonic crack detection system, Probe A is positioned on a lucite wedge module so as to transmit into the bimetallic test specimen a nonevanescent longitudinal wave, L_a, in addition to the usual shear wave, S_a. A second probe is placed strategically behind the first so that Probe B receives the shear wave reflected from the base of the surface-breaking crack, S_b, on the average at the same time when S_a is received by Probe A. The adjustable lucite paths are used to compensate for the metal path differences between the S_a and S_b beams. The proper values for the probe separation, platform angles α_1 and α_2, and bearing angles β_1, β_2, and γ_1 depend mainly, but not critically, on the pipewall thickness h.

The interference echoes received by the probes will generally be statistically independent time functions governed by separate metal path effects. The degree of coherence of the interference field is dependent upon the probe separation distance and the spatial characteristics of the interference field in neighboring examination volumes. Probe separation distances of 15 mm or greater have been found to reduce the coherence of the interference field in the cladded test plates to negligible levels.

Multiple-beam techniques yield more reliable results than single-beam techniques because the former smooth out the random phase and amplitude fluctuations. With the simple addition of waveforms received by the two probes, which amounts to real-time signal averaging, more decorrelation of the interference field than that of the signal field is expected to occur. The result is an enhancement in SIR. Figure 11 illustrates the SIR-enhancement which can be achieved by temporal averaging (i.e., without any probe movement) in the detection of a 5 percent deep sawcut in a double-cladded plate.

(5) Use of Multiple Frequencies

Unlike the crack echoes, the interference echoes are stronly influenced by the ratio of the dominant wavelength present in the transmitted L or S wave to the mean grain size and the mean roughness of the clad-base and the weld-base material fusion lines. While the reverberation level is less at lower frequencies, it is easier to transmit short pulses at

higher frequencies. It may be advantageous to use one resonance frequency for Probe A and another for Probe B ("frequency wobbling").

(6) Array Processing

Interference level fluctuations can be reduced by the use of multi-element arrays, since each element in the array yields extra information about the location of the surface-breaking crack to be detected. A three-element, nonplanar array arranged in the form of a triangle provides, for example, three opportunities for pairwise cross-correlation. The output SIR available for crack detection depends on the directivity pattern of the array, the space-time-frequency characteristics of the signal field, and the space-time-frequency characteristics of the interference field. The bearing angle errors associated with the amplitude and phase fluctuations can be reduced by the use of directional arrays. Useful redundancy and supplemental bearing angle information can be obtained without having more than three elements in the array. The probes should be connected in parallel to the same transmit-and-receive electronics. The detection process for surface-breaking cracks becomes a relatively simple matter of recognizing the characteristic LS pulse pair or doublet which is uniquely associated with surface-breaking cracks (see Fig. 10 and lowest trace in Fig. 11).

(7) Spatial Averaging

A small change in the position of the MBA-array may change the interference field significantly but leave the crack echoes basically unchanged. The LS pulse pair recognition process may be further aided by averaging the output of the MBA-array over several hundred statistically different array positions. Spatial averaging is recommended when the LS doublet is not clearly evident from the individual waveforms. Proof-of-principle results on the SIR-enhancement achievable with spatial averaging are presented in Fig. 12.

REFERENCES

/1/ Edelmann, X., "Application of Ultrasonic Testing Techniques on Austenitic Welds for Fabrication and Inservice Inspection", Third International Conference on Nondestructive Evaluation in the Nuclear Industry, February 11-13, 1980, Salt Lake City, Utah

/2/ Edelmann, X., "The Practical Application of Ultrasonic Testing of Austenitic Weld Joints", Materials Evaluation, 37, 47-51, September 1979

/3/ Lapides, M. E., "Improved Ultrasonic Inspection Methods for Stainless Steel Piping", Electric Power Research Institute Project NP-1153-SR Special Report, August 1979

/4/ Potter, E., "Ultrasonic Examination of Austenitic Stainless Steel Welds", Third International Conference on Nondestructive Evaluation in the Nuclear Industry, February 11-13, 1980, Salt Lake City, Utah

/5/ Saitoh, T., "Measuring the Depth of Cracks in Austenitic Stainless Steel Overlays by Ultrasonic Technique", Third International Conference on Nondestructive Evaluation in the Nuclear Industry, February 11-13, 1980, Salt Lake City, Utah

/6/ Johnson, L., "Ultrasonic Testing of Dissimilar Metal Welds", paper presented at 1979 EPRI Nondestructive Evaluation Meeting, October 22-23, 1979, EPRI NP-1234-SR Special Report, December 1979

/7/ Hudgell, R. J. and H. Seed, "Ultrasonic Longitudinal Wave Examination of Austenitic Welds", British Journal of Nondestructive Testing, 22, February 1980, pp. 78-85

/8/ Urick, R. J., Principles of Underwater Sound for Engineers, Chapter 8, McGraw-Hill Book Company, New York, 1967

/9/ Ol'shevskii, V. V., Characteristics of Sea Reverberation, Consultants Bureau Translation from the Russian, New York, 1967

/10/ Smith, J. H., "Ultrasonic Evaluation of Dissimilar-Metal Transition Joint Welds", Oak Ridge National Laboratory Report ORNL/TM-6679/R1, June 1979

/11/ Überall, H., Surface Waves in Acoustics, Chapter 1, Physical Acoustics -- Principles and Methods, Volume X, Mason, W. P. and Thurston, R. N. editors, Academic Press, 1973

/12/ Gruber, G. J., "Defect Identification and Sizing by the Ultrasonic Satellite-Pulse Technique", in Proceedings of 1979 DARPA/AFML Review of Progress in Quantitative Nondestructive Evaluation, Report No. AFML-TR-80-55, May 1980

/13/ Kuppermann, D. S., et al., "Evaluation of Ultrasonic Techniques for Detection of Stress-Corrosion Cracks in Stainless Steel Piping", Electric Power Research Institute Project NP-761 RP449-1 Special Report, June 1978

/14/ Kraus, S. et al., "Fast Signal-Averaging Unit for Ultrasonic Testing. Characterization of Materials Properties and SNR-Improvement for Coarse-Grained Materials", paper presented at ARPA/AFML Review of Progress in Quantitative Nondestructive Evaluation, Rockwell Science Center, July 8-13, 1979

/15/ Kraus, S. and Goebbels, K., "Signalmittelungs-Verfahren zur Unterdrückung des kohärenten Untergrundes bei der US-Fehlerprüfung grobkörniger Werkstoffe", Institut für zerstörungsfreie Prüfverfahren, Saarbrücken, West Germany, Report No. 760717-TW, 1976 (available: Gesellschaft für Reaktorsicherheit mbH, Glockengasse 2, D-5000 Köln 1)

/16/ Linzer, M. et al., "Development of High-Sensitivity Ultrasonic Techniques for In-Service Inspection of Nuclear Reactors", U.S. Nuclear Regulatory Commission Report NUREG/CR-1076, November 1979

/17/ Goebbels, K., "On the State-of-the-Art and Advanced Techniques to Improve the Signal-to-Noise Ratio for the Ultrasonic Testing of Coarse Grained Materials", Third International Conference on Nondestructive Evaluation in the Nuclear Industry, February 11-13, 1980, Salt Lake City, Utah

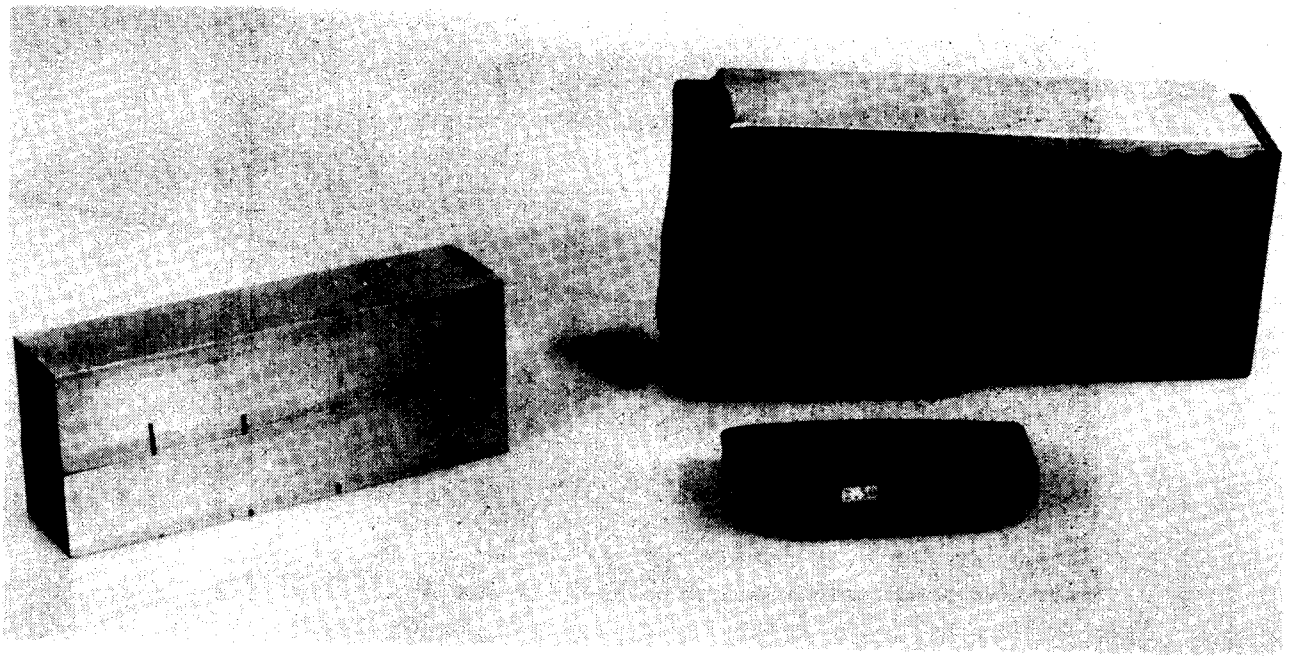


Fig. 1. Cladded Pressure Vessel, Pipe, and Test Plate Samples

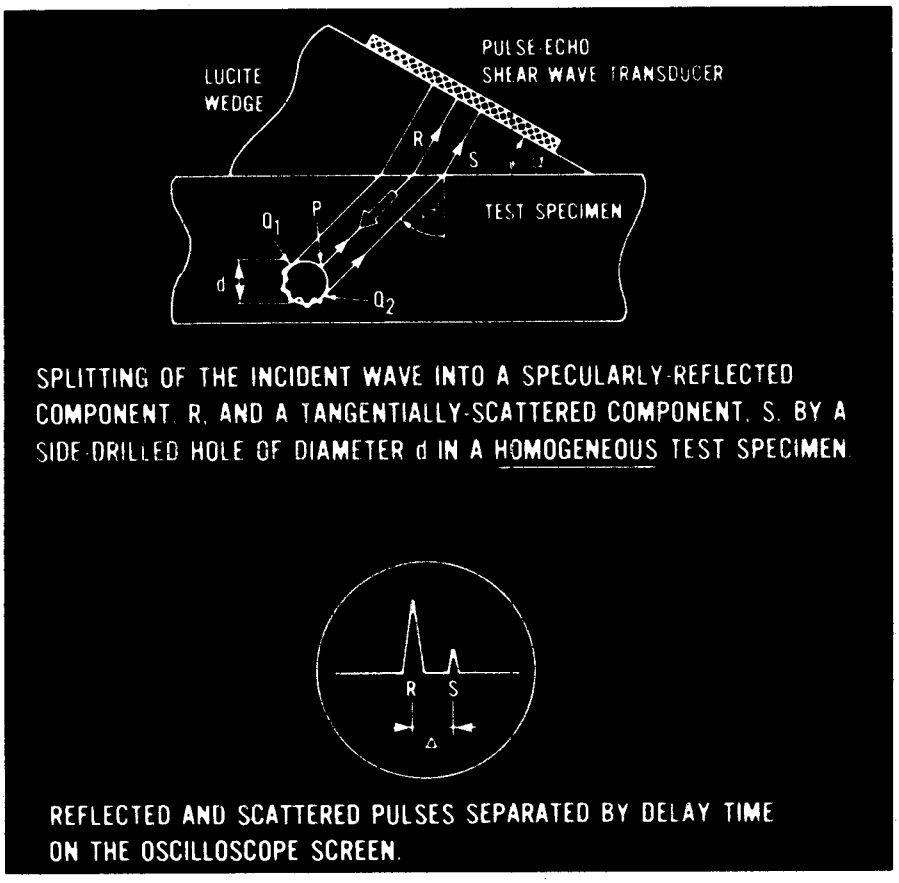


Fig. 2. Generation of a Pair of Echoes by a Side Drilled Hole in a Homogeneous Test Specimen

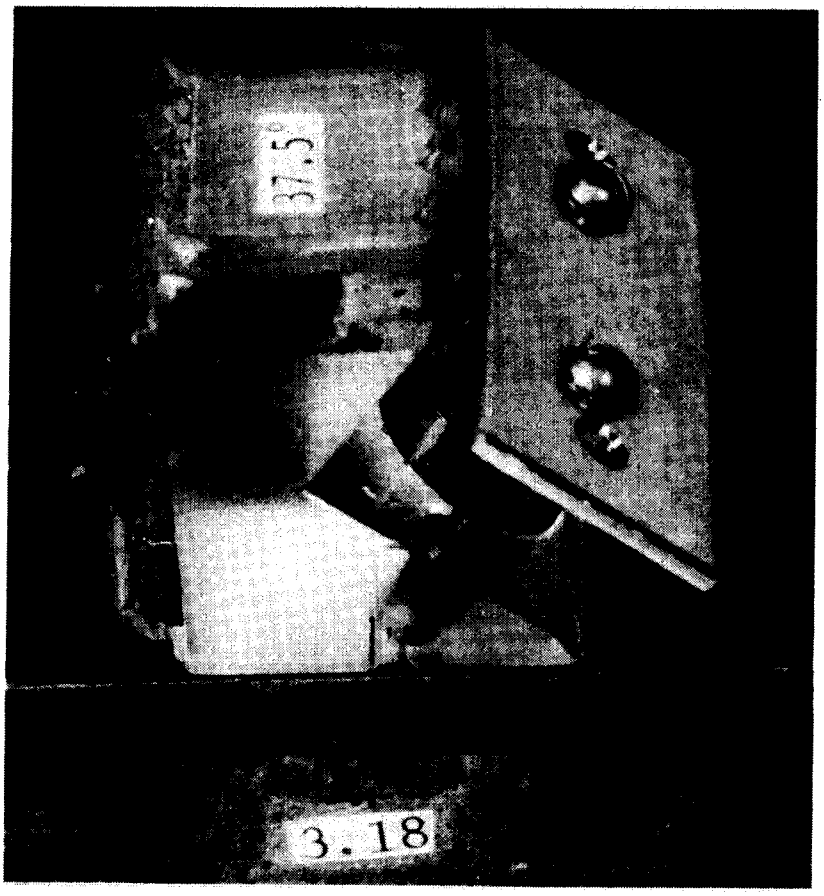


Fig. 3. Pulse-Echo Shear Wave Probe Aimed at a 3.18 mm Diameter Side Drilled Hole in a Homogeneous Test Specimen

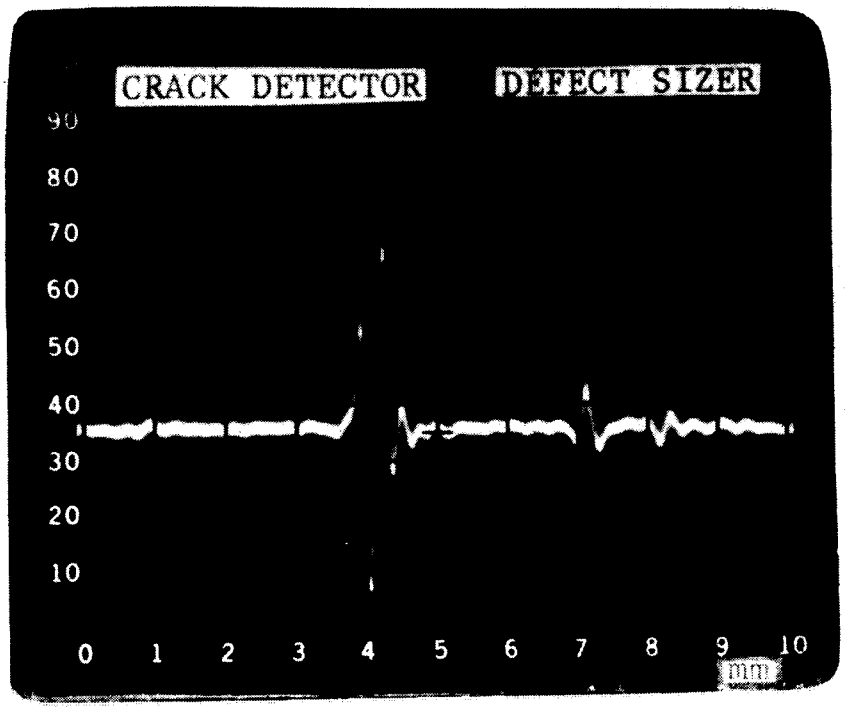


Fig. 4. Reflected and Satellite Pulses from a 3.18 mm Diameter Side Drilled Hole

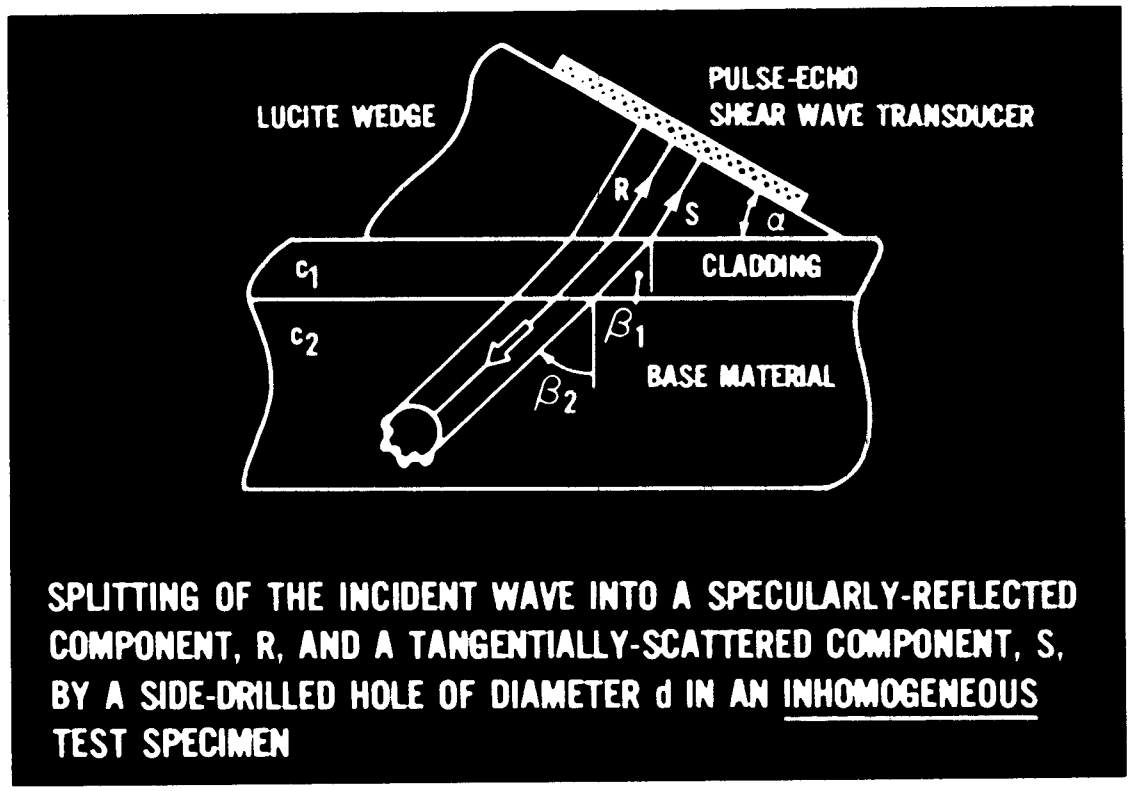


Fig. 5. Generation of a Pair of Echoes by a Side Drilled Hole in an Inhomogeneous Test Specimen

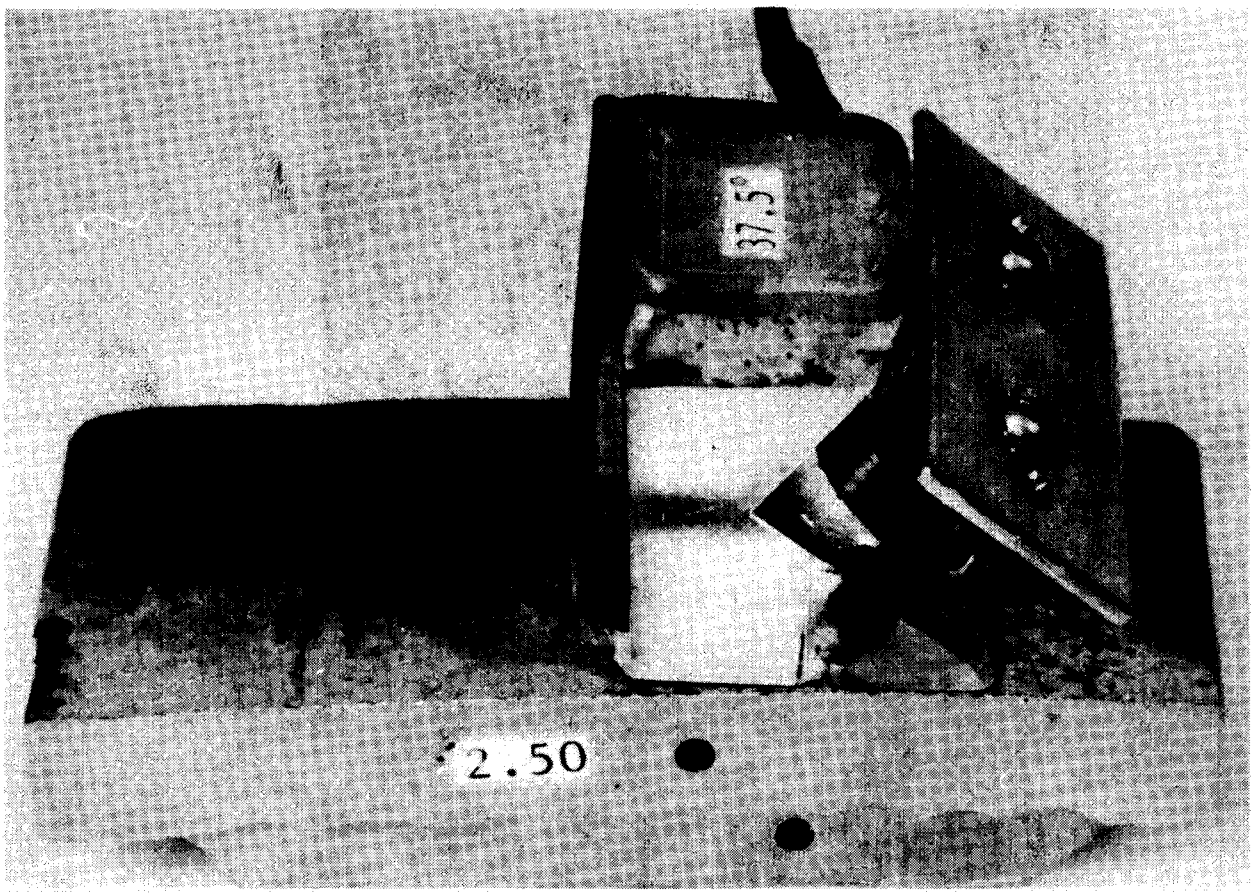


Fig. 6. Pulse-Echo Shear Wave Probe Aimed at 2.50 mm Diameter Side Drilled Holes in a 304-308L Bimetallic Test Specimen

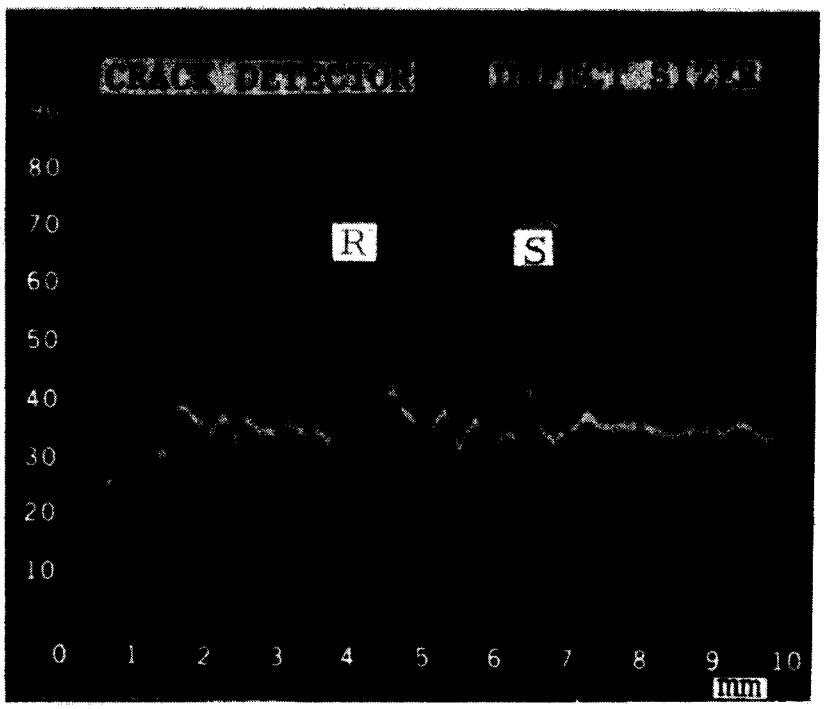


Fig. 7. Reflected and Satellite Pulses from a 2.50 mm Diameter Side Drilled Hole in the Base Material

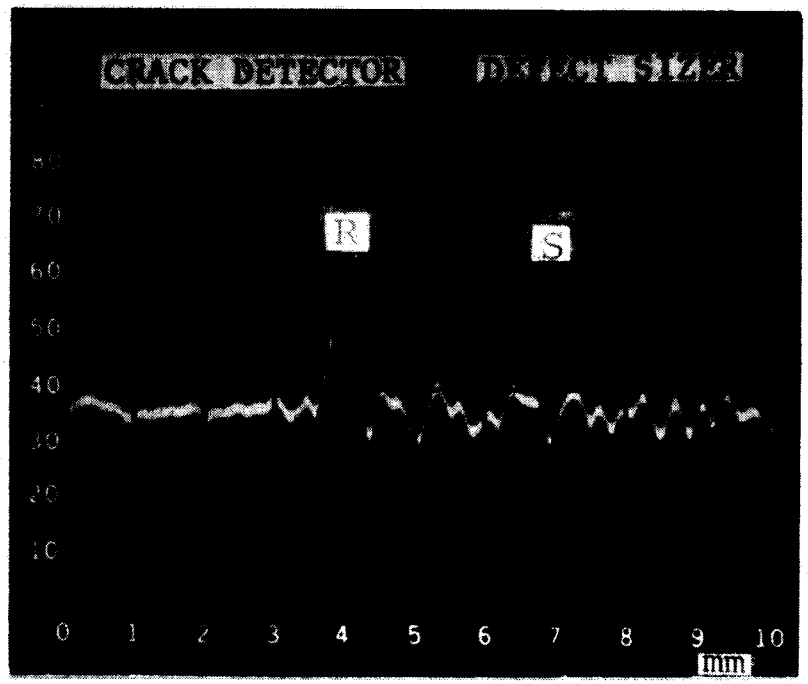


Fig. 8. Reflected and Satellite Pulses from a 2.50 mm Diameter Side Drilled Hole in the Clad Material

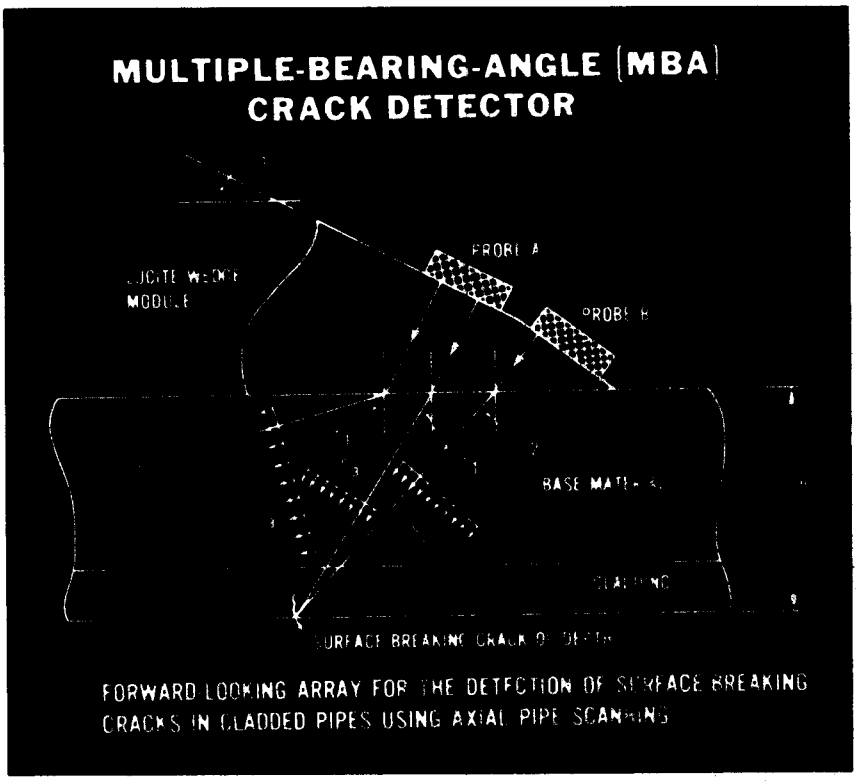


Fig. 9. Two-Element Array of Multiple-Bearing-Angle (MBA) Crack Detector

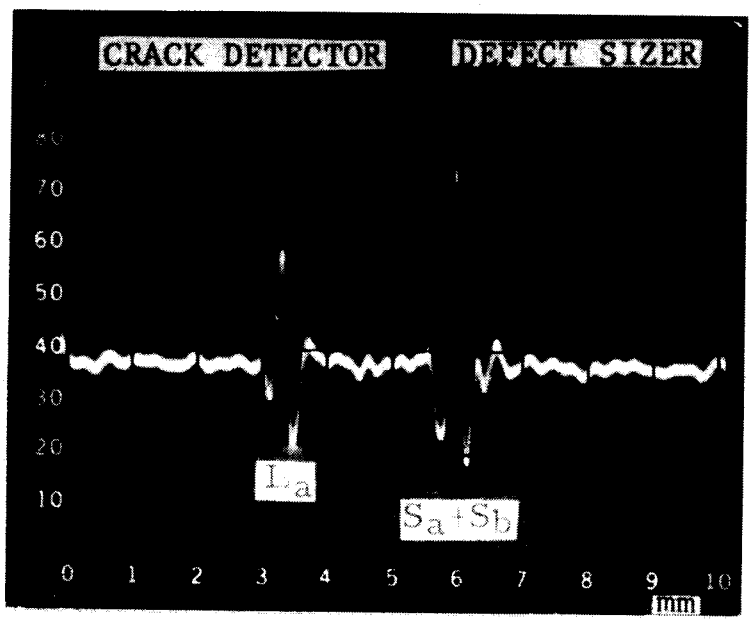


Fig. 10. Superposition of Three Beams Received by the MBA Array of Fig. 9

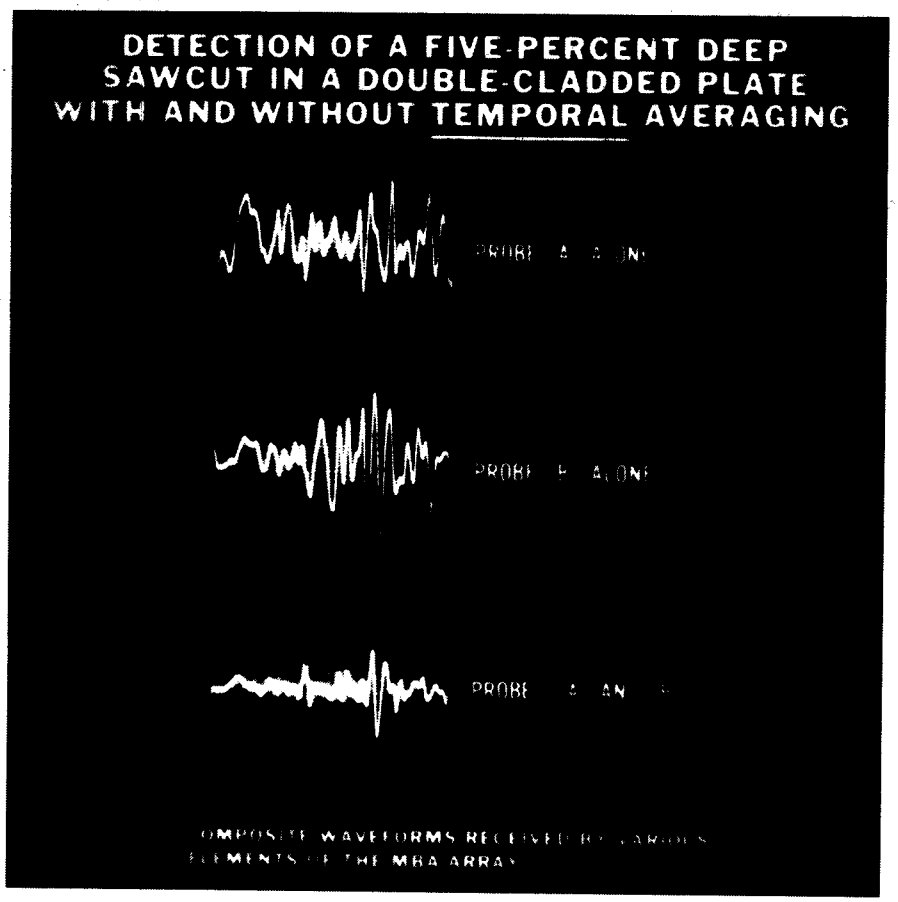


Fig. 11. Signal-to-Interference Ratio Enhancement Achievable by Temporal Averaging

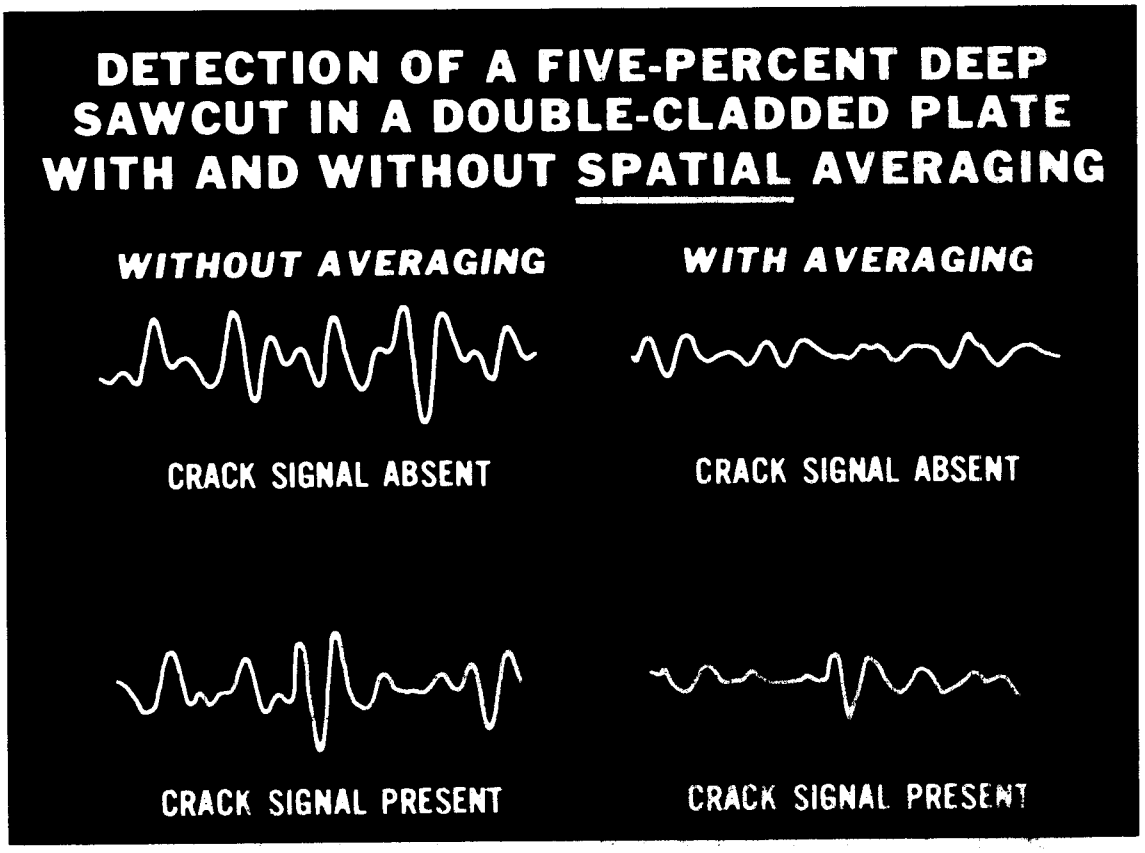


Fig. 12. Signal-to-Interference Ratio Enhancement Achievable by Spatial Averaging

Flaw-to-grain echo enhancement by split-spectrum processing *

V.L. NEWHOUSE, N.M. BILGUTAY, J. SANIIE
Purdue University, USA

ABSTRACT

A split-spectrum processing technique for an ultrasonic flaw detection system is demonstrated which improves the flaw-to-grain echo ratio in large grained materials. The enhancement is achieved by partitioning a wide band received spectrum, to obtain uncorrelated or partially correlated bands, which are then processed to suppress the grain echoes with respect to the flaw echo. Simulation data and experimental results for titanium are presented showing improved flaw detection capabilities.

Note of the editor : full paper not submitted for publication.

Introduction:

When the range cell of an ultrasound system contains many unresolved and random reflectors such as grains, the overlapping echoes which result make the detection of flaws within the range cell difficult even when the flaws are substantially larger than the grains.

A similar problem exists in radar when targets are embedded in smaller random targets, known as clutter, which like grains result in unresolved and randomly distributed reflections that conceal the desired target. To improve the detection of targets in clutter, techniques known as frequency diversity or agility have been used where clutter echoes are decorrelated by simultaneously transmitting with two or more channels centered at different frequencies or by shifting the transmitted frequency between pulses. The resulting decorrelated signals are then averaged, which results in signal-

* Supported by EPRI project number RP1395-4 and Purdue NSF-MRL Program DMR 77-23798.

to-clutter enhancement [1,2]. The application of frequency agility to flaw visibility enhancement was suggested by Koryachenko [3] and successful experimental results were reported by Goebbels [4].

In this paper we describe a split-spectrum processing technique first reported at a recent conference [5], which gives results superior to frequency averaging. This technique operates by plotting the minimum amplitudes of different frequency segments of a broad band echo signal as a function of time.

Experimental Technique:

In previous work [4] the frequency agility technique has been applied to r.f. flaw detection systems simply by shifting the center frequency of the transmitted signal within the bandwidth of the transducers and processing the data by time averaging as in radar. Since each output function must be sampled and stored individually, this process has the disadvantage of being both time consuming and requiring a large storage space in the computer. However, a significantly simpler technique is possible for obtaining the individual output functions when a wide band signal is transmitted. Thus, it can be shown theoretically that the filtering necessary to obtain the output functions corresponding to adjacent frequency bands can be achieved at the receiver by computer processing rather than at the transmitter by real filters, with equivalent results.

In the work described here a wide band transmitted noise signal centered at 5 MHz with 3 MHz half-power bandwidth was used in a previously described random signal correlation system [6]. A typical output of this system as a function of range is shown in Fig. 1. This wide band output of the correlation system is Fourier transformed and split into adjacent spectral bands by means of Gaussian shaped digital filters. These spectral

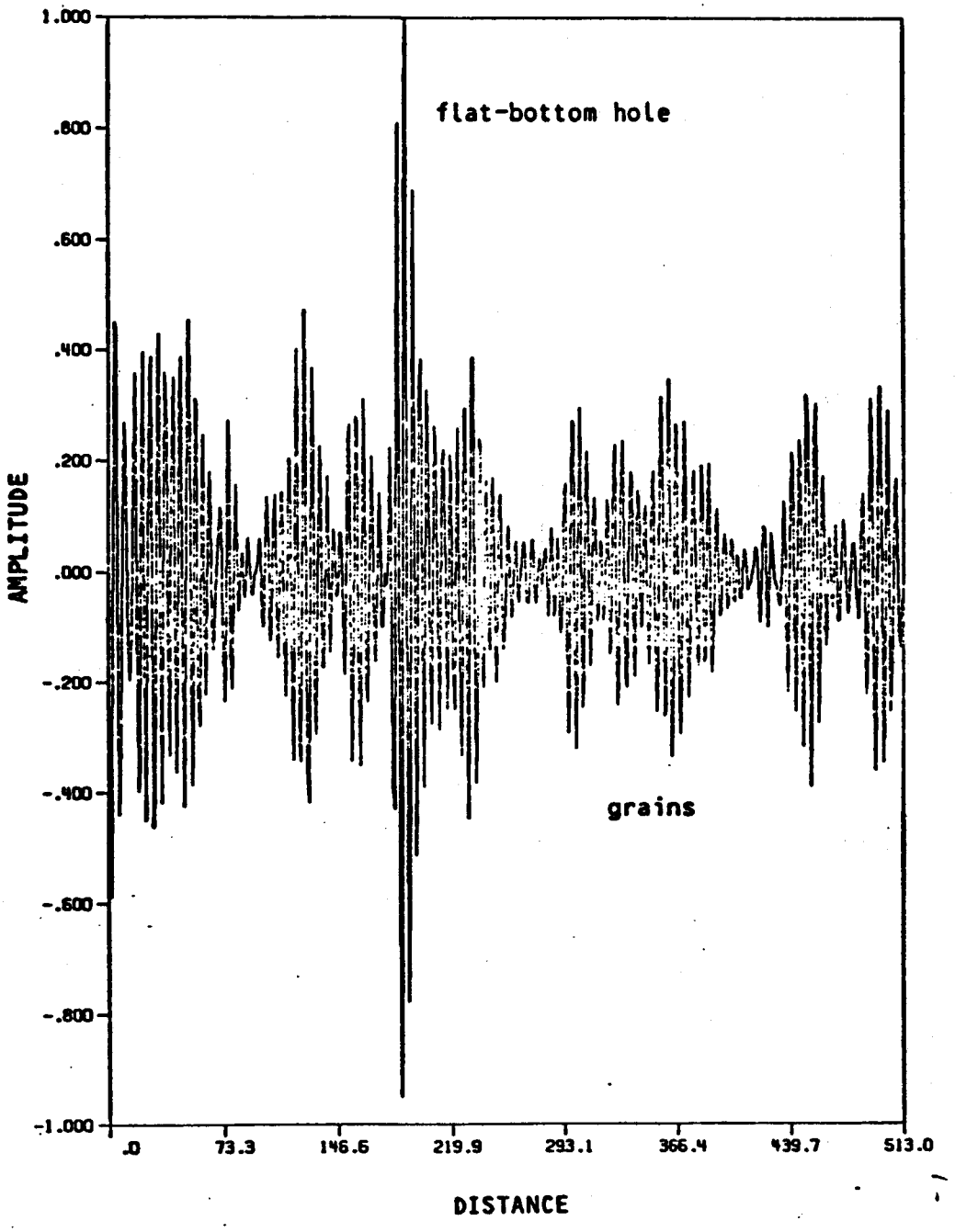


Fig. 1 Correlator output for a titanium sample with 3/64 inch diameter flat-bottom hole.

bands are then inverse Fourier transformed and the resulting separate correlation functions are normalized to a single amplitude. This normalization procedure has the effect of enhancing the effective bandwidth of the system. Using these individual correlation functions, the algorithms described below are used to obtain a single correlator output with improved flaw visibility.

Experimental Results:

The algorithms whose performances are described here will be referred to as the averaging and the minimization techniques respectively. The averaging technique is similar to the square law detection followed by n-pulse integration used in radar systems. In this technique, the received signals corresponding to different frequency bands are first squared and then averaged. The minimization technique which was originally introduced by this group [5], selects and plots the minimum squared amplitude from among the frequency bands at each point. The two algorithms have been applied to titanium samples with average grain sizes between 0.01-0.02 mm, containing flat-bottom holes simulating flaws.

Fig. 1 shows the unprocessed correlator output for a 3/64 inch diameter hole at 3 inch depth surrounded by grain echoes. The correlation functions used in the processing algorithms are obtained by filtering the amplitude spectrum of the wide band echo shown in Fig. 1 with Gaussian shaped filters having selectable bandwidths b and center frequency spacing Δf. Therefore, the number of bands m used for split-spectrum processing is determined by the frequency jump Δf and the total available bandwidth B, which is 2 MHz in these experiments and lies between 4-6 MHz.

An example of a processed output using the minimization algorithm with b = 500 KHz and Δf = 100 KHz is shown in Fig. 2. The output shows significant improvement in flaw-to-grain echo ratio as well as enhanced resolution

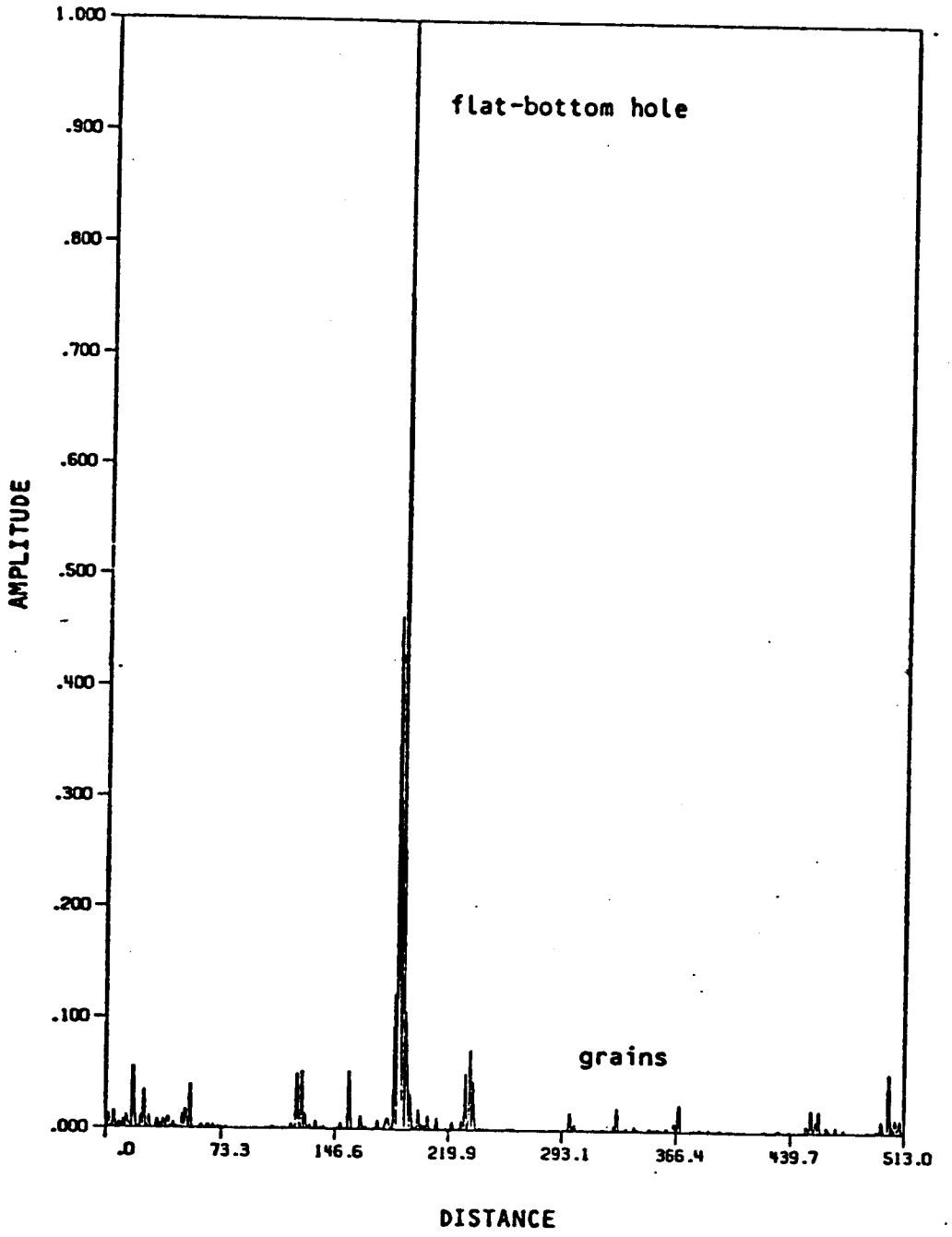


Fig. 2 Signal of Fig. 1 processed with the minimization algorithm. b = 0.5 MHz, Δf = 0.1 MHz, B = 2.0 MHz, m = 21.

compared to the original output shown in Fig. 1.

Fig. 3 shows the plots of experimental flaw-to-maximum grain echo ratio enhancement (F/G) vs. bandwidth b for various values of frequency jump Δf. The enhancement factor, F/G, is calculated by determining the ratio of the flaw echo to the maximum grain echo in the processed output and dividing it by the corresponding ratio in the squared correlator output.

Results for the same titanium sample using the averaging algorithm are shown in Fig. 4 as F/G vs. b for various values of Δf. We see that the maximum value for F/G is distinctly smaller than that given by the minimization algorithm shown in Fig. 3. These two figures are discussed further in the theoretical section.

The effect of the average grain size on the performance of the minimization algorithm was investigated by simulation. Fig. 5 shows the plot of F/G vs. b with Δf = 143 KHz for average grain sizes of 0.05, 0.1 and 0.2 mm corresponding to 25, 50 and 100 grain boundaries within the scan range, respectively. These results show that for average grain size Δx = 0.2 mm the F/G results are significantly worse than those for Δx = 0.1 mm and Δx = 0.05 mm. Although the peak values of F/G for all three cases occur between b = 300-400 KHz indicating that the optimum bandwidth is independent of the average grain size, the peak values are higher for smaller Δx. These results indicate that the performance of the minimization algorithm is affected in a positive manner as the average grain size is reduced.

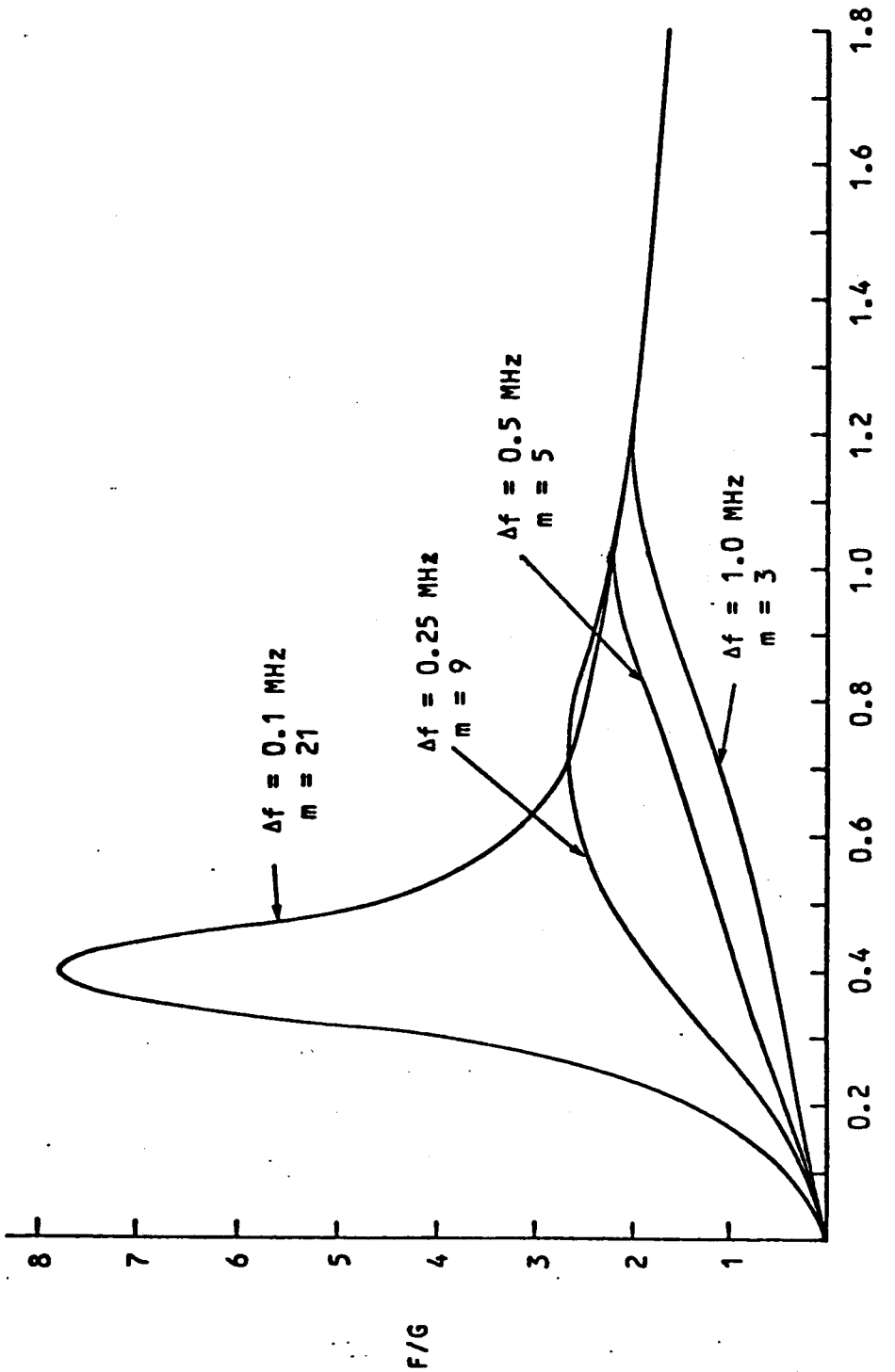


Fig. 3 Flaw-to-maximum grain echo ratio enhancement vs. bandwidth in titanium sample for the minimization algorithm. Available bandwidth B = 2.0 MHz, Δf = frequency spacing between spectral samples, m = number of spectral samples.

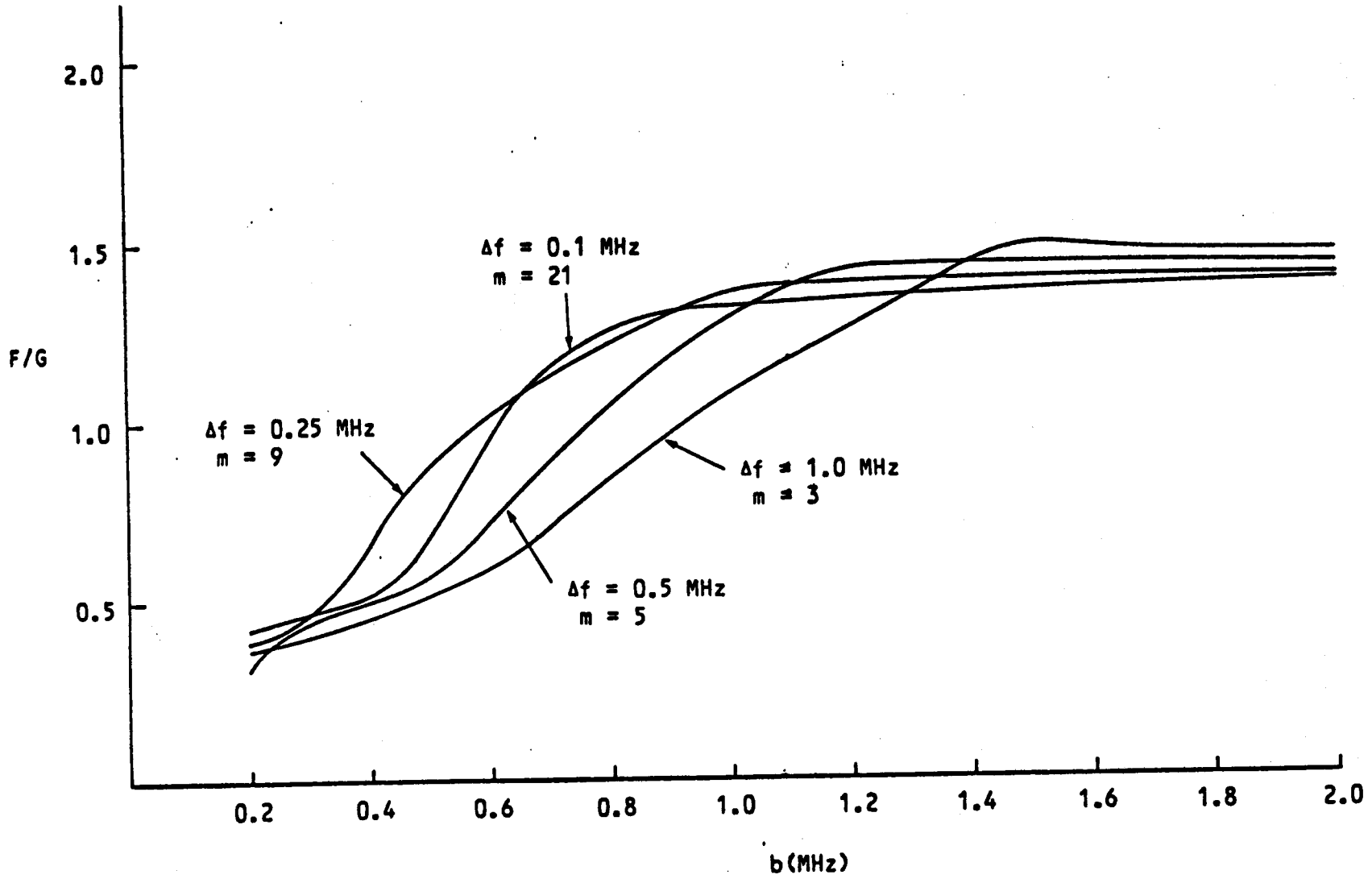


Fig. 4 Flaw-to-maximum grain echo ratio enhancement vs. bandwidth in titanium sample for the averaging algorithm.
Available bandwidth B = 2.0 MHz, Δf = frequency spacing between spectral samples, m = number of spectral samples.

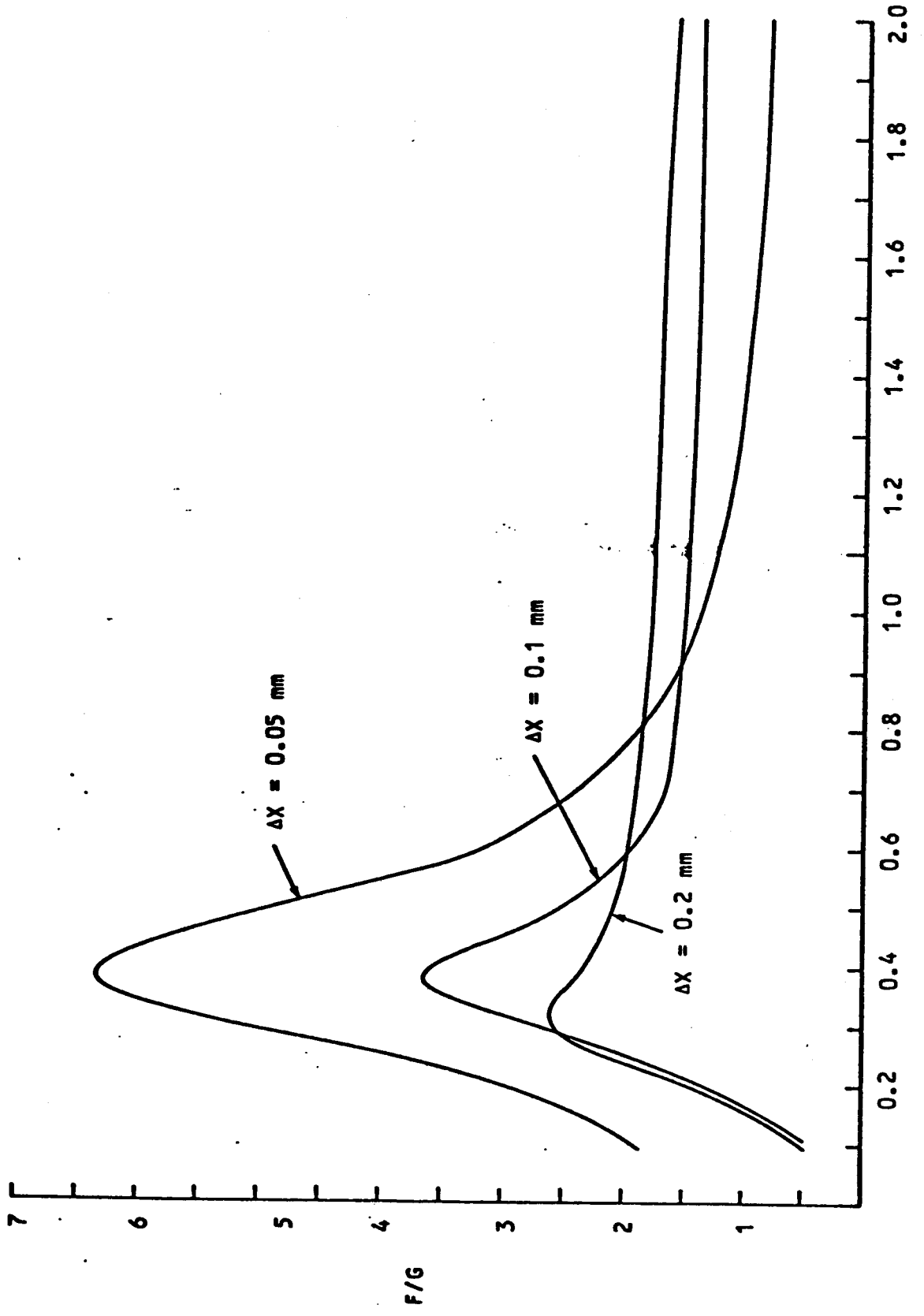


Fig. 5 Flaw-to-maximum grain echo ratio enhancement vs. bandwidth for simulated minimization algorithm with selected values of Δx (average grain size).

Conclusion:

This paper has addressed itself to the task of detecting the presence of a single relatively strong sound reflector (i.e. flaw) situated in the range cell of an ultrasound echo system, under circumstances where the echo from the strong reflector is dominated by the sum of echoes resulting from smaller, unresolved reflectors (grains) which fill the range cell. We have demonstrated that the flaw-to-maximum grain echo ratio can be enhanced by nearly an order of magnitude by procedures in which the echo of a broad band transmitted ultrasound signal is split into many spectral components which are processed and subsequently recombined. Two algorithms have been described which make use of the fact that echoes from scatterers which are too close to be resolved, are dominated by interference effects such that their amplitudes strongly with frequency. Since the amplitudes of the echoes from the large and well separated scatterers are relatively unaffected by frequency changes, a mechanism is available for extracting a large scatterer echo from the combined echo of many smaller scatterers.

The results presented here show the feasibility of split-spectrum processing for ultrasonic applications. Further research may lead to even more powerful algorithms, matched to the different classes of flaws and grain structures.

Acknowledgements

The authors would like to thank Dr. Peter Winchell for his assistance in estimation of the grain size for the titanium samples used in the experiments and Dr. Eric Furgason for his suggestion of the minimization algorithm.

References

[1] E. W. Beasley and H. R. Ward, "A Quantitative Analysis of Sea Clutter Decorrelation with Frequency Agility," IEEE Transactions on Aerospace and Electronic Systems, Vol. AES-4, pp. 468-473, 1968.

[2] H. Ray, "Improving Radar Range and Angle Detection with Frequency Agility," Microwave Journal, Vol. 9, pp. 63-68, 1966.

[3] V. D. Koryachenko, "Statistical Processing of Flaw Detector Signals to Enhance the Signal-to-Noise Ratio Associated with Structural Reverberation Noise," Soviet Journal of Non-Destructive Testing, Vol. 11, pp. 69-75, 1975.

[4] S. Kraus and K. Goebbels, "Improvement of Signal-to-Noise Ratio for the Ultrasonic Testing of Coarse Grained Materials by Signal Averaging Techniques," First Int. Symp. on Ultrasonic Materials Characterization, NBS, Gaithersburg, Maryland, June 7-9, 1978.

[5] N. M. Bilgutay, J. Saniie, E. S. Furgason and V. L. Newhouse, "Flaw-to-Grain Echo Enhancement," Proc. Ultrasonics International '79, Graz, Austria, pp. 152-157, 1979.

[6] N. M. Bilgutay, E. S. Furgason and V. L. Newhouse, "Evaluation of Random Signal Correlation System for Ultrasonic Flaw Detection," IEEE Trans. Sonics and Ultrasonics, Vol. SU-23, pp. 329-333, 1976.

[7] V. L. Newhouse and E. S. Furgason, "Ultrasonic Techniques in Flaw Detection," Ch. III, Research Techniques in Non-Destructive Testing, (R. S. Sharpe, ed.), Academic Press, 1977.

Figure Captions

Fig. 1 Correlator output for a titanium sample with 3/64 inch diameter flat-bottom hole.

Fig. 2 Signal of Fig. 1 processed with the minimization algorithm. $b = 0.5$ MHz, $\Delta f = 0.1$ MHz, $B = 2.0$ MHz, $m = 21$.

Fig. 3 Flaw-to-maximum grain echo ratio enhancement vs. bandwidth in titanium sample for the minimization algorithm. Available bandwidth $B = 2.0$ MHz, Δf = frequency spacing between spectral samples, m = number of spectral samples.

Fig. 4 Flaw-to-maximum grain echo ratio enhancement vs. bandwidth in titanium sample for the averaging algorithm. Available bandwidth $B = 2.0$ MHz, Δf = frequency spacing between spectral samples, m = number of spectral samples.

Fig. 5 Flaw-to-maximum grain echo ratio enhancement vs. bandwidth for simulated minimization algorithm with selected values of Δx (average grain size).

Ultrasonic imaging techniques in non-destructive evaluation

S. GANAPATHY
University of Michigan, USA

ABSTRACT

Recent progress in the development of a synthetic aperture focusing system for ultrasonic pulse-echo evaluation is described in this paper. This paper describes results in some selected areas of our work towards the design of a real-time field implementable system. Deconvolution combined with synthetic aperture processing shows enhanced resolution of flaw images. Several techniques have been designed and implemented for graphical display of flaws. An order of improvement in processing speed has been obtained and work is continuing in this direction. Initial results have been obtained in our work on defining the effect of synthetic aperture processing on flaw images and resolution.

1. INTRODUCTION

A synthetic aperture focusing technique for ultrasonic testing, SAFT-UT, has been under development at The University of Michigan over the past 5 years [Refs 1, 2, 3, 4, 5]. The system is capable of imaging discontinuities in pressure vessel steel with high lateral and longitudinal resolution, namely, about 1 wave length. With conventional focused transducers the resolution is a function of the size of the active element, assuming a constant focal length. In a synthetic aperture system, the equivalent of a very large diameter transducer is synthesized by combining the responses of a small diameter transducer which has been mechanically scanned over an area. Since the synthetic aperture focusing process is performed after the scan has been completed, the SAFT-UT technique has the feasibility of focusing at any and all depths without rescanning.

High signal to noise ratios are achieved in the SAFT-UT system through the use of signal averaging. Signal averaging in the SAFT-UT system is a simple operation since each A-scan is stored digitally during data acquisition. Signal-to-noise ratio improvements of 20 to 30 dB are readily obtainable. It then becomes feasible to use higher frequency transducers and to obtain greater sensitivity for detecting small discontinuities.

In a synthetic aperture system it is necessary that a discontinuity be scanned over a large subtended angle in order to obtain the optimum resolution. This is accomplished in the SAFT-UT system by the use of a wide beamwidth transducer. A wide scanning angle has an added advantage

in that discontinuities which have orientations that are not optimum can still be imaged by the SAFT-UT system in a single scan. In such a case the ultrasonic beam is incident upon a discontinuity at many angles simultaneously, thus improving the reliability of the inspection results. The use of broadband highly-damped transducers and digital deconvolution techniques makes it possible to identify discontinuities located close to another reflector, such as a front surface interface or another discontinuity.

SAFT-UT is inherently quantitative and volumetric. The digital nature of the SAFT-UT data acquisition, processing, and display makes it ideally suited for quantitative analysis. The speed and accuracy of the minicomputer assure reliability and repeatability. A two dimensional scanning apparatus makes possible a truly volumetric scan of the material. When combined with an interactive display system, the operator is able to thoroughly scrutinize suspect areas. In addition, since the system records the RF A-scans in digital form, they can be stored indefinitely on magnetic tape for comparison with subsequent inspections. Such a capability is of extreme importance in monitoring a growing crack.

Discontinuities are sized and located independently of the relative amplitude of the echoes from the discontinuities. Unlike the conventional UT approach in which the amplitude of the echo from a discontinuity is used to determine the size of the discontinuity, the SAFT-UT system uses the image of the discontinuity's boundaries to determine its size. In this respect the amplitude of response is of secondary importance. As long as enough energy is reflected by the discontinuity so that it can be detected, an accurate determination of its size is possible.

2. SYNTHETIC APERTURE IMAGING

Synthetic aperture imaging can be illustrated by considering the case of a transducer which is scanned in a straight line over a test specimen containing a point target. As shown in Figure 1, the echoes for those scan positions that are laterally displaced from the target location are delayed in time due to the greater distance they have to travel. The locus of echo phase shifts created by the scanning process is generally hyperbolic in form with its apex position at the location corresponding to minimum echo travel time.

If the scanning and surface geometries are known, it is possible to accurately predict the shape of the locus of the echoes. If the individual A-scan signals are now shifted forward in time by an amount equal to their predicted phase delays, they will come into phase with one another. Then, if the signals are coherently summed, the result will be a single large response as shown in Figure 2. The A-scan signals included in this process constitute a synthetic aperture. The same process is repeated with a new synthetic aperture displaced by one scan position from the previous aperture as shown in Figure 3. In this case, however, the phase shift compensation does not produce a set of in-phase echoes. Destructive interference occurs during summation

which results in a significantly smaller response. The process is directly analogous to that which occurs in a conventional transducer with a focusing lens. Repeatedly shifting the new aperture by one scan position and producing a new output signal each time has the effect of producing a scanning synthetic aperture.

The achievable lateral resolution ρ_x will be approximately equal to $[\lambda/(4\sin(\Delta\theta/2))]$, where λ is the ultrasonic wavelength in the medium in which the target is located, and $\Delta\theta$ is the total angle over which the target is insonified. If we assume an insonification angle of 30°, a reasonable value for a focused transducer in steel, then ρ_x is approximately equal to λ, or 2.6 mm (0.10 in) in stainless steel at 2.25 MHZ.

3. EXPERIMENTAL SETUP AND DATA COLLECTION

3.1 Experimental Setup

In this section we will very briefly describe the experimental setup. The data collection is done in a scanning tank using a true 5 axis scanner (Figure 4). The scanner can be moved in X, Y, or Z axis and also has two rotational degrees of freedom, one in the XY plane and one in the YZ plane. The specimen to be scanned is immersed under water and the transducer is pulsed and the echoes coming back from the specimen are digitized and stored. The Electronics hardware consists of a Panametrics (10 MHZ bandwidth, maximum gain of 60 dB) amplifier and pulser and a transient recorder with a maximum sampling frequency of 20 MHZ with 8 bit accuracy. Typical transducers used are 2¼ MHZ or 5 MHZ focused transducers.

Currently this data set is typically written on to a disk and processing and display are done off line. The processing is done on an Interdata 7/32 minicomputer with 256Kbytes of 750 nanosecond main memory. Synthetic aperture processing itself takes of the order of a few hours (3 to 6) currently and efforts are underway to drastically reduce that time. The synthetic aperture processing and the subsequent steps produce a four dimensional data set. Namely the X, Y, Z coordinates at any point inside the specimen and the associated amplitude of the echo pulse. It is from this information that we have to reconstruct the size, shape, orientation, etc., of the flaw. To enable us to do this we have designed and implemented various interactive graphics techniques. These are the perspective contour plot, gray scale imaging, pseudo color imaging and shaded surface technique. These have been implemented on appropriate graphics hardware. Our graphics hardware consists of a high resolution (512x512x12) RAMTEK color graphics terminal, a medium resolution (256x256x8) gray scale terminal, a Tektronix 4010 and an HP plotter. We will soon be adding a color hard copy device (to make slides, transparencies, etc.). Besides these the laboratory has the usual assortment of line printer, DEC Writers, video terminals, tape drive, etc. . All of the devices are interfaced to the Computer and constitute a flexible and yet reasonably powerful facility to carry out our research goals in Nondestructive Evaluation.

3.2 Data Collection

All data collection and management is currently done digitally with an Interdata 7/32 minicomputer. A flow chart for the system is shown in Figure 5. During data acquisition a test specimen is immersed in a tank of water and scanned under computer control by a single scanning transducer operating in pulse-echo mode. Highly damped, focused transducers are used in a raster scan. Scanning is done in a single plane with the test specimen oriented so that the focal point of the transducer is located on the specimen surface.

At each scan position the minicomputer causes the ultrasonic transducer to be pulsed. The resulting A-scan RF signal is sampled and converted to a digital value at equal time intervals as shown in Figure 6. The time delay between the pulsing of the transducer and the first sample (ID), the subsequent delay increment between successive samples (DI), and the number of samples (NP) are recorded for future use. Additionally, the operator may choose to employ signal averaging to reduce the random noise introduced by wideband amplifiers in the system. In this case, at each scan position, the transducer is pulsed repetitively and the resulting sampled signals are averaged. For random noise a signal-to-noise ratio improvement equal to the square-root of the number of signals averaged can be achieved.

Thus far, the discussion of the synthetic aperture focusing technique has been described in terms of a linear scan. In reality, the typical data scan is two-dimensional and requires a two-dimensional aperture. The locus of echoes from a point target is therefore actually a hyperboloid and the phase shifts are calculated accordingly.

4. DECONVOLUTION OF A-SCAN SIGNAL

Since the resolution of A-scan signal is primarily limited by the bandwidth of a transducer, higher longitudinal resolution can be achieved by use of highly damped transducer with a price of reduced sensitivity. An alternative approach to improve the longitudinal resolution is the use of signal processing technique known as deconvolution. The purpose of deconvolution is to remove the effect of transducer characteristics out of A-scan signal so that the deconvolved A-scan signal reveals more details of discontinuities which had been obscured by the transducer response. There are several ways to derive a deconvolution filter. The method developed here (linear predictive deconvolution) is based on linear prediction analysis which is a system modeling technique using linear least square criterion. The method consists of two steps; (1) estimate transfer function of a transducer by calculating linear prediction coefficients of the transducer impulse response, (2) build a finite impulse response (FIR) filter whose coefficients have been obtained in step 1. Figure 7 shows the block diagram of these steps. The results of the deconvolution are shown in Figure 8. Figure 8-a is an impulse response of a 2.25 MHZ transducer taken at the front surface of an aluminum block and the deconvolution filter coefficients were calculated using this signal. Figure 8-b is the result of the

deconvolution when input is the signal in Figure 8-a, Figure 8-c is the result of a bandpass filter after the deconvolution showing certain clean up effect. Figure 8-d is the envelope detection of the original signal in Figure 8-a and Figure 8-e is the envelope detection of Figure 8-c. Since one of the limitations in this method is the minimum phase requirement for an impulse response, further improvement of the method has been made to remove this restriction by including complex cepstrum computation which is a class of generalized linear system analysis and it can separate an impulse response into minimum and maximum phase components. Then linear prediction analysis is applied separately to each of these components. Thus the final form of the deconvolution filter (homomorphic predictive deconvolution) becomes the cascade of two deconvolution filters; one for a minimum phase component and the other for a maximum phase component. Figure 9-a is the result of homomorphic predictive deconvolution method using the signal in Figure 8-a as an input, Figure 9-c is a simulated A-scan data generated by taking convolution of Figure 8-a and two impulses shown in Figure 9-b. Figure 9-d shows the result of deconvolution of the data in Figure 9-c.

5. IMAGING NEAR FRONT SURFACE DISCONTINUITY

For the ultrasonic nondestructive testing using longitudinal wave, it is difficult to detect discontinuities located close to the front surface of a specimen. This is due to the fact that a reflection from a flaw is likely to be buried in the front surface reflection which has much larger amplitude than that from a flaw and it also takes certain amount of time to decay. Two approaches have been investigated to solve this problem; (1) use of deconvolution method, (2) application of two dimensional filtering to B-scan images. As described in this paper, deconvolution can remove the ring down of a transducer response, thus increasing the detectability of small reflectors near a larger reflector. However, since in the deconvolution process a transducer response is modeled by a linear system, A-scan data to be deconvolved must be free of saturation, which requires additional modifications to the data acquisition system. The second approach deals with a gray scale image of B-scan data and does not require saturation free condition. We have made an initial study of the second method. This method applies a two dimensional filter to a B-scan image to remove the region caused by front surface echoes. In a typical B-scan image as shown in Figure 10, a bright region caused by front surface echoes extends over the entire X direction with a finite width in Z direction. Two dimensional Fourier transform of this image will generate a spectrum as shown in Figure 11. As illustrated by these figures, frequency component of the front surface image is mostly concentrated on a thin line. Thus, by filtering out this portion of the spectrum and getting back to the spatial domain we can remove the front surface signal while keeping most of information regarding flaws. We have implemented a two dimensional filtering program which utilizes two dimensional FFT and two dimensional Hanning window, and it was applied to a B-scan image of part of a inconel pipe. The result indicates that most of front surface echo has been removed. However, more experiment

on this method using artificial flaws will be necessary in order to evaluate the improvement in detectability of near front surface flaw.

6. GRAPHICAL DISPLAY OF FLAWS

There are several techniques that have been designed and implemented for the graphical display of flaws. The four techniques that we will discuss in this paper are:

(a) Perspective Contour Plot
(b) Gray Scale Imaging
(c) Pseudo Color Imaging and
(d) Shaded Surface Representation

6.1 Perspective-Contour Plot

A perspective-contour plot is a composite picture of a sequence of contour plots, each contoured at the same intensity level, rotated as defined by user, and displayed after hidden line elimination. Given an inspection volume defined by three spatial coordinates, X, Y, and Z, one can construct a perspective-contour plot by using any set of either XY, XZ, or YZ planes that intersect the volume. For example, Figure 12 shows two different perspective-contour plots of the same inspection volume. Each plot is contoured at the same intensity level and rotated by the same amount. The difference between the two plots is the number and type of planes that compose the plots. The top plot is composed of four XY planes while the bottom plot is made up of nine XZ planes.

The computer algorithm which produces a perspective-contour plot has been implemented as an interactive software program which uses a command language to set up the various necessary parameters. The user-defined parameters remain in force until specifically changed. This allows the user to produce a series of plots for various values of certain parameters while holding the other parameters constant. For example, a user might specify the planes he wants, the contouring level desired, and then proceed to produce a series of plots for various rotations (See Figure 13). It is also possible to specify a region within the inspection volume to be enlarged for closer scrutiny. After enlargement, rotation can again be made to optimize the view.

6.2 Gray Scale Imaging

The gray scale display unit was designed, built and debugged at The University of Michigan. For a complete description of the design and potential capabilities of the unit the reader is directed to reference [3]. A fairly powerful and useful interactive software has been designed and has been in use for looking at cross sectional information. The basic idea is to look at any one plane (XY, YZ or ZX) of a specimen at a fixed value of the third coordinate and convert the echo amplitude into gray levels. This has proved to be a more effective technique than contour plots for visualizing and understanding the flaw information (See Figures 14 and 15).

Unlike the contour plot where one has to decide on the slicing level, in gray scale imaging one is not throwing any information away. Because of the look-up table feature of the hardware one can zoom in and look at any amplitude range in greater detail. The disadvantage is that one does not get a three dimensional view of the whole flaw at once. Improvements can be made to overcome this deficiency and efforts are underway to implement such techniques as walk-thru the object, etc. .

6.3 Pseudo Color Imaging

This is really an extension of gray scale imaging technique. Instead of using gray levels to represent amplitudes one uses a color coding scheme to represent amplitudes. The basic idea is to use cool colors such as blue or green to represent low amplitudes and hot colors such as red or pink to represent the higher amplitudes. Since the human visual system is capable of seeing more colors at one time than the number of distinct gray levels, color does add an important dimension to comprehension of flaw information. Our own results and experience to date indicates that Pseudo Color Imaging is a far better display technique than the previous two techniques. This too suffers from the disadvantage of not presenting a true three dimensional image.

6.4 Shaded Surface Representation

A true three dimensional display technique is to display the three dimensional flaw geometry as a shaded surface with varying gray levels across the perspective image. The subtle change and rate of change of intensities would then convey a very powerful depth cue to the visual system. Our work in this area is not complete yet bet we do have preliminary results that show promise.

7. REAL-TIME STUDY

In order to determine the potential for real-time imaging using the synthetic aperture technique, several interrelated problems must be addressed. One problem concerns the aperture size and its effect on resolution. Smaller apertures clearly require less time to process but give less resolution. Another problem is data input/output (I/O). If computer memory is limited, data must be obtained from an external device at a considerable sacrifice in speed. Hence the theoretical lower limits to processing are more dependent on the access time of storage devices than on execution time of machine instructions.

However, the time required for synthetic aperture processing may or may not be the bottleneck in the design of a real-time field implementable system. There could be potential computational bottlenecks such as in scanning, display or subsequent image processing. All of these must be carefully studied and evaluated before one can design a complete SAFT-UT system. Such an investigation is under way at The University of Michigan and in this paper we will present some of our findings.

7.1 Faster Aperture Processing

We have identified a definite bottleneck in our system which involves the synthetic aperture processing itself [Ref 3]. To understand the basic computational porblem, refer to Figure 16. The heart of the computation revolves around vector addition where elements of vectors have to be shifted by varying amounts. As the figure shows the shift depends on the depth (or the element that is under consideration) and the distance ρ between the two vectors. For flat surfaces these shifts (as a function of ρ and n) could be computed ahead of time and stored in look up tables. For other geometry, it might be better to compute on the fly. This is still under investigation.

Nevertheless, it is this shift and add cycle that has to be executed a few million times. As an example consider the EDM block scan (page 111 of reference [3])which has an X-Y grid of 61 by 71 points (See Figure 17). Each A-scan is digitized to 406 points in Z. If we use an aperture size of 25x25, the number of such shift and add operations are approximately equal to 61x71x406x25x25 i.e., 1×10^9 or a billion times. It has been possible through very efficient programming of the inner loop and use of double buffering techniques to effectively hide the I/O time under processing time and execute each shift and add operation (programmed instructions) in approximately 15 μ sec. That gives us an execution time of 15000 seconds or a little more than 4 hours just to do the aperture processing. The details of our analysis and solution can be found in reference [3] and [4].

We are currently working on improving the execution time even further and identifying other problem areas where we might be compute bound. A careful analysis and an extension of the above ideas indicates that further speed can be obtained only by switching to the use of array processors or better still the design of a special purpose processor.

8. CALIBRATION AND PARAMETER STUDY

Part of the motivation for this study is to more clearly define the effect of the synthetic aperture processing program on the final processed image and to be able to more conveniently characterize the resolution of the processing by methods which more closely correspond to the methods used for characterizing a linear system. In particular, it would be useful to characterize the synthetic aperture by its impulse response, or, in the terminology used in characterizing an optical system, by a point-spread function.

Once the procedures for characterizing the effects of the synthetic aperture on processed images have been developed, it then becomes possible to measure the effects of changes in the various parameters used in data collection and processing by noting the effects these changes have on the point-spread function. For example, it would be desirable to know how much random error can be tolerated in the scanning device which locates the transducer at each successive position in the scan at data collection time. How rough can the front surface of the sample be?

What are the effects of the chain of electronics in the data collection system? What is the effect of the decrease in amplitude of the echo pulse with distance? What are the effects of pulse shape and pulse width? Some of these questions have been addressed [4,5] and we will present some of our results in this paper.

In order to obtain the point spread function of our synthetic aperture processing system a data generating program has been developed to create data sets. The data generating program used in this study can build data sets that simulate one or more point reflectors distributed throughout a scanned volume. The operator can choose the number and locations of these points. Ohter parameters which the operator can specify are: (a) the frequency of the simulated transducer pulse, (b) the envelope of the pulse (presently limited to Gaussian or rectangular), (c) the phase of the RF within the pulse envelope (measured relative to the center of the pulse), (d) the amplitude and width of the pulse envelope, (e) the amount of attenuation of the pulse amplitude due to absorption and scattering within the simulated volume, (f) reciprocal r or reciprocal r^2 attenuation, (g) sampling intervals in X, Y, and Z directions (these can be specified independently), and (h) randomization of the simulated transducer X-Y position and/or height. In this paper, X, Y, and Z are the spatial coordinates of the inspection volume, the surface of the test piece and the scan being in an X-Z plane. r is then the distance from the point target to the point on the surface directly below the transducer. Note also in this paper all the plots were made after the RF waveforms were envelope detected. The last feature allows the generation of data sets which simulate sets produced by a scanning mechanism which has random position and/or height errors associated with each position in the scan grid. For details of the program and the testing procedure the reader should refer to [4].

Several experiments were carried out using the simulated data generated by this program to better understand the effect of processing parameters. Figure 18 shows a sequence of processed ideal data sets containing random position errors. From top to bottom in the figure, one standard deviation in the error distribution equals, respectively, 20 percent, 50 percent and 100 percent of the horizontal sampling intervals (X and Y sampling intervals are 2.54 mm). Comparing these plots with the same size aperture of Figure 19, it can be seen that the side lobes are affected first and that the effect is to wash these out into an overall background level around the central peak. The central peak is also broadened. The top result in Figure 18 is surprisingly good and suggests that the requirements on scanning mechanism precision are not at all extreme. Also, the deeper the flaw lies, the more error that can be tolerated since a given error in scan position produces smaller phase shift errors at deeper depths. The overall effect is to reduce the signal-to-noise ratio and reduce the side lobes in the point spread function.

It is possible to deliberately introduce slight random variations into the positions of a scanning device in order to reduce the side lobes in the response if it is possible to tolerate a slight reduction

in the signal-to-noise ratio. It was also observed that the point spread function deteriorates rapidly when the standard deviation of local random variations of a front surface of a specimen exceeds 0.5 mm, while global variations are not as serious as local variations.

Our efforts in this direction is still continuing and one is referred to [4] and our forthcoming annual report [5] for additional results.

9. CONCLUSIONS

The above represent some of our results in our efforts to design a field implementable real-time Ultrasonic Imaging System using synthetic aperture processing to automatically infer the size, shape, orientation and type of flaw in reactor material. Our work is system oriented and spans a number of areas such as Ultrasonics, Signal Processing, Computer Graphics and Image Processing and Computer Architecture. Our results to date are very encouraging and our experience leads us to conclude SAFT-UT is indeed a viable tool for real-time Ultrasonic inspection of reactor components and that more automated graphics and image processing and a deeper understanding of SAFT processing and the interrelationships amongst various parameters in SAFT and resolution of imaging are problems that need further attention. The current state of the art and trends in Computer and Electronics technology and our experience so far with SAFT leads us to be optimistic about the design of a real time SAFT-UT system for field implementation.

ACKNOWLEDGEMENTS

Thanks are due to the various members of the Ultrasonic Imaging Laboratory who contributed to several aspects of the broad research objectives discussed above. In particular Mr. Nobuo Hamano has collaborated very closely on major aspects of this research and I am grateful to him for several suggestions and some of the results. All of the above research has been supported by the Metallurgy and Materials division of the Nuclear Regulatory Commission and I wish to thank them for their continuing support.

REFERENCES

1. J.R. Frederick, R.C. Fairchild, B.H. Anderson, "Improved Ultrasonic Nondestructive Testing of Pressure Vessels," NUREG-0007-2, September 1977.

2. J.R. Frederick, C.J. H. Vanden Broek, R.C. Fairchild, M.B. Elzinga, "Improved Ultrasonic Nondestructive Testing of Pressure Vessels," NUREG/CR-0135, May 1978.

3. J.R. Frederick, C. Vanden Broek, M. Elzinga, S. Ganapathy, et. al., "Improved Ultrasonic Nondestructive Testing of Pressure Vessels," NUREG/CR-0581, January 1979.

4. J.R. Frederick, C. Vanden Broek, S. Ganapathy, M. Elzinga, et. al, "Improved Ultrasonic Nondestructive Testing of Pressure Vessels," NUREG/CR-0909, September 1979.

5. S. Ganapathy, N. Hamano, et. al., "Ultrasonic Imaging Techniques in Nondestructive Testing," Forthcoming Annual Report, July 1980.

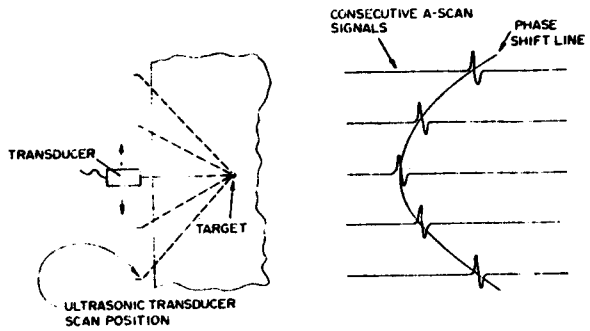


Fig. 1 Scanned transducer response

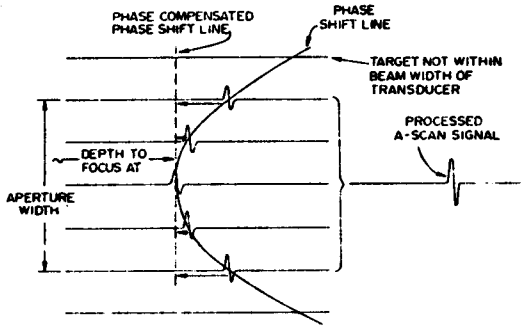


Fig. 2 Single aperture phase correction

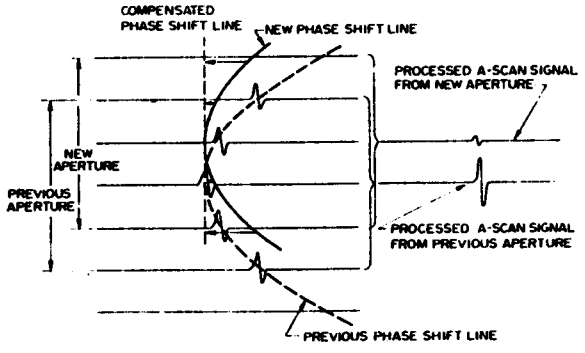


Fig. 3 Consecutive synthetic apertures showing resolution improvement

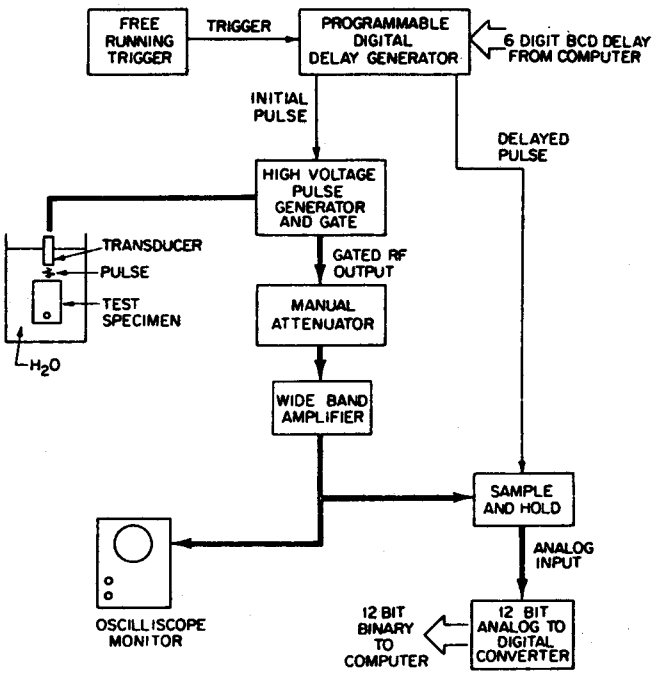


Fig. 5 Data acquisition system block diagram

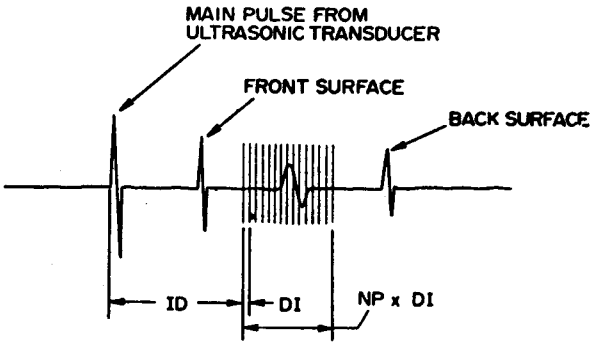


Fig. 6 Sampling of an A-scan RF signal

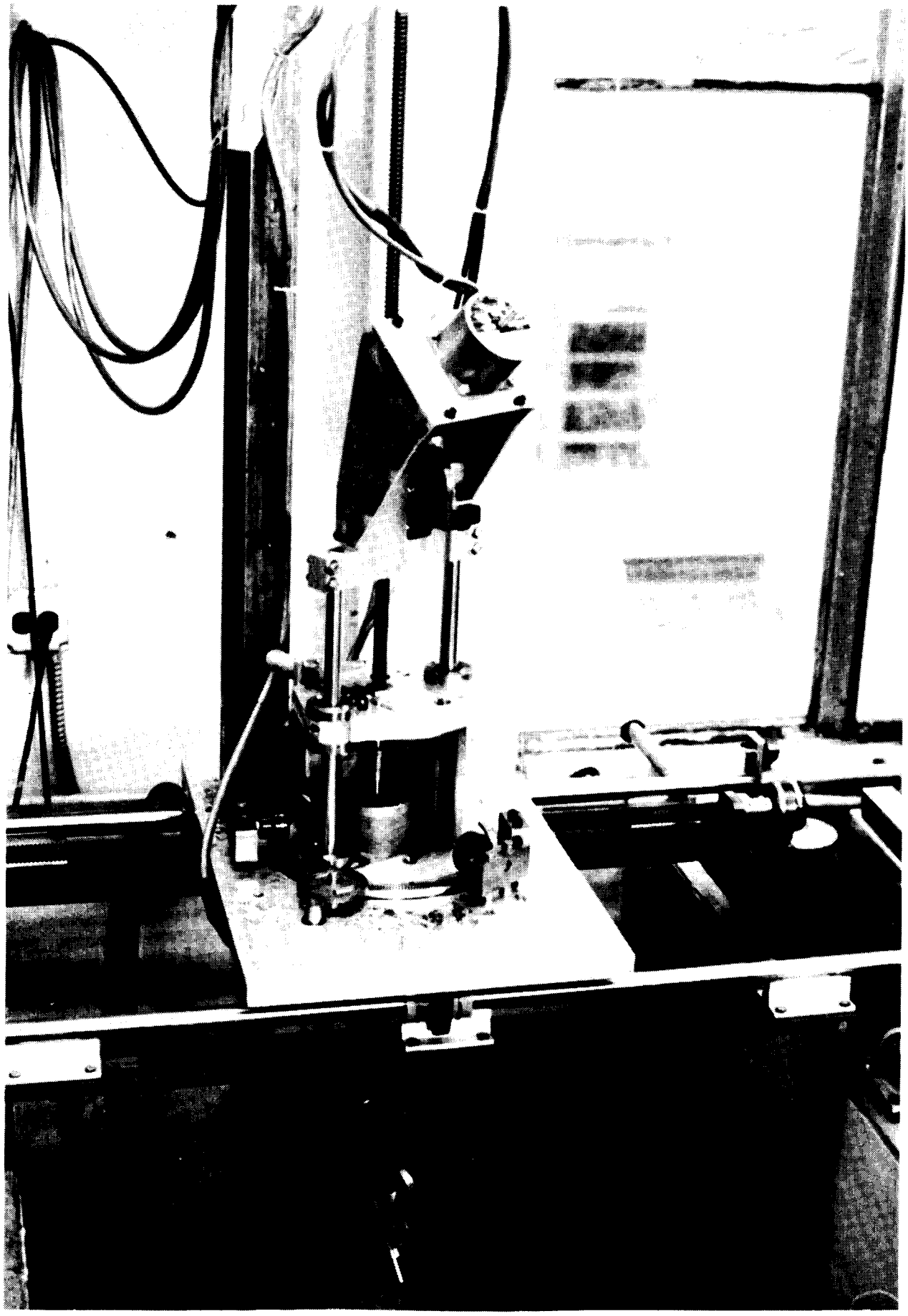


Figure 4 : Scanning Mechanism .

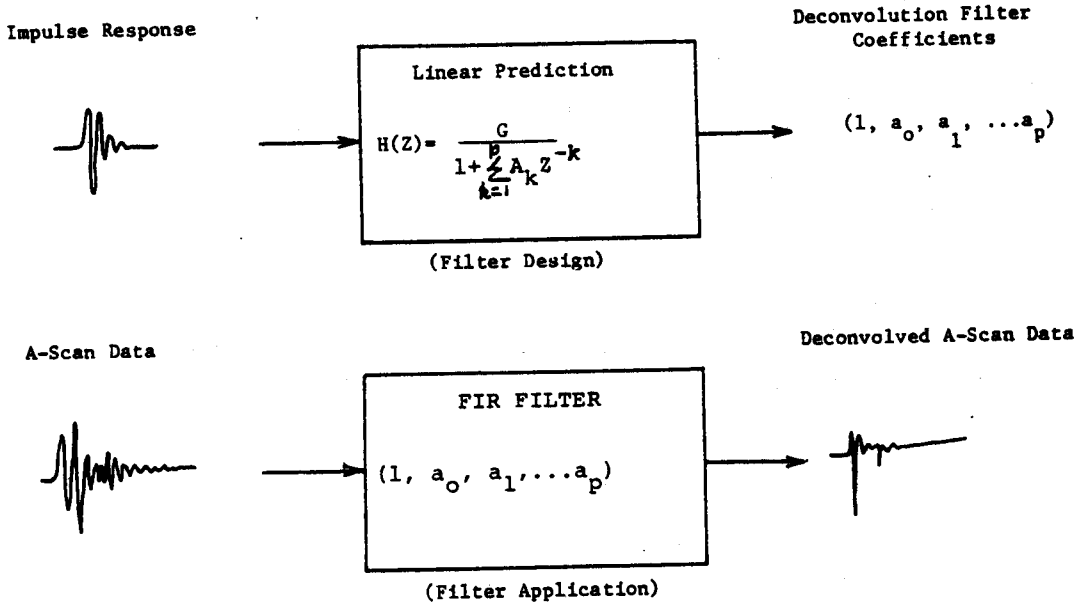


Fig. 7 Linear Predictive Deconvolution

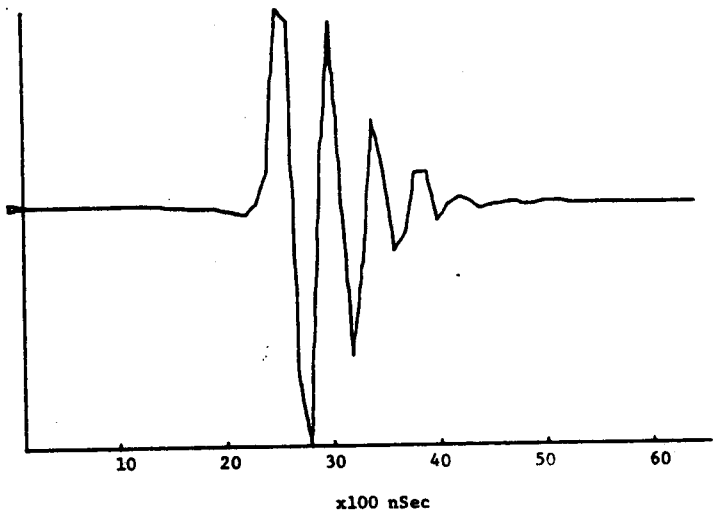


Fig. 8-a Impulse Response of 2.25 MHZ transducer (100 n sec sampling rate)

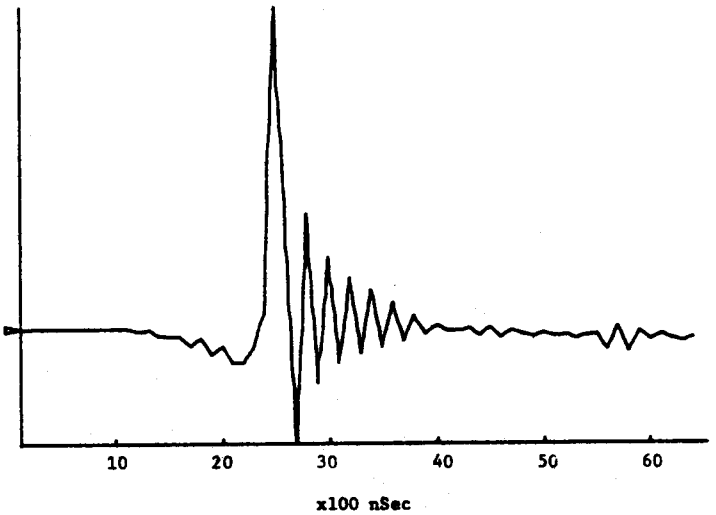


Fig. 8-b Result of Linear Predictive Deconvolution

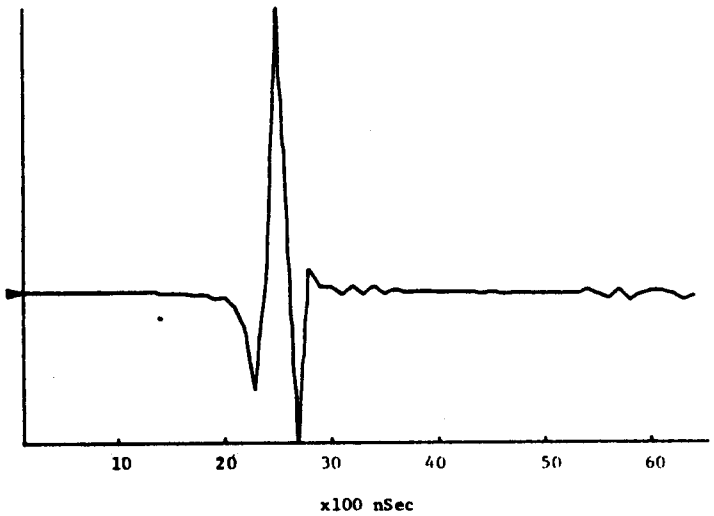


Fig. 8-c Result of Bandpass Filtering after Deconvolution

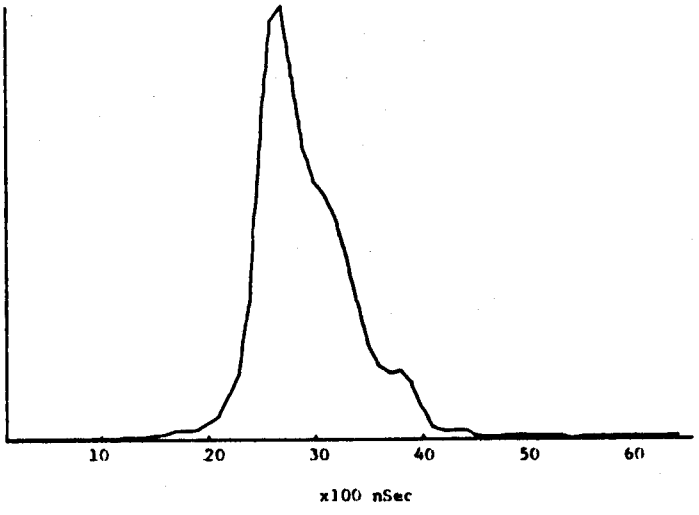


Fig. 8-d Envelope of Original Signal in Figure 8-a.

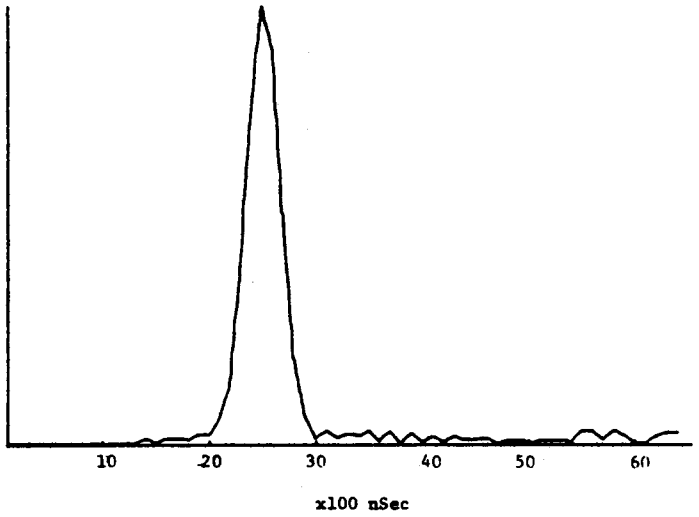


Fig. 8-e Envelope of Deconvolved Signal in Figure 8-c.

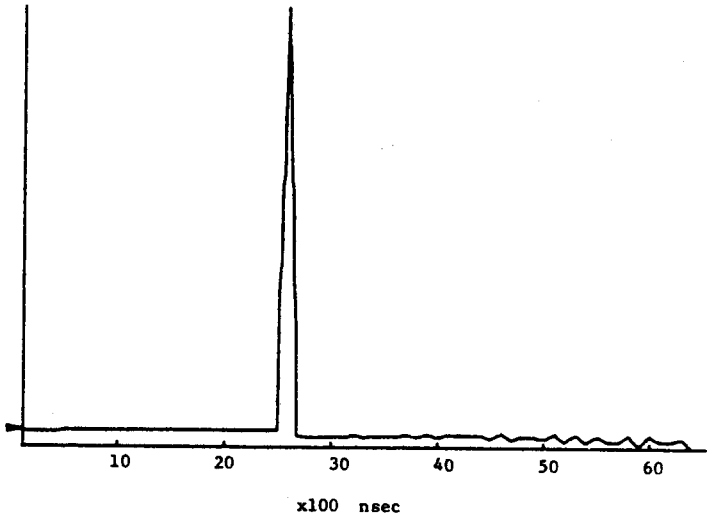


Fig. 9-a Result of Homomorphic Predictive Deconvolution on the Signal in Figure 8.

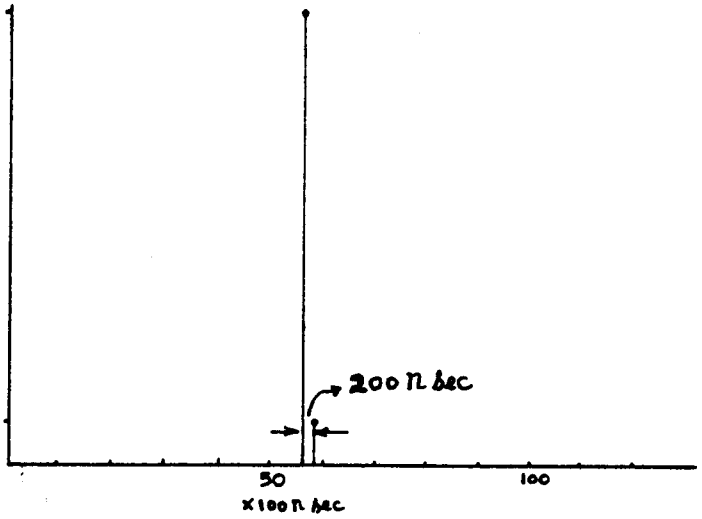


Fig. 9-b Impulse Train Used to Generate Figure 9-c.

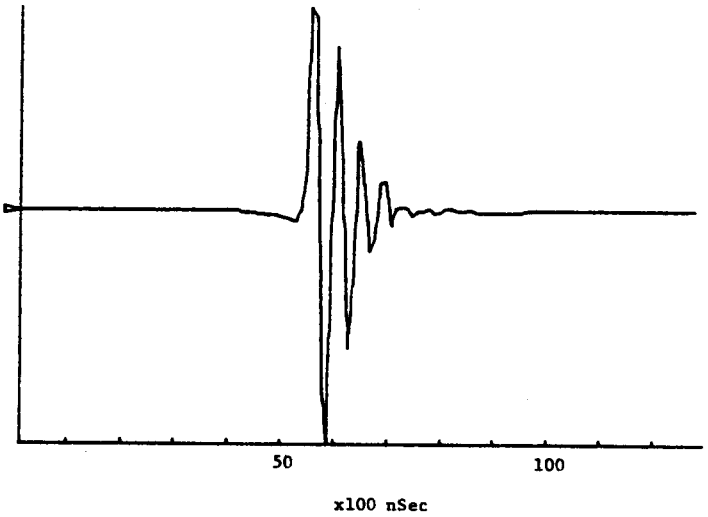


Fig. 9-c Synthesized A-scan Data (Convolution of Fig. 8-a and Fig. 9-b).

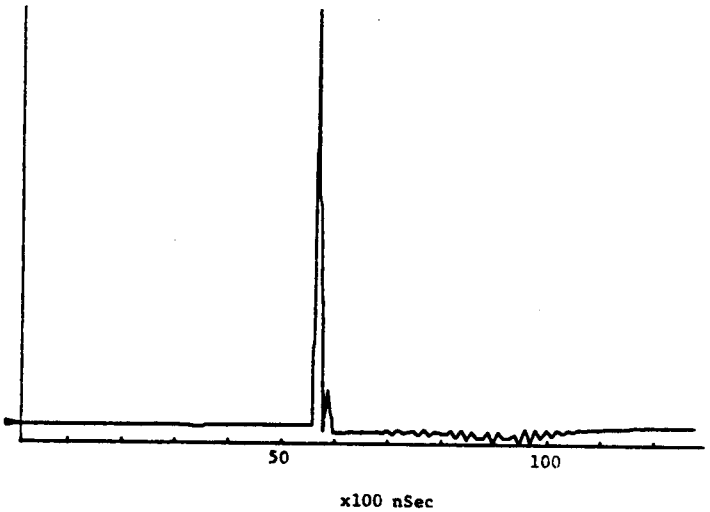


Fig. 9-d Result of Homomorphic Predictive Deconvolution on the Synthesized A-scan Data in Figure 9-c.

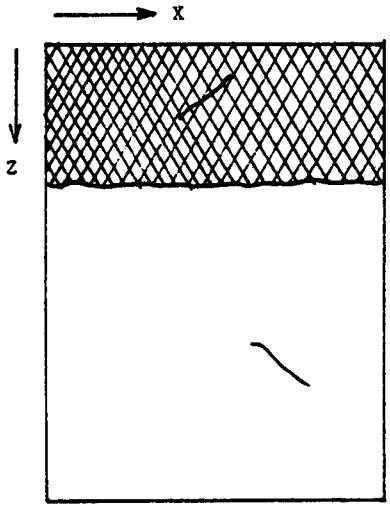


Fig. 10 Typical B-scan Image

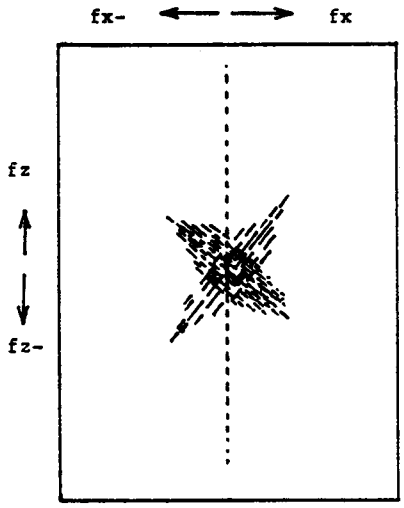
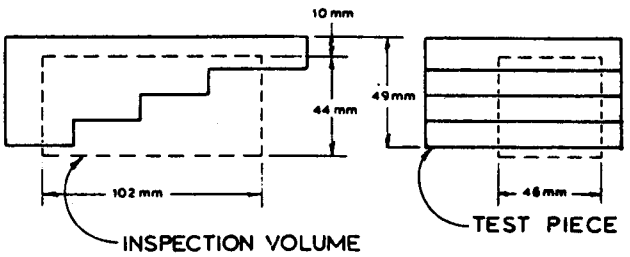
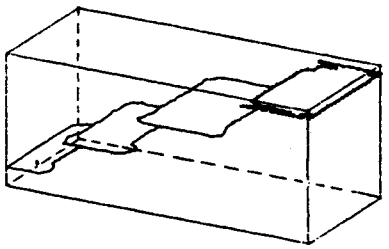


Fig. 11 Two dimensional Spectrum of Figure 10





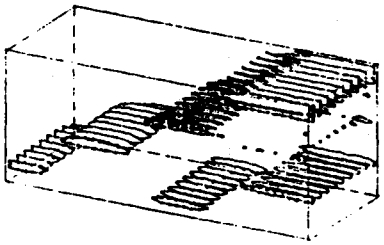


Fig. 12 **Examples of the perspective-contour plot**

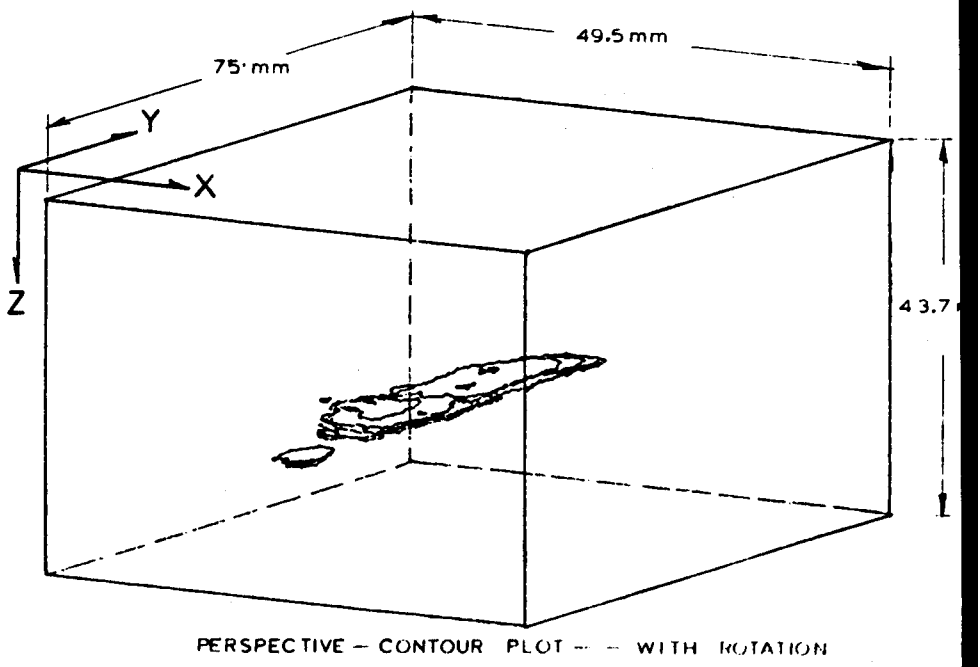


Fig. 13 **Perspective-contour displays of a slag inclusion**

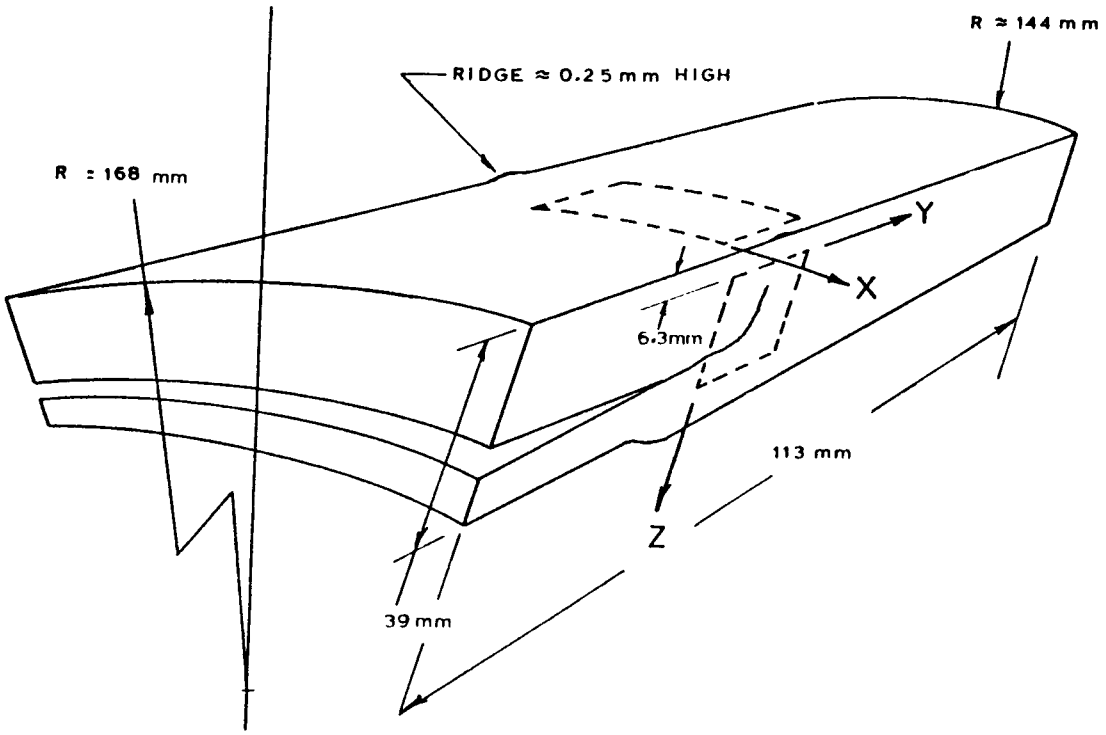


Fig. 14 Test piece for Inspection Volume INCPIP.3 (2.25 MHz scan)

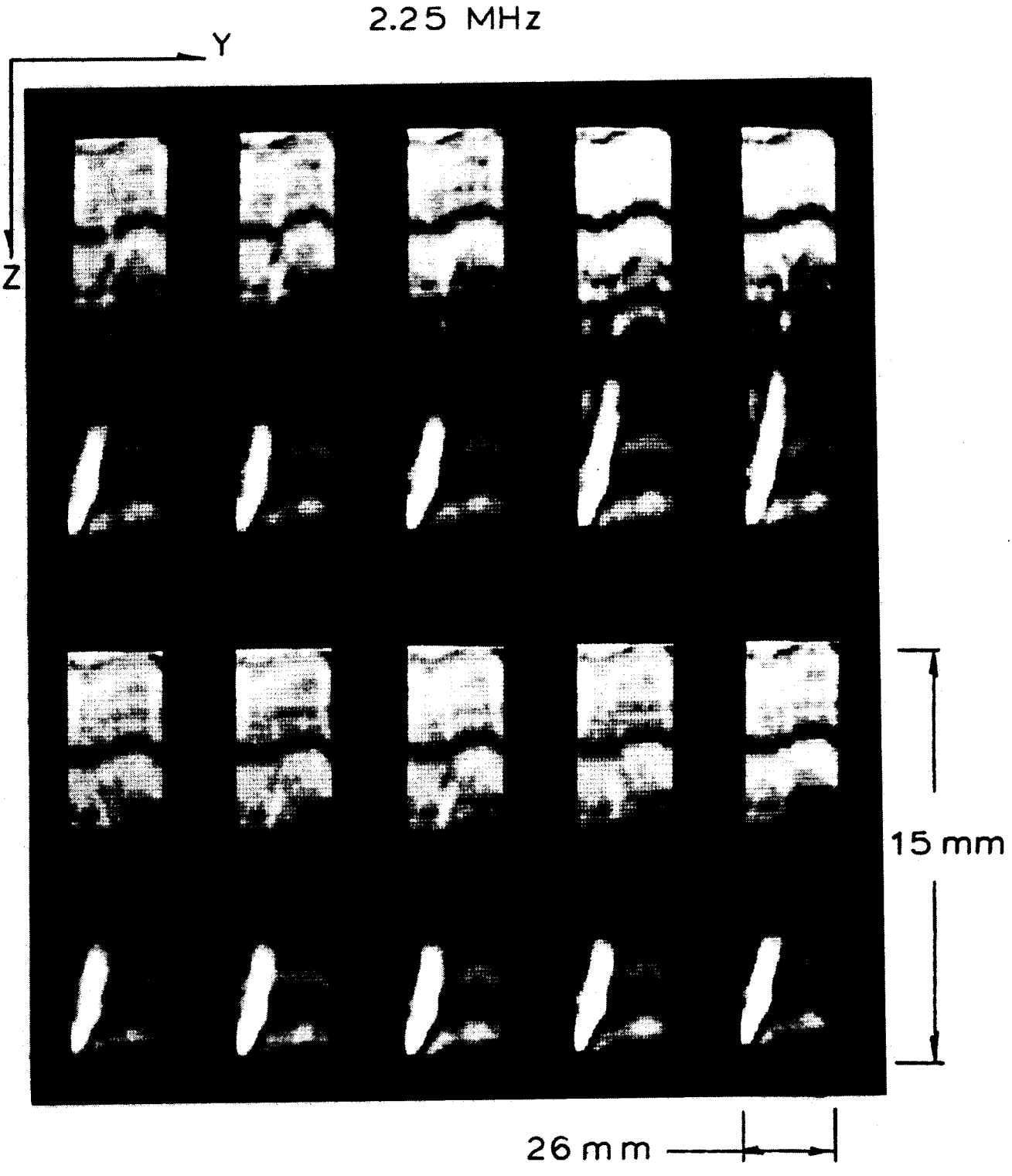


Fig. 15 Gray-scale display results for Inspection Volume INCPIP.3

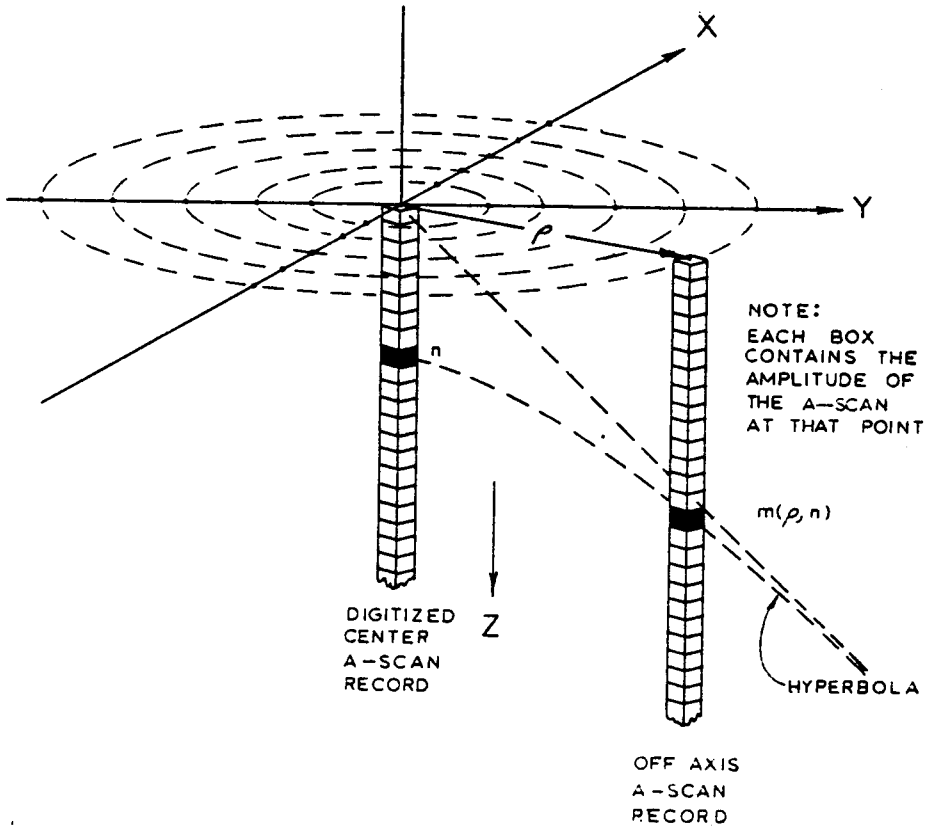


Fig. 16 Diagram showing the relationship between off-axis A-scan and center A-scan in a synthetic aperture

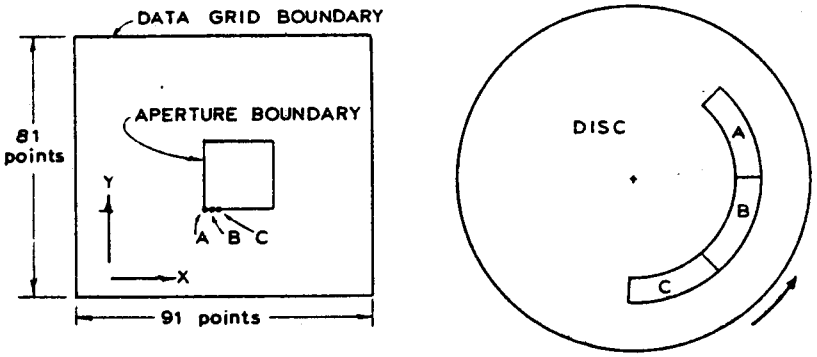


Fig. 17 Diagram showing relation between data records within an inspection volume and the data organization on disc.

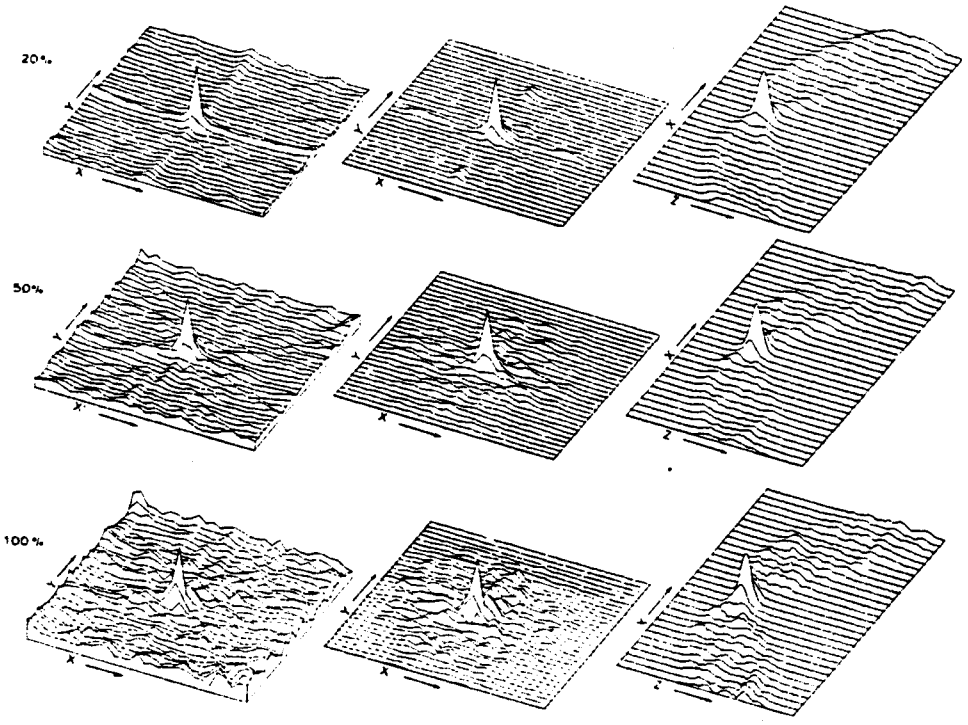


Fig. 18 The effect of random position errors on the point spread function. From top to bottom, one standard deviation in the error distribution is, respectively, 20 per cent, 50 per cent, and 100 per cent of the horizontal sampling interval which is 2.54 mm (approximately one wavelength of sound in the material). Processing was done with an 11 x 11 aperture in each case.

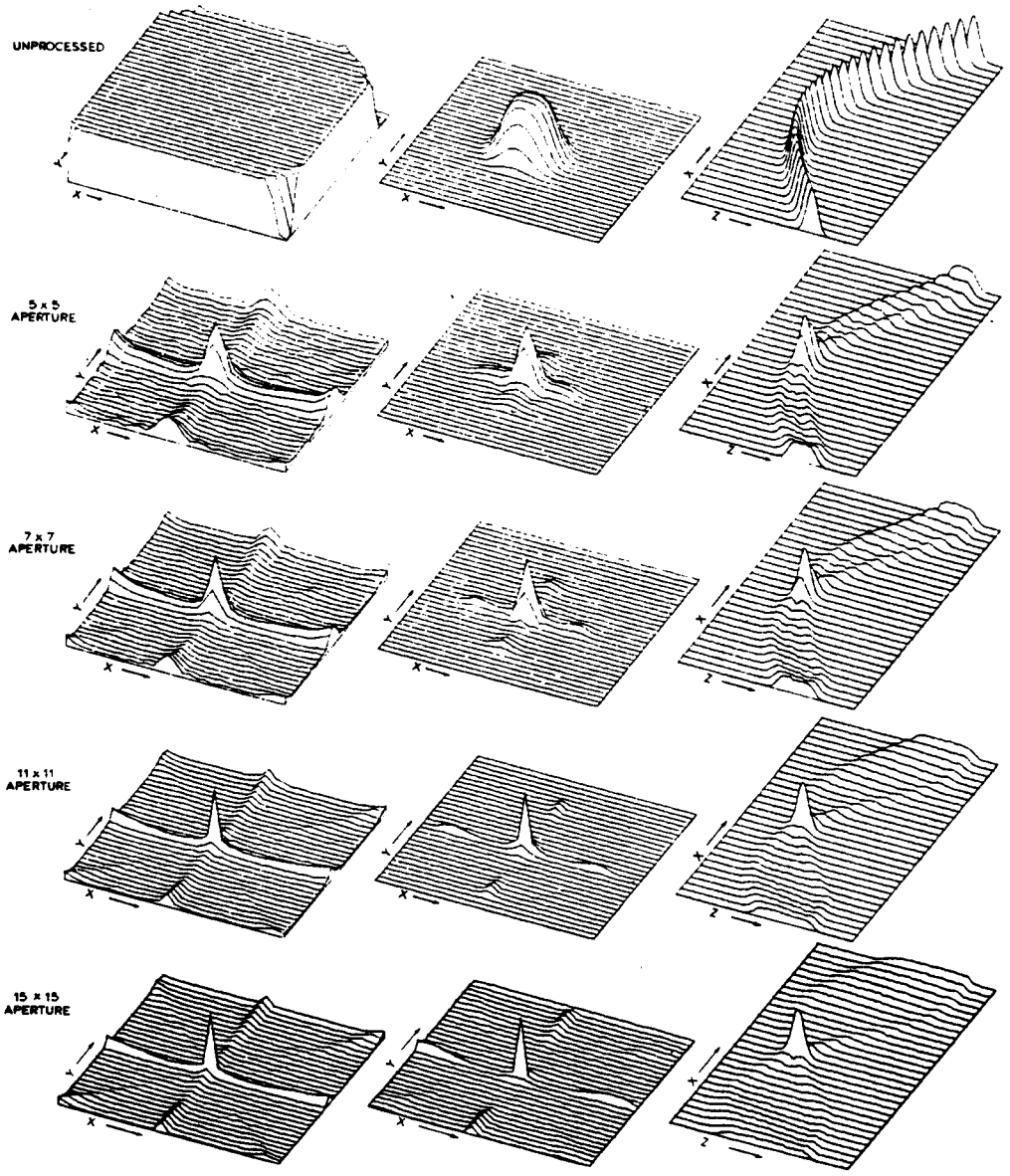


Fig. 19 Plots showing the effect of aperture size on the point spread function of the synthetic aperture processing. The center plot in each row is an x-y slice through the point target and is the plot representing the point spread function

Ultrasonic inspection of stainless steel pipe weldments for IGSCC

M.E. LAPIDES
Electric Power Research Institute, USA

Written contribution shortly introduced by

J.L. ROSE
Drexel University, USA

NOTE

These notes have been prepared for the use of EPRI contractors and have been released to CSNI for purposes of discussion at a European specialist meeting. These notes represent a summary of work in process as of April 1980. However, they are not intended to serve as any official program evaluation, nor should they be cited as a basis for quantitative or qualitative assessment of any particular UT method.

1.0 Introduction: During the past several years EPRI has conducted a series of research programs aimed at improving the reliability of detection of intergranular stress corrosion cracking (IGSCC) found in austenitic, stainless steel, Type 304 nuclear power plant piping. The purpose of this paper is to record some salient observations from this work which can serve as a guide to those concerned with similar investigations and with the development of advanced signal processing methods. Note that some of the work discussed is still in process. In such cases, the opinions expressed are those of the author as opposed to being fully-validated conclusions.

2.0 Flaw Characteristics: IGSCC in the reference material results from a composite of material sensitization, environment and stress. The sensitization requirement primarily restricts IGSCC to the weld heat-affected zone (HAZ). The complete spectrum of environmental factors is not currently known. However, IGSCC can occur at BWR operating temperatures in the presence of oxygen normally present in the coolant and in PWR borated water at temperatures of approximately 100°F. The actual enabling chemistry in the PWR units is not currently known.

IGSCC growth appears to be driven by a composite of residual stress and applied loads; the crack orientation will vary with the magnitude and distribution of these forces. The most common situation is that IGSCC appears as a circumferential crack in the HAZ; axial components of the crack are not uncommon in large pipe sizes.

A useful perspective is provided by thinking of IGSCC as being a tree-like growth with 'branches' extending in all directions into the intergranular medium. At any particular radial depth either the 'branch' or the 'trunk' may be the predominant physical flaw and acoustic reflector. Under high stress intensity conditions the 'trunk' section usually dominates; the crack being akin to a saw cut or notch with roughened sidewalls. At low stress intensity both 'trunk' and 'branches' may be

extremely 'tight' with barely any physical separation in evidence,

3.0 Basic UT Detection Considerations: The usual pipe wall thicknesses of interest to these investigations range from about 6 mm to 32 mm. (BWR pipe sizes are nominally 4"-28", Schedules 80-100. PWR sizes are approximately the same, but vary significantly from unit to unit, and the schedules are typically 10-60 in the affected lines.) Thus, attenuation and scattering is a significant issue, but not nearly so much as is the case with cast materials or thicker sections. By implication, crack signal-to grain noise is not as significant an issue as it might be in alternate cases noted, except for cracks which are a small percentage (3-5%) of the pipe wall thickness. As a corollary, crack signal-to grain noise enhancement techniques, while valuable, are generally not the critical issue in this IGSCC detection case. Instead, the more substantial issue is the differentiation of IGSCC returns from the potentially large number of geometric reflectors which will generally present themselves during volumetric examination of the HAZ.

There are probably a large number of search unit configurations applicable to the successful detection of IGSCC in reference piping. For the BWR pipe sizes EPRI has concentrated on low frequency (1.8-2.5 MHz) units of either single or dual crystal types; the latter often being referred to as 'dual, low frequency' and being differentiated from more conventional 'dual' or 'pitch-catch' units by the presence of a roof angle which serves to partially focus energy in the HAZ area. A 45° shear wave is utilized for the BWR sizes. The dual unit is recommended, except where interference between it and a weld crown preclude HAZ examination. The smaller, single crystal unit is adequate for these cases (usually smaller pipes with undressed crowns). A document describing the analysis, development, specifications and experience with these search units has been published (1).

A search unit for the thinner wall pipes (i.e. PWR case) has not yet been fully evaluated.

4.0 Some In-Service Inspection Considerations: Normally, it might be expected that firm detectability and sizing requirements might exist as derived from the fracture mechanics analyses associated with specific inspections. However, this is not currently the uniform case for various reasons, foremost among which are the limited knowledge of crack propagation rates and the general indication that through-wall leakage does not result in a safety issue. Accordingly, the targets currently specified are somewhat arbitrarily defined and are: 99+% detection of all IGSCC greater than 10% through wall with less than 2% false calls. Tacitly, this is an operational utility-oriented performance set which places high emphasis on a low false alarm rate (e.g., decreasing the minimum through-wall size while accepting a higher false alarm rate would be no more technically demanding). Alternatives may be considered as the understanding of the impact of IGSCC is better illuminated. However, the present set appears reasonable in light of the indications that IGSCC will arrest in large pipes (16" diameter or larger) - and will propagate rapidly in smaller pipes (4"-10", normally welded). The minimum detectable crack for techniques noted is believed to be 3% through wall.

Pragmatic ISI requirements also dictate the overall UT apporach since it is clear that the pulse height recording level can substantially influence performance expectations as suggested by the following:

Recording Level	No. Recordable Calls	Probable Error Source
50% DAC	High*	Missing Small Cracks
20% DAC	Higher*	Miscalling Cracks (False Alarms)

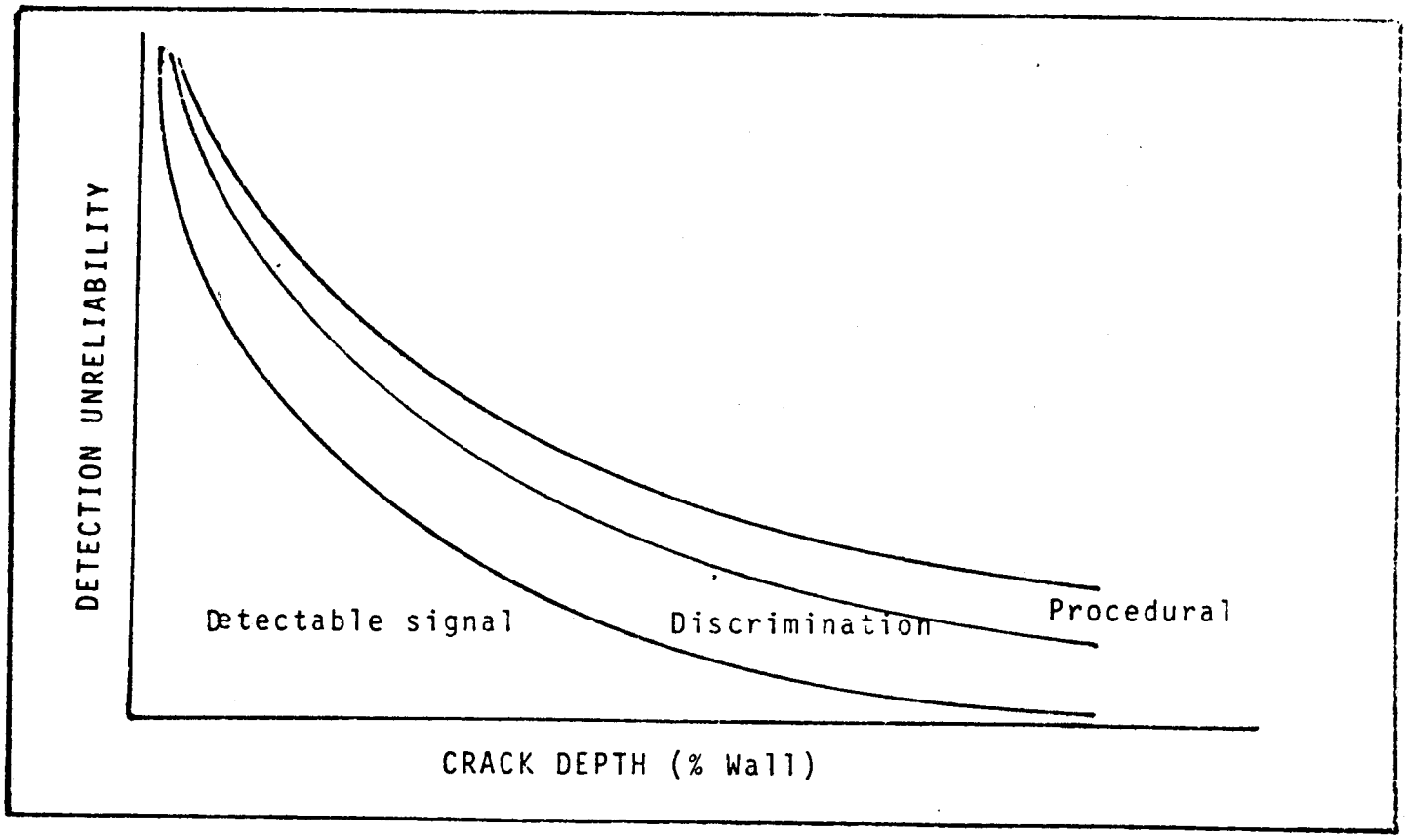
*Quantitative value varies substantially with welding quality.

Thus, considering the realities of ISI, there is a premium on achieving target performance with the maximum recording level. Correspondingly, there is no guarantee that decreasing recording level will improve prospects for achieving target requirements previously noted (although obviously decreasing recording level tends to insure that all cracks are [illegible].

There are many reasons why the optimization study implied in the tabulation has not been performed; one being the wide variability of welding practice and resultant number of 'geometric' calls (e.g., weld crown, root, counterbore) encountered. However, the primary reason is the belief that much higher pay-off techniques than a simple reduction in recording level appear to exist. These are discussed in subsequent sections.

It appears of importance to note that the assessment of the reliability of a single inspection method does not of necessity establish the reliability of ISI; the reason being that in ISI flaw calls are invariably subject to one or more reinspections, using either alternate methods, or people of higher skill levels, or both. (Such interpretation error, which is believed to stem from incorrectly equating ISI to more conventional, on-line quality inspections, appears prevalent in formalized nuclear safety studies.) Consideration of the actual ISI process has fostered thoughts on the use of a two-step process to achieving performance goals. The objective of the first phase would be ~100% crack detection, but with a higher-than-end-target false call ratio. The second procedure would be optimized to discriminate the remaining, restricted set of geometric calls. Although nominally complex, this approach is completely compatible with large-scale ISI as currently performed - and could substantially conserve time and radiation exposure.

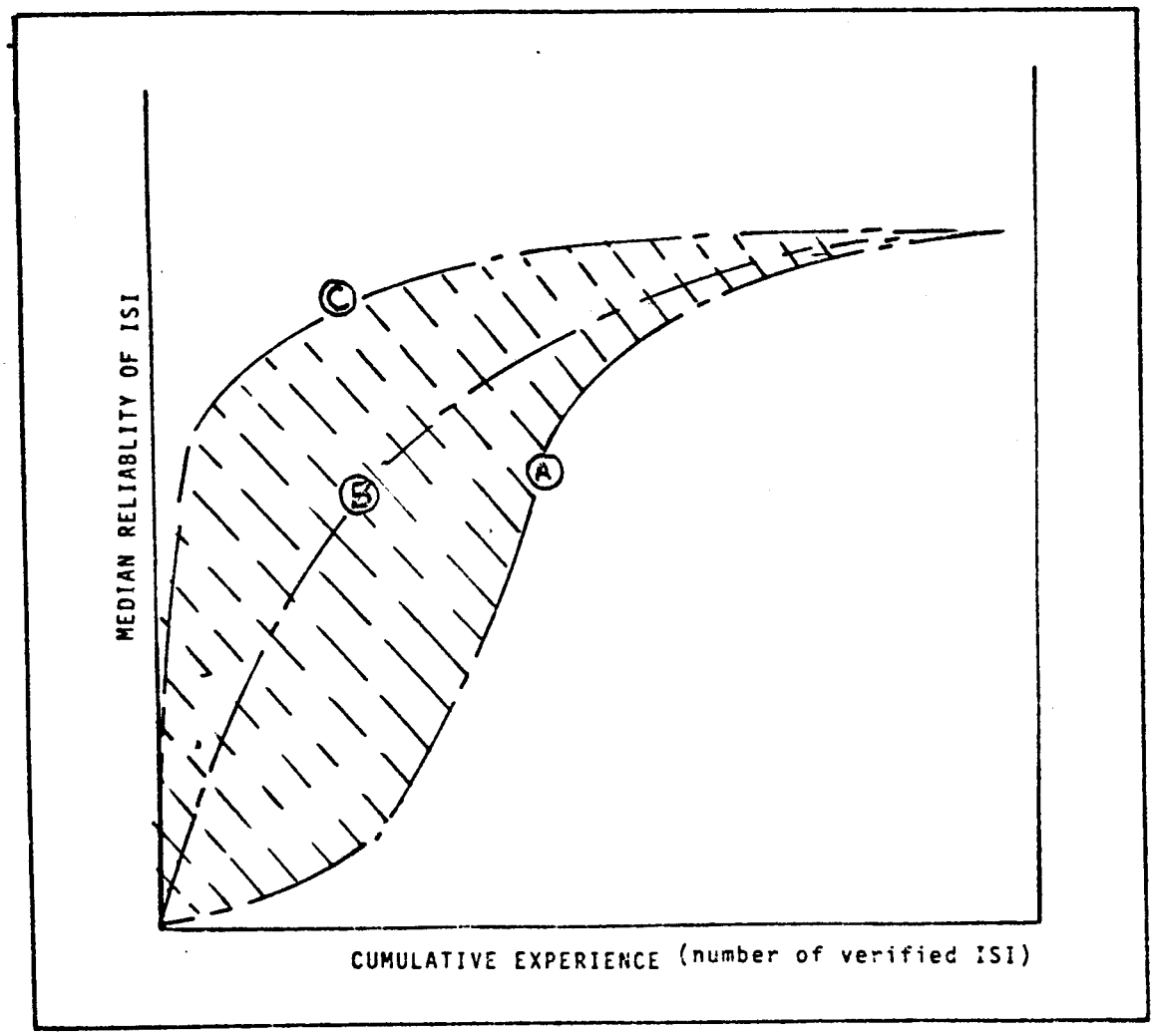
5.0 Basis of Advanced Development: The following, somewhat simplified sketch, which integrates prior comments, serves as a basis for discussion of advanced development. The sketch illustrates the relative sources of unreliability for IGSCC detection as a function of wall penetration.



At low percentage penetration, the major source is obtaining measurable reflected energy from the crack. This source of unreliability drops rapidly with increasing crack depth, at which point discrimination (i.e., differentiating crack and geometry calls) and procedural error sources predominate. Since the reflected energy limit generally occurs at crack sizes below the target of interest, the logical emphasis of advanced work is on the reduction of the other two remaining error sources.

ISI personnel will normally perform manual operations or computations to aid in discriminating 'calls'. Actions could include finger damping (to eliminate responses from weld crowns) and plotting of the location of calls to eliminate those whch are exterior to HAZ. The extraction and extension of these supplementary crack 'features' by signal processing methods - and their use to reduce discrimination errors, provides one basis for advanced development. Two somewhat similar, but separable, paths are involved. The first examines 'features' which can be utilized in companion with present manual inspection methods; the second, using automation of search unit movement and position determination, permits address of more diverse detection and discrimination techniques.

ISI procedural errors can derive from many sources including training and skill level of operators, the methods used by the inspection team to insure the quality of their work and other factors. However, for the reference piping EPRI experience suggests a more basic problem, related to calibration standards, which is illustrated in terms of the following 'learning curve' sketch.



Curve (A) is a typical utlity industry learning curve which results when the initial basis for inspection procedure development is suspect and must be verified on the basis of destructive assay results from service withdrawals. Curve (C), the other extreme, is the case where an existing, code-acceptable inspection method is known to be fully applicable when the flaw inspection campaign is initiated. Historically,

IGSCC efforts were tracking Curve (A), largely because of: (a) generic unfamiliarity and (b) the fact that conventional UT calibration standards (e.g., slots EDM notches) proved to be much better ultrasonic reflectors than did actual 'tight' IGSCC frequently found in service. Since the size of the shaded area shown in the sketch is a measure of the economic penalty the utilities pay for ISI unreliability, it is considered important to reduce the time required to substantially improve 'reliability' in addition to achieving an ultimately '100% reliable' technique. Curve (B) illustrates the first approach selected which was simply the generation of true equivalents of the IGSCC flaws in piping weldments - and the distribution of these samples to ISI and utility groups as qualification standards. Retrospectively, this action provided more rapid upgrading of capability than would the development and distribution of a single procedure to be used by all ISI groups. There are probably a number of applicable procedures; the diverse availability of samples facilitates 'tuning' of available procedures as well as training and acceptance testing by ISI customers.

The two 'feature' extraction methods previously mentioned can also be rationalized in terms of the preceding sketch. Basically, both are techniques of achieving performance representative of Curve (C). Although not intrinsically so, the companion methods are usually less powerful than fully automated methods. However, with the present state of technology, they can be more rapidly distributed to ISI users- and have been developed on this basis. In simulated field tests the companion or 'call confirmer' methods have already demonstrated the tenets of the learning curve sketch in excellent fashion.

6.0 Flaw Samples: The availability of valid flaw samples is a major problem in all ISI work; the necessity of true replication of a flaw(s) becomes of critical significance when 'features' are utilized in the inspection procedure; the number of samples required to quantitatively qualify an ISI procedure can easily become a prodigious fiscal and time burden if a large number of interrelated features are involved. Accordingly, a substantial effort has been devoted to flaw manufacture and to the verification of 'true' equivalents.

From the standpoint of UT, IGSCC varies substantially in ultrasonic transmission or reflectivity essentially with crack 'tightness'. (See Section 2.0). Conservatively, information should always be obtained from 'tight' specimens but this is neither necessary or feasible in many cases. Specifically, existing information on welding procedures, pipe sizes and applied loads can be used with reasonably high confidence to predict the expected 'tightness' of the crack.

The more common IGSCC samples (4"-diameter pipe obtained from General Electric's Pipe Test Laboratory) were prepared under high load conditions and are typically too open to serve as conservative samples (although they are probably accurate replicas of 4" pipe cracks found in service). The primary samples utilized had IGSCC grown in under BWR service environment conditions (except for applied loads) using an artificial crevice, crack initiation acceleration technique. These samples are believed to be near identical replications of IGSCC found in service before the crack is 'opened' by service loads. IGSCC locations and length can be precisely controlled, crack depth can be controlled to a one sigma variation of approximately 0.5 mm. Hence, destructive assay for most confirmation work is not required. Insofar as can be determined, the manufactured IGSCC are identical to large pipe service removals in the 12"-28" diameter range except that the crack is somewhat tighter.

The ultrasonic response of service withdrawal, artificial crevice, chemically corroded and mechanical flaws is being acquired and cross-correlated in order to determine where sample interchangeability is feasible. The measured parameters are: a) the search unit characteristics and calibration, b) the relative amplitude of the return (for conventional UT approaches), c) the power spectra of the return, and d) variants of (b) and (c) as a function of search unit-flaw location parameters. The latter two items are considered mandatory for 'feature'-based system evaluation. A standard recording protocol has been developed as well as a computer-based data retrieval system to permit permanent retention and flexible usage of these data. The pragmatic

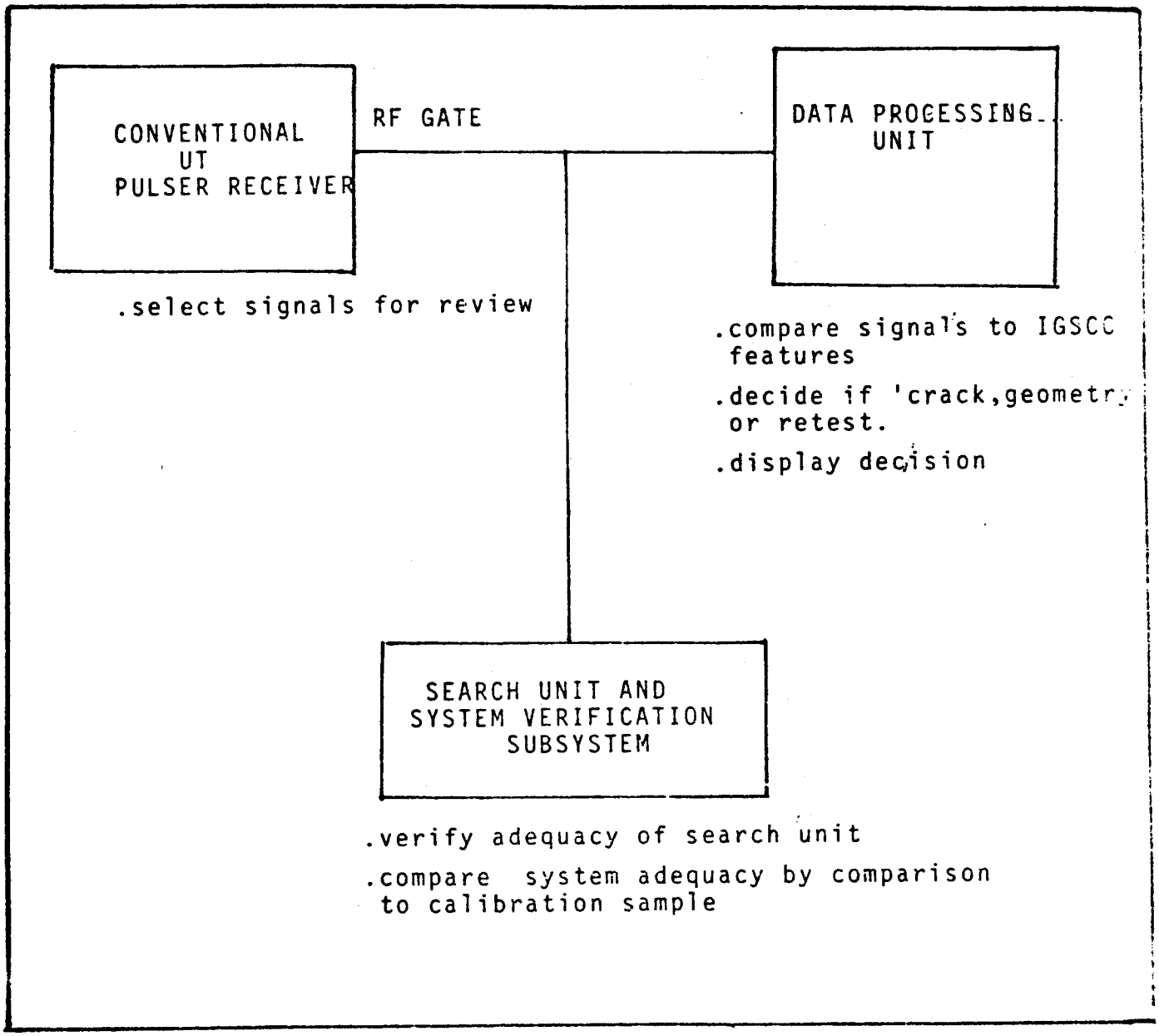
reason for this approach (based largely on the estimate of the number and types of samples required to qualify a feature-based system) is suggested by the following tabulation:

Flaw Sample Type	Availability	Unit Cost	Comments
o Service Removals	Poor	Very High	Diversity not possible
o Service Replicas	Good	High	
o Physical Equivalents	Excellent	Moderate-High	
o RF Waveforms (from physical samples)	Derives from above	Low	Also available from equipment in service
o RF Waveforms (synthetic)	Excellent	Very Low	Implies simulation will be used to qualify systems

Fundamentally, the cost and time of using physical samples exclusively for qualification at high confidence levels could easily become excessive. It appears mandatory to be able to substitute computer simulation, with waveforms perturbed to permit variational and sensitivity studies, to overcome these limitations (referred to as 'synthetic waveforms'). Note also that since IGSCC reliability is discrimination limited (see Section 5.0) the qualification test base must be appropriately diverse in both cracks and 'geometry' (e.g., crown, root, counterbore, surface finish, etc.).

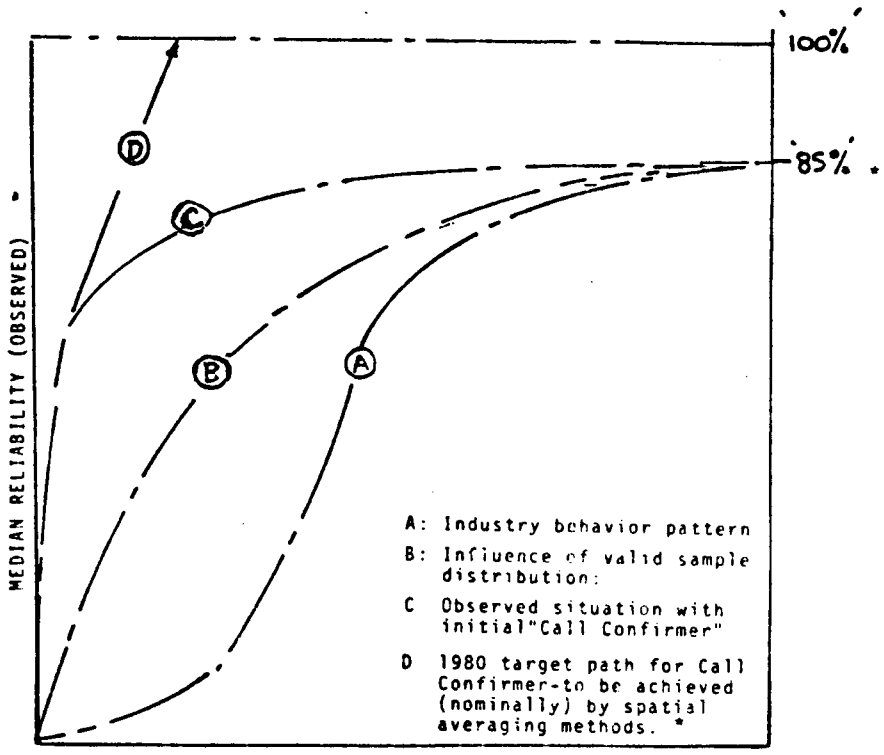
7.0 Feature Extraction Systems: Companion Methods: The signals acquired in conventional, ultrasonic pulse-echo approaches contain more 'information' (both time and frequency domain) than is normally used by the operator. This is well-known; there is a major body of existing analyses and signal processing techniques (largely from radar related efforts) available to demonstrate feasibility and the potential value of the 'information' in laboratory-scale operations. What does not appear to be available are integrations of these equipments adaptable to field usage and perhaps more importantly the identification of a method for qualifying such

equipments for ISI by diverse users. The latter factor appears to be unique in that it is without precedent and poses some distinctly new questions (e.g., assuming a signal processing algorithm is substituted for operator judgment, what is the liability of the third party, algorithm creator?). In recognition of the aforementioned considerations and because the instrument was believed to be independently valuable and capable of rapid field introduction, a decision was made to evaluate what has come to be identified as a 'call confirmer' shown schematically in the following sketch.



The 'call confirmer' consists of three basic functional elements: a) a conventional pulse-echo UT set, b) an auxiliary data processing unit (DPU), and c) a search unit verification subsystem. The DPU connects to the UT set thru an RF gate; it performs by comparing an operator-selected flaw signal to 'features' which have been found to characterize IGSCC. In one implementation, these features include pulse envelope duration and rise times, and the relative power in selectable frequency bands - all of which are combined to form a discriminant function. The DPU declares whether the signal call is judged to be a 'crack' or a 'geometry' - or whether retest is necessary for such determination. The response is noted by flashing lights.

The 'call confirmer' is now being readied for field testing as part of its development for reasons suggested by the following sketch which, in turn, is a recasting of that shown in Section 5.



*Note that 'median reliability' refers to the total spectrum of IGSCC encountered in BWR piping. However, errors are not random; '100%' performance can virtually be guaranteed with some pipe sizes and classes at the present time.

In its present physical embodiment, the 'call confirmer' scores 85-100% on crack calls with 0-20% false calls when operated by various users with little prior training. (By way of reference, skilled operators score from 0-100% on cracks and 0-40% false calls using conventional methods; the primary reason for the low scores being the lack of substantial prior experience with the 'tight' cracks tested.) This performance suggests a basic value of acceleration of a learning curve as previously noted as well as other direct usage options. However, a higher priority concern is achieving the nominal '100%' instrument based on the following considerations:

Qualification

a) The unit has been tested on some 150 flaws, an impressive number which probably exceeds that for many methods accepted as 'qualified'. However, neither the overall performance figure, nor the number of tests can be considered significant by themselves unless it can be insured that the test flaws exhibit sufficient diversity. In context, diversity means: 1) the cracks and geometries are representative in size and type of those expected in service, 2) those geometries which are 'suppressed' in the discrimination are represented by extremes to which the discrimination process is most sensitive (i.e., a means of performing sensitivity studies in critical areas), and 3) pipe size, fabrication processes, and material variants of interest are included.

b) A computer simulation of the 'call confirmer' has been developed to aid in design and to contribute to the qualification program described, notably sensitivity studies.

c) As a result of using (a) and (b) preceding, it is anticipated that qualification results will be presented as a reliability and false call ratio at a specified, quantifiable confidence level.

d) The 'call confirmer' includes signal averaging (temporal) once the 'call' has been selected. However, such averaging does not occur during 'wiping,' and the operator must select the calls to be confirmed. The qualification of these procedures (i.e., determination of error sources); the compatibility with existing codes (or equivalent) remain to be established.

e) The feasibility of using spatial averaging or an additional discriminant to achieve the '~100%' capability instrument has been demonstrated. What remains to be determined is whether this step requires measured and recorded search unit movement or simply approximate movement under operator control. Nominally, this will be a second procedure initiated when the unit indicates 'retest' as being required.

Instrument Design

a) With the exception of any physical implementation for 'retest' response, the unit is presently configured for field use. Acceptability by operators remains to be established.

b) Transducer drift from nominal calibration is a standard field problem, made more significant in this instrument because 'features' may be more sensitive to drift than is pulse formation. The target is to have the unit operate with any serial number of a special transducer model; to have transducer acceptance criteria (or to desensitize performance to transducer variations by a deconvolution technique) and to have a pre-usage operator check referenced to an IGSCC calibration standard.

c) The present physical implementation is referred to as an analog unit (even though considerable digital signal processing componentry is used) since a conscious decision was made to eliminate a high speed A/D converter and fast Fourier transform unit in the interest of cost of the end unit. However, an all-digital system is also under investigation - and has been subject to preliminary evaluation using the

higher speed equipment subsequently described. The decision to implement the all-digital unit (which uses somewhat different 'features' for discrimination) is considered to be cost-based; the exception being that deconvolution (or equivalent) appears to be substantially easier in digital configuration. Parenthetically, the 'cost' of the unit defined appears to be more dependent on the number and type of alternate flaws (i.e., other than IGSCC) to which the unit can be adapted than on component costs per se (since application diversity should be the market determinant).

d) Specific 'features' of the pulse showing high discrimination value can obviously be displayed for discretionary use of the operator in conventional UT approaches. This subject has not been addressed specifically to date, but information necessary for this option implementation will be made available once more data on qualification and, more significantly, transducer sensitivity influences, have been obtained.

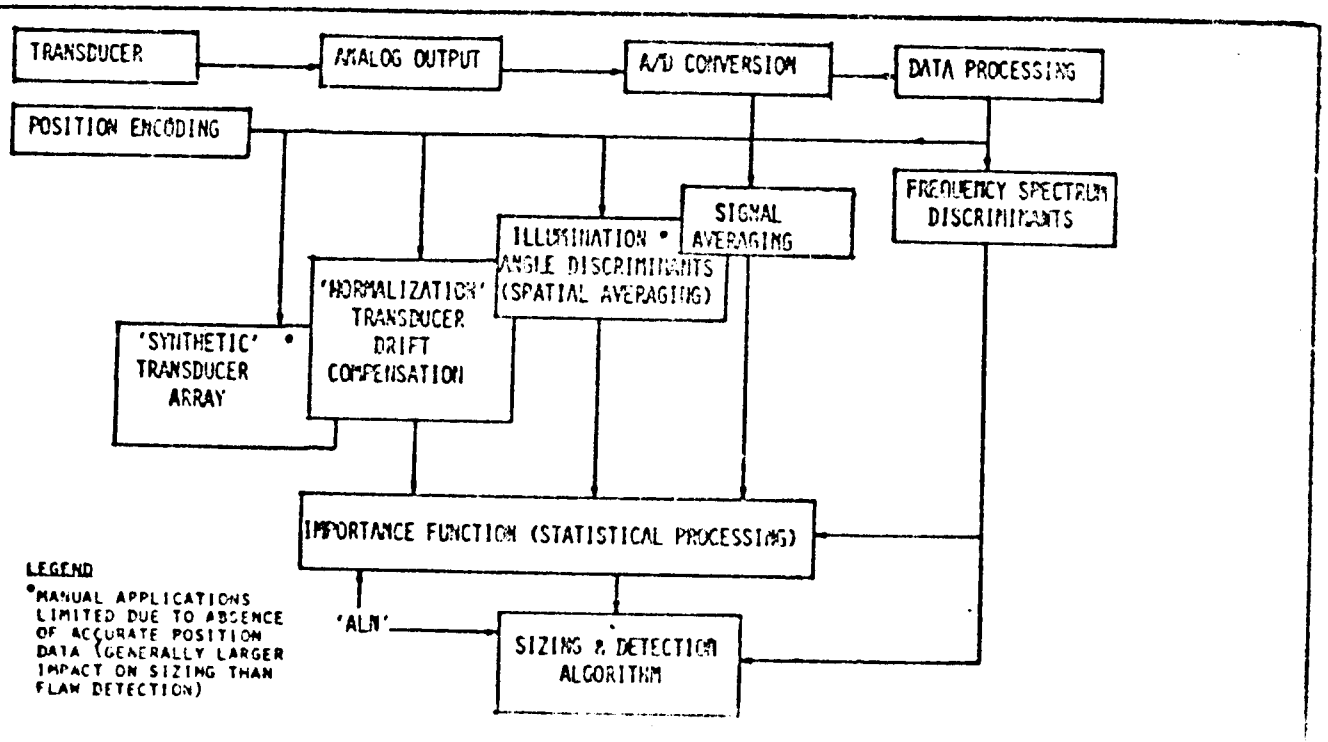
The major contributors to the work described are as follows:

M. E. Lapides, EPRI, Concept, Functional Approach
J. Rose, M. Avioli, Ultrasonics International, Analysis & Design
B. Abrams, A. Zeger, Zeger-Abrams, Instrument Design & Implementation
G. P. Singh (now SwRI), Analysis
M. Behravesh, Battelle Columbus, Qualification

8.0 Feature Extraction Systems: Automated Systems: The fully-automated system being developed by EPRI is intended to be a diverse NDE instrument rather than one uniquely intended for reference pipe IGSCC. However, this discussion is limited only to the latter application. Viewed in this context, the fully-automated system has many program characteristics in common with the manual unit previously discussed and many which are unique to itself. The primary common element is the 'qualification' requirement, which, in this case, is substantially more demanding since no human operator is in a decision loop, nor is an operator presented with supplementary information to track or compare the automated decision with conventional practise.

The fundamental functional elements of the fully-automated system include a) an electromechanical positioning system capable of moving and precisely determining the position of a search unit on a pipe under command of b) an interface controller connected to c) a digital, signal processing unit operated and integrated by a programmable microprocessor section, all of sufficient speed and capacity to permit essentially real-time processing of acquired signals with search unit movement rates of the order of 100 inches/minute. This basic equipment (item c) exists as fieldable hardware, appropriately engineered for transport, operator interfacing; data display and recording and supervisory review, all as might be required in ISI operations inside containment of nuclear plants. This equipment is described in Reference (2) and is not further delineated herein.

The signal processing unit/scanner complex is potentially capable of providing or simulating virtually all of the ultrasonic detection and sizing techniques which can derive from combined knowledge of a signal and its position as suggested by the following sketch.



General Format for Digital Waveform Analysis of Ultrasonic Test

Representative signal/position combinations which can be accommodated range from mimicking operator motions through to precision illumination angle studies and/or achievement of synthetic transducer arrays. As suggested by the sketch, the processing assumes emphasis on frequency domain information as well as the need for both 'predetermined' and 'statistical' methods of developing software programs for flaw characteristics. (i.e., A 'statistical' approach would involve the determination of the relative discrimination value of arbitrarily selected techniques or 'features' - and, by iteration, select those features of most significance to the flaw characterization; one method of doing this is the Adaptive Learning Network as marked in the sketch.)

An integrated, fully automated unit has not yet been subject to intensive reference pipe IGSCC testing. However, there is little reason to believe that it does not have the same potential - or indeed, even more than the previously described manual unit. Hence, the more significant issues are related to how the potential is realized, how the unit is 'qualified', and the programs required or in being for these objectives.

The IGSCC detection and sizing method utilized in the automated system is not yet fully developed, but consists of the following essential steps: 1) A series of scans of the HAZ are made to detect flaws of interest; this series utilizes ranging to select signals from the HAZ, a form of matched filter to differentiate IGSCC and geometry signals and correlation methods to integrate the results of overlapping scans. 2) The targets selected on the first series are reexamined for sizing using a diffraction method. Preliminary testing of the system data processing on restricted samples for purposes of status assessment suggest that target performance levels should be achievable. However, a substantial qualification effort is required, in part because comparatively few investigators have examined the frequency domain approaches used and, in part, because of the current necessity of developing algorithms by an iterative approach.

In contrast to conventional pulse-echo techniques, a diverse frequency-based UT technique favors the use of a broad band transducer since,

theoretically, the information content is proportional to the bandwidth. This poses no problem to the technique in use, but difficulty can arise in correlating results with those obtained by more conventional methods. Specifically, the transducer currently used yields crack calls which would usually be ignored by an operator; in the automated system these 'calls' are readily enhanced by established signal-to-noise enhancement techniques. The practical consequences of this situation are:

a) Initial development of the algorithm should be conducted on true flaws of broad diversity, coupled with destructive assay in order to avoid initial errors. Unfortunately, this situation is not easily achievable.

b) A premium exists on developing accurate (in the frequency spectrum sense) physical replicas of flaws which do not require destructive assay, signal 'signatures' of flaws and/or search unit cross-correlation techniques - all as a means of avoiding the limitations inherent in item (a) preceding.

These observations were perhaps the strongest motivation for accelerated development of a basic catalog of frequency spectrum signatures of flaws of various, sizes and types. Ideally, these signatures should accelerate algorithm development and are expected to be vital in 'qualification.'

Once an algorithm has been developed, it is important to attempt to derive sound, physical acoustics interpretations of the more important discriminant functions, primarily to insure that a satisfactory flaw sample base or equivalent is in hand for development and qualification. Stated alternatively, it is clearly feasible to develop an excellent detection or sizing algorithm solely from empiric pattern recognition based techniques. However, this severely complicates the qualification process by expanding the number of flaw-pipe variants which must be utilized.

The present state of microprocessor/programming technology is such that reprogramming is nowhere near as convenient in either time or cost as is desirable. The practical implication of this observation is that high confidence in the algorithm viability is desired before commitment to microprogramming.

All of the preceding notations reflect the 'first-time through' nature of the undertaking (and parenthetically the difference between laboratory demonstrations and ISI instrument development); a situation which should be considerably relieved by completion of the effect undertaken. A similar, if not more formidable situation recognized, is that of the mechanical scanner itself. Currently, very few mechanized scanners for utility UT work exist throughout the world. Those that do exist were not specifically developed for the type of data acquisition discussed. Hence, one dimension of effort is simply basic scanner development and verification. The second dimension is that while it is most convenient to develop detection and sizing algorithms for pipe circular geometries, the probable IGSCC detection requirement is for examination of pipe-to-component weld areas. The first consideration is reflected in present limited ability to utilize some 'spatial averaging' methods in initial algorithms (e.g., present scanners are capable of moving a search unit axially and circumferentially; skewing of the search unit, a motion of formation value has contemporarily been excluded since such motion is not available).

Many generating plants were not built to facilitate ISI; those that were nevertheless provide very limited space for scanner introduction and movement. These considerations, plus the indicated incidence of IGSCC at pipe-to-component and pipe-to-fitting weldments, all serve to place in question the diverse applicability of algorithms which depend on both flexible and precise location capability - or which predicate comparatively minor variations of diameter with axial movement. A comprehensive evaluation of scanner potential and plant accessibility, now in process, is expected to resolve this issue.

As previously noted, these comments relate to the use of the fully-automated system for ISI, a recognized long-term objective. From an alternative viewpoint the system hardware is proving to be of immediate value in data acquisition as an aid in the configuration of alternate instruments - and, most particularly as a tool to address the critical issue of flaw sizing in addition to detection.

The major contributors to the work described are as follows:

Various, Adaptronics Inc., Analysis, Signal Processing Equipment Design (A. Mucciardi, Project Manager)

M. Fleming, Amdata Systems, pipe scanning equipment

S. Doctor, Battelle Northwest, frequency spectrum 'signature' catalog

R. Beverly, SwRI, flaw sample and data management

M. Behravesh, Battelle Columbus, qualification

All R&D efforts involved are directed by Gary Dau of EPRI; the qualification and ISI application efforts are primarily part of a separately funded BWR Owner's Group Project managed by M. E. Lapides

REFERENCES

1) EPRI NP-1153 'Imroved Ultrasonic Inspection Method for Stainless Steel Piping (August 1979)

2) EPRI NP-1234-SR "Nondestructive Evaluation Program Progress in 1979" (December 1979)

SESSION 3 : INDUSTRIAL PRACTICE

Chairmen : A. JUVA, Technical Research Center of Finland

J.R. TOMLINSON, Central Electricity Generating Board, United Kingdom

Application of ultrasonic testing techniques on austenitic welds for fabrication and inservice inspection

X. EDELMANN
Sulzer Brothers Limited, Switzerland

ABSTRACT

The demand for safety and operational surveillance of nuclear power installations, in particular with regard to leaks in austenitic pipes which are mainly caused by intergranular stress corrosion cracking, is forcing engineers to find ways and means to test austenitic weld joints as well.

In view of advantages of ultrasonic testing, which is used with great success for weld joints from carbon steel, its application on austenitic welds seems to be obvious. Subsequent operational surveillance can be rendered even more effective by using the experience in instrumental response gathered during testing at the stage of fabrication.

Sulzer Brothers Limited is a manufacturer of components for nuclear power plants. The laboratory for nondestructive testing gained its experience in ultrasonic testing of austenitic welds on components in fabrication which often undergo an ultrasonic examination. Furthermore, inservice inspections were performed on austenitic components of Swiss nuclear power plants, both BWR as well as PWR.

Examples of ultrasonic applications both for inservice and fabrication inspections are given. The possibilities and the limitations are discussed. The problems met in course of testing for intergranular stress corrosion cracking are dealt. The difficulties met during an inservice inspection of the austenitic primary coulant piping of a Westinghouse typ pressurized water reactor are described.

There are a lot of cases where ultrasonic testing of austenitic components is possible. But one is far away from a general solution. Development has to be performed on a case by case basis.

It is very important that each factor influencing the test result is taken into consideration. One has to differentiate between parent metal and weld metal. Manufacturing process, welding technique and heat treatment are very important for the testability. Control of the grain configuration by measurements of the sound transparency may indicate an incorrect manufacturing process. Differentiation between fabrication and inservice inspection is most important. For both, adequate reference

blocks are absolutely necessary. On these blocks the testing problem can be analysed and a suitable testing technique and sensitivity laid down.

Unforeseen difficulties on the components to be tested are complicating the examination problem. Often, the definite technique can be set down only in course of the actual examination because of geometrical and metallurgical problems. In older plants the manufacturing of adequate reference blocks is a difficult task. These facts demand a lot of the testing personnel. Therefore a special training is necessary.

Experience has to be gathered with the new testing techniques on actual flaws. Exact documentation and critical analysis of findings will allow a judgement of possibilities and limitations and will also help in taking corrective actions in the development of testing techniques.

Further research for the testing of strongly attenuating cast structures and for the distinction of false indications from real flaws is urgent. These developments must be tested in practice. The testability must be influenced in the stage of fabrication of a component in relation to geometry, accessibility, metallurgy and surface condition. Furthermore, mechanized equipment must be provided to reduce radiation doses of testing personnel. Most important is a careful pre-service inspection of new components.

1. INTRODUCTION

The demand for safety and operational surveillance of nuclear power installations, in particular with regard to leaks in austenitic pipes which are mainly caused by intergranular stress corrosion cracking, is forcing engineers to find ways and means to test austenitic weld joints as well (1).

In view of advantages of ultrasonic testing, which is used with great success for weld joints from carbon steel, its application on austenitic welds seems to be obvious. Subsequent operational surveillance can be rendered even more effective by using the experience in instrumental response gathered during testing at the stage of fabrication.

Sulzer Brothers Limited is a manufacturer of components for nuclear power plants. The laboratory for nondestructive testing gained its experience in ultrasonic testing of austenitic welds on components in fabrication which often undergo an ultrasonic examination (2,3). Furthermore, inservice inspections were performed on austenitic components of Swiss nuclear power plants, both BWR as well as PWR (4).

2. PROBLEMS INVOLVED

The difficulties in connection with ultrasonic testing of austenitic welds and parent metals are well-known. The problems are connected with the metallurgical structure. The elastic anisotropy of the different grains leads to a scattering coupled with mode conversion.

Disturbing echos are met as "noise". The sonic energy is attenuated, while scatter echos and grain boundary ("grass") patterns appear. A very important factor is the signal-to-noise (S/N) ratio, which denotes the ratio between the evaluated ultrasonic indication of the actual signal "S" and the noise "N" due to scatter and interference echos. For a reliable examination the S/N-ratio should be as good as possible.

Differences in grain sizes and orientations influence the testability. Weld zones are characterized by columnar grains which behave quite differently compared to the grain structure in the parent metal.

For ultrasonic testing a very clear distinction must be made between parent metal and weld metal, and between fabrication and inservice inspection.

3. AUSTENITIC MATERIALS AND WELD JOINTS

When talking about the testability of austenitic structures, the term "austenitic" covers a variety of materials. It includes stainless steels and nickel-chromium alloys, such as "Inconel", "Incoloy" etc., as well as dissimilar weld metal joints. The distinction between different materials and between parent metal and weld metal is very important (Fig. 1); whereas parent metal may be rolled, drawn, forged or cast, a wide range of processes is used for welding. The problems of testing differ according to material, production and process method. In the manufacturing process a component may undergo one or more heat treatments which can influence grain structure, especially the grain size.

Fig. 2 shows a Nimonic forging with varying grain size and its effects. At two positions on the forging, an attempt was made to obtain four backwell echos with a 4 MHz straight beam probe. In one position the only indications which can be seen are those from the coarse-grained structure. From our point of view a control of the grain configuration is at least as important as the searching for flaws, e.g. laminations. Grain configuration can vary from component to component even within one workpiece. Great differences can be met. This possibly points towards an incorrect production process, e.g. incorrect forging or a false heat treatment.

The following example (Fig. 3) shows such an influence on the grain configuration. A heat treatment was specified as solution heat treatment which, in this case, should not have influenced the grain size. Comparative measurements with ultrasonic showed remarkable differences in sound transparency between the plate with and the other without heat treatment. An investigation in the macrographic section showed the very different grain configuration, which led us to conclude that something went wrong with heat treatment. In this connection two facts have to be pointed out:

(1) Grain sizes in the parent metal from ASTM 2 to 1,0 and 00 together with a certain content of impurities such as phosphorus and sulfur can produce great problems during welding. Often, microfissures may occur to a large extent. These fissures are intergranular in the heat affected zone of the weld beginning perpendicularly at the fusion line. There are cases where, in the stage of inspection of the parent metal, testability can only be reached by reduction of the testing frequency. Instead of investigating why these difficulties have occurred and what could be possible consequences for welding and for later use in service of the component, the efforts are concentrated, possibly unwisely, on sufficient sound transparency.

(2) Incorrect heat treatment and larger grain sizes can have a bad influence on the occurrence of intergranular stress corrosion cracking.

4. TESTING OF AUSTENITIC WELDS DURING FABRICATION OF A COMPONENT

4.1 Variety of Austenitic Welds

The following figures show some macrographic sections through different types of welds as they can be found in boiling water (Fig. 4) and pressurized water (Fig. 5) reactors. One can state that great differences occur both in parent as well as in weld metal. There are dissimilar metal welds, connecting different types of base metals. Carbon steels are buffered against the weld joint. It is obvious that each kind of weld joint has to be investigated separately.

4.2 Reference Blocks

For the development of an examination method, one of the most important step is the fabrication of an adequate number of reference blocks. These blocks must be of the same parent and welding materials as the object to be examined. Welding must also be carried out with the same welding techniques, the weld seam geometry must be the same, and welding parameters, welding position, weld temperature gradients etc. must be kept practically identical. It is also of great importance that the reference blocks are heat treated in the same manner as the component.

4.3 Advanced Ultrasonic Testing Techniques

When choosing a suitable technique for a given examination problem, the use of conventional probes should always be considered first. If no success can be obtained, special techniques have to be applied. Fig. 6 shows some possibilities. They can be divided into two groups: special probes and signal processing. Both special probes as well as signal processing can bring improvements. In Europe good results have been achieved by angle probes with longitudinal waves, often by means of the transmitter/receiver technique (5,6,7). Fig. 7 gives an impression of the variety of angle probes with longitudinal waves available on the market. One difficulty for the practical application of these special probes is the shear wave part which appears together with longitudinal waves in oblique incidence.

The great amount of probes makes it difficult to judge whether a certain probe is the best for a specific application or not. Therefore, reference blocks are absolutely necessary.

4.4 Development of a Testing Technique

The testing technique can be developed by using the reference blocks. These reference blocks and reflectors are necessary both for longitudinal

and transverse defects; the most suitable reflectors are side-drilled holes at different depths and, for defects close to or at the surface, notches. The best position for the side-drilled holes is at the transition line between the parent and weld material. Fig. 8 shows an example of a DAC (distance-amplitude-correction) curve from such holes on dissimilar weld metal joint. The indications from the various reflectors with the beam passing through the weld have been exposed successively on a photograph of the screen. The DAC curve from the opposite direction, i.e. only through the fine-grained base material, is quite different. A comparison of the two DAC curves gives the opportunity of assessing the absorption, scattering and refraction effects of the materials. In addition, a decision can be made as to whether the weld is to be examined with one procedure or in different depth zones with different probes.

4.5 Spurious Indications

When examining welds in the field, spurious indications are frequently met. These indications are caused mainly by the metallurgical structure conditions or by the weld seam geometry. When using longitudinal wave angle probes, the shear wave component can also be the cause.

An example of a spurious indication is shown in Fig. 9. Here, during examination of a weld with 45° longitudinal waves, a part of the waves is deflected at the transition between the stainless steel parent metal and the Inconel weld and hits the opposite surface vertically. This effect can be confirmed by dabbing the spot in question on the opposite surface with contact medium, so that the indication is influenced on the screen. As soon as the beam exit point of the probe is moved over the transition line, this indication disappears immediately.

4.6 Test Results Gained by Special Probes

The following two examples show the possibilities of the application of angle probes with longitudinal waves.

Fig. 10 shows a section through a 3 mm deep vertical crack in an austenitic submerged arc weld together with the corresponding ultrasonic indication on the screen. The heights of the reference holes with the beam passing through the weld have been marked on the screen. For this type of defect, the most suitable probe is a small transmitterreceiver longitudinal wave 70° angle probe with 4 MHz. Such probes can be used as well for the examination of cracks in or under cladding. Even surface cracks can be found in this way.

The next example is shown in Fig. 11 where a comparison is made among three different types of probes on a 45 mm thick automatically welded TIG-Inconel weld. The investigation was made with longitudinal wave 45° probes from different manufacturers. Of course, each probe produces a different DAC curve from the 2 mm side-drilled holes (7, 17, 27 and 37 mm from the surface in weld/parent metal transition) with the beam passing through the weld. As noted previously the pictures of the screen have been exposed succesively showing in each case all four indications. The probes were then set to find the 1 mm high lack of fusion defect shown, using the individual DAC settings. The resulting indication is shown for each probe

alongside. Due to the orientation of this defect, it is best found and gives the strongest indication through the weld. Differences in the relationship between the DAC curve and the indication height for each probe are obvious due to the difference in probe characteristics (frequency).

As can be seen, some good results have been achieved by the application of special techniques in the stage of fabrication. But one is still far away from a general solution of the problem. Further experience must be gained in the very near future. Above all, a reasonable sensitivity setting must be determined for the various probes in relation to the flaws to be found. It is therefore important to make as many sections as possible through defects found and to closely follow and record any grinding out of defects during repair. Information about the position, size and nature of defects thus investigated can then be compared with the ultrasonic examination results. By a critical analysis of test results, we can make a step forward to a successful testing procedure. This requires, however, effective collaboration between manufacturer, customer and acceptance authorities.

5. INSERVICE INSPECTION

An inservice inspection is often performed under less than ideal circumstances. Apart from the surrounding conditions such as radiation and temperature,additionally the components to be tested have not been designed and made to facilitate testing. For instance the actual metallurgical structure may not be accurately known.

Furthermore, geometric conditions at the inner and outer surface can bring problems. Often one has to decide during an inspection how to go on because actual circumstances do not correspond exactly to those prescribed in the drawing. Particular difficulties are caused by the special type of expected flaws which can differ dramatically from those met during fabrication of a component.

5.1 Principle for Inservice Inspection

An inservice inspection should - from our point of view - be concentrated to the areas near the inner and outer surfaces. Fig. 12 shows the realisation with the help of a reference block. Suitable reference reflectors are notches at the inner and outer surface and side-drilled holes (SDH) in the fusion line between parent and weld metal.

The surface area can be covered by special transmitter/receiver longitudinal (TRL) angle probes with an incidence angle of 70° or greater (creeping wave probes, head type waves). With these probes, depending on the case of application, cracks which are going down from the upper surface or coming up near the surface can be found even when the beam crosses the weld area. For the inner surface a 45° shear wave probe with a suitable frequency can be applied because the service induced flaws occur mostly beside the root of the weld.

When applying longitudinal waves - which are able to cross the weld metal - special care has to be taken. For the examination with the corner effect under 45° for flaws at the inner surface, some effects have to be taken into consideration. Fig. 13 shows the comparison of the amplitude of notches with different depths in a test block with a thickness of 50 mm. A 2.25 MHz crystal, size 0.5 x 0.75" with two wedges producing shear waves and longitudinal waves under an incidence of 45° in steel is used. The results using the shear wave probe show an increase of amplitude with increasing notch depth. The longitudinal (compressional) angle probe results in oscillations which do not even allow to dimension notches by the amplitude, not to speak of cracks. A very important fact for application of shear wave probes is the region of saturation which begins in this case at a notch depth of about 3 mm. These results are very important for the sensitivity setting for an inservice inspection. The behaviour of notches in the sound field of a probe has to be taken into strict consideration. If this is not the case, large errors in the test result can be the consequence. The fact of saturation is important too for the notch depth of 10% after ASME Code XI, which in this case is 5 mm (in the region of saturation!)

5.2 Intergranular Stress Corrosion Cracking (IGSCC)

The ultrasonic testing for IGSCC identification still creates great problems. The effects considered in all of the former paragraphs are unfortunately valid also for components with IGSCC. Fig. 14 shows the most important factors which impede the testability and have great influence on the test result. One meets different grain sizes again from component to component and even within one component with corresponding influence on attenuation. The crack has under certain circumstances an unfavourable shape and orientation, which makes it a bad reflector. This can go so far till the occurrence of a crack network may, together with grain desintegration, prevent any reflection because the material can no longer oscillate.

For a correct ultrasonic testing one should have a reference block as similar as possible to the object to be tested. One cannot use a certain piece of austenitic steel with reference reflectors. Furthermore, a comparison of sound attenuation from the reference block to different locations on the object to be tested has to be performed (Fig. 15). Such a comparison can be made with two identical shear wave probes set in V-path, both on the reference block and on the test object. If the different sound transparency is not corrected, the examination result can be worthless.

Another point which has to be taken into account is the often not ideal geometry (Fig. 16). The objects to be tested seldom have machined inner and outer surfaces. Thickness can change, counterbores, excessive penetration at the root of the weld and the weld bed surface limit the possibilities of ultrasonic testing. In many cases these factors are identified at the beginning of an actual examination only. Each weld must be investigated as an individual problem which expects a lot from the testing personnel. In our company we have built up a special training program.

Another fact has to be kept in mind: Even today it is not possible to give a reliable value for crack depth by ultrasonic means!

5.3 Thick Wall Cast Components

A special problem is the ultrasonic testing of cast components. In Westinghouse type pressurized water reactors the main cooling pipes are made of austenitic steel in a thickness range of 60-85 mm. At the Beznau power plants I and II an ISI of austenitic welds of the primary coolant system was performed in 1979. Cast elbows welded together with different types of austenitic pipe materials are encountered. A report about this problem has been published (4). Here, the most important results will be mentioned only.

Fig. 17 shows the attenuation for different frequencies in a 40 mm thick piece of austenitic casting - which is typical for elbows. It is obvious that 1 MHz is the most suitable frequency. But great differences in attenuation may occur in the various components. Fig. 18 demonstrates the reference block with reference reflectors, side-drilled holes and notches, for cast components welded together. Examination of the surface and near surface region is done by a special 70° TRL-probe. A 2 mm deep reference notch in the cast material at the surface andthe 5 mm diameter SDH in the depth of 15 mm with sound waves incident through the weld metal produce indications with a good signal to noise ratio (Fig. 19). This probe has been developed for the detection of subcladding cracks (8).

The volume and the root area are examined by a special transmitter/receiver probe with longitudinal waves of 45° at a frequency of 1 MHz (9). The indications of the 5 mm dia sidedrilled holes in 15, 30 and 45 mm depth with sound waves incident through weld and parent metal can be seen in Fig. 20. In this case the sound transparency through the cast parent metal is worse than through the weld metal. This demonstrates that there exist cases where the problems in the parent metal are more pronounced than in the weld metal. The applied probe was the best available for the cast material in the above mentioned elbows. But even this probe is not sufficient for a thickness of 60 mm as can be seen in Fig. 21. On the left side the noise level is shown and on the right side an indication which could be associated with the 4 mm deep notch. The notches of 1, 2 and 3 mm and in actual testing also the 4 mm notch would not be found. With shear waves there is no possibility of detecting either the side drilled holes or the notches through the cast parent metal. These facts together with those demonstrated in Fig. 13 (notches as reference reflectors) forced us to concentrate the ISI on those components which have a better sound tranparency. Such components with a much better sound transparency than that of the reference blocks shown in Fig. 17 and 18 were found during inservice inspection and were carefully investigated.

The problems described show the possibilities and limits of the testing techniques available today.

6. SUMMARY

There are a lot of cases where ultrasonic testing of austentitic components is possible. But one is far away from a general solution. Development has to be performed on a case by case basis. It is very important that each factor influencing the test result is taken into consideration. One has to differentiate between parent metal and weld metal. Manufacturing process, welding technique and heat treatment are very important for the testability. Control of the grain configuration by means of measurements of the sound tranparancy may indicate an incorrect manufacturing process. Differentiation between fabrication and inservice inspection is most important. For both, adequate reference blocks are absolutely necessary. On these blocks the testing problem can be analysed and a suitable testing technique and sensitivity laid down.

Unforeseen difficulties on the components to be tested are complicating the examination problem. Often, the definite technique can be set down only in course of the actual examination - especially for ISI - because of geometrical and metallurgical problems. These facts demand a lot of the testing personnel. Therefore a special training is necessary.

In older plants the manufacturing of adequate reference blocks is a difficult task.

7. CONCLUSIONS

Experience has to be gathered with the new testing techniques on actual flaws. Exact documentation and critical analysis of findings will allow a judgement of possibilities and limitations and will also help in taking corrective action in the development of testing techniques.

Further research for the testing of strongly attenuating cast structures and for the distinction of false indications from real flaws is urgent. These developments must be tested in practice. The testability must be influenced in the stage of fabrication of a component in relation to geometry, accessibility metallurgy and surface condition. Furthermore, mechanized equipment must be provided to reduce radiation doses of testing personnel. Most important is a careful pre-service inspection of new components.

References

(1) M. E. Lapides "Improved Ultrasonic Inspection Method for Stainless Steel Piping". EPRI NP-1153 Special Report August 1979

(2) X. Edelmann and R. Hornung, "Erfahrungen im Prüfen von austenitischen Schweissverbindungen", Material und Technik, Vol. 5, No. 1, 1977, p. 19.

(3) X. Edelmann, "The Application of Ultrasonic Testing of Austenitic Weld Joints", Materials Evaluation, Vol. 37, No. 10, 1979, p. 47.

(4) X. Edelmann, "Wiederkehrende Prüfung mit Ultraschall an austenitischen Schweissverbindungen im Hauptkühlmittelsystem von Druckwasserreaktoren", International Symposium "New Methods of Non-Destructive Testing of Materials and their Application Especially in Nuclear Engineering". Saarbrücken FRG 17th - 19th of September 1979, Conf. Proc. p. 177.

(5) H. Wüstenberg, T. Just, W. Möhrle and J. Kutzner, "Zur Bedeutung fokussierender Prüfköpfe für die Ultraschallprüfung von Schweissnähten mit austenitischem Gefüge" Materialprüfung, Vol. 19, No. 7, 1977, p.246.

(6) T. Just, M. Römer, E. Neumann, K. Matthies, and B. Kuhlow, "Leistungsfähigkeit verschiedener Ultraschallprüftechniken an austenitischen Probeschweissungen mit natürlichen Testfehlern", Materialprüfung, Vol. 19, No. 12, 1977, p. 488.

(7) G. Herberg, W. Laufer et al., "Statusbericht zur Ultraschallprüfung an austenitischen Schweissnähten", Materialprüfung, Vol. 20, No. 3, p. 120.

(8) H. Wüstenberg and E. Schluz "Versuche zur Feststellung plattierungsnaher Reflexionstellen an Reaktorteilen mit Ultraschall. DGZfP-Vortragstagung 1972, Saarbrücken.

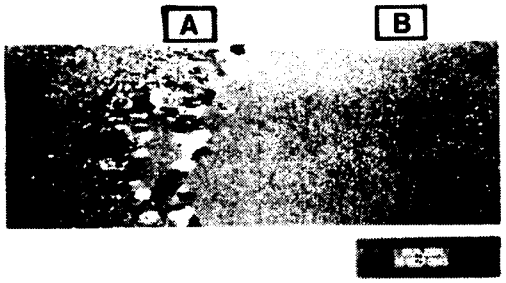
(9) P. Caussin and J. Cermak, "Performances of the Ultrasonic Examination at Austenitic Steel Components" Conference on the Periodic Inspection for Pressurized Components" London 8 - 10 May 1979, I Mech I 1979, C 49/79, p. 207.

Parent Metal	Weld Metal
Material	Material
Manufacturing Process : rolling drawing forging casting etc.	Welding Technique : shielded metal arc submerged arc tungsten inert gas electron beam etc.

Heat Treatment

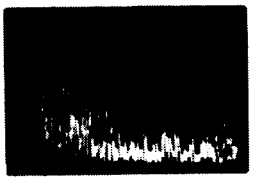
SULZER ZFMP	Austenitic Weld Joints	1

Nimonic - forging

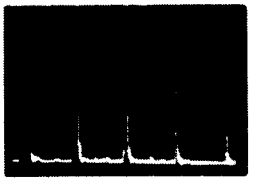


Indications:

A Only grain indications



B 4 back echos



Probe:
Krautkrämer B4F

SULZER ZFMP	Nimonic with Coarse Grain	2

Austenitic weld joint

TIG mech. Material : X5CrNi 18 9



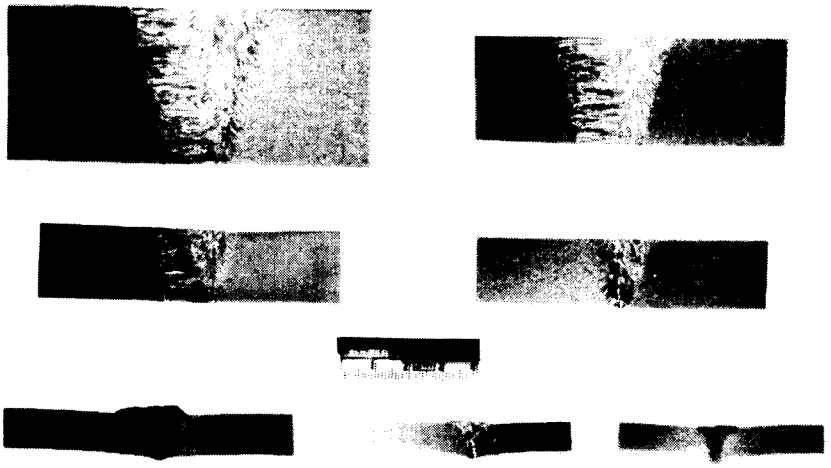
without heat treatment



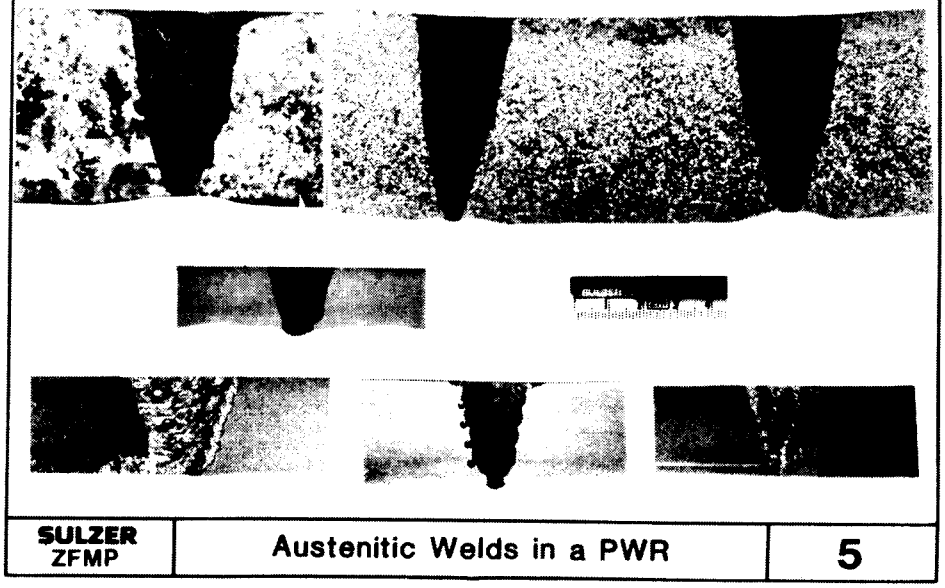


with h.t.

SULZER ZFMP	Influence of Heat Treatment	3



SULZER ZFMP	Austenitic Welds in a BWR	4



SULZER ZFMP	Austenitic Welds in a PWR	5

Advanced

Ultrasonic Testing Techniques

Special Probes

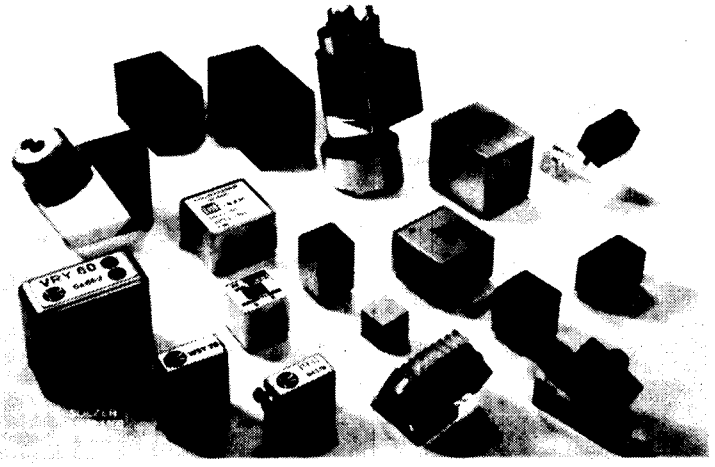
angle probes with longitudinal waves
short pulses
polarized shear waves
reduction of the testing area by:
transmitter-receiver technique
focussing probes
etc.

Signal Processing

signal analysis
signal averaging
adapted learning networks
frequency variation
etc.

SULZER ZFMP	Austenitic Welds	6

Ultrasonic Testing of Austenitic Welds



Angle Probes with Longitudinal Waves

SULZER ZFMP	Variety of Special Probes	7

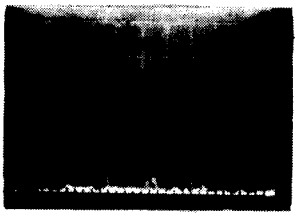
DAC - curve

DAC = Distance - Amplitude - Correction

Material :

X 20 CrMoV12 1 Inconel 10 CrMo 9 10





—x— —x DAC through parent metal

—●— DAC through weld metal

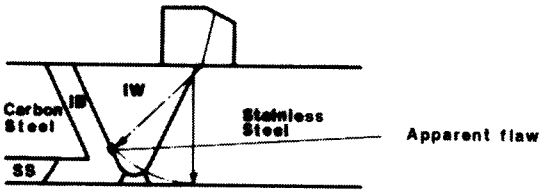
Probe : RTD TRL 45° 4 MHz
f ~ 30 mm

SULZER ZFMP	DAC - Curve	8

Dissimilar Metal Weld Joint

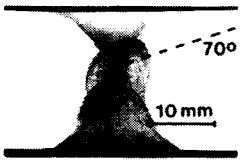


Spurious indication with 45° long.



IB = Inconel Butter Weld
IW = Inconel Weld

SULZER ZFMP	Spourious Indication	9



Submerged - arc weld

Crack

Material:
X2CrNiMo18 12

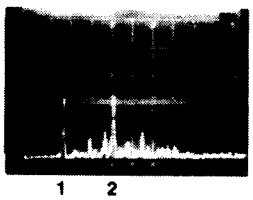


Magnification

Crack

Probe:
Krautkrämer
WSY 70° TRL 4MHz

Indications:

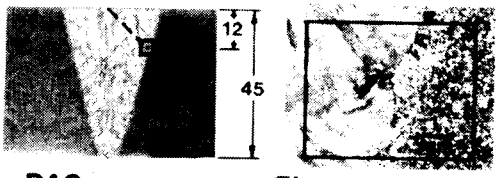


X Reference holes 2 mm dia.
1 Flaw indication long.
2 Spurious indications trans.

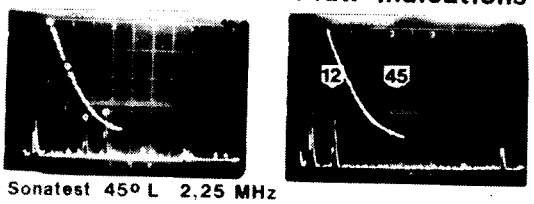
SULZER ZFMP	Weld with Crack	10

Lack of fusion

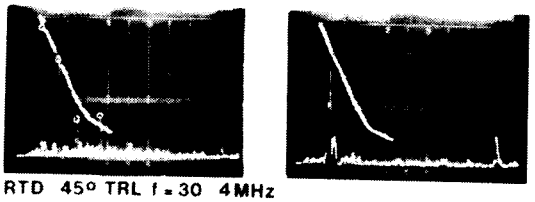
Magnification 10 x



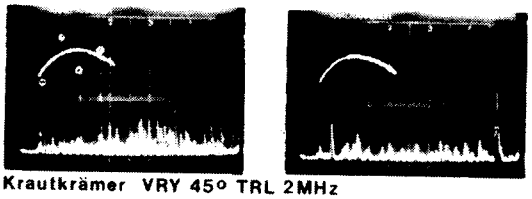
DAC - curves **Flaw indications**



Sonatest 45° L 2,25 MHz



RTD 45° TRL f = 30 4MHz

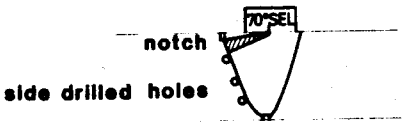


Krautkrämer VRY 45° TRL 2MHz

SULZER ZFMP	Inconel Weld Joint	11

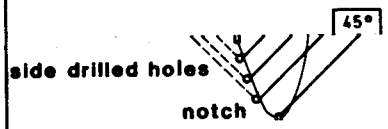
Ultrasonic Testing of Austenitic Welds

surface and near surface area



70° dual search unit long. waves

root area incl. volume



45° search unit

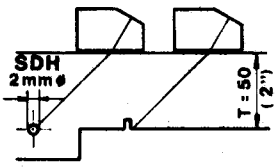
shear: through parent metal

long. : through weld metal

SULZER ZFMP	Inservice Inspection	12

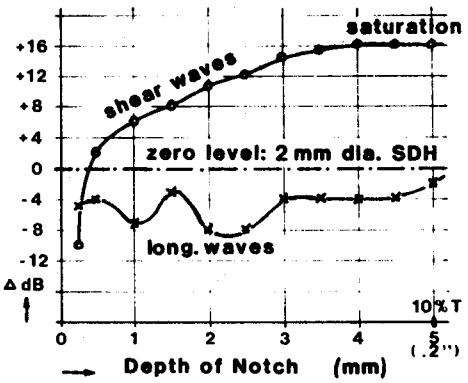
Angle Probes 45°, Corner Effect

Shear- and Longitudinal Waves



Probe: 0.75 x 0.5"
Dapco 2.25 MHz
Shoe: 45° Shear
45° Long.

Relative Amplitude Height



SULZER ZFMP	Notches as Reference	13

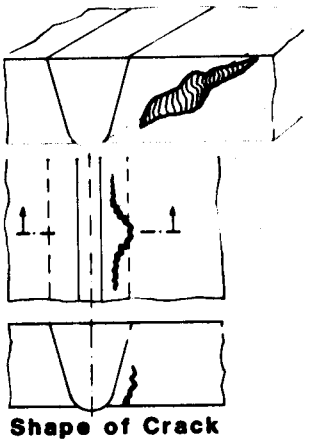
Intergranular Stress - Corrosion Cracking



Grain Size

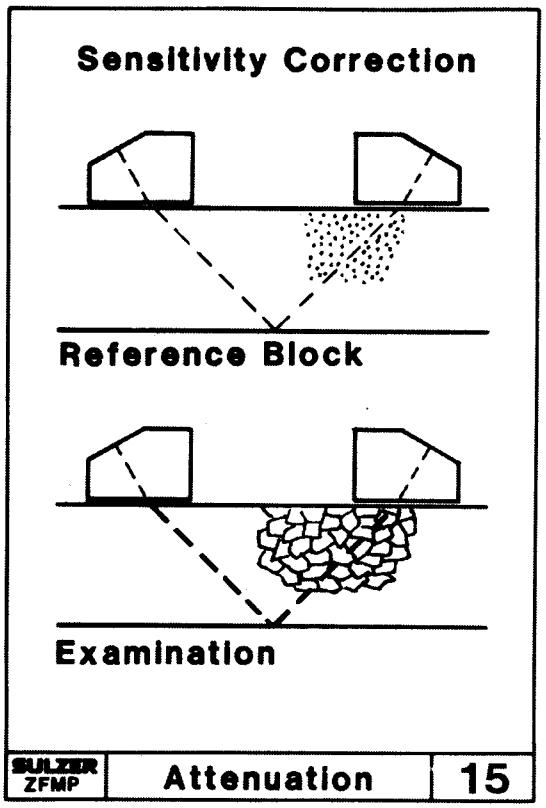


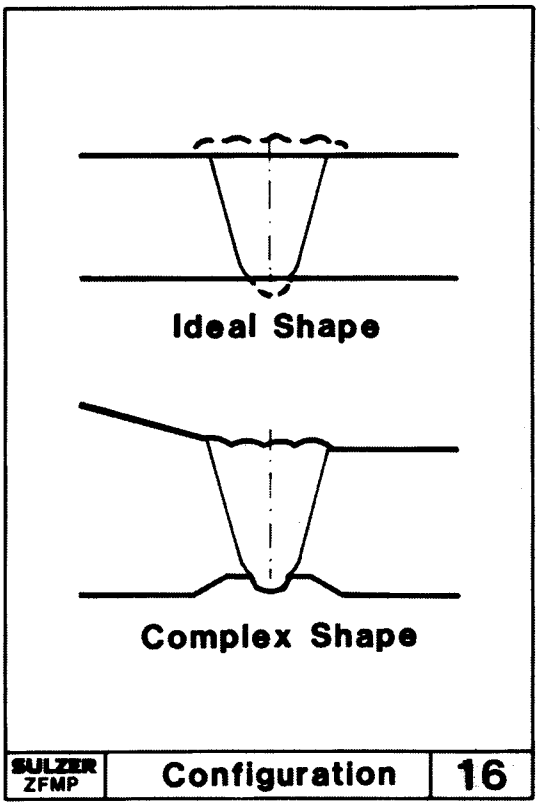
Network of Cracks
Grain Desintegration

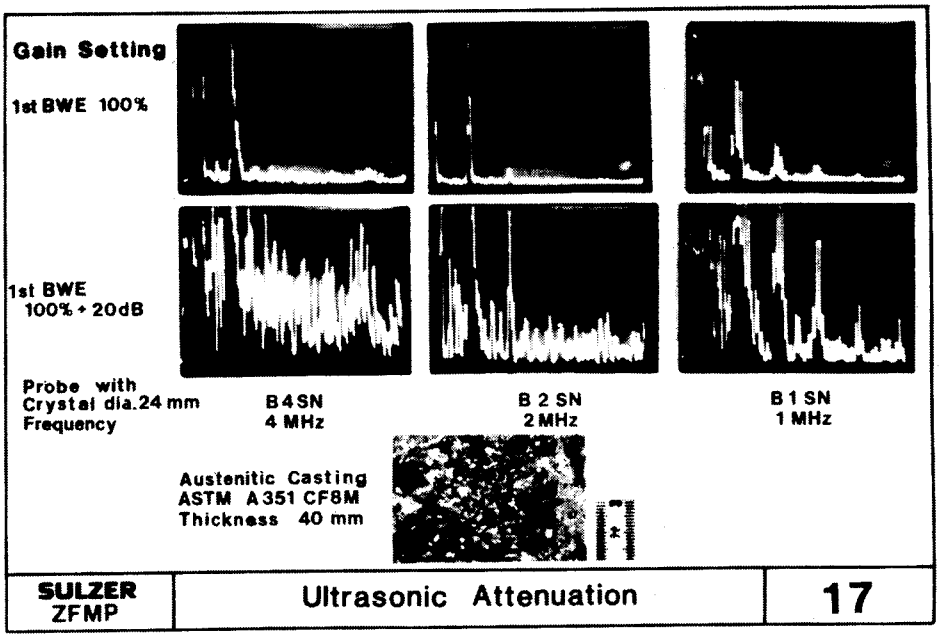


Shape of Crack

SULZER ZFMP	Influencing Factors	14


Sensitivity Correction
Reference Block
Examination
SULZER ZFMP
Attenuation
15


Ideal Shape
Complex Shape
SULZER ZFMP
Configuration
16

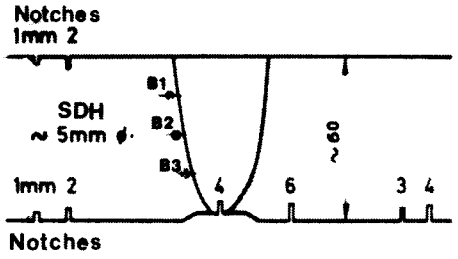

Gain Setting
1st BWE 100%
1st BWE 100% + 20dB
Probe with Crystal dia. 24 mm Frequency
B4SN 4 MHz
B 2 SN 2 MHz
B 1 SN 1 MHz
Austenitic Casting ASTM A351 CF8M Thickness 40 mm
SULZER ZFMP
Ultrasonic Attenuation
17

Austenitic Weld Joint in the Main Cooling System

Casting	Weld	Casting
G-X5CrNiMo 1810 A-351 Gr CF8M	X2CrNiMo 1810 316L	



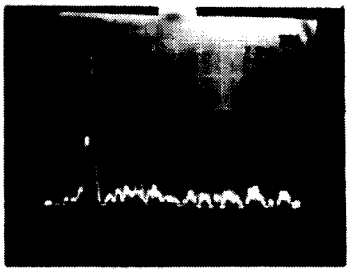
Reference Reflectors



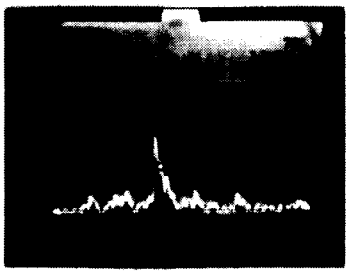
SULZER ZFMP | UT Reference Block | 18

Testing of the Near Surface Area

Main Cooling Pipe



Indication of the 2mm deep Surface Notch through cast parent metal

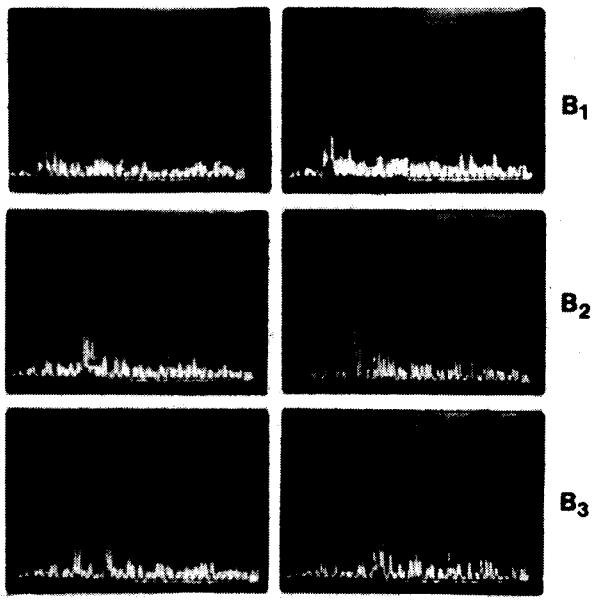


Indication of the 5mm dia. SDH in 15mm depth through weld metal

Probe: RTD BAM 70°SEL
Subcladding Crack Probe

SULZER ZFMP | UT-Indications | 19

Vinçotte Probe V 45°L SE 85F 1MHz



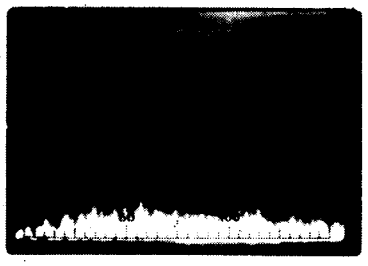
through parent metal **through weld metal**

Reference Block for Main Cooling Pipe
Austenitic Casting with Weld

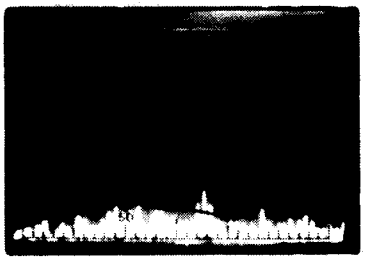
SULZER ZFMP | UT-Indications | 20

Vinçotte Probe V 45°L SE 85F 1MHz

Reference Block: Austenitic Casting
Main Cooling System PWR
Notch (4 mm deep) at inside surface



Noise Indications



Notch Indication

SULZER ZFMP | UT - Indications | 21

Recent experiences in the ultrasonic examination of austenitic steel components

M. KROLL, E. FISCHER, M. STERNISCHA, H-D. WALLHEINKE
Kraftwerk Union, F.R. Germany

ABSTRACT

During manufacture, nuclear power plant components made of austenitic stainless steels are subjected to a comprehensive ultrasonic examination based on the stipulations of both the Federal German Reactor Safety Commission and the KTA Safety Standards. This is, however, not applicable to austentitic castings.

In general, the ultrasonic examination of austenitic plates and seamless pipes presents few problems if the parts involved are of standard dimensions. Difficulties are, however, often encountered in the examination of forgings and welds. Not enough information is available on the type and scope of these difficulties prior to examination to enable an examination technique to be specified in the form of examination instructions. The selection and stipulation of an optimum ultrasonic examination technique is, therefore, based on measurements taken on the part to be examined or on test specimens whose dimensions and manufacturing technique are in essential agreement with those of the part to be examined.

Experience was gained in the field of ultrasonic examination of austenitic welds from a relatively large number of test pieces (circumferential pipe welds and butt welds on plates).

This involved the determination of the signal-to-noise ratio for the various test pieces as a rule on a 3 mm cylindric hole. Results of reference measurements performed with longitudinal-wave dual search units (SEL) produced as a rule better signal-to-noise ratios. The differences to results obtained with transverse-wave search units containing a single oscillator were, however, in some cases only a few dB. According to the experience already gained, both the welding method (submerged arc or manual electrode welding) and

welding parameters (energy per unit length) do not influence the ultrasonic examination as much as local differences in beam attenuation.

In addition, considerable differences in amplification occur in some cases dependent upon the type and location of the reflectors (longitudinal or transverse discontinuities, location in the base material or within the weld) which may considerably complicate the evaluation of the signal amplitude even with the use of the DAC method. The surface waviness of ground welds, especially when relatively large SEL search units are used, often introduces an additional difficulty into actual test performance and evaluation of results. In spite of these difficulties and restrictions, welds on austenitic components with average wall thicknesses are generally amenable to a meaningful ultrasonic examination if the fine-grain quality of the base materials is adequate and thus also amenable to examination. The amount of work involved in this case is, however, as a rule considerably higher than that for ferritic components.

1. Introduction

The extensive use of ultrasonic examination for in-process and in-service inspection of austenitic components constitutes a considerable part of the quality assurance system and safety philosophy in the construction of nuclear facilities.

The requirements made of non-destructive examination and those to be made of the components of the reactor coolant pressure boundary of nuclear power plants in the Federal Republic of Germany with regard to safety are specified in a guideline of the German Advisory Committee on Reactor Safeguards (RSK = Reaktor-Sicherheitskommission). The RSK has been set up by the Federal Ministry for the Interior. This guideline gives, amongst other things, a wealth of details for the non-destructive examination of components of the reactor coolant pressure boundary of pressurized water reactors. The following paragraph refers to the ultrasonic examination of austenitic weld connections in the edition valid since the beginning of 1979:

"The ultrasonic examination may be replaced by the radiographic examination for welds with nominal diameters less than 500 mm in which the material properties are impaired to such a degree that no conclusive examination can be made when using the techniques of the pulse echo method available according to the present state of the art such as the single probe technique, focussing probes, transmitter-receiver technique, wide-band probes and the use of longitudinal waves."

This guideline means that the suitability for ultrasonic examination of welds must be demonstrated in every single case.

Using two examples it shall be illustrated in the following that the performance of such a demonstration necessitates costly examination programs.

2. Examination Examples

At this point there shall be no detailed references to the particular difficulties encountered in the ultrasonic examination of austenitic materials as the type and size of the interaction between ultrasonic waves and austenitic materials is described in many references. Likewise it is important to keep clearly in mind, with regard to the much-quoted distinction between the search and analysis technique, that the interest of industry must be seen to lie in demonstrating the integrity of austenitic components with justifiable economic expenditure. Thus the approach for solving examination problems must of necessity accord greater consideration to the choice of existing examination techniques than to the optimization of a particular technique on the basis of only a few test blocks. In the selection of the available examination method, preference is given furthermore to that method which necessitates the least expenditure in its performance with the same degree of demonstrability.

2.1 Accumulator

In the first example, the effects of the welding parameters on the ultrasonic examination of 25 mm thick plates are investigated. The findings should be taken into consideration in accordance with the guideline already referred to in the manufacturing process of accumulators. The material is a niobium-stabilised austenite with the material no. 1.4550. (X 10 Cr Ni Nb 18/9).

As coarse grain and dendrite growth certainly are the factors governing the suitability for ultrasonic examination in the case of austenitic weld joints and as it must be possible to limit these parameters by local heat treatment, the energy per unit length and the welding process were varied to enable

the effect on ultrasonic examination to be interpreted. A verification of the mechano-technological material characteristics would have to show whether the results obtained lay within the scope of the prescribed tolerance ranges even from this point of view.

2.1.1 Welding

In determining the welding process for the investigation program, it was necessary to consider primarily the welding techniques envisaged for the manufacture of the accumulator, namely the submerged-arc welding process and manual arc welding. So that it was also possible to assess idealised welding conditions in respect of ultrasonic examination, an automatic tungsten inert gas welding head (automatic TIG welder) was developed which permits lower base metal heating and a lower rate of weld metal deposition. Furthermore, it is possible to keep the parameters constant for the duration of the weld.

Attention was also paid to keeping the interpass welding temperature low with a view to only slight grain enlargement.

The following table shows a comparison of the individual parameters. A wire or electrode diameter of 4 mm and 3.25 mm was used for both the 3 submerged-arc welds and the 3 manual arc welds. In each case one of the plates with very low energy per unit length, no. 2 of the submerged-arc welds and no. 6 of the manual arc welds, was welded with the smaller wire diameter or smaller electrode. A wire with 1.0 mm diameter was used for the automatic weld. The energy per unit length of approx. 18500 $\frac{Ws}{cm}$ for the submerged-arc weld and approx. 8000 $\frac{Ws}{cm}$ for the manual arc weld correspond to normal weld data. One may see from the table that the energy per unit length was reduced by a factor of 2 for two plates in each case.

Welding edge preparation may be seen in the next diagram. The double-U butt weld, the weld geometry which occurs by far the most often, was performed for all manual arc welds and 2 out of 3 submerged-arc welds.

We shall not go into details here of the wire and flux combination nor into the analyses of the filler metals. It should, however, be mentioned briefly that the procedure usually found in practical application was also adhered to here.

2.1.2 Non-Destructive Examination

The correlation of these welding parameters with the result of the non-destructive examination was performed in accordance with the pragmatic procedure referred to above.

All plates were subjected to a radiographic examination which, however, produced no results other than isolated pores in plates nos. 2 and 3. The pores were permissible in accordance with valid codes and standards. No. 3 of the test plates, the submerged-arc weld with the compound single-U and single-V butt weld preparation, was radiographically examined both perpendicularly and parallel to the V.

Before fabrication of the test specimens necessary for performance of the ultrasonic examination, sound attenuation measurements were undertaken on the plates. The welds of the test plates were ground flush with the plates on both sides. A deviation from the standard fabrication sequence arose however, due to the relatively great "distortion" of the plates during welding. This rendered subsequent straightening of the plates and additional mechanical surface finishing necessary. This resulted in the quality of the specimen surface no longer corresponding to that of the component. It was optimum for the

ultrasonic examination with a peak-to-valley height of < 10 µm and ripple of < 0.1 mm related to the probe contact surface.

The sound attenuation measurements should be taken here to mean the deviation of the transmission echos and should make a statement on the stability of the structural configuration of a single plate or on the comparison of the plates with one another. They were performed with 45° angle probes in V transmission. The result may be seen from the diagram. The V transmission values were recorded at both 2 and 4 MHz for the transverse waves and 2 MHz for the longitudinal waves. In spite of optimum surface conditions, the measurement for the transverse wave probes shows no satisfactory results. Since greater amplitude deviations are recorded as the wave length becomes shorter, as is to be expected, it is understandable that the longitudinal wave probes with 2 MHz provide the best results, namely the least variations.

An evaluation of the V transmission values recorded in all seven plates both perpendicularly and parallel to the weld shows that it was not possible to prove any relationship between the ultrasonic signal and the welding process or parameter settings used.

The proof of suitability for ultrasonic examination linked with a selection of the most suitable examination techniques was provided by the recording of DAC curves. Six test blocks were made from each plate with which reference responses for longitudinal and transverse defects could be recorded. In accordance with the basic code for the examination of welded plates of these dimensions, the transverse holes with 3 mm diameter were distributed as in the diagram. The test reflectors which represent 4 depth zone areas including the groove for the

demonstration of surface cracks in half the skip distance, lie on the one hand in the filler metal and on the other in the weld groove face.

The examination techniques used are derived from commercially available probes. The tables shown provide a list of the transverse and longitudinal wave probes with various beam angles and frequencies. One can see that in the case of the longitudinal wave probes the choice of beam angle results from the desire to demonstrate all test reflectors directly, i.e. at half the skip distance.

The individual test holes were examined using each of these probes and the "gain reserve" and signal-to-noise ratio were recorded as decisive parameters.

An evaluation of the results summarised at first in table form shows that preference must be given to the longitudinal probes and in this case the transmitter-receiver examination technique. Although it was also possible to detect a great number of reflectors using the simpler single ultrasonic crystal examination technique with transverse waves, the examination failed completely in the detection of transverse defects.

Preference of the TRL examination technique with division into two depth zones as opposed to the single ultrasonic crystal-longitudinal wave probe is based on the far greater signal-to-noise ratio of the transmitter-receiver method.

Much more interesting than the result of comparing examination techniques, which is on the whole identical to the theoretical predictions, is the fact that it was not possible to find any influence of the welding procedure or weld parameter settings on the suitability for ultrasonic examination. The results which it was possible to achieve by reducing the

energy per unit length are smaller than the deviations which must be attributed to the performance of a manual ultrasonic examination.

A change in the welding procedure aimed at reducing base metal heating is unnecessary from the point of view of examination at least for plate thicknesses as investigated in this case.

A comparison of the notch toughness values determined in ISO-V specimens and metallographic evaluation of macro and microsections likewise reveals only slight differences for the various welding processes. Only in the automatic TIG welds is the structure somewhat altered. As opposed to the submerged-arc and manual arc welds, the crystallite orientation is not quite as uniform.

Due to the realisation that reduction of base metal heating has a negligible influence on the structure of the weld and non-destructive examination, four more test plates were made to supplement this series of investigations. They were also subjected to examinations depending on welding parameter settings but this time in addition taking into consideration the increase in base metal heating.

This time the welding procedure was limited to the performance of submerged-arc welds. The energy per unit length and the filler pass temperatures may be seen in the table. The weld parameters were chosen to enable a comparison to be made with the tests carried out previously. The energy per unit length of $\sim$ 17000 $\frac{Ws}{cm}$ again corresponds to generally used weld parameter settings. The interpass temperature of approx. 20° was achieved by H_2O quenching after welding of each pass.

The ultrasonic examination proceeded analogously with the test program already described, and the results of both sound attenuation measurements and the determination of an optimum

examination technique are directly comparable. As a result of the attempt to achieve as high a signal-to-noise ratio as possible, the transmitter-receiver technque with longitudinal waves and subdivision of the wall thickness into two depth zones had to be chosen as the most suitable examination method. The evaluation of the effect of welding parameter variation on the suitability for ultrasonic examination shows no impairment of the ultrasonic examination even in this case with extreme increase in base metal heating.

A comprehensive assessment of the tests on 11 test plates with a total weld length of 5.5 m shows that DAC curves for the TRL technique provide adequate values for all beam incidence positions and that the welding parameters have no effect on suitability for ultrasonic examination.

The mechano-technological values also lay above the minimum requirements.

One may conclude provisionally from this investigation that it is not necessary to manufacture separate test blocks for each welding procedure, each weld profile and for different welding parameter settings.

2.2 Piping

In a further case we have tackled the problem of demonstrating the integrity of austenitic pipe welds. In a program similar to that of the plates, the aim is to demonstrate suitability for ultrasonic examination. You can see a list of the nominal diameters and wall thicknesses in the following table. As in the previous test, different welding procedures were used. As may be seen from the table, submerged-arc, manual arc and automatic TIG welds were compared with one another. A table of the welding parameters is unnecessary in this case as

various procedures have to be used due to fabrication conditions and not because optimisation of the welding procedure was the reason. The automatic weld was intended in turn to enable us to interpret any improvement in the ultrasonic examination due to constant setting parameters.

The second point which must be considered in its effect on the suitability for ultrasonic examination was the manufacturing process of the pipes. Some were made from forged bars by drilling whilst others were manufactured by the pilger method.

Before the investigations on the suitability of the weld connections for examination were begun, the first difficulties were already in evidence due to great sound attenuation discrepancies both amongst the individual pipes and also at different positions on the same pipe. The metallographic results showed grain sizes of - 1 to 6 according to the ASTM classification. The coarse grain areas or partially-crystallized structure may be attributed to deviations during the forging process as a result of exceeding or falling short of the hot working temperatures, the furnace dwell times and the critical degree of deformation of the material concerned.

As an approach as near as possible to normal practice was a prerequisite for performance of the welds, the test block pipe sections were selected at random to simulate the joining of different pipes. This diagram shows the consequences for the existing grain size deviations.

The two pipe sections with fine grain and coarse grain and the problems of the filler metal clearly illustrate the difficulties encountered in attempting to provide a conclusive ultrasonic examination.

In addition to the problems encountered in the structure of the austenite, one may anticipate further difficulties in the ultrasonic examination of piping. The pipe bend, surface waviness and the shape of the weld root limit the possibilities of solving such problems. The following list provides an overview of the examination techniques used. As, on the whole, the amplitude height represents the only evaluation variable, the gain reserve of the ultrasonic examination device and the signal-to-noise ratio was determined once again at 3 mm transverse holes.

Adaptation to the pipe curvature was undertaken on all probes. Thus in the investigation phase the adaptors used were exclusively wedges to keep probe wear to a minimum. Thus it was possible to use the same ultrasonic probes for longitudinal and transverse defect examination and for the various dimensions.

I do not want at this point to go into details about the "usual" difficulties encountered in ultrasonic examination, e.g. the theoretical examination of the transmission curve in transverse defect examination, accuracy of defect location relative to pipe curvature, the change in the angle of incidence at a groove as a function of the pipe diameter and the wall thickness for constant beam angle, as they are not specifically related to austenite.

On the other hand the problem of surface waviness due to the great weld reduction in welds ground quasi-flush with the pipe are not negligible. Although the probe shoe must be adapted for these pipe dimensions, the contact problems are not lessened. Waviness of less than 0.5 mm per probe contact surface permissible in our case signifies impairment of manual examination even with relatively well ground final passes. All these boundary conditions prejudiced the use of ultra-

sonic probes of miniature design. That preference was given once again to the TRL examination technique as the choice of the most suitable examination method may be attributed not least to the formation of the arithmetic mean value. However, the result should not obscure the fact that variations in gain in the order of magnitude of only 1 dB were decisive for individual cases of application. It is easy to see from the example of the DAC curves that this result represents a compromise.

If one considers the example of the weld referred to above with the two different structures for the adjacent materials, it is easy to appreciate that DAC curves of the same reference hole recorded from different positions vary quite considerably from one another.

The next diagram shows, for the purpose of clarity, which four incidence positions are possible for the detection of longitudinal and transverse defects when using probes ground to fit the contact surface. Tilting or meandering is also greatly limited when using adapted transducer shoes. If one still takes reflector locations in the other side of the weld root face and in the filler metal itself into consideration, it is easy to appreciate that the selection of a reference source involves a high content of unsharpnesses.

The following diagram shows an example of DAC curves recorded using different incidence positions.

The two diagrams show an examination technique used for one pipe dimension. As the selected TRL technique necessitated in its turn a division into 2 zones, it was also necessary to prepare two adaptor scales. The use of a TR probe with a focussing range of 60 mm transmission path with wall thicknesses up to 30 mm resulted from the desire to keep the

number of examination techniques used small and to determine one procedure applicable to all cases of application. The relatively long focussing distance and also the 45° beam angle may be attributed to the problems already mentioned encountered in the examination of transverse defects.

Each of these two diagrams shows not only the DAC curve applicable for the component examination which must be made extremely conservative to avoid at all costs the risk of falling short of the detection threshold, but also the 4 reference sources for the 4 possible incidence positions. However, in an amplitude height evaluation there is a distinct rise in the detection threshold for other areas.

This may lead to considerable indication recordings particularly in austenite examination with an in part greatly reduced signal-to-noise ratio and very definite structural noise locally. Thus in the manual examination of austenite, too, one must begin to correct the great deviations in the echo height by making allowances as is similarly the case with the automatic examination. That means that if an indication which must be recorded has to be allocated to an overestimated area due to its location, the corresponding allowance must be subtracted from the overall detection threshold for the conservative detection height.

Otherwise one would have to record separate reference responses not only for every individual pipe section but also for every dimension and every incidence position of every depth zone.

It was not possible to single out any influence of the condition of the processed material on the performance of the ultrasonic examination. Although performance of the examination was facilitated on the pilger rolled bars due to the generally

smaller degree of sound attenuation in the base material, it is understandable that such influences play a subordinate role as a result of the sound attenuation caused by the HAZ (heat affected zone) linked with the high gain deviations.

Discussion

In the present report on our practical experiences in the preparation of examination concepts for the ultrasonic examination of austenitic components we have attempted to illustrate the course of examination in relation to the specified legal requirements. As the RSK guideline referred to at the beginning of the report has not yet been made binding in a KTA safety rule (KTA = Kerntechnischer Ausschuß = Nuclear Safety Standards Commission), these in-process inspections are performed as part of the requirements of a KWU specification. In both examples, that of the 25 mm thick plates and that of the pipe weld joints, we have paid as much attention to the examination of the effect of differing welding processes, weld edge preparations, variable interpass temperatures and energy per unit lengths as to the influence of the condition of the processed material. The procedure for determining the optimum examination technique is often rendered more difficult with forged parts as test blocks must be manufactured for calibration of the detection threshold.

Although the two examples have shown that a series of fabrication parameters during welding have only slight effects on the suitability for ultrasonic examination, everyone who is involved with the ultrasonic examination of austenitic materials knows the dreaded inconstant connection between material and suitability for ultrasonic examination. For this reason it is still advisable, at least on the basis of these results, to observe all important fabrication parameters such as

- material (base material and filler metal)
- fabrication process (base material and weld)
- dimensions important for examination
- surface conditions

for the test block, too.

The empirical determination of suitability for examination derived from this procedure and the optimum examination technique in each case are necessary as we are not yet able to extrapolate the optimum procedure from our wealth of experience due to the large number of variables.

The choice of examination techniques must be made with the aim of being able to detect possible fabrication defects with certainty. As the occurrence of hydrogen-induced transverse cracks is impossible in the case of austenitic welds, we shall be able in future to leave out ultrasonic examination for transverse defects.

As the empirical procedure to demonstrate the suitability for ultrasonic examination necessitates considerable expense and a high incidence of risks related to fabrication and deadlines, we are planning a research and development program jointly with research institutes and other system manufacture's in which both the effect of material variables on the suitability for ultrasonic examination shall be determined, as comparative investigations with various examination techniques tested on selected austenitic components.

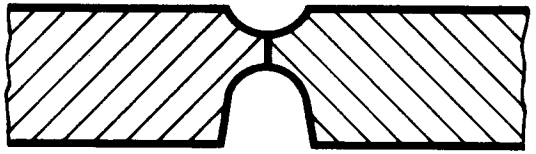
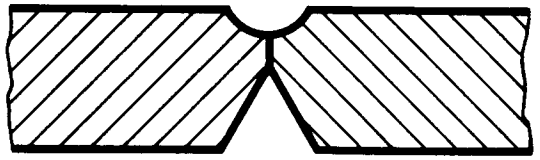
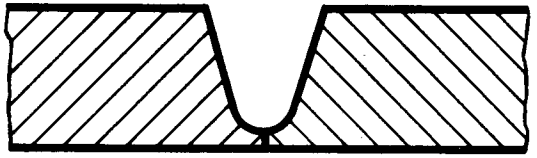
State of the Art for Ultrasonic Examination of Austenitic Welds in Accordance with the RSK - Guideline

- Fokussing Probes
- Transmitter – Receiver Technique
- Special Probes with Short Pulses
- Longitudinal Wave Probes for Oblique Incidence

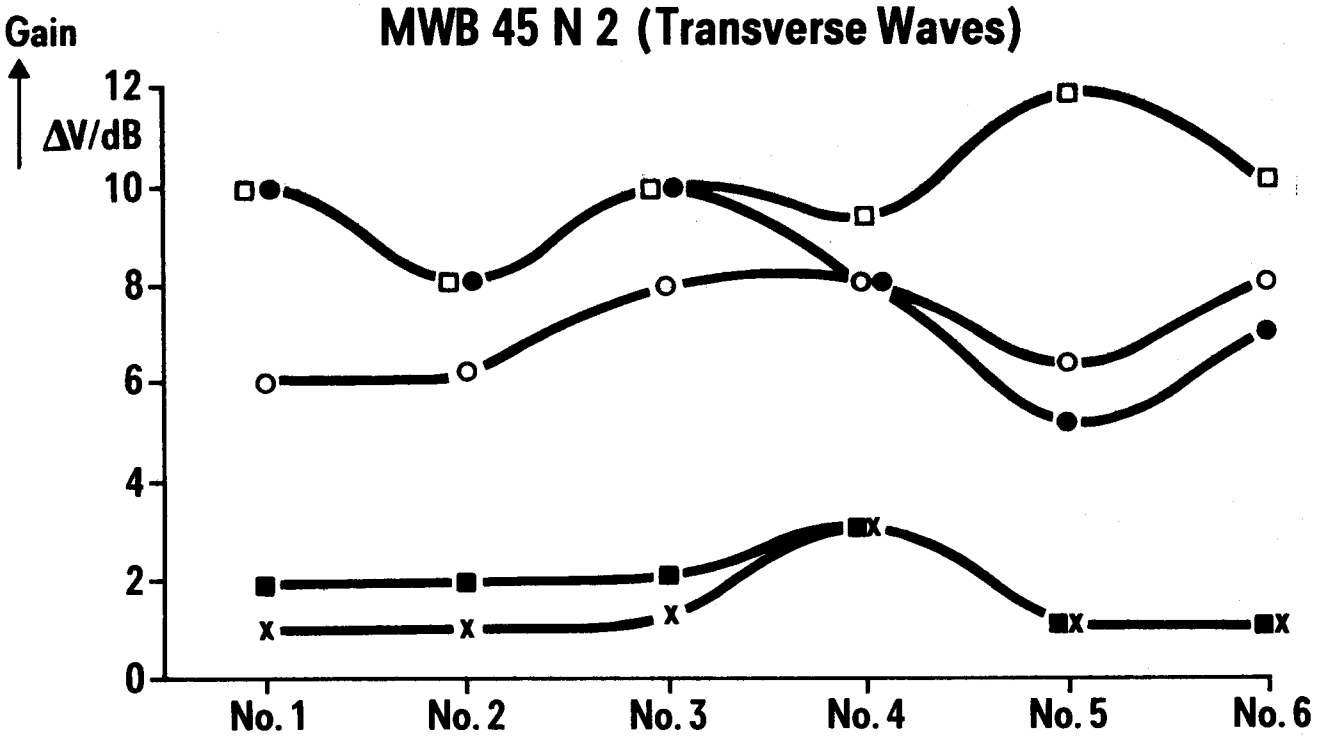
RSK - Guideline (RSK = German Advisory Committee on Reactor Safeguards)

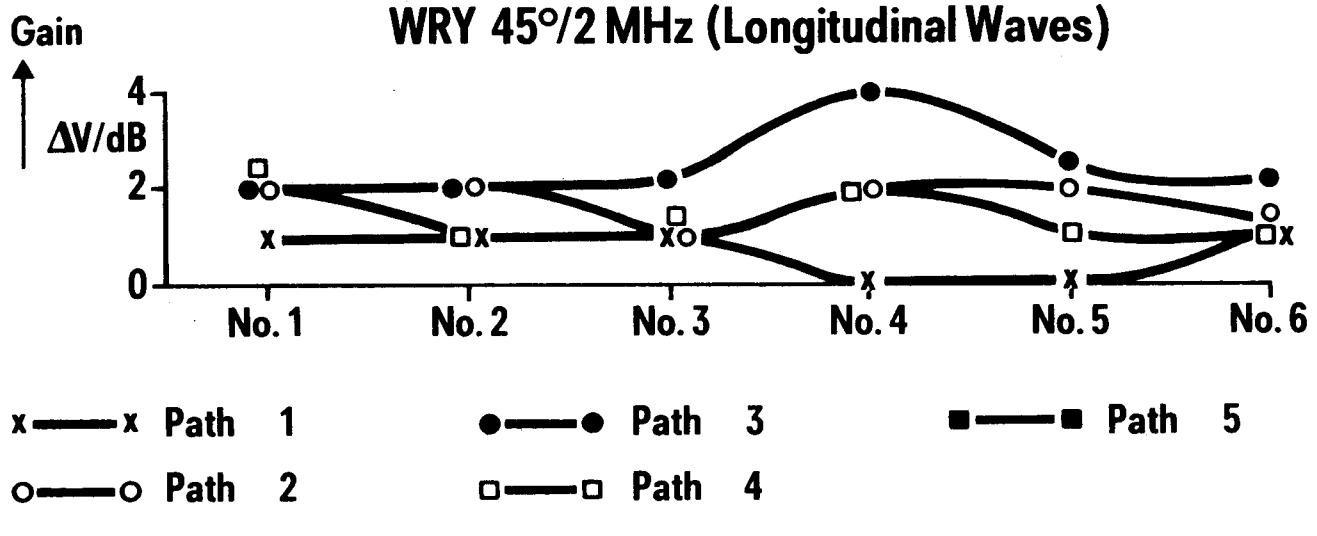
No.	Welding Process	Interpass Temperature	Energy per Unit Length
1	SAW	46°C	~18 500 Ws/cm
2	SAW	41°C	~ 9 350 Ws/cm
3	SAW	36°C	~10 000 Ws/cm
4	MAW	58°C	~ 8 000 Ws/cm
5	MAW	57°C	~ 4 750 Ws/cm
6	MAW	54°C	~ 5 000 Ws/cm
7	Automatic TIG	100°C	~ 7 200 Ws/cm

Welding Parameters (Plates I)

Weld Joint Design	Sketch	Adapted to:
Double - U Butt Weld		No. 1, No. 2 } SAW No. 4, No. 5, No. 6 } MAW
Compound Single - U, Single - V Butt Weld		No. 3 SAW
Single - U Butt Weld		No. 7 Automatic TIG

Welding Edge Preparation

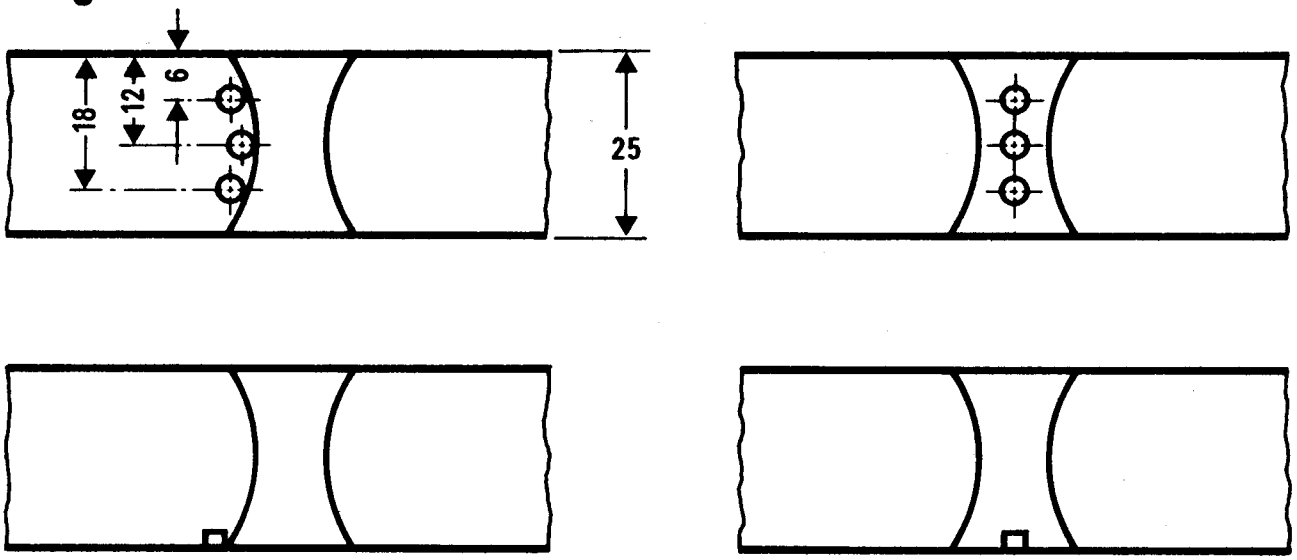




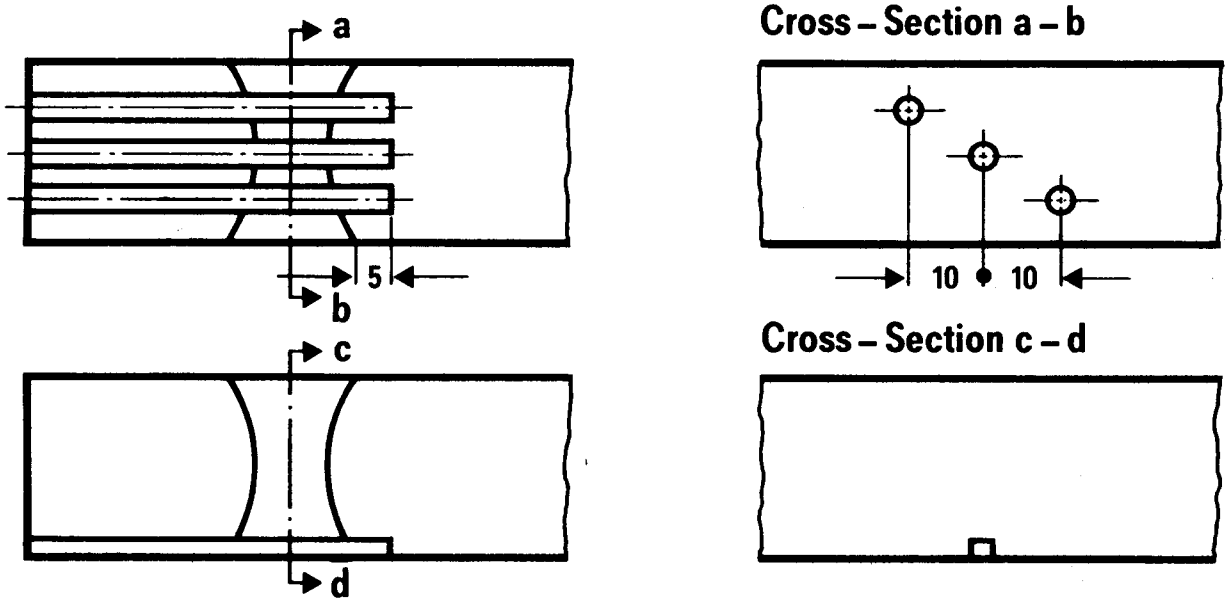
Relative Attenuation Curves

E80 586e

Longitudinal Defects



Transverse Defects



Test Blocks for Ultrasonic Examination

E80587e

Probe	Frequency/MHz	Wave Mode	Technique	Beam Angle
MWB 45 N 2	2	Transverse	Single	45°
MWB 45 N 4	4	Transverse	Single	45°
WRY 45	2	Longitudinal	Single	45°
WRY 60	2	Longitudinal	Single	60°
WRY 70	2	Longitudinal	Single	70°
SM TRB 4 H	4	Longitudinal	TR	0°
BAM TRL 70	2	Longitudinal	TR	70°
RTD 70 TRL 2	2	Longitudinal	TR	70°
RTD 60 TRL 2	2	Longitudinal	TR	60°

Probes Used (Plates)

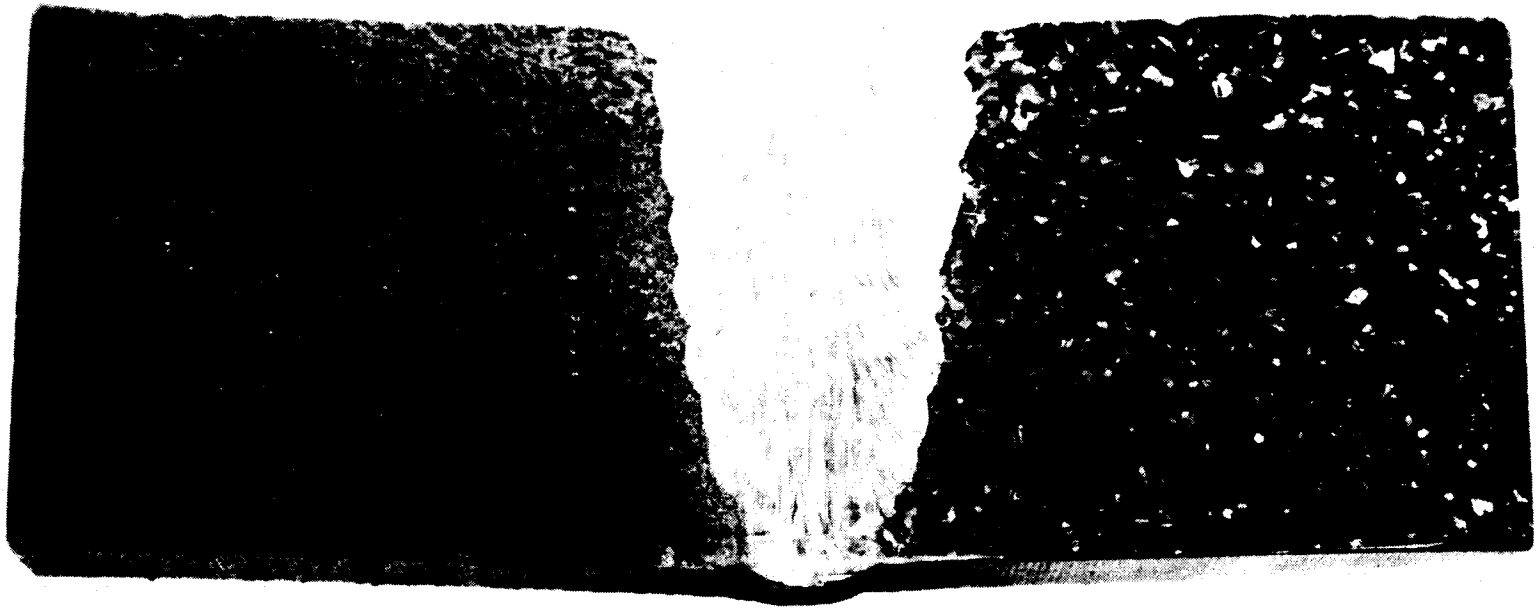
No.	Welding Process	Interpass Temperature	Energy per Unit Length
1	SAW	46°C	~18 500 Ws/cm
2	SAW	41°C	~ 9 350 Ws/cm
3	SAW	36°C	~10 000 Ws/cm
4	MAW	58°C	~ 8 000 Ws/cm
5	MAW	57°C	~ 4 750 Ws/cm
6	MAW	54°C	~ 5 000 Ws/cm
7	Automatic TIG	100°C	~ 7 200 Ws/cm
8	SAW	150°C	~16 800 Ws/cm
9	SAW	100°C	~ 8 900 Ws/cm
10	SAW	~20°C (H_2O – Quenched)	~16 800 Ws/cm
11	SAW	max. 200°C	~29 750 Ws/cm

Welding Parameters (Plates II)

E80583e

Weld No.	Dimensions	Welding Process
201	250 li ⌀ × 31	SAW
204	250 li ⌀ × 31	MAW
205	234 li ⌀ × 28	SAW
207	234 li ⌀ × 28	MAW
208	234 li ⌀ × 28	Pulsed TIG
212	108 li ⌀ × 16	Pulsed TIG
301	325 li ⌀ × 40,5	SAW
302	325 li ⌀ × 40,5	MAW
308	230 li ⌀ × 29,5	MAW

Grain Size ~5 (ASTM) Weld Grain Size ~1 (ASTM)

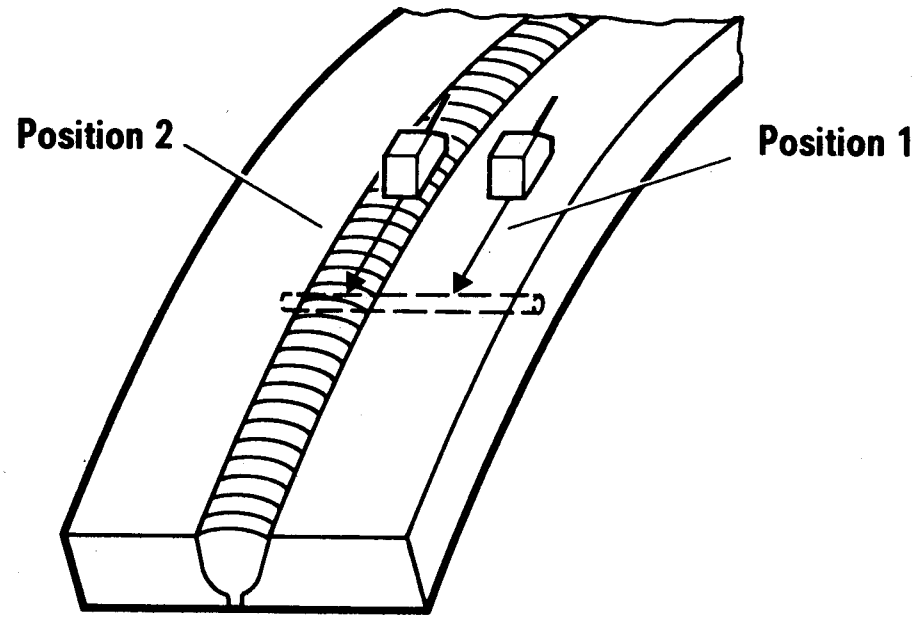


Example of a Pipe–to–Pipe Weld with Different Grain Sizes

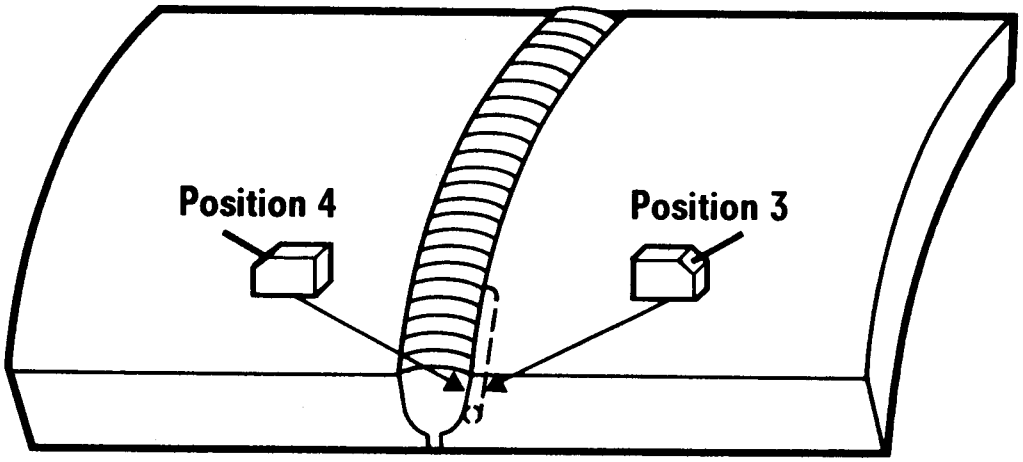
Probe	Frequency/MHz	Wave Mode	Technique	Beam Angle
WRY 60	2	Longitudinal	Single	60°
WRY 70	2	Longitudinal	Single	70°
Panametrics	2,25	Transverse	Single	45°
BAM UPM 65	2	Longitudinal	TR	65°
BAM UPM 70	2	Longitudinal	TR	70°
RTD 45 TRL 2	2	Longitudinal	TR	45°
RTD 60 TRL 2	2	Longitudinal	TR	60°
RTD 70 TRL 2	2	Longitudinal	TR	70°

Probes Used (Piping)

Transverse Defects

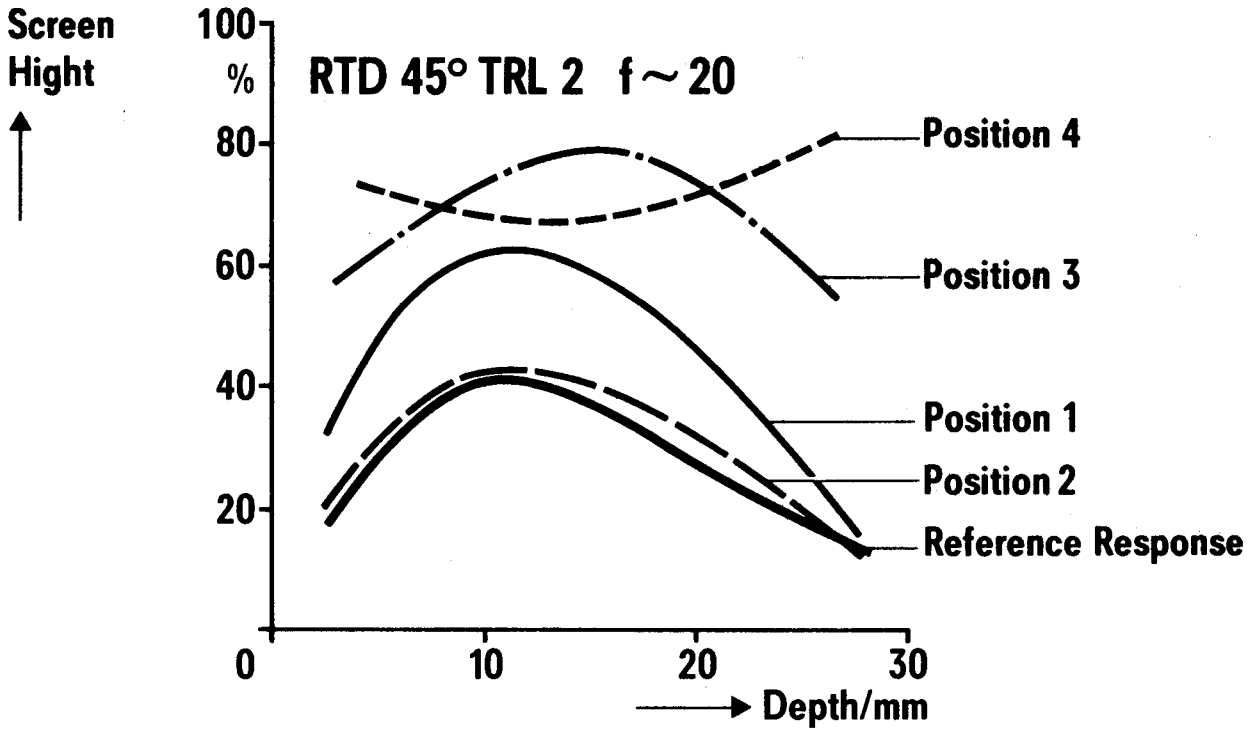


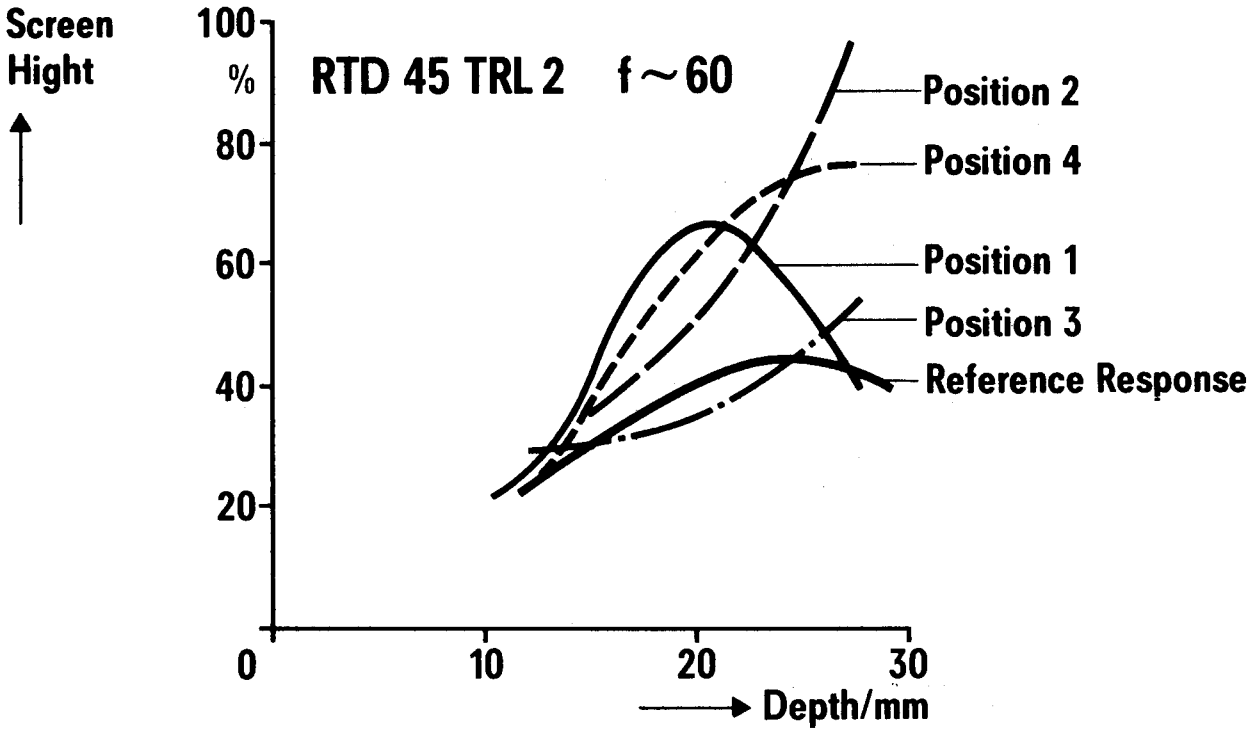
Longitudinal Defects



Scanning Directions (Piping)

E80590e





DAC – Curves

E80588e

Plates	Pipes
● Welding Process	● Welding Process
● Interpass Temperature	—
● Energy per Unit Length	—
● Examination Technique	● Examination Technique
—	● General Problems in UE of Pipes
—	● Condition of Material after Processing

List of Examined Parameters

Present practice on ultrasonic in-service inspection through austenitic stainless steels on nuclear piping in Spain

J.B. PEREZ PRAT
Tecnatom S.A., Spain

ABSTRACT

1. CALIBRATION PROBLEMS IN RELATION TO CODES

The code used is ASME section XI and section V as references. There are no requirement of calibration blocks with weld and big differences between blocks with or without welds have been found.

2. RESEARCH DEVELOPED

Systematic research has been carried out on calibration blocks with welds manufactured with the same welding procedure as on site. Drilled holes at differents depths inside and outside the weld metal have been manufactured to demonstrate the detectability of those reference reflectors. Moreover notches at the weld root, weld crown and counterbore have also been manufactured.

Longitudinal and transverse waves ultrasonic probes with several angles were used.

3. DESIGN PROBLEM

Welding design is a very important factor in testing reliability. Weld crown must be ground flat to allow welding inspection and the counterbore must be minimum.

However with the older design nothing of that can accomplished and therefore additional scans must be carried out as well as surface examinations.

1. INTRODUCTION

On 1976 Tecnatom started the preoperational inspection of the first Spanish Nuclear Power Plant of the 1000 MWe generation, built at Almaraz with a PWR Westinghouse type reactor, and was faced with the problems arising from the need of including more than 1000 welds with ultrasonic inspections on the base line program with near 60 % of austenitic stainless steel. On 1978 and 1979, the same work was started at two other similar type and size plants, Lemóniz and Ascó.

Up to 1979 our research on inspection of austenitic stainless steels have been limited to be a part of the work preparation, with the normal time and man power limitations of a private emerging inspection organization. Work preparation was iniciated as follows:

In addition to the official inspection requirements limited to enforcement of ASME XI, at the stage of preparation of the first inspection we asked the utility to provide us with a complete set of welded mock-ups, easily obtained during the installation stage, to be used as ultrasonic calibration and procedure development blocks, allowing consideration of the weld and base metal and HAZ different ultrasonic performance. As a result of the request, near 20 different welded pipe spools covering different materials, thicknesses and diameters were supplied by the plant owner, and mechanized by us, with base metal and weld located refectors consisting on side drilled holes and notches with depths and dimensions as propposed by ASME XI for base metal calibration blocks. This practice has been repeated and improved for the other new plants (see fig. 1)

The calibration blocks are made from the same base material, and with welding procedure, counterbore and weld crown finish similar to the production welds. All recently built nuclear power plants in our country are providing us with a

complete set of welded spools for obtaining the ultrasonic calibration blocks. Usually, one set of blocks is used for field PSI and ISI and mantained on the plant. A duplicate collection of blocks is retained on our laboratory allowing improvement of techniques and work preparation, as well as comparison of ultrasonic performance between similar lines from different power plants. The carbon steel blocks show minimum effect for ultrasonic distorsion or through weld defect detectability, while the stainless steel welds and materials show different ultrasonic distorsion and defect masking effects, which we intend to define and optimize case by case. At present we are intending to correlate with general metalographic structure by heat treatment and welding parameters.

2. INSPECTION OF CAST STAINLESS STEEL PRIMARY PIPING

The primary piping of Almaraz NPP was made from SA351 CF8A centrifugally cast straingth runs, elbows being statically cast, 66 to 90 mm thick. The same material was found at Zorita NPP with regular ISI since 1972. Some available longitudinal refracted wave transducers, were tried and later on, a mechanized sample of primary piping material drop-out was send, together with a reduced specification, to various potential transducers suppliers in Europe in early 1976. The best result was obtained by a combination of RTD SEL type transducers, using 45º, 52º and 72º refracted angles.

The weld metal (root TIG SFA-5-9 type 308 and manual or sub arc type 308) found on the primary piping was ultrasonically much better than the base metal, who presented apparent attenuations of nearly 1 db each 4 mm distance. Statically cast material bends produce higher noise and spurious indication levels than centrifugally cast parts.

Presently some slight improvements have been provided for the primary piping inspection of the second and third plant, but inspection effectiveness is considered still seriously limited (see fig. 2). New SEL transducers as well as other new special types, show improved performance while signal filtering and transducer matching, for further improvement of signal to noise ratio, has been intended.

Metalographic examinations of weld and base metal have been performed, looking for grain preferred orientarions. Results show no preferent orientations but a completely differenciated zone on the lower or inside part of the centrifugally cast base material (see figs. 6 and 7).

Machined notches on the lower surface cannot be detected by angled beams what is considered as the most serious limitation of this ultrasonic inspection.

When preparing the mechanized inspection of safe end to pipe weld from inside the reactor vessel, it was found that the transducers selected for inspection from the upper surface were not the adequate ones when they were used from lower surface.

Even the K1G strai ght beam transducer used normally for O.D. inspection was needed to be substituted by the SEB1. This asymmetry on through thickness direction was also atributed to through thickness differences of grain size.

Transducer selection is made on the plant mock-up weld by outlining the calibration curves on the ultrasonic screen, followed by a complete scan on base metal calibration block with a memory device or photographic long time exposure recording the envelope of single puntual spurious indications appearance. The calibration is considered admissible when DAC curve is at least 6 db over the envelope of the spurious indications which are additionally around 4-8 db over grass level (see fig. 3).

3. INSPECTION OF TRI-METAL WELDS

Tri-metal welds found until now on the PWR with stainless or inconel buttering show acceptable ultrasonic transmission capabilities. Shear wave pitch and catch 45º signals are not found substantially more affected by these welds than by welds between two carbon steel materials.

On the contrary inconel or tri-metal welds of BWR reactor vessel safe ends,are presenting special difficulties to ultrasonic inspection: Longitudinal refracted wave twin crystal shape wedged, transducer assemblies are being manually tested presently and, later on, they will be tested in a mock-up where calibration blocks or welded spools will be inserted and mechanically scanned with the ISI equipment and Data Adquisition System.

Curvature of safe ends provides additional dificulties and requires, specially for twin crystal transducers, a different perpendicular and parallel mounting for each different diameter.

4. OTHER WELDS ON AUSTENITIC STAINLESS STEELS

Ultrasonic inspections of other austenitic pipe welds from 8 to 36 mm thick, mainly 376 types 304 and 316, have been dealed up to now using only shear waves 2 or 4 MHz completing ocassionally the inspection with 70º longitudinally refracted SEL 2 MHz.

In on our third PWR, where the weld crown have been made near flush smooth on almost all welds, and the counterbore have been machined to 2T distance from weld root and where few use of ring inserts have been made, the weld and weld interface ultrasonic scanning difficulties have become more strong and evident, and the use of longitudinal refracted waves from single miniature transducers WSY type has been started; nevertheless there are still reflectors inside sample welds that are not detectable after extensive trials performed on the weld mock-ups using different longitudinal refracted wave transducers (see fig. 4).

Longitudinal refracted (LR) waves are used instead of shear waves only when some of the reflectors cannot be detected through weld by shear waves and they are detectable by longitudinal waves or when any of the gain corrections, needed for obtaining the same amplitude on the same or equivalent reflector by traversing weld metal, is more than 8 db. However the use of LR waves is restricted by their limitations on use on a full skip scan.

Changes up to 8 degrees on ultrasonic beam apparent angle have been observed to differ on base material, from angle measured on stainless steel standard V type block. Some metalographic correlation seams to identify bigger deviations with material showing through thickness sharp grain size changes. When crossing welds, even bigger deviations appear, such as a 70º transducer with a 38º measured through weld angle.

On figure 5, three structures of 376-304 identical specification materials are shown; the first structure corresponds to material with a normal ultrasonic performance. The second and third ones correspond to one specimen on two different through thickness positions (total thickness of 19 mm), showing different grain size and grain boundary segregation levels, and producing a 5º - 8º change on the apparent refracted angle.

5. METHODOLOGY FOR AUSTENITIC MATERIAL ULTRASONIC CHARACTERIZATION

We have started a cooperation with the INTA's (1) materials and NDT laboratory, subsidiary of the Spanish Defense and Air Forces, which facilities include an ultrasonic spectroscopic installation.

The first attempt on the field of austenitic piping materials characterization has been to obtain a series of slice cuts 10 mm thick on different positions and with different orientations from a section of primary piping weld and base metal (see fig. 12).

(1) Instituto Nacional de Técnica Aeroespacial Esteban Tarradas Ref. Dr. F. Ramírez, Mr. F. Soler and C. Valdecantos.

We initially asked for ultrasonic attenuation measurements from 1 to 5 MHz frequency range, and velocity measurements and noise spectrum analysis on the different specimen sections. A discouraging variability without appearance of possible correlation was initially found. See fig. 8 and 11. Afterwords the INTA laboratory has been working on the following approach technique:

Using a broad band transducer, the signal of the water-steel incident echo signal is p otted by a XY devi e showing a continuous amplitude versus frequency shape. By gating on the oscilloscope the water-steel interface signal together with the first backwall signal the resulting amplitude-frecuency curve is shape modulated and plotted on the same frequency or Y scale. By parallel moving of the specimen a modulated amplitude frequencv curve is obtained on each different point (see fig. 10), with a small manually induced X displacement for presentation.

From these curves the following information is obtained and easily analized.

a) The local velocity is easily obtained by measuring the distance between e.g. 10 modulation peaks on the Y scale. Variations of velocity are made evident by comparing modulation peak relative position on the different curves.

b) The attenuation is shown simultaneously on all the available frequency ranges by the modulation intensity.

Attenuation and velocity comparison between different points with no significant position differences show up the dispersion of these values while differences found consistently between different slice orientations, or in depth or weld different positions, will be used for knowledge of ultrasonic performance.

Presently, a lot of 30 specimens obtained for CF8 cast and welded spools of 304 type forged materials are in course of ultrasonic velocity and attenuation characterization.

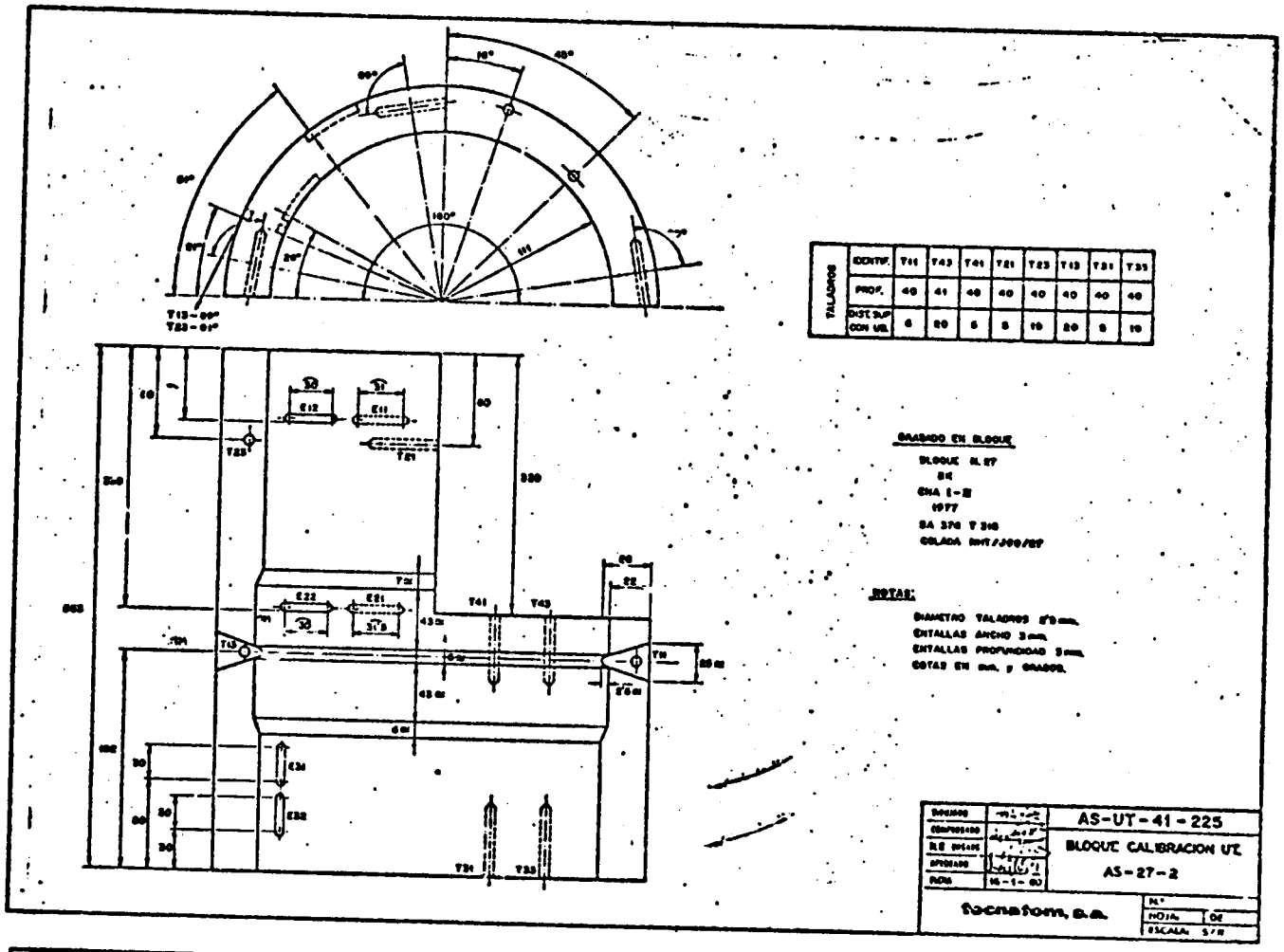
7. CONCLUSION

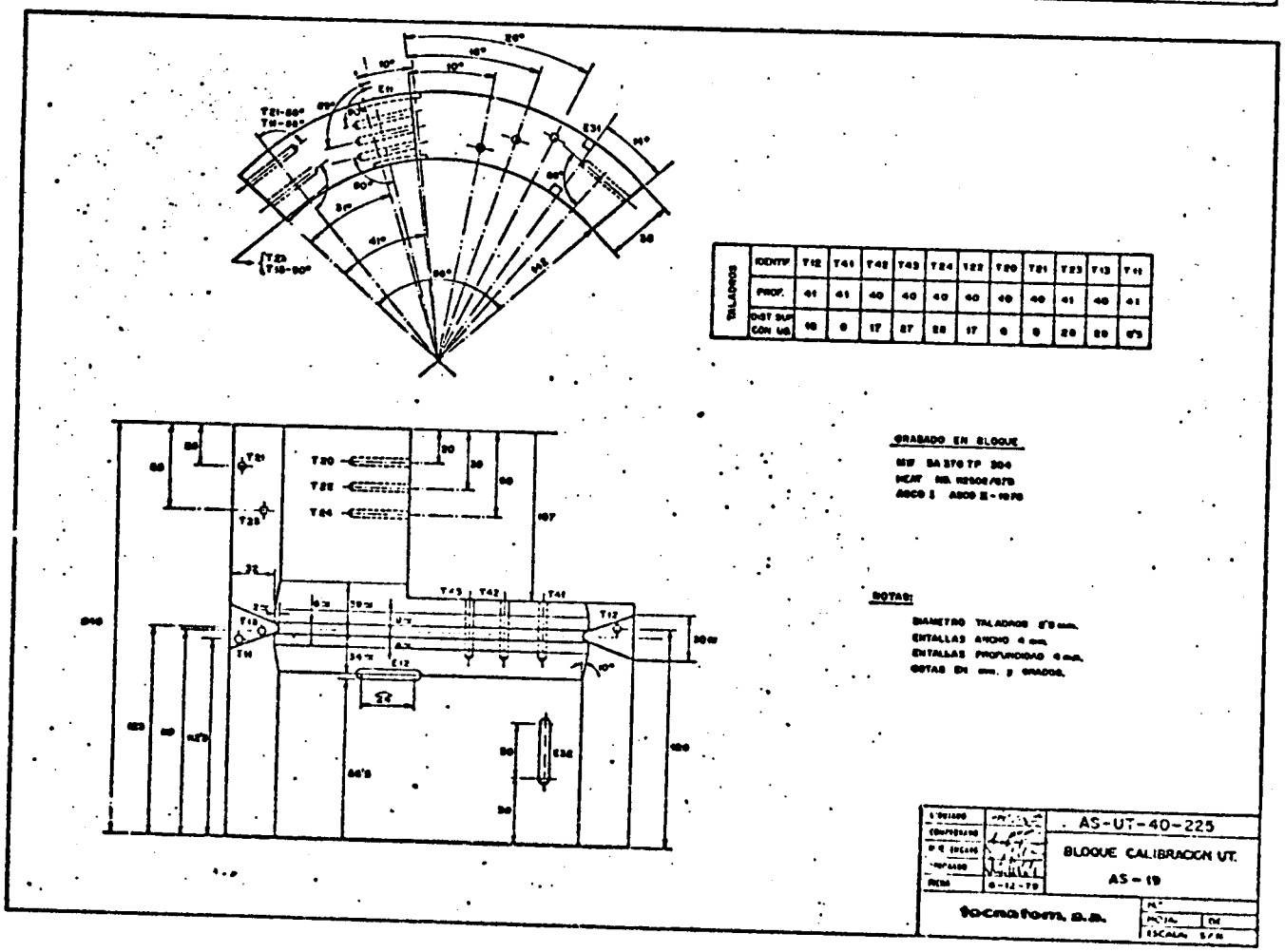
Ultrasonic Inservice Inspection of a Nuclear Power Plants generally required and practiced, present a series of different problems emerging from the simple fact that ultrasonic beams suffer directional attenuation and deviations when used through austenitic stainless steels, with intensity depending on both the base material and the weld structure themselves and their non-uniformity.

Cast as well as extruded or forged pipe when sectioned for metalographic study, in addition to dispersion values, show variations on grain size on through thickness direction due to the fabrication or heat treatment processes.

Our performance, during the past four years, in ultrasonic field inspection of austenitic stainless steels, from the point of view of an inspection company user of commercially available equipments, as well as from the point of view of an utility related group, intending to assure by ISI the control of defects significant for the plant integrity, and, at the same time assuring the efficiency of man power and equipment investments for ISI, sho up an evident unclear balance. Rate on progress observed even appreciable and high praised, is as a whole not paying the considerable effort observed on this field at international level.

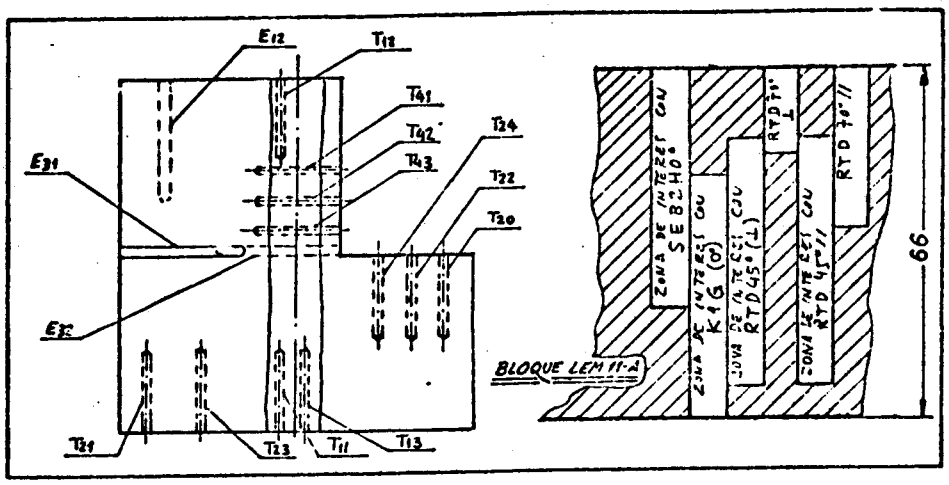
Even when the same rate of effort is required until assuring adecuate levels of confidence on ISI of our presently pressure resisting or just installed austenitic welded materials it seems at this point that there is a evident need to require from pipe fabrication processes, specially heat treatment specification tolerances, as well as welding processes the prevention of the observed anomalies produced on the ultrasonic beams when actually crossing such materials. Ultrasonic inspectability more than a challenge to ultrasonic specialist must be a part of nuclear (procurement) fabrication or welding specifications. In nuclear industry ISI accesibility has been strongly considered as part of the quality of the plant some years ago, and in the same way as ultrasonics is clearly the ISI most extended technique, the ultrasonic "visibility" should be considered at least on the welding procedure qualifications acceptance, until the ultrasonic inspectability conditions can be objectively translated into manufacturing parameters.





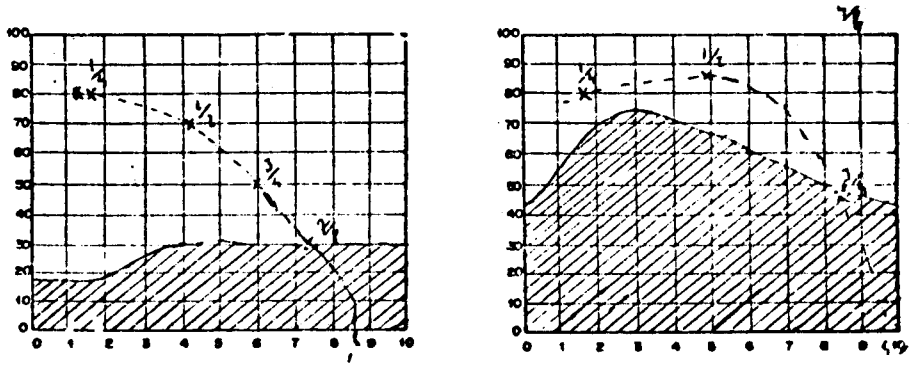
tecnatom Fig. 1. Welded mock-ups used as ultrasonic calibration blocks

Procedimiento UT-64 Rev. 2 Bloque LEM-11A Material SA-351 CF8A Ø / espesor 36" / 66mm



TIPO DE EXPLORACION	PALPADOR	CAMPO mm.	REFL. REF.	CORRECCION GANANCIA	FORMA CAD	REVISION 0	1	2
PREVIA	K1G	100	ECO DE FONDO	——	——	X		
0°	SEB2H0°	100	TALADRO T12 AL 80%	— —	T20; T22; T23	X		
	K1G	100	TALADRO T22 AL 80%	——	T22; T23; T24	X		
PERPENDICULAR	RTD45SEL1	100	TALADRO T21 AL 80%	——	T21; T22; T23; T24	X		
	RTD70SEL2	50	TALADRO T20 AL 80%	——	T20; T21	X		
PARALELO	RTD45SEL1	100	TALADRO T42 AL 80%	——	T41; T42; T43	X		
	RTD70SEL2	100	TALADRO T41 AL 80%	——	T41; T42	X		

tecnatom Fig. 2. Scan plan for CF8 Primary Piping Inspection



2. 45°/Frec. 1MHz Ganancia db 52
Dimensiones 2(12x22) Campo mm 100
Nº Serie 38-091 Cable 2PK10

Refl	V/8	Distancia mm	Recorrido mm	Altura div
1/1	7/8	17	16	90
1/2	5/8	28	42	30
1/3	3/8	41	59	50
2/1				

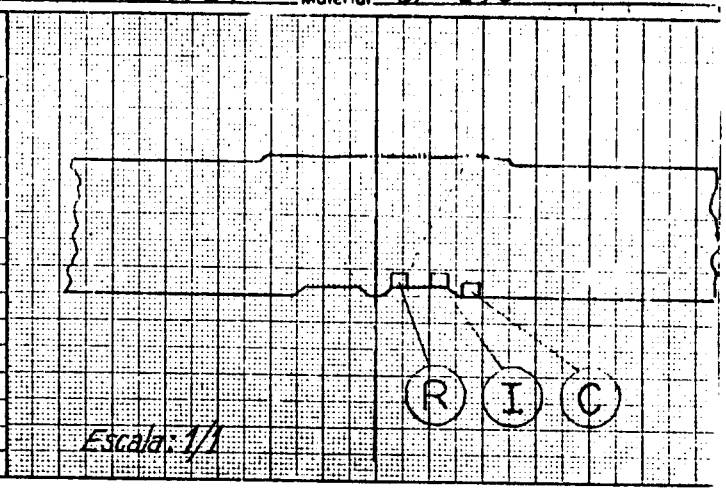
52º
Angulo / Frec. 2MHz Ganancia db 54
Dimensiones 2(12x25) Campo mm 100
NºSerie 38-122 Cable 2PK10

Refl	V/8	Distancia mm	Recorrido mm	Altura div
1/1	7/8	13	16	90
1/2	5/8	35	49	85
1/3	3/8			

tecnatom Fig. 3. Relation CAD to spurious echos with both new probe of 1 MHz, 45º (left) and former probe of 2 MHz, 52º (rigth)

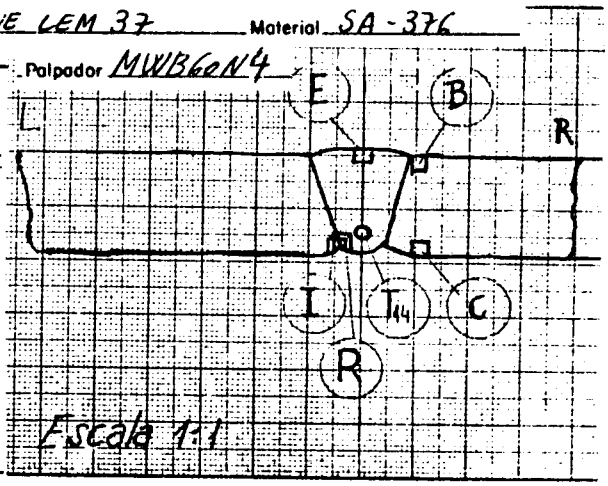
Soldadura BLOQUE LEM 37 Material SA-376

Max. % PANTALLA	Distancia en pantalla	Posición palpador mm	REFLECTOR	
70	54	51	R	B.M
80	49	57	I	B.M
60	65	79	C	B.M
55	60	53	R	T.W.
80	58	44	I	T.W.
20	65	43	C	T.W
10	57	46	RAIZ	
120	20	18	T_{21}	
50	55	39	T_{23}	
				± 60%



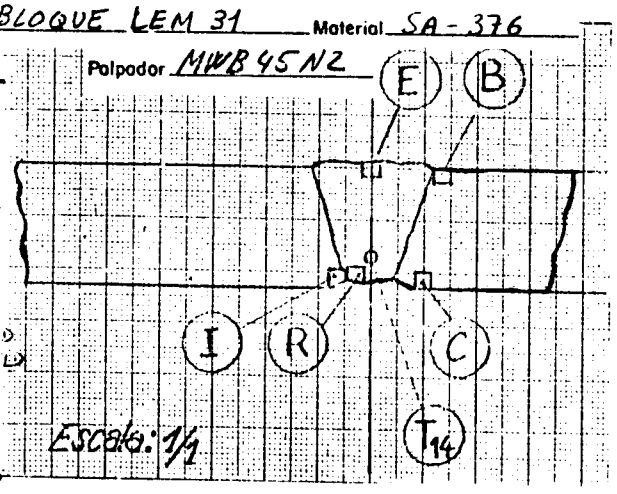
Max. C.A.D. %	Distancia en pantalla	Posición palpador mm	REFLECTOR	Soldadura BLOQUE LEM 37 Material SA-376
75	33	42	C	B.M.
180	35	24	R	B.M.
75	33	32	I	B.M.
60	35	38	GEO.	FROM RIGHT SIDE
70	32	32	GEO.	FROM LEFT SIDE
50	64	67	B	B.M.
25	66	56	E	FROM LEFT SIDE
100	22	21	T_{14}	
9	63	52	E	FROM RIGTH
0	-	-	R	THROUGH WELD
0	-	-	I	THROUGH WELD
0	-	-	C	THROUGH WELD

Palpador MWB60N4

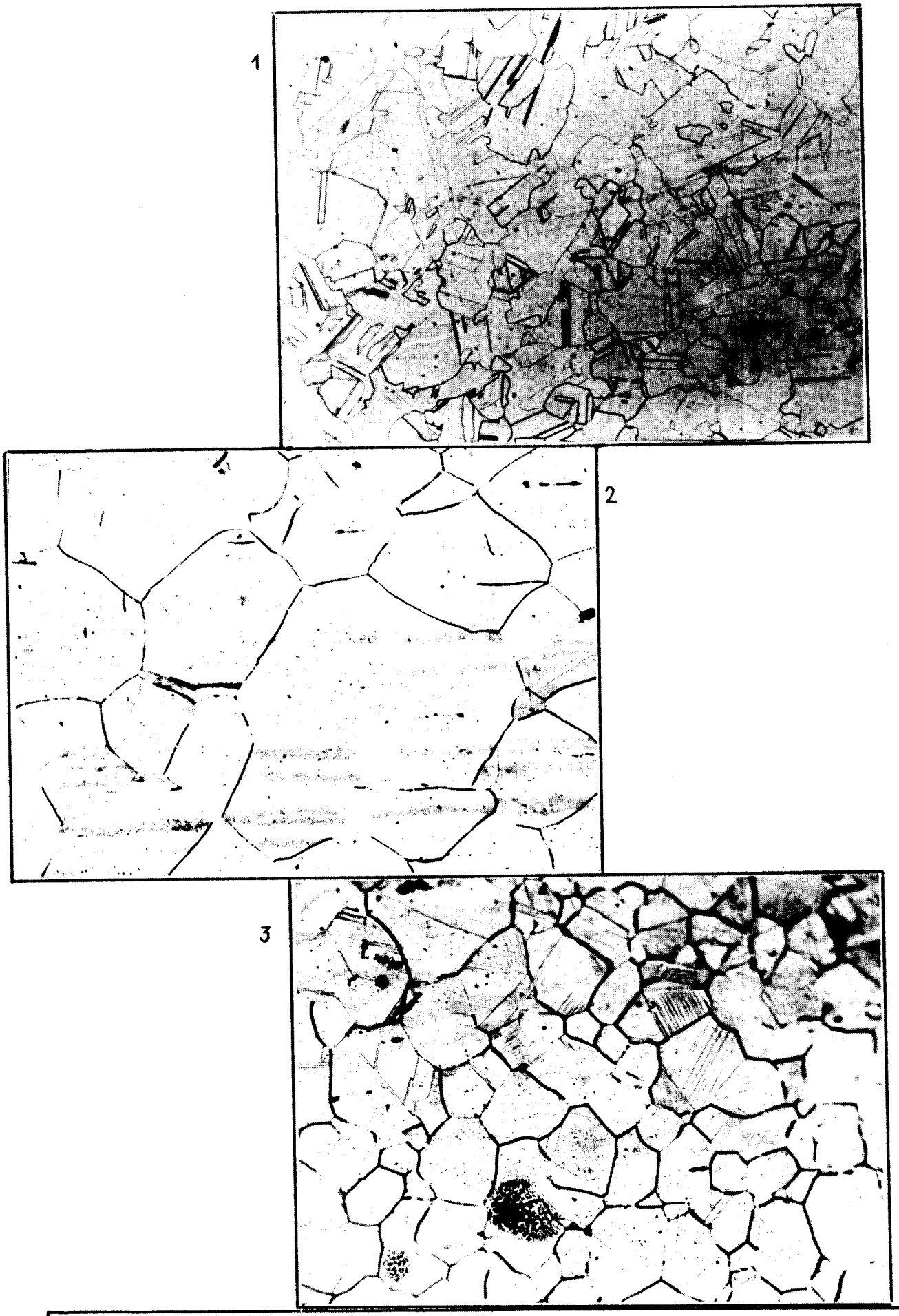


Max. C.A.D. %	Distancia en pantalla	Posición palpador mm	REFLECTOR	Soldadura BLOQUE LEM 31 Material SA-376
110	28	26	C	FROM B.M.
70	30	25	I	FROM B.M.
45	31	25	R	FROM B.M.
90	58	43	B	FROM B.M.
45	35	61	E	FROM B.M.
100	44	83	[illegible]	
0	-	-	I	THROUGH WELD
0	-	-	C	THROUGH WELD
0	-	-	R	
45°	APPEARING	AS 3		

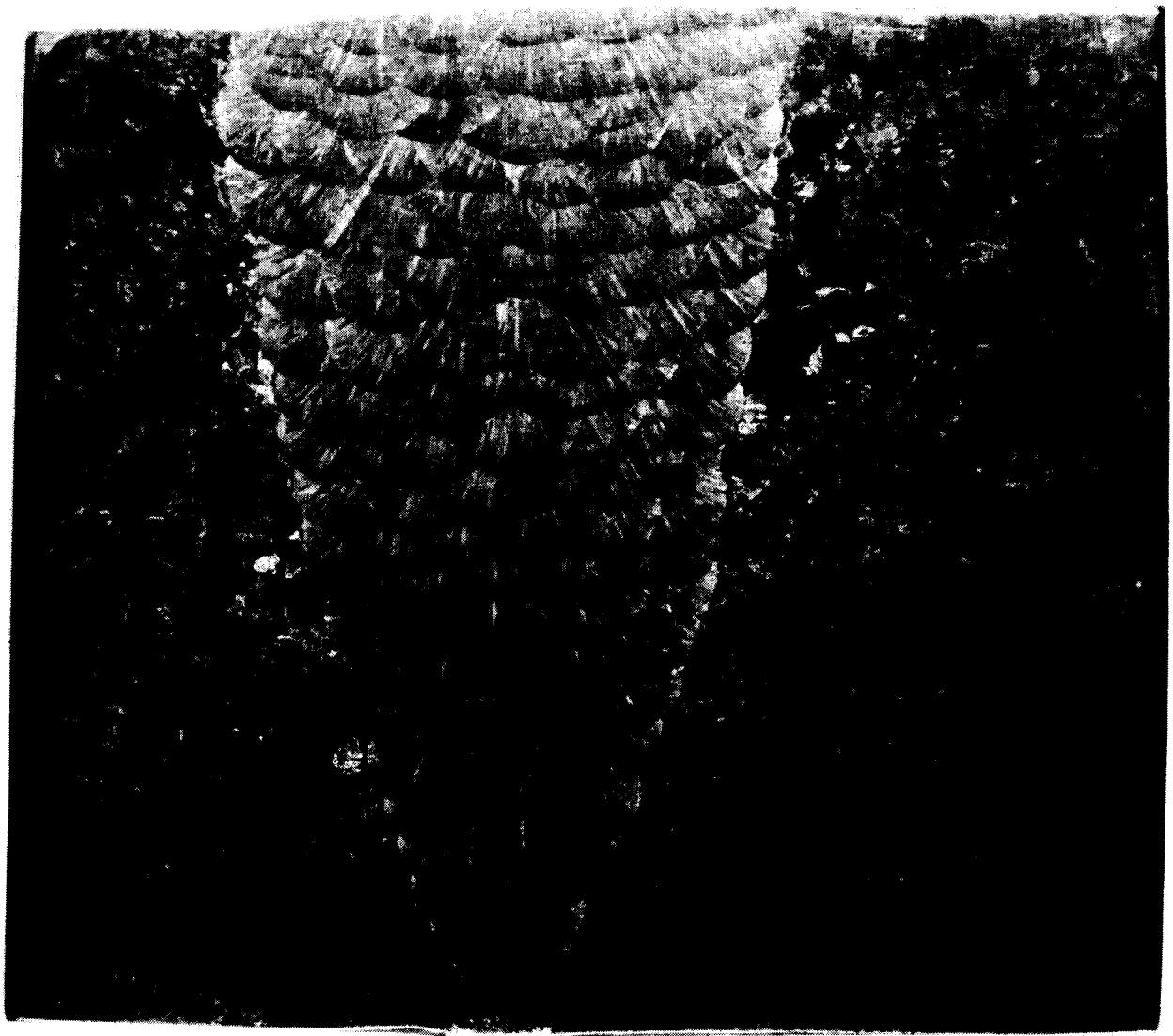
Palpador MWB45N2



tecnatom Fig. 4. Mock-up schemes used for ascertaining through weld detectability



tecnatom Fig. 5. Three austenitic structures with different UT performance all corresponding to SA-376 304. Structures 2 and 3 are from same specimen but at different thickness posit.



SA.351

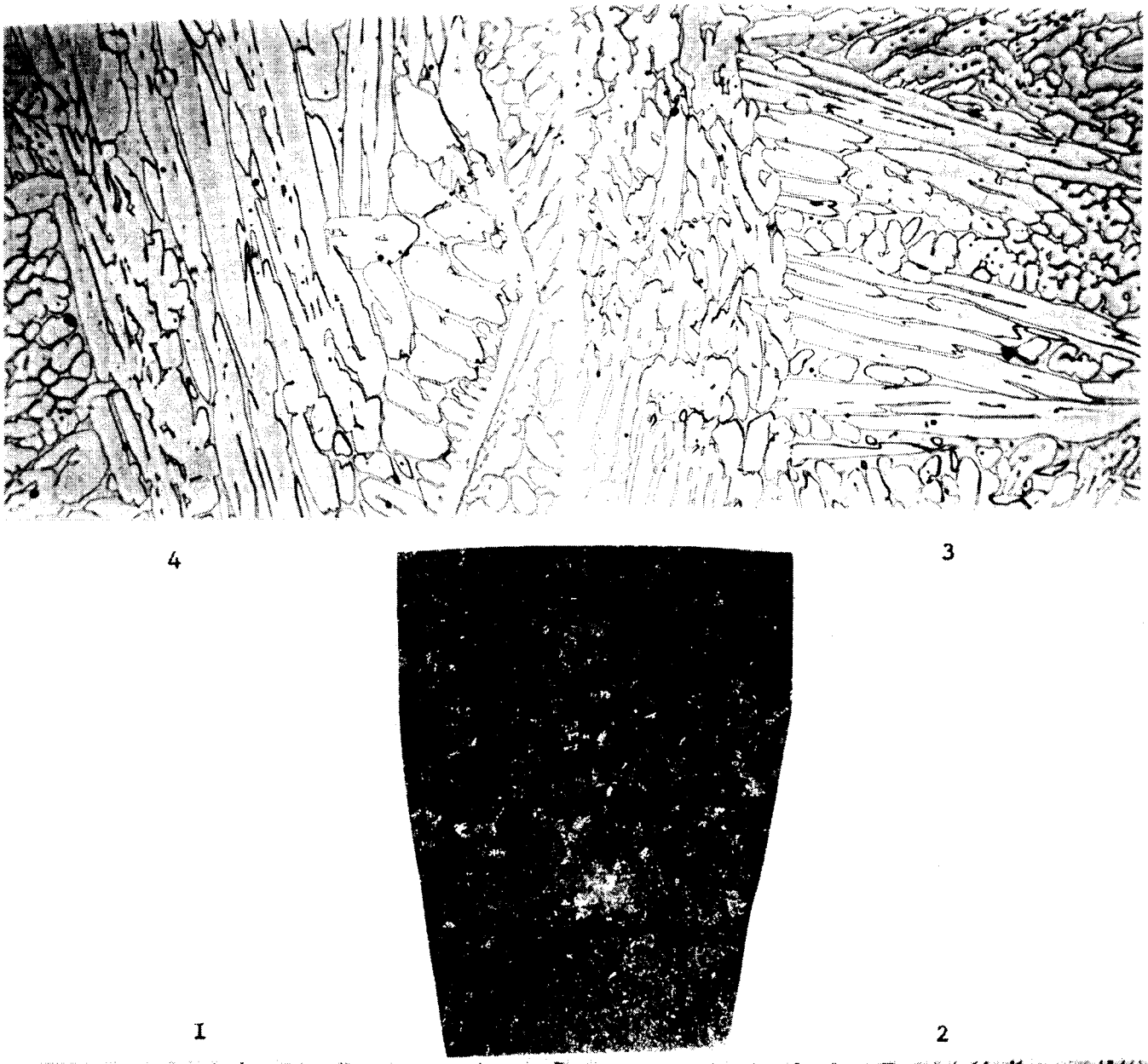


SA.351

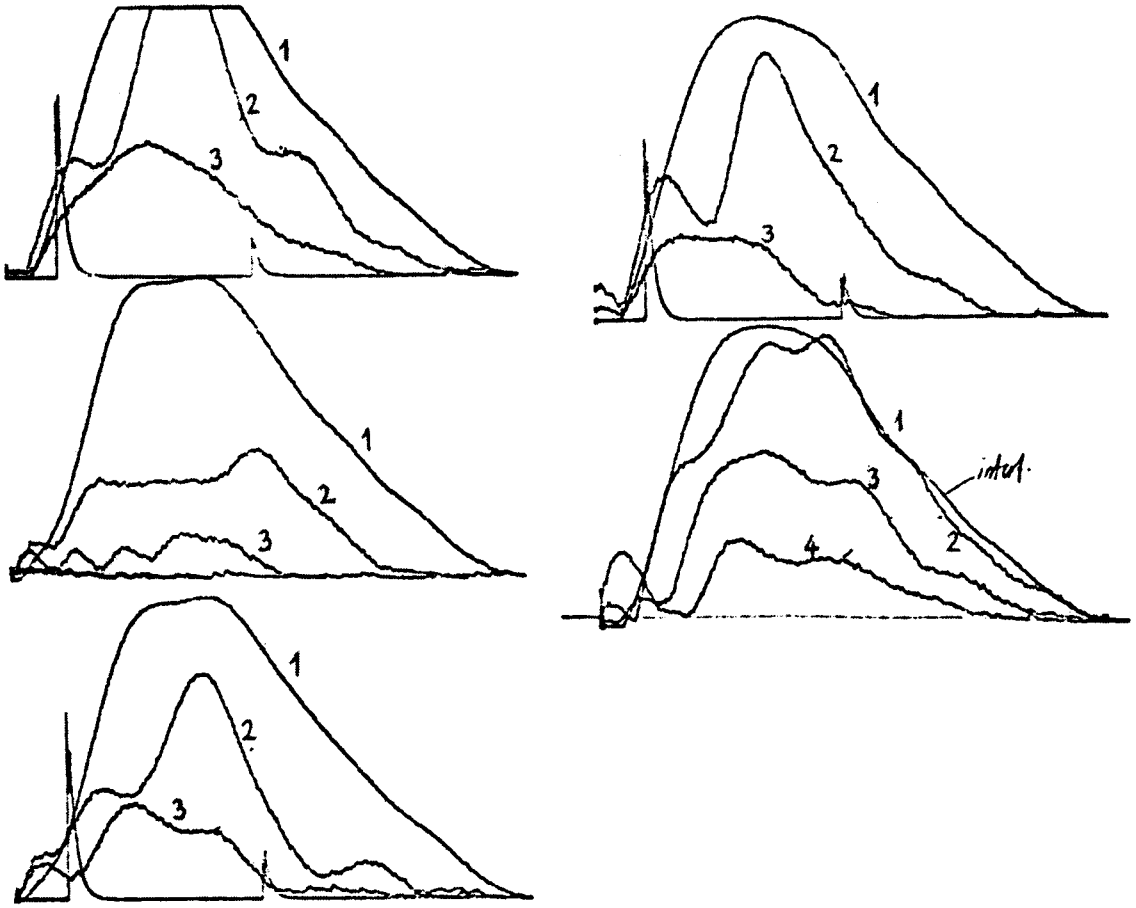


SA.376

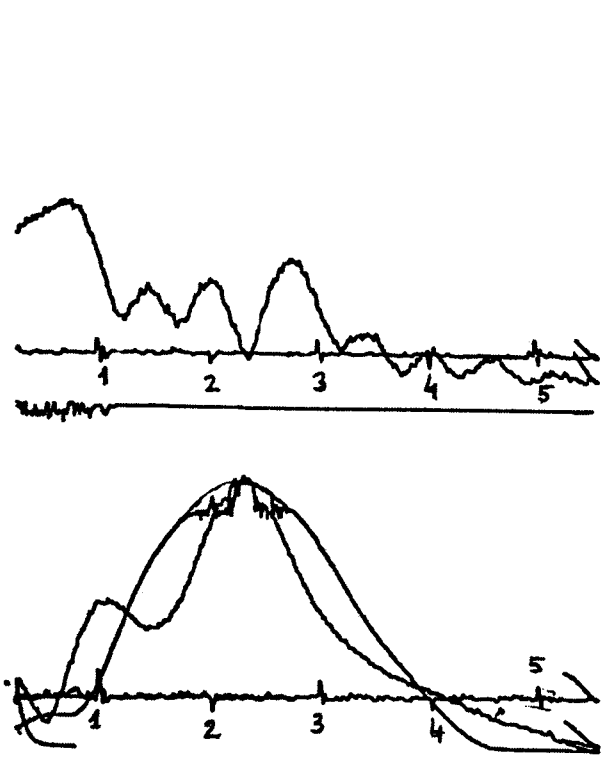
tecnatom Fig. 6. Macrographs of SA351 CF8 and SA376 304 structures, both with different in depth grain size.

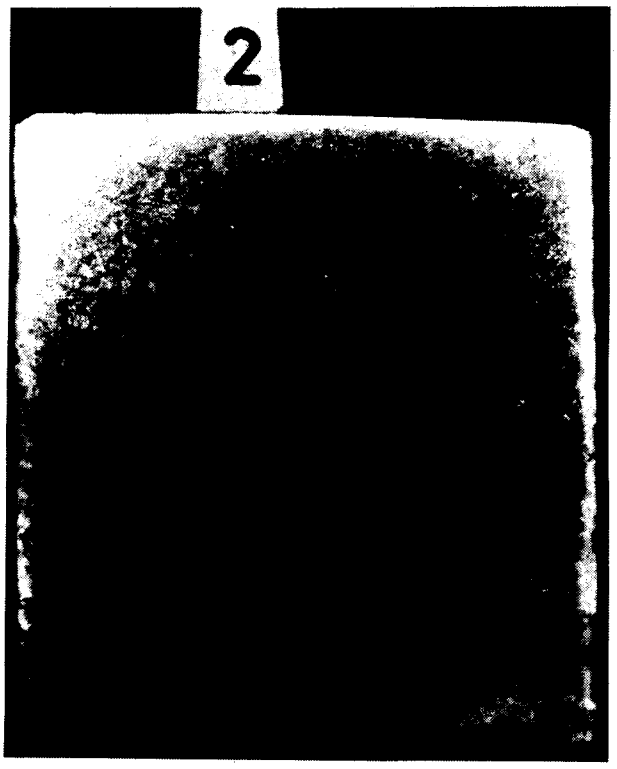


tecnatom Fig. 7. Structure at four different thickness positions from a SA351 CF8 sample (x 60)

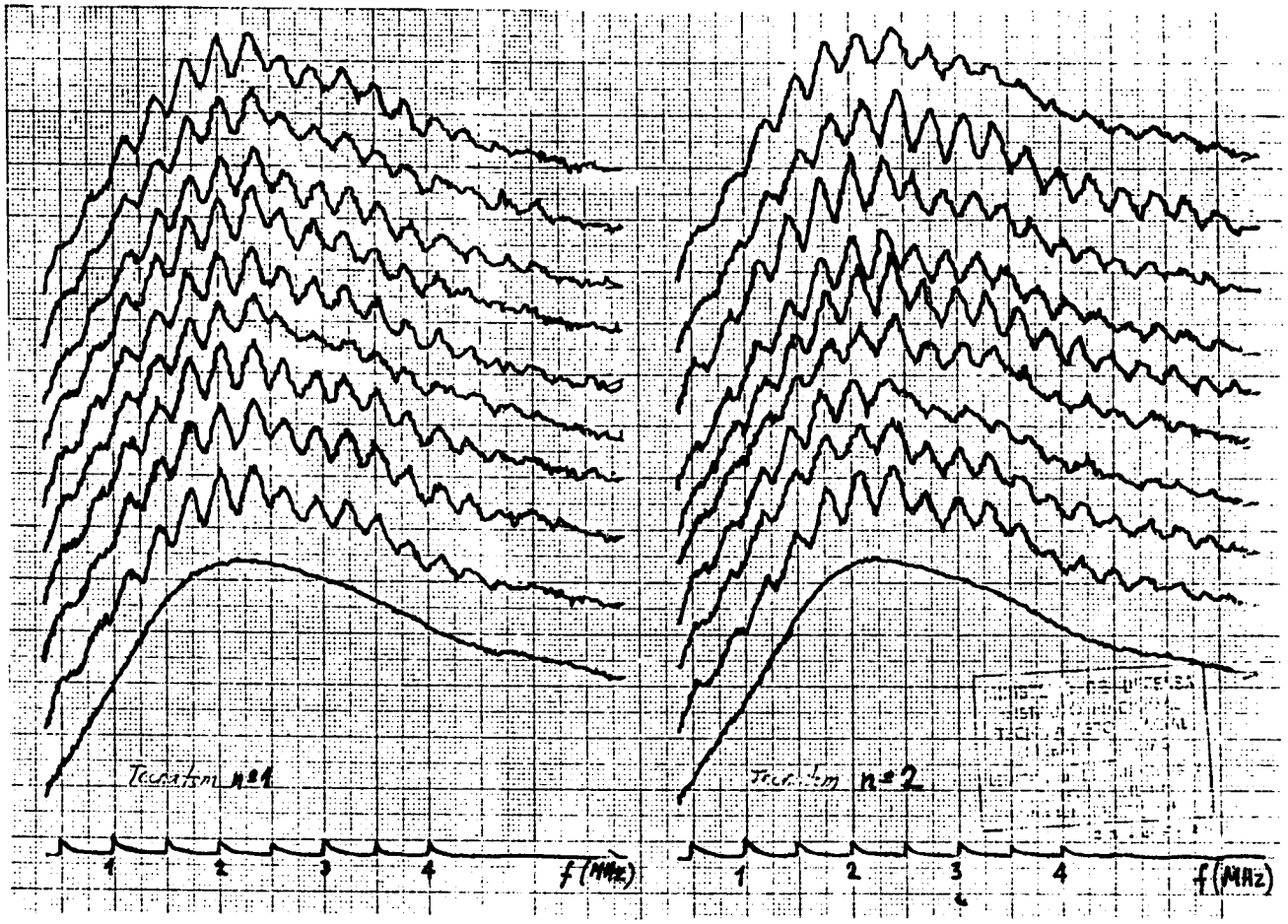


tecnatom Fig. 8. Spectrum from: 1. interface 2.1st backwall echo 3.2nd backwall echo 4.3rd backwall echo in 5 different places at the same slice cut.

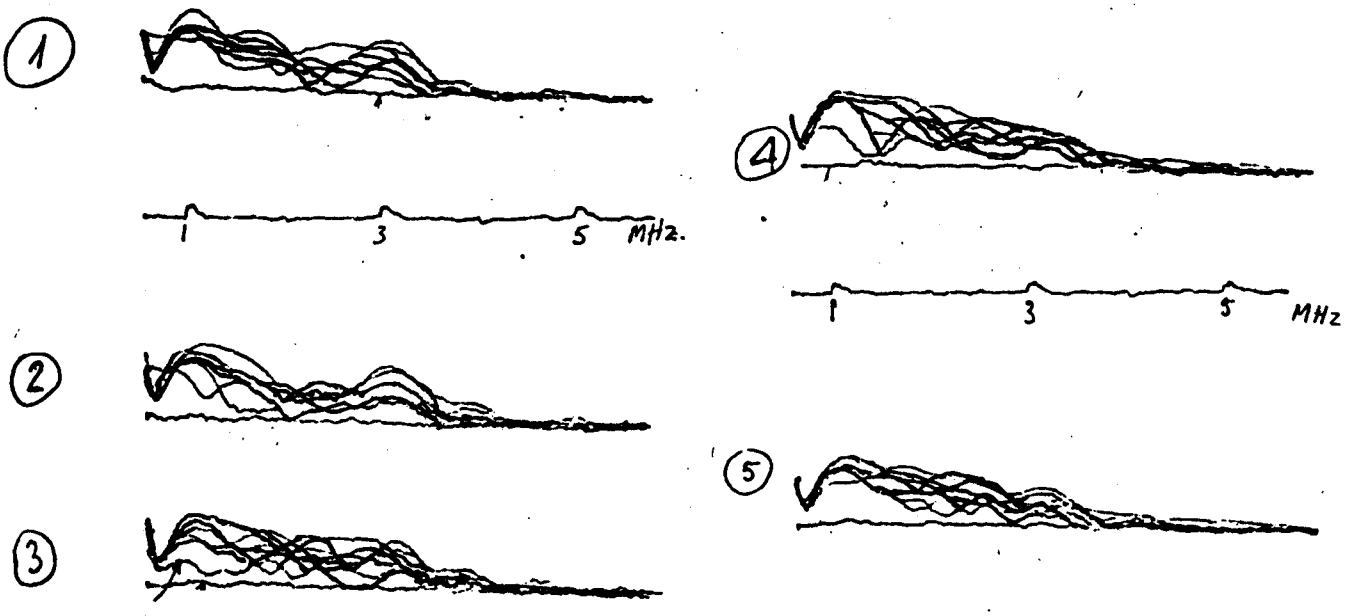




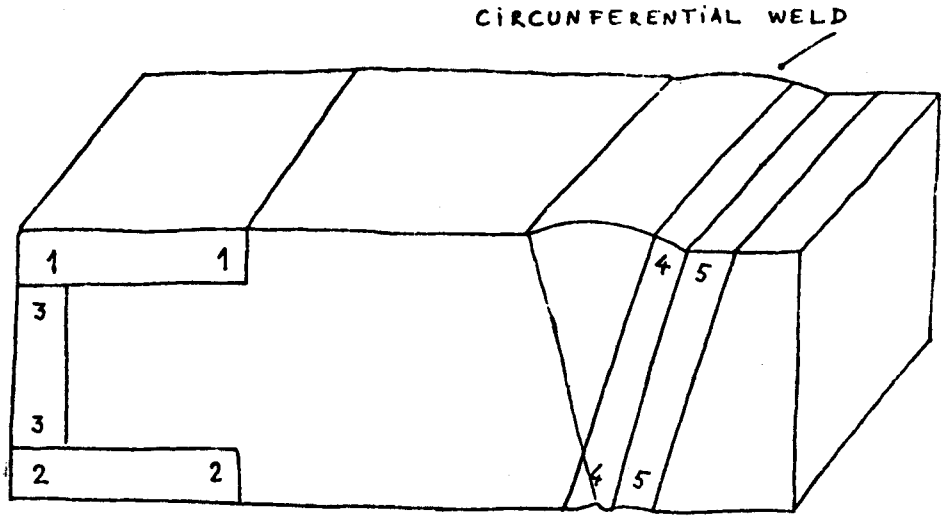
tecnatom Fig. 9. Noise frequency distribution on SA351 CF8 material sample



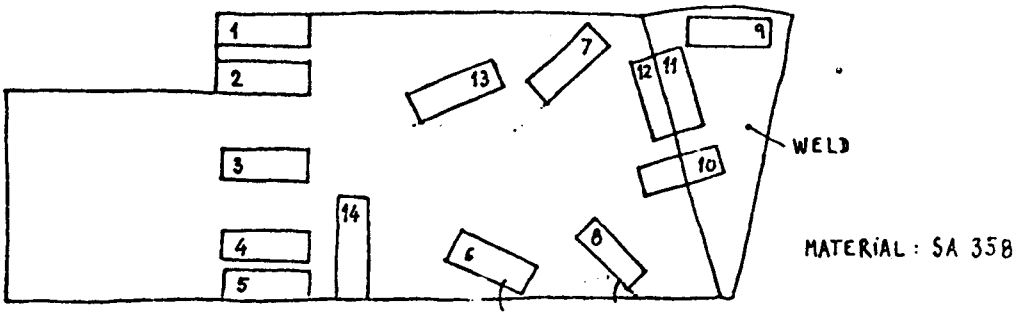
tecnatom Fig. 10. Frequency response from initial pulse to backwall echo in order to measure local velocity and ascertaining attenuation differences.

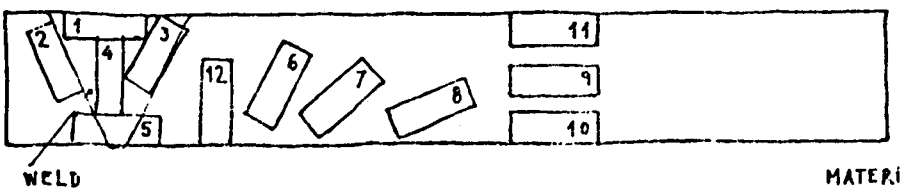


tecnatom Fig. 11. Noise frequency spectrum at different position on 5 different orientated sample of welded SA351 CF8.



PRIMARY SLICE CUTS





SIZE OF SLICE CUT: 15 × 15 × 6

tecnatom Fig. 12. Drawings of slice cuts to characterization of both ultrasonic velocity and attenuation.

Detection of underclad defects by non-destructive testing

J.P. LAUNAY, J.C. LECOMTE, P. MARTIN, A. THOMAS
Framatome, France

ABSTRACT

Following discovery of underclad defects in various reactor vessel nozzles and steam generator tube sheets, FRAMATOME undertook a lengthy test program to perfect and qualify non destructive test methods for detecting and characterizing this type of detect.

Methods were studied to satisfy examination needs of both shop and site. The following situations were analysed :

- Reactor Vessel Nozzles :
  - . Manual UT (shop and site)
  - . Automatic UT (shop and site)
- Tube sheets
  - . Manuel UT before sheet drilling (shop)
  - . Automatic Eddy Current Testing after tubing (shop and site)

The technique chosen for ultrasonic examination uses 2 MHz longitudinal waves with about 70° refraction angle in the cladding thickness. The probes used are of the "Double Probe" or "focalised single probe" types. This method can detect defects with surface larger than or equal to 2 mm2. Examination of tube sheet by Eddy Current is performed using a probe placed inside the tubes. In this case, only open defects in drilled tube sheet holes can be detected.

The feasibility of detection using both methods has been demonstrated on artificial representative defects and qualification has been obtained through numerous tests on natural defects.

All methods and resources presently available to FRAMATOME allow an excellent detection rate for underclad defects.

1 - INTRODUCTION -

Discovery of underclad cold cracking phenomenom in steam generator tube sheets (fig. 1) and under the cladding of reactor vessel nozzles (fig.2) led FRAMATOME to study, develop and qualify non destructive examination methods capable of detecting and charecterizing these types of defects. To reach this objective, FRAMATOME started by studying the possibilities of various NDT methods, after which the following two techniques were retained :

a) ultrasonic testing for examination of tube sheet before drilling and of reactor vessel nozzles

b) Eddy current testing by internal probe for examination of drilled tube sheets with tubes installed.

2 - CHARACTERISTICS OF DEFECTS TO BE DETECTED -

The type of defects to be detected originated from the same source for both tube sheets and reactor vessel nozzles : a cold cracking phenomenom was involved in both cases.

The tube sheets have an inconel cladding with an average thickness of 8 mm, and the base metal was up of SA 508 cl. 3 type steel.

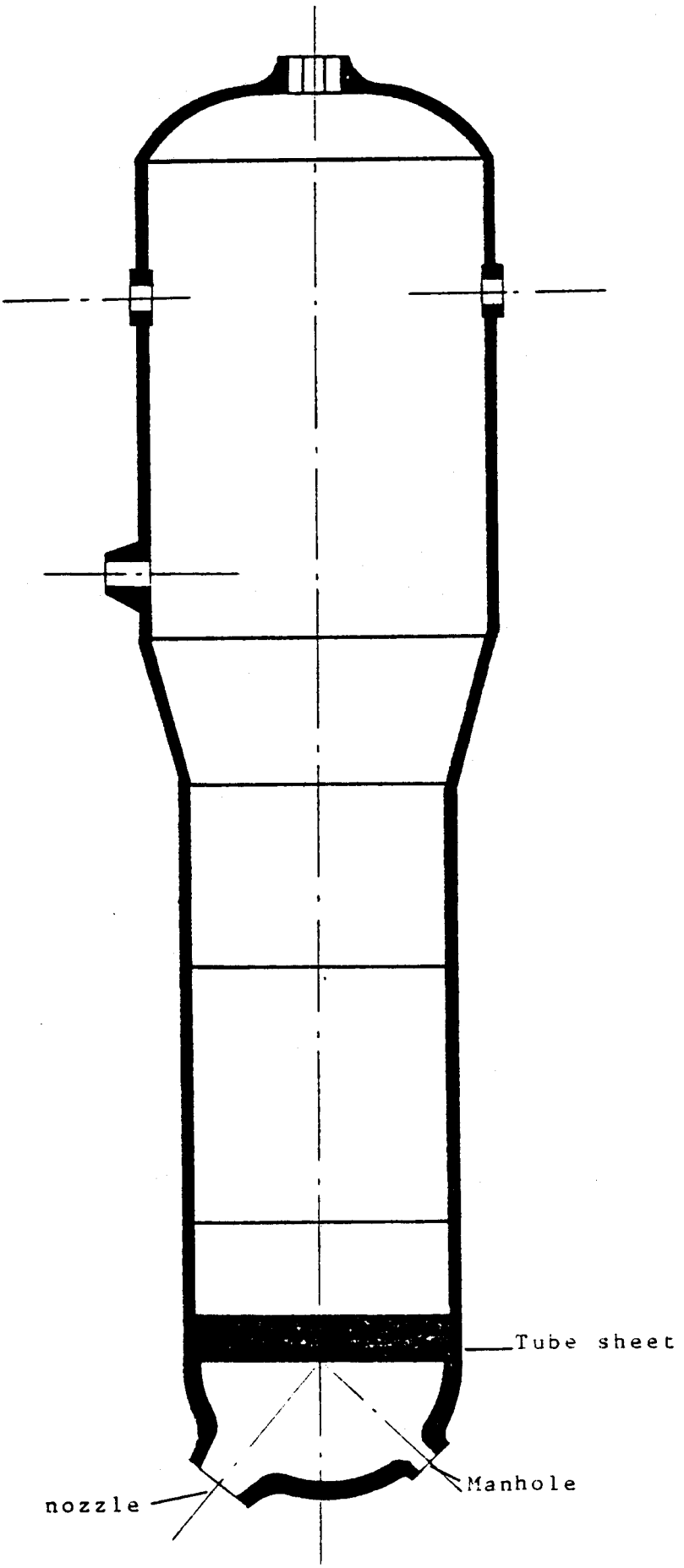


FIG. 1 - STEAM GENERATOR

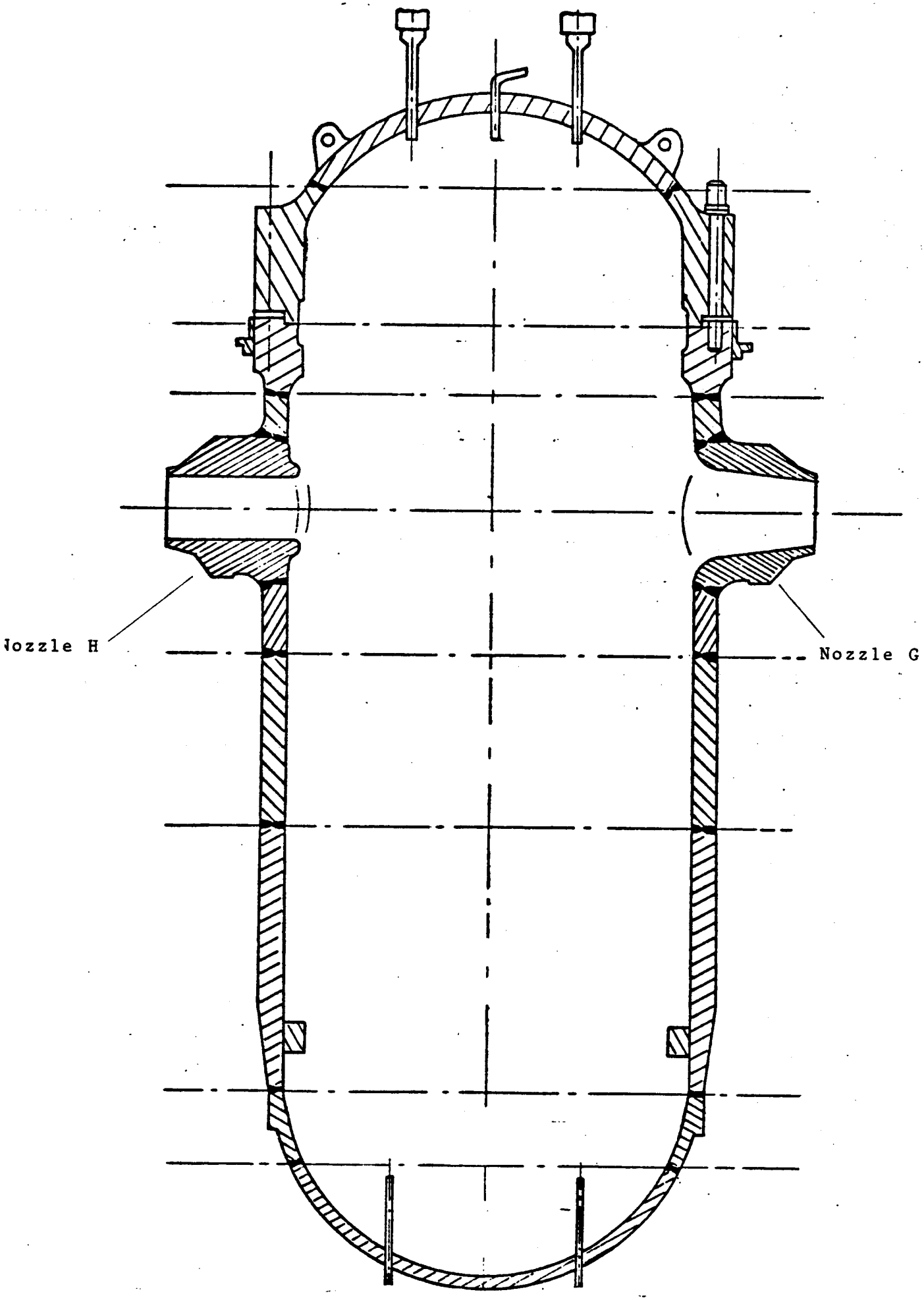


FIG 2 - REACTOR VESSEL

The reactor vessel nozzles have a stainless steel cladding which is also about 8 mm thick. The base metal was also made up of SA 508 cl. 3 type steel.

In both cases the cracks are situated in the base metal and stop at the interface between the base metal and cladding. They are perpendicular to the cladding - base metal interface.

3 - ULTRASONIC INSPECTION METHODS -

The ultrasonic method was chosen for the detection of underclad cracking :

a) in non drilled tube sheets

b) in reactor vessel nozzles.

3-1. Principles of method -

Various tests were performed by FRAMATOME in cooperation with the French Atomic Energy Commission (CEA) and Electricite de FRANCE (EDF). These tests were performed on models and on parts containing artificial and actual defects. The tests were mainly concerned with the choice of refraction angle in steel, wave mode and the types of probes to be used. Following these tests FRAMATOME chose the ultrasonic method using inclined longitudinal waves at angle of about 70° in the base metal for detection of cracks. It should be noted that this method was advocated by various research organisations notably for reheat cracking.
FRAMATOME studied and adapted two test techniques based on the inclined longitudinal wave principle :

a manual inspection method with separate transmitter/receiver probes.
an automatic inspection method with underwater focalised probes (in cooperation with CEA)

3-2. Manual ultrasonic inspection -

Two SE type inclined longitudinal wave probes were used depending on the kind of surfaces to be tested :

- the first type of probe is used to inspect even or large radii curved surfaces
- the second type of probe is used to inspect small radii curved surfaces.

3-2-1. Probes used for inspection of even or large radii curved surfaces.

The probes used by FRAMATOME are BAM SE 70 L2 150 or SONATEST SE 2.25 Mhz (the latter attached to a plexiglass probe shoe inclined at an angle of 26°) of the transmitter receiver type.

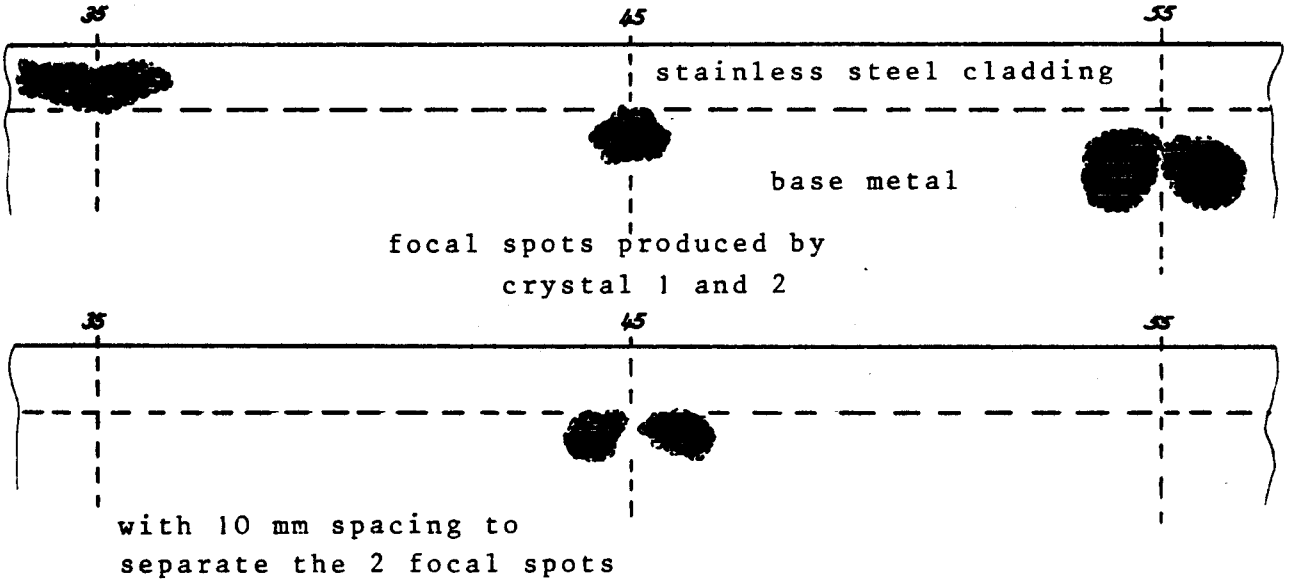
To compare the different probes used, FRAMATOME performed analysis of acoustic beam behaviour in stainless steel and base metal for both crystals in each probe. The results were recorded at -6, -12 and -18 dB. fig.3 shows beam charecteristics at -6 dB for both probes (BAM and SONATEST). Analysis of experimental results produced the following data :

- the refraction angle of both probes is identical : about 61° (fig.4)
- the crossing of the stainless steel - base metal interface did not appear to affect beam homogeneity
- for each probe isoenergetic curves generated by both crystals were very similar.
- for BAM probe :

  the beams crossed each other at a depth of about 10 mm. At about this depth each beams' dimensions for - 6 dB were smallest (limit of near field). Therefore, it is at this depth that the best detection sensitivity and signal to noise ratio is obtained ; this is confirmed by the curves given in fig.5

BAM Probe

Focal spots at - 6 dB



"Modified stainless steel"
SONATEST Probe -

Focal spots at - 6 dB

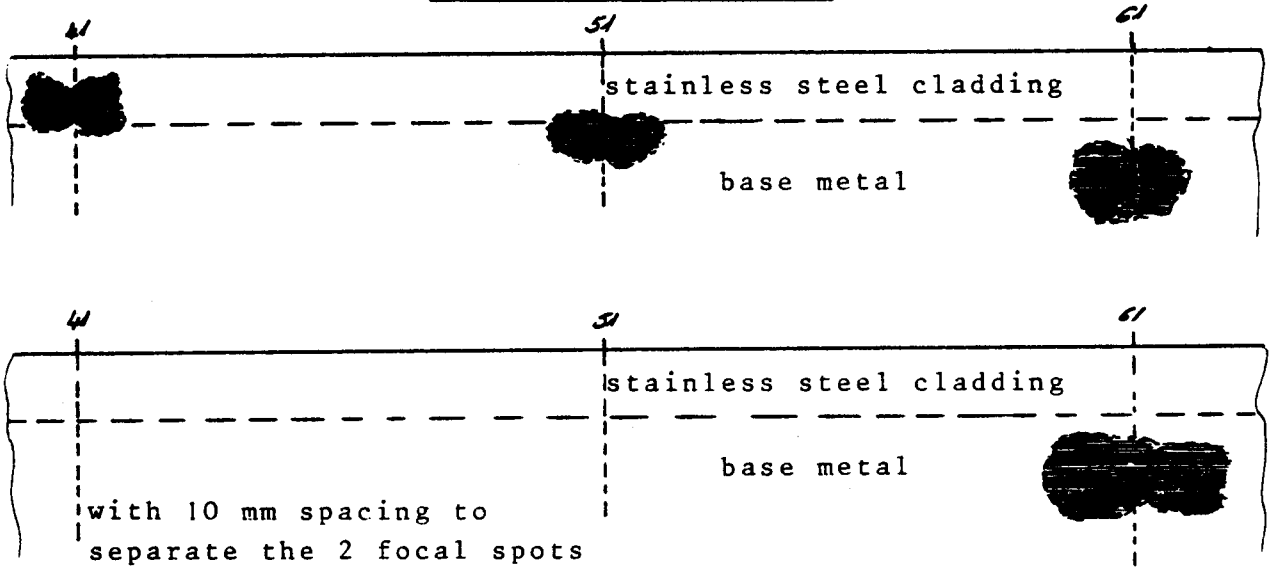


FIG. 3 - FOCAL SPOTS

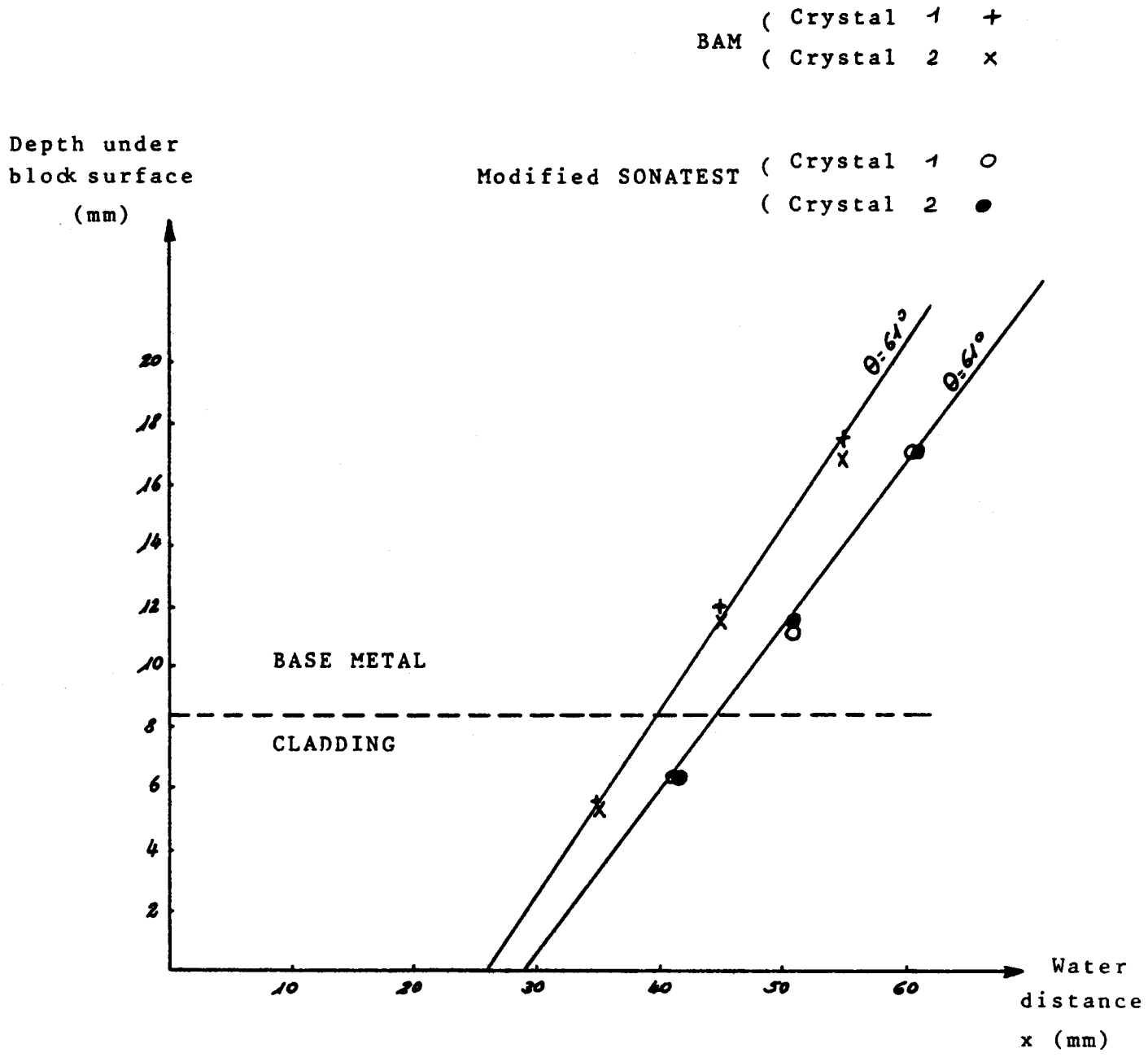
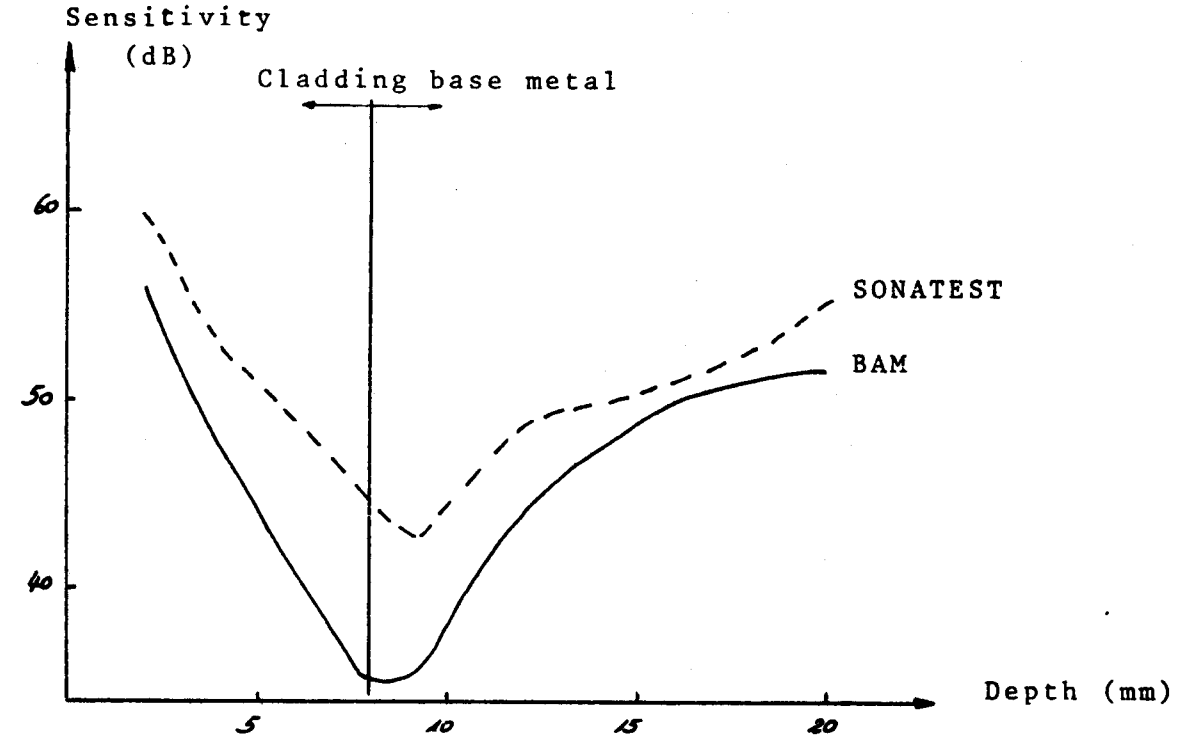


FIG. 4 - ANGLES OF REFRACTION



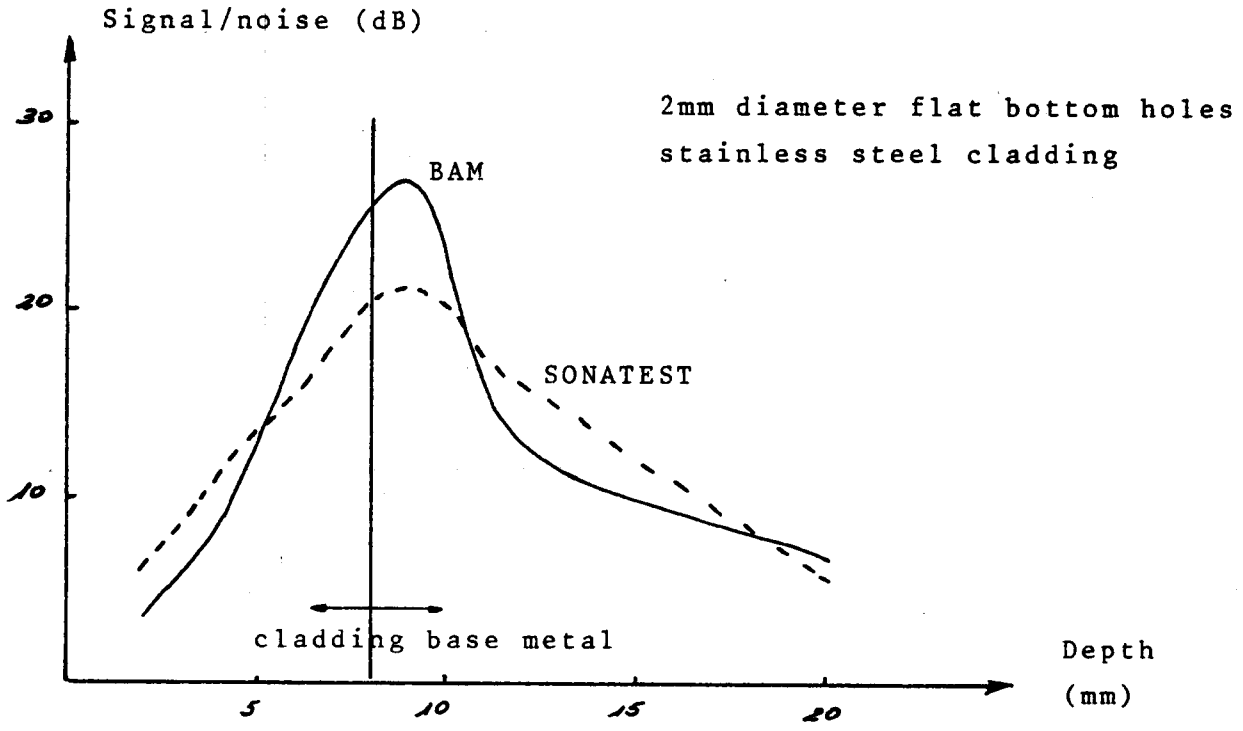


FIG. 5 - GRAPHS : Signal to noise ratio
Sensitivity

However beyond this 10 mm depth zone, the beams rapidly separate and this becomes even more marked the deeper one goes.
Therefore, outside this zone, detection sensibility and signal to noise ratio strongly decreases. This is confirmed by the curves given in fig. 5.

- For SONATEST probe "modified stainless steel".

The beam axes crossed each other at a depth of 16 mm. On the other hand the beams emitted by each half - crystal started to converge at a depth of less than 5 mm and the minimum dimensions for - 6 dB for each beam is located at a depth of about 6 mm. Optimal detection sensitivity level and signal to noise ratio is therefore situated at a depth of between 5 and 20 mm i-e at a depth where marked beam intersection occurs. This takes place at a depth of 10 mm which is confirmed by the curve given in fig.5

Below 10 mm, single beam dimensions further decrease as well as the intersection zone. Above 10 mm these parameters increase. This phenomenom leads in the case of the SONATEST "modified stainless steel probe" to a lesser reduction in detection sensitivity level and signal to noise ratio at a depth of about 10 mm than for the BAM probe.

If the BAM probe appears to be best suited for detection of defects located at the limit of the interface zone (because at this depth beams cross and dimensions are minimal whilst acoustic pressure is at a maximum) its range of use at depth is extremely reduced.
Therefore, a reflector with a large vertical measurement risks to have this latter dimension greatly underestimated by the BAM probe (if the -6 dB method is used).

If, however, none of the SONATEST "modified stainless steel" (sensitivity, beam dimensions, common surface) do not appear well suited for applications at the limit of the interface zone, on the other hand, large defects measured in the vertical direction should be evaluated much more accurately than with BAM probe.

This is because the depth of the detection range is much greater. It should be noted that the BAM probe is more sensitive for the detection of defects located at the limit of cladding area but that the SONATEST "modified stainless steel" probe performs more efficiently when identifying serious defects located at depth.
Therefore the two probes appear to have complementary functions.

3-2-2. Probes for inspections of small radii curved surfaces.

Probes developed for inspection of even or large radii curved surfaces are not suitable for small radii curved surfaces due to their flat crystals and the small size of shoes used. Therefore FRAMATOME was called upon to develop special probes and to demonstrate that test sensitivity for all radii of curves was equivalent.

The probe developed by FRAMATOME has the following charecteristics :

- contact probe with shaped shoe
- diameter crystal : 30 mm half cut
- dome shaped crystal
- crystal material : PZT
- frequency : 2MHZ
- type of waves : longitudinal
- separate transmitter and receiver.

A beam analysis (fig.6) shows that the FRAMATOME probe has almost the same characteristics as BAM'S :

- the refracted angle in the block : 66° (BAM : 61°) (fig.7)
- depth of beam convergence : 9,5 mm (BAM : 10 mm)

With a more detailed approach it can be seen that minimum dimensions at - 6 dB for each beam are located at a depth of 3 mm but these beams do not cross.

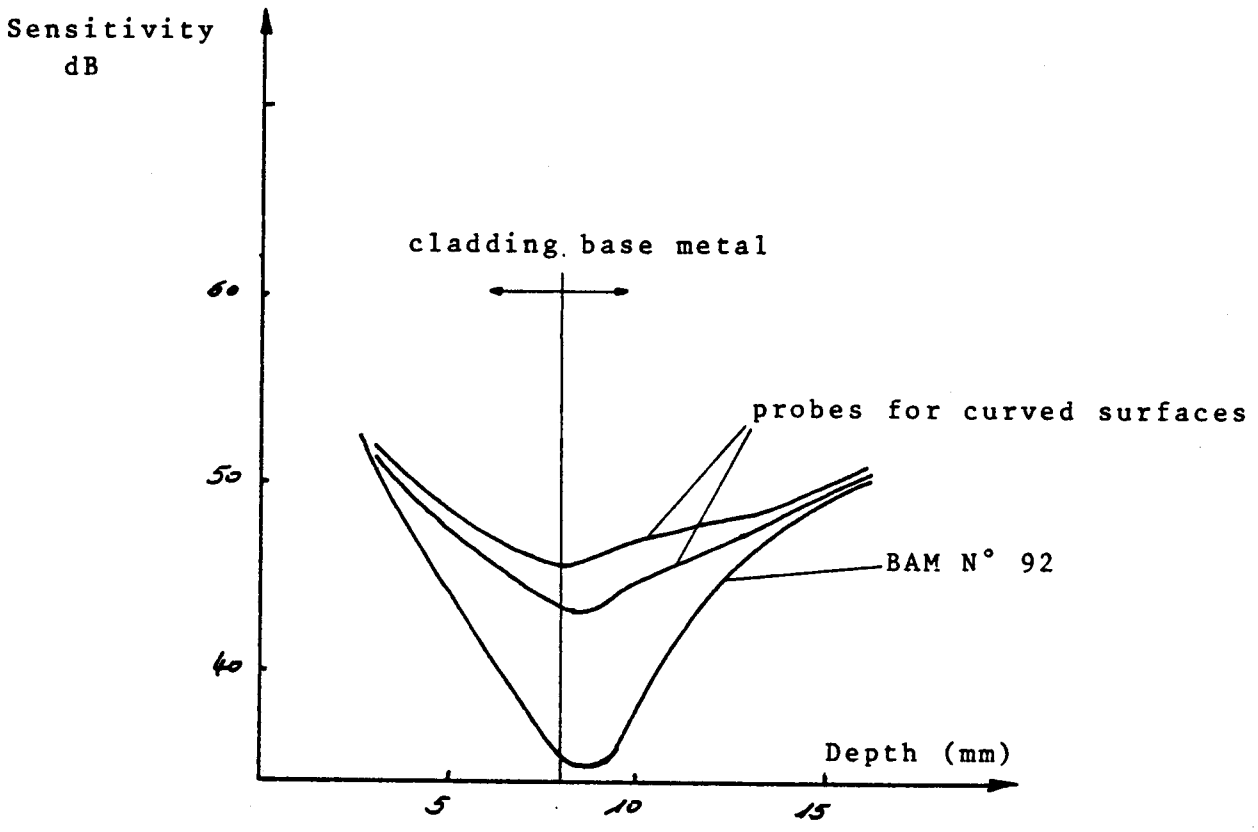
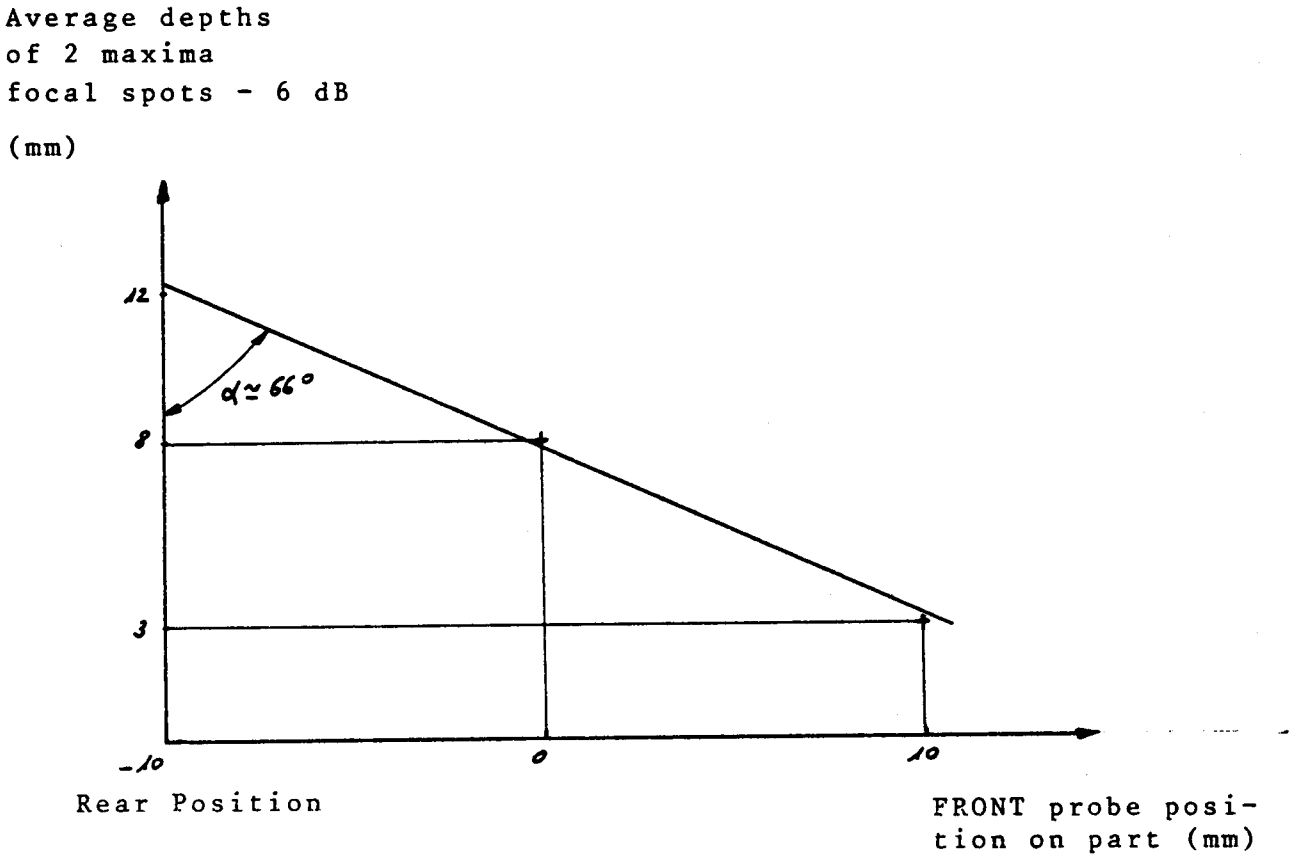


FIG. 6 - COMPARISON BETWEEN PROBES USED FOR :
- 1) Small radius curved surfaces
2) Even and large radius surfaces

==========



The refraction angle in part is 66°

FIG. 7 - REFRACTION ANGLE IN PART

However, a marked beam intersection can be observed at a depth of 8 mm. At this depth detection sensitivity should be at its most efficient and this is confirmed by the curves given in fig.6.

To conclude, although the most efficient sensitivity level is not obtained at the depth where the beam dimensions are at their lowest point (BAM probe's characteristics), their dimensions are however lower tham BAM'S at a depth of 8 mm (fig.6).

The refraction angle is slightly larger than BAM'S and at a first sight is more efficient for detecting defects which are perpendicular to the scanning surface.

The inspection methods used on (1) even and large radii curved surfaces and on (2) small radii curved surfaces are identical except for the following two differences :

- the type of probe to be used
- the surface condition of the zone to be inspected and consequently the calibration block which is needed to set the sensitivity level for examination.

All other parameters are identical and may be applied to either of the two surface types. The type of probe which was specially developed to inspect small radii curved surfaces has characteristics which are comparable to or slightly more efficient than the Bam probe's.
In fact :

- at the same convergence depth the beam's measurements are smaller at -6 dB
- the loss of sensitivity around maximum sensitivity is less marked (fig.6). Therefore at a depth of 5 mm, sensitivity level is only 4.4. dB whereas with the Bam probe a comparable loss occurs at 10.8 dB.This gives greater range for detection at depth.

- the signal to noise ratio for holes located at a depth of between 4 to 12 mm is greater for 12 dB.

Calibration, which is performed using blocks representing the curves (radii - surface condition), ensures a severity level (detection - characterisation) comparable to that obtained when inspecting even or large radii curved surfaces.

3-2-3. Operation of manual inspection.

Inspection is performed in two parts :

part 1 : inspection with inclined longitudinal wave probe of the BAM or "modified SONATEST" types

part 2 : inspection using KRAUTKRAMER SEB 4 KF 8 type probe at right angles to the indications detected in part 1.

The setting of apparatus is performed on blocks which represent the part to be inspected and which contain flat bottomed 2 mm diameter holes.

The characterisation of indications into inclusion or non inclusion types is based on the comparison of responses obtained from the above two inspection operations.
The following are considered as being inclusions :

- all indications whose vertical measurements determined by the BAM probe are lower than or equal to the thickness of cladding as determined by the difference between bore radii before and after covering.
- all indications whose vertical measurements are greater than the thickness of cladding when a response, obtained at right angles to the defect with the SEB 4 KF 8 probe, is greater than 50 % for a vertical measurement equal to within 2 mm of that obtained with the BAM probe.
  In all other cases, indications are to be considered as being cracks.

3-2-4. Results obtained.

Inspection can only be performed using machined or ground surfaces having a roughness of 6.3 Ra

- when inspecting tube sheets the manual U.T. method which was developed allowed detection of cracks up to 0,7 mm deep and 5 mm long.
- when inspecting reactor vessel nozzles, the inspection method applied to the machined surface allowed stainless steel underclad cracks to be detected when their area was slightly greater than 2 mm2.

A small number of cracks were not detected during inspection because of difficulties relating to the small dimensions of the beam in the scanning zone. Nevertheless, efficiency could be improved by increasing the number of tests. Performance of two successive examinations ensures detection of all cracks which are ~~lesser~~ greater than or equal to a height of 3 mm.

The inspection method applied to ground surfaces gives results which are comparable to those obtained from machined surfaces. Comparative tests performed showed, however, that difference in surface condition lead to an average loss in sensitivity of 2.5. dB which can reach 3.4. dB in places. The extent of this difference only has a negligeable effect on inspection operations.

The manual method may be applied with equal efficiency to either even or small and large radii curved surfaces.

3-3. Automatic inspection using underwater focalised probes -

Detection of underclad cracks with contact probes becomes complicated very quickly as it involves repeated inspection over large surface areas, as is the case with plant and site equipment.

The small diameter of SE type probe's focal spot size leads, in fact, to excessively long examination times.

These factors led FRAMATOME to study and develop automatic inspection methods for examination of reactor vessel nozzles. These studies were performed in cooperation with Electricite de FRANCE (EDF) and Compagnie Générale de Radiographie (C.G.R.) insofar as in plant test applications are concerned, and with EDF and CEA for site testing applications.

3-3-1. Technique used.

The method used is again based on use of inclined longitudinal waves entering the steel at an angle of about 70°. These waves are produced by focalised underwater transducers mounted on an automatic testing apparatus.

- One of these transducers is adjusted at right angles to the inspection surface. It is designed to obtain an echo from the wall upon which the window is synchronised
- The two other transducers which are located on each side of the first transducer, are inclined at an angle of 14°. The axes of these two transducers converge with that of the first transducer on the scanning surface. These transducers are designed to detect cracks (fig.8).

The equipment chosen by FRAMATOME is as follows :

- the synchronisation transducer is referenced PANAMETRICS 308 R and has a 9 mm diameter crystal working at a frequency of 5 MHZ.
- the other two transducers are both referenced PANAMETRICS V 395 equipped with highly damped crystals 38 mm in diameter.

They function at a nominal frequency of 2.25 MHZ. Focalisation is obtained through a masked lens. The radii of the lens curve allows a focal distance of 260 mm to be obtained underwater. The focal spot is 6 mm in diameter at -6 dB. The purpose of the mask is to eliminate spurious echos originating from the condition of the scanning surface.

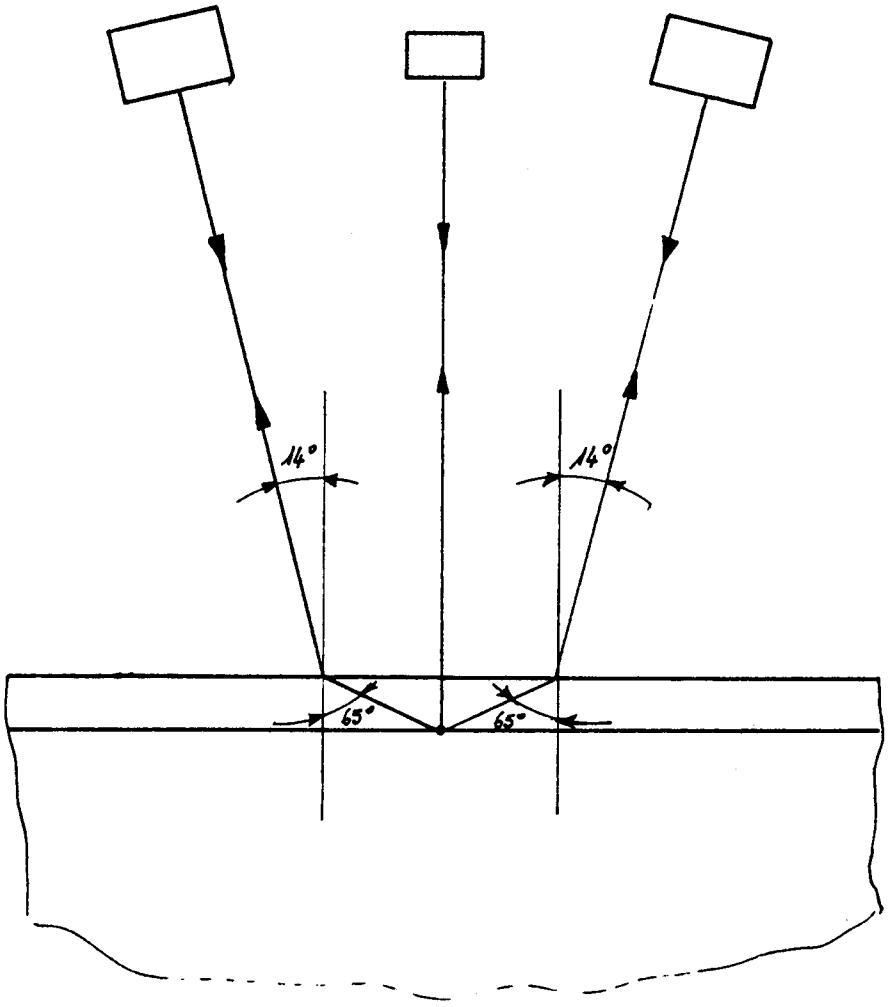


FIG. 8 - DIAGRAM OF THE MOBILE PROBES SYSTEM

The analysis of the transducer beam which is used for automatic inspection of the nozzles was also performed. Cross sections of beams were established at the point where the beam enters the part, i-e after travelling 180 mm underwater. These cross sections were established at -2, -6, -12 and -18 dB and are given in fig.9 for a masked and a non masked transducer (underwater incidence angle of 14°).

It can be seen that the existence of the mask leads to beam decay. From the cross section of the 130 mm radii it can be noted that the focus spot increases laterally to about 10 mm at -6dB.

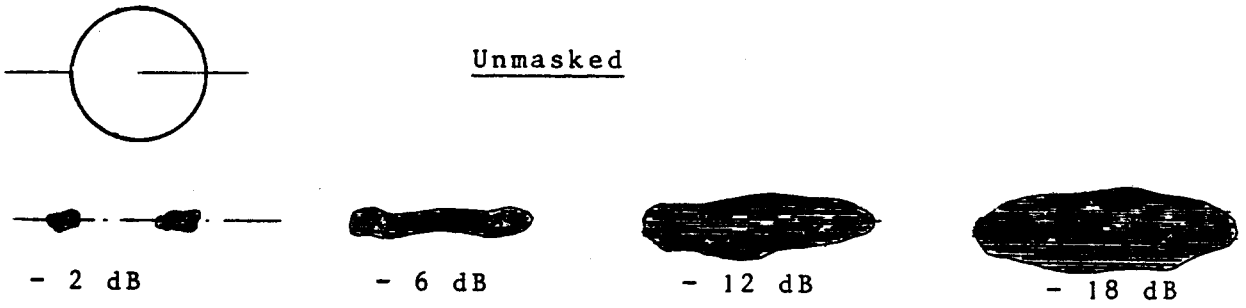
In the cross section through the generatrix of the cylindrical lens, the crystallength changes from 38 to 28 mm and the apparent near field in this direction is 300 mm in length. The 180 mm cross section approaches the near field limit (about 2/3) and only measures 17 mm at -6dB.

3-3-2. Results obtained.

As is the case with manual inspection using SE probes, the qualification test for the method using focalised transducer was performed on those nozzles having a great number of cracks of various sizes. Insofar as crack detection is concerned, the sensitivity of this method for identifying 2 mm2 surface cracks was proven and no cracks greater than 3 mm in height remained undetected.
These results were obtained from both ground and machined surface conditions.
The characterisation into inclusion and non inclusion type indications is not possible, however, at the present time. FRAMATOME is directing its efforts in this direction as well as in the measurement of crack height.

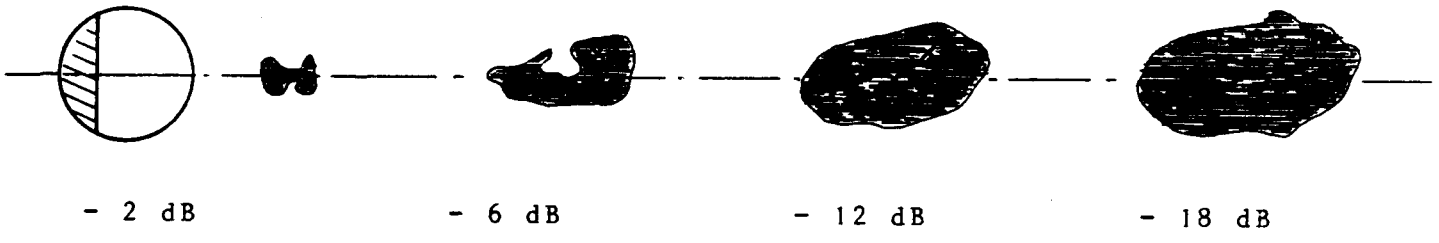
Transducer V 395 N° 24.341

R_1 = 130 mm R_2 = 00



Angle of incidence = 14°

A5K = 32,7 dB



Angle of incidence = 14°

A5K = 36,4 dB

Water Path = 180 mm

FIG.9 -BEAM CROSS SECTIONS

4 - EDDY CURRENT INSPECTION METHOD -

The specific geometry of drilled steam generator tube sheets with tubes installed raised a delicate problem for the development of a suitable underclad crack detection method. Methods such as R.T., U.T. thermography and Eddy current testing on cladding surfaces were envisaged but dropped after preliminary studies and tests. Finally FRAMATOME chose the eddy current testing method applied to the inside of a tube. The principles of this method were developed by the CEA.

4-1. Description of method.

The method developed uses a differential probe which is rotated inside the tube. This method only allows cracks which emerge on the surface of the tube sheet holes to be detected.

A diagram of the inspection equipment used is given in fig.10 It includes a probe with a mobile operation system and control bay.

The probe (fig.11) includes two coils electrically connected to a balanced impedance bridge.

If a discontinvity causes a break in the electromagnetic field, the bridge is unbalanced and gives rise to a variation in measurable voltage.

Calibration is performed using a reference block containing a defect produced by E.D.M. This reference defect is located in the base metal at the limit of the clad - base metal interface. It is 3 mm high and 1 mm long.

A frequency of 25 KHz is used for inspection.

4-2. Tests performed and results obtained.

Several tests were performed on :

- representative test blocks with artificial defects produced by E.D.M.

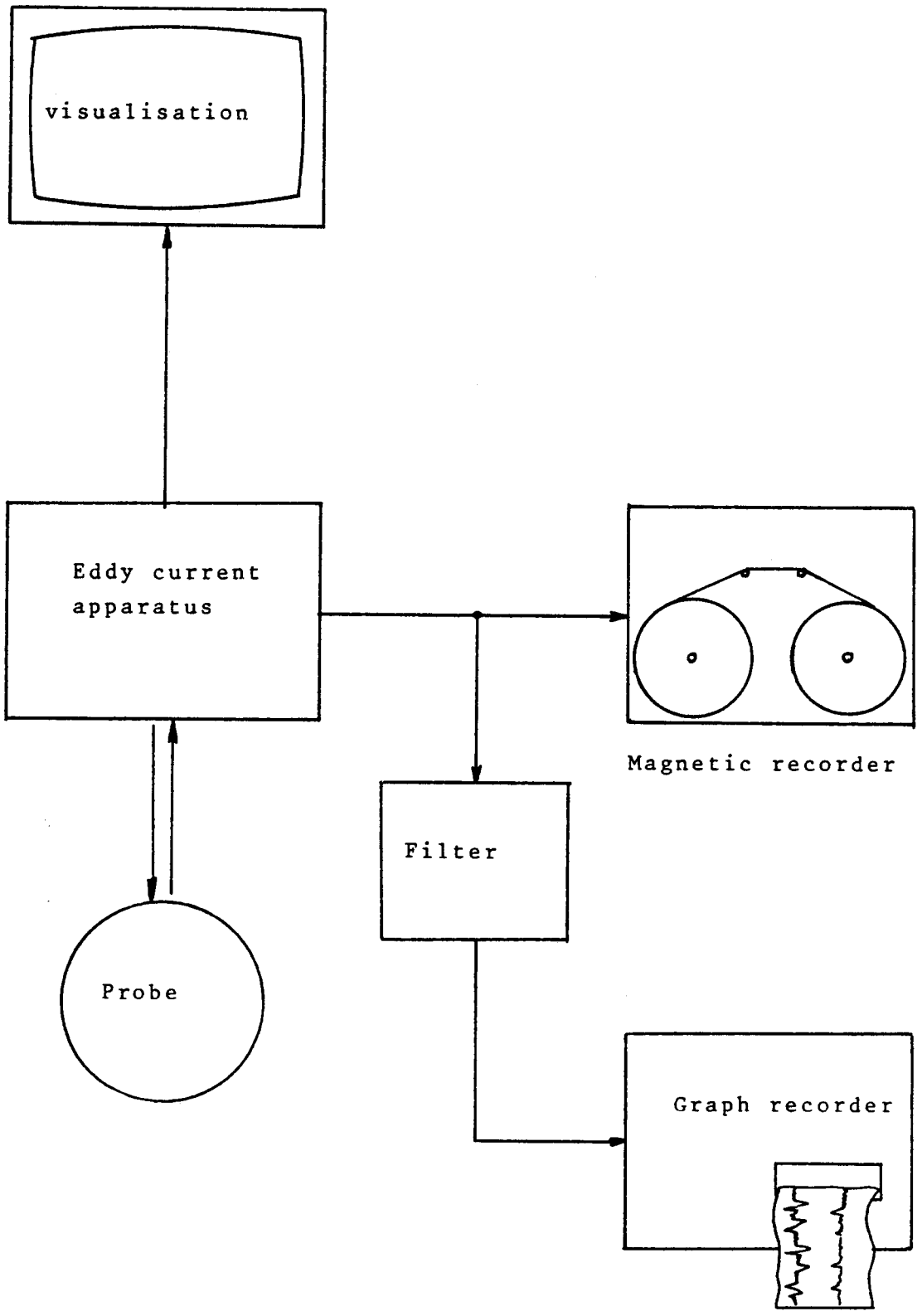
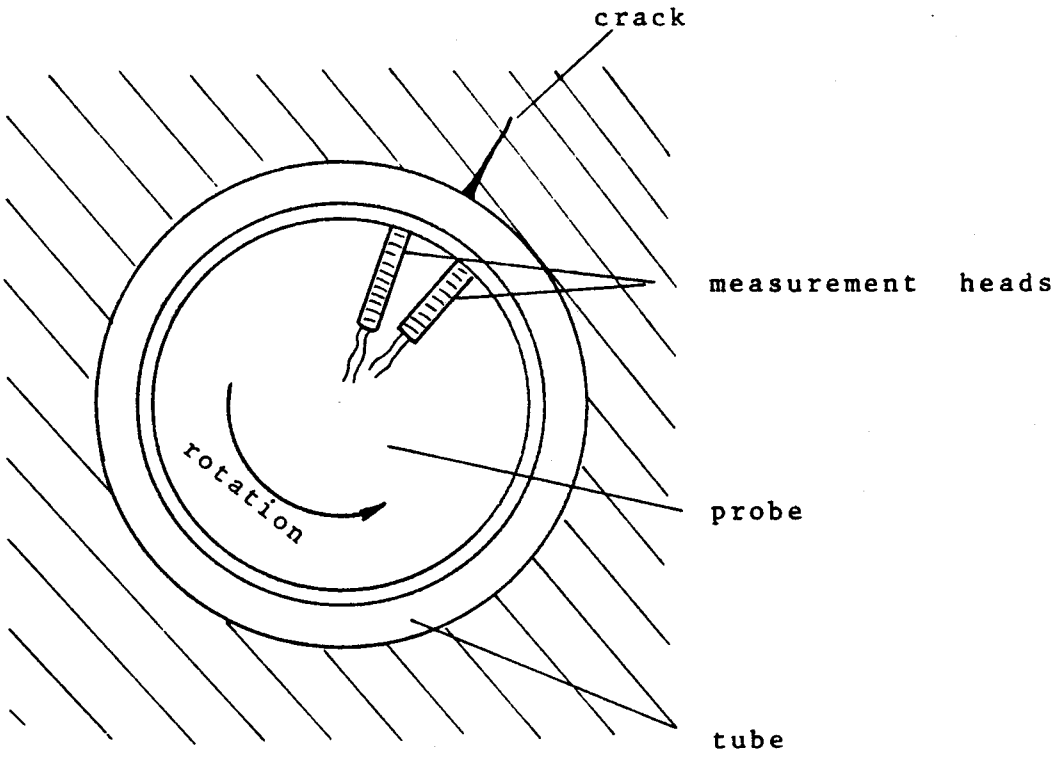
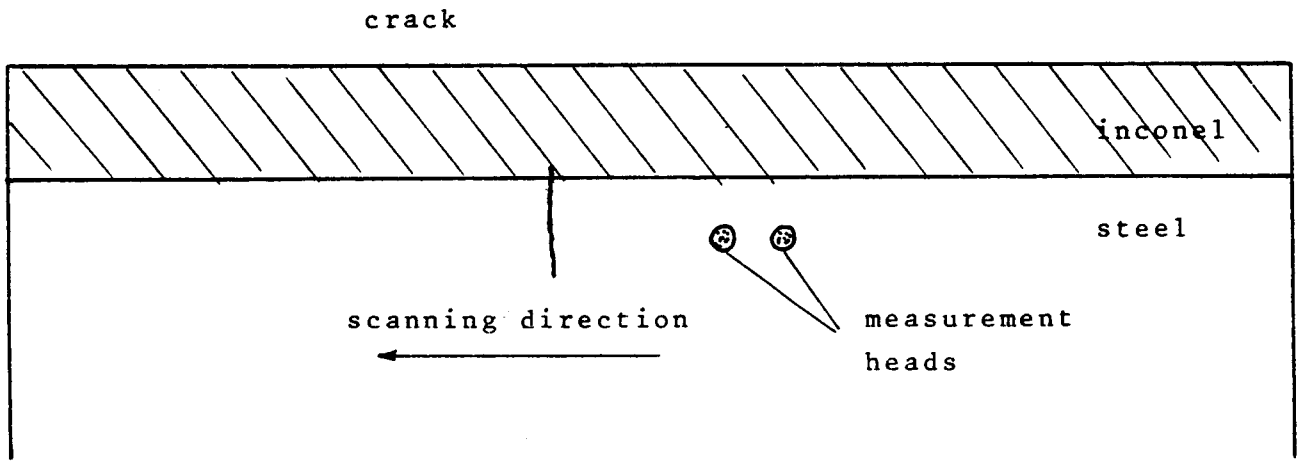


FIG. 10 - DIAGRAM OF THE EDDY CURRENT TESTING SYSTEM



View from above



Open view of the hole

FIG. 11 - DIFFERENTIAL MEASUREMENT PRINCIPLE USED

- a tube sheet containing natural defects
- representative models with fatigue cracks obtained from notches produced by E.D.M. and subjected to fatigue test.

4-2-1. Crack detection

Defects identified by dye penetrant test and situated at right angles to the metal base - clad interface were located on tube sheets. Before tubing, all defects were redetected using eddy current.
After tubing and tube expansion, almost all previously detected indications were located.

For the representative model having defects produced by EDM, it can be seen that fatigue cracks are able to be detected when cracks are propagated in inconel and steel sides with or without stressing of test piece.

4-2-2. Characterisation of indications.

Possible defects other than cracks cannot be detected by eddy current.
Characterisation of crack height obtained from a signal following several rotations of the Eddy current probe gave rise to a signal which overestimated height by about 2 mm for the inconel side and by about 5 mm for the steel side when compared to visual estimation and to results obtained from eddy current examination before tubing. This overestimation occurs systematically and can be attributed to the air-gap caused by the tube thickness and by the difference in magnetic permeability between inconel and steel.

4-3 - Conclusions -

Following the work performed by FRAMATOME concerning :

a) the selection of a method well suited to solving problem

b) the qualification of a well suited method for Eddy current testing from inside tubes

FRAMATOME considered it possible to inspect steam generator tube sheet using this method as all significant crack type indications normally detected by P.T. were located by eddy current after tubing.

Automatic testing apparatus which allows inspection to be performed in both radioactive and non radioactive environments has been specially developed to permit on site inspection.

Sizing of cracks perpendicular to stainless steel overlay by ultrasonic testing

T. SAITOH, Japan Steel Works
S. TAKAHASHI, Chiyoda Chemical Engineering and Construction Co, Ltd, Japan

ABSTRACT

In the petroleum industry, many pressure vessels with stainless steel overlay are in service and small cracks are often found on the surface of the overlay after some years of service.

In the past few years, a method of accurately measuring the crack depth of coarse grain stainless steel overlay has been sought because it is impractical to obtain the depth of these cracks by ultrasonic testing.

The present paper describes the technique which measures the depth of cracks in austenitic stainless steel overlay from the overlay side by ultrasonic testing.

1. INTRODUCTION

A number of refineries operates with direct desulfurization or hydrocracking reactors that are overlayed inside with austenitic stainless steel to cope with the high temperature and high pressure hydrogen.

In the turnaround maintenance inspection of these reactors, dye penetrant tests (PT) are performed to confirm that the overlay welds are sound. When a crack is detected by PT, it is necessary to measure the depth and length of the crack and ascertain from fracture mechanics whether the reactor is sound or requires repairs before operated again.

Measuring the depth of the crack with the shear wave angle beam technique is acceptable for ferritic steels, but not for austenitic stainless steel welds because of the coarse grain. Therefore, plant operators have been seeking a reliable inspection technique for overlay welds both from software and hardware aspects. Such a technique would be essential to measure the crack depth and foresee the life of the reactor, a basis for ascertaining when restarting the reactor.

The present paper reports the technique which measures the depth of cracks in austenitic stainless steel overlays from the overlay side by ultrasonic testing, using the longitudinal wave twin crystal angle probe.

Two probes having different focal distance are provided to measure the depth of cracks from 2 to 30 mm. The probes are featured as below.

Twin crystal	Longitudinal wave technique
Focal distance	10 and 20 mm, respectively
Angle of refraction	45°
Frequency	4 MHz
Probe size	20 mm x 35 mm x 20 mm each, distance between front of probe and probe index, 9 mm

The newly developed technique has been evaluated by test pieces with overlay having natural cracks and in several reactors with cracks on overlay.

The results have been satisfactory and, by this technique, data for analyzing safety of reactors and for countermeasures were obtained. Though developed for chemical pressure vessels, the technique would also be applied to nuclear pressure vessels with proper remote manipulating system.

2. PRINCIPLE OF ULTRASONIC MEASUREMENT OF CRACK DEPTHS

In general, the crack observed in the welds of the reactor has a considerable rough crack surface compared with that of high cycle fatigue crack as shown Fig. 1 and is oriented perpendicular to the testing surface.

Therefore, the depth of cracks in ferritic steel is generally measured by capturing the crack tip by the tip-peak-ehco-method[1)2)], which uses the echo caused when ultrasonic waves hit the crack tip as shown in Fig. 2, and calculating the depth from the beam path length (W).

$$d = W \cdot \cos. \theta \quad \ldots\ldots\ldots\ldots\ldots\ldots \quad (1)$$

θ : angle of refraction

3. PROBLEMS IN THE ANGLE BEAM TECHNIQUE

3.1 Grass Echo in Austenitic Stainless Steel Welds

In austenitic stainless steel welds, there is no transformation for making the grain fine. In addition to this, the grain become coarse because the dendrite formed during welding remains until the weld cools to the ambient temperature.

In such a case, if the shear wave angle beam technique shown in Fig. 3 is applied to the austenitic stainless weld, many noises called the grass echo appear only at the weld. Because most of the time, its response exceeds the echo response of the defect, the signal to noise ratio decreases, making it difficult to identify the defect. [3) 4)]

3.2 Shear Wave Angle Beam Technique from Overlay Side

Even in overlays, the coarse dendrite lies perpendicular to the interface, and the occurrence of grass echo cannot be avoided.

When a crack (depth = 10 mm) occurring in the overlay through a base metal of ferritic steel is measured by the tip-peak-echo-method shown in Fig. 4, the grass echo occurs within the beam path length (w), penetrating the overlay.

The cathode ray tube (CRT) pattern for the sanning shown in Fig. 4 is shown in Fig. 5 (a) and is compared with the test for ferritic steel shown in Fig. 5 (b).

For ferritic steel, the spurious echo unavoidable in the angle beam technique is generated from the probe housing and dead zone (4 mm) including the transmission pulse (T) occurs, but its length is small. Its interference is negligible, (See Fig. 5 (b)) because the tip-peak-echo can be observed.

For the overlay, the grass echo which occurs overlaps with the spurious echo generated from the probe housing and the transmission pulse (T) and forms a dead zone having a length of ℓ_1 (25 mm) (See Fig. 5 (a)). Therefore, the tip-peak-echo is hidden in this zone. This dead zone (ℓ_1) depends on the probe characteristics, overlay thickness, and sensitivity. When ℓ_1 is 25 mm, the limited depth of the crack that can be measured is about 18 mm from equation(1). When the depth of the crack is smaller than the limited depth, it cannot be measured. The cause of this dead zone is mostly grass echo from the overlay.

4. COUNTERMEASURES AND FINDINGS

The important task is to eliminate the dead zone shown in Fig. 5 (a), that is, the transmission pulse, spurious echo, and the grass echo, and to improve the characteristics for capturing the tip-peak-echo without missing.

For this purpose a technique for measuring with a longitudinal wave twin crystal angle probe of a special design is studied (Fig. 6).

Basis of Longitudinal Wave Twin Crystal Angle Probe Specification

a. Twin crystal angle probe [5]

Using this type of probe, the transmission pulse and the spurious echo were erased, and the beam of the sound is narrowed to improve directivity so that the crack tip-peak-echo shown in Fig. 4 can be detected and the depth of the crack measured accurately.

b. Longitudinal wave

The use of longitudinal wave in the sound mode to detect flaws in austenitic stainless steel welds has been studied by many researchers in the world for the past few years, and it become generally to be accepted. The sound velocity of longitudinal wave in metals is about twice the sound velocity of shear wave; therefore, the wave length (λ) of a longitudinal wave will be about twice of that of a shear wave when the frequency is fixed. Generally, a long wave length (λ) has less grass echo. Also, even with equal wave length (λ), the longitudinal wave is said to cause less grass echo. [5] Further, since the directivity improves with higher frequency, it is considered that the longitudinal wave is advantageous over the shear wave in decreasing the occurrence of grass echo and improving the signal to noise ratio.

The difference between the conventional method (shear wave technique) and the focused longitudinal wave technique is shown in Fig. 7.

The signal to noise ratio of the focused longitudinal wave technique is improved compared with the conventional method.

c. 45° angle of refraction

A check of the directivity theory [6] on the angle probe revealed that the directivity varies depending on the refraction angle (θ) of the angle probe.

The Fig. 8 shows the width of the ultrasonic beam when the depth of the crack is 10 mm. Thus, a narrow beam with sharp directivity is decisive for the tip-peak-echo-method [7]. For this reason, the refraction angle was set at 45°.

d. Focal distance

The echo response from a vertically oriented crack surface is expected smaller and to improve echo response and signal to noise ratio, two probes having different focal distance (10 and 20 mm respectively) are provided to measure the depth of crack from 2 to 30 mm.

Distance-Amplitude Curves of these probes obtained using wedge type test block are shown in Fig. 9.

e. Probe size

Considering that this technique is to be applied to In-Service Inspection, probe size is minimized to increase the useability.

5. RESULTS OF MEASUREMENT

Three types of test pieces are provided to verify the capability of new probes and tested.

Type 1 test pieces : Having natural crack without overlay

Type 2 test piece : Having artificial flaws with overlay

Type 3 test pieces : Having natural crack with overlay

Blocks having naturural cracks were cut out from the reactor which was used for several years and had been preserved in our Muroran Plant.

These blocks had natural cracks which had been induced during the investigation of local heating stress in the research center.

Type 1 and Type 3 test pieces were cut out from these blocks as shown on Fig. 10.

Examination condition

Equipment : Krautkrämer USIP-11

Probe : Longitudinal wave twin crystal angle probes

Couplant : Glycering

5.1 Type 1 Test Pieces

Type 1 test pieces are shown in Fig. 11.

Actual depth of crack in Fig. 11 is measured by magnetic particle examination.

Results of measurement by ultrasonic testing are shown in Table 1.

Table 1 Correlation between actual depth of cracks and depth by UT on type 1 test pieces

Test piece No.	Actual depth of crack (mm)	Depth by UT (mm)	
		FD : 10 mm	FD : 20 mm
1	5	6.3	-
2	10	10.9	-
3	15	14.7	16.5
4	20	-	23.5
5	30	-	30

FD : Focal distance

5.2 Type 2 Test Piece

A test piece with a 8 mm thick overlay of type 309 and type 347 provided with 1 mm width saw cuts of various depths shown in Fig. 12 (a) was made and tested.

Fig. 12 (b) and (c) show the CRT pattern (with a time base of 50 mm) of the test piece with 2 mm and 4.5 mm saw cuts in the overlay.
As expected, the grass echo disappeared and with improved signal to noise ratio, it was possible to measure the depths of the artificial flaws (saw cuts) in the overlay.

Results of measurement of ultrasonic testing are shown in Table 2.

Table 2 Correlation between actual depth and depth by UT on type 2 test piece

Test piece No.	Actual depth of saw cuts (mm)	Depth by UT (mm) FD : 10 mm
6	2	2.1
	4.5	4.6
	8	8.8
	10	10.6
	12	12.7
	14	14.8

FD : Focal distance

5.3 Type 3 Test Pieces

Two test pieces are the 8 mm thick weld overlay on the block having natural cracks whose depths are 6 mm and 14 mm respectively, cut out from the reactor as described in Para. 5.

These test pieces are shown in Fig. 13 and results of measurement by ultrasonic testing are shown in Table 3.

Table 3 Correlation between actual depth and depth by UT on type 3 test pieces

Test piece No.	Actual depth from testing surface (mm)	Depth by UT (mm)	
		FD : 10 mm	FD : 20 mm
7	14	16	-
8	22	-	23.3

The figures shown in Table 3 have a little variation compared with the results of type 2 test block, however, it is considered that these values are fairly accurate for the application of fracture mechanics analysis.

The several CRT patterns obtained from the test piece No. 8 shown in Fig. 14 (a) to (e).

Fig. 14 (a) shows the CRT pattern when scanning sensitivity is adjusted.

The grass echo or noise echo from the sound area is set to 20 % of CRT height.

Fig. 14 (b) shows the reflection from the crack tip of the overlay side.

Fig. 14 (c) shows the reflection from the crack surface.

Fig. 14 (d) shows the reflection from the crack surface at focal distance.

Even from the crack surface, we can expect a large echo at focal distance.

Fig. 14 (e) shows the reflection from the crack-tip, and when the probe is moved away from the crack further, all reflections disappear.

By reading the beam path length, the crack depth can be calculated.

6. CONCLUSION

It has been practically impossible to measure the depth of cracks that start from overlay surface and lies within the overlay, those that extend into the base metal, or those that start at the interface and extend into the base metal. By developing a longitudinal twin crystal probe with a refraction of 45°, it has been confirmed that cracks of 2 mm or more in depth could be measured accurately.

The newly developed technique has been evaluated in several reactors with cracks on overlay. The results have been satisfactory, and it has been confirmed that by this technique, data for analyzing safety of reactors and for countermeasures to be taken can be obtained.

It is emphasized that this problem raised by the operator, researched and developed by the reactor manufacturer and engineering and construction company, and confirmed by the operator as practical is a sample of implementing terotechnology.

REFERENCES

1. F. H. Dijkstra, "Flaw Evaluation with Particular Reference to Flow Size Estimation", IIW-Colloguium, Copenhagen, (1977).

2. Y. Ishii and T. Fujimori "An Introduction to Determination of Height of Weld Defects by the Ultrasonic Angle Beam Examination ", J. of The Japanese Society for Non-Destructive Inspection, 26 (1977) 308.

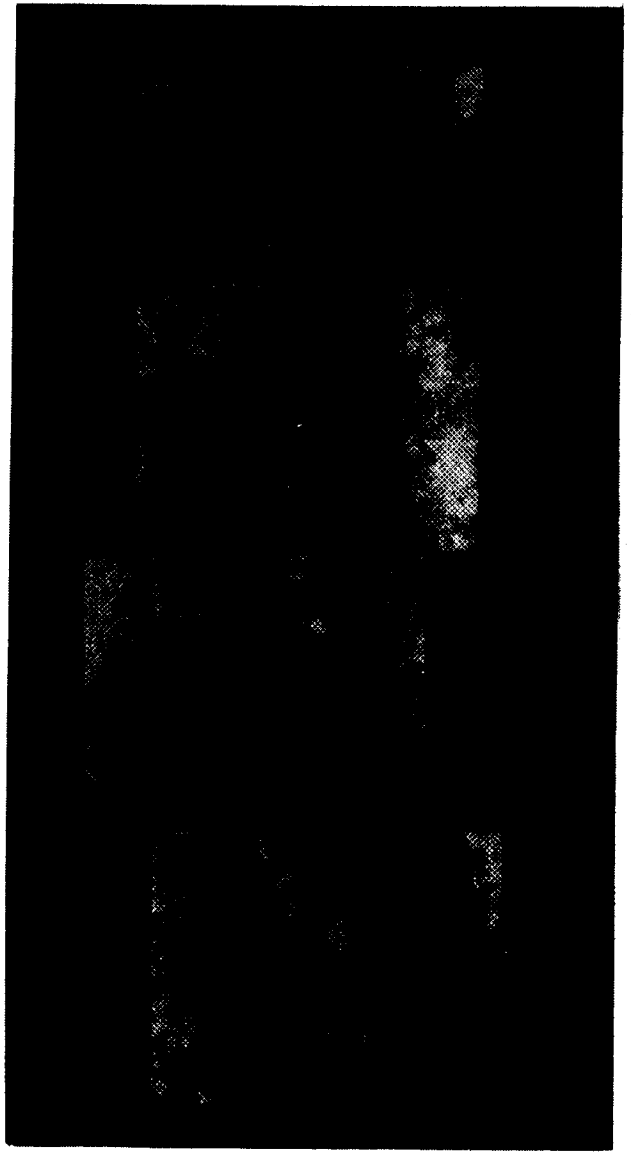
3. H. V. Richter, "Zur Ultraschallprüfung Austenitischer Schweiss-Verbindungen", Die Technik 23 (1968) 610.

4. Sub-Committee 202 Working Group - 7 of The Japanese Society for Non-Destructive Inspection, "Ultrasonic Testing of Weld in Austenitic Steels", Report No. 2661 (1977).

5. B. Kuhlow, "Ultrasonic Testing of Austenitic Steel Weld Joints", Preprints of eighth World Conference on Non-Destructive Testing (1976), Cannes, Report No. 2B6.

6. K. Kimura, "Sound Field of Ultrasonic Angle Probe", Report of National Research Institute for Metals, (1974).

7. K. Kimura, a. Fukuhara and S. Matsumoto, "Point Focusing Angle Probe", J. of The Japanese Society for Non-Destructive Inspection, 27 (1978) 126.



(x 50)

Fig. 1 Micro-observation of typical crack detected in the pressure vessels

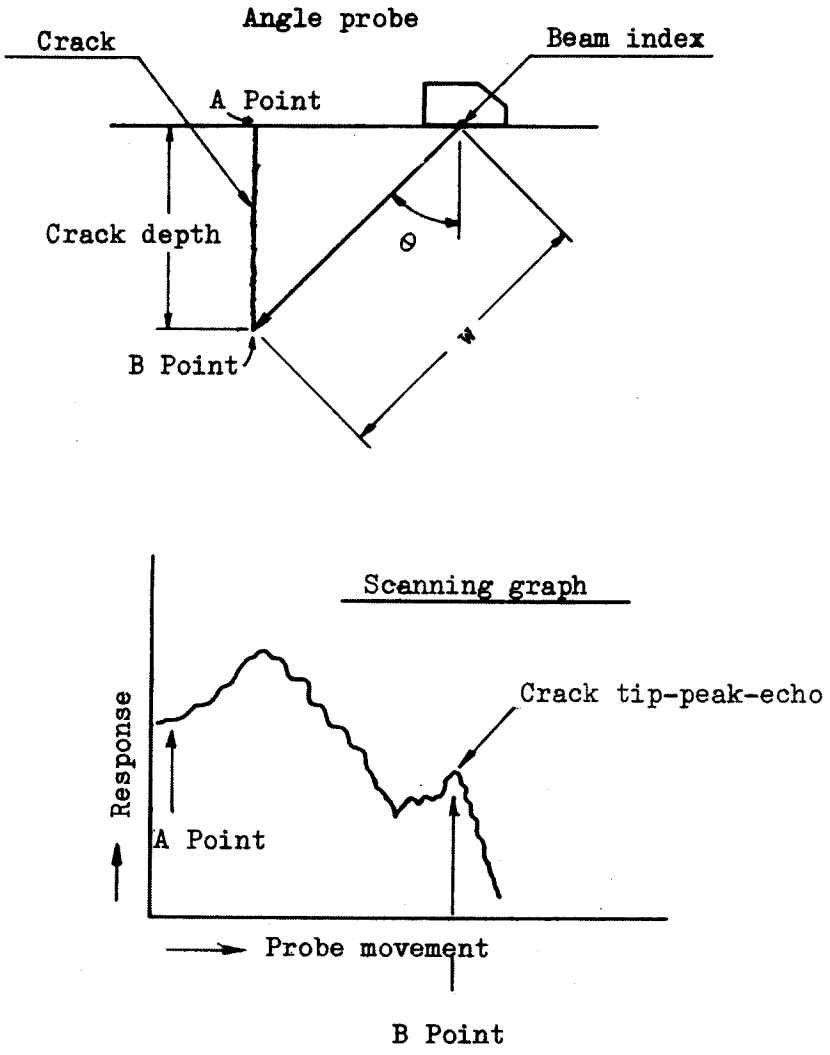


Fig. 2 Measurement of crack depth by tip-peak-echo method

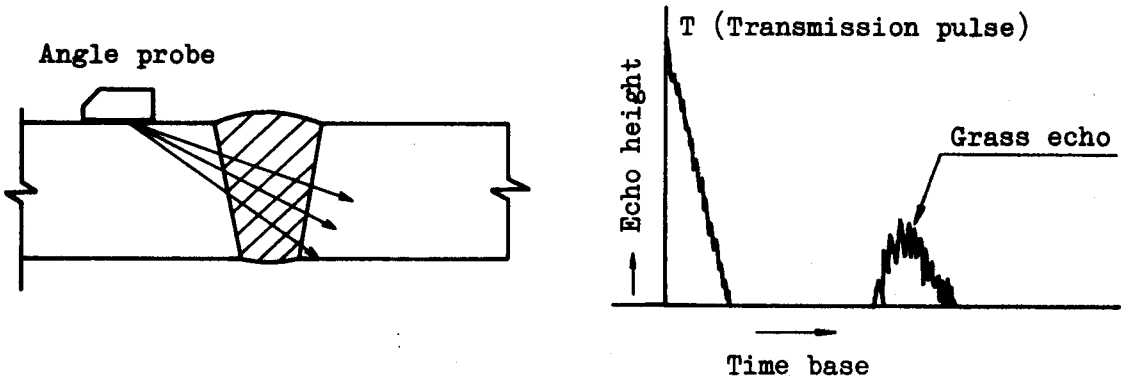


Fig. 3 CRT pattern from grass echo in coarse grain weld by shear wave angle beam technique

(CRT : Cathode ray tube)

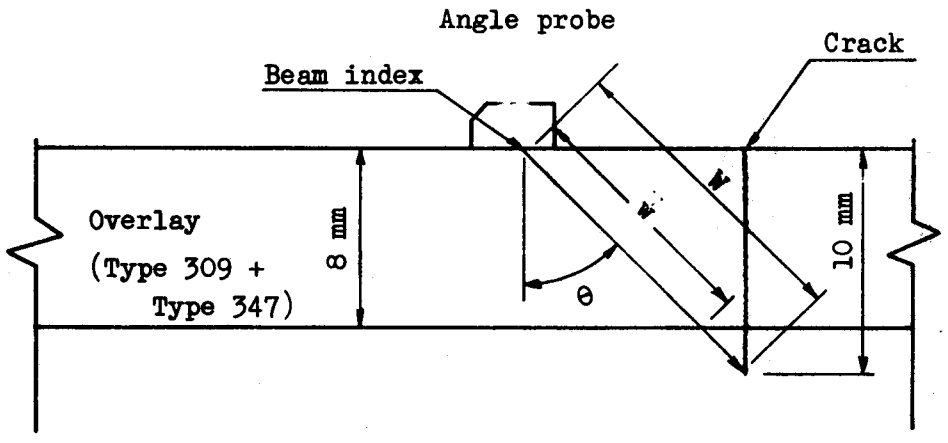
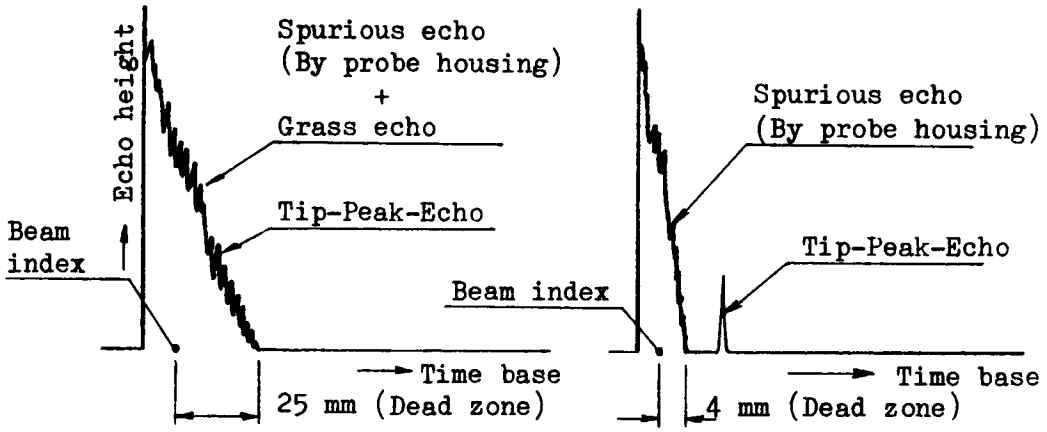
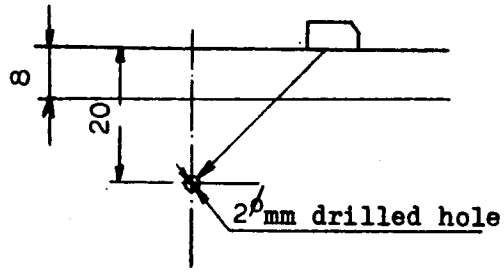


Fig. 4 Measurement of crack depth for ferritic steel with overlay



Sensitivity : Reflection from drilled hole - 80 % of CRT height

for overlay



for ferritic steel

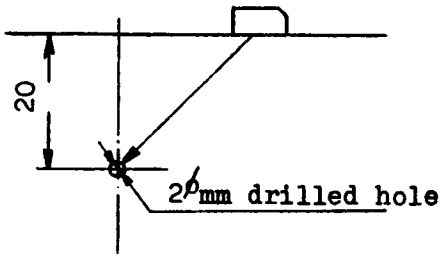


Fig. 5 CRT pattern from shear wave angle probe

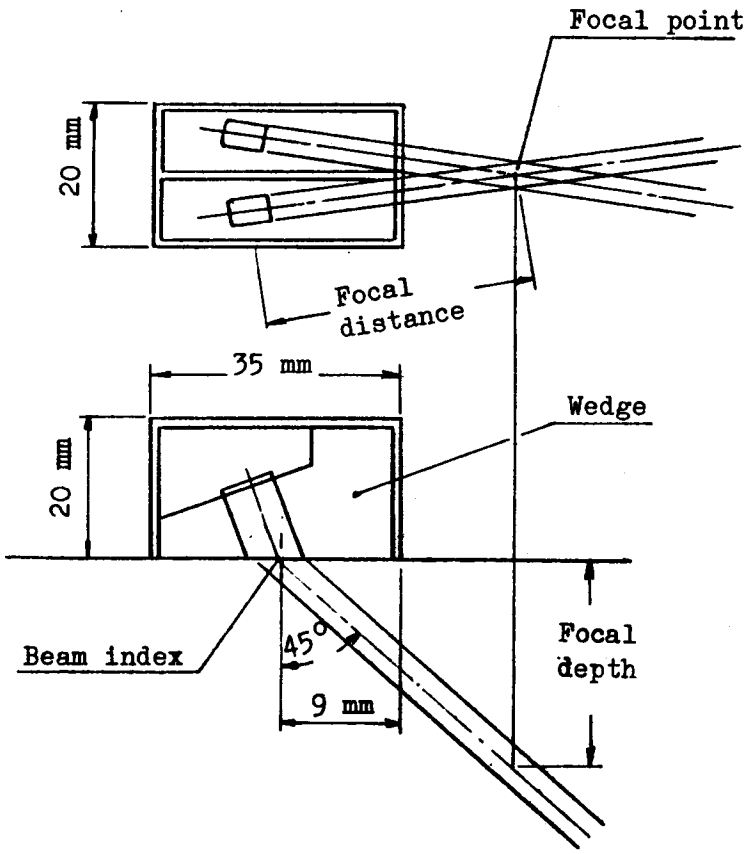
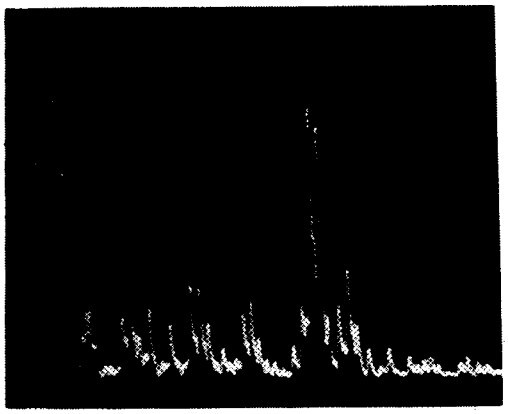
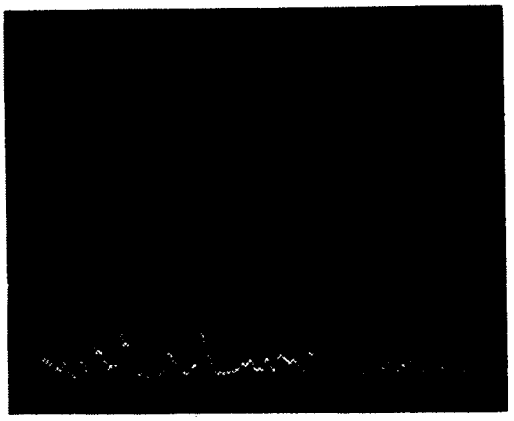


Fig. 6 Mechanism and dimensions of longitudinal wave twin crystal angle probe



WB45-N1 (1 MHZ)
Conventional method



WRY45-L2 (2 MHZ)
Focused longitudinal method

Fig. 7 CRT pattern of reflection from 4.5 side hole in coarse grain weld

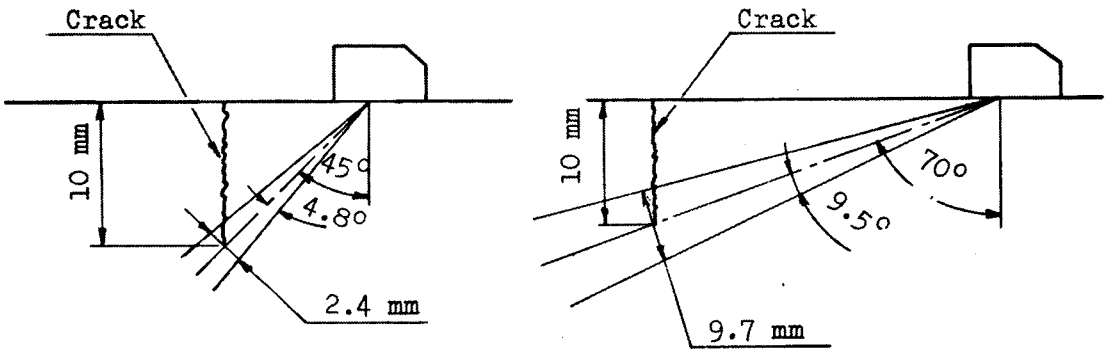
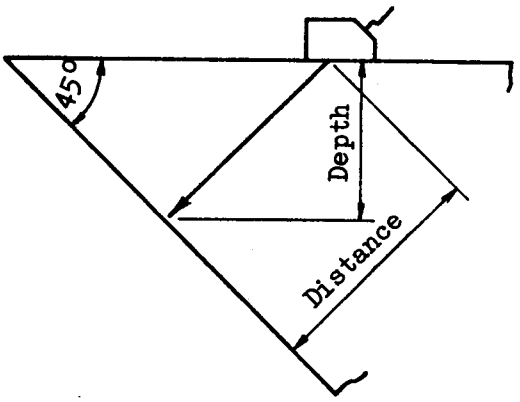
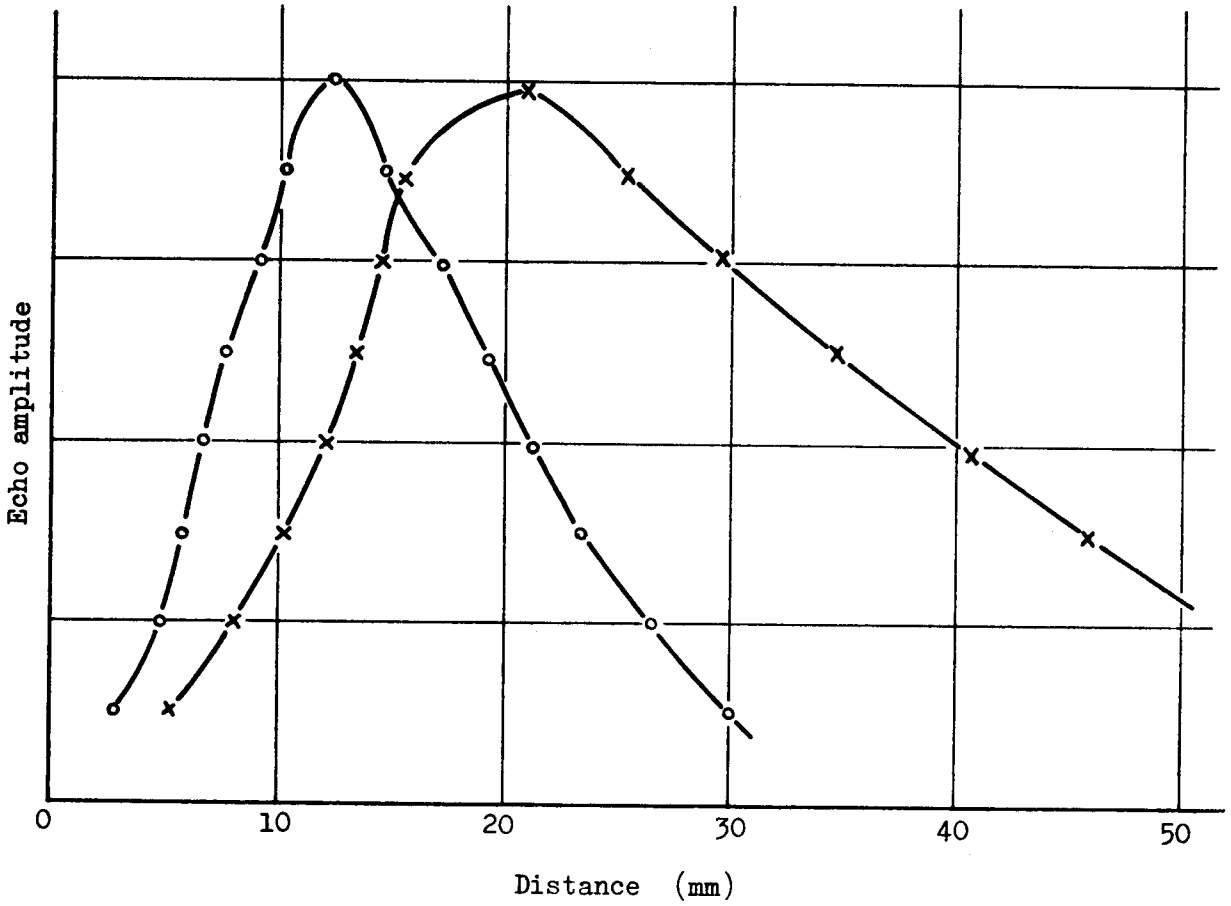
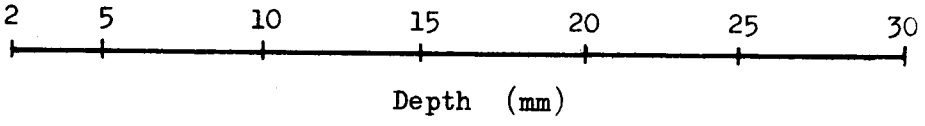


Fig. 8 Variation in directional characteristics from difference in refraction angle of angle beam probe



Wedg type test block was used to determine the Distance-Amplitude Curves.





For 10 mm focal distance probe

For 20 mm focal distance probe

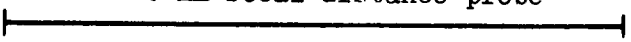


Fig. 9 Distance-Amplitude Curves for new probes

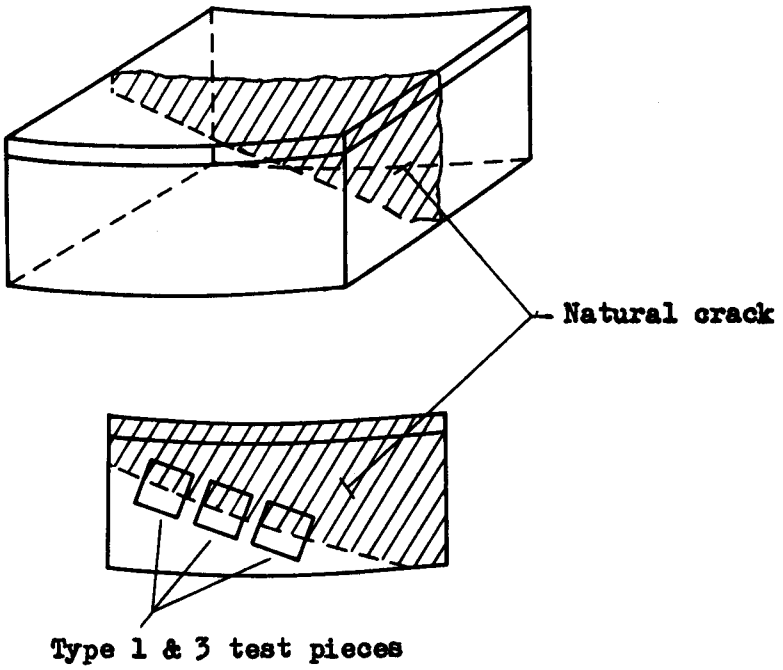
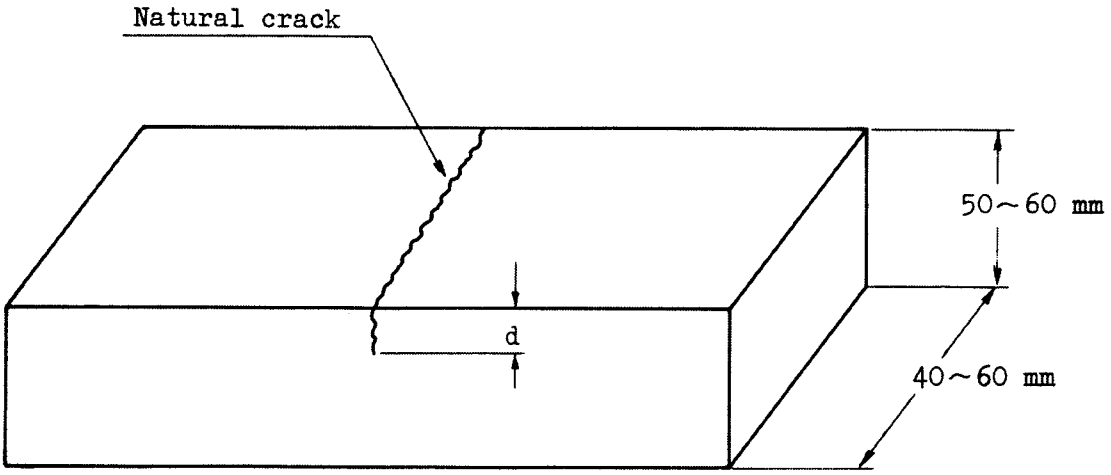


Fig. 10 Block having natural crack cut out from used reactor



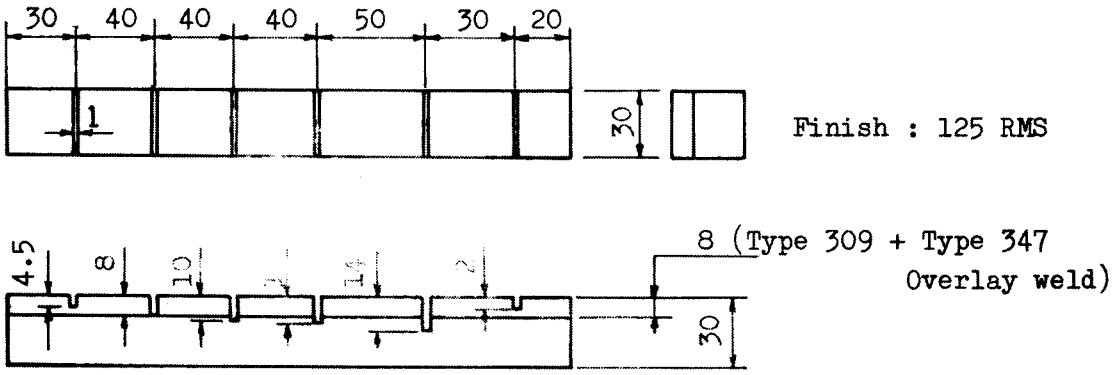
Depth (d) : 5, 10, 15, 20, 30 mm

Finish : 125 RMS

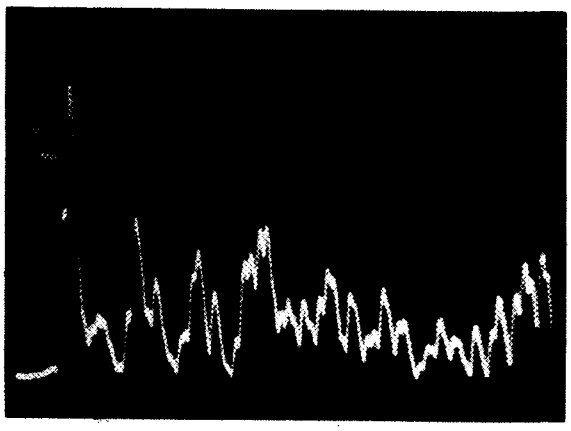


(In case of 10 mm crack test piece)

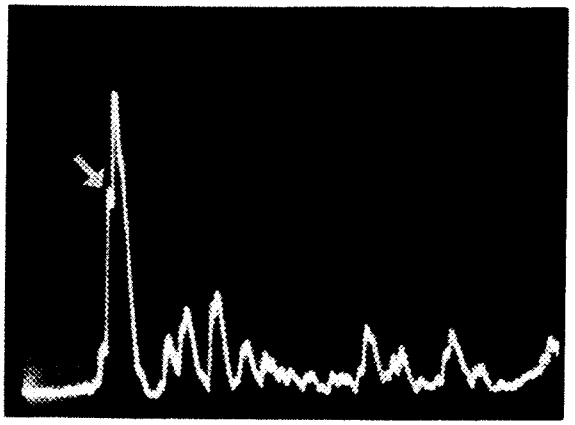
Fig. 11 Test pieces with natural crack



(a) Test piece with overlay and artificial flaws



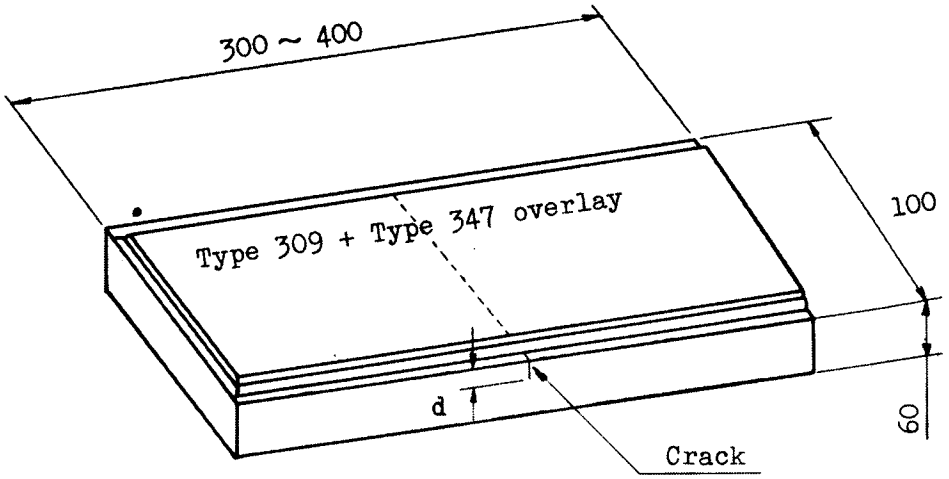
(b) depth 2 mm



(c) depth 4.5 mm

CRT pattern of test piece with overlay and artificial flaws

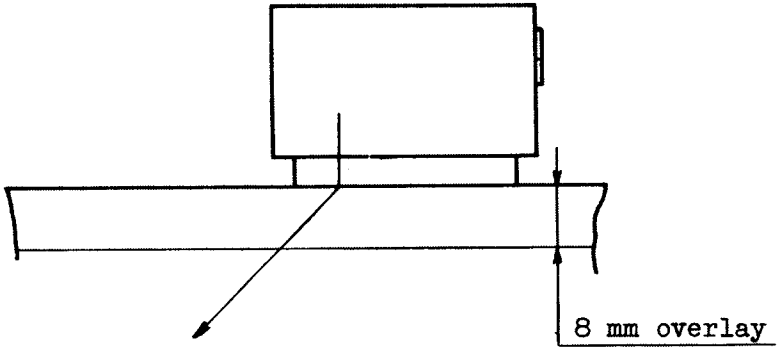
Fig. 12 Test piece with overlay and artificial flaws

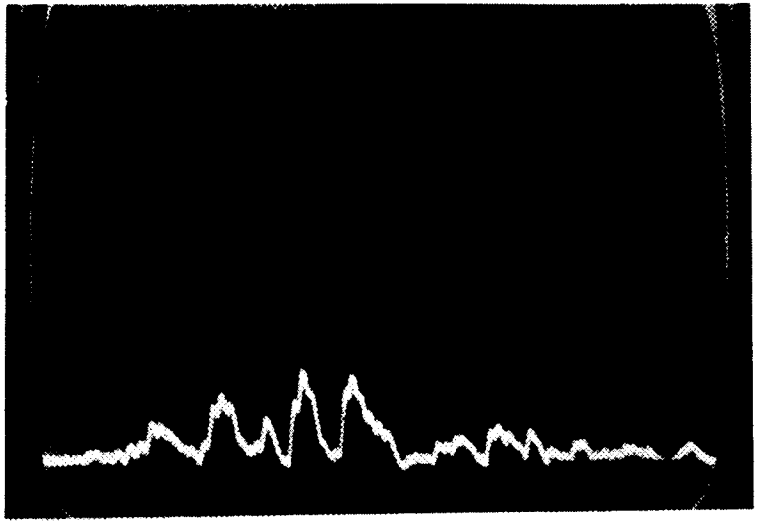


Depth (d) : 6. 14 mm

Finish : As weld

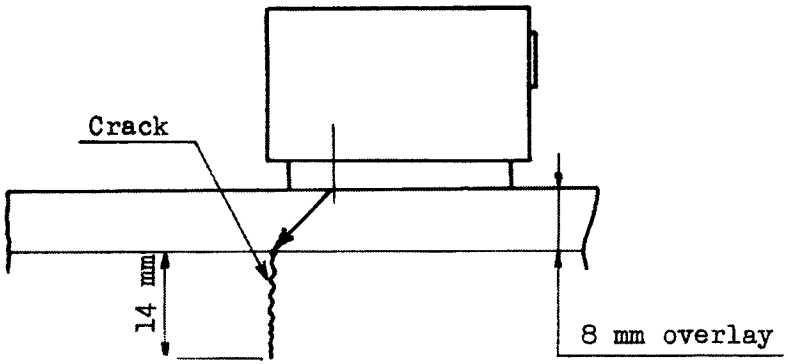
Fig. 13 Test pieces with natural crack and overlay

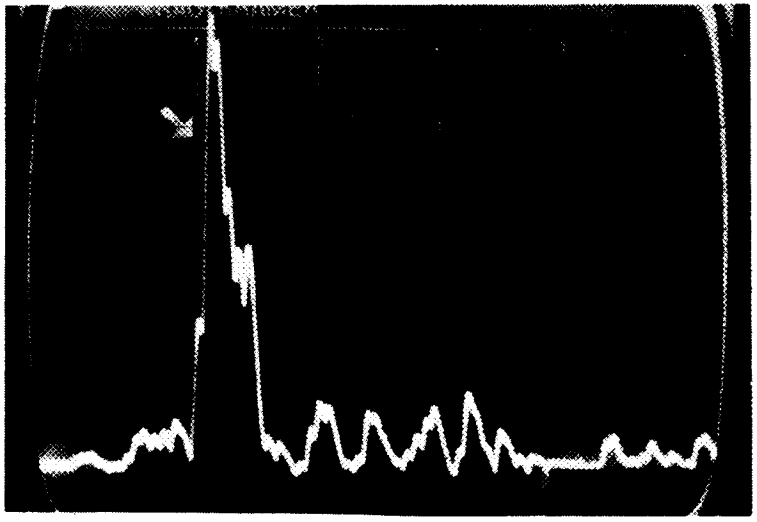




CRT pattern from sound area

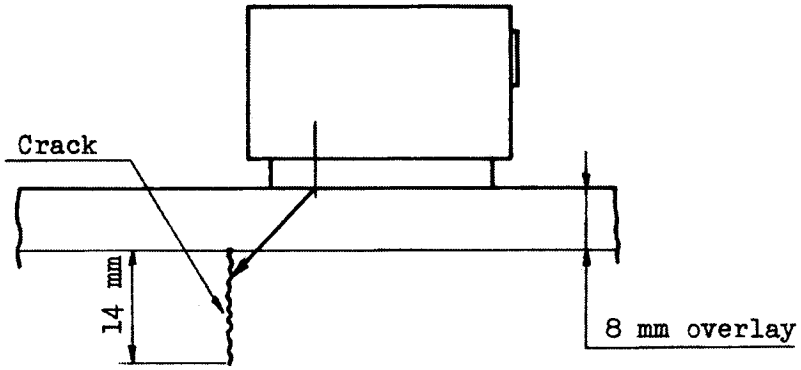
Fig. 14 (a)

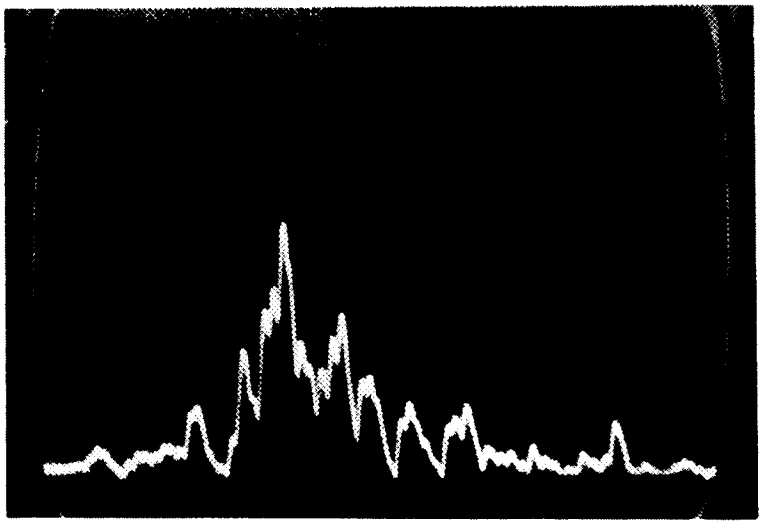




Reflection from crack tip (overlay side)

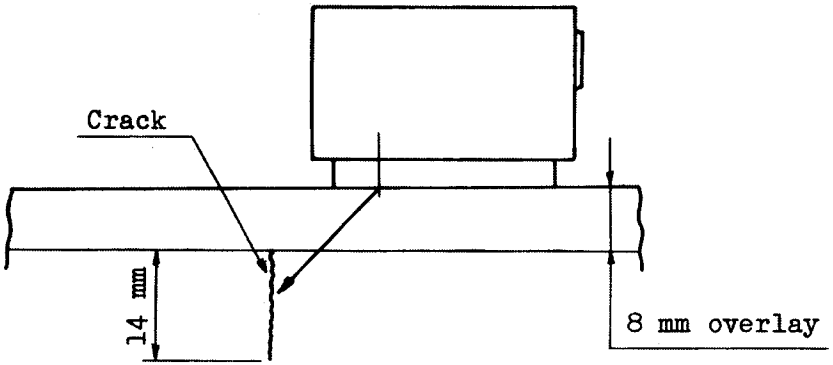
Fig. 14 (b)

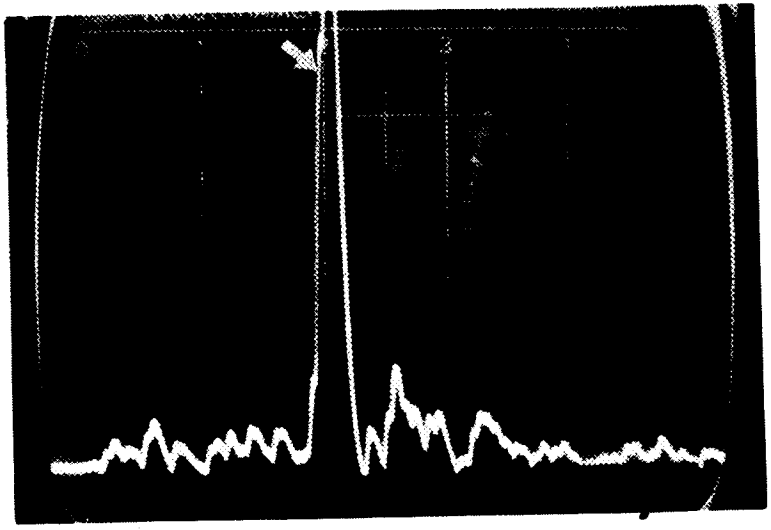




Reflection from crack surface

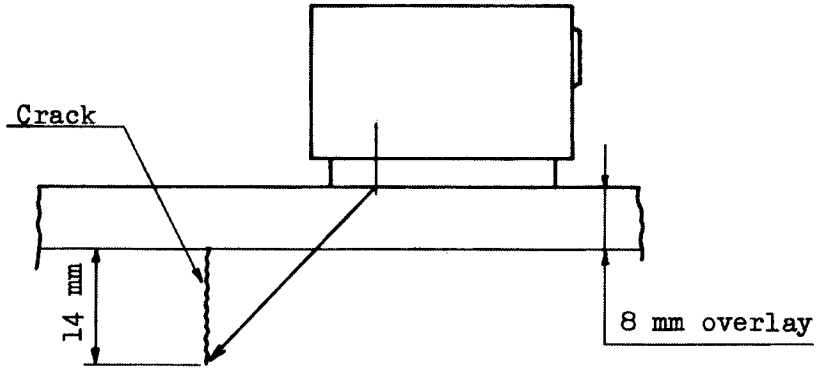
Fig. 14 (c)

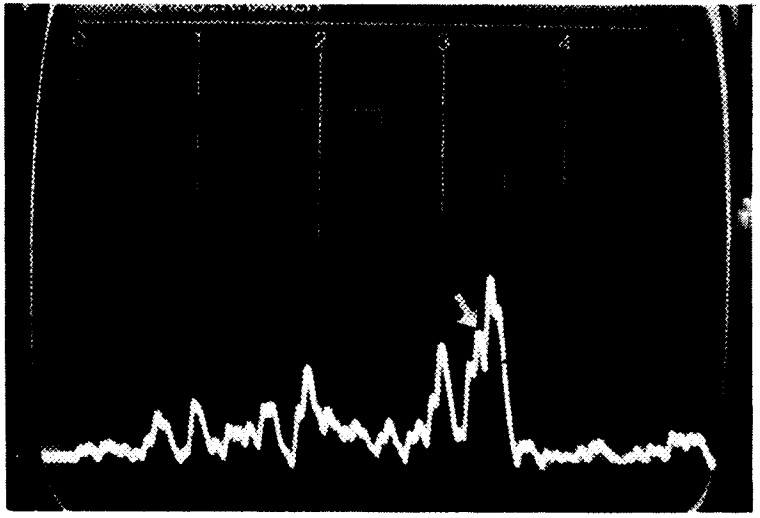




Reflection at focal distance

Fig. 14 (d)





Reflection from crack tip

Fig. 14 (e)

SESSION 4 : RELIABILITY

Chairmen : I.P. BELL, United Kingdom Atomic Energy Authority

J. MUSCARA, Nuclear Regulatory Commission, USA

Report on a survey of ultrasonic testing in austenitic weld materials

S. SANDBERG
Tekniska Roentgen Centralen, Sweden

ABSTRACT

Buttwelds in austenitic stainless steel plats containing machined-in flaws were ultrasonicly examined partly at 1.5 MHz by special ultrasonic methods including 3-dimensional imaging, focused image holography and C-scan imaging with a segmented annular array search unit partly at 0.5 MHz, 1.0 MHz, 2.0 MHz and 2.25 MHz by focused and non-focused probes of varying bandwidth in transverse and longitudinal mode with frequency analysis performed on the UT signal. In addition the plates were examined by radiography, liquid penetrant and conventional ultrasonic puls echo methods to characterize the reflectors in the welds.

It was shown that the primary problem in the detection of the known flaws in these specimens was the presence of numeruous false indications, not the lack of ultrasonic penetration. Examination with refracted longitudinal rather than refracted transverse wave ultrasound enhanced flaw detectability by minimazing the number of flase indications yet leaving the number of true indications intact.

A focusing device increases detectability for both transverse and longitudinal modes. The metalurgical parameters studied do not significant affect the detectability of the machined-in flaws.

1. INTRODUCTION

This is a report on a section of a research program sponsored by the Swedish Nuclear Power Inspectorat covering ultrasonic testing of austenitic weld material with the objective to assess the ability of several UT methods to detect and characterize artificial flaws in austenitic stainless steel welds. The program was conducted as a cooperative research program by TRC, STK and SwRI.

The weld panels used are of type 316 stainless steel 39 mm thick butt welded with different submerged arc welding techniques to give a variety of metallurgical parameters.

The following four weld panels were used in this program :

SMAW LG : Submerged arc welded Large Grain size

SMAW FG : Submerged arc welded Fine Grain size

SMAW MGHC : Submerged arc welded Medium Grain size
High carbon content to give grain boundary precipitates

SMAW MGLC : Submerged arc welded Medium Grain size
with a low carbon content

The configuration of the weld panels is shown in figure 1.

Side drilled holes 2.0 and 3.2 mm in diameter and short notches with a depth of 1.0 and 2.0 mm were machined into the weld panels after an initial UT-RT-PT examination.

The weld panels were examined with the following ultrasonic techniques :

1) Imaging with a focused phased array search unit of 1.5 MHz, 38 mm in diameter, 8-ring annular array manufactured by SwRI.
2) Imaging with refracted longitudinal waves with twin crystal quasifocused 2.0 MHz probes manufactured by RTD.
3) Imaging with refracted longitudinal waves with lensfocused 1.5 MHz probes manufactured by SwRI.
4) Imaging with refracted transverse waves with lensfocused 1.0, 1.5 and 2.25 MHz probes manufactured by SwRI and Panametrics.
5) Imaging with refracted transverse waves with flat 0.5, 1.0, 2.0 and 2.25 MHz probes of different bandwidths, manufactured by TRC, SwRI, Panametrics and Krautkrämer, and use of a Karl Deutsch variable Narrow Bandwith transmitter.

The evaluated parameter was signal to noise ratio. The S/N relationship is defined as the maximum signal amplitude from the observed defect divided by the maximum structural noise from the weld volume observed.

2. RESULTS

Table 1 is a simplified overall picture of the results grouped according to flaw type and location, probe type, angle and mode. A "yes" means an average S/N greater than 6 dB for all or almost all scans.

The results are rather ambiguous but it is quite obvious that refracted longitudinal waves are preferable to transverse waves when possible to use. Bandwidth considerations indicate that a narrow bandwidth is preferable to a broad bandwidth. Analyses with the Karl Deutsch Narrow Bandwidth transmitter and transverse wave mode show an increase of sensitivity of 10-15 dB in spite of a decrease in transmitted amplitude. No significant increase in detectability is observed.

Considering frequencies the results of this program show no significant trend between 1.0 and 2.25 MHz. 0.5 MHz does not indicate the machined in defects of the sizes used.

The frequency spectrum analysis shows in the weld material a frequency shift of 200 kHz towards higher frequency for a 0.5 MHz probe and a frequency shift of 200 kHz towards lower frequencies for a 1.0 MHz probe. For a 2.25 MHz probe the shift is also towards lower frequencies. The maximum frequency may vary between 0.8 and 2.25 MHz when penetrating weld material. Metallurgical reflectors cannot be separated from flaw reflectors with the frequency analysis applied.

Considering sizes of machined defects a 3.2 mm side drilled hole seems possible to detect with both transverse and longitudinal modes but an amplitude variation of 12 dB should be anticipated when scanning a side drilled hole in transverse mode. A 1 mm notch (2 % T) in the weld root seems possible to detect if one chooses his parameters carefully and a 2 mm notch (5 % T) is reasonably easy to detect. Notches in the weld crown are only possible to detect with longitudinal wave mode.

It should be noted that one needs a different set of UT parameters for the weld root and weld crown using longidutinal waves.

Figure 2 shows a serie of scans with a flat and a lens focused 2.25 MHz broadband transducer over a 1.0 mm notch in the weld root of the SMAW MGHC weld panel. The figure indicates that a focusing device does help detectability. This figure is typical for all focusing devices used in this program.

The above mentioned results are averaged over several weld panels with different metallurgical parameters. Different weld specimens do give different test results but it is not so that one set of metallurgical parameters is preferable to another for several types of machined defects. The results rather suggest the contrary, if a set of ultrasonic parameters will detect the machined defects in one weld specimen it will also detect similar set or machined defects in another.

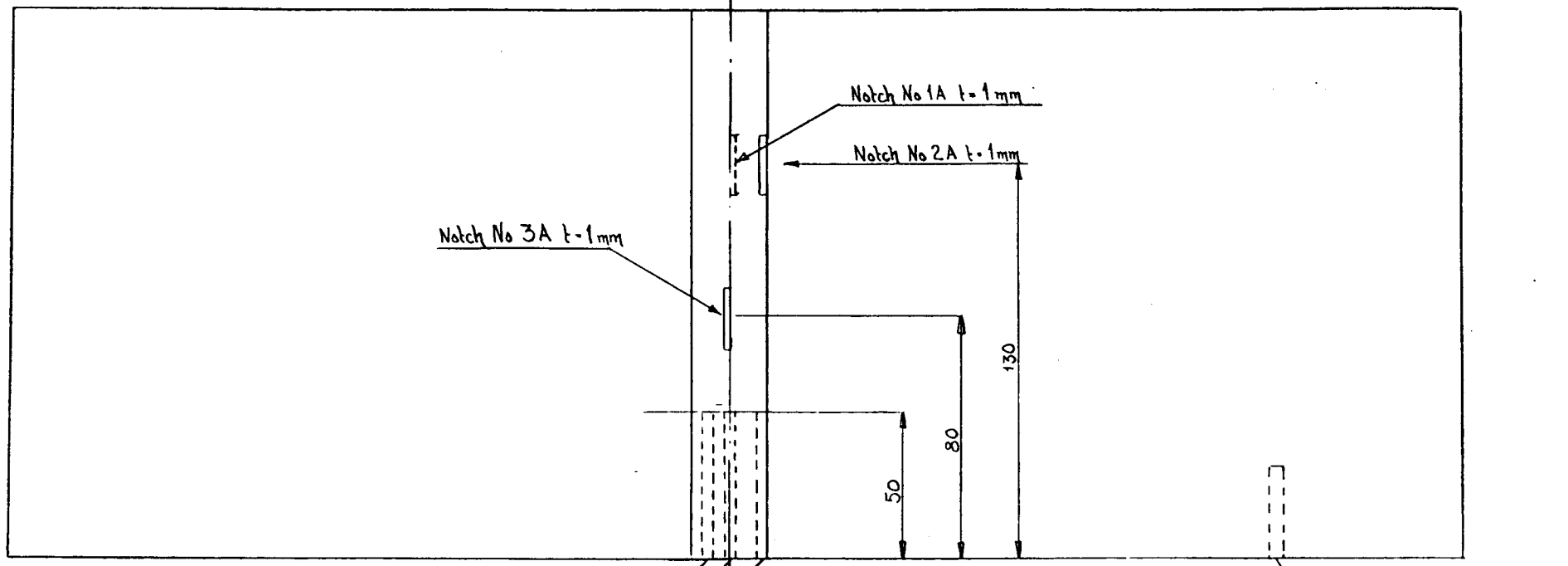
A great effort was made to use signal processing to help separate metallurgical noise from flaw indications. 3 dimensional imaging and holographic imaging with a holosonic 200 instrument was used, and frequency spectrum analysis with a Tektronix 7L12 frequency spectrum analyser was conducted with signals from different types or reflectors.

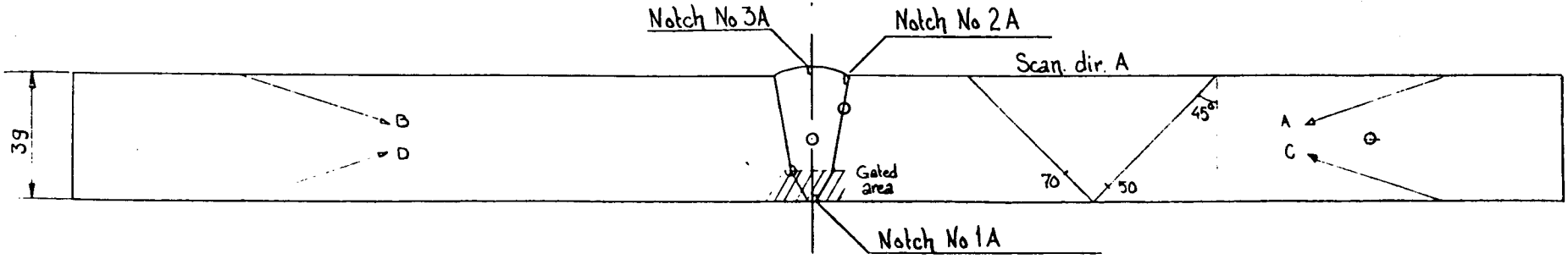
The signal processing used does not significantly help raise the detectability of the machined defects in the weld specimens.

This document must not be passed on to any person not authorized by us to receive it, nor be copied or otherwise utilized by such person without our authority.
AB Sveriges Tekniska Kontrollinstitut

SMS. 715

Ytjämnhet där ej annat angives Ra V





A, B, C and D : Scanningdirections

Dat.-nr	Ant.	Benämning		Material	Mod.-nr Ämne Dimension	Anm.
Konstr.	Ritad	Kop.	Konstr.	Stand.	Godk.	Skala 1:1,5	Ersatter	Ersatt av

STK
AB Sveriges Tekniska Kontrollinstitut

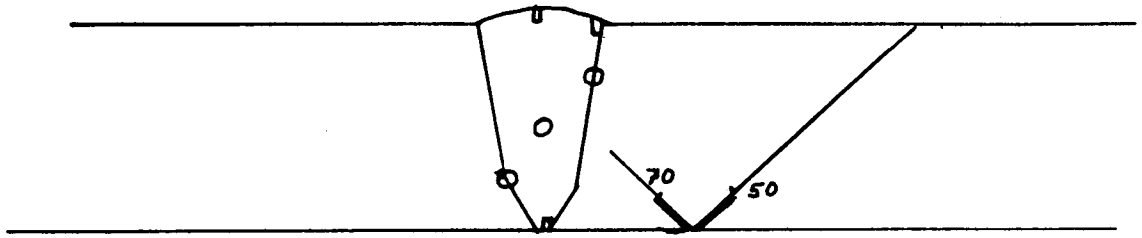
Figure nr 1
Weldspecimen SMAW MGHC
Gated area : weldcast

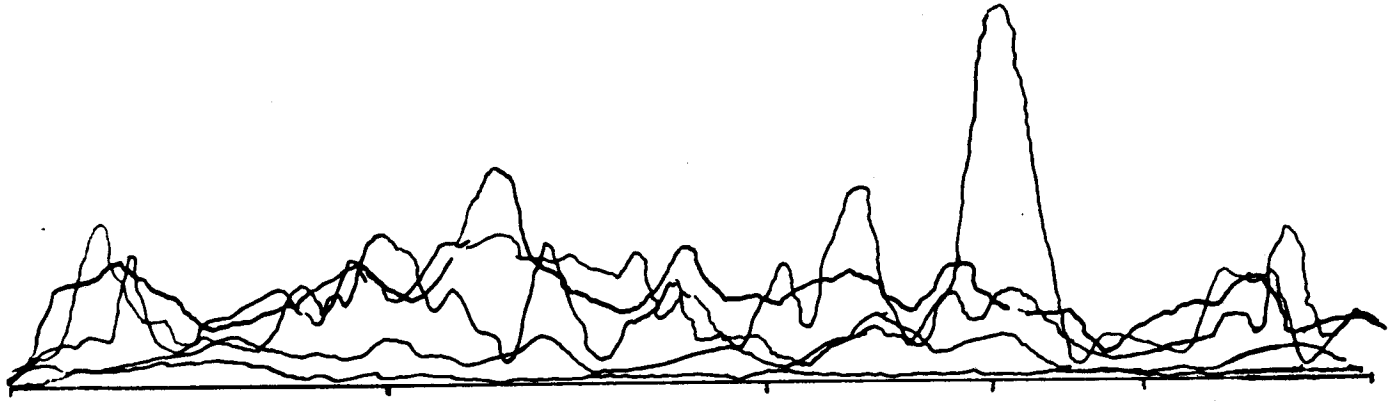
Dat.
Ritn.-nr

FIGURE 1

Denna handling är vår egendom och får enligt gällande lag inte kopieras, visas eller utlämnas till tredje person.
AB Sveriges Tekniska Kontrollinstitut

-007-





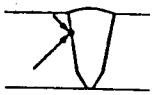
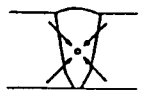
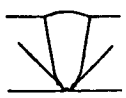
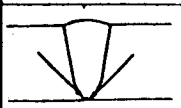
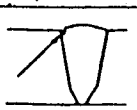
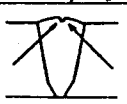
SMAW MGHe
Pan V 395 foc
2,25 MHz Gate 50-70 mm



SMAW MGHe
Pan V 395 flat
2,25 MHz Gate 50-70 mm

FIGURE 2.

Table 1: Result digest

Result digest shows defect location and size, scanning direction and if the machined defect is possible or not to detect for each probe. A yes represents an average S/N greater than 6 dB detected in all or almost all scans.		SDH No 3 HAZ Ø 3,2 mm	SDH No 2 Weld center Ø 3.2 mm	SDH No 1 HAZ Ø 3,2 mm	SDH SWRI HAZ Ø 2 mm	Notch weldroot depth 1,0 mm	Notch weldroot depth 2,0 mm	Notch Weld-crown, HAZ depth 1,0 mm	Notch weld-crown/weld-center,dep2,0
									
Pan V 395 2,25 MHz	flat 45° T immersion	Yes	Yes	No		No	Yes	Yes	No
Pan V 395 2,25 MHz	focused 45° T immersion	Yes	Yes	Yes		No	Yes	Yes	No
Pan V 392 1,0 MHz	flat 45° T immersion	No	No	No		No	No	No	No
Pan V 392 1.0 MHz	focused 45°T immersion	—	--	No		No	--	—	--
Pan V 389 0,5 MHz	flat 45°T immersion	No	No	No		No	--	No	No
Pan A 403-S 2,25 MHz	flat 45° T contact	Yes	No	No		Yes	Yes	Yes	No
Pan A 401-S 1,0 MHz	flat 45° T contact	Yes	No	No		Yes	Yes	No	No
Pan V 395 2,25 MHz	flat 55° T immersion	Yes	Yes	Yes		No	Yes	--	--
Pan V 395 2,25 MHz	flat 70° T immersion	Yes	Yes	Yes		No	Yes	--	--
Pan V 395 2,25 MHz	focused 70° T immersion	Yes	--	Yes		No	--	--	--
Pan V 392 1,0 MHz	flat 70° T immersion	Yes	No	Yes		--	No	—	--
RTD 76-38 2,0 MHz	quasi foc 45° L contact	Yes	Yes	Yes		No	No	Yes	Yes
RTD 76-40 2,0 MHz	quasi fac 50° L contact	Yes	Yes	Yes		No	Yes	No	No
RTD 76-45 2,0 MHz	quasi foc 70° L contact	--	Yes	—		---	—	--	—
SWRI 1,5 MHz	flat 45° T contact				No	No			
SWRI 1,5 MHz	flat 60° T contact				No	No			
SWRI 1,5 MHz	focused 45° T immersion				No	No			
SWRI 1,5 MHz	focused 60° T immersion				No	No			
SWRI 1,5 MHz	focused 45° L immersion				No	No			
SWRI 1,5 MHz	phased array 45L immersion				Yes	Yes			
SWRI 1,5 MHz	phased array 45T immersion				No	No			
SWRI 1,5 MHz	phased array60 T immersion				No	No			

Ultrasonic examination of stainless steel E.B. welds by an immersion technique *

G. TORRIDA, G. ANTONIOLA, D. LATERZA
Fiat TTG S.p.A., Italy

ABSTRACT

An ultrasonic examination method of austenitic stainless steel electron beam (E.B.) welds is being developed. The method is based on an automatic immersion technique employing focused transducers and aimed at detecting both the weld soundness and penetration.

The scope of this examination is the quality control of E.B. welds of different geometries performed in the fabrication of nuclear reactor components at Fiat TTG.

Equipments used are :

- ultrasonic apparatus with dual trace display
- four track recorder
- immersion system to move the pieces and transducers so to have an 100 % volume scanning of the welds

The examination procedure, firstly set up for E.B. butt welds in AISI 304 pipe 10 mm thick, 110 mm O.D., consists of :

1) Calibration of the ultrasonic equipment with recorder (the minimum detection level shall be ascertained) by means of a first calibration block with holes (to verify the weld soundness) and a second calibration block with circumferential notches on the inside diameter (to verify the weld penetration);
2) Examination of the welded joint;
3) Repetition of the calibration as per item 1. to verify the calibration constancy of the equipment.

The reliability of the examination procedure has been checked as follows :

1) Weld soundness - The recorded indications, mostly due to porosity defects, are verified by means of radiographic examinations in addition to sectioned specimens. This comparison gives an approximate correction coefficient depending upon the dimensions of the defect. At present, the soundness control is able to detect, with good signal/noise ratio, porosities of about 0.8 mm diameter.

* Work done within the activities of the CNEN-FIAT Industrial Promotion Program

2) Weld penetration - The penetration control is at present able to detect an artificial defect 0.5 mm in depth on the inner surface of the welded specimen.
The comparison between real lacks of penetration and the corresponding ultrasonic indications has brought us to study and prepare four types of calibration blocks welded in particular ways so to simulate the real defects better than the usual artificial defects obtained by machining. The specimens welded in these ways are then equatorially cut to examine and compare the actual defects with the recorded indications. This type of investigation is still in progress because it is deemed it necessary to enrich our case record. Subsequent step will be to obtain a significant correlation between lack of penetration and calibration notches indications.

In conclusion, the establishment of adequate acceptance standards for the ultrasonic inspection of E.B. welds by means of automatic immersion techniques suitable to lot fabrication purposes requires, in our opinion, an accurate experimentation to arrive at a correct interpretation of defect indications. This is particularly true for the lack of penetration defect.

1. INTRODUCTION

An ultrasonic examination method of austenitic stainless steel electron beam (E.B.) weld is being developed. The method is based on an automatic immersion technique employing at the same time two focused transducers traveling to examine both the weld soundness and penetration.

The scope of this examination is the quality control of E.B. weld of different geometries performed in the fabrication of nuclear reactor components at Fiat TTG.

Equipments used (Fig. 1 and 2) are:

- ultrasonic apparatus with dual trace display
- four track recorder
- immersion system to move the pieces and transducers so to have a 100% volume scanning of the welds.

The examination procedure described in this paper is being evaluated for the quality control of a first lot of 150 E.B. butt welds in AISI 304 pipe 10 mm thick, 110 mm. O.D. Reliability of results is also discussed.

2. EXAMINATION PROCEDURE

The examination of the immersed welded tube is performed employing at the same time two focused transducers positioned at 90 degrees from each other (see Fig. 3). Each transducer is connected to one channel of the ultrasonic apparatus and to one of the recorder. The oscilloscope pattern can be visualized both separately (one channel per time) and contemporaneously (both channels) on the TRC of the apparatus. Each rotation of the weld is signaled by a proximity switch connected with the external marker of the recorder.

The choice of the focused transducers has been aimed at diminishing the extent of the reception noise without sensitivity losses due to the attenuation thanks to the point energy concentration obtainable with this kind of transducers. An additional reason for this choice is the good side definition of the ultrasonic beam which allows an accurate evaluation of the defect size. The choice of the focused transducer type (narrow or broad band) has been performed according to the following conclusions of a previous investigation:

i) The weld soundness is better detected by means of a broad band focused transducer with the following characteristics:

- 1 in. diameter
- 2.25 MHz frequency
- 76.8 mm focusing
- 0.7 mm focal spot.

This choice, in addition to the results of the experimental investigation, is supported by the fact that the reflecting (or attenuating)defects have different dimensions and, therefore, to each dimension would correspond an ideal frequency value as far as maximum reflection is concerned. Ideally, one should therefore control the weld by means of several narrow band transducers, each tuned in a particular frequency. Of course, this would be very costly and could arise interpretation problems. It is preferable to employ broad band transducers which, even if slightly less sensitive, can work covering a large frequency band. In addition, broad band transducers have the advantage of an high resolution.

ii) The weld penetration is better detected by means of a narrow band focused transducer with the following characteristics:

- 3/4 in. diameter
- 5 MHz frequency
- 44 mm focusing
- 1.1 mm focal spot

The above mentioned choice takes into account of the reflector type, i.e. the lack of penetration to be ideally considered as a plane reflector, and of the necessity of compromising between the sensivity which requires high frequencies and the noise level which is low with low frequencies.

The examination is performed with the two transducers focused at the tube inner surface (weld root) as follows:

i) For the weld soundness testing the ultrasonic beam is positioned perpendicular to the longitudinal axis (rotation axis) of the tube and possible attenuations of the bottom echo due to detected defects are recorded in A scan. Typical defects of E.B. welds in tubes are, for example, porosities in the zone of overlapping beads.

ii) For the weld penetration testing the ultrasonic beam is positioned with 21° tilt (Fig. 3) so to scan the weld root zone and possible reflections due to lacks of penetration are recorded in A scan. It should be noticed that in E.B. welds lack of penetration defects may just occur at the weld root.

The following calibration blocks are used:

i) For the weld soundness testing: block with three series of trepanned holes as shown in Fig. 4;

ii) For the weld penetration testing: block with two slits obtained by ECM as shown in Fig. 5.

The examination procedure is the following:

1. Calibration of the ultrasonic equipment with the recorder (the minimum detection level shall be ascertained) by means of both the "soundness block" and the "penetration block";

2. 100 per cent weld scanning with a tube rotation of 6 rpm and a longitudinal feed of 0.2 mm per revolution of the two rigidly linked transducers; a complete scanning of the weld zone requires a 10 mm pass;

3. Repetition of the calibration as per 1. in order to verify the calibration constancy of the equipment.

3. INTERPRETATION OF THE RESULTS

Results are interpreted according to the following:

i) Weld soundness (Fig. 6 shows an example of calibration recording)

Attenuation levels, recorded as peak heights, are caused by holes 2.5 mm in depth and 0.8 - 1 - 2 mm in diameter, whereas attenuations of other holes 5 and 7.5 mm in depth are not to be considered being erroneous (higher attenuations due to the side effect of the hole).

Signal repetition (R number) is defined as the number of longitudinal scan passes where the attenuation signal (peak height H) becomes higher than the detection threshold ("zero level") given by the 0.8 mm dia., 2.5 mm in depth hole.

For correct interpretation of the results after the calibration, a table shall be prepared as follows:

Hole dia. (mm)	Hole depth (mm)	Peak height H(mm)	Signal repetition numb. (R number)
0.8	2.5	0	0
	5.0	15*	5
	7.5	21*	6
1.0	2.5	6	4
	5.0	12*	6
	7.5	23*	8
2.0	2.5	34	8
	5.0	41*	10
	7.5	47*	13

* Values not to be considered

In this way one has two different kinds of data:

a) The attenuation level of the bottom echo (actually recorded as peak height) as a function of the flaw reflecting area: with equal reflecting areas maximum attenuation occurs at the weld root.

b) Repetitions, whose number is a function both of the flaw reflecting area (particularly its dimension referred to the longitudinal axis) and the flaw position in the wall thickness (with equal dimensions, the number of repetitions is lower toward the weld root).

In conclusion, one can summarize the situation as follows:

a) With equal reflecting areas but different depth of the flaws in the wall thickness:

Flaw at weld root: Max. peak heigh; Min. repetition number

Flaw at weld surface: Min. peak height; Max. repetition number

b) With different reflecting areas but equal depth of the flaws in the wall thickness:

- Peak heights proportional to the reflecting areas
- Repetition numbers increase with the increasing of the longitudinal dimension of the reflecting areas. The other dimension (circumferential) affects only the permanence time of the attenuation signal.

The evaluation of the flaw equivalent diameter is performed by means of the DAC curves (distance-amplitude curves) shown in Fig. 7A. In order to obtain these curves we have determined the peak heights of the two holes 1 and 2 mm dia., 2,5 mm in depth (H = 6 and 34 mm respectively). A specimen has been prepared by machining one production tube so to have three thickness steps 2.5-5-7.5 mm in addition to the nominal wall

thickness of 10 mm. Moving the transducer focused at the tube inner surface longitudinally on the stepped zones we have recorded the variation of the bottom echo height and obtained the DAC reference curve from the three experimental values H = 97, 92, 89. Assuming that this variation is valid also for the reflecting flaws at different levels in the wall thickness, we have described the two curves having this variation and going through the H = 6 and 34 values determined as mentioned above.

The combined use of these DAC curves and of the Repetition Curves (Fig. 7 B) allows to evaluate the flaw equivalent diameter as described in the following example:

H = 9; R = 4 (Weld F of table on page 8)

The intersections of the line H = 9 with DAC curves (Fig. 7A) determine four possible cases:

- Equiv. dia: 1.0 mm; depth of the flaw: 0 mm (weld root)
- " " 1.1 mm; " " " " 2.3 mm
- " " 1.2 mm; " " " " 3.9 mm
- " " 1.3 mm; " " " " 5.8 mm.

Definite R number values correspond to each of these values (Fig.7B):

- Flaw dia. : 1.0 mm R = 3.0
- " " 1.1 mm R = 4.3
- " " 1.2 mm R = 5.8
- " " 1.3 mm R = 7.9.

R =4.3 is the closest value to the one (R = 4) determined for the flaw under consideration which, therefore, should have an 1.1 mm equiv. dia. and a 2.3 mm depth from the weld root.

ii) Weld penetration (Fig. 8 shows an example of calibration recording).

The detectionthreshold is given by the peak height corresponding to the slit 0.5 mm in depth at the inner surface of the calibration block. The evaluation of the penetration lack is obtained by means of both the peak height and the repetition number.

3. RELIABILITY OF THE EXAMINATION PROCEDURE

The reliability evaluation has been performed on the recorded indications from 150 E.B. welds automatically scanned. Each significant indication has been reexamined by means of RT and PT methods.

Results obtained so far can be summarized as follows:

i) Weld soundness - 15 per cent of the examined welds have shown indications exceeding the "zero level".The checking has been performed by means of the RT method, in this case considered 100 per cent reliable as far as tridimensional flaws is concerned. Some typical examples of relevant comparisons are the following:

Weld	RT indication (mm) RT equiv. dia. (mm)	UT indications H (mm) - R	UT equiv.dia. (mm)	Equiv.dia. change from RT (%)
A	0.9 x 0.8 0.96	7 - 6	1.1(half thick ness)	+ 15
B	1.2 x 1.3 1.41	30 - 5	1.8 (root)	+ 28
C	1.6 x 1.2 1.56	14 - 4	1.2 (root)	- 23
D	1.8 x 1.2 1.66	9 - 13	1.4 (surface)	- 16
E	2.5 x 1.2 1.95	9.5- 13	1.4 (surface)	- 28
F	dia 1.2	9 - 4	1.1 (toward root)	- 8
G	1.8 x 0.5 1.07	12 - 2	1.1 (root)	+ 3

It is concluded that the ultrasonic immersion technique, in the conditions of our experimental setup, can detect tridimensional flaws having an equivalent diameter of 0.8 mm, and that this technique, conceived for a production control, can afford results affected by a maximum error of about 30% for flaws within the 0.8 - 2 mm equiv. dia. range.

ii) Weld penetration - This part of the reliability evaluation is the one that has experienced most difficulties. Various types of defective welded tube specimens have been prepared as a reference for real lack of penetration defects such as:

- specimen with beads increasingly deep from zero (no weld) to the wall thickness (complete penetration)
- four lobes specimen, i.e. a specimen with four lacks of penetration positioned at 90 degrees, and obtained by changing a welding parameter (thickness)
- specimen welded with a tilted beam
- specimen welded with a lack of penetration corresponding to a beam deflection obtained by means of a magnetic field.

According to our experience, the four lobes specimen (Fig. 9) is the most representative. A comparison has been made between the indication of the 0.8 mm slit in the calibration block and those of the four lobes specimen. The transfer of the calibration peak height from the 0.8 mm slit has located on the four lobes specimen recording lacks of penetration that, after cutting the weld apart, resulted to have real values of approx. 1.6 mm.
The limited representativeness of the calibration slits induced us to investigate the only two production welds showing lacks of penetration at the UT examination. Both RT and PT testings have been performed: the radiographic testing detected no defects whereas the liquid penetrant testing detected lack of penetration in one of the two production welds. The cutting apart of this weld evidenced that to the UT evaluated 2.2 mm lack of penetration corresponded a real defect of approx. 3 mm.

In conclusion, it can be stated that the method under development is able to detect lack of penetration defects with a sensitivity which is higher for 0.5 and 0.8 mm calibration slits than for the real defects. Anyway, the method appears to be able to detect lacks of penetration on the order of 1 mm.

4. CONCLUSION

The establishment of adequate acceptance standards for the ultrasonic inspection of E.B. welds by means of automatic immersion techniques suitable to lot fabrication purposes requires, in our opinion, an accurate experimentation to arrive at a correct interpretation of defect indications.

At Fiat TTG ultrasonic examination of stainless steel E.B. welds by the described immersion technique employing two focused transducers is still under development. Anyway, the work done so far allows us to be confident of the reliability of the method. The interpretation of the results appears to be somewhat critical in the detection of very small lack of penetration defects at the weld root whereas the weld soundness control has already reached a satisfactory stage of development.

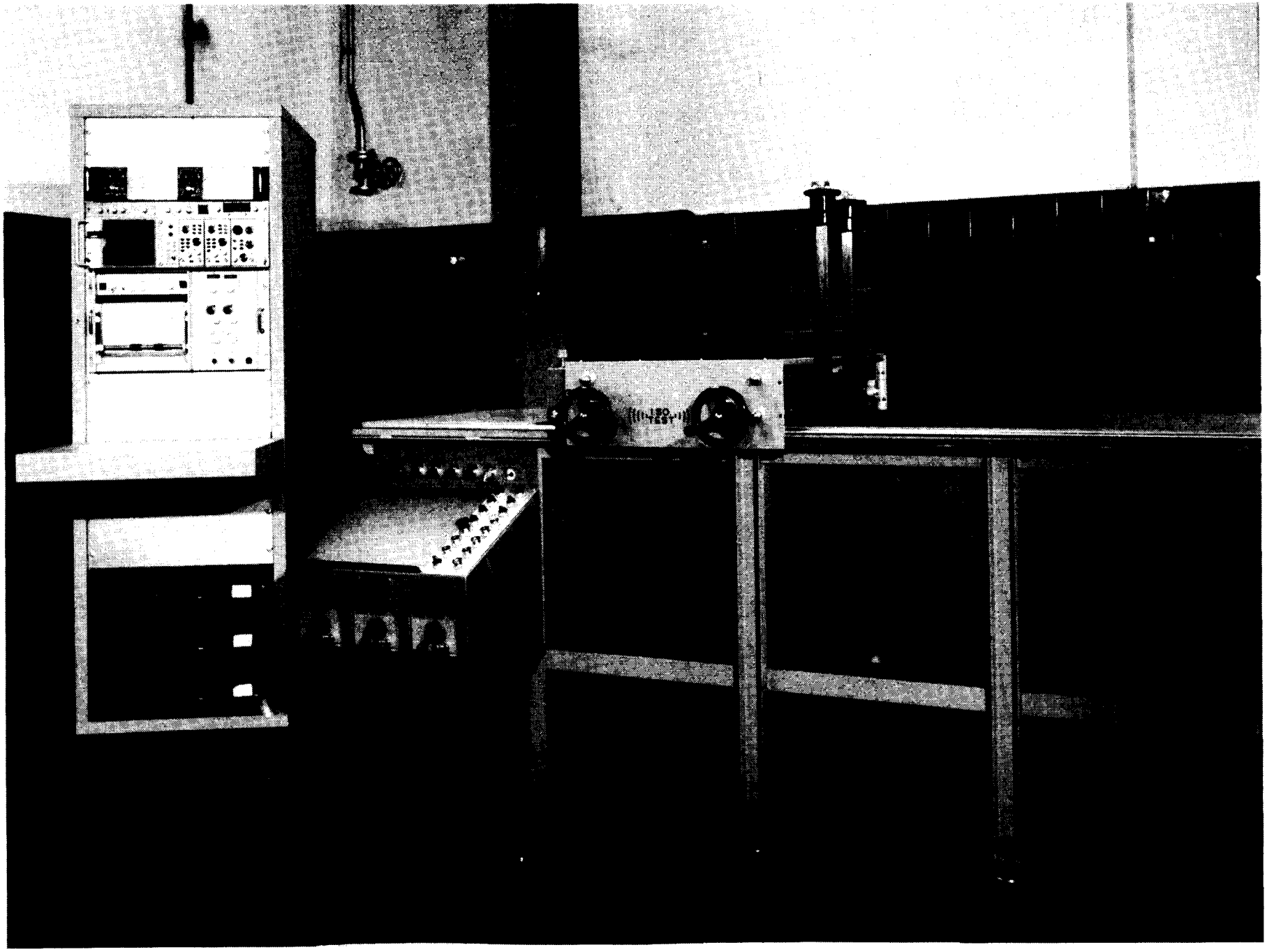


Fig. 1 - Experimental setup for ultrasonic examinations.

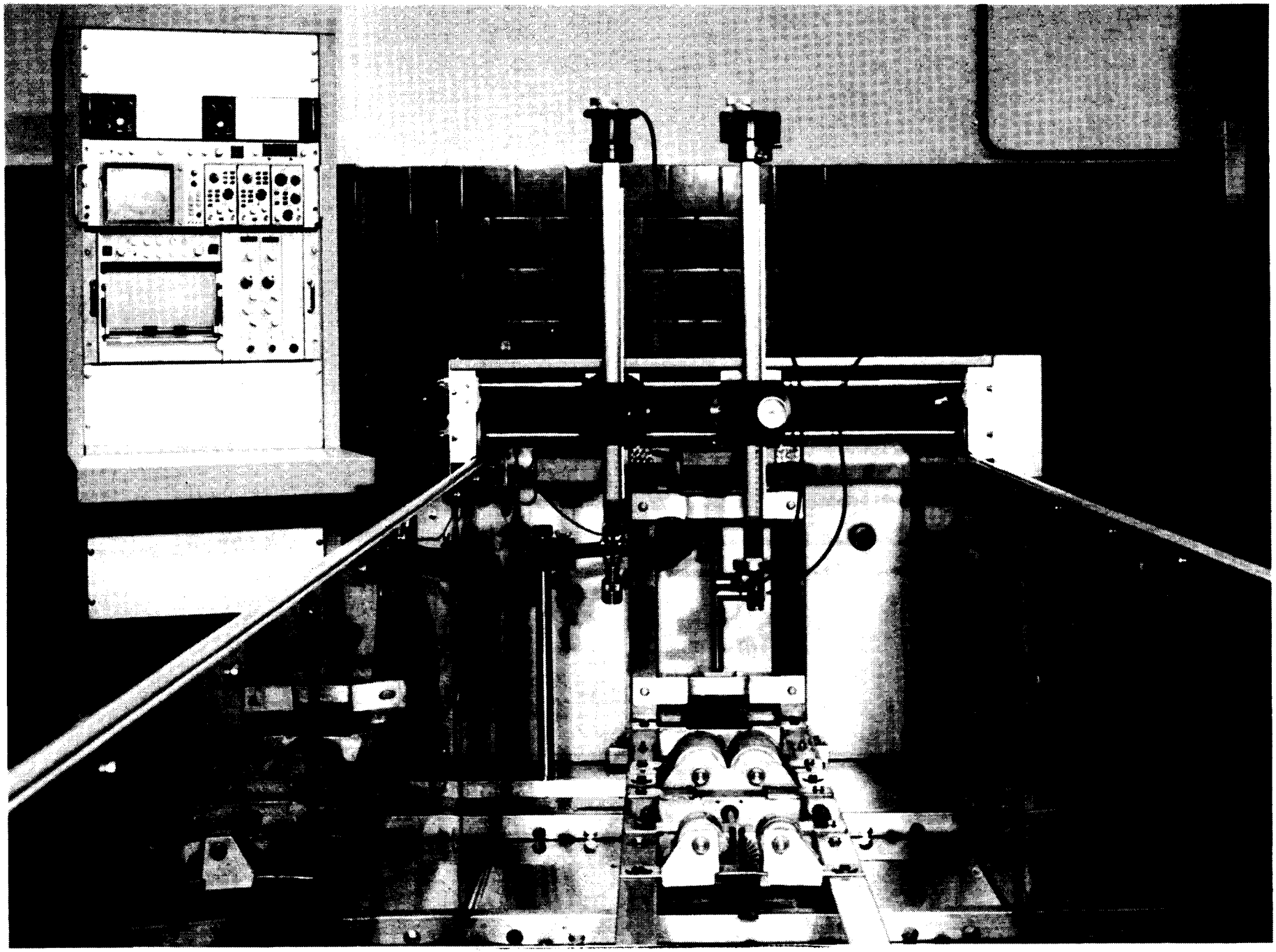


Fig. 2 - Immersion system at the interior of the tank

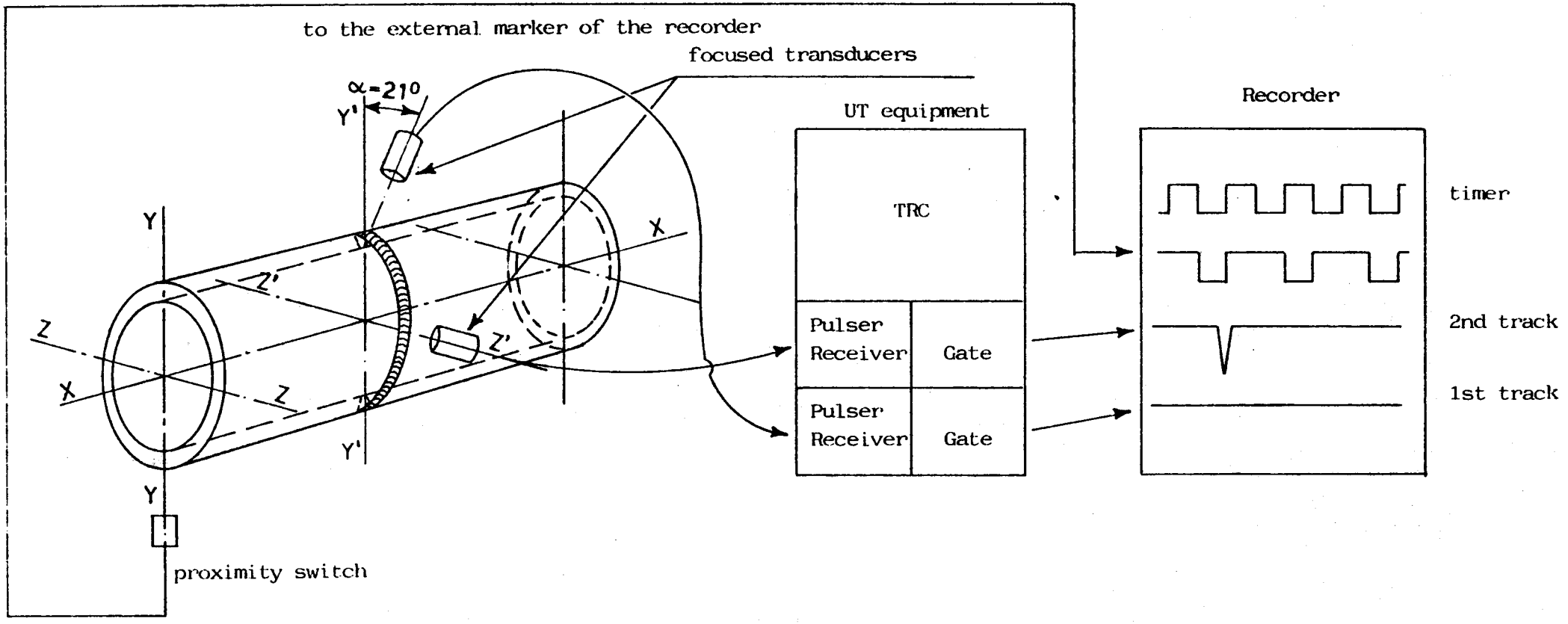


Fig. 3: Experimental setup for the ultrasonic examination of the immersed welded tube.

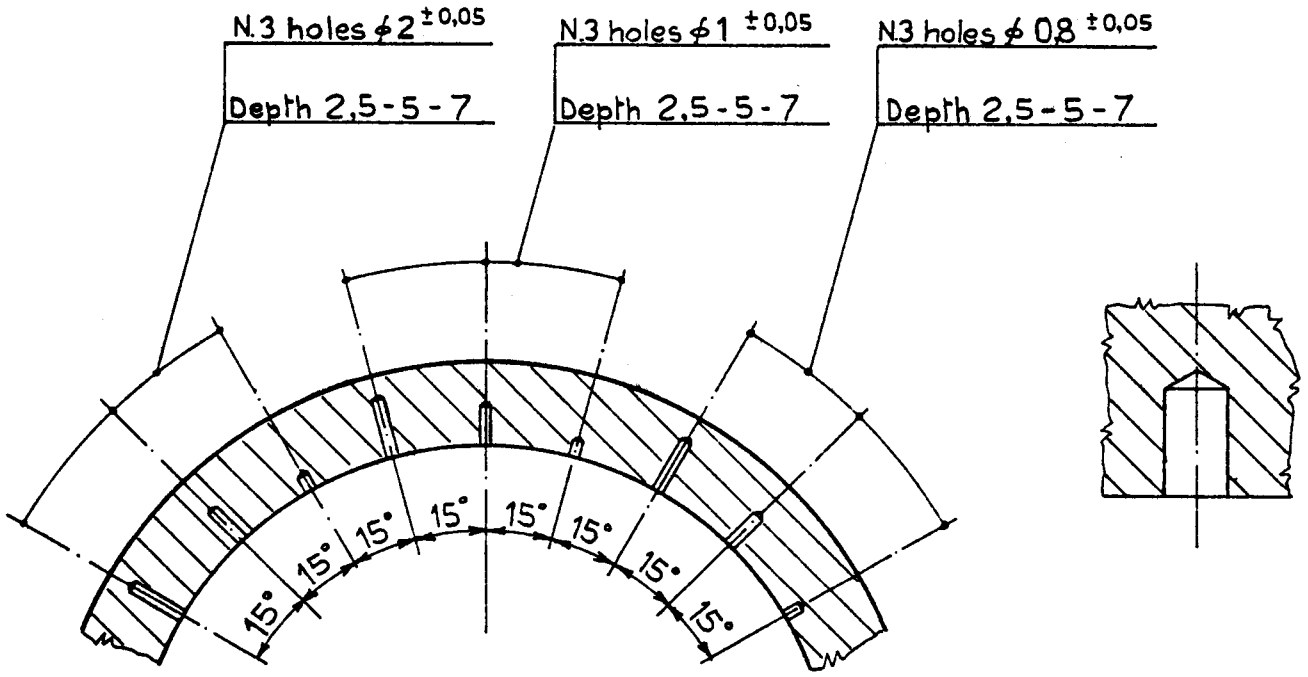


Fig. 4 - Calibration block for the weld soundness testing
(dimensions in mm)

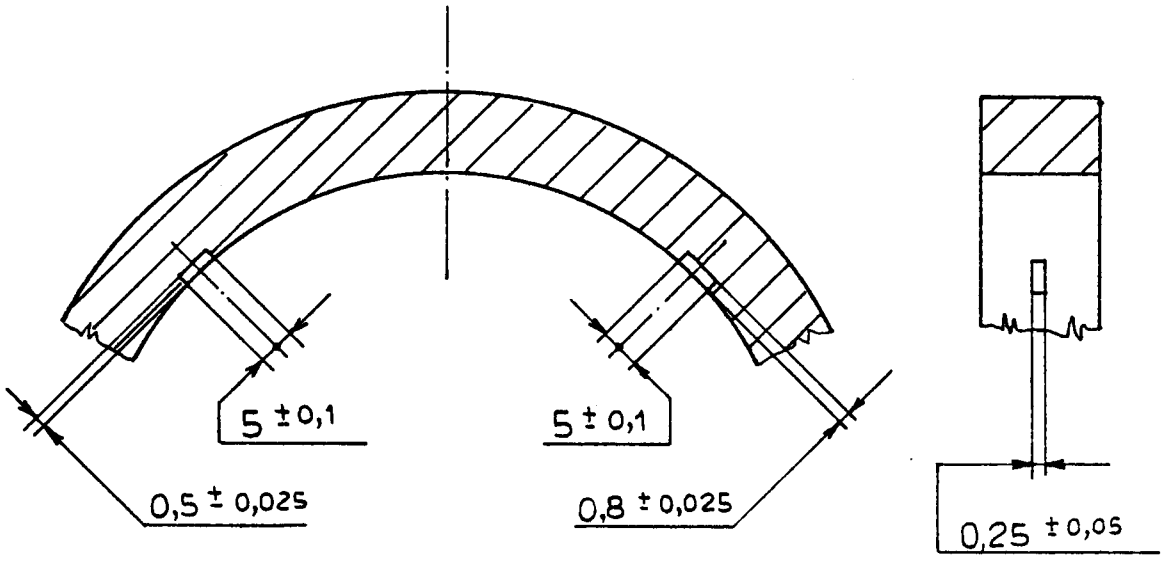


Fig. 5: Calibration block for the weld penetration testing
(dimensions in mm)

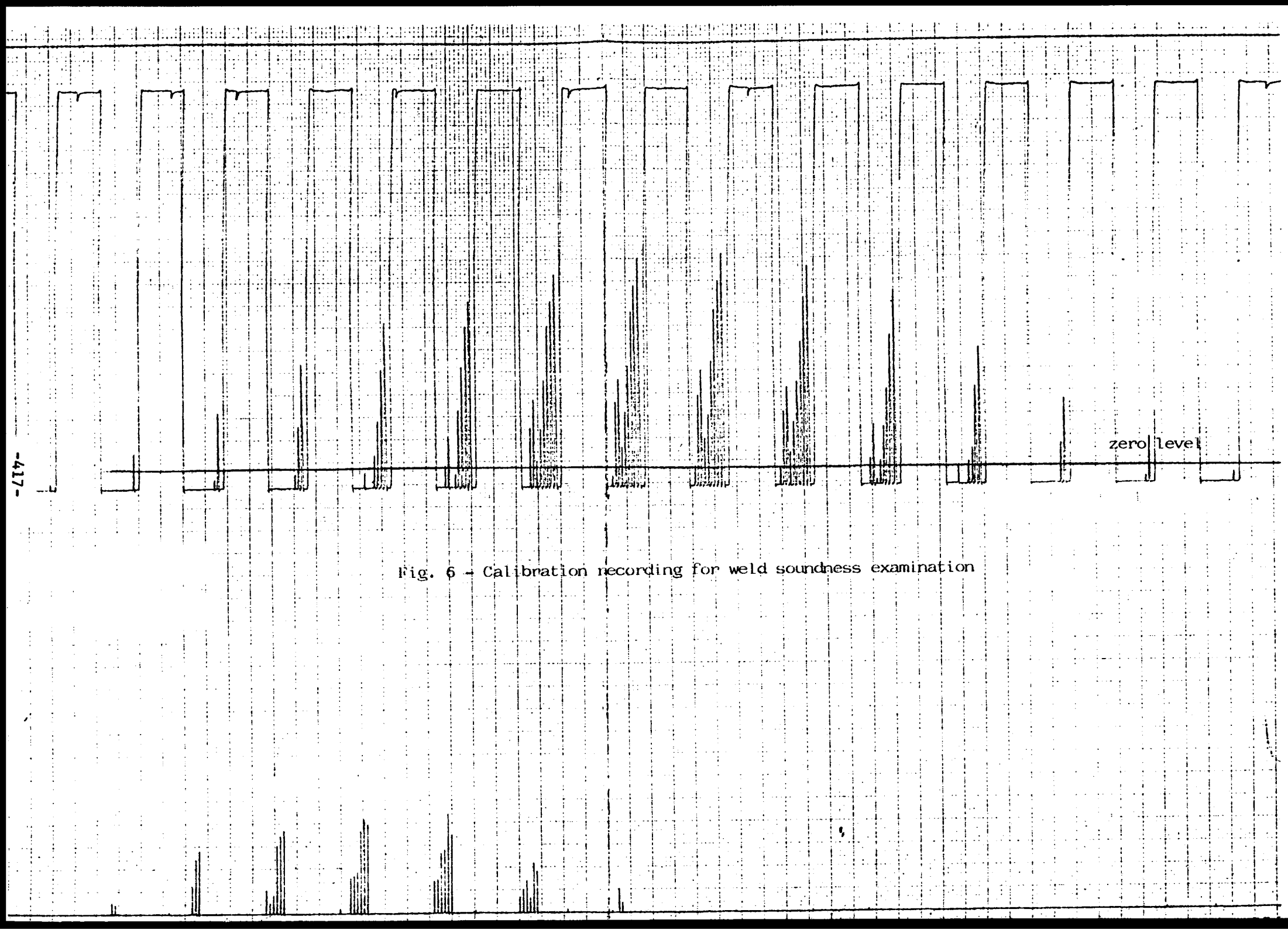


Fig. 6 - Calibration recording for weld soundness examination

Fig. 7 A - Distance Amplitude Curves (DAC)

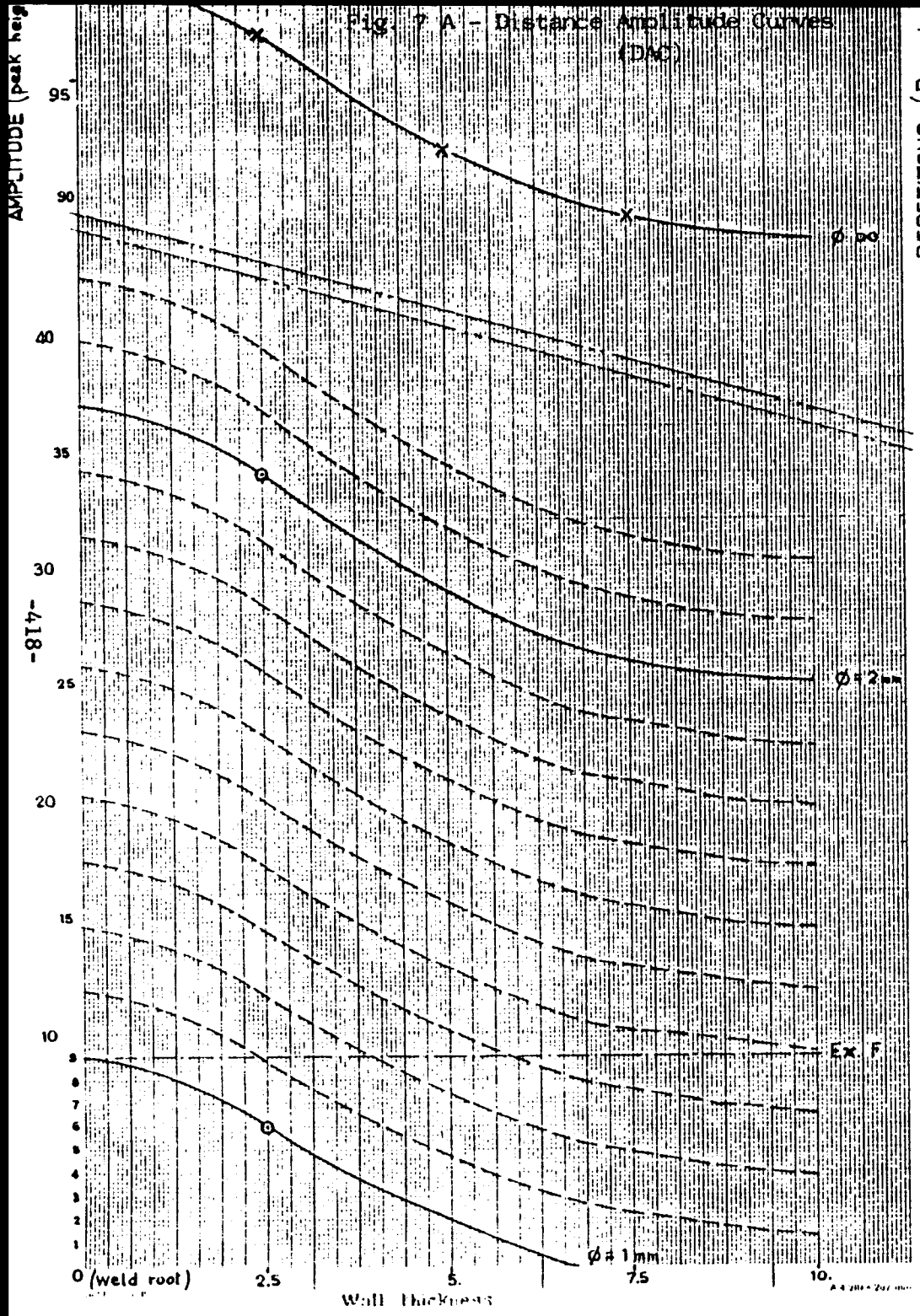


Fig. 7 B - Repetition Curves

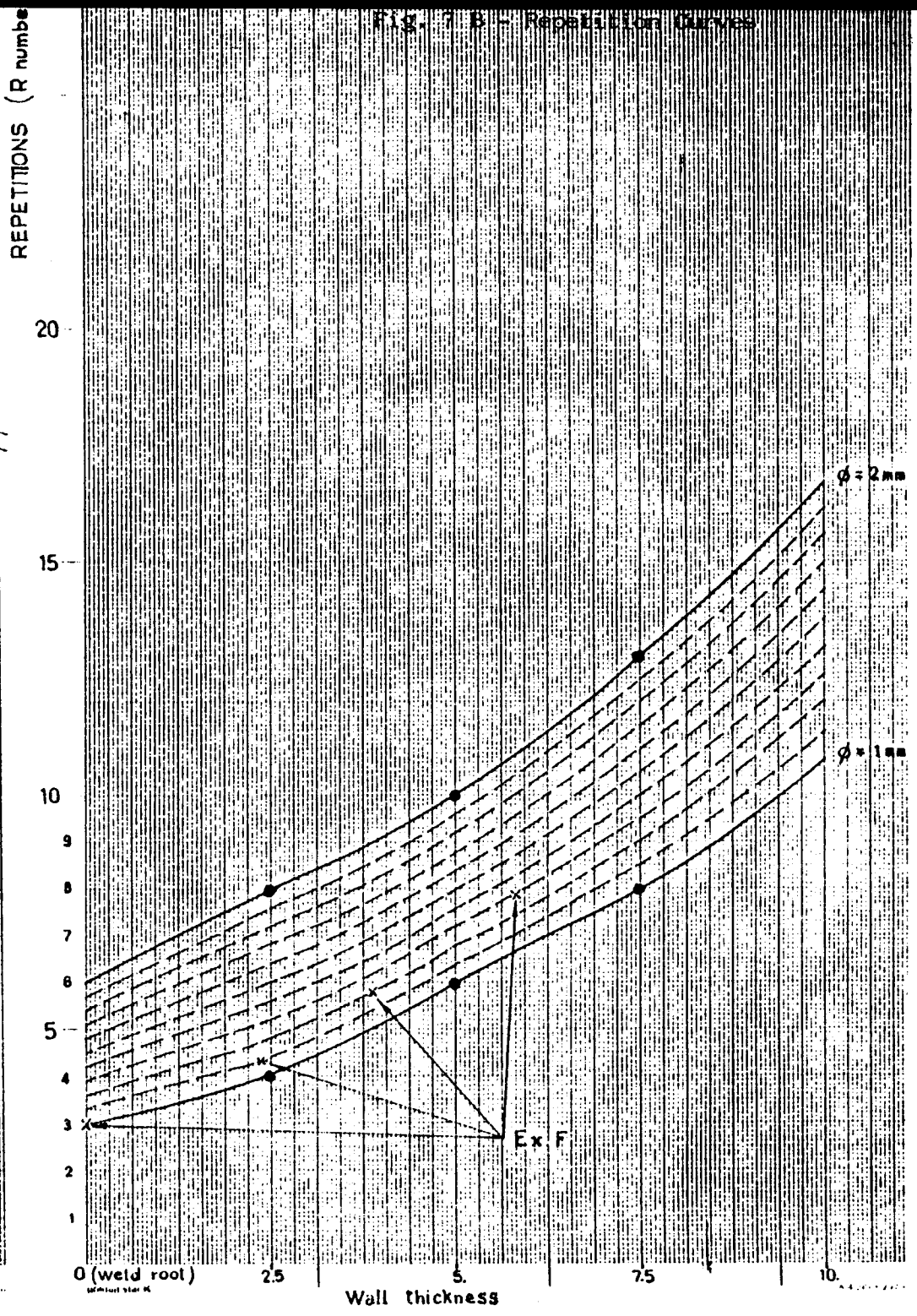
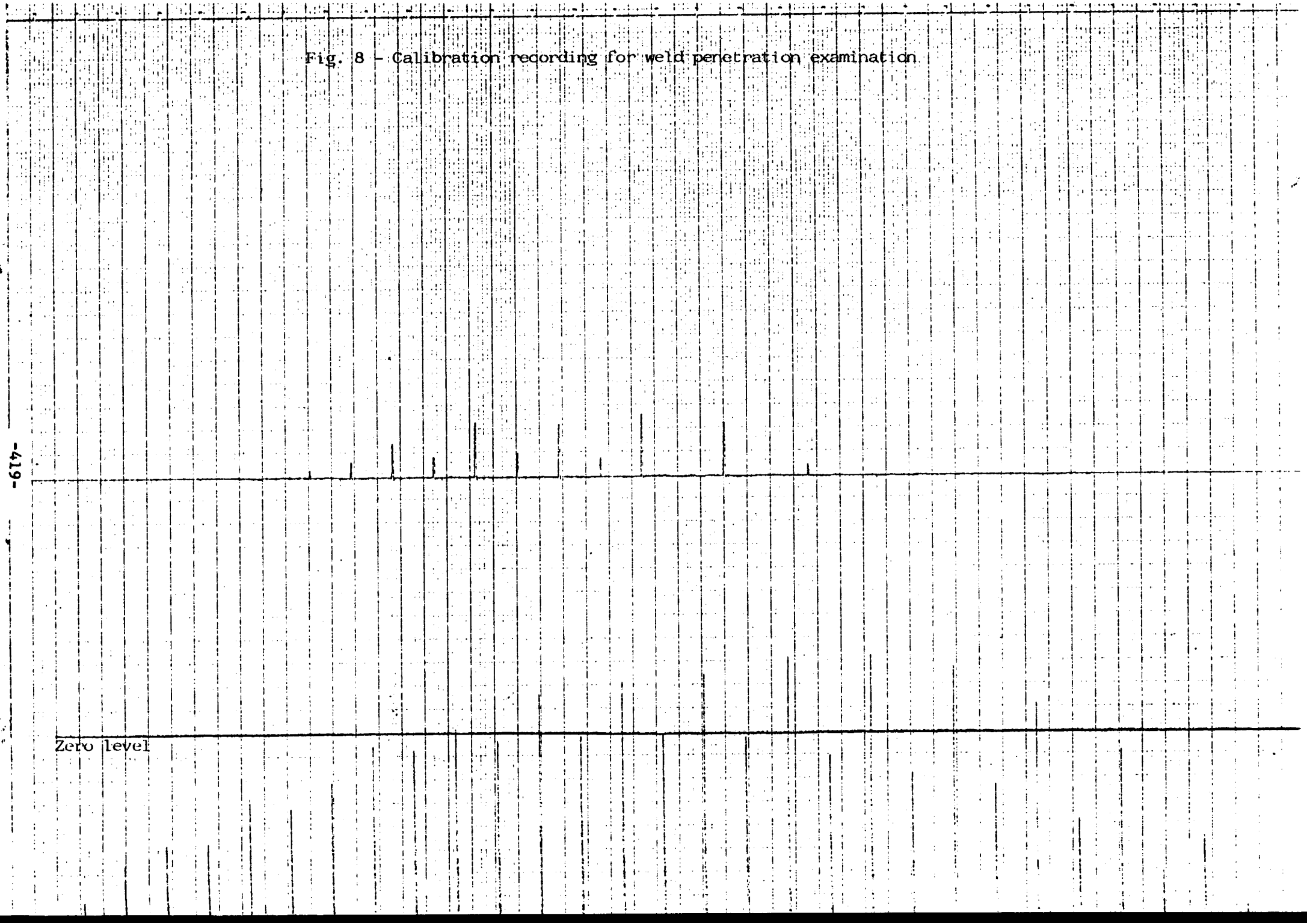


Fig. 8 - Calibration recording for weld penetration examination



L = 5 mm

H_{max} = 4 mm

h_{min} = 2 mm

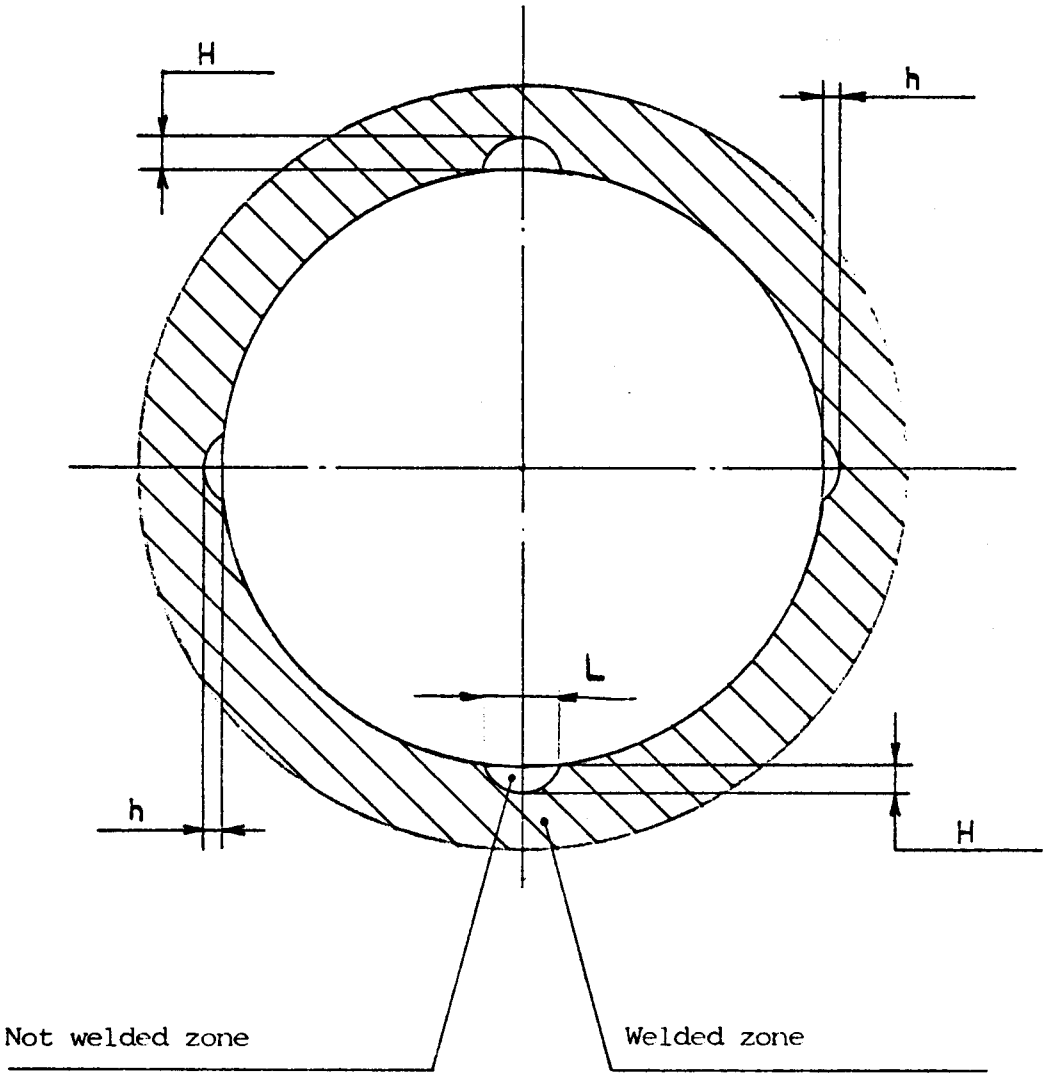


Fig. 9 - Four lobes specimen for the reliability evaluation of lack of penetration defects.

Factors affecting the reliability of the ultrasonic examination of austenitic components

P. CAUSSIN, J. CERMAK, D. VERSPEELT
Association Vinçotte, Belgium

ABSTRACT

Except in special cases (heavy castings for example) the ultrasonic testing technique is already able to reveal major flaws present in austenitic steel components. The detectability of small flaws has been demonstrated, as has surprisingly good location and sizing capability. However it has not been possible until now to draw any general rules about the real performance of the ultrasonic technique in view of the number of problems reported all over the world.

Following some 10 years of research and field practice it appeared that the reliability of ultrasonic inspection of stainless steel items depended mainly of three factors :

(i) The metallurgical microstructure of the test specimen, which complicates the inspection and which is generally unknown at the time of the test;

(ii) The test procedure, which should provide unambiguous results;

(iii) The instrumentation, which needs to be thoroughly checked, at the manufacturing stage and before every inspection.

The effects of these three parameters are discussed and possible solutions for improved reliability drawn.

1. INTRODUCTION

The ultrasonic technique is commonly applied for inspecting austenitic steel components of nuclear and petrochemical installations. It is often the only method practically applicable in nuclear environments for testing welds and pipes of the primary and auxiliary circuits. The latter are generally made of austenitic material which were considered for a long time as particularly difficult to inspect. The particular crystallographic structure of the material and the size of the grains are generally recognized as the major cause of high ultrasonic attenuation (mainly scattering) and low signal-to-noise ratio [1]. In the early 70's custom-made ultrasonic probes showed great promise [2]. At present such probes, using low-frequency refracted longitudinal (compression) waves, make possible the inspection of pieces of 5 to 100 mm in thickness, including centrifugally cast item [3, 4]. However, if the sensitivity level required by most of the codes can be met in most of the cases, if detection of small flaws was demonstrated, if sizing capabilities were shown reasonable regarding the difficulties encountered, very little is known about the reliability of the testing method.

In this presentation, three major parameters affecting that reliability will be discussed.

2. METALLURGICAL STRUCTURE

The manufacturing processes of austenitic steel items generally lead to the appearance of large crystallographic domains. The latter can be larger than the ultrasonic wavelength used for the inspection. In that case, the properties of single crystals will govern the ultrasonic propagation [5, 6].

In welds these grains have been shown to grow with a preferential crystallographic direction (< 100 >) along the heat dissipation lines. From that process results a peculiar texture with properties similar to the ones of single crystals. These properties affect both the apparent attenuation and the velocities of ultrasonic waves. An example is shown in figure 1 where both the longitudinal wave attenuation at 2.25 MHz (0 dB for ferritic steel) and the velocity (5940 m/s for ferritic steel) was plotted against the orientation of the ultrasonic beam. In that case the grains were mainly oriented at 35° from the 0° reference. That diagram shows a periodical variation of both parameters and a good correlation between them. In figure 2 similar results are compared for samples with grains larger and smaller than the wavelength of longitudinal waves. In the second case, the variations were much less important, which revealed that the appearance of such fluctuations depends on the grain size to wavelength ratio. A detailed analysis of these results will be published elsewhere.

The austenitic steel microstructure not only causes fluctuations of both ultrasonic attenuations and velocities but also affects the frequency content of the ultrasonic signals and the beam structure. Figure 3 shows frequency spectra of bottom wall echoes in pieces in carbon and cast austenitic steel of 60 mm in thickness. It can be seen that in the austenitic casting the high frequencies were much more attenuated than in the ferritic steel.

The same samples were used to measure the structure of the ultrasonic beam after 60 mm of carbon and cast austenitic steel. The plots obtained with an electrodynamic sensor are presented in figure 4. Obviously the austenitic casting has severely distorted the ultrasonic beam.

These results not only demonstrate that the austenitic structure can drastically affect the parameters of the ultrasonic examination but also that their importance can be evaluated when knowing the microstructure of the piece to be inspected. However a weld can join very different microstructures as in the example of figure 5 where a multi-pass weld connects a casting to an extruded pipe (ASME 316). Furthermore, knowing the grade of the material, the elaboration process and the manufacturer does not mean that the microstructure is known. Figure 6 shows the microstructure of two centrifugally cast ASTM A351 - CF8M steels of the same thickness made by the same manufacturer. It is obvious that the resulting microstructures were quite different.

3. TESTING PROCEDURE

It is generally agreed that the reliability of an ultrasonic inspection strongly depends on the testing procedure. The latter must involve adequate probes and unambiguous evaluation methods, and also take account of geometrical problems.

Since about 10 years probes specially designed for testing austenitic items have been intensively developed and are now available on the market. Figure 7 shows an example of the signal-to-noise ratio improvement gained with a home-made probe when testing centrifugally cast pieces. In practice, the difficulty of inspecting austenitic material has led to the development of more than 20 different probes adapted to the numerous test conditions encountered when inspecting a structure as complex as the primary and the auxiliary circuits of nuclear plants. Besides these, standard probes are also used.

Having the appropriate probe is the first step when planning a test, the second step is to elaborate a testing procedure which will guarantee that known testing problems are solved. As an example, let us consider the preparation of the search for undercladding cracks. Generally the probe recommended for such an inspection is a Transmitter - Receiver (TR) probe using longitudinal waves refracted at 70° and having a beam crossing point positioned at the average cladding to base material interface (fig. 8). In such a test, the inspector should be able to discriminate an echo of a crack (rejectable) and of a cladding defect (usually acceptable). A possibility for solving that problem is to use a straight beam probe designed for inspecting the cladding and measuring its thickness. In that case the results gained with both probes can be combined for improving the echo interpretation. As a matter of fact, a combination of probes has always augmented the reliability of the ultrasonic examination and should be applied whenever possible.

Another problem mainly relevant to the inspection of pipe welds is the geometry of the weld. Usually, achieving the necessary strength of a weld does not require very accurate geometry of the weld assembly. In practice, large deviations can be tolerated. This can lead to a situation such as the one described in figure 9, where the as built weld profile significantly differs from the initial design. In such a case, geometrical echoes can be generated on surface discontinuities and will disturb the inspection, complicating the echo evaluation, extending the inspection time requested, and tiring the inspectors. These consequences can only have a negative effect on test reliability.

4. INSTRUMENTATION

4.1. Checking program

Assessing the performances and the reproducibility of an inspection requires that the instrumentation meet the specified standard and be stable over a long period of time. In ultrasonic testing the first problem comes from the fact that very little is specified for the instrumentation although variabilities were known and reported [7].

Five years ago a house program was initiated to evaluate the actual variabilities of ultrasonic instrumentation. For that purpose, a special equipment was designed and acquired. Since then a series of characteristics of probes, cables and electronic circuits (hereafter called apparatus) are regularly checked. The same equipment is used for checking at the construction stage the special probes made for inspecting austenitic materials. The extension of the checking program is indicated in table 1.

In this presentation only indicative results of that program will be described.

4.1.1. Beam characteristics

The angular characteristics of a single crystal angle probe are measured in a semi-cylindrical steel block of 100 mm in radius. The probe under evaluation is coupled to the flat axial surface and an electrodynamic sensor scans the cylindrical surface, measuring the energy distribution in the plane of incidence and in the axial plane perpendicular to the latter. A typical result of a defective 45° angle probe is indicated in figure 10. Not only an error in the refraction angle of 2.5° was measured but also a squint angle of 4° as well as a reinforcement of the secondary lobe.

The beam characteristics of T.R. probes are measured in triangular steel blocks using also an electrodynamic sensor and custom-made recording system. The set-up used is indicated in the insert of figure 11. That figure shows the energy distribution when the beam crossing point is accurately positioned. In cases where the crystals were not accurately mounted in the probe, beam divergences similar to the one indicated in figure 12 are measured. Such a probe cannot be accepted for ultrasonic testing.

4.1.2. Apparatus

The apparatus check covers a large number of items which requires special procedures. As an example, two disturbing results will be mentioned as examples of characteristics which must be avoided.

The first example concerns the frequency sensitivity of the amplifier. Whatever that sensitivity, it can be assumed that it is independent of the gain setting used. However, in practice, situations like the one described in figure 13 can be found. In that case the frequency bandwidth was shortened when the gain increased.

In the second example of figure 14, it is shown that the complex input impedance of the amplifier can vary not only from one apparatus to another but also in a single apparatus depending on the amplifier setting.

4.1.3. Instrument

Is called instrument the assembly of apparatus, probe and cable. The resulting characteristics of an instrument depend on the characteristics of its individual components. A proper operation would theoretically require a reasonable impedance matching between these three components. In practice it appears that very little attention is paid to that kind of requirement. Indeed both the input and output impedance of the apparatus vary with the setting used as shown above. The result is that major parameters of an ultrasonic inspection such as beam characteristics, testing frequency, resolution, etc..., can be modified without notice. As an example, figure 15 shows what happened to the waveform and the frequency spectrum of an echo when the apparatus input impedance was modified. This modification corresponds to two different power settings of the apparatus. It can be seen that the real effect of that setting is to modify the harmonic content in the signal instead of applying more or less power to the probe.

4.2. Influence of instrumentation characteristics on inspection performances and reproducibility

If fluctuations of instrumentation characteristics can be measured in the laboratory, it is difficult to quantify a priori which will be their influence on the performances and the reproducibility of an inspection. To get a preliminary idea of that influence, an exploratory program was initiated. For that program a special apparatus was built. The main advantage was that three parameters - the output impedance, the input impedance and the frequency response - can be independently varied as indicated in table 2. Two straight beam probes were selected together with two connection cables for each. One cable had the nominal length and the other half that length. The combination of these characteristics gave for each probe 36 possible configurations.

To evaluate the influence of these characteristics, a plate made of austenitic steel, 35 mm thick, was selected. Each probe was permanently coupled to the block in order that when changing the apparatus settings or the cables the probe coupling did not affect the results.

With that set-up, two tests were made. The first one concerned the gain necessary with each configuration to obtain a bottom wall echo at 80 % of screen height (SH). For the second one, the transfer adaptation between the austenitic plate and a standard carbon steel calibration block of the same thickness was measured.

The results of the sensitivity measurements are indicated in figure 16 for both probes. Differences in the range of 15 to 20 dB can be seen. Furthermore, the high damping probe was not operational with a capacitive load. For the rest, the major influence came as expected from the frequency response. However, differences of 6 to 10 dB were also accountable to the other variables.

With the transfer measurements it is generally expected to determine the difference in ultrasonic attenuation in two different blocks. In that case, this measurement would have had to give equal results for all 36 configurations. That was not confirmed as indicated in figure 17 where differences of 4 dB were recorded.

Further details on that program will be published elsewhere.

5. CONCLUSION

In this presentation attention has been drawn to three parameters which obviously can affect the reliability of ultrasonic inspection of austenitic steel components.

If it is now recognised that the metallurgical microstructure of an austenitic piece plays a definite role in the inspectability of that piece, it has also been shown that it is difficult to know which is exactly that structure at the time of inspection. To efficiently use the laws of ultrasonic waves behaviour in an austenitic structure it would therefore be desirable to be capable of measuring the actual characteristics of the tested structure. Alternatively, a solution could be found by developing testing methods less sensitive to the effect of microstructure.

To assess both the efficiency and reliability of an inspection, the testing procedure must be carefully prepared and take account of known possible problems. However, it is not always possible to have a previous knwoledge of the exact geometry of a weld profile due to actual construction tolerances. In these circumstances, a conservative evaluation of results should be made. It is thus recommended that for new plants more attention be paid to weld preparation. Secondly, means should be found to measure in situ the real geometry as an aid both for the elaboration of the testing procedure and for the evaluation of results.

The third parameter analysed is the effect of equipment characteristics. It was shown that the equipment must be carefully checked if the main parameters of the inspection have to be known. If not, successive inspections will be carried out with equipment objectively different but nominally identical. It was indicated that these differences affect the inspection results. To avoid such interference, it is recommended to prepare, on an international basis, standards on both the instrumentation characteristics and the methods to measure them.

REFERENCES

1. Ultrasonic testing applied to austenitic steel
   P. CAUSSIN
   Proceedings of the SMIRT-5 Post Conference Seminar on Non-destructive Examination, Berlin, FRG, August 22, 1979.

2. Ultrasonic testing of austenitic steel castings and welds
   J-P. PELSENEER, G. LOUIS
   Br. J. NDT, July 1974, pp. 107-113.

3. Field efficiency of ultrasonic testing of austenitic steel components
   P. CAUSSIN, J. CERMAK
   Proceedings of Nuclex 78, Basle, Switzerland, October 2-9, 1978.

4. Performances of the ultrasonic examination of austenitic steel components
   P. CAUSSIN, J. CERMAK
   Proceedings of the I Mech E Conference on Periodic Inspection of Pressurized Components, London, Great Britain, May 8-10, 1979, paper C49/79.

5. Ultrasonic inspection of austenitic welds
   B.L. BAIKIE, A.R. WAGG, M.J. WHITTLE, D. YAPP
   Proceedings of the IAEA, IWGFR on in-service inspection, Bensberg, FRG, March 1976.

6. Effects of microstructure on ultrasonic examination of stainless steel
   D.S. KUPPERMAN, K.J. REIMANN
   Proceedings of the CSNI - Specialist Meeting on the Ultrasonic Inspection of Reactor Components, Risley, Sept. 27-29, 1976.

7. The calibration of equipment used in ultrasonic flaw detection in steel
   R.D. LEDGE, H.L. CARSON
   NDT, August 1967, pp. 35-44.

TABLE 1 : INSTRUMENTATION CHECKING PROGRAM

. Probes : - Complex impedance versus frequency
- Frequency spectrum
- Beam characteristics

. Cable : - Capacitance
- Characteristic impedance

. Apparatus : - CRT : Distortion
- Generator : - Pulse characteristics
- Output impedance
- Time base : - Linearity
- Amplifier : - Input impedance
- Frequency response
- Linearity
- Gain accuracy
- Dead zone of main bang and echoes
- Resolution
- Sensitivity and dynamic range

. Instrument : - Apparatus + cable + probe
- Sensitivity
- Characteristic echo

TABLE 2 : CHARACTERISTICS INDEPENDENTLY VARIABLE

Apparatus

- Output impedance :	12.5, 25.-, 50.- Ohm
- Input impedance :	Resistive : 50.- Ohm
	Capacitive : 800.- Ohm at 2.- MHz
- Frequency response :	Low Pass : 0.65 - 2.25 MHz (-3 dB)
	High Pass : 1.25 - 4.45 MHz (-3 dB)
	Wide Band : 0.29 - 9.76 MHz (-3 dB)

Cable

- Nominal length
- Half nominal length

Probes

Straight beam :

- 4 MHz, 10 mm dia, low damping
- 2.25 MHz, 25.4 mm dia, high damping

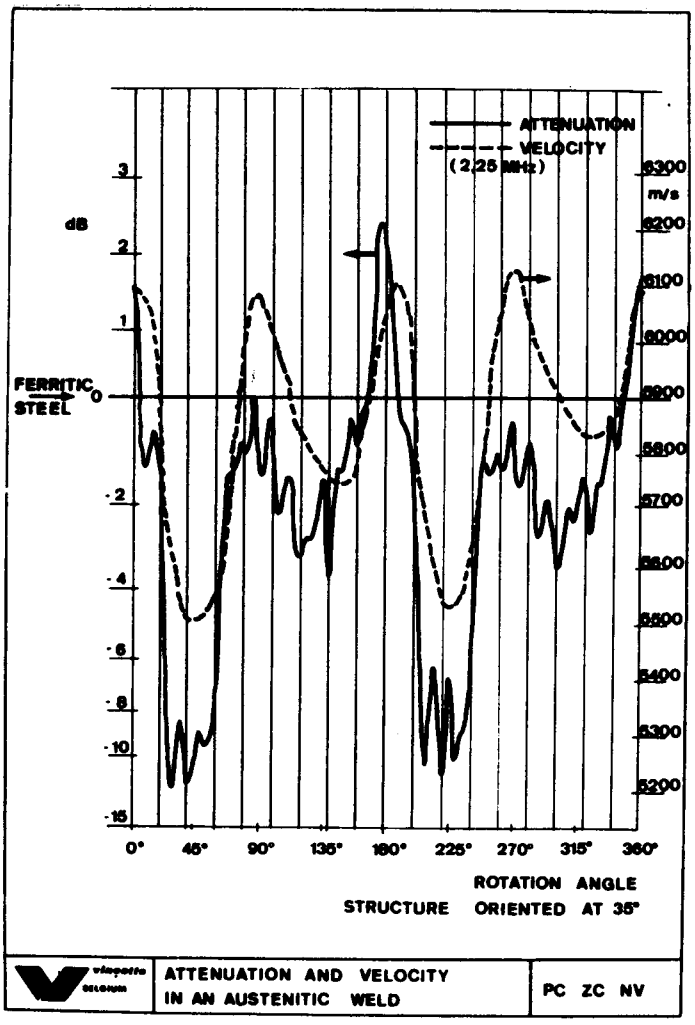

ATTENUATION
VELOCITY
(2,25 MHz)
dB
m/s
FERRITIC STEEL
3
2
1
0
-2
-4
-6
-8
-10
-15
6300
6200
6100
6000
5900
5800
5700
5600
5500
5400
5300
5200
0°
45°
90°
135°
180°
225°
270°
315°
360°
ROTATION ANGLE
STRUCTURE ORIENTED AT 35°
ATTENUATION AND VELOCITY IN AN AUSTENITIC WELD
PC ZC NV

Fig.1

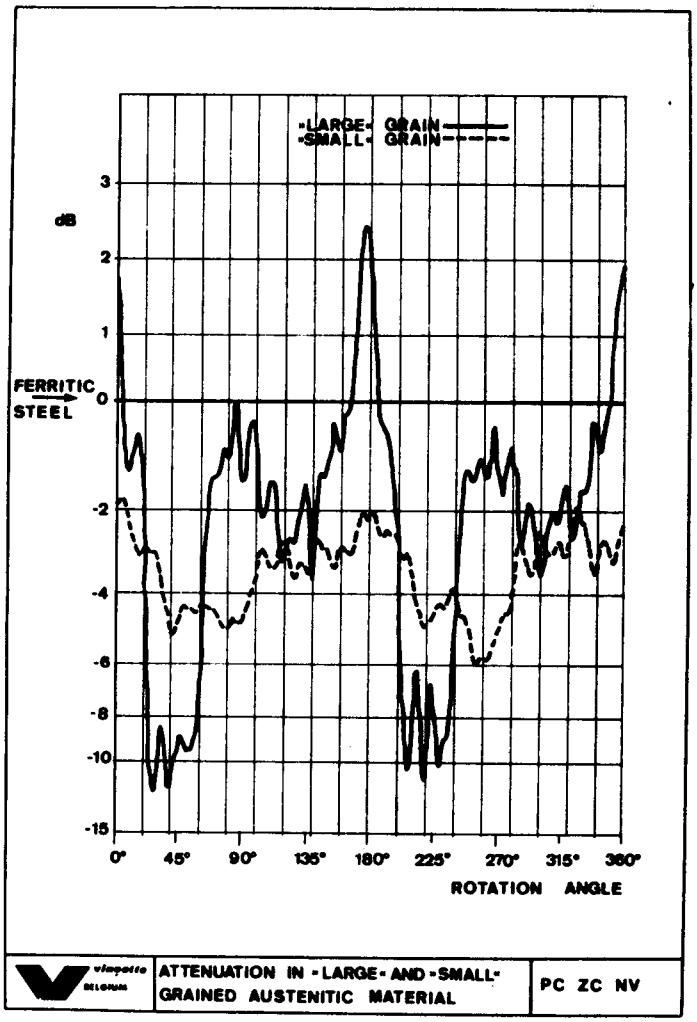
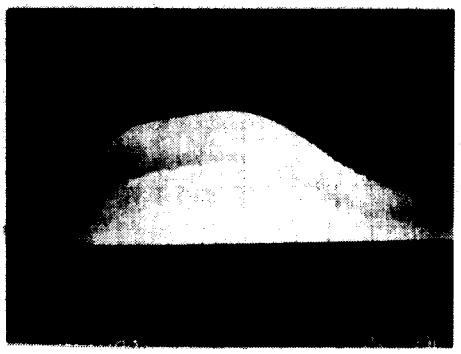
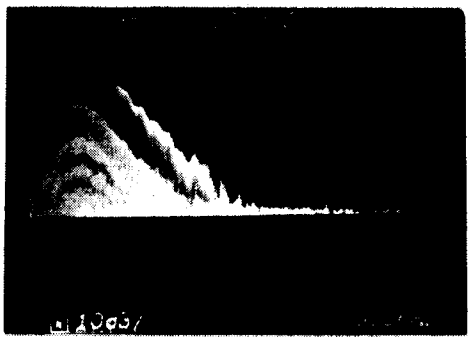

-LARGE- GRAIN
-SMALL- GRAIN
dB
FERRITIC STEEL
3
2
1
0
-2
-4
-6
-8
-10
-15
0°
45°
90°
135°
180°
225°
270°
315°
360°
ROTATION ANGLE
ATTENUATION IN -LARGE- AND -SMALL- GRAINED AUSTENITIC MATERIAL
PC ZC NV

Fig.2



a



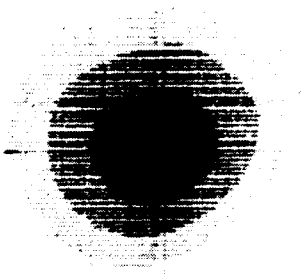
b

Bottom wall echo spectrum analysis for a 25.4 mm dia., 2.25 MHz normal beam probe for 60 mm of metal path.

a. Fine grain ferritic steel

b. Centrifugally cast austenitic steel

vinçotte	Figure 3	PC ZC NV



a



b

IO mm

IO mm

Beam spread of a 25.4 mm dia., 2.25 MHz normal beam probe at 60 mm of metal path. Limits at -2, -6 and -I4 dB drop.

a. Fine grain ferritic steel

b. Centrifugally cast austenitic steel

vinçotte	Figure 4	PC ZC NV



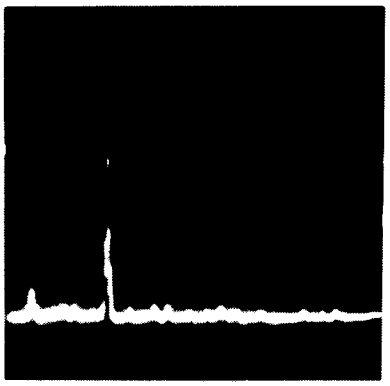
Macrograph of a 35 mm thick butt weld. Left : ASME TP3I6 extruded pipe, right : ASTM A35I-CF8M cast pipe

vinçotte	Figure 5	PC ZC NV

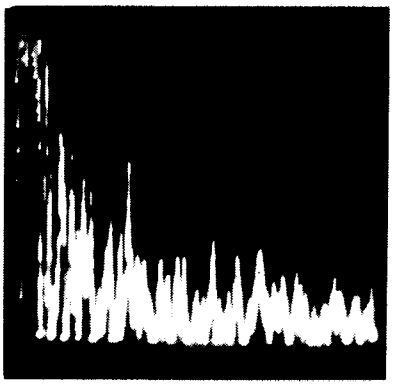




Full thickness macrographs of centrifugally cast austenitic steel pipes, 800 mm diameter, 62 mm thick. Material ASTM A35I-CF8A. (Internal surfaces at top of macrographs, external surfaces at bottom)



a



b

Echoes from a 4.7 mm diameter, 30 mm deep hole drilled in a centrifugally cast block.

a. longitudinal wave, I MHz, 45° angle probe

b. standard, 2 MHz, 45° angle probe

vinçotte	Figure 7	PC ZC NV

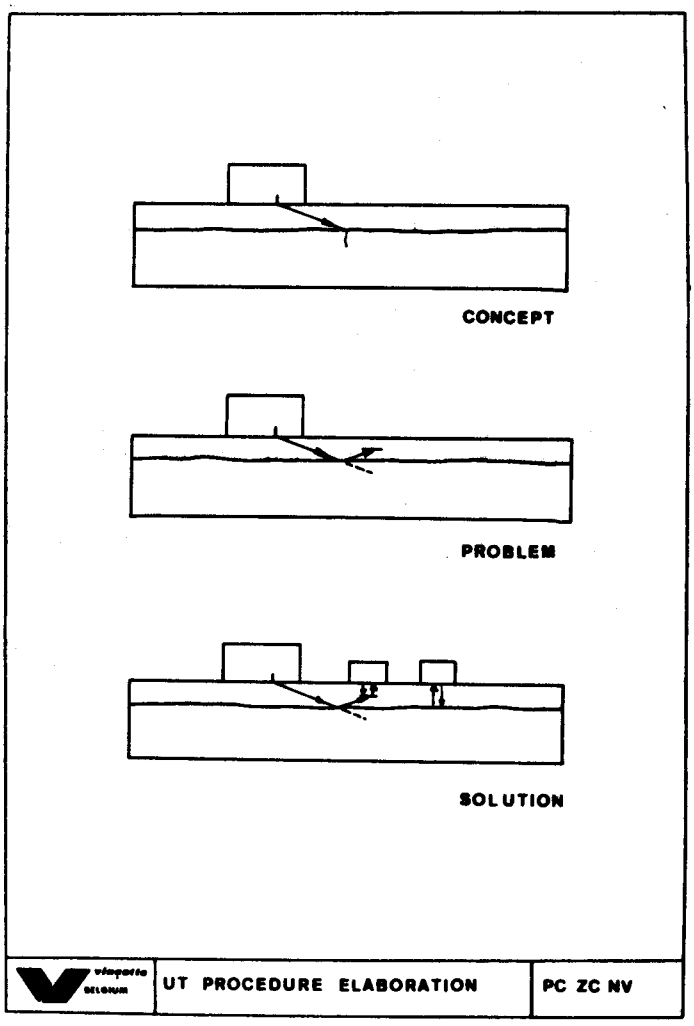

CONCEPT
PROBLEM
SOLUTION
UT PROCEDURE ELABORATION
PC ZC NV

Fig. 8

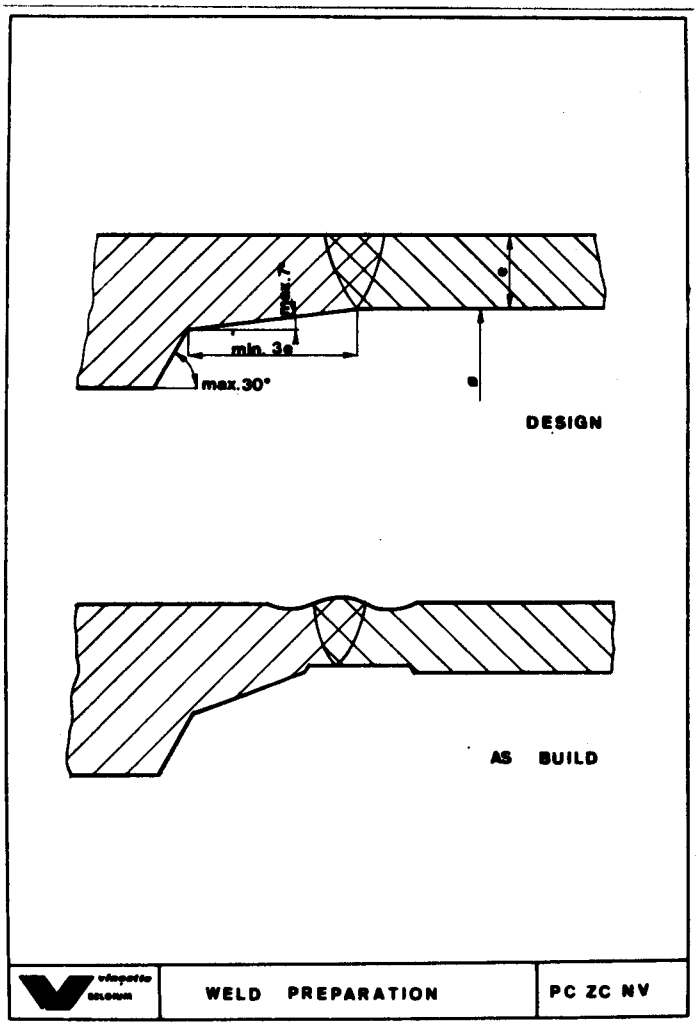

min. 3e
max.30°
e
DESIGN
AS BUILD
WELD PREPARATION
PC ZC NV

Fig. 9

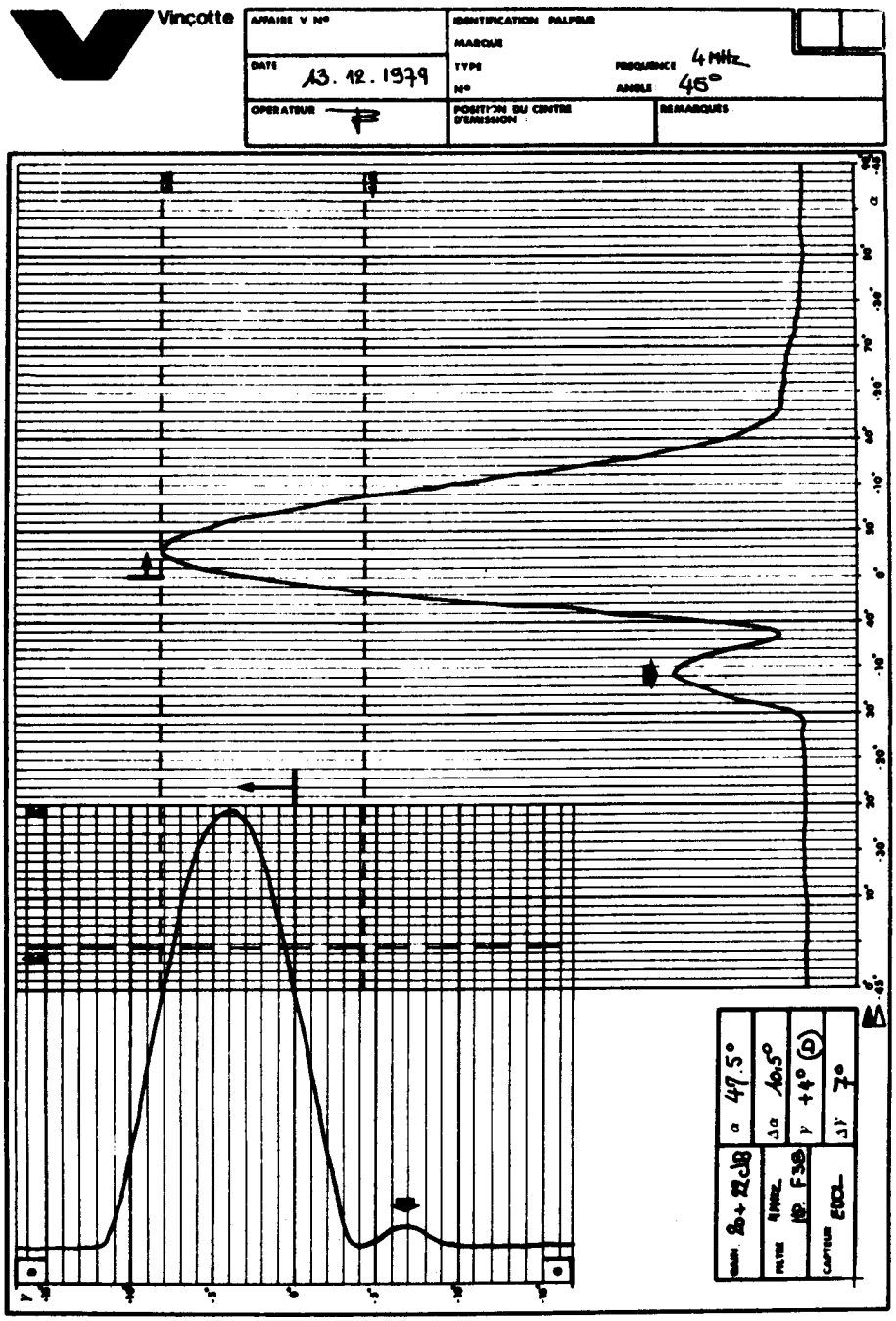
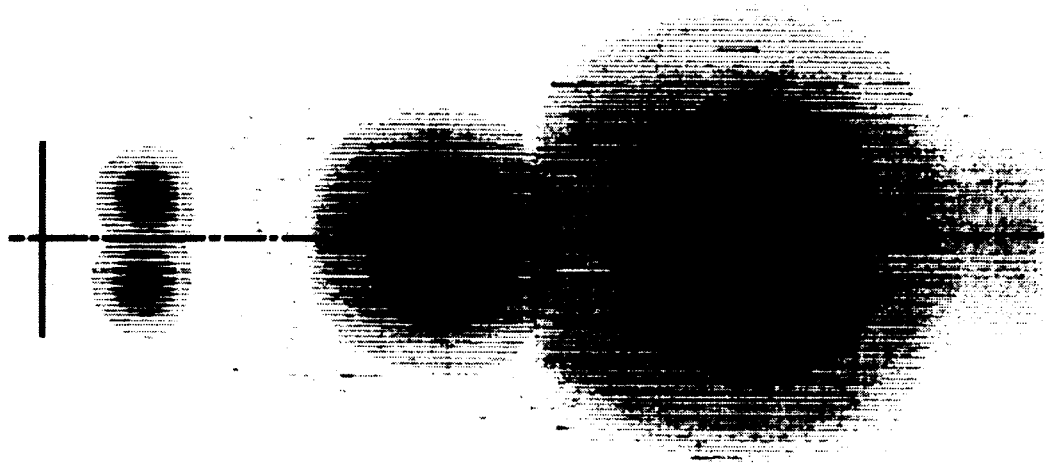

Vinçotte
AFFAIRE V N°
IDENTIFICATION PALPEUR
MARQUE
DATE
13.12.1979
TYPE
FREQUENCE 4 MHz
N°
ANGLE 45°
OPERATEUR
POSITION DU CENTRE D'EMISSION
REMARQUES
α 47.5°
Δα 10.5°
γ +4° (D)
Δγ 7°
GAIN 20+12dB
FILTRE 4 MHz
MP F36
CAPTEUR E80L

Fig.10

SE PROBE , 45°, LONGITUDINAL WAVES , 1MHz



D(mm) 42 122 207

10mm

vinçotte BELGIUM	CORRECT BEAM CARACTERISTICS	PC·ZC·NV

Fig. 11

SE PROBE , 45 , LONGITUDINAL WAVES , 1MHz

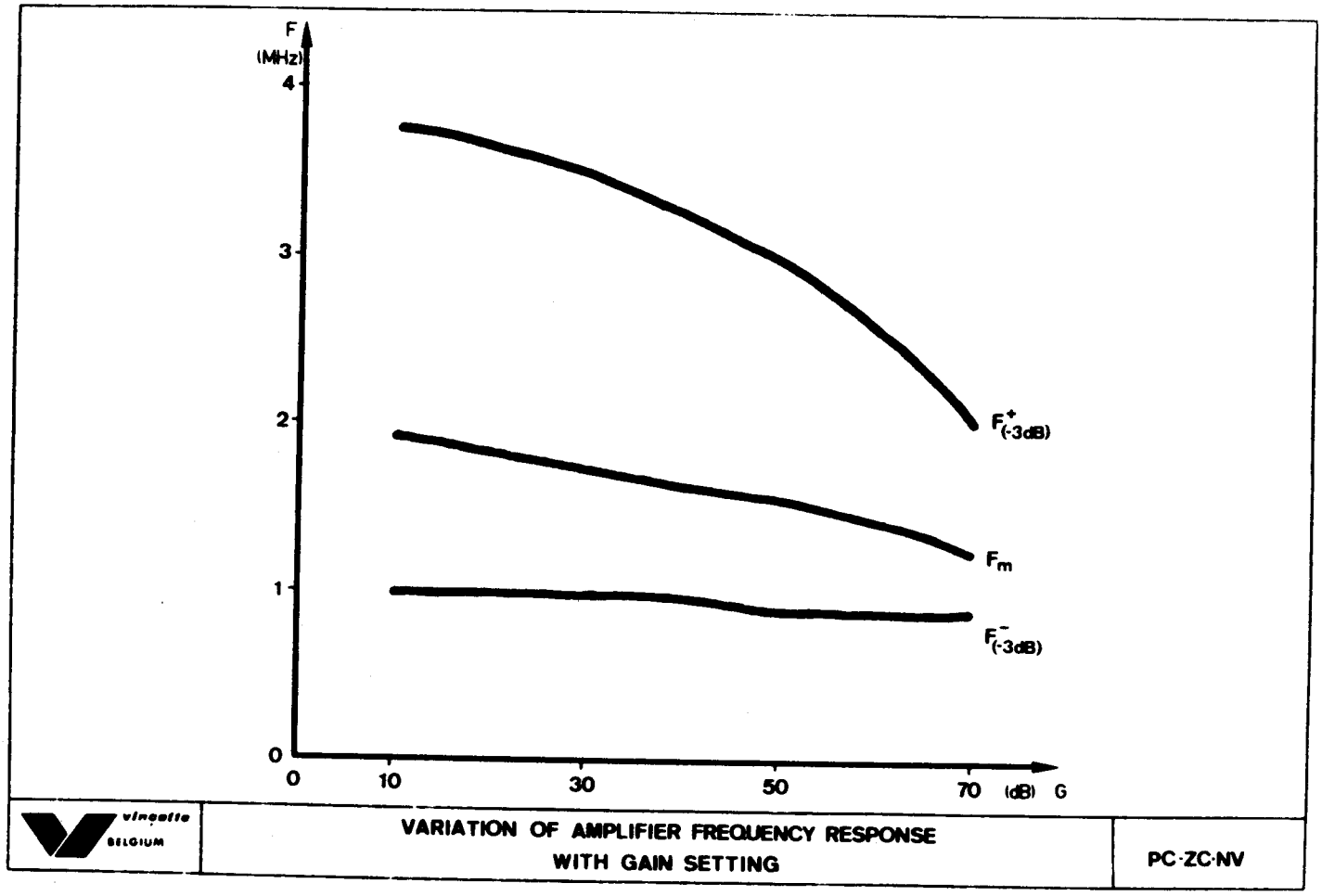


D=33mm D=119mm D=205mm

10mm

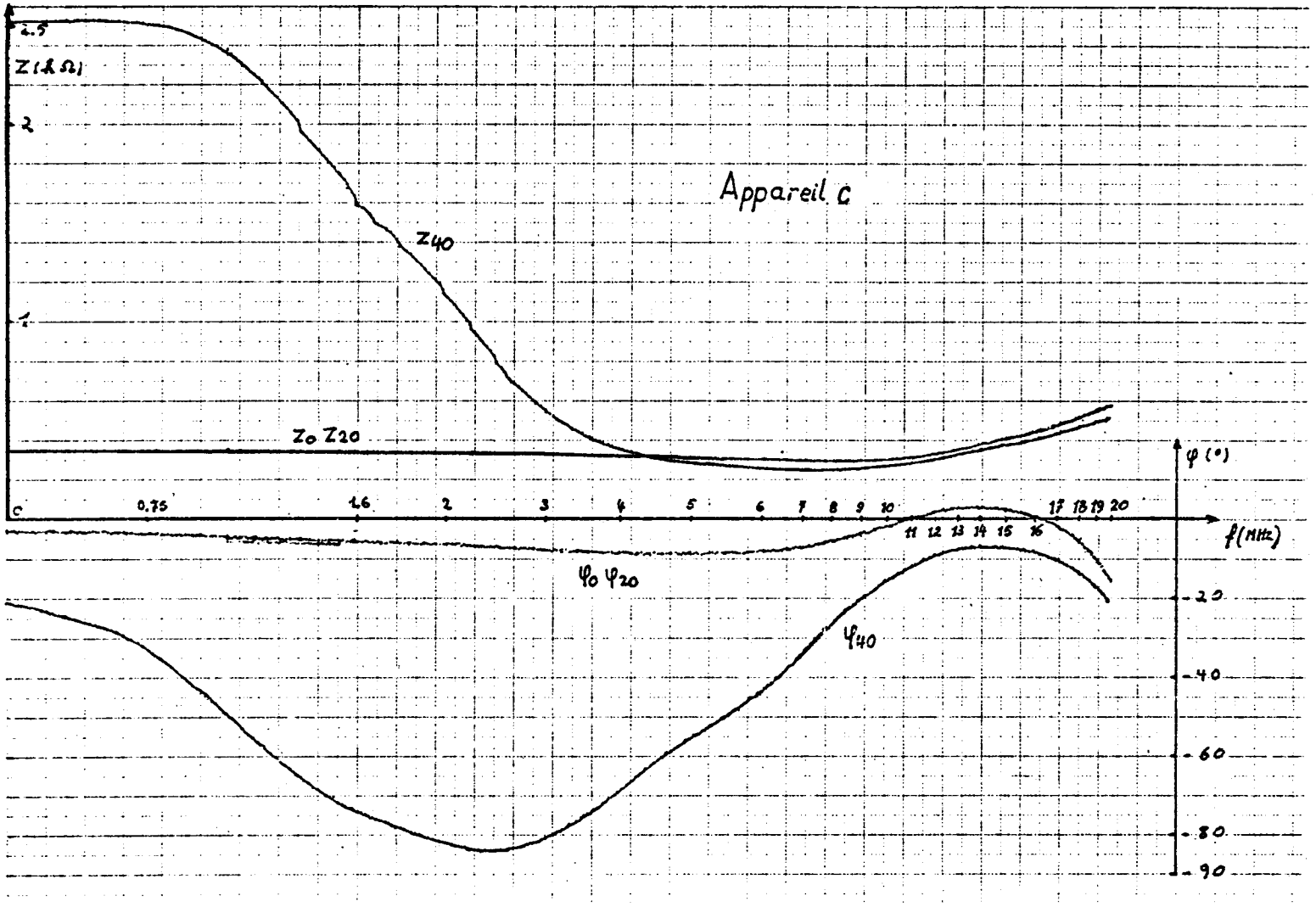
vinçotte BELGIUM	BEAM ANALYSIS ERROR ON SQUINT AND REFRACTION ANGLE	PC·ZC·NV

Fig. 12



vingotte BELGIUM	VARIATION OF AMPLIFIER FREQUENCY RESPONSE WITH GAIN SETTING	PC-ZC-NV

Fig. 13



vinçotte BELGIUM

Fig. 14 : ULTRASONIC UNIT INPUT IMPEDANCE VARIATION

PC ZC NV

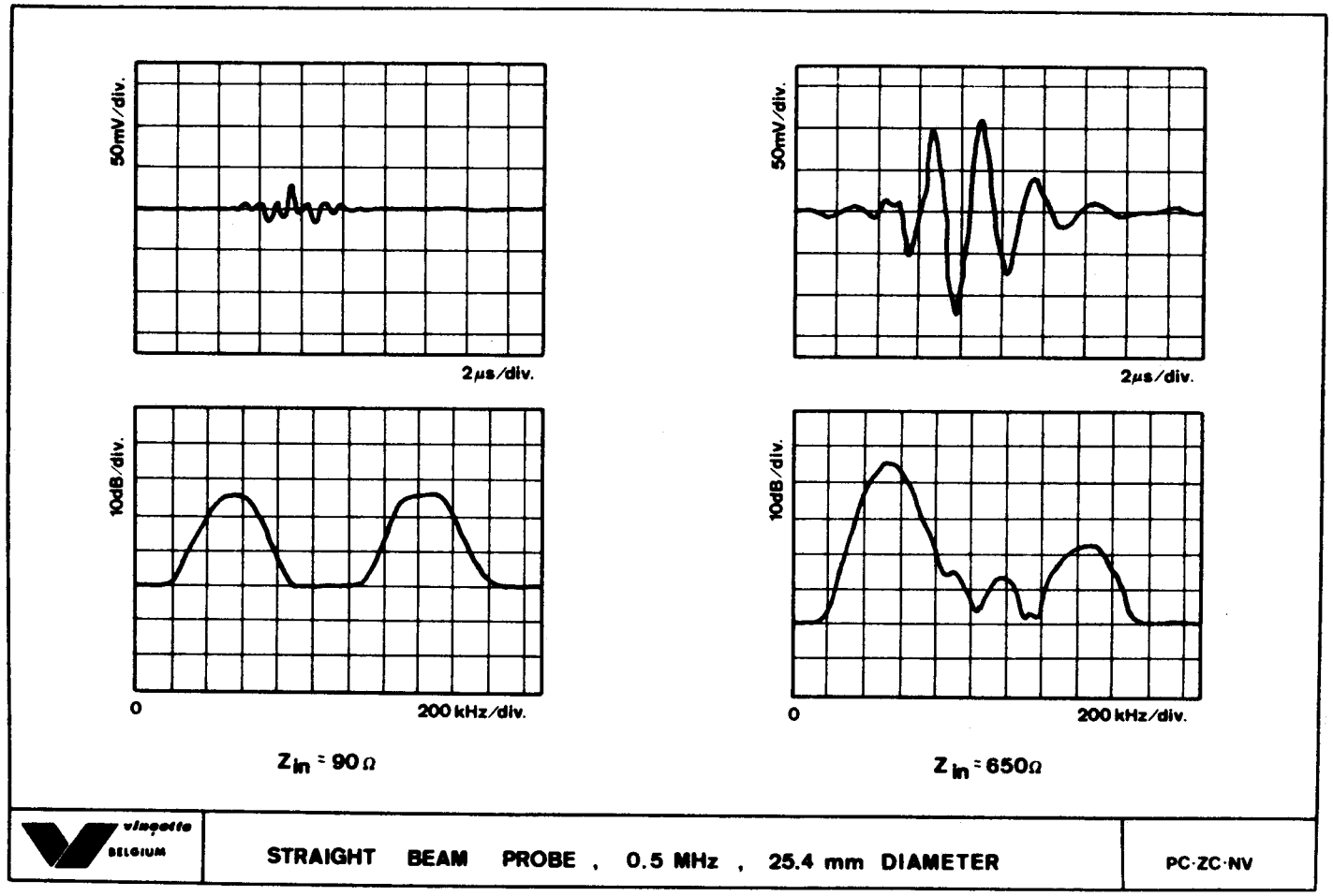


Fig . 15

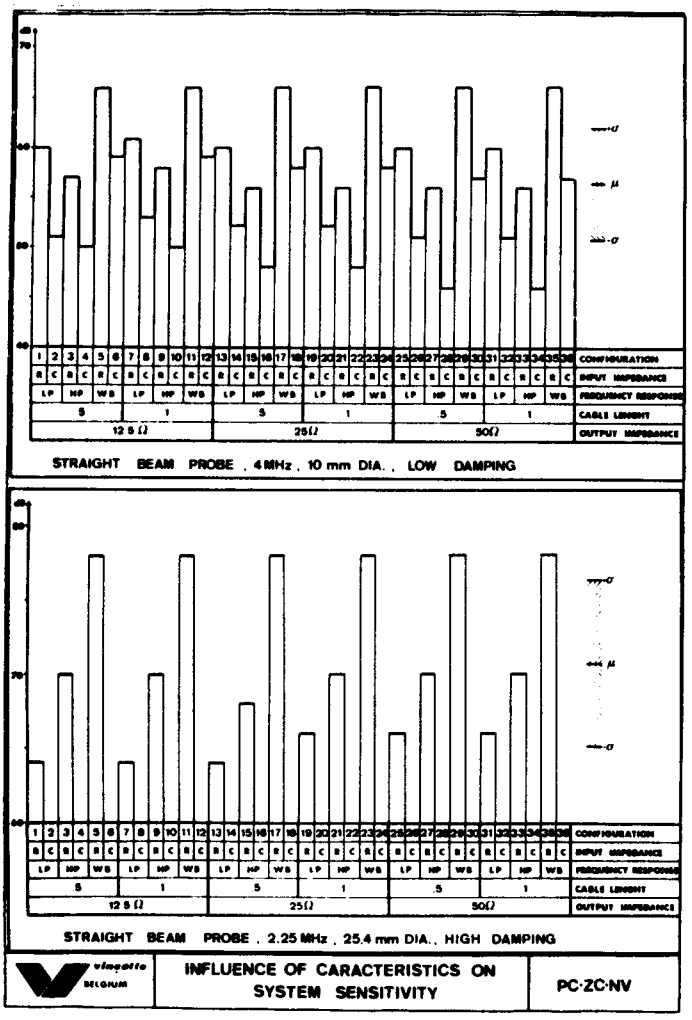


Fig.16

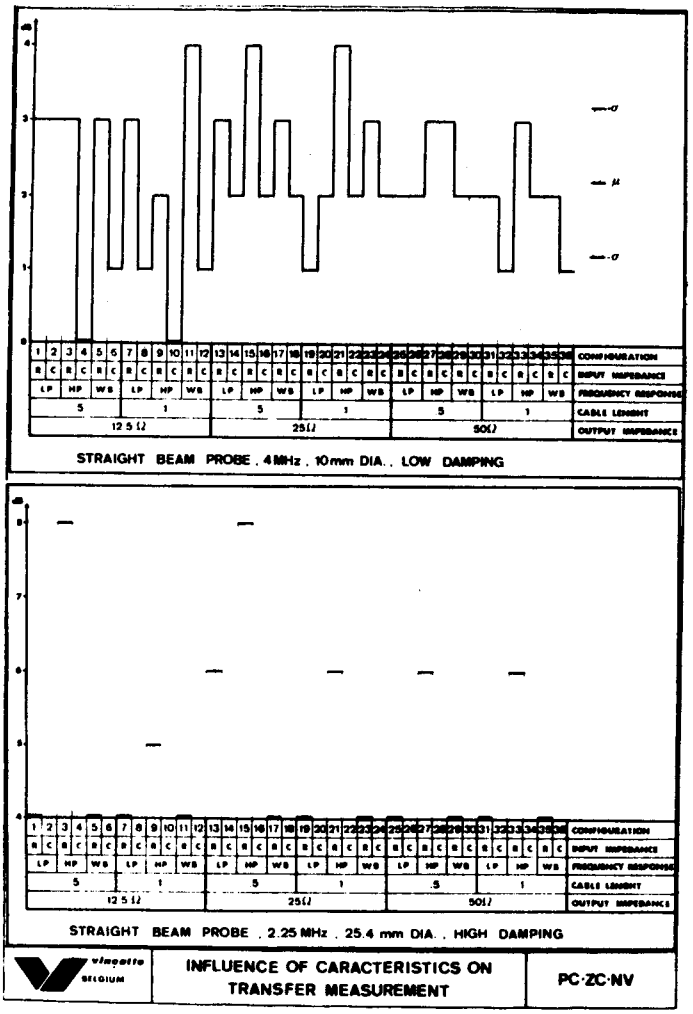


Fig.17

Detectability of intergranular stress corrosion cracking using field proven ultrasonic techniques

C.E. LAUTZENHEISER, W.C. Mc GAUGHEY
Southwest Research Institute, USA

ABSTRACT

Experience over the past four years has shown that a conscientiously applied surveillance program of ultrasonically examining pipe welds can effectively detect intergranular stress corrosion cracking and allow for timely corrective action; the appropriate surveillance program is the use of trained personnel following detailed procedures. This statement is based on the fact that no stainless steel pipe welds examined by Southwest Research Institute (SwRI) have developed significant leaks due to undetected intergranular stress corrosion cracking (IGSCC). Furthermore, in all instances except one, the presence of cracking defined by such an ultrasonic examination program has been confirmed when destructive evaluation was made.

Exhaustive laboratory research programs have identified many problems with detecting IGSCC with conventional ultrasonic procedures. Recommendations have been developed for the use of focused dual element ultrasonic search units and other specialized approaches. Unfortunately, the use of dual element search units on piping systems requires a very high degree of specialization in the design of those search units. This specialization, while practical under laboratory conditions, becomes exceedingly difficult to accommodate under field conditions. The need for specially designed search units to fit the wide range of pipe diameters and wall thickness encountered necessitates having a very large number of special search units available for each field examination series. Furthermore, normal wall thickness variations as encountered in the field can negate the applicability of many of the previously designed and constructed search units. The net effect of these difficulties is such that the effectiveness of highly specialized search units is largely diminished by field conditions.

Fortunately it has also been found that single element search units are only slightly less effective than dual element search units when evaluated in laboratory conditions. The adaptability of single element search units to field conditions more than compensates for the potential of reduced sensitivity observed under laboratory conditions.

A properly designed inspection program includes use of 45° and 60° angle beams. It was earlier observed and subsequently confirmed by field experience that most cracks are detected using the 45° shear waves. However, it has been found that in 9% of the cases the IGSCC was detected only with the 60° angle beam and not with the 45° beam.

The total surveillance program must include control of the procedure, and equipment and the training of the ultrasonic technicians. It has also been found to be extremely important that a highly experienced Level III analyst carefully review the ultrasonic examination record and evaluate each individual indication to determine if the indication is due to IGSCC or is simply a benign geometric reflector. This is unfortunate because it encourages the accumulation of the very important analysis experience in a very small number of people. However, it appears nothing less will allow the necessary high degree of ability to be developed and applied in a way that will maintain this successful technique for identifying IGSCC.

INTRODUCTION

The ASME Code provides rules for the calibration and recording of the examination, but leaves open such procedural matters as search unit frequency, beam angle, and search unit size. This is done to permit development of an improved examination. For comparison with previous examinations, it would be best not to change procedures; however, when service-induced cracks are found which do not respond well to the examination, the procedure must be improved.

PROCEDURE IMPROVEMENT

Southwest Research Institute (SwRI) developed a thin-wall examination procedure using a dual 55-degree angle beam search unit. As shown in Figure 1, the angle was selected to reach under the weld crown to the weld root on a 4/8 vee path. The dual search unit gave good resolution and apparently improved examinations, but the improvement was not free of problems. Surface waves were generated in addition to the 55-degree angle beam shear waves. The surface waves sometimes reflected from crown grinding marks at the same time as the 55-degree beam reflection from the root. If the indication could be reduced by damping, the indication was from the surface and not a root indication which should be undampable.

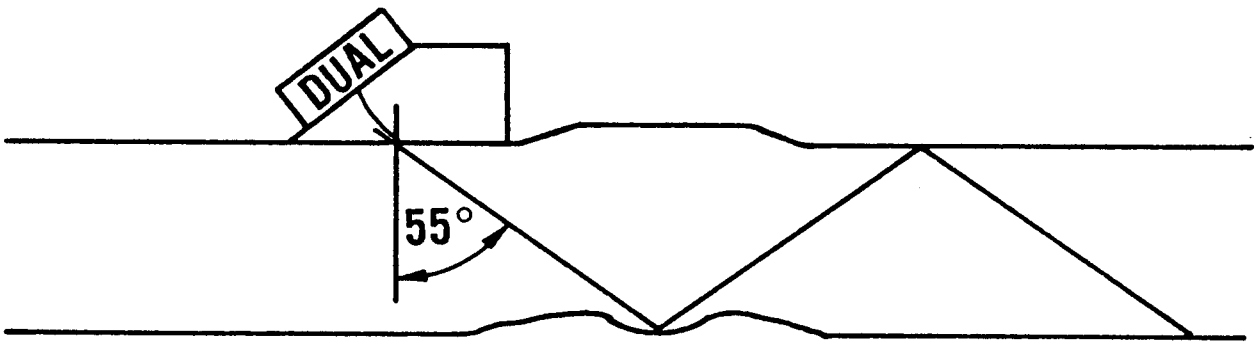


FIGURE 1. THIN WALL PROCEDURE

A through-wall transgranular crack specimen examined with the dual 55-degree search unit detected the crack with a low amplitude. A 2.25 MHz, 45-degree search unit with a single 1/4-inch diameter piezoelectric element gave higher amplitudes and enhanced the probability of detecting, recording, and identifying such indications. Therefore, the procedure was improved to use this search unit. Subsequent use of the 2.25-MHz, 1/4-inch diameter, 45-degree examination disclosed several additional crack-like indications in the system. Some of these indications were confirmed radiographically. Areas containing thirty-two ultrasonic indications were removed from the line, and all but one of them were confirmed as cracks by liquid penetrant examination.

This experience confirms that a specimen containing a service-induced flaw indication is the best proof device for procedure evaluation. Until such a specimen is available, the reflectors in the calibration block are the best available reflectors for procedure qualification.

ON-THE-JOB PROCEDURE DEVELOPMENT

Unfortunately the availability of service-induced flaw indications during procedure development does not insure that the procedure will be capable of differentiating geometric from crack-like indications. In the summer of 1979 an examination agency working on Three Mile Island Unit 1 had five throughwall service-induced flaw indications which they used in the development of a procedure using a 5 MHz 50° angle beam search unit pulsed at 1 MHz. Examination of welds in the line containing the five coolant leaks indicated that other welds had cracks which had not penetrated the pipe wall. Metallographic examination confirmed the presence of cracks on the inside surface of the pipe adjacent to the welds.

The procedure was used in the examination of 946 welds and "UT indications characteristic of cracking" were found in 206 of these welds. This resulted in IE Bulletin No. 79-17, dated July 26, 1979, which gave the following schedule for all PWRs:

1. Review Report due August 25, 1979

2. Visual, surface and volumetric examinations by October 24, 1979

3. Examination and Repair Report by November 23, 1979

Shortly after the Bulletin was issued, information was made available that 7 of the TMI welds which UT interpretation indicated were cracked 360° intermittently had been removed and metallography revealed that none were cracked. By this time 1902 welds had been examined and "UT indications characteristic of cracking" had been found in 350 welds. These welds were reexamined with a 2.25 MHz 60° angle beam search unit. This procedure found that 38 of the welds had ultrasonic indications inducive of IGSCC and the remaining 312 welds contained only geometric reflectors. IE Bulletin No. 79-17, Revision 1, dated October 29, 1979, stated "Further metallurgical analysis of these welds is required to verify the adequacy of the UT procedures and to determine the nature of the cracking," and extended the completion date to October 19, 1980, for the examination of PWR systems.

The procedures used on the Three Mile Island Unit 1 stainless steel pipe systems did not take advantage of developments in detection and identification of stress corrosion cracking made during the past four years. Early reports of

Bulletin No. 79-17 examinations of other unit systems by other examination agencies using their own ultrasonic procedures revealed no indications identified as cracks and no geometric reflectors were mistakenly identified as crack-like indications.

DEVELOPMENT OF THE 1.5 MHZ EXAMINATION FOR DETECTION OF STRESS CORROSION CRACKING

In order to improve the reliability with which stress corrosion cracking could be detected and identified, a significant procedure evaluation was undertaken in conjunction with the Electric Power Research Institute (EPRI). Evaluation of the frequency characteristics of the reflected indication was of prime concern. The frequency spectrum analysis of the reflected ultrasonic pulse indicated that the stress corrosion cracks in the EPRI specimens were most reflective to a frequency of 1.5 MHz. The small size and tightness of the stress corrosion cracks would lead one to believe that they would be detected best with higher frequencies. However, investigation has shown that this is not the case.

The EPRI cracked pipe specimens, which were removed from boiling water reactor systems, were subjected to ultrasonic examination with a set of specially developed search units. These search units varied in frequency from 1.0 to 10 MHz and in piezoelectric element size from 1/4 to 1/2 inch in diameter. Shear beam angles used were 45 and 60 degrees. Use of this set of search units on the EPRI cracked pipe specimens showed that the 1.5-MHz search units provided ten times the amplitude obtained with a 2.25-MHz examination; that is, cracks which gave 20 to 40 percent distance amplitude correction curve (DAC) amplitudes at 2.25 MHz gave 200 to 400 percent DAC amplitudes at 1.5 MHz.

Field application of the 1.5-MHz examination was not without problems. Examinations on small diameter pipes were attempted using 1/4-inch diameter search units which, due to increased beam spread, caused an increase in recording of geometric reflectors. In addition, the beam spread generated surface waves from the leading edge of the angle beam wedge, adding to the confusion. Increasing the search unit size to 3/8-inch diameter solved most of this problem; however, a surface wave indication is recorded occasionally from a 1.5-MHz, 3/8-inch diameter, 60-degree search unit and rarely from a 45-degree search unit.

Amplitude enhancement with the 1.5-MHz frequency required numerous reexaminations with 1.5 MHz to check the measurements and with 2.25 MHz for comparison with previous examination records. In the first inservice inspection (ISI) in which the 1.5-MHz frequency was used, one 4-inch bypass indication and three 12-inch core spray indications were called and confirmed as cracks. In addition, another crack was found in one of the removed specimens. This indication had been detected and recorded. But it was one grain width from the weld base metal interface, had a maximum amplitude of 178 percent during a 60-degree shear wave examination, and appeared to be a root indication; so it was miscalled in analysis.

The 1.5-MHz 45-degree and 60-degree angle beam examinations gave stress corrosion crack amplitudes equal to or greater than those obtained with 2.25 MHz 45-degree and 60-degree examinations. Most stress corrosion cracks give higher

amplitudes from the 45-degree angle beam examination and the 60-degree angle beam examination provides confirmation of the reflector at a lower amplitude. However, in about 10 percent of cases the 60-degree angle beam examination of the stress corrosion crack provides a higher amplitude and permits identification of the reflector. The 1.5 MHz examination consistently provided improved detection of stress corrosion cracks, so in spite of the requirement for additional examinations, the change was justified.

SINGLE VERSUS DUAL ANGLE BEAM EXAMINATION

SwRI has not found consistently improved detection with the 1.5-MHz dual 45-degree angle beam examination. When the 1.5-MHz 45-degree single and dual angle beams are compared on different stress corrosion cracks, the dual gives higher, lower or equal amplitudes compared to those from the single angle beam. When the weld crown dimensions prevent a 4/8 vee path examination of the weld root area, the 12/8 vee path examination can be used with the single angle beam. However, the focusing effect of the dual search unit limits the depth of field and prevents extension of the examination from the 4/8 to the 12/8 vee path without a change of search units. Since we have not found consistent convincing evidence that the dual improves detection of the condition, our procedures require the single angle beam examination for detection of stress corrosion cracks.

ANALYSIS

Indications 100 percent of the DAC and greater are analyzed to determine the origin of the indication. In addition, all of the recorded indications are analyzed in areas which have a history of cracking in similar plants. As shown in Figure 2, analysis uses the thickness and weld crown dimensions taken at one point on the weld to draw the cross section through which the examining beam passes. The beam centerline position "W" from the weld centerline and indication metal path are plotted. The 60-degree examination metal path corrections must be determined from the calibration record. The 45- and 60-degree examination calibrations are usually recorded on the same sheet. The wedges sometimes have different beam path distances; so the delay control that is set for the 45-degree examination does not provide the right delay for the 60-degree wedge, and the 60-degree metal paths must be corrected by 1/10 or 2/10 of an inch.

The metal path is plotted as an angular line extending from the examination surface to or through the opposite surface. Metal paths terminating at the opposite surface on the far side of the weld centerline (such as indications 1 and 5) are identified as root indications. Metal paths terminating more than 1/2 inch on the near side of the weld centerline (such as indications 3 and 7) are identified as inside surface geometry.

Metal paths terminating at the inside surface between those limits may be root suckback, inside surface geometry, or crack-like indications. In order to determine the indication identity, the preservice radiographs must sometimes be used. In one instance, the indication was found to have come from weld spatter deposits on the inside surface. An ultrasonic reexamination may be performed by repeating the examination which found the indication as a check on the metal path, "W", and "L" measurements. If this examination is different from previous PSI or ISI examinations, an additional reexamination like the previously recorded examination may be performed to determine if a change to the reflector has occurred, or if the change is due to an improved examination. At the time

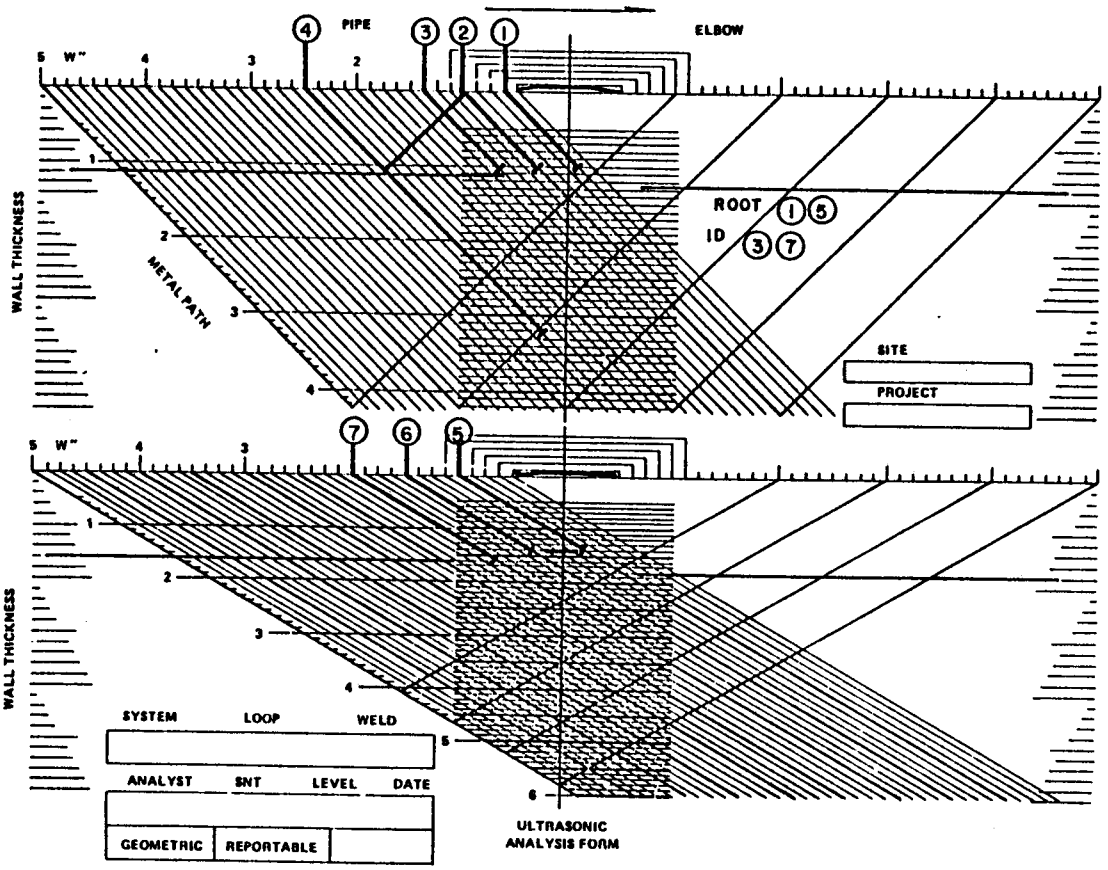


FIGURE 2. INDICATION ANALYSIS

the reexamination is made, thicknesses and profile gauge measurements of the surface at the indication position are made to permit plotting the indication in the geometry applicable to that indication. If the indication cannot be explained geometrically, radiographs are called for. The new radiographs may show a geometric reflector, a crack-like indication, or no indication. In the latter two cases, the ultrasonically called, crack-like indication must be removed whether or not it is confirmed radiographically since it has been proven that the ultrasonic examination has better sensitivity for detection of stress corrosion cracks. Radiography can confirm, but cannot deny the presence of a stress corrosion crack.

Metal paths which extend through the opposite interface may reflect to the examination surface and back to terminate at the opposite surface on an "N" path such as indication 4. The weld crown sometimes prevents the search unit from approaching close to the weld centerline to permit examination of the inside surface on the slant path. When this occurs, the "N" path may show the indication more readily than the slant path. This condition has occurred on some 4-inch recirculation bypass piping weld cracks.

Many indications have metal paths which terminate at positions other than the inside surface. So far, these have proven to be geometric reflectors from the crown and outside surfaces. The probable beam path and source of the indication must be determined by analysis.

In analyzing indications, it must be kept in mind that geometric reflectors in piping occur approximately 1,000 times more often than flaw indications. Figure 3 shows some of the geometric conditions which give indications requiring recording and analysis to determine if they are defect indications. It shows both the 45- and 60-degree angle beam shear wave reflected from a 14-degree weld prep conical bore into the weld crown. Such indications are commonly detected.

CONICAL BORE ANGLE AFFECT ON THE EXAMINATION BEAM

The pipe weld inside surface preparation is generally a cylindrical bore extending approximately 1/2 inch in from the end, to the conical bore which extends to the inside surface of the pipe. The conical surface angle may be specified as no greater than 10 degrees, or a 4-to-1 slope, or a 3-to-1 slope. These slopes are approximately 14 and 18 degrees, respectively; therefore, the conical surface angle may vary from 0 to over 20 degrees in some piping systems.

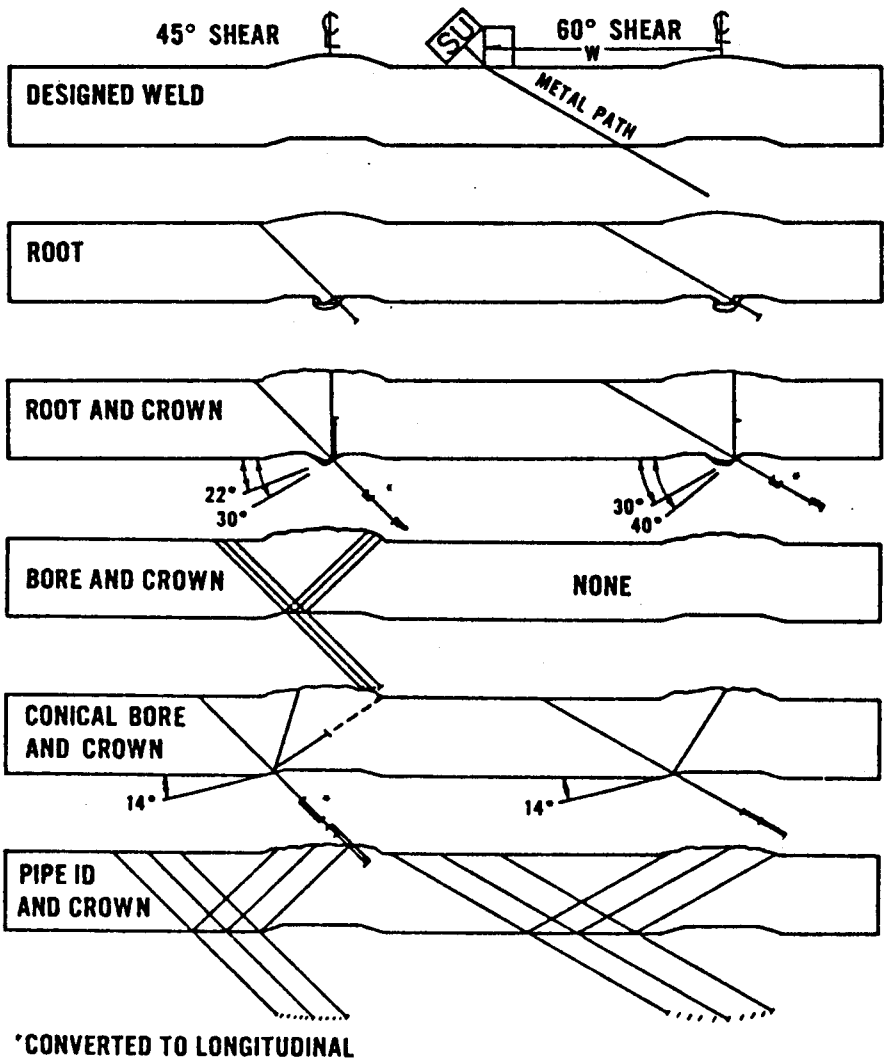


FIGURE 3. GEOMETRIC REFLECTORS IN PIPE-TO-PIPE WELDS

Appendix III to Section XI of the ASME Code appeared in the Winter 1975 Addenda. Appendix III relies on the 45-degree angle beam examination of pipe welds. As shown in Figure 4, the weld crown may prevent coupling the search unit so that the 4/8 vee path portion of the beam examines the weld root. When this occurs, the search unit must be coupled farther from the weld so that the 12/8 vee path portion of the beam examines the weld root. The remainder of the weld volume is examined by moving the search unit toward the weld until stopped by the crown. During this scan, the 4/8 vee path portion of the beam is incident on the conical bore and will be deflected from the beam path shown in Figure 4.

Shear waves incident on a steel-water interface at angles between 34 and 89 degrees from the normal to the interface will reflect at the same angle on the other side of the normal. However, Figure 5 shows that shear waves at angles between 1 and 33 degrees will partially mode convert into longitudinal waves. Longitudinal waves at angles between 1 and 89 degrees will partially mode convert into shear waves. The percent of energy converted is read vertically above the longitudinal wave beam angle regardless of whether the longitudinal angle is incident or mode converted.

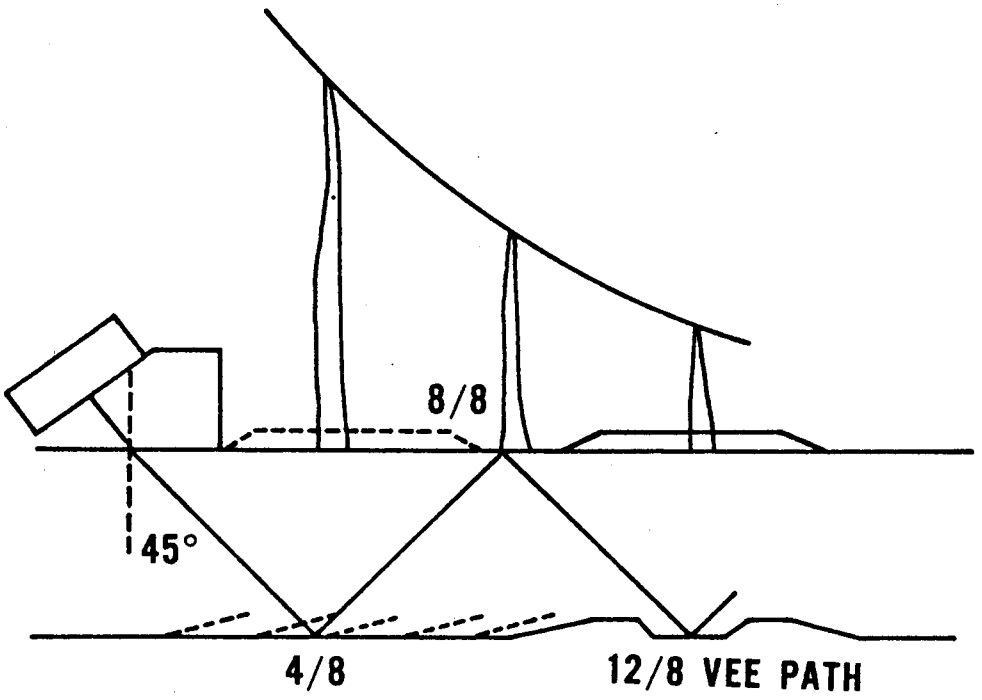


FIGURE 4. "N" PATH EXAMINATION

Figures 6, 7, and 8 show the deflection and mode conversion of a 13/8 vee path beam as the conical bore angle is changed from 0 through 29 degrees in 1-degree steps. Frames are identified by their chamfer angle number in degrees. Beam paths are drawn for flat and flush weld crowns and roots. Crown and root geometric other than flat and flush will produce additional geometric reflectors.

Increasing the dimension of the inside surface weld preparation cylindrical bore to two times the nominal wall thickness would permit examination of the

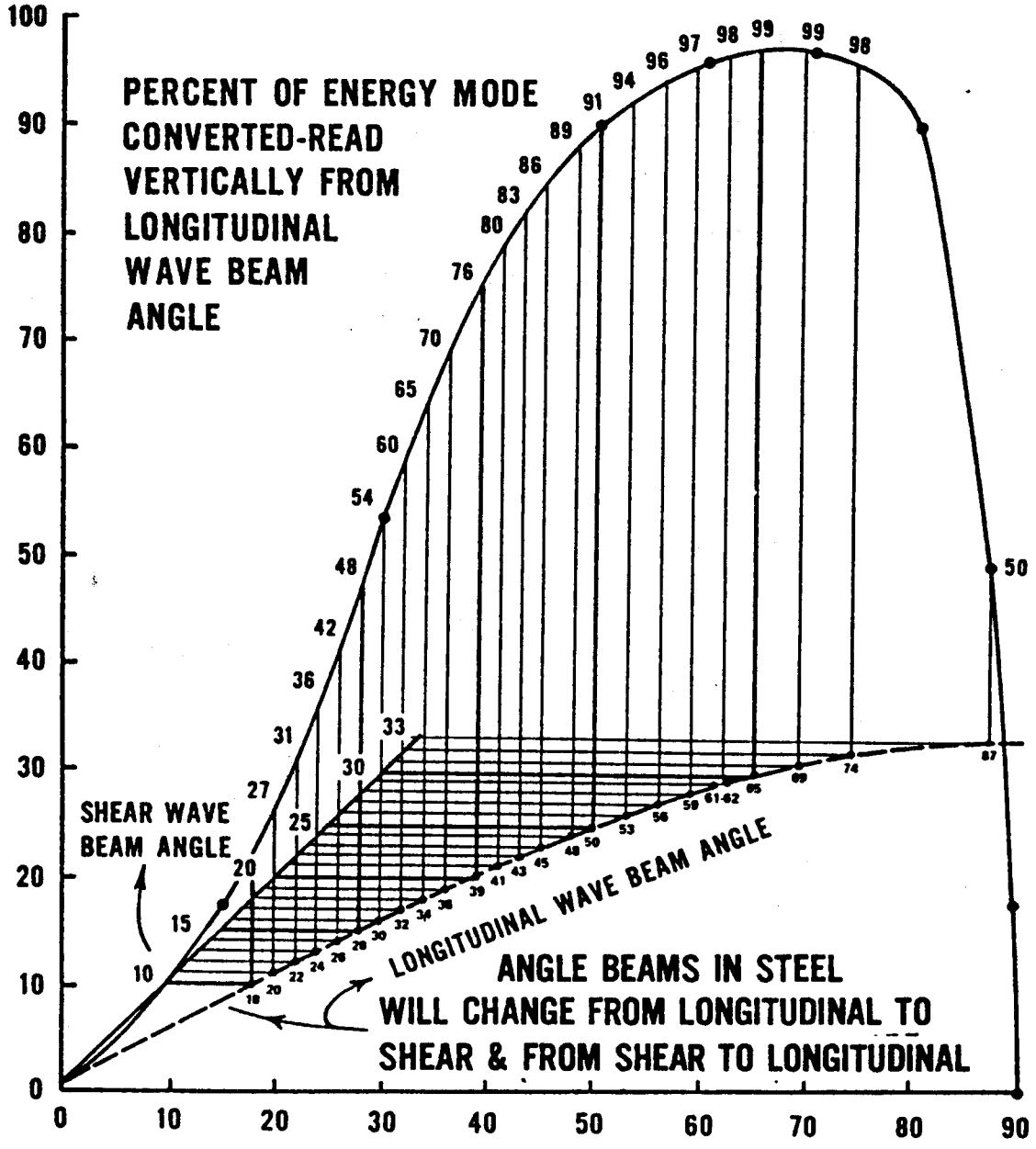


FIGURE 5. MODE CONVERSION

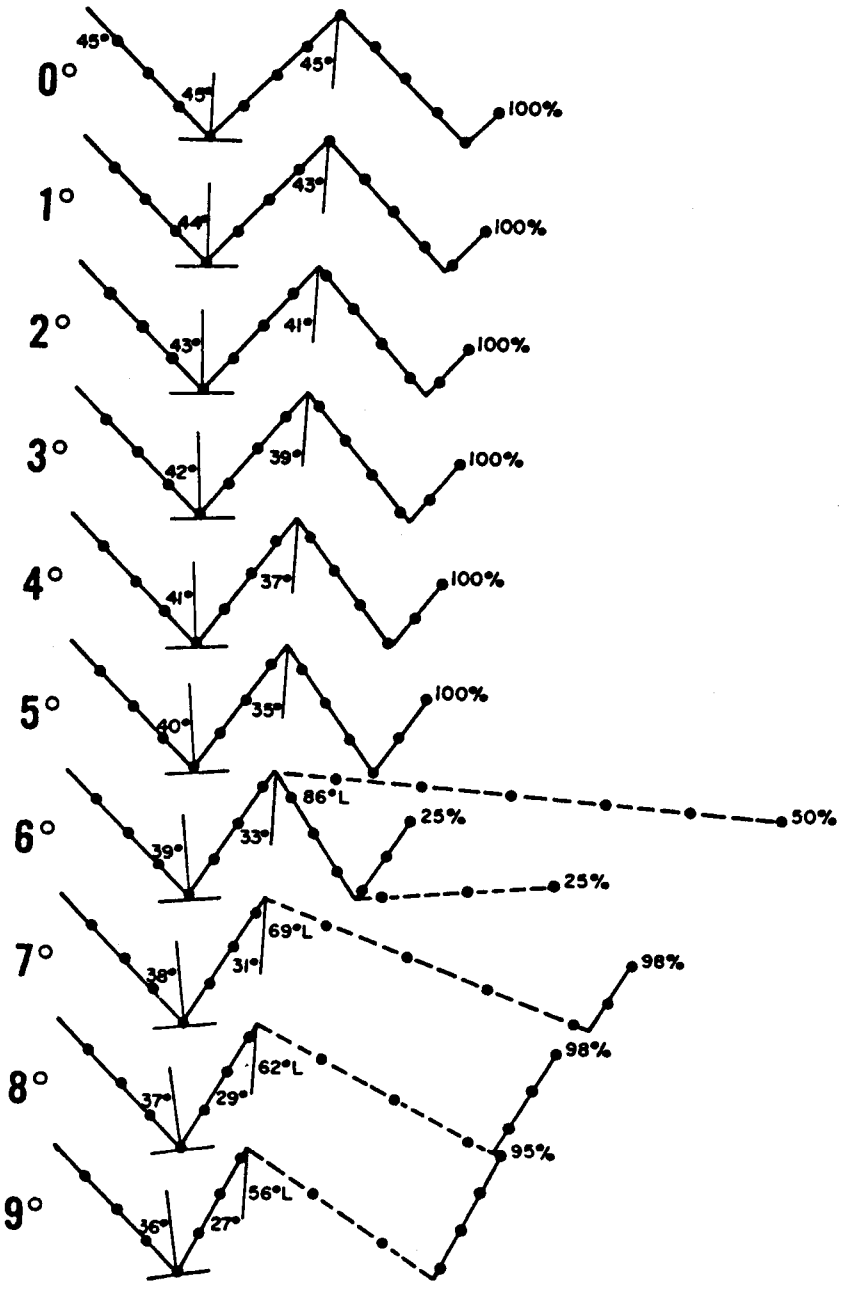


FIGURE 6. BEAM PATHS 0° TO 9° CONICAL BORE

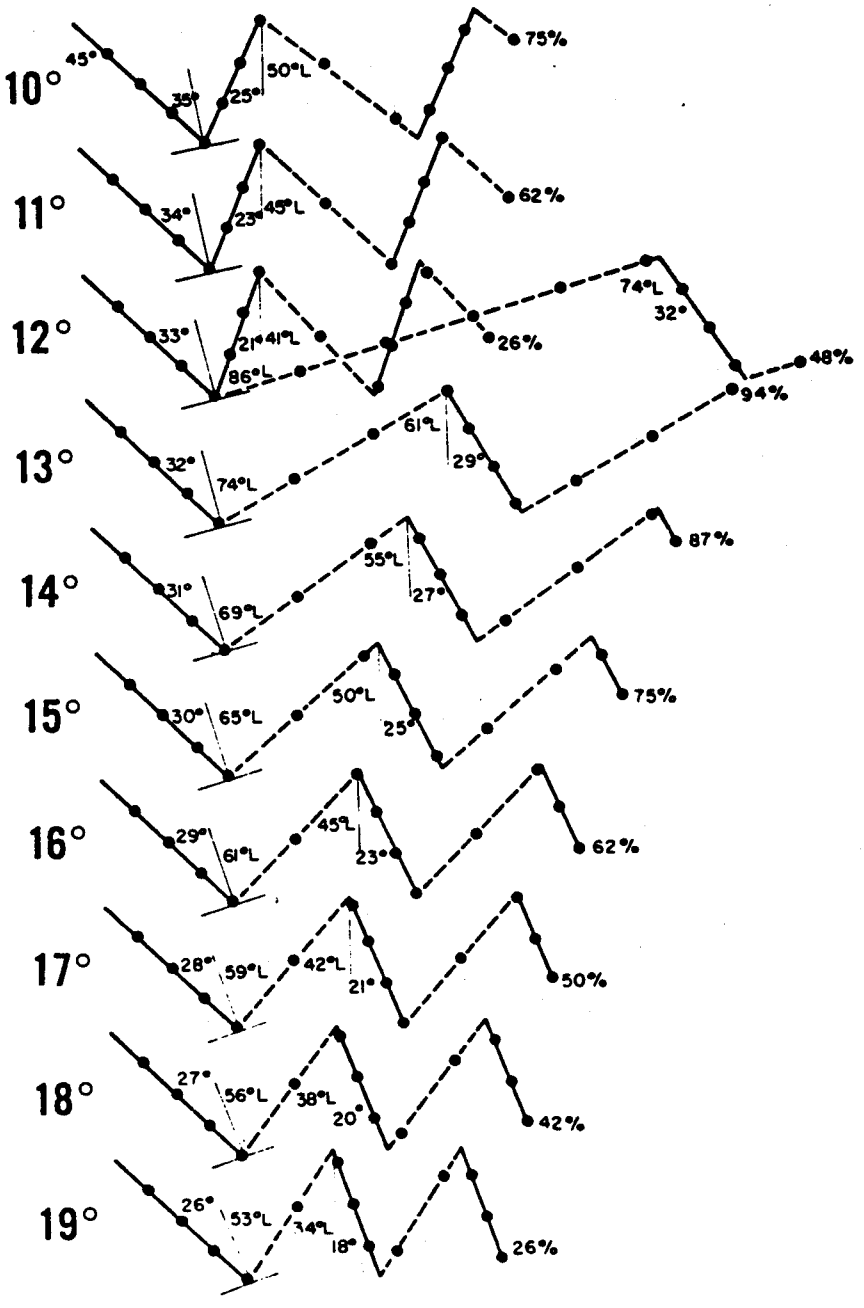


FIGURE 7. BEAM PATHS 10° TO 19° CONICAL BORE

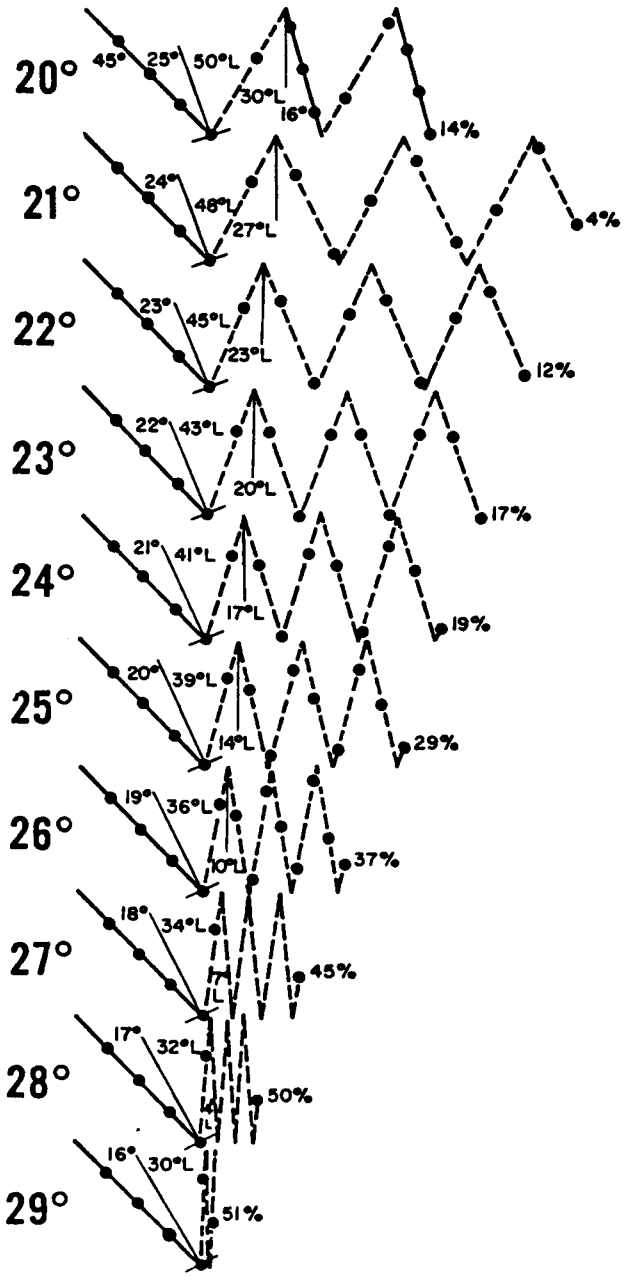


FIGURE 8. BEAM PATHS 20° TO 29° CONICAL BORE

weld without bouncing the beam from the conical bore. We have recommended this change for several years. A plant which used the 2t cylindrical bore weld prep has been examined, and significantly fewer geometric indications were recorded.

From 0 through 5 degrees, the shear beam is deflected along a gradually changing path. At 6 degrees, the angle beam shear wave is incident at 33 degrees to the outside surface normal and converts 50 percent of its energy to longitudinal. At 7 degrees, the beam is incident at 31 degrees to the outside surface normal and converts 99 percent of its energy into longitudinal which hits the inside surface and converts to shear. From 8 through 11 degrees, the alternate shear and longitudinal beams proceed along a gradually changing path. At 12 degrees, the angle beam shear wave is incident at 33 degrees to the inside surface normal and converts 50 percent of its energy to longitudinal. At 13 degrees, the beam is incident at 32 degrees to the inside surface normal and converts 98 percent of its energy to a 74-degree longitudinal which hits the outside surface at 61 degrees to the normal, converting 98 percent to shear at 29 degrees, then it returns to the inside surface and another 98 percent energy conversion to longitudinal. From 14 through 20 degrees, the alternate shear and longitudinal beams proceed along a gradually changing path with a lower percentage of the energy converted.

At 21 degrees, the angle beam shear wave is incident at 24 degrees; 89 percent of the energy converts to 48 degrees longitudinal which is incident on the outside at 27 degrees, and 54 percent of this energy reflects. At 13/8 of the vee path, only 4 percent of the energy is left. The remainder has been scattered by reflection from the conical bore and mode conversions at the five longitudinal wave reflection interfaces. From 22 through 29 degrees, progressively less energy is converted at the conical bore; but more energy is reflected in the longitudinal mode at the interfaces, so the 13/8 vee path energy percentage increases.

On conical angles of 22 and 23 degrees, about 15 percent of the energy is reflected in shear, normal to the outside surface, appearing between 6/8 and 7/8 of the vee path. On a conical angle of 29 degrees, about 54 percent of the energy is converted to longitudinal, approximately normal to the outside surface, and appearing between 5/8 and 6/8 of the vee path.

Increasing the dimension of the inside surface weld preparation cylindrical bore to two times the nominal wall thickness would permit examination of the weld without bouncing the beam from the conical bore.

ANALYSIS THROUGH THE CONICAL BORE

In some existing plants, the conical bore is known to be approximately 1/2 inch from the weld centerline, but the conical angle is not known. As shown in Figure 9, indications which have metal paths extending through the conical bore area may be identified by using a compass to swing an arc pivoted at the conical surface. The arc crossing a reflecting surface indentifies the shear wave reflector if the damping note confirms the identity such as crown Indication 8. The shear wave need not damp at the reflector if its direction is normal to the reflector such as outside surface Indication 9. If the arch reaches halfway from the conical surface to a reflector identified by damping such as crown Indication 10, the indication is caused by a mode-converted longitudinal wave which must damp regardless of incident angle to the damping surface. When the arc narrowly missed the damping-identified reflecting surface, the pivot point

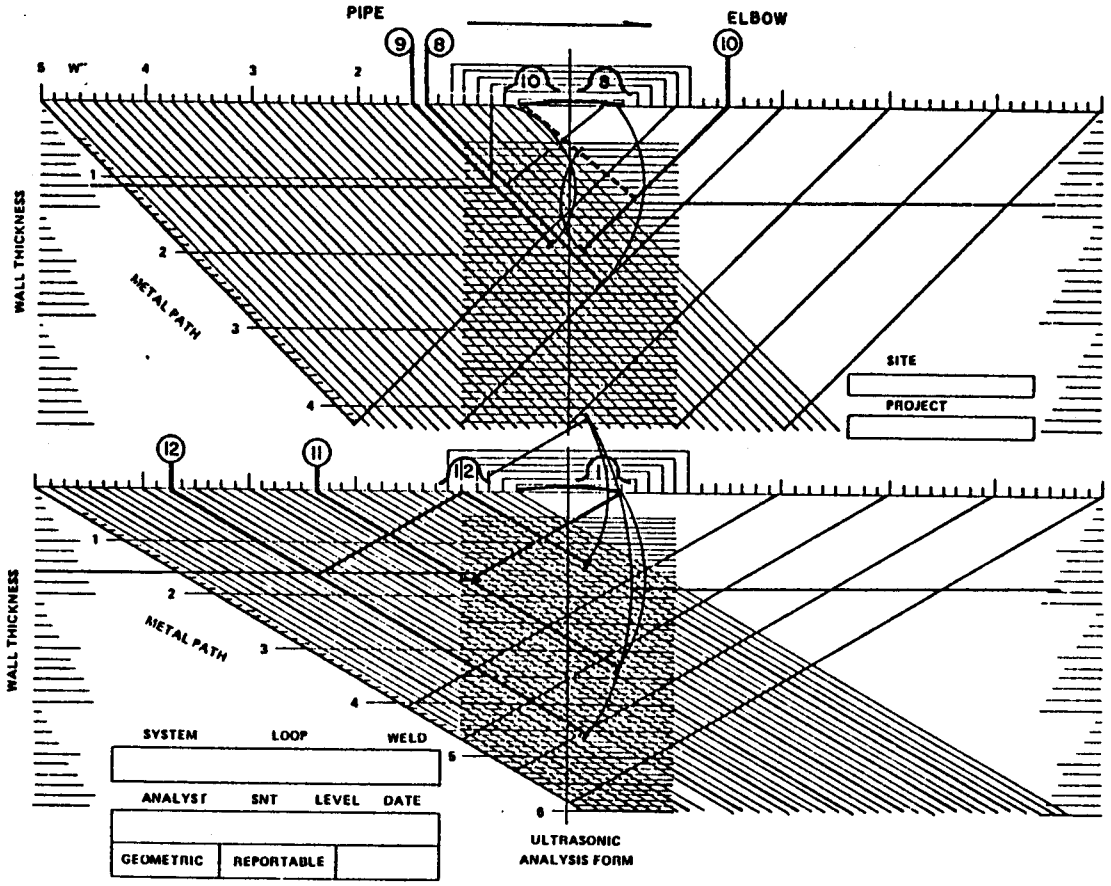


FIGURE 9. BEAM SWINGING

may be moved up or down 12-1/2 percent since the pipe thickness tolerance is ±12-1/2 percent of nominal thickness such as crown Indication 11. When the arc extends far beyond the damping surface, a second arc pivoted at the damping spot will generally identify the inside surface reflecting the indication such as root Indication 12.

IDENTIFICATION OF STRESS CORROSION CRACKS

The developed procedures and analysis techniques have permitted us to identify stress corrosion cracks. We have called and destructively confirmed intergranular stress corrosion cracks in the 4 inch recirculation bypass lines on three out of six units examined.

IGSCC in the 4-inch recirculation bypass has been attributed to the combined influence of the sensitization in the heat-affected zone and the inside surface weld preparation grinding/machining stresses, welding stresses coupled with a high oxygen concentration in the stagnant lines.

Also, we have called and destructively confirmed intergranular stress corrosion cracks in the 10 inch core spray lines of two out of six units examined. An ultrasonic indication in a third unit was confirmed radiographically but was not confirmed by penetrant or metallographic examinations.

IGSCC in the 10-inch core spray piping has been attributed to the combined influence of the sensitization in the heat-affected zone and the inside surface weld preparation grinding/machining stresses, welding stresses with a high oxygen concentration in the water.

In addition, we have called and destructively confirmed transgranular stress corrosion cracks in the 8 inch safety injection lines on one of five units examined. These cracks were reported to be due to the presence of chlorides during construction.

In addition, one core spray pipe crack was detected by visual examination when a wet surface was wiped dry and became wet again prior to ultrasonic examination. The cracks which have been called from the ultrasonic examinations have been between 0.015 and 0.187 inch in depth between 0.5 and 4.0 inches long and the lengths are generally in the top half of horizontal run lines.

CONCLUSIONS

The procedures used in examination and analysis of flaw indications have resulted in many cracks being removed from the examined piping systems. SwRI believes that some minor cracks may have been missed in examination or analysis; however, no significant leaks have occurred between our periodic examinations of pipe.

REFERENCES

Floyd A. Firestone, "Tricks with the Supersonic Reflectoscope," Non-Destructive Testing, Fall 1948.

W. C. McGaughey, "Pipe Weld, Ultrasonic Examination, ID Weld Prep," SwRI Internal Report, May 1975.

Wayne T. Flach, William T. Clayton, and Joel G. Godwin, "Development and Refinement of Ultrasonic Examination Techniques to Detect Intergranular Stress Corrosion Cracking in Austenitic Piping," Paper presented to ASNT Symposium, April 1977.

EPRI Report NP676-SR, "Detailed Analysis of the Fundamental Ultrasonic Response Data from Stainless Steel Corrosion Crack Specimens."

EPRI Preliminary Report NP-1153, "Improved Ultrasonic Inspection Method for Stainless Steel Piping," August 1979.

NRC IE Bulletin No. 79-17, "Pipe Cracks in Stagnant Borated Water Systems at PWR Plants," July 26, 1979 and Revision 1 October 29, 1979.

Ultrasonic inspection reliability for primary piping systems *

F.L. BECKER
Battelle Northwest Laboratory, USA

ABSTRACT

This report describes the results of the first year's effort of a five year program which is being conducted by Battelle, Pacific Northwest Laboratories, on behalf of the U.S. Nuclear Regulatory Commission. This initial effort was directed toward identification and quantification of inspection uncertainties, which are likely to occur during inservice inspection of LWR primary piping systems, and their influence on inspection reliability. These experiments were conducted on 304 stainless steel samples, however, the results are equally applicable to other materials. Later portions of the program will extend these measurements and evaluations to other materials and conditions. Initial conclusions of this study are as follows:

1. ASME Section XI, Appendix 3 calibration requirements coupled with a lack of search unit selection and control, provide no assurance that even ideal reflectors of reportable size will produce a reportable indication.

2. Ultrasonic transparency produced by flaw tightness and/or fluid in the crack can reduce reflected signal amplitudes by as much as 32 dB. This effect is qualitatively similar to the theoretical calculated reflection from closely spaced, smooth plane parallel surfaces.

3. Non-optimum orientation of surface-connected reflectors can produce substantial loss in signal amplitudes, compared to ideal reflectors, and exhibit little relationship to reflector depth for 45° incidence. In all cases, the condition is less severe for 60° incidence. This condition is frequency and search unit dependent.

4. The influence of crack roughness in the range of 10 to 30 μm RMS can reduce relfected signal amplitude by as much as 12 dB relative to an ideal reflector of the same size. The amplitude decreases monotonically as the degree of surface roughness increases.

Round robin inspections for the purpose of measuring the effectiveness of current ISI procedures are in progress. Future program efforts will employ fracture mechanics analysis to calculate the required level of ISI reliability. Revision in the ASME Section XI Code will be recommended to assure that the required inspection reliability will be achieved.

*Work supported by U.S. Nuclear Regulatory Commission under a Related Services Agreement with U.S. Department of Energy, Contract DE-AC06-76RLO 1830.

INTRODUCTION

Inservice inspection of U.S. light water reactor (LWR) primary and secondary system piping is performed to the requirements of ASME Section XI. Inspections are performed at periodic intervals on a sampling of pipe joints. The objective of these inspections is to provide assurance that cracks of unacceptable size are not present, as well as the identification of generic-type defects which may be present in the remainder of the system or other similar systems. In some instances flaws as large as 25% of wall thickness[1] may not be detrimental to the integrity of the pipe, even under conservative assumptions of material properties and service conditions. In other instances, smaller flaws could lead to rapid failure. In either case, flaws of small size must be reported to assure the discovery of generic defect conditions.

Recent events have raised considerable doubt as to the effectiveness of ASME Section XI requirements. Round robin inspections conducted by the Pressure Vessel Research Committee (PVRC),[2] the Plate Inspection Steering Committee (PISC)[3] and Nordtest[4] have shown very low levels of effectiveness for procedures based on the requirements of ASME Section XI. The PVRC and PISC trials were performed on samples typical of pressure vessel inspection, while the Nordtest samples were more typical of piping systems.

Recent failures[5] (leaks) in BWR and PWR systems due to intergranular stress corrosion cracking (IGSCC), PWR feedwater pipe cracking and BWR recirculation riser safe end cracking also serve to demonstrate the inadequacy of ASME Section XI requirements. None of these flaws were initially discovered by inservice inspection techniques. In many instances, the character of the flaws was such that they would not be reportable according to ASME Section XI requirements.

The U.S. Nuclear Regulatory Commission (NRC) sponsored program, "Integration of NDE Reliability and Fracture Mechanics", has been initiated to address this current lack of effectiveness for inservice inspection of LWR primary piping systems. The principal objectives of this program are:

1. Determine the reliability of ultrasonic inservice inspection (ISI) performed on commercial, light water reactor primary piping systems.

2. Using fracture mechanics analysis, determine the impact of NDE unreliability on system safety and determine the level of inspection reliability required to assure a suitably low failure probability.

3. Evaluate the degree of reliability improvement which could be achieved using improved and advanced NDE techniques.

4. Based on material, service and NDE uncertainties, formulate recommended revisions to ASME Section XI and Regulatory requirements needed to assure suitably low failure probabilities.

Results of the first phase of this program are reported below.

PROGRAM RESULTS

Before discussing specific results of the program, it is instructive to discuss the various components of inspection reliability, shown grapically in Figure 1. Six components or blocks of the inspection are shown. These could, of course, be subdivided further. In the first block, we have included ID geometry, material characteristics (i.e., attenuation and signal-to-noise ratio), and most importantly, the characteristics of the flaw (i.e., length, depth, tightness, roughness and orientation). The second block considers O.D. geometry and coupling efficiency. Thirdly, the characteristics of the search unit and instrument. The fourth area is the operator and his training, certification, experience, integrity and the conditions under which he must work. The fifth area includes the procedures and requirements governing the inspection, as well as other records and reports of fabrication and previous inspections. And lastly, the decision of acceptability. Each of these components contribute significantly to the overall inspection reliability.

In this paper, we shall discuss our results concerning flaw characteristics and equipment variables, as well as the influence of inspection procedures on inspection reliability. Analytical predictions of inspection reliability (recording probability) are also presented.

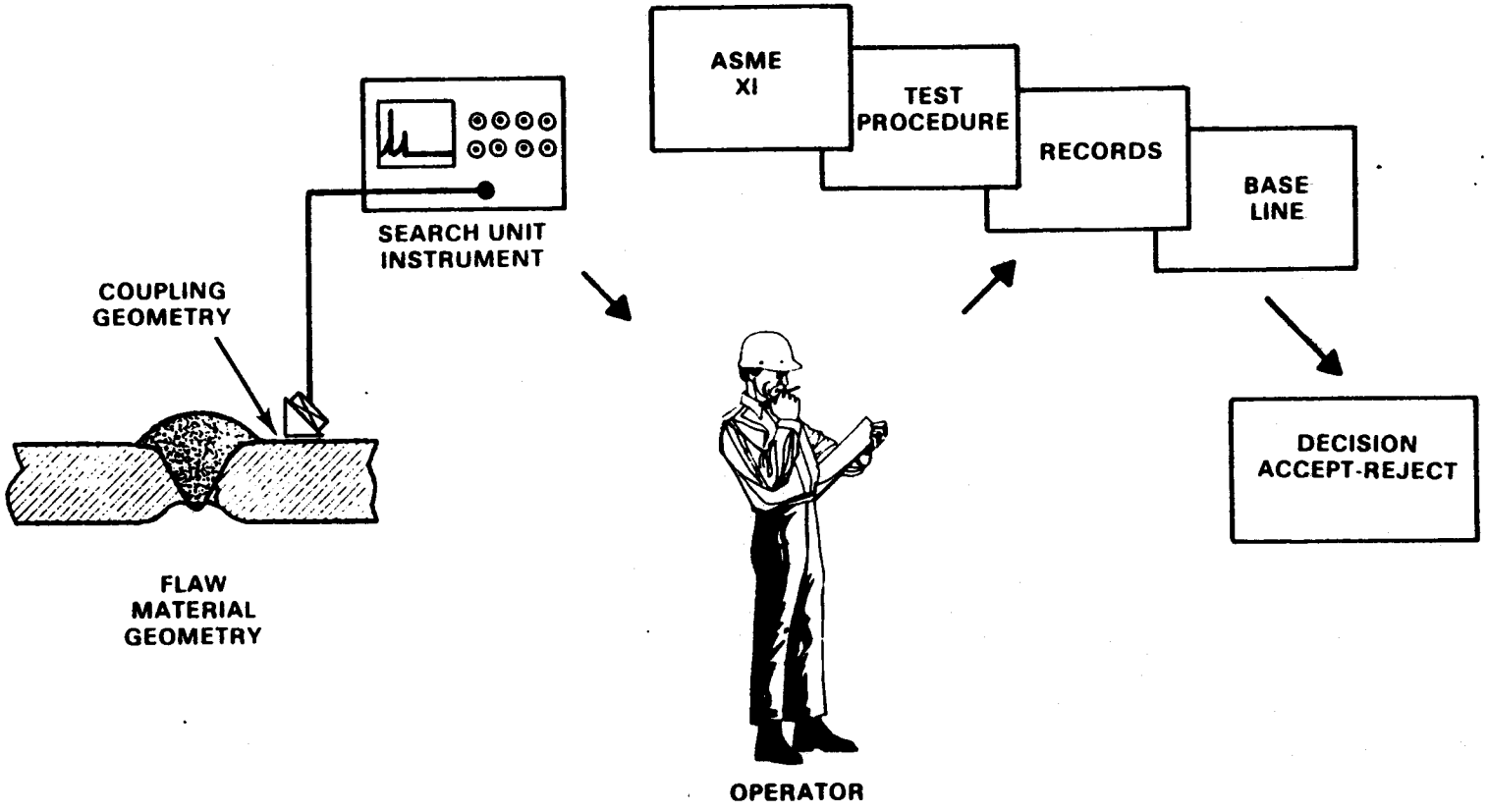


FIGURE 1. COMPONENTS OF INSPECTION RELIABILITY.

STATE-OF-PRACTICE

At the inception of the program, it was felt that the state-of-practice of ISI was highly variable and should be documented. Interviews with five utilities, four commercial ISI organizations and three reactor manufacturers were conducted. The results of this investigation will be published shortly. Highlights of the review are as follows:

- Test procedures are very similar and not substantially different from code minimums. Supplemental tests (after an indication has been located) are substantially different.
- Selection of search units is highly variable.
- Confidence in the inspections were highest for ferritic piping and lowest for cast stainless steel.
- Only one company characterizes or periodically evaluates search units.
- Recording of geometrical indications during basline (PSI) or ISI is not consistent and, therefore, of limited value.
- Nominal and worst case counterbore conditions were described and are shown in Figure 2.

FLAW GEOMETRY

Flaw geometry conditions considered in these experiments include: aspect ratio $a/\ell = .2$, circular segment, orientation $0° \pm 30°$ from perpendicular and back surface angle $0° \pm 20°$. Sample geometries are shown in Figure 3. The EDM method was used to fabricate the notches. Maximum signal amplitude from each notch was recorded using four different search units at 45° and 60°. The results of these evaluations are shown in Figures 4-7. The influence of search unit diameter for nonperpendicular reflectors (Figures 6 and 7) follow the same trends shown in Figures 4 and 5.

Conclusions which can be drawn from this data, Figures 4-7, included the following:

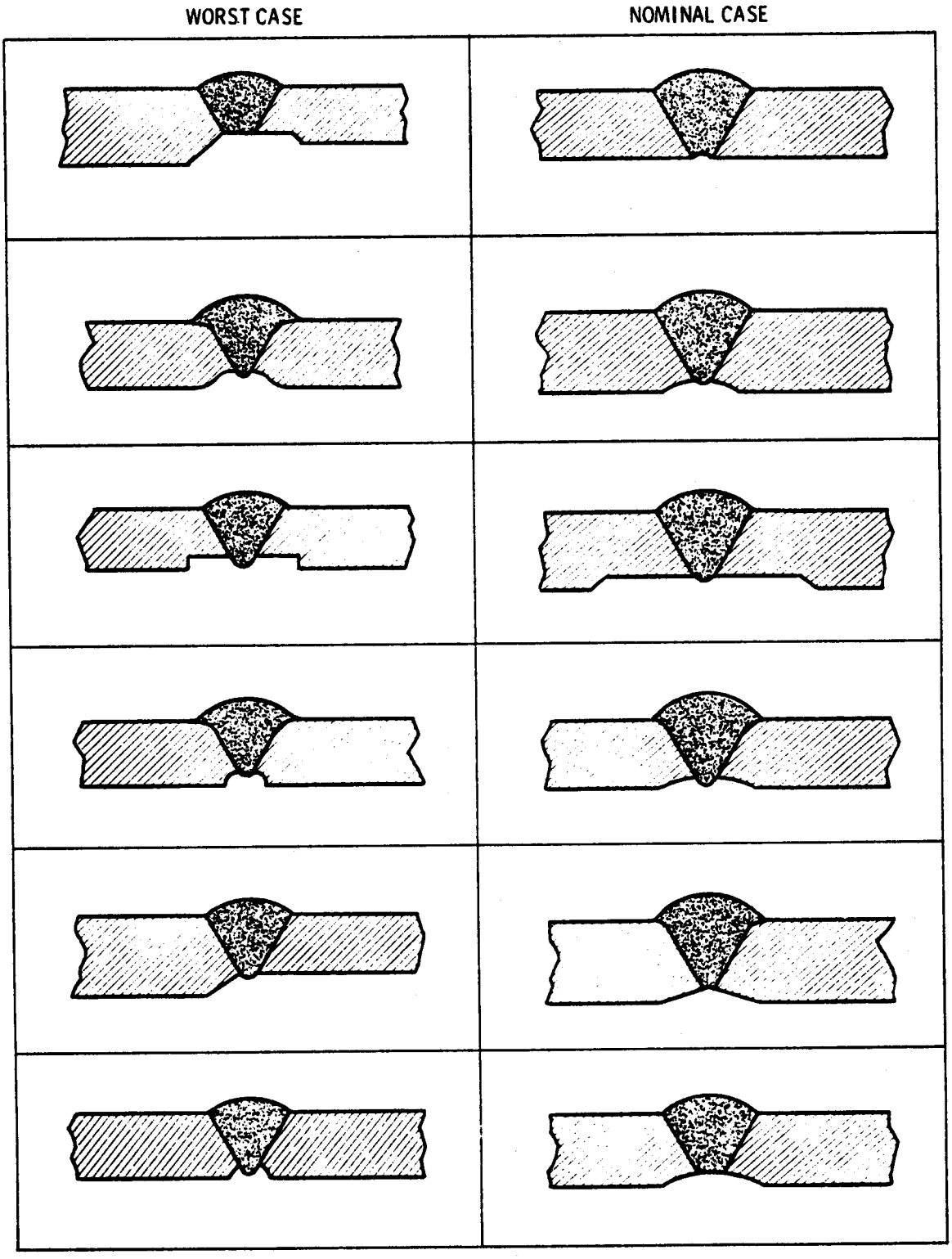


FIGURE 2. COUNTERBORE CONDITIONS.

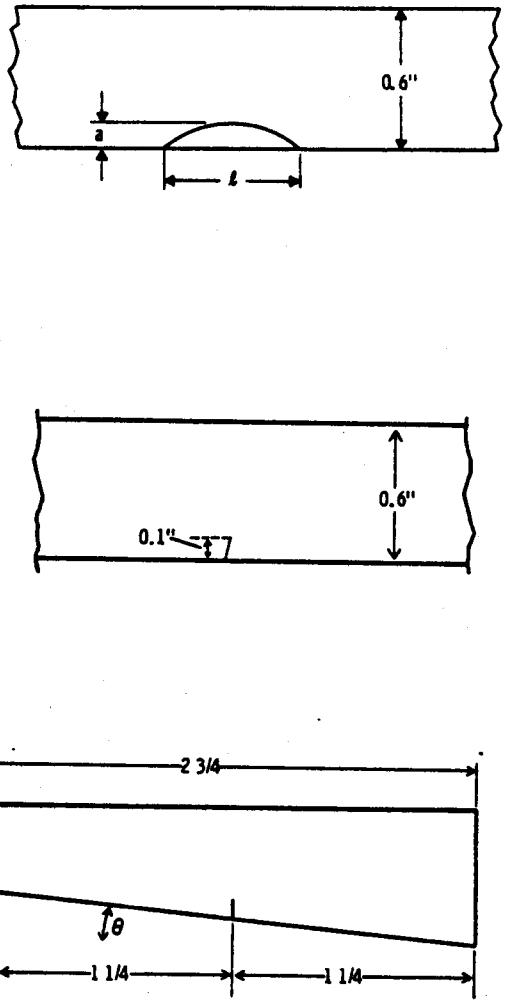


FIGURE 3. EDM NOTCH CONFIGURATIONS.

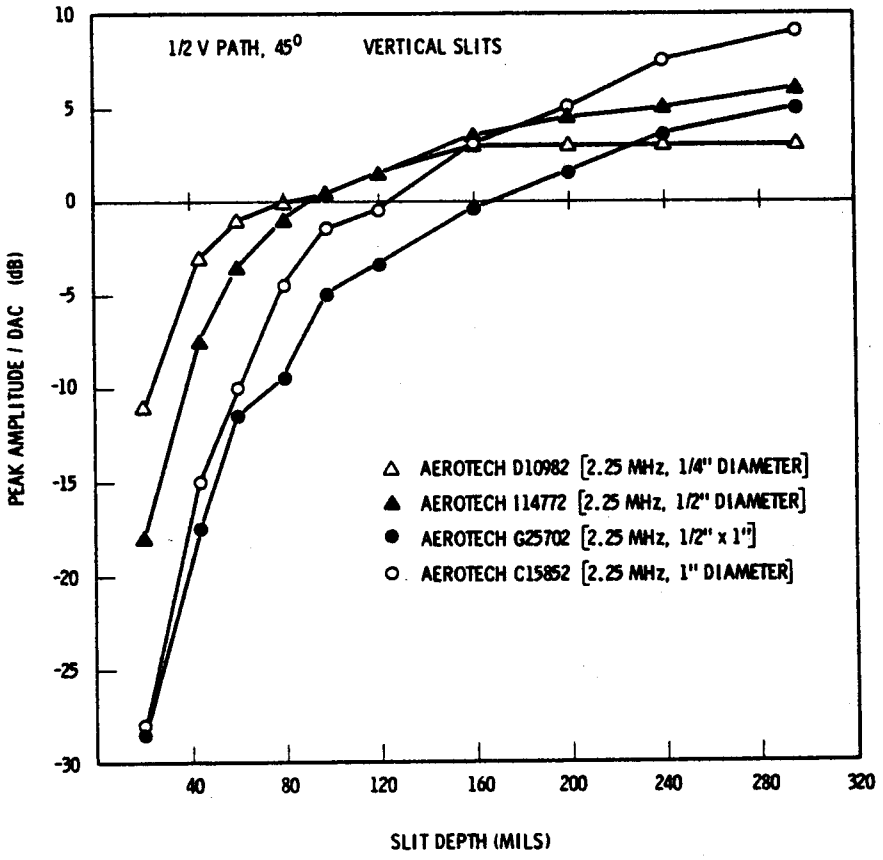


FIGURE 4. PEAK AMPLITUDE RESPONSE FOR VERTICAL EDM SLITS USING FOUR DIFFERENT 45° SEARCH UNITS.

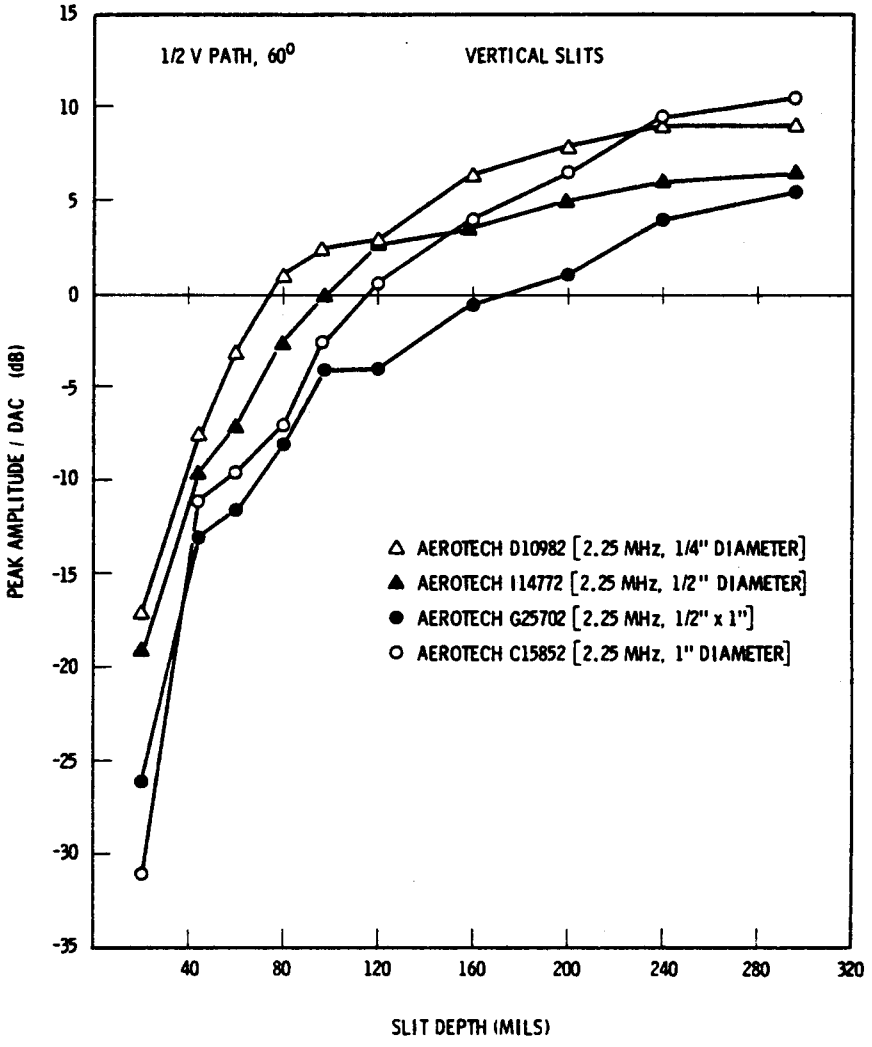


FIGURE 5. PEAK AMPLITUDE RESPONSE FOR VERTICAL EDM SLITS USING FOUR DIFFERENT 60° SEARCH UNITS.

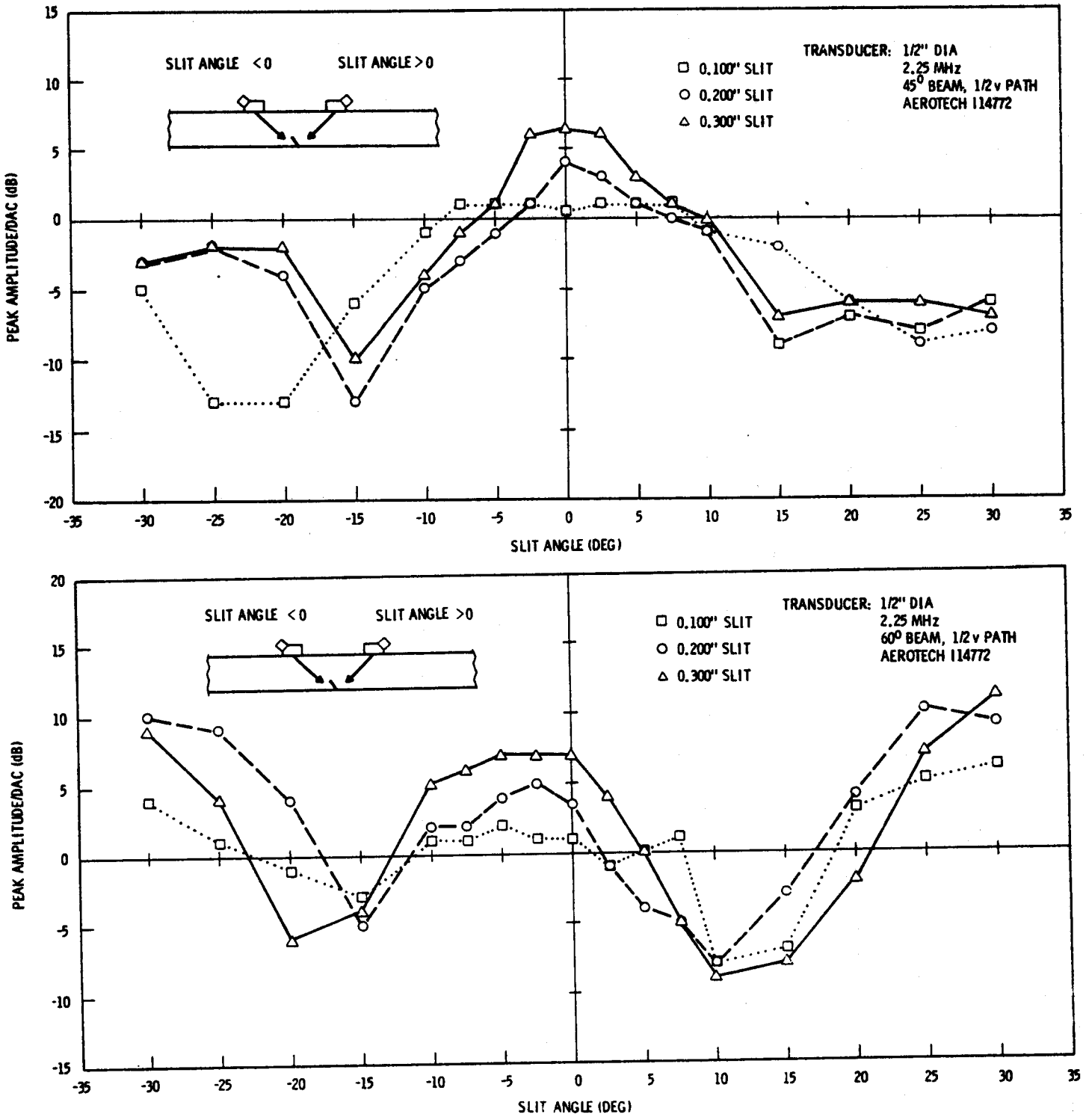


FIGURE 7. RESPONSE FROM ANGLED SLITS USING 45° AND 60° SEARCH UNITS.

1. ASME Section XI, Appendix III, 1977 calibration, recording and reporting requirements are nonconservative considering the allowable flaw sizes of Tables IWB-3514.

2. Search unit selection (presently uncontrolled) results in highly variable (nonconservative) test results.

3. Sensitivity to off angle conditions increases with flaw depth.

4. Flaw orientation has much less influence on the reflected amplitude for 60° shear 1/2 V path inspection than for 45° inspection.

FLAW CHARACTERISTICS

The objective of this experiment is to quantify the influence of crack characteristics on the ultrasonic response. By applying a tensile stress to the flaw, it is possible to separate the influence of crack tightness from all other crack variables. We shall call these two quantities tightness and flaw character.

Thirty 0.6 inch thick 304 stainless steel samples were prepared for this experiment. 24 samples were produced by fatigue in bending at flaw growth rates of 10^{-4} inch/cycle (rough) and 10^{-6} inch/cycle (smooth). Six samples were fabricated by the thermal fatigue method. Flaw depths were from 10 to 42% of the through-wall thickness.

The ultrasonic response measured from the 24 bending fatigue samples, using a 1/2 inch, 2.25 MHz, 45° search unit is shown in Figure 8. These points average 1.15 dB below the EDM notch curve with a standard deviation (σ) of 1.35 dB. The EDM notches have approximately the same aspect ratio ($a/\ell = .2$) as the cracks but are circular segments rather than semi-elliptical like the cracks. Semi-elliptical notches would produce a larger difference between notches and cracks. The responses shown in Figure 8 are in fact the maximum signals which can be achieved, as tensile stresses beyond yield produce no further increase in signal amplitude. Therefore, this data represents the flaw characteristics in the absence of crack tightness.

Before proceeding further with the discussion of crack tightness, it is instructive to consider the theoretical influence of this effect. As the faces of the crack

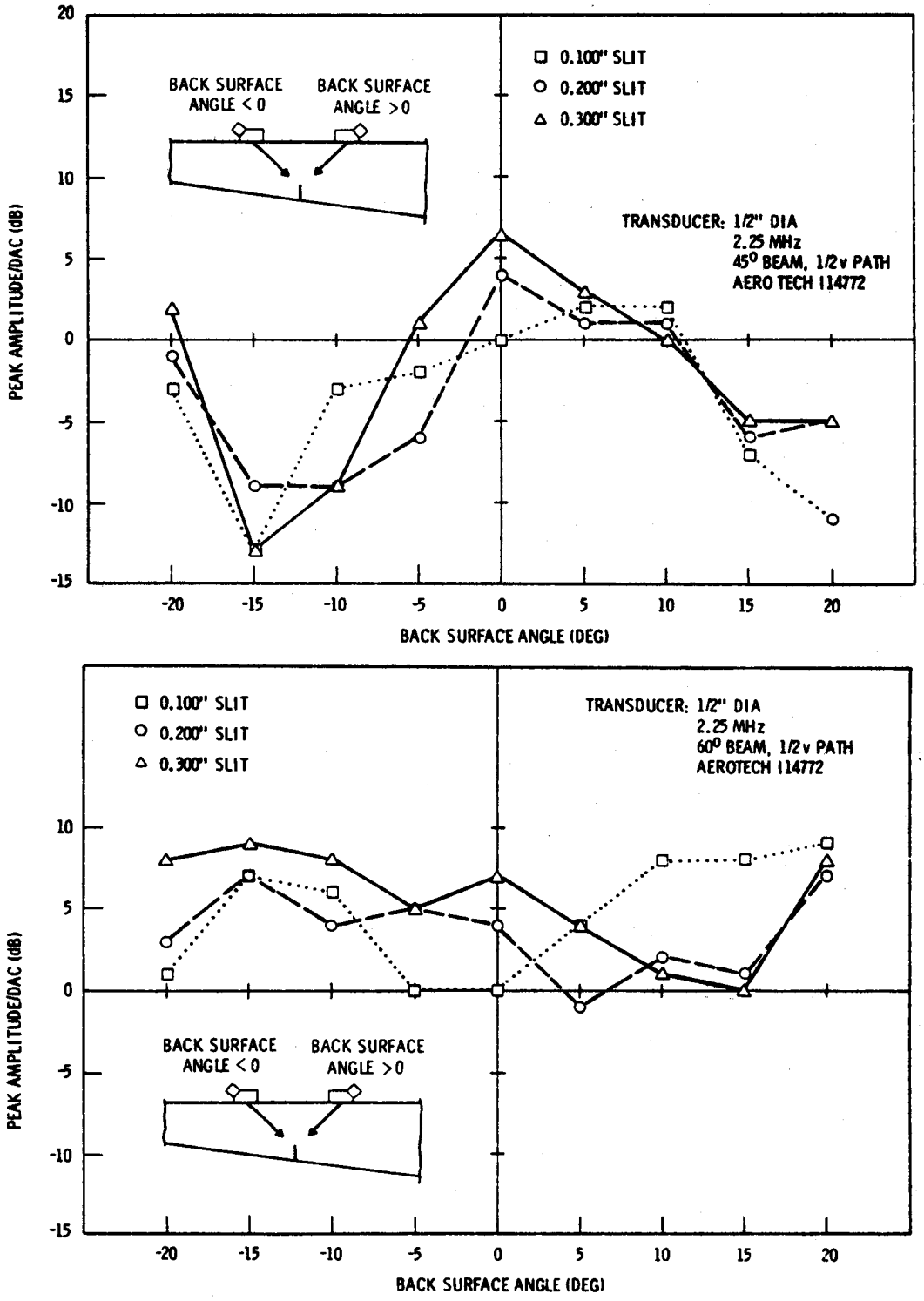


FIGURE 6. RESPONSE FROM VERTICAL SLITS ON AN ANGLED BACK SURFACE (COUNTERBORE CONDITION) FOR 45° AND 60° SEARCH UNITS.

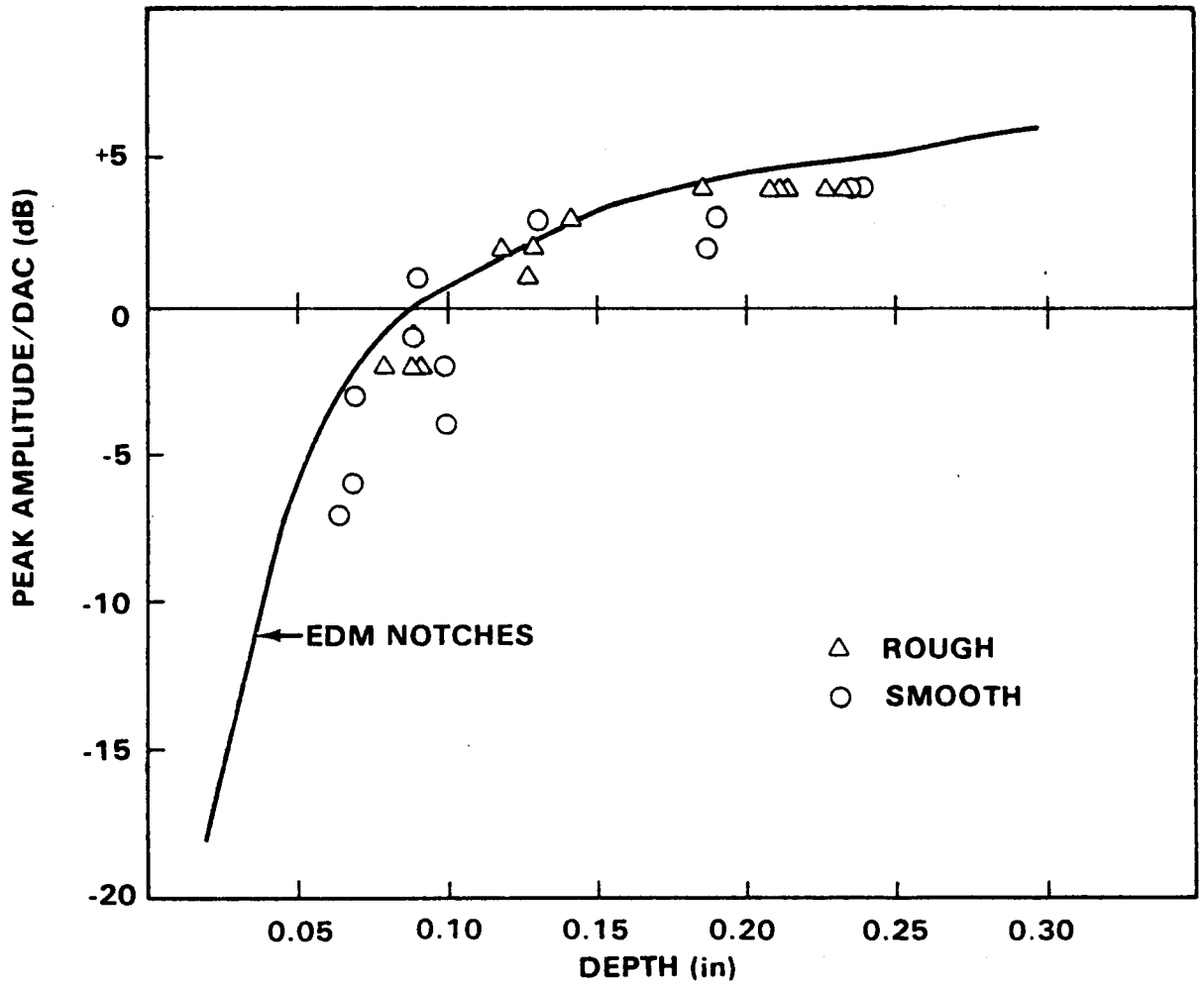


FIGURE 8. RESPONSE OF BENDING FATIGUE CRACKS AND EDM NOTCHES USING 1/2 INCH 2.25 MHz 45° SEARCH UNIT.

are forced into closer proximity, the influence of the intervening medium is reduced. For smooth plane parallel surfaces, it is possible to calculate the reflectivity as a function of the distance between the two surfaces. Figure 9, after Brekhovskikh,[6] represents the case for water-filled and air-filled gaps between stainless steel surfaces for 45° incident shear waves. The theoretical considerations are mentioned here only as an illustration. The crack is more truly represented as a statistically rough surface with some points in intimate contact. Increasing the contact pressure forces more points into contacts and results in a higher degree of ultrasonic transparency.

The influence of crack tightness on the ultrasonic response was determined using a four-point bending fixture. All of the samples were measured in compression up to approximately 75% of yield and 50% of yield tension. One half of the samples (those which were to be destructively tested) were tested at 200% of yield in compression and 100% of yield in tension. Figures 10 and 11 are typical examples of the results from the cracks which were produced by bending. In each case, tensile stress produced no increase in signal amplitude while the plateaus are separated by 32 $\pm$ 2 dB regardless of flaw size. The mean difference between tension and 75% of yield in compression was 7 dB with a standard deviation of 4 dB. Figures 10 and 11 also show the effect of mechanical hysteresis for stresses beyond the yield (in this case, 25 kip).

For the case of thermal fatigue cracks as illustrated by Figure 12, the response is considerably different than for bending fatigue cracks. The crack in the sample shown in Figure 12 was 0.193 inch deep. The response, as fatigued, is 18 dB below DAC, and 22 dB below an equivalent EDM notch. The two plateaus are separated by 15 dB with the lower 26 dB and the upper 12 dB below an equivalent EDM notch. A tensile stress equal to 33% of yield was required to open the crack to its maximum reflectivity.

The large differences in amplitude between the bending fatigue and thermal fatigue samples are due to the initial crack tightness and the crack characteristics. The bending fatigue cracks are planar and have a surface roughness of approximately 10 microns. The thermal fatigue cracks are considerably rougher and deviate from a planar reflector by an amount which is significant compared to the wavelength.

INSTRUMENT AND SEARCH UNIT CHARACTERISTICS

Experiments are currently in progress to evaluate the influence of instrument and

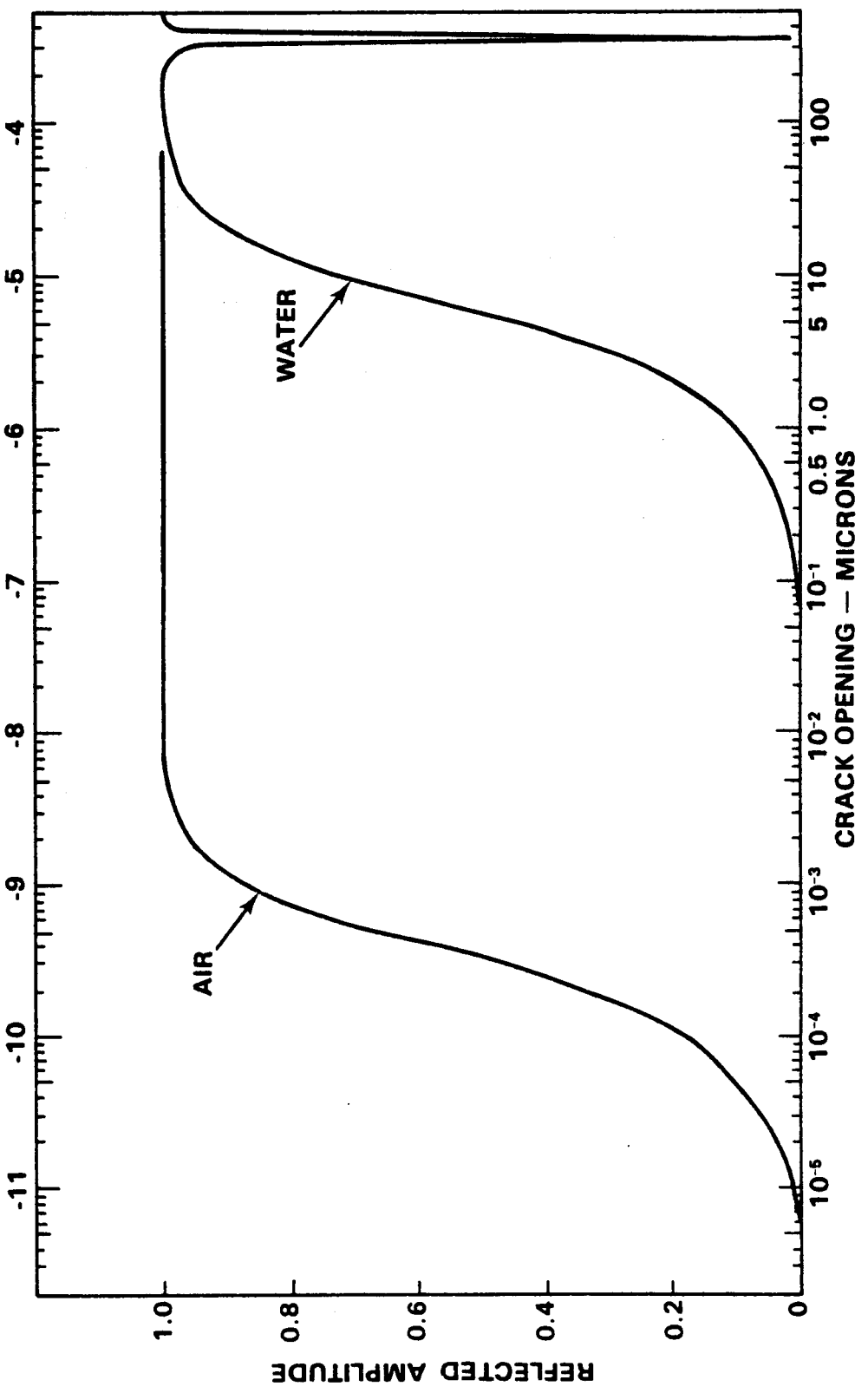


FIGURE 9. REFLECTION FACTOR AS A FUNCTION OF SPACING BETWEEN TWO PLANE PARALLEL SURFACES SEPARATED BY WATER AND AIR, FOR 2.25 MHz SHEAR WAVES AT 45° INCIDENCE.

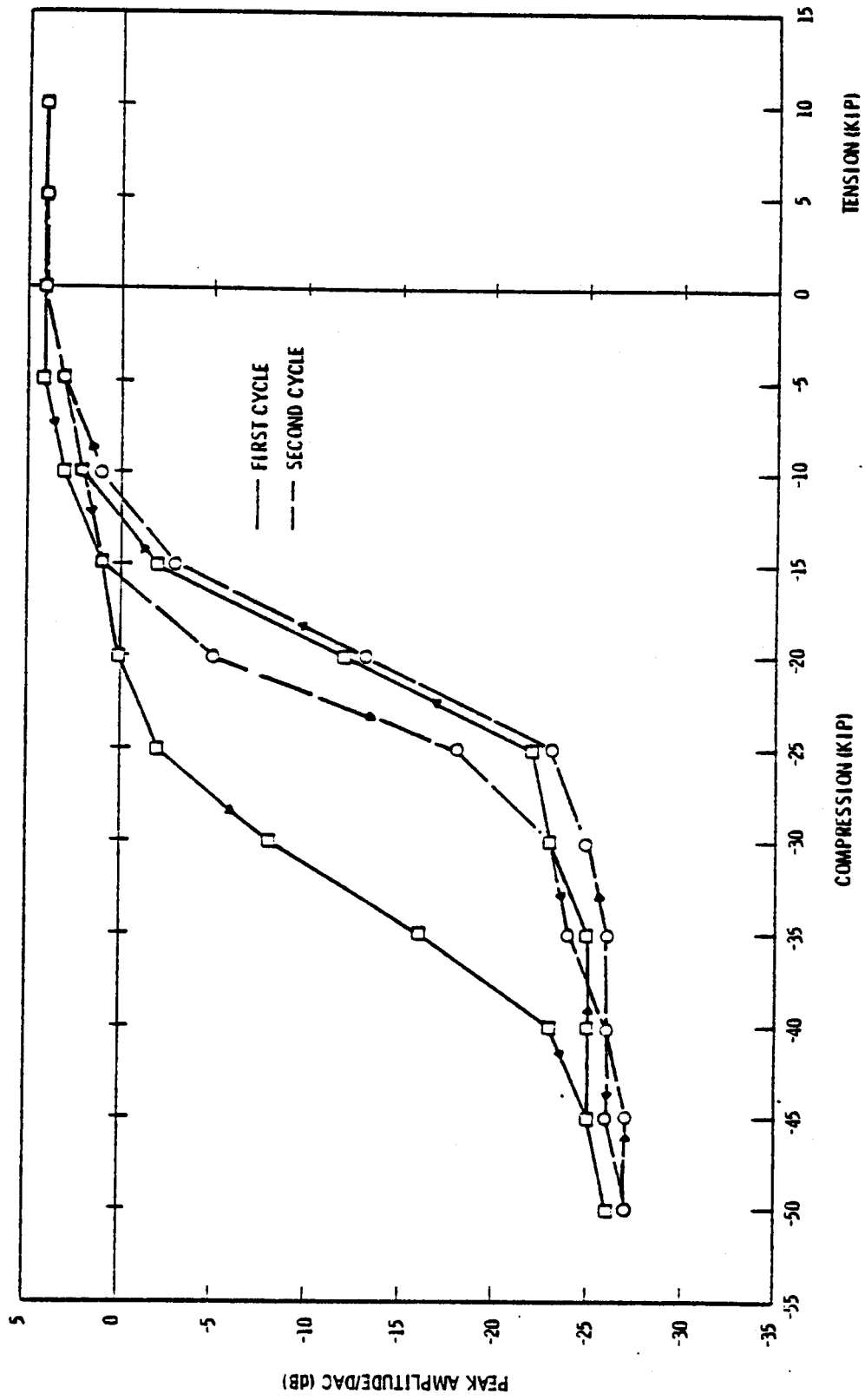


FIGURE 10. Reflected Amplitude From a Fatigue Flaw as a Function of Load in Bending. Yield Stress is Equivalent to a Load of 25 KIP. Flaw Size is 0.232 Inch Deep (39% Through Wall).

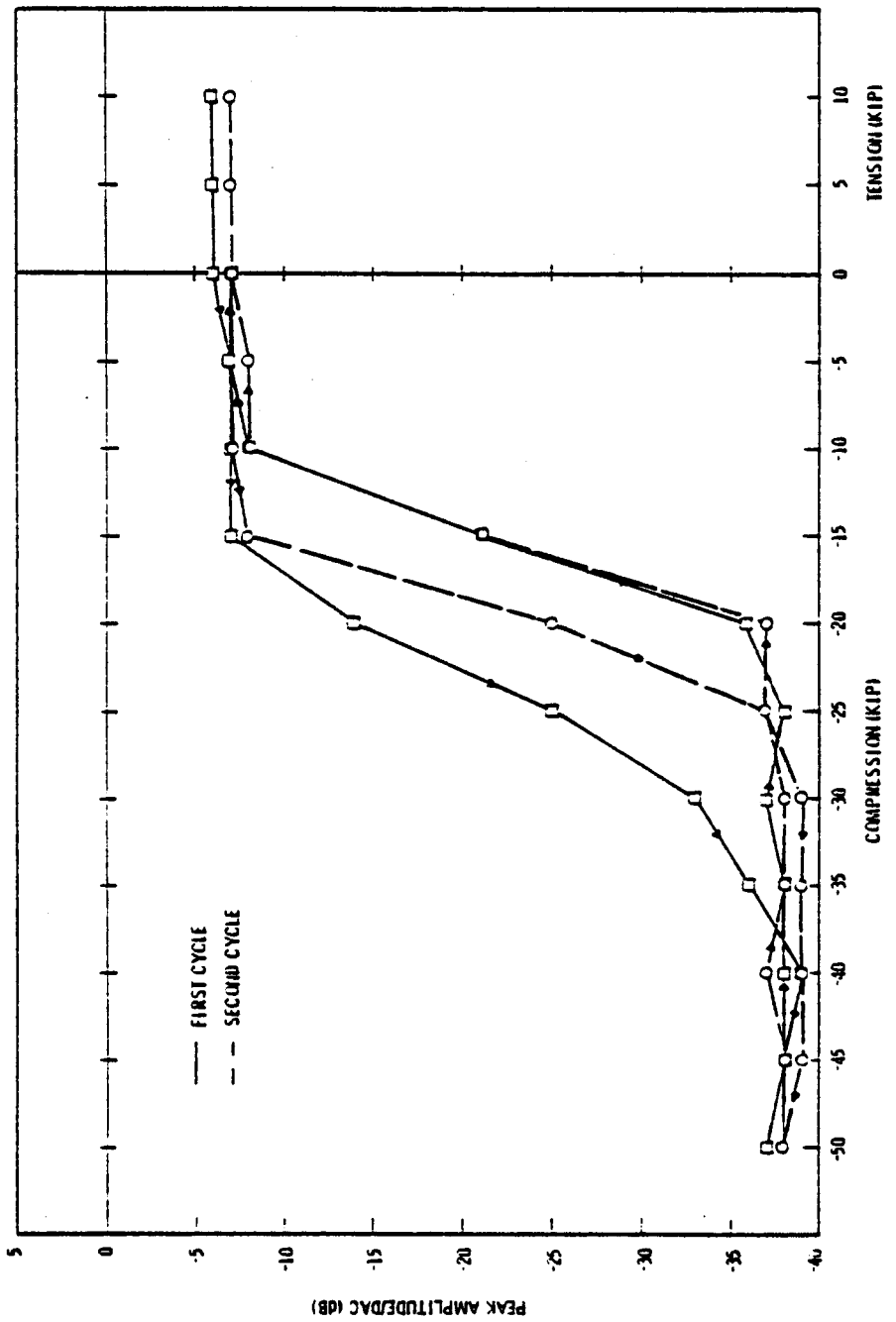


Figure 11. Reflected Amplitude from a Fatigue Flaw as a Function of Load in Bending. Yield Stress is Equivalent to a Load of 25 KIP. Flaw Size is 0.068 Inch Deep (11.3% Through Wall).

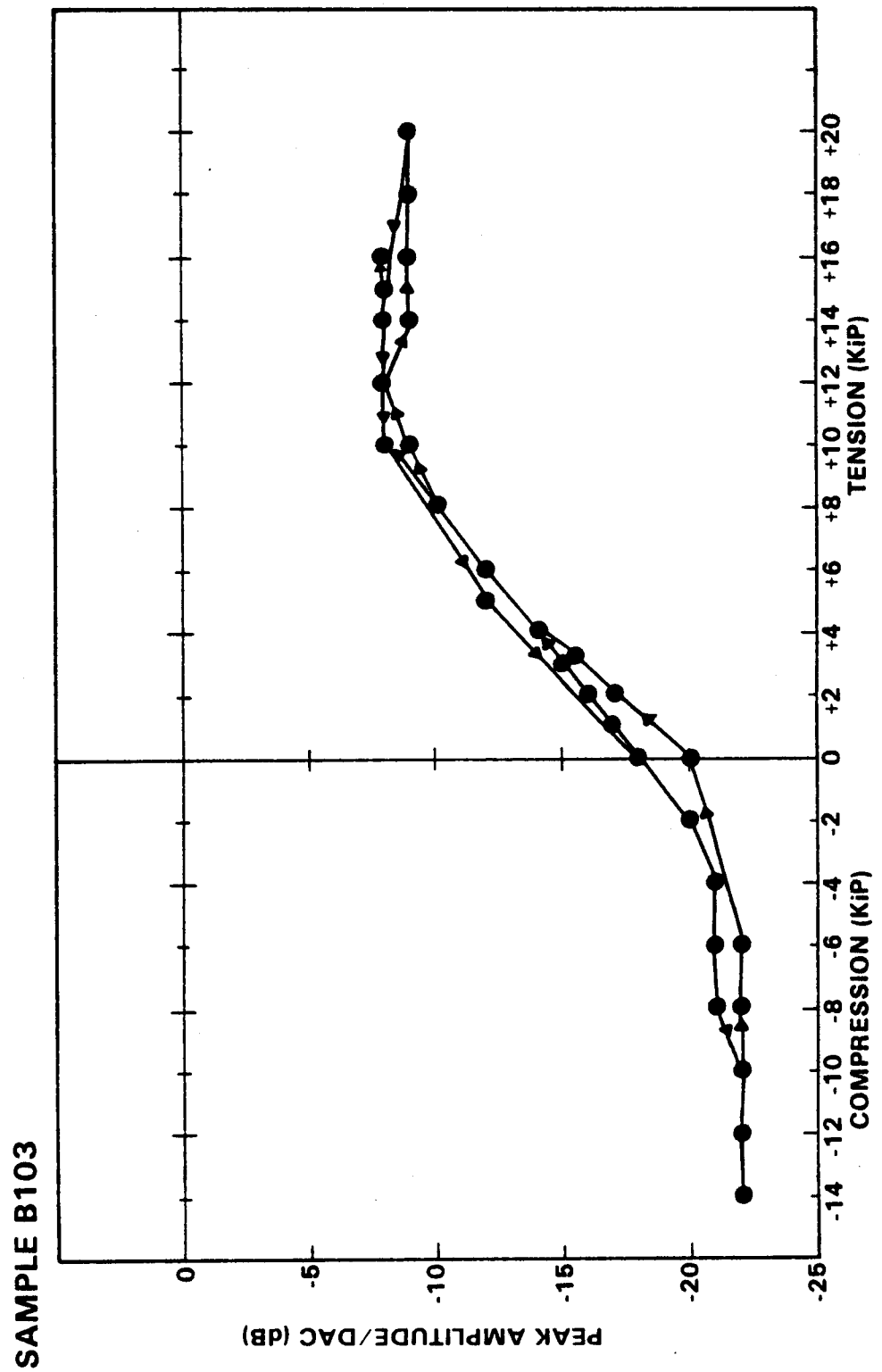


FIGURE 12. REFLECTED AMPLITUDE FROM A FATIGUE FLAW AS A FUNCTION OF LOAD IN BENDING. YIELD STRESS IS EQUIVALENT TO A LOAD OF 33 KIP. FLAW SIZE IS .193 INCH DEEP (32% THROUGH WALL).

search unit variables on inspection reliability. Extensive characterization measurements were performed on the two most commonly used instruments and a limited range of search units. The two most important effects defined to date are horizontal beam diameter and the effective operating frequency of the search unit-instrument combination.

ASME angle beam calibration techniques using notches of lengths greater than 1.0 inch do not compensate for the effective beam width along the length of the flaw (horizontal beam spread). This factor becomes important when the flaw length is less than the horizontal beam spread of the search unit. This effect is demonstrated by Figure 4, where 1/4 to 1 inch search units were calibrated using a 10% notch. The minimum acceptable flaw size according to ASME Section XI, IWB 3514-3 is 11.4% or 68 mils. These data represent EDM notches of aspect ratio (a/ℓ) of .2; real flaws and aspect ratios from greater than .2 to .5 will produce lower response curves relative to DAC.

The second factor of imporatnce is that of frequency response of the search unit-instrument combination. The two instruments evaluated were the sonic Mark 1 and the Nortec 131. Both instruments are portable and would be considered medium bandwidth units. However, they differ slightly in their pulse output and receiver bandwidth. When used with the same search unit, these conditions produce a center frequency shift of approximately .3 MHz (2.4 to 2.1 MHz). This shift may be responsible for the response differences shown in Figure 13. The lower frequency of operation of Unit 2 is less sensitive to flaw orientation.

ESTIMATES OF INSPECTION RELIABILITY

If we assume that variability due to inspection errors is normally distributed about some mean response, $\mu(d)$, the probability that a flaw of a given depth (d) will produce a response greater than the recording threshold can be calculated. This is defined as the recoding probability, RP(d). We assume that the crack response, r, is given by:

$$r = \mu(d) + \sigma_1^2 + \sigma_2^2 + \sigma_3^2 \qquad (1)$$

where: $\mu(d)$ = mean dB response for a crack of depth d; σ_1^2 = crack-to-crack

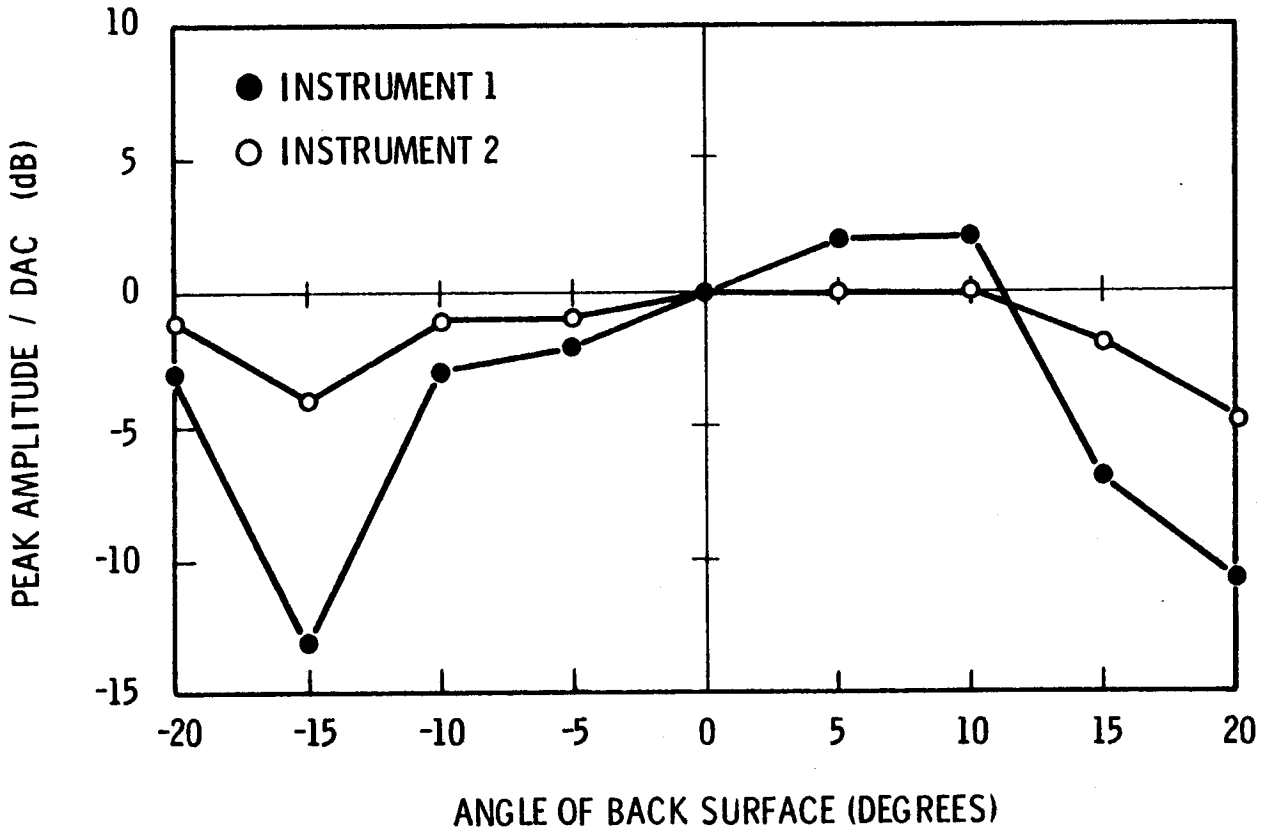


FIGURE 13. RESPONSE FROM .1 INCH DEEP ANGLED BACK SURFACE NOTCHES USING THE SAME SEARCH UNIT AND TWO DIFFERENT BUT SIMILAR UT INSTRUMENTS.

variability; σ_2^2 = variability between inspectors; σ_3^2 = variability within inspections and $\sigma_r^2 = \sigma_1^2 + \sigma_2^2 + \sigma_3^2$.

The recording probability is then calculated as follows:

$$RP(d) = \frac{1}{\sqrt{2\pi}} \int_{\infty}^{Zo} e^{-1/2\, r_{dr}^2}$$

where $Zo = \frac{\mu(d)-c}{\sigma_r^2}$ and c is the recording threshold.

Our estimate of the mean response curve, $\mu(d)$, is based on 24 fatigue crack samples and their measured response under comparessive loading of 75% of yield. While the 75% compressive stress may appear to be very conservative, it should be noted that the data is for dry cracks. Cracks filled with liquid (the condition applicable for ISI of ID surface connected cracks), IGSCC and tight thermal fatigue cracks may produce larger losses in signal amplitudes with no external stress applied. The experimental data is shown in Figure 14, along with fitted curve $\mu(d)$ and the response curve for ideal reflectors of aspect ratio .2. The mean of the measured data is 7 dB below the ideal response curve with a standard deviation of 4 dB.

Estimation for the various sources of inspection error are shown in Table 1, along with similar estimates made by Forli[4] and Silk.[7] The standard deviation, σ_r, is suprisingly close for each of the estimates even though they are derived from substantially different sources.

Estimates of recording probability for DAC threshold levels of 100, 50 and 20% are shown in Figure 15. These estimates are based on the results of this study. However, those of Forli and Silk are not substantially different. The range of applicability of these estimates include most materials and thicknesses of primary system piping welds, but excludes flaws on the far side of austinitic welds and cast austinitic piping.

ROUND ROBIN INSPECTIONS

Preparations are currently in progress for round robin insepctions to determine the effective ness of current ISI practices. The results of these tests should be available early in 1982.

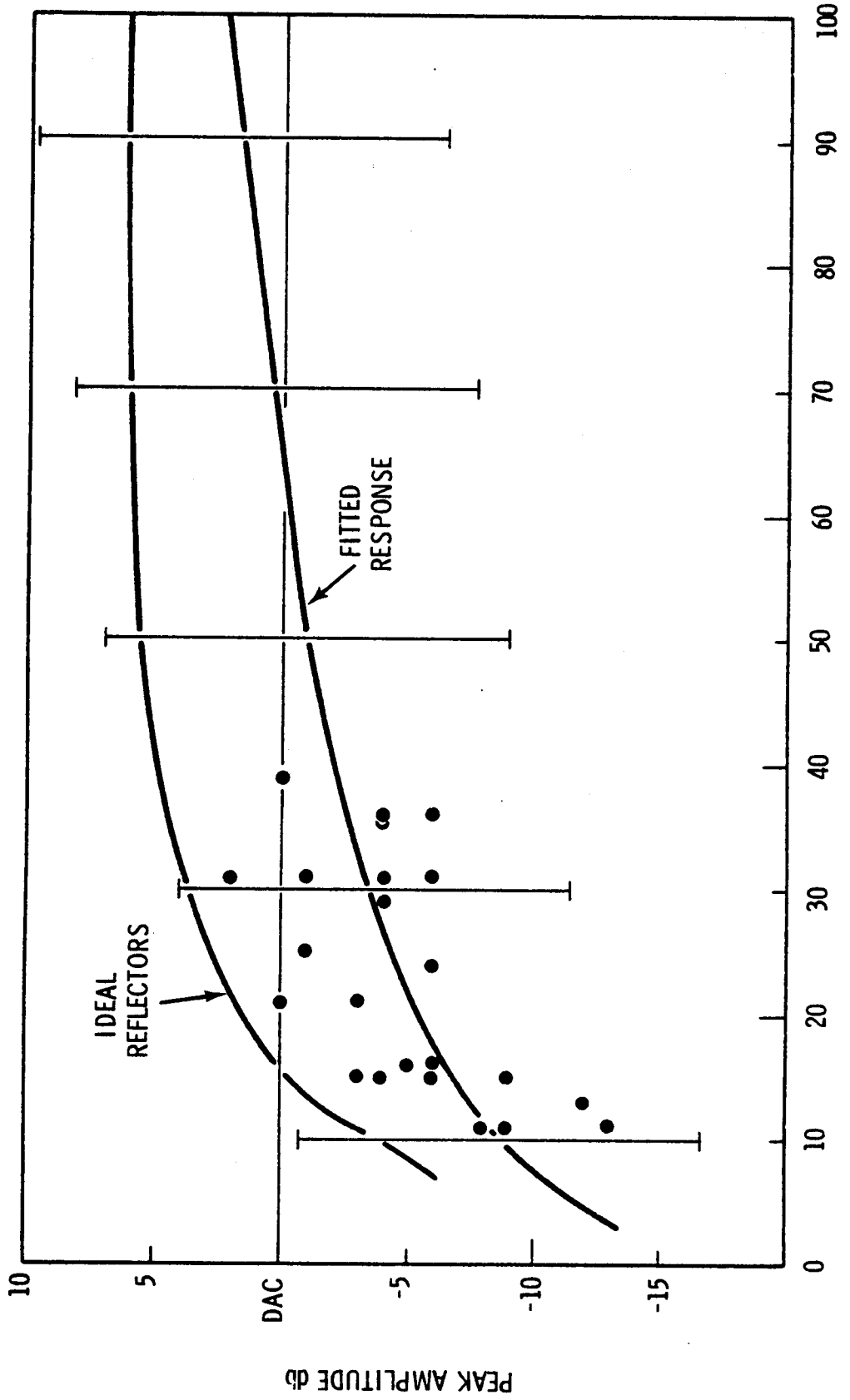


FIGURE 14. Adjusted Response Curve for Fatigue Flaws Under Compression, Shown with 2σ Error Bounds. The Upper Curve (ideal reflectors) is the Response Curve for Notches of Aspect Ratio (depth/length) .2.

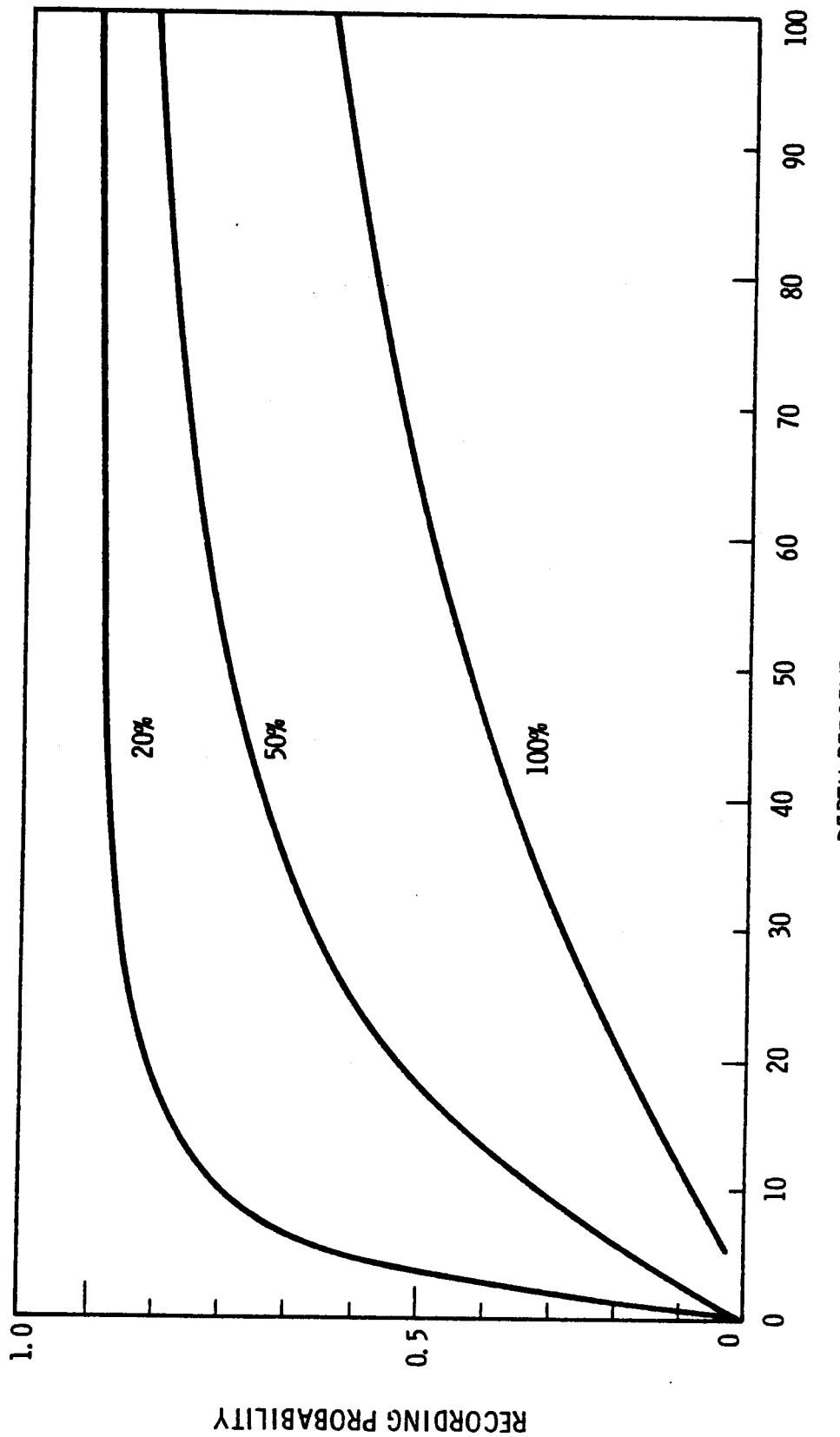


Figure 15. Estimated Recording Probability (i.e., the probability that the ultrasonic response will exceed a threshold value) versus flaw depth for 100, 50 and 20% DAC recording or reporting thresholds.

TABLE I

ESTIMATE OF STANDARD DEVIATION
OF INSPECTION VARIABLES

	This Study ± dB	Silk[7] ± dB	Forli[4] ± dB
Defect Orientation	3.6	3.5	---
Defect Roughness	1.4	3.0	---
Transparency	3.7	4.0	---
σ_1 Crack-to-Crack Total	5.4	6.1	3.3
σ_2 Between Inspection Teams	2.0	---	4.4
σ_3 Within Inspector	2.0	2.0	2.6
Coupling	---	2.0	---
σ_r Total Inspection	6.1	6.7	6.0

REFERENCES

1. Mayfield, M.E., et al, "Cold Leg Integrity Evaluation," NUREG/CR-1319, 1980.

2. Buchanan, R.A., "Analysis of Nondestructive Examination of PVRC Plate Weld Specimen 251J-Part A," Welding Research Council Bulletin 221, November, 1976.

3. Plate Inspection Steering Committee PISC, "Evaluation of the PISC Trial Results," EUR 6371, Volume V, Commission of the European Communities, Brussels, 1979.

4. Foreli, O, "Comparison of Radiography and Ultrasonic Testing," 2nd Nordiske NDT Symposium, Kobenhaun, May 21-23, 1979.

5. Bush, S.H., "Nondestructive Examination and Component Reliability: What Should We Be Looking For," Third International Conference on NDE in the Nuclear Industry, sponsored by the American Society for Metals, Salk Lake City, UT, February 11-13, 1980.

6. Brekhovskikh, L.M., "Waves in Layered Media," Academic Press, New York, NY, 1960, pg. 47.

7. Silk, M.G., "Estimates of the Magnitude of Some of the Basic Sources of Error in Ultrasonic Defect Sizing," AERE-R-9023, Feb. 1978.

PANEL SESSION

Chairman : P. CAUSSIN, Association Vinçotte, Belgium

Panelists: X. EDELMAN, Sulzer Brothers Limited, Switzerland

K. GOEBBELS, Fraunhofer - Institut für Zerstörungsfreie Prüfverfharen, F.R. Germany

C.E. LAUTZENHEISER, Southwest Research Institute, USA

J. MUSCARA, Nuclear Regulatory Commission, USA

A. THOMAS, Framatome, France

J.R. TOMLINSON, Central Electricity Generating Board, United Kingdom

WARNING

This part of the proceedings was made up from notes of the session chairmen and from major points of discussion arising during the panel session. The panel session chairman collected all notes and gathered them in the following paragraphs.

None of them have been reviewed by their authors and these should not be taken responsible for possible errors or omissions.

1. SESSION 1 : FUNDAMENTALS

1.1. Chairmen notes

1.1.1. X. EDELMANN

The paper of Mr. TRUMPFF dealt with the problem of ultrasonic testing of mixt welds between forged or cast stainless steel and ferritic steels.

In course of the investigations a metallographic study of the different regions was performed. Furthermore ultrasonic wave propagation was studied by measuring of attenuation and sound velocity again in the different regions. Then optimal condition for the detection of artificial reflectors investigated. The best suitable technique for the described welds is the application of longitudinal waves with a refracted angle of 45° in steel, at a center frequency of 1.5 MHz. Works are going on to determine the best commercial available probes.

The paper of J. ROSE dealt with the utilization of a Fisher linear discriminant function in intergranular stress corrosion cracking detection. The application of this technique allows to separate geometric indication from IGSCC indications in 304 stainless steel piping. A transducer selection criterion has been worked out. Excellent signal to noise ratios have been achieved with these transducers. Fisher linear discriminant functions as algorithms make use of features as rise time, pulse duration, fall time, partial power between 1.5 MHz and 2.0 MHz in the power spectral response and a second partial power between 2.0 and 2.5 MHz.

There are test specimens used for training of the system. Excellent results have been achieved on unknown cracked specimens.

These technique must be tested in practice, this means that the transformation from the laboratory into the field has to be performed. The final development is the so called "call confirmer", a black box which takes the decision : crack indication or geometric indication. The performance of the present system seems to be pretty far in front of the capability of an usual level two ultrasonic inspector.

In the paper of D. KUPPERMAN data are given on sound velocity and signal amplitude variations and deviations of longitudinal and shear beams in stainless steel weld metal. These measurements are compared with model calculations. Good agreement between both has been achieved. Application of spatial averaging was described. Furthermore results of an investigation of ultrasonic testing technique for IGSCC were presented.

General recommendations

- Realization of simple means for discrimination of cracks from geometrical indications (call confirmer) for ISI.
- Transformation of the new developed techniques into field application.
- Metallurgical work - study of the physical nature of the weld material. Influencing grain structure to guarantee better testability.

1.1.2. K. GOEBBELS

Fundamental aspects were treated during the meeting in most of the sessions. Therefore, some details in this summary are not only restricted to Session 1.

The problems of coarse grained materials NDE, especially of austenitic stainless steel components, are due to

- elastic anisotropy (direction dependence of velocity v in the single crystal) and
- grain size d (scattered intensity, "grass", proportional to mean grain volume for d $\leq$ wavelength λ).

They both together are leading to

- high attenuation α ,
- high scattering α_S ,
- beam skewing θ and
- beam splitting.

Only the last effect ("Frielinghaus-Ganglbauer" effect : 9. WCNDT, Melbourne, Nov. 1979) was not dealt with at the Specialists Meeting.

Several papers discussed θ : JUVA, LAUNAY, KUPPERMAN, additionally GRAY (Session 2), CAUSSIN (Session 4) on the background of BAIKIE's work from 76. The problem is well understood now, but general conclusions have to be drawn (the reader who is more interested in this, is referred to SILK's contribution to Volume 4 of Research Techniques in NDT by R.S. SHARPE, Ed. A.P. London 1980). As the signal-to-noise ratio (SNR) or signal-to-interference ratio (SIR, GRUBER in Session 2) is proportional to (KRAUS, Session 2) :

$$\text{SNR, SIR} \sim (\alpha_S \cdot \Delta \cdot D^2_x)^{-1/2}$$

with Δ = pulse length, D_x = beam diameter at distance x,

each method to decrease α_S , Δ and D_x is appropriate to increase the SNR. This was shown by many contributions :

- "design for inspection" (TOMLINSON, panel discussion) and

- fine grained structure are demanded to decrease α_S ,

- longitudinal waves instead of shear waves (NEUMANN et al.) are reducing the grass amplitude and they are used by most people in practice,

- pulse shaping by the so-called controlled signals (CS) - technique reduces α_S and optimizes the choice of frequency (CROSTACK and OPPERMANN),

- there is no doubt that short pulses are one of the easiest and most appropriate ways to enhance signals,
- reducing D_x by focussing (lenses, transmitter-receiver probes; NEUMANN et al.) will be used now in practice very often,

- analysing beam skewing, the advantage of shear horizontal waves (SH-waves, polarized vertical to the plane of incidence) is clearly seen (KUPPERMAN). The problem is to excite and detect them with ultrasonic probes. Electromagnetic acoustic transducers (EMATs) seem to be the only way in this direction,

- surprising results for the SNR, SIR could be obtained in a study by NEWHOUSE et al. (Session 2), using communication theory (like radar) algorithms,

- a totally different problem, the discrimination between geometrical indications and defect signals during ultrasonic testing of tube weldments (the counterbore problem) was treated by ROSE et al. : pattern recognition algorithms evaluated with training sets and applied to test sets showed promising results in the relations false accepted/false rejected indications.

The final discussion came to the conclusion that each of the methods developed for signal enhancement has its merits, but that none of these methods can solve the outstanding problems alone. Therefore combinations of different methods should be one keyword for the future. GRUBER, KRAUS, NEWHOUSE (Session 2), KUPPERMAN pointed out that especially the combination of signal averaging techniques with other developments is an encouraging step forward.

Several basic problems not yet solved were mentioned during all the sessions, not only in session 1 :

- physics of scattering for $d \geqslant \lambda$, physics of interference, propagation in columnar grains, mode-conversions L-SV-SH, beam splitting,

- interdisciplinary work design-metallurgy-NDE,

- quantitative grain size determination for ASTM 1, 0, -1,...

- possibilities to improve SNR, SIR by communication theory techniques,

- classification and sizing of defects, if the problem signal-enhancement is reasonably solved.

1.2. Discussion

Most of the questions addressed both signal to noise ratio (S/N) enhancement and flaw discrimination techniques. It was also recognized that before speaking about S/N improvement, a signal should be obtained.

Proposals for reducing the noise level (mainly discussed in this session) were though to mask efforts for pushing up the signal level as was proposed earlier. B. GRAY, UKAEA, also stressed the fact that better S/N should eventually lead to efficient sizing techniques.

In the discussion of intergranular stress corrosion cracking (IGSCC) detection, J.L. ROSE, Drexel University, USA, answering questions of M. KROLL, KWU-FRG, made clear that his results were only based upon the crack samples he had access to. As the test pieces were not destructively examined yet, he could not comment on their specific geometry. F.L. BECKER, BNW USA, answering also a question of M. KROLL precised that usually IGSCC roughness was in the range of ultrasonic wavelength, whereas notches can be ten times smoother.

2. SESSION 2 : INSTRUMENTS AND METHODS

2.1. Chairmen notes

2.1.1. C.E. LAUTZENHEISER

Note not delivered.

2.1.2. A. THOMAS

During the second part of Session II, we heard four reports concerning either the state of the art on signal processing or recent developments in UT methods.

1. For Mr. KRAUS' paper, I want to point out the two following points, relating to signal averaging methods :

   - first, an effort is made to develop an industrial device able to make these methods applicable on the whole,
   - then, it seems that further improvements of these methods and good applications could be obtained by the combination of other methods which are also known to help to signal-to-noise ratio improvement.

2. In the paper of Mr. GRÜBER, I noticed the use of 2 probes in the same casing which are both used for producing interference effects on the screen and for reducing noise.
   We are expecting additional results to check the efficiency of this method.

3. From the paper of Mr. NEWHOUSE, it appears that with a good computer, we are able to get many signal processings.
   The new algorithm Mr. NEWHOUSE uses seems to be very interesting for signal-to-noise ratio improvement and we await further results on its application.

4. Concerning the paper of Mr. GANAPATHY, it is to be feared that I will have to make further efforts to understand it very well.
   Nevertheless, it seems to be very interesting to check if the pictures obtained on low attenuation materials may bring some improvements in the interpretation of screen patterns from high attenuation austenitic components.

2.2. Discussion

There has been considerable discussion about the different techniques and new approaches presented. Most participants tried to make clear either the relative advantages and drawbacks of each approach or the interest of combining different solutions. However no definite answers have been given. Indeed it was appearing that most of the new techniques presented were still in an early stage of development.

The general feeling was however that major improvements should be expected from signal processing although industrial practicallity of that approach was still questionable. On the other hand, adapted pulse echo techniques only involving special probe design based upon metallurgical effects were shown to be readily available and far more efficient than standard UT techniques.

Several attendees also pointed out remaining problems such as detection of ID surface connected defects with angled longitudinal waves (F.L. BECKER), effect of varying metallographic conditions in a given piece (N. THOMSEN, Danish Welding Institute) or suggested other techniques such as phase analysis (S. CRUTZEN, Commission of European Communities).

F.L. BECKER also stressed the appearing disagreement about the use of short and long pulses to improving signal to noise ratios. Unfortunately the question could not be talked over due to time lack.

3. SESSION 3 : INDUSTRIAL PRACTICE

3.1. Chairman note : J.R. TOMLINSON

The papers in this session fell into two groups : those by EDELMANN, KROLL et al and PRAT were concerned with inspection of austenitic forgings, pipes and welds; those of LAUNAY et al and SAITOH et al considered the detection and sizing of underclad cracks.

EDELMANN noted that a case by case consideration of components was still necessary to ascertain their inspectability. More data is needed from destructive examination of components rejected by NDT to correlate the UT indications with the actual defects. There should be more consideration given to the needs of NDT in the design process - both in respect of geometrical form and in choice of metallurgical processing. It may be that by minor modification of heat treatments many of the difficulties of ultrasonic inspection could be removed.

KROLL examined the effect of varying the heat input in welding on the attenuation of sound. He found little effect. This apparently surprising result was understandable when it was recognised that there was little variation in the grain structure of the welds produced.

PRAT illustrated the difficulty of devising suitable inspection techniques for components where the requirements of NDT had not been considered at the design stage. He proposed that specifications for fabrication should include requirements on ultrasonic penetrability alongside the usual mechanical properties.

These three papers all illustrated the importance of employing an approach to problems in which the skills of NDT engineers, metallurgists welding engineers and fracture analysts are combined. Advances in NDT alone are likely to be inefficient means of enhancing plant integrity.

LAUNAY et al and SAITOH and TAKAHASHI both demonstrated some success in detection and measurement of underclad cracks. At least on isolated cracks in the base material it appears that cracks deeper than 3 mm can be detected and sized reasonably well. It would appear that extension of defect into the cladding is not detectable by ultrasonics alone - eddy current methods will have to be employed and further development work is needed in this field.

3.2. Discussion

The discussion was naturally divided into two parts. The first one concerned the three first papers. Many comments supported the views of the lecturers on the necessity to take into consideration since the design stage all inspection requirements. Once again the emphasis was put on the lack of specification on the metallurgical structure of components. It was suggested that acceptance standards include NDT of matallurgical structures in view of assessing both inspectability and conformity to expected mechanical and chemical toughness.

In the second part, the inspectability of cladding to base material joints was questioned. Answering a question of G. LOUIS, Cockerill, Belgium, J.P. LAUNAY precised that the Framatome's evaluation criteria are very conservative. In the exemple given, UT indication being obtained in only one scanning direction with SE probes and no indication with the straight beam probe, the indication would be called crack.

Both J.P. LAUNAY and T. SAITOH agreed that the diffraction technique described by the latter can not be used for sizing the french sub-cladding cracks due to the difference in morphology of both crack types. In any case the Japanese experience was the only success reported till now in this conference in sizing flaws in components involving austenitic material.

A. DE STERKE, RTD-Netherlands, criticized the way in which T. SAITOH measured the focal distance of its S.E. probes, namely using a reflection on a flat plane. Instead he recommended to use side drilled holes which would give more realistic results. (N.E. : the shape and morphology of the reflector used influence the focal distance measured. In this case, the choice of an artificial reflector is a matter of personnal judgment, since no recognized standard is presently available).

4. SESSION 4 : RELIABILITY

4.1. Chairman notes : J. MUSCARA

SANDBERG reported the results of an experimental survey of a number of UT methods to detect and characterize artificial flaws in 39 mm thick butt weldments incorporating metallurgical variability produced by various submerged arc welding techniques. The basis of judgment was S/N.

The important conclusions were :

1. Longitudinal waves gave better results than transverse ones.

2. Frequency analysis failed to separate metallurgical and flaw reflectors.

3. Weld crown notches could only be detected with longitudinal waves.

4. Focusing does help detection of weld root defects.

5. The results are not sensitive to metallurgical parameters.

TORRIDA et al paper described an ultrasonic immersion technique employing two focussed transducers to examine (a) the weld soundness (b) the penetration of electron beam welded austenitic steel for nuclear components. In relation to weld soundness it was shown that the technique can detect volumetric flaws of diameter 0.8 mm, and gives a maximum error of 30 % for 0.8 - 2 mm flaws as judged by comparison which radiography. Weld penetration presented more difficulties but the method can detect 1 mm lack of penetration.

In the CAUSSIN et al paper it is argued that despite advances made in the detection of small flaws and in sizing capabilities, little is known about the reliability of NDT of austenitic weldments. The paper discusses three factors affecting this reliability

1. Variability of metallurgical structure. There are two related aspects (a) the microstructure plays a vital role in determining the inspectability of the weldment (b) it is often difficult to know what the structure is - this point was also made by Mr. GRAY in his paper, when he pointed out that nominally identical welding can give quite different grain structures at different times.

2. Testing procedure. A difficulty here is knowing precisely enough the geometry of a weld profile due to construction tolerances. Means of measuring the real geometry in situ are advocated.

3. Equipment characteristics. The importance of thorough equipment characterization is emphasized. The preparation of, and agreement on, international standards is recommended.

4.2. Discussion

The discussion started on the comments of J. MUSCARA on the reliability of the ASME code techniques. He declared that in his personnal opinion, those techniques have been proved unreliable as well for austenitic steel as for ferritic steel inspection.
In the mean time NRC establishes a data base on actual service flaws and NDT indications and will probably requires in the near future that any new technique designed for ISI be proven on realistic flaws. In that purpose NRC has installed a pipe crack study group of which conclusions will be released soon.

M. KROLL asked how P. CAUSSIN could measure the cladding thickness of reactor pressure vessel (N.E. : P. CAUSSIN uses a specially designed SE probe. Presently the thickness range covered is 4 to 12 mm with an accuracy of 0.5 mm).

5. GENERAL DISCUSSION

S.J. CRUTZEN, Commission of European Communities, and S. GANAPATHY, University of Michigan, USA, stressed the fact that it is very difficult to have an objective appraisal of the different techniques presented. Indeed on one hand every experimentator uses his own collection of test pieces and on the other hand it was shown by several lecturers that most test pieces suffer from great variability in microstructure and thus in acoustic properties. To solve this problem, the participants recommended that test pieces be collected on an international basis and be used to get comparable data.

Answering a question of S.J. CRUTZEN, the participants mentioned several international cooperative programmes already in existence.

- Ad hoc Working Group on ultrasonic inspection of austenitic steel welds.
  Australian - Belgian - Dutch - German - Swiss participants.

- Framatome - Electricité de France - Commissariat à l'Energie Atomique - Westinghouse : quadripartite programme.

- Framatome - Vinçotte programme

- French - German cooperative programme

- German - Japanese cooperative programme

- International Institute of Welding group on the ultrasonic inspection of austenitic welds.

- STK - TRC - Westinghouse programme.

In view of this amount of efforts, H.J. DE NORDWALL, Commission of European Communities, mentioned the possibilities of the European Communities to provide an adequate forum for some international harmonization. Following the same line, the participants were of the opinion that within 5 years a cooperative programme should be organized on a worldwide basis to objectively compare all techniques already in use or newly developed. The chairman promised to bring that conclusion to the attention of the sponsor of this meeting, the Committee for the Safety of Nuclear Installation of the Organization for Economic Co-operation and Development.

APPENDIX

PROGRAMME GROUP

P. CAUSSIN, chairman	Association Vinçotte Belgium
X. EDELMAN	Sulzer Brothers Limited Switzerland
K. GOEBBELS	Fraunhofer - Institut für Zerstörungsfreie Prüfverfharen F.R. Germany
A. JUVA	Finland Technical Research Center
C.E. LAUTZENHEISER	Southwest Research Institute USA
J. MUSCARA	Nuclear Regulatory Commission USA
R. NICHOLS	United Kingdom Atomic Energy Authority
P. OLIVER	Organization for Economic Co-operation and Development
J. TOMLINSON	Central Electricity Generating Board United Kingdom
H.D. WALLHEINKE	Kraftwerk Union F.R. Germany